AN INVESTIGATION OF CONICAL DIFFUSER PERFORMANCE WITH SWIRLING INLET FLOW

A. THAKKER

A thesis
presented for the degree of
Doctor of Philosophy of
The City University

Department of Mechanical Engineering
The City University
London

February, 1980.

ABSTRACT

A research programme was conducted to investigate extensively the effect of "solid-body" and Rankine vortex swirl addition on the performance of conical diffusers.

An extensive survey of available literature on theoretical and experimental work has been presented with particular emphasis on areas not covered by previous surveys. Criteria used for defining performance have been reviewed and extended to swirling flow cases. Some degree of ambiguity exists in the estimation of performance; thus experimental results were assessed against all the theoretical models to seek a trend.

Flow visualization studies have indicated that both types of swirl improve the diffusion process of the 10^{o}, 20^{o} and 30^{o} diffusers. The degree of improvement depends on double conical angle and degree of swirl induced.

The experimental analyses have indicated that solid-body swirl modifies the pressure drop in the inlet pipe, improves the diffusion process, eliminates separation tendencies completely or partly, improves the diffuser performance and there is a prospect of further improvement with higher swirl severity.

The characteristics of the free vortex generator showed that the optimum influence of Rankine vortex swirl on diffuser performance was obtained when the number of blades was 8 and the blade angle of the generator was 6^{o}, 10^{o} and 10^{o} for the 10^{o}, 20^{o} and 30^{o} diffusers respectively. The flow in the diffusers deteriorated when the blade angle was increased above its appropriate optimum angle. The

experimental analysis indicated that optimum Rankine vortex swirl eliminates the separation tendencies completely or partly, improves the diffusion process, modifies the pressure drop in the inlet pipe, improves the diffusers' performance and for the 20^{o} and 30^{o} diffusers, the axial velocity at the centre of the vortex was found to be low and the solid-body core of the Rankine vortex approximately coincided with the displacement area of axial velocity to the centre.

Application of experimental data to theoretical analysis showed that for 10^{o} and 20^{o} diffusers, optimum Rankine vortex swirl was seen to be best whereas for the 30^{o} diffuser, best improvement resulted from solid-body swirl 3.

PRINCIPAL NOMENCLATURE

A	Cross-sectional area of duct
AR	Area ratio $(=A_2/A_1)$
B	Inlet blockage factor (=blockage area/total cross-sectional area)
C_p	Pressure recovery coefficient
C_{p_I}, $C_{p_{ideal}}$	Ideal pressure recovery coefficient
C_{pRS}	Diffuser performance coefficient based on area average $(= (1/A_2 \int p_2 dA_2 - 1/A_1 \int p_1 dA_1)/(\rho/2A_1 \int \tilde{V}_1^2 dA_1))$.
D	Diameter
DF	Distortion factor $(=u_{max}/\bar{u})$
k	Calibration scale factor
L	Diffuser length along centre-line
$\dot{m}$	Mass flux
M	Angular momentum
p	Static pressure
$\bar{P}$	Mass averaged static pressure
P_o	Total pressure
$\bar{P}_o$	Mass averaged total pressure
$\hat{P}$	Centre-line total pressure
q	Dynamic head $(=\frac{1}{2}\rho\bar{u}^2)$
Q	Volumetric flow rate
r, R	Radius of duct
RR	Radius ratio $(= R_2/R_1)$
s	Swirl number $(= V_z/V_\theta)$
u	Axial velocity
$\bar{u}$	Mean axial velocity
u_{max}	Maximum axial velocity
$\hat{u}$	Centre-line axial velocity

v	Tangential velocity
$\bar{v}$	Mean tangential velocity
V_m	Maximum velocity of undisturbed Poissieulle flow
V_{zc}	Diffuser inlet centre-line velocity
$\tilde{V}$	Total velocity
$\bar{\tilde{V}}$	Mean total velocity
V_z, V_r, V_θ	Velocity components in the cylindrical co-ordinate system
V_e	Velocity magnitude external to boundary layer
x	Axial length

Greek symbols

α	Kinetic energy factor
α_s	Kinetic energy weighting factor, equation (3.3.2.17)
β	Blade angle of free vortex generator
δ^*_{ax}	Axisymmetric boundary layer displacement thickness, equation (2.1). Note δ^*_{ax} does not have the same physical interpretation as that used for plane boundary layer unless $R \gg \delta^*_{ax}$
ε_o	Overall diffuser effectiveness
η	Diffuser efficiency
η_e	Diffuser energetic efficiency
η_E	Diffuser overall energy efficiency, equation (3.5.1.1.)
η_{total}	Efficiency of conical difuuser defined by Peters (6) $(=(\int p_2 V_{z2}\,dA_2 - \int p_1 V_{z1}\,dA_1)/(\frac{1}{2}\rho\int \tilde{V}_1^2 V_{z1}\,dA_1 - \frac{1}{2}\rho\int V_2^2 V_{z2}\,dA_2))$
θ	Momentum thickness
θ_3	Axisymmetric boundary layer momentum thickness $(= \int_o^R (V_z/V_{zc})(1-V_z/V_{zc})(r/R)dr)$
λ	Pressure loss coefficient
ρ	Fluid density
ϕ	Cone angle of diffuser

ψ	Swirl angle (= $\tan^{-1} v/u$)
$\bar{\psi}$	Mean swirl angle (= $\tan^{-1} \bar{v}/\bar{u}$)
$\hat{\psi}$	Projected maximum swirl angle (= $\tan^{-1}(R\omega/\bar{u})$)
γ	Diffusion factor
ω	Angular velocity
Ω	Angular velocity of swirler at onset of instability

Subscripts

1	Inlet section
2	Exit section
$\mathfrak{L}$	Centre-line
c	Value at vortex core

ACKNOWLEDGEMENTS

The author wishes to express his deep grateful thanks to Dr.R.S. Neve for his guidance and encouragement throughout this project.

Special thanks to [redacted] for developing and modifying the control system and to [redacted] and his staff for their assistance with modifying the test apparatus. Thanks are also extended to all those who have assisted at various times including the library staff and the computer staff.

The research project was carried out in the Mechanical Engineering Department of The City University and the author is grateful to its Senate for provision of the necessary facilities and to the Science Research Council for their support.

Thanks are due to [redacted] for the efficient manner in which this manuscript was typed.

Finally, my sincere thanks to [redacted], for her devoted support, patience and encouragement throughout the project.

CONTENTS

LIST OF FIGURES

Page

CHAPTER FOUR (cont'd).

CHAPTER FIVE

CHAPTER SIX

Page

CHAPTER SIX (cont'd)

Page

CHAPTER SIX (cont'd)

CHAPTER SEVEN

Page

CHAPTER EIGHT

CHAPTER NINE

Page

CHAPTER TEN

LIST OF TABLES

Page

CHAPTER TEN (cont'd.)

CHAPTER ONE

INTRODUCTION

In fluid mechanics, a diffuser is a duct in which the cross-sectional area increases in the direction of the flow. In subsonic flow it produces both a reduction in the velocity level of a fluid stream and an increase in its static pressure. Which of these is the primary objective is dependent on the particular diffuser installation; however each of these objectives needs to be achieved with the minimum of losses. The expansion can be achieved using many different wall contours, but conical diffusers have the advantage of simplified geometry and construction which makes them attractive for practical applications.

In many internal flow systems, it is desirable to reduce the velocity level in some components so that large losses will not occur. Diffusers are used for such a purpose and a common example is found in closed-circuit wind tunnels. In these systems,it is desirable to reduce the velocity level at the test-section discharge so that the fluid stream can be returned to the test-section inlet with as low a power requirement as possible. Diffusers are also used between the compressor and burner of gas turbine engines, and sometimes between the two turbines in a free-turbine arrangement of these engines. In the first case, the objective is to reduce the velocity of the stream to avoid blowing out the flame while in the second it is to produce a velocity that coincides with the efficient operating regime of the downstream turbine.

The rotating and stationary blade passages in the compressor of such engines are also diffusers since they produce an overall reduction in the relative velocity of the working medium. The amount of energy that can be transferred to the fluid is determined by the magnitude of the velocity reduction which can be produced in the rotor; the maximum reduction is often sought so as to minimise the number of stages required for a particular work output. The use of a diffuser downstream of a turbine is an example of an application where the pressure rise produced is the primary objective. In this instance, it serves the same function as a condenser in a steam power plant; i.e. to reduce the back pressure on the turbine, thereby increasing the expansion ratio across it and increasing its work output.

Diffuser performance is a strong function of many flow variables as well as geometric ones. In seeking an optimum diffuser for a given situation, the design engineer must be able to account for the effect of each variable. For uniform axial inlet flows, the effect of geometry on conical diffuser performance is fairly well established. The effect of inlet boundary layer thickness and of simple axial profile distortions has been established for plane-wall diffusers. However, for conical and annular units, and for more complex inlet flow distortions, little design information exists. An important practical case of inlet flow distortion is that of swirling inlet flow. Many times, for example, in flow downstream of a pump or hydraulic turbine, some swirl will be present, and the designer must try to remove it or live with its consequences, for few guidelines are available.

In many engineering applications, the designer of a conical diffuser often comes across a situation when a large pressure rise has to be obtained with a short diffuser, because of severe space limitations. Such a situation calls for the use of wide angle diffusers. Unfortunately, the process of conversion of kinetic energy into pressure energy is very inefficient in such diffusers. This is due to the presence of a strong adverse pressure gradient which causes a rapid growth of boundary layer thickness along the diffuser wall and its eventual separation from the wall.

The problem of obtaining proper flow spreading together with useful pressure recovery across rapidly expanding diffusers is of considerable practical importance. Many different approaches to this end have been reported in literature, e.g. vortex generators, screens or baffles, surface roughness, corrugations, etc. apart from the use of direct boundary layer control. These methods have the common aim of preventing separation from the wall of the diffuser. With increasing expansion angle and area ratio, however, the effectiveness of these methods either break down or it is obtained at a high cost of pressure recovery.

The current research programme arose from the view that it may be possible to improve the performance of the fluidic vortex amplifier by attaching a diffuser at its exit. The discharge from a switched vortex amplifier possesses a very high degree of swirl and the aim is to generate a higher impedance in the chamber by diffusing the discharge. Following recent work on the performance of fluidic vortex amplifiers by Neve (63) and swirling and non-swirling flow in conical diffusers by Wirasinghe (52) who laid down the overall guidelines of research, it was decided to

conduct a comprehensive research programme to investigate the character of swirling flow in wide angle diffusers and in a pipe (diffuser with zero divergence angle),and also to contribute to the existing knowledge on performance without swirl.

An extensive survey of relevant previous experimental work is presented in Chapter Two. A discussion on diffuser performance and the role of swirling flow in pipes, conical diffusers and annular diffusers is included. At the end of the chapter, the foundation of the present research programme is laid.

A considerable degree of ambiguity still exists in the manner in which diffuser performance is evaluated. In Chapter Three, various analytical models presented by previous investigations have been developed logically. Some of the models are further extended for evaluating performance of diffusers with swirl.

The flexibility of the test apparatus, design information and instruments used for experimental work are reported in Chapter Four.

Chapter Five describes the flow visualization work conducted in air to observe the influence of different severity of solid-body swirl, on flow patterns in pipe and wide angle diffusers. The discussion throws light on difficulties associated with such work. Detailed experimental analysis as to the effect of solid-body swirling flow and structure of flow in the diffusers are reported in Chapter Six.

Performance of the free vortex generator and formulation of suitable guidelines for the experimental work are reported in Chapter Seven. The flow visualization work conducted in air to observe the effect of Rankine vortex severity on flow patterns in pipes and wide angle diffusers is described in Chapter Eight. The experimental analysis associated with the presence of optimum Rankine vortex swirl in wide angle diffusers is reported in Chapter Nine.

Theoretical models developed in Chapter Three were used in Chapter Ten to evaluate performance of the diffusers.

The work carried out is reviewed in Chapter Eleven and the results are presented. Possible extensions in the various areas are also discussed.

CHAPTER TWO

LITERATURE SURVEY

2.1 INTRODUCTION

For a very long time, researchers in various disciplines have been working quite independently with applications involving swirling flows. In the early sixties the subject was attacked from every conceivable angle. Suggestions have been made that, in certain flow regimes, the effect of swirl is to improve diffuser performance, while in others, the performance is reduced. However, caution must be exercised in defining efficiency as the extra energy introduced to produce swirl must be taken into consideration in an efficiency definition. A pipe may be treated as a special case of a diffuser, the work associated with swirling flow in pipes warrants a survey and discussion.

The object of the discussion which follows is an attempt to present relevant information from previous work in an informative manner, and it is hoped that this will form a useful foundation for the work to follow.

2.2 DIFFUSER PERFORMANCE

In fluid mechanics, a duct in which the cross-sectional area increases in the direction of the flow is termed a diffuser. A diffuser is concerned with the conversion of kinetic energy into pressure energy through the deceleration of flow. Thus the efficiency of the diffuser is based on the amount of total pressure recovered for a given inlet flow situation.

The first known performance chart for conical diffusers was a map drawn by Eiffel (1). The method by which the performance curves were obtained was not completely described, but it was suggested (2) that the results were obtained analytically by accounting separately for flow losses due to friction and diffuser shape. Eiffel suggested that the best compromise diffuser for use in a wind tunnel was one with an area ratio of 9.0 and an included angle of 7 deg.

Patterson (5) compared the data of Gibson (3, 4) and Peters (6). He stated that maximum efficiency, for a conical diffuser with axial flow, occurs for about an 8 deg. included angle. According to him, Gibson was the first to indicate that energy conversion is not complete at the exit of the diffusers; a further discharge length in the form of a tail-piece is necessary. Peters made a complete investigation of this and suggested a discharge length of four to six times the maximum diameter of an 8 deg. diffuser. The gain in efficiency is about 5-7%.

McDonald and Fox (7) determined the effect of diffuser geometry on performance and effectiveness for a wide range of geometries. Fig.(2.1) shows contours of constant recovery and also the line of maximum pressure recovery at constant L/R_1 (line α-α). Data also were presented on flow regime, or degree of separation, as a function of diffuser geometry. This information is particularly important when there is equipment operating downstream of the diffuser that might be adversely affected by velocity profile non-uniformity.

In addition to the effects of geometry, the performance of a diffuser is affected by the condition of the inlet flow. Performance is strongly affected by variation in inlet

boundary layer thickness. Cockrell and Markland (8) verified the effect of diffuser inlet boundary layer thickness by the addition of inlet pipe lengths. They claimed that diffuser performance is adversely affected by increasing boundary layer thickness up to the point of $\theta_3/R_1 \approx 0.06$. Further increase in θ_3/R_1 results in a slight performance increase until the inlet flow becomes fully developed.

Sovran and Klomp (9) correlated diffuser performance as a function of inlet blockage as defined by equation (2.1). They felt that performance

$$\delta^*_{ax} = \int_o^R \left(1 - \frac{V_z}{V_e}\right) \frac{r}{R}\, dr \qquad (2.1)$$

reduction was the result of insufficient rather than inefficient diffusion. The blockage concept also suggests the possibility of using experimental information from a diffuser of one cross sectional form to calculate the performance of a diffuser of another cross sectional form.

Wolf and Johnston (10) investigated the effect of non-uniform, but still axial, inlet velocity profile on the performance of two-dimensional diffusers. The diffuser inlet velocity profiles were of uniform shear, wake, jet and step shear types. The result in general showed that the diffuser performance was reduced for inlet flows which produced regions of separation near the walls. For wake type flows with a low velocity region in the centre of the inlet, a performance increase was found for some diffuser geometries.

Migay (11) and Livesey and Turner (12) investigated the influence of inlet turbulent mixing on the performance of wide angle two-dimensional diffusers, the inlet flow being generated with coarse grids and wall obstructions respectively. Both noted an improvement in flow stability with separation eliminated and, in the case of Migay's tests, the consequent reduction in outlet blockage resulted in an improvement in static pressure recovery (C_p) from 0.30 to 0.60. William and Stevens (13) contributed brief details of preliminary tests carried out to assess the influence of a high level of inlet turbulence on annular diffuser performance.

Nicoll and Ramaprian (14) put forward data on the gross performance of conical diffusers subject to annular secondary injection at inlet. Tests indicate that the improvement in diffuser performance is significant even at moderate rates of injection. Duggins (15), although he used an injection technique in a somewhat different geometry, confirmed the above findings. In addition, he also assessed the effect of cone angle and slot width and established the optimum rate of injection. Fielder and Gessner (16) carried out similar investigations on two-dimensional diffuser.

Rao (17) describes a method, making use of radial splitters to achieve flow stabilization, applicable to large area ratio and wide angle conical diffusers.

Krasinski and Aziz (18) carried out a study of the efficiency of a radial diffuser, which has the advantage of extreme shortness and the possibility of noise abatement, and found that, applying boundary layer control, the stability of the diffuser is greatly improved when the flow is disturbed and uneven at entry, which often occurs in reality.

Vyas, Samba Siva Rao and Raghunathan (19) presented some new data on the effect produced by straight vanes placed before the inlet of straight conical diffusers at various inlet blockages, B. They found that the efficiency of the diffuser increases as the inlet blockage increases up to the peak recovery as noted by Johnston and Powars (20) and the straight-vane system improves the pressure efficiency for high values of non-dimensional diffuser length but for low values of non-dimensional length, it is more suited to higher area ratios.

2.3 SWIRLING FLOW IN PIPES

Considerable study of swirling compressible flow in tubes (the Ranque-Hilsche tube) has been carried out since 1950. However, relatively little work in the area of swirling incompressible pipe flow is to be found in the literature; the bulk of the compressible flow work has been aimed mainly at characterising and understanding the ability of the Ranque-Hilsche tube to produce temperature separation, rather than investigating the phenomena of axial flow reversal in swirling pipe flows.

In the study of swirling incompressible tube flow conducted by Peck (21) and Beal (22), dye injection was used to identify a region of reversed axial flow near the centre line of the tube. Nuttal (23) and Binnie (24) likewise noted axial flow reversal in swirling incompressible pipe flow, along with the existence of a third flow regime. Under the most extreme swirl conditions, they found that the axial flow was normal (downstream) at the centre of the tube and at the wall, but reversed in an intermediate region.

Talbot (25) investigated the decay of vortex motion superimposed on Poiseuille flow in the laminar range. He observed instability using a dye filament, and defined a stable region for combination of Reynolds and swirl numbers (Fig.2.2). He also related his experimental work to a linearised theory and found good agreement with its prediction.

Bresan (26, 27) studied the swirling incompressible flow of water in a tube, with the swirl induced by tangential injection of the water into the test section. He obtained static pressure and velocity profiles and developed a simple model for predicting axial flow reversal as a function of the swirl strength and decay rate. King, Rothfus and Kermode (28) investigated a system somewhat similar to that of Bresan's. They added a back-mixing to their system and used an improved probe technique to determine pressure and velocity profiles. In the light of their work, they discuss the model presented by various investigators to explain the flow reversal phenomenon.

Menis (29) studied the decay of swirl in a pipe with air as the fluid. He showed that the tangential velocity profile satisfied the theoretical profiles obtained by Prandtl (30) using a heat conduction analogy. Kreith and Sonju (31) investigated the decay of a liquid turbulent swirl which was induced by twisted metal strips along the centreline of the tube and correlated their results with a linearized model. They found that swirl was sufficiently strong to produce flow reversal.

It is fair to say that Harvey's (32) work was the first major contribution to swirling flow in pipes. He was the first to trigger off a breakdown phenomenon in a tube flow. He studied the stability of a swirling flow in a straight

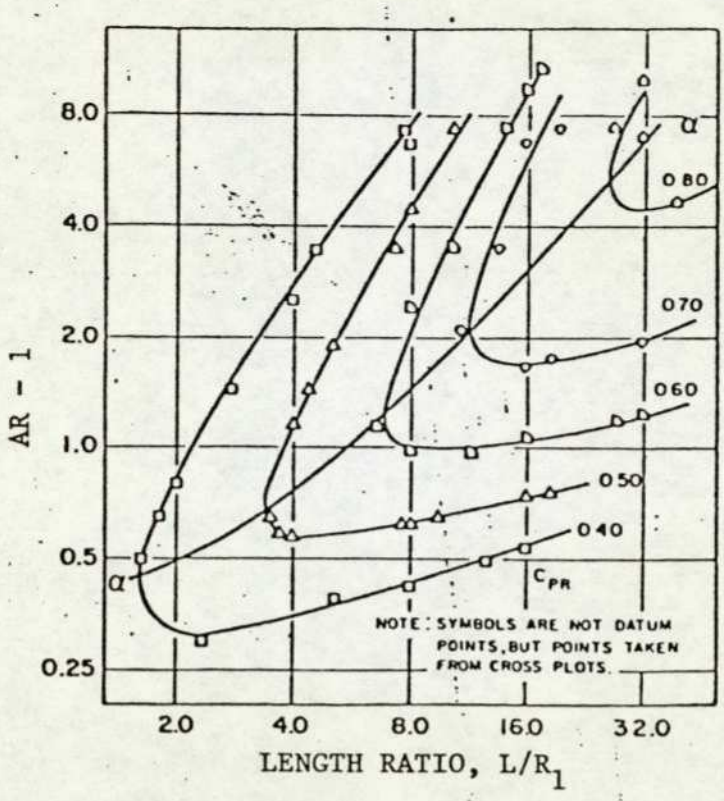

FIG.2.1 CONTOURS OF CONSTANT PERFORMANCE COEFFICIENT FOR CONICAL DIFFUSERS WITHOUT SWIRL (Ref.7).

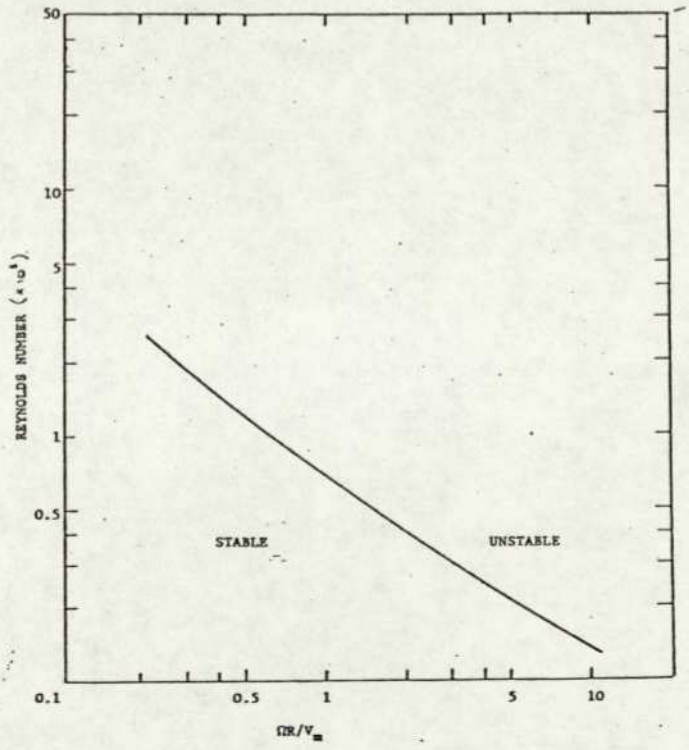

FIG. 2.2 CRITICAL CURVE FOR SWIRL INSTABILITY IN PIPE.

pipe and found that increasing the maximum swirl angle produced a stagnation bubble at the centreline of the pipe. This resulted from the low pressure region created at the pipe centre due to the swirl. With sufficient swirl the difference between the wall and centreline static pressures become equal to or greater than the dynamic pressure of the axial flow. The total pressure of the centreline flow then is lower than the surrounding flow, leading to stagnation or backflow. Harvey gave the criterion for the onset of the stagnation bubble as

$$\frac{\text{angular momentum}}{\text{axial momentum}} > 1.0$$

For solid body rotation and uniform axial flow this is exactly equivalent to saying that the maximum swirl angle is greater than 45°. However, this 45° swirl angle criterion holds only approximately for real swirl distributions. Work done with pipes by Youssef (33) gave results similar to those of Harvey.

The swirling pipe flow results can give an indication of the limiting conditions for swirling diffuser flow. Since it was found (49) that swirl angle increases slightly through the diffuser, the stagnation bubble should first appear at the diffuser exit and then move up to the inlet with increasing swirl. Precisely this behaviour was reported by So (34) for a laminar swirling flow in a conical diffuser with $2\phi = 6^{\circ}$. Flow visualization showed the stagnation bubble and its movement upstream with increasing swirl. Unfortunately, So did not give the swirl condition when the stagnation bubble first appeared. His data showed no backflow for a maximum swirl angle of 20°, but did show backflow for a maximum swirl angle of 50°. Therefore his work neither confirmed nor

contradicted the work of Harvey.

From these considerations, one can hope that for maximum swirl angle less than 40^{o} to 45^{o} there will be no problems with diffuser blockage caused by a stagnation bubble or backflow along the centreline.

Using Harvey's apparatus, Kirkpatrick (35) investigated pressure gradient associated with breakdown. He concluded that viscous flow plays an important part at low Reynolds number and there is loss of total pressure at the centre. His result shows that the distribution of the angle of swirl across the vortex is, in the inner part of the vortex, similar to that of an exponential vortex whose swirl is proportional to

$$\frac{1}{r}\left(1 - e^{-r^2}\right)$$

He found that when a breakdown was present there were axial pressure gradients fore and aft of it; positive upstream and negative downstream. However, when the breakdown was eliminated by reducing the swirl, the pressure gradient was found to disappear.

Gore and Ranz (36) carried out a preliminary study of backflow in rotating fluids moving axially through expanding cross-sections. They were mainly concerned with the conditions for existence and characteristics of backflows. They found that for rotating water in a short tube, when the swirl ratio was increased beyond unity, the region near the axis started to oscillate and when increased beyond a critical value the flow reversed on the axis.

Lavan, Nielsen and Fujer (37) studied analytically the motion of a laminar incompressible viscous flow in a circular duct. They developed a linearized analytical solution, valid for flow having small Reynolds numbers and large swirl ratios. They obtained, by numerically solving the discretized angular momentum and vorticity transport equation, solutions for a wider range of Reynolds number and swirl ratios. The occurrence of flow reversal on the axis and near the tube wall is studied, in particular, and conditions for incipient flow reversal are published.

Weske and Sturov (38) examined turbulent swirled flow of air in a long cylindrical tube at different inlet degree of swirl. They found that the flow behaves differently depending on the swirl intensity. This is manifested among others in different contributions of the fluctuations of different velocity components to the total velocity fluctuations.

Bellamy-Knight (39) investigated vortex breakdown in a cylindrical tube. His flow visualization methods, experimental apparatus and flow conditions are similar to that of Sarpkaya (42, 43), except that he used a cylindrical tube of 1 inch (2.54 cm) inner diameter. He found that his work gave results in close agreement with Sarpkaya's experiments in a divergent tube; in particular, regarding the bubble flow and the existence of a hysteresis region.

2.4 SWIRLING FLOW IN CONICAL DIFFUSERS

According to Peters (6), Andres (40) was the first to say that there is a marked improvement in efficiency of conical diffusers with swirling inflow. However, he did not venture to investigate the behaviour under such conditions. Peters investigated the effect of swirling inlet flow on efficiency

of a conical diffuser with an area ratio of 2.35 and total divergence angle between 5.2 and 180 degrees. His results, showing η_{total} as a function of diffuser divergence angle, are shown in Fig.(2.3). Although they show a definite increase in efficiency with increasing inlet swirl, there are ambiguities in the results. However, Peters' work gives a strong indication that diffuser efficiency might increase with swirling inlet flow.

Vullers (41), according to Patterson (5), suggested that for a free vortex an improvement in efficiency is realised only when the rotation is small and that the present design of diffuser is not efficient when the rotation is large since it does not transform the rotational kinetic energy.

So (34) carried out an experimental study of the behaviour of rotating flow in a 6^{o} cone angle conical diffuser. His study resulted in establishing five distinct flow regimes representing three basic types of vortex flow and two transitional phenomena. They are as follows

Regime 1, the flow is a laminar, one-celled vortex

Regime 3, the flow is also a one-celled vortex but turbulent

Regime 5, the flow is a turbulent, two-celled vortex

Regime 2, represents the transition of a one-cell vortex flow from laminar to turbulent and is characterised by the breakdown of a two-celled vortex into a one-celled vortex.

Regime 4, the other transitional phenomenon, characterised by the breakdown of a two-celled vortex into a one-celled vortex.

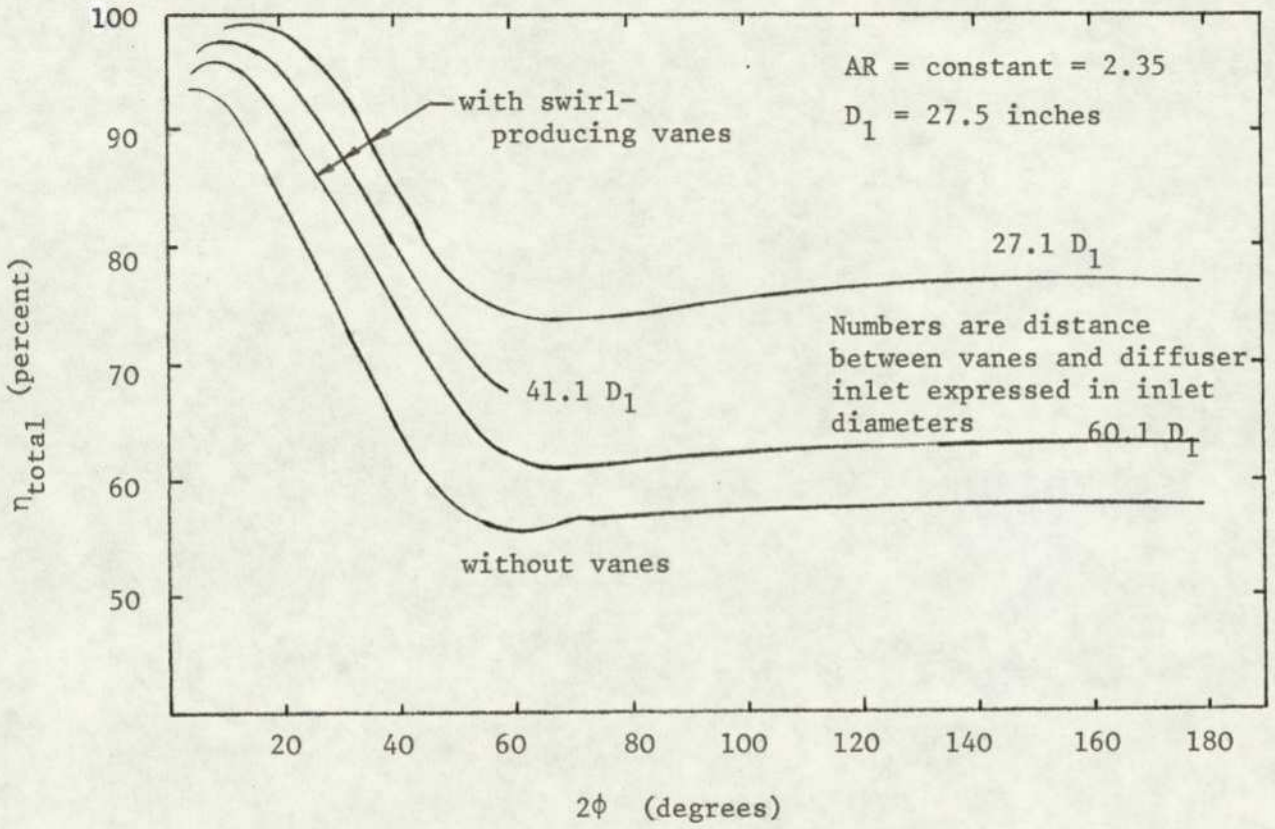

FIG. 2.3 TOTAL EFFICIENCY FOR CONICAL DIFFUSERS WITH SWIRLING INLET FLOW MEASURED BY PETERS (6).

The exponential type of vortex distribution was produced by guide vanes. He did not differentiate between the effects of Reynolds number and swirl number. According to him, if either the flow rate or the blade angle or both are large, then the flow is characterised as strong swirl. The above flow regimes are characterised as weak, medium and strong swirl. In view of this, several investigators feel that his conclusions must be interpreted with some caution.

Sarpkaya (42, 43) investigated experimentally the swirling flow in a mildly diverging cylindrical tube, in which he observed three types of vortex breakdown: double helix, spiral form and axisymmetric form. Guide vanes were used to generate swirl. He found that the type and location of the breakdown was dependent upon the Reynolds and circulation numbers of the flow. The axisymmetric breakdown is basically a finite transition between two sequent states of flow, from a uniform state of swirling flow to one featuring a series of standing waves of finite amplitude. The double-helix and spiral forms, which occur in a region well defined by Reynolds and Circulation numbers, appears to be a consequence of the instability of the vortical viscous flow to spiral disturbances.

Bossel (44) investigated swirling flows in streamtubes of variable cross-section. He concentrated on the behaviour of vortex flow at high swirls. He concluded that the occurrence of vortex breakdown depends on

(1) the initial swirl parameter of the vortex

(2) the subsequent expansion of the stream tube containing the vortex (or equivalently, a corresponding pressure gradient).

These results are completely in agreement with viscous computations, his earlier work, and with experimental observations of Harvey, Sarpkaya, Orloff & Bossel and Lambourne & Bryer.

Gore and Ranz (36) carried out a preliminary study of backflows in rotating fluids moving through expanding cross-sections. They concentrated on the conditions for the existence and characteristics of such backflows. According to them, Peters in his treatment of divergent flow under different conditions of inflow reported no backflow with swirling inflow, possibly because his nozzles did not allow visual observation. Binnie, Hooking and Kamel (45) have observed swirling flow through short divergent sections and reported no backflow.

They identified two important effects for the swirling flow in diffusers. First, axial backflow originated from axial pressure gradients created when the rotating fluid moved through increasing flow cross-section. When the swirl ratio exceeded the critical value, a pattern of reversed flow replaced these pressure gradients. Second, backflow could be stopped at a stagnation point on the axis by controlling the distribution of axial velocities and pressure at some cross-section upstream.

The first of these effects must be interpreted with caution as it tends to limit flow reversal to expanding cross sections. Binnie et al (45), showed that not only does flow reversal occur in diverging and constant cross-sections, but it does so even in convergent cross-sections. They also showed that at low swirl, the flow was unstable, but the flow stabilised when

the swirl was high enough to establish an air core. The reversal of flow does not replace the pressure gradient. Kirkpatrick (35) showed that pressure gradient is very much a part of reversal and is present even after reversal. It is however true that it is the pressure gradient that causes flow reversal.

In internal flow, Sprenger (46), Velentina and Carroll (47) improved diffuser performance with vortex generators. However, those experiments were made only for specific diffusers. Senoo and Nishi (48) attempted to answer the question: what is the optimum configuration of vortex generators for a conical diffuser, and how much increase of pressure recovery is expected with the vortex generators?

The first comprehensive work on the effect of swirling flow in conical diffusers was investigated by Van Dewoestine (49) and by McDonald and Fox (50). Swirl was generated by a rotating honeycomb. They found that swirling did not affect the performance of some diffusers (e.g. 32.2° diffusers) but caused a rather large increase in performance of other diffusers. The most drastic performance increases with swirl took place in diffusers which contained a considerable degree of separation (e.g. the higher area ratio 12° and 15.8° diffusers). They also found that at swirl angles higher than those necessary to produce optimum performance, performance decreased. The reason for this was put forward by them, determined from the previous investigation of Harvey, discussed in section (2.3) (Swirling flow in pipes). To show the effect of swirl on performance, they presented performance maps, Fig.(2.4), (2.5) and (2.6) corresponding to swirl 1, 2 and 3 (i.e. swirl angle of 9°, 13° and 22°) respectively. For comparison, Fig.(2.3)

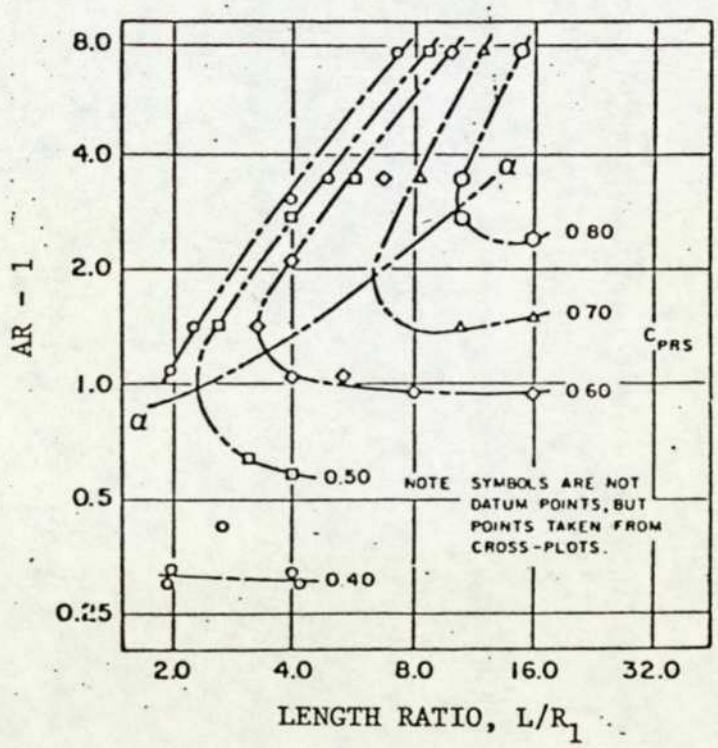

FIG.2.4 CONTOURS OF CONSTANT PERFORMANCE COEFFICIENT FOR CONICAL DIFFUSERS WITH SWIRLING INLET FLOW (SWIRL 1)

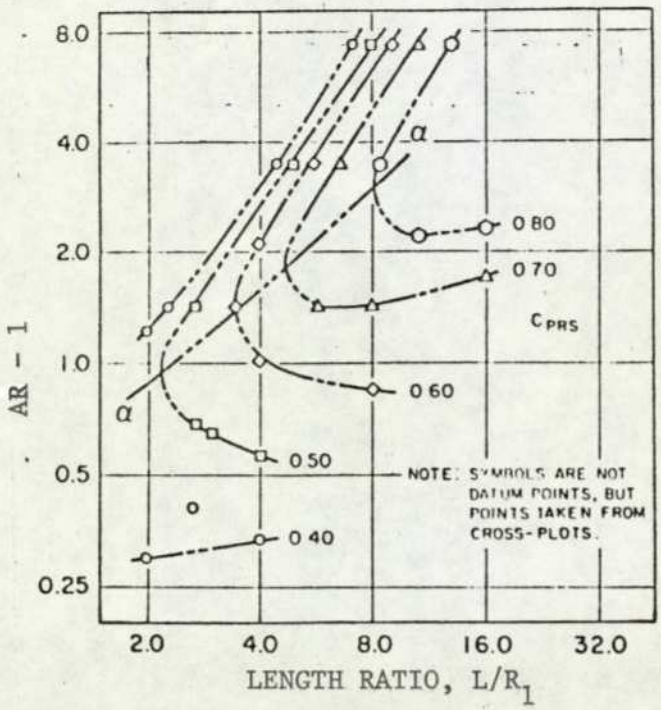

FIG.2.5 CONTOURS OF CONSTANT PERFORMANCE COEFFICIENT FOR CONICAL DIFFUSERS WITH SWIRLING INLET FLOW (SWIRL 2).

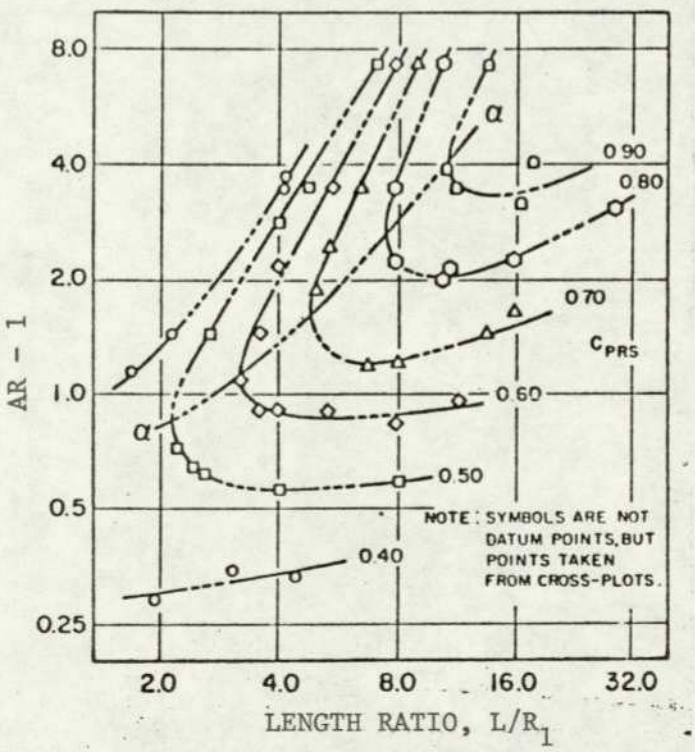

FIG.2.6 CONTOURS OF CONSTANT PERFORMANCE COEFFICIENT FOR CONICAL DIFFUSERS WITH SWIRLING INLET FLOW (SWIRL 3).

corresponds to the performance map from McDonald and Fox (7) with no swirl. Note that the line α-α, the optimum line, drawn through the points of infinite gradient is a measure of the shortest diffuser length required for a given area ratio to obtain the best performance. Fig.(2.7) shows the physical diffuser dimensions required, for a specific swirl strength, to obtain a given performance (in this case 0.70). Finally Fig.(2.8) shows a comparison of lines of optimum performance.

Samba Siva Rao, Vyas and Raghunathan (51) investigated the effect of inlet circulation, varying linearly with radial distance from the axis of the tube at inlet, on the performance of conical diffusers of area ratio 2.35 to 4.0, having cone angle 5-30 degs. The introduction of swirl at the inlet of the diffuser improved the performance of the diffuser considerably. For a linear variation of circulation at the inlet, the optimum vane angle for maximum efficiency lies between 6 deg. and 12 deg. for area ratios in the range 2.24 - 4.0.

Wirasinghe (52) investigated experimentally and theoretically swirling and non-swirling flow in conical diffusers. Swirl was generated by rotating honeycomb. For swirling flow in a conical diffuser, he used a 10^{o} diffuser and found that mild swirl has a definite effect on eliminating separation tendencies. This confirms the past work of Van Dewoestine ,McDonald and Fox (49) (50). Wirasinghe's research also indicates that there is a scope for further increase of performance with increase of swirl. He also found that swirl modifies the wall static pressure drop in the inlet pipe immediately upstream of the diffuser.

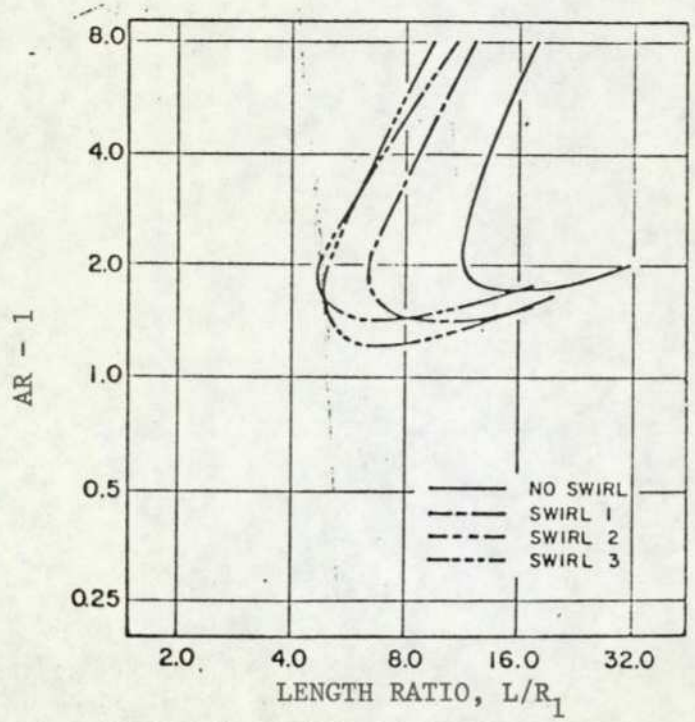

FIG.2.7 EFFECT OF SWIRLING INLET FLOW ON CONTOUR OF CONSTANT PERFORMANCE COEFFICIENT

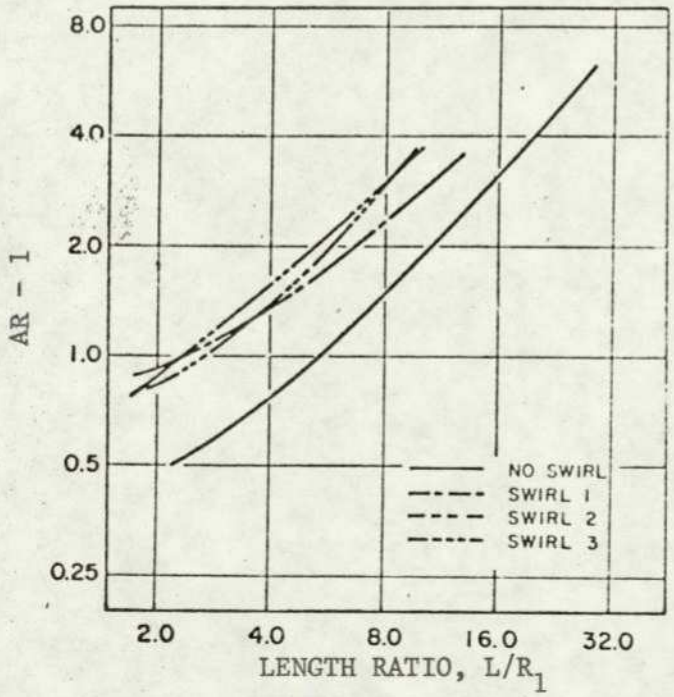

FIG.2.8 EFFECT OF SWIRLING INLET FLOW ON LINE OF OPTIMUM PERFORMANCE AT CONSTANT LENGTH RATIO.

Domkundwar, Sriramulu and Gupta (61) undertook a study to find the effect of swirl strength, angle of diffuser, secondary mass flow and the presence of combustion on the strength and size of the recirculation zone inside a diffuser. They found that increase in both swirl strength and diffuser angle lead to an increase in the strength and size of the recirculation zone.

Senoo, Kawaguchi and Nagata (62) investigated five conical diffusers with different divergence angles to find the influence of swirl on the pressure recovery coefficient. They observed that the pressure recovery of all diffusers were improved by swirl and the highest coefficient was found in a 8 degree diffuser when the flow had a moderate swirl.

2.5 SWIRLING FLOW IN ANNULAR DIFFUSERS

Diffusers of the annular type appear in turbomachinery applications wherein the fluid is to flow over and around a hub, a central shaft, and bearings. These latter types of diffuser are thus expected to deal with flows of varying degrees of swirl. It is important for the designer to have good understanding of the behaviour of an annular diffuser through which a swirling fluid is to flow.

The swirling flow in an annular diffuser was first examined by Hoadly and Hughes (53). They tested one with conical casing, having 10 deg. cone angle, and a cylindrical hub. Introducing a free-vortex swirl into the diffuser passage, they concluded that the centrifugal effect of the swirl was to stabilize the flow on the outer wall thus delaying or even preventing separation there. Moreover, Hoadley and Hughes observed that the performance of their diffuser improved as the inlet swirl angle increased, up to 10 deg. but deterioration took place thereafter. Similar

conclusions were drawn by Honami et al (54) who studied the fluid flow in a mixed flow diffuser (one with both the casing and the hub being conical).

Shaalan and Shabaka (55) used the same configuration as that of Hoadley and Hughes (53) but investigated the effect of widening the angle of divergence on the reaction of swirl in the flowing fluid. They found that the overall performance of the diffuser was markedly improved with swirl up to a certain limit and then deteriorated remarkably.

2.6 CONCLUSION

It has been established that even though the subject of diffusers has been widely studied, there are areas in which, although studies have been performed, generality is not claimed and more theoretical and experimental work is needed.

The areas which were thought to be worthy of further research are as follows:

1. Effect of vortex type on flow properties and diffuser performance.
2. Effect of swirl angle on diffuser performance.
3. Effect of geometry (area ratio, length, angle of divergence, entry and exit length).
4. Flow visualization.
5. Evaluation of diffuser performance.

Some experimental equipment was already available; modifications and additions were needed to enable the five topics to be dealt with. The central question to be answered is whether the addition of swirl really improves performance or not.

CHAPTER THREE

THEORETICAL ANALYSIS OF DIFFUSER PERFORMANCE WITH AXIAL FLOW & SWIRLING FLOW

3.1 INTRODUCTION

Diffusers are concerned with regaining as much static pressure as possible from the dynamic pressure of a moving fluid, this being carried out in subsonic flow by an increase of cross-sectional flow area with downstream distance.

A number of different parameters have been proposed by various researchers, for and used in diffuser investigations, and as a result a certain degree of ambiguity has been introduced. Most of the parameters are measures of the static pressure rise that is produced across the diffuser with, less often, information on the total pressure loss and the outlet flow condition. This static pressure rise can usually be unambiguously defined and easily measured since experience shows that the static pressure is essentially uniform over any cross-section of a diffuser. On the other hand, any attempt to use the reduction in velocity produced by a diffuser encounters considerable difficulty in evaluation, since the velocity generally varies over diffuser cross-sections. Relative measures of pressure regaining capability are obtained by comparing the measured pressure rise with either the maximum value that could be theoretically obtained at the particular flow rate or with the ideal pressure rise that it was possible to achieve with the particular diffuser geometry. In each case an inviscid flow process is presumed, with the first also implying the use of an infinite area ratio to produce complete diffusion; i.e. essentially zero exit velocity. This, however, is not sufficient to prescribe these reference pressure rises unless the inlet flow to the diffuser is uniform, i.e. one-dimensional.

The pressure rise produced in the absence of losses is determined by the reduction in kinetic energy flux that occurs in the diffuser. With non-uniform inlet flow the kinetic energy flux entering a diffuser is greater than it would be if the same flow rate entered under uniform conditions and a knowledge of the inlet profile is therefore required in order to determine the maximum pressure rise that can be achieved. For the ideal pressure rise to be determined, the ideal exit velocity profile must also be established. This presents difficulty in both defination and evaluation and the non-uniform ideal process does not, therefore, lend itself to convenient usage in diffuser performance parameters. A more convenient, though possibly less meaningful, reference process can be defined on the basis of uniform flow conditions. This permits a simple evaluation of the decrease in kinetic energy which takes place in an ideal diffuser and therefore of the corresponding increase in static pressure. Only the mass averaged velocity at the inlet and outlet are required and both are readily obtained from the flow rate and particular geometric areas, quantities which are usually known in diffuser applications.

The object of this chapter is to present in a logical manner relevant theories for expressing diffuser performance from previous work. The analysis will also concentrate on developing a suitable basis for presenting such information when the flow at entry of the diffuser possesses a whirl component of velocity. It is hoped that this will form a useful analytical foundation for the work to follow in latter chapters.

3.2 COCKRELL AND MARKLAND'S MODEL

3.2.1 Introduction

Nearly half a century ago, Patterson (**5**), with the help of Gibson (4), formulated an acceptable guide to diffuser design. Patterson's paper was broad in scope and made clear reference to the effect of parameters which were not fully investigated until much later. In 1963, Cockrell and Markland (8) reviewed the experimental work, much of it being along the lines formulated by Patterson, and indicated improved analytical understanding of diffusers.

It is thought that a brief summary of their theoretical analysis may be beneficial for the discussion to follow and at later chapters.

3.2.2 Analysis

The approach of Cockrell and Markland is shown below. The problem is to derive suitable performance parameters for non-uniform entry flow into diffusers but without swirl.

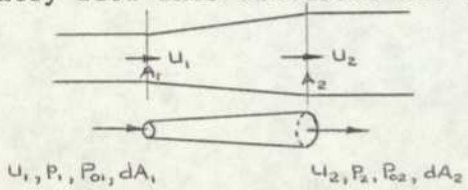

Consider an elementary stream tube with imcompressible flow. Mass weighted energy is given by

$$u_1 p_1 + \tfrac{1}{2}\rho u_1^3 = u_1 p_{o1} = \delta e_1 / dA_1 \qquad \text{at entry}$$
$$u_2 p_2 + \tfrac{1}{2}\rho u_2^3 = u_2 p_{o2} = \delta e_2 / dA_2 \qquad \text{at exit} \qquad (3.2.2.1)$$

Energy loss is thus

$$de = \delta e_1 - \delta e_2 = u_1 p_{o1} dA_1 - u_2 p_{o2} dA_2$$
$$= u_1 p_1 dA_1 - u_2 p_2 dA_2 + \tfrac{1}{2}\rho(u_1^3 dA_1 - u_2^3 dA_2)$$

Integrating this equation to obtain the total energy loss, for constant p_1 and p_2 across inlet and exit

$$\Delta e_{loss} = \int_{A_1} u_1 p_{o1} dA_1 - \int_{A_2} u_2 p_{o2} dA_2$$
$$= p_1 \int_{A_1} u_1 dA_1 - p_2 \int_{A_2} u_2 dA_2 + \tfrac{1}{2}\rho\left(\int_{A_1} u_1^3 dA_1 - \int_{A_2} u_2^3 dA_2\right)$$
$$= Q(p_1 - p_2) + \tfrac{1}{2}\rho\left(\int_{A_1} u_1^3 dA_1 - \int_{A_2} u_2^3 dA_2\right) \qquad (3.2.2.2)$$

where Q is volume flow rate. We now define the mean velocity $\bar{u}_1$ at inlet and $\bar{u}_2$ at exit.

$$\bar{u}A = \int_A u dA = Q \qquad (3.2.2.3)$$

and we define a parameter α (kinetic energy factor) which represents the extent of non-uniformities in the velocity profile

$$\alpha \bar{u}^3 A = \int_A u^3 dA \qquad (3.2.2.4)$$

Introducing equation (3.2.2.3) and equation (3.2.2.4) into equation (3.2.2.2) we have finally

$$\Delta e_{loss}/Q = \Delta P_t$$

where ΔP_t is the energy loss per unit volume, or "normalised total pressure loss".

$$\Delta e_{loss}/Q = p_1 - p_2 + \tfrac{1}{2}\rho(\alpha_1 \bar{u}_1^2 - \alpha_2 \bar{u}_2^2) \qquad (3.2.2.5)$$

we may write this as an energy equation

$$(p_1 - p_2) + \tfrac{1}{2}\rho(\alpha_1 \bar{u}_1^2 - \alpha_2 \bar{u}_2^2) - \Delta P_t = 0 \qquad (3.2.2.6)$$

α_1 is close to unity, provided the velocity distribution at inlet is uniform, but α_2 differs increasingly from unity as the area ratio and expansion angle of the diffuser increase. Writing the energy equation in the simplified form

$$(p_1 - p_2) + \tfrac{1}{2}\rho(\bar{u}_1^2 - \bar{u}_2^2) - \Delta P = 0 \qquad (3.2.2.7)$$

ΔP now absorbs the real loss of stagnation pressure and the apparent losses associated with non-uniformities. Thus

$$\Delta P = \Delta P_t - \tfrac{1}{2}\rho\bar{u}_1^2(\alpha_1 - 1) + \tfrac{1}{2}\rho\bar{u}_2^2(\alpha_2 - 1) \qquad (3.2.2.8)$$

From equation (3.2.2.7) and equation (3.2.2.3) we have

$$\Delta P = (p_1 - p_2) + \tfrac{1}{2}\rho\bar{u}_1^2(1 - A_1^2/A_2^2)$$

If we define

$$q = \tfrac{1}{2}\rho\bar{u}_1^2 \qquad (3.2.2.9)$$

and the pressure recovery coefficient

$$C_p = (p_2 - p_1)/\tfrac{1}{2}\rho\bar{u}_1^2 = (p_2 - p_1)/q \qquad (3.2.2.10)$$

then the above equation becomes

$$\Delta P = qC_p + q(1 - A_1^2/A_2^2)$$

$$= q(1 - A_1^2/A_2^2 - C_p) \qquad (3.2.2.11)$$

We now define λ, the pressure loss coefficient as

$$\lambda = 1 - C_p/(1 - A_1^2/A_2^2) \qquad (3.2.2.12)$$

thus from equation (3.2.2.11)

$$\Delta P = q(1 - A_1^2/A_2^2)[1 - C_p/(1 - A_1^2/A_2^2)]$$

thus introducing equation (3.2.2.12)

$$\Delta P = \lambda q(1 - A_1^2/A_2^2)$$

If a tail pipe is fitted at the end of a diffuser, then the static pressure will continue to rise beyond the diffuser exit as the velocity distribution changes due to turbulent mixing. Let p_3 be the maximum pressure achieved in the tailpipe, then the combined pressure loss coefficient for diffuser plus tailpipe is

$$\lambda' = 1 - C_p'/(1 - A_1^2/A_2^2) \qquad (3.2.2.13)$$

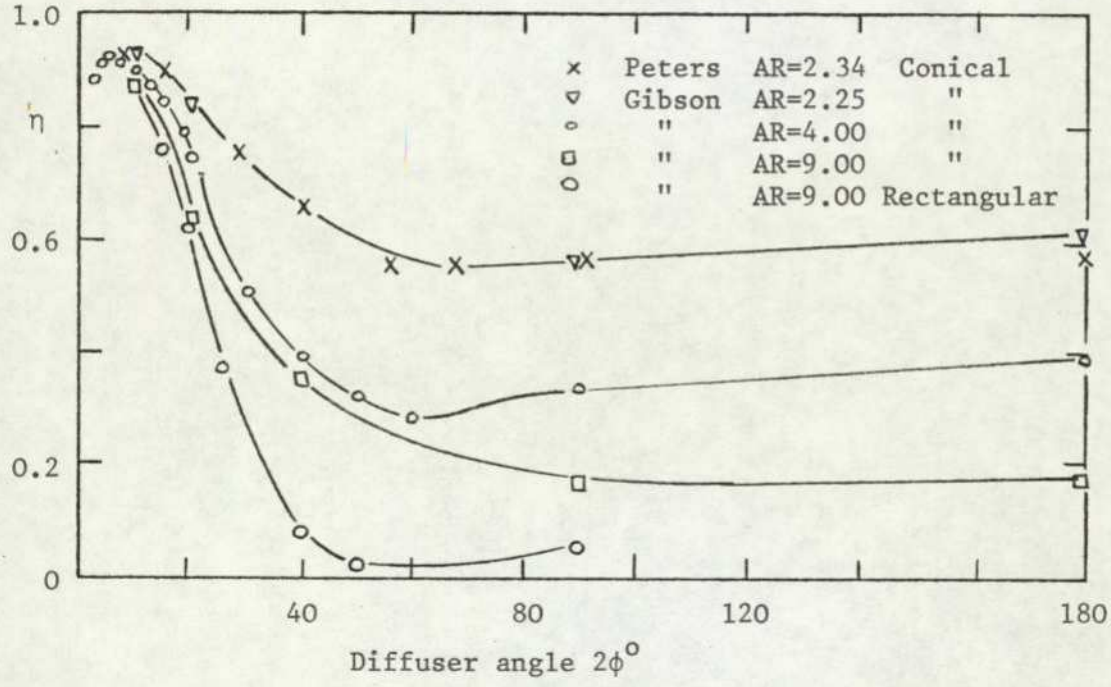

FIG.3.1a DIFFUSER PERFORMANCE CURVES; PATTERSON (5)

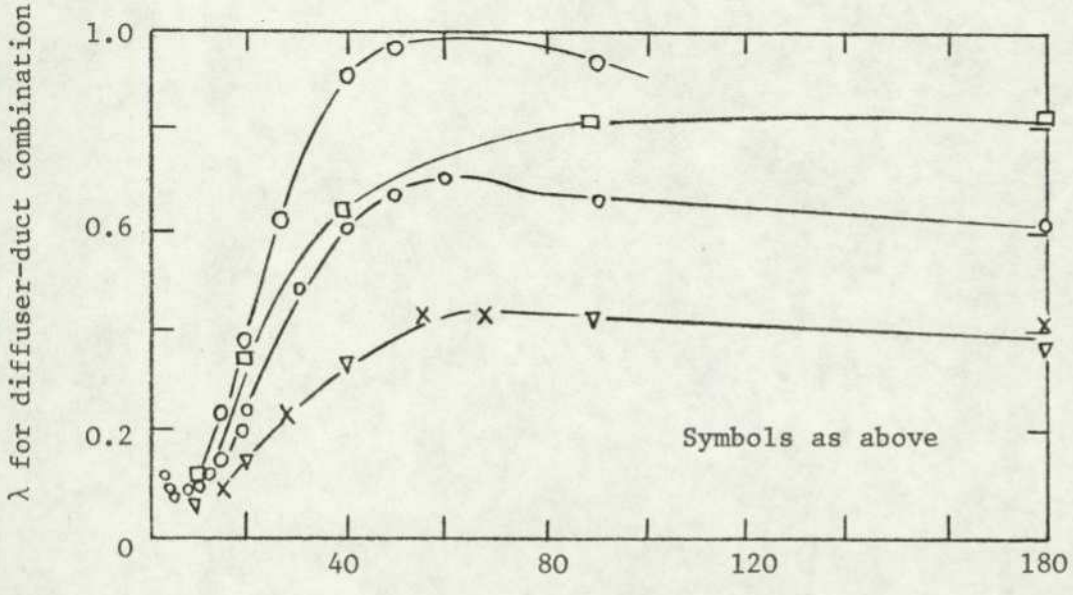

FIG. 3.1b PATTERSON'S CURVES EXPRESSED AS LOSS COEFFICIENTS; COCKRELL AND MARKLAND (8).

where now the pressure recovery coefficient is defined by

$$C_p' = (p_3 - p_1)/q \qquad (3.2.2.14)$$

The accepted definition for diffuser efficiency is that given by Patterson (5); it is the ratio of power transformed (in the form of flow work) to kinetic energy difference between inlet and outlet sections.

$$\eta = \left(\int_{A_2} pudA - \int_{A_2} pudA\right) \Big/ \left[\int_{A_1} \tfrac{1}{2}\rho\tilde{V}^2 udA - \int_{A_2} \tfrac{1}{2}\rho\tilde{V}^2 udA\right] \qquad (3.2.2.15)$$

If the flow is axial at inlet and outlet sections, then $\tilde{V} = u$ and as the uniform pressure is in addition transmitted through the boundary layer, the above equation yields

$$\eta = (p_2 - p_1)\bar{u}_1 A_1 \Big/ \left[\int_{A_1} \tfrac{1}{2}\rho u^3 dA - \int_{A_2} \tfrac{1}{2}\rho u^3 dA\right] \qquad (3.2.2.16)$$

Introducing equation (3.2.2.3) and equation (3.2.2.4)

$$\eta = (p_2 - p_1)/q\alpha_1(1 - A_1^2\alpha_2/A_2^2\alpha_1) \qquad (3.2.2.17)$$

If the velocity distribution is uniform at inlet and exit section $\alpha_1 = \alpha_2 = 1.0$ and the above equation reduces to

$$\eta = (p_2 - p_1)/q(1 - A_1^2/A_2^2) \qquad (3.2.2.18)$$

Introducing equation (3.2.2.12), it can be seen that

$$\eta = 1 - \lambda$$

Figure (3.1a), from Patterson, shows the variation of the diffuser efficiency with expansion angle and Fig.(3.1b) by Cockrell and Markland shows the variation of loss coefficient λ' for diffuser plus tailpipe combination.

3.3 SOVRAN AND KLOMP'S MODEL

3.3.1 Introduction

Sovran and Klomp (9) suggested that the overall diffuser effectiveness relates to the actual pressure rise to that achieved from the same geometry with ideal, one-dimensional flow at the same flow rate, i.e.

$$\varepsilon_o = (p_2 - p_1)/(p_2 - p_1)_{ideal}$$

$$= C_p/C_{p_{ideal}} \qquad (3.3.1.1)$$

where the ideal pressure recovery is a function of only the geometric area ratio of the diffuser, i.e.

$$C_{p_{ideal}} = 1 - 1/(AR)^2 \qquad (3.3.1.2)$$

where $AR = A_2/A_1$.

But it is well known that the actual pressure recovery is strongly influenced by the inlet flow, thus they presented procedures based upon kinetic energy profile to assess the effect of non-uniformity of inlet velocity profile on performance of conical diffuser, i.e.

$$\varepsilon_o = \frac{\alpha_1\left[1 - \frac{\alpha_2/\alpha_1}{AR^2}\right]}{\left[1 - \frac{1}{AR^2}\right]} - \frac{\bar{\omega}}{\left[1 - \frac{1}{AR^2}\right]} \qquad (3.3.1.3)$$

where $\bar{\omega} = (\bar{P}_{o_1} - \bar{P}_{o_2})/q_1$ is the pressure loss coefficient, and $\bar{P}_o$ is the mass averaged stagnation pressure. If the static pressure is considered constant across the fluid stream, a condition which very nearly exists for flow in uncurved ducts, then the averaged stagnation pressure can be expressed as

$$\bar{P}_o = p + \alpha q \qquad (3.3.1.4)$$

The above analysis was further developed by (66) to accommodate the effect of free vortex swirl at diffuser inlet. The next section deals with the analysis in detail and its application to conical diffuser geometry for both free and forced vortex swirl.

3.3.2 Extension of Sovran and Klomp Model to Take Account of Swirling Flow in Conical Diffuser

Consider the flow along a stream tube of a conical diffuser to be isentropic, incompressible and swirling with uniform velocity profile. The energy equation is then:

$$p_1 + \rho\tilde{V}_1^2/2 = p_2 + \rho\tilde{V}_2^2/2 \qquad (3.3.2.1)$$

thus

$$p_2 - p_1 = \rho/2u_1^2[1 - u_2^2/u_1^2] + \rho/2v_1^2[1 - v_2^2/v_1^2]$$

From the velocity diagram Fig.(3.2)

$$u = \tilde{V}\cos\psi \qquad (3.3.2.2)$$

and

$$v = \tilde{V}\sin\psi \qquad (3.3.2.3)$$

From continuity equation

$$u_1A_1 = u_2A_2 \qquad (3.3.2.4)$$

and if the tangential velocity is that of a free vortex, then

$$vR = \text{constant} \qquad (3.3.2.5)$$

thus

$$v_1R_1 = v_2R_2$$

Substituting into equation (3.3.2.1) for the entire section, yields

$$p_2 - p_1 = \rho/2\tilde{V}_1^2\cos^2\psi_1[1 - 1/AR^2] + \rho/2\tilde{V}_1^2\sin^2\psi_1[1 - 1/RR^2]$$

The coefficient of pressure recovery is given by

$$C_{p_I} = (p_2 - p_1)/\rho/2\tilde{V}_1^2$$

$$= \cos^2\psi_1[1 - 1/AR^2] + \sin^2\psi_1[1 - 1/RR^2] \qquad (3.3.2.6)$$

The above equation reduces to the familiar relationship for ideal pressure recovery coefficient when the flow is one dimensional (i.e. zero swirl)

$$C_{p_I} = [1 - 1/AR^2] \qquad (3.3.2.7)$$

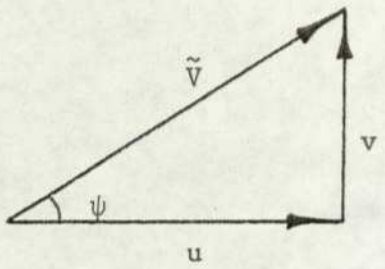

FIG.3.2 VELOCITY DIAGRAM

Velocity triangle varies over the cross-section

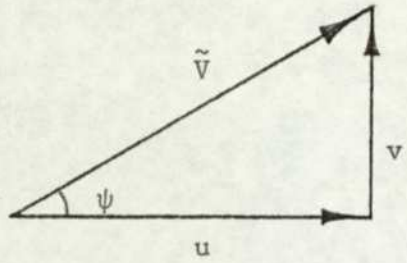

Velocity triangle constant over the cross-section

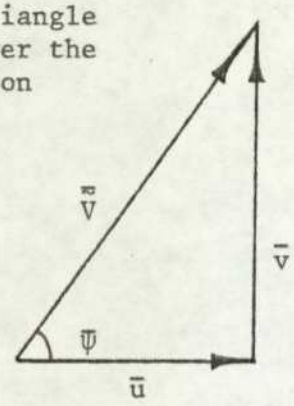

FIG.3.3 VELOCITY TRIANGLE AT DIFFUSER INLET.

Similarly, when losses are included in the energy equation, it can readily be shown that equation (3.3.2.6) becomes

$$C_p = \cos^2\psi_1 \left[1 - 1/AR^2\right] + \sin^2\psi_1 \left[1 - 1/RR^2\right] - \omega \quad (3.3.2.8)$$

where in this case

$$\omega = (P_{o_1} - P_{o_2})/(\rho/2\tilde{V}_1^2 \quad (3.3.2.9)$$

Consider the flow to be non-uniform, then both C_{P_I} and C_p are reduced by a distorted velocity profile as shown by Sovran and Klomp. The next step is to quantify the effect on diffuser performance.

In case of non-swirling (zero ψ) flow, a real flow with non-uniform velocity distribution

$$\alpha = \frac{\text{kinetic energy flux for non-uniform flow}}{\text{kinetic energy flux for uniform flow}}$$

However, in the case of swirling flow, an equivalent uniform stream cannot be defined merely by equating axial mass flow rates. The so-called uniform swirling stream must also have an angular momentum equal to that of the real (non-uniform) flow. The velocity component $\bar{u}$ is thus defined as usual by

$$\bar{u} = \int u dA/A \quad (3.3.2.10)$$

but the mean flow angle $\bar{\psi}$ is obtained by equating angular momenta.

For non-uniform flow, the angular momentum is given by

$$M = \int_A \rho uvr dA \quad (3.3.2.11)$$

from velocity diagram, Fig.(3.2) $v = u\tan\psi$, thus

$$M = \rho \int_A u^2 \tan\psi r dA \quad (3.3.2.12)$$

The angular momentum for the equivalent uniform flow is given by

$$M = \dot{m}R\bar{v}$$

$$= \rho A\bar{u}^2 \tan\bar{\psi}R \qquad (3.3.2.13)$$

where R is the mean radius of the cross section. Thus equating equation (3.3.2.12) and (3.3.2.13)

$$\tan\bar{\psi} = \int_A (u/\bar{u})^2 \tan\psi r dA/R.A. \qquad (3.3.2.14)$$

Equation (3.3.2.10) giving $\bar{u}$, and equation (3.3.2.14) giving $\bar{\psi}$, then fully define the velocity triangle of the equivalent uniform stream. The kinetic energy flux, for the two flows can then be compared. For the non-uniform flow, the kinetic energy flux is

$$KE = \int_A \tfrac{1}{2} \tilde{V}^2 d\dot{m}$$

$$= \int_A \rho/_2 u\tilde{V}^2 dA$$

But from the velocity diagram, Fig.(3.3), $\tilde{V} = u/\cos\psi$, thus

$$KE = \rho/_2 \int (u^3/\cos^2\psi) dA \qquad (3.3.2.15)$$

Now consider the kinetic energy flux for equivalent uniform flow.

$$KE = \tfrac{1}{2} \dot{m}\bar{\tilde{V}}^2$$

$$= \rho/_2 (\bar{u}^3/\cos^2\bar{\psi})A \qquad (3.3.2.16)$$

Thus the ratio of equation (3.3.2.15) and (3.3.2.16) yields the kinetic energy weighting factor α_s

$$\alpha_s = \int_A (u/\bar{u})^3 (\cos^2\bar{\psi}/\cos^2\psi) dA/A \qquad (3.3.2.17)$$

Let us now consider the evaluation of pressure recovery coefficient based on mass averaged pressures.

$$C_p = (p_2 - p_1)/\rho/_2 \bar{\tilde{V}}_1^2 \qquad (3.3.2.18)$$

considering a stream tube, then

$$P_o d\dot{m} = p d\dot{m} + \rho/2 u\tilde{V}^2 dA \qquad (3.3.2.19)$$

dividing by $\dot{m}$

$$P_o(d\dot{m}/\dot{m}) = p(d\dot{m}/\dot{m}) + (\rho u\tilde{V}^2 dA)/(2\dot{m}) \qquad (3.3.2.20)$$

defining the mass averaged pressure as

$$\bar{P}\dot{m} = \int P d\dot{m} \qquad (3.3.2.21)$$

If one is to take account of the whole cross-section, then one integrates across the section. Thus for whole section (taking account of all the stream tubes within the section) equation (3.3.2.20) becomes

$$\int_A P_o(d\dot{m}/\dot{m}) = \int_A p(d\dot{m}/\dot{m}) + \int_A (\rho u\tilde{V}^2 dA)/(2\dot{m})$$

substituting equation (3.3.2.21) and static pressure being constant across a cross-section

$$\bar{P}_o = p + (\rho/2A) \int_A (u/\bar{u})\tilde{V}^2 dA \qquad (3.3.2.22)$$

from the velocity triangles, Fig.(3.3)

$$\cos\bar{\psi} = \bar{u}/\bar{\tilde{V}} \quad \text{and} \quad \cos\psi = u/\tilde{V}$$

equation (3.3.2.17) becomes

$$\alpha_s \bar{\tilde{V}}^2 = \int (u/\bar{u})\tilde{V}^2 dA/A \qquad (3.3.2.23)$$

from equation (3.3.2.22) and (3.3.2.23)

$$\bar{P}_o = p + \rho/2 \bar{\tilde{V}}^2 \alpha_s \qquad (3.3.2.24)$$

Applying the above equation to the inlet and exit of a diffuser yields

$$p_2 - p_1 = \rho/2 [\bar{\tilde{V}}_1^2 \alpha_{s1} - \bar{\tilde{V}}_2^2 \alpha_{s2}] - [\bar{P}_{o1} - \bar{P}_{o2}]$$

substituting into equation (3.3.2.18)

$$C_p = \alpha_{s_1} [1 - (\bar{\tilde{V}}_2^2 \alpha_{s_2} / \bar{\tilde{V}}_1^2 \alpha_{s_1})] - [\bar{P}_{o_1} - \bar{P}_{o_2} / \rho/2 \bar{\tilde{V}}_1^2]$$

But $\tilde{\bar{V}} = \bar{u}^2 + \bar{v}^2$, thus

$$C_p = \alpha_{s1}\left[1 - (\alpha_{s2}\bar{u}_2^2/\alpha_{s1}\tilde{\bar{V}}_1^2) - (\alpha_{s2}\bar{v}_2^2/\alpha_{s1}\tilde{\bar{V}}_1^2)\right] - \bar{\omega}$$

$$= \alpha_{s1}\left[(\bar{u}_1^2/\tilde{\bar{V}}_1^2) - (\bar{u}_1^2\bar{u}_2^2\alpha_{s1}/\bar{u}_1^2\tilde{\bar{V}}_1^2\alpha_{s1}) + (\bar{v}_1^2/\tilde{\bar{V}}_1^2) - (\bar{v}_1^2\bar{v}_2^2\alpha_{s2}/\bar{v}_1^2\tilde{\bar{V}}_1^2\alpha_{s1})\right] - \bar{\omega}$$

$$= \alpha_{s1}\,\bar{u}_1^2/\tilde{\bar{V}}_1^2\left[1 - (\alpha_{s2}\bar{u}_2^2/\alpha_{s1}\bar{u}_1^2)\right] + \alpha_{s1}\bar{v}_1^2/\tilde{\bar{V}}_1^2\left[1 - (\alpha_{s2}\bar{v}_2^2/\alpha_{s1}\bar{v}_1^2)\right] - \bar{\omega} \qquad (3.3.2.25)$$

Substituting into equation (3.3.2.25)

(a) the continuity equation, i.e. $\bar{u}_1A_1 = \bar{u}_2A_2$

(b) conservation of angular momentum with downstream travel

(c) neglecting the small effect of frictional dissipation

(d) $R_1\bar{v}_1 = R_2\bar{v}_2$

yields

$$C_p = \alpha_{s_1}\cos^2\bar{\psi}_1\left[1-(\alpha_{s2}/\alpha_{s1}AR^2)\right] + \alpha_{s1}\sin^2\bar{\psi}_1\left[1-(\alpha_{s_2}/\alpha_{s_1}RR^2)\right] - \bar{\omega} \qquad (3.3.2.26)$$

Now for isentropic flow, where $\bar{\omega} = 0$, the ideal pressure recovery coefficient for non-uniform flow will be

$$C_{p_I} = \alpha_{s1}\bar{u}_1^2/\tilde{\bar{V}}_1^2\left[1-(\alpha_{s2}\bar{u}_2^2/\alpha_{s1}\bar{u}_1^2)\right] + \alpha_{s1}\bar{v}_1^2/\tilde{\bar{V}}_1^2\left[1-(\alpha_{s_2}\bar{v}_2^2/\alpha_{s1}\bar{v}_1^2)\right] \qquad (3.3.2.27)$$

Again substituting into equation (3.3.2.27)

(a) the continuity equation

(b) conservation of angular momentum with downstream travel

(c) neglecting the small effect of frictional dissipation

(d) $R_1\bar{v}_1 = R_2\bar{v}_2$

yields

$$C_{p_I} = \alpha_{s1}\cos^2\bar{\psi}_1\left[1-(\alpha_{s2}/\alpha_{s1}AR^2)\right] + \alpha_{s1}\sin^2\bar{\psi}_1\left[1-(\alpha_{s_2}/\alpha_{s_1}RR^2)\right] \qquad (3.3.2.28)$$

Thus the overall diffuser effectiveness

$$\varepsilon_o = C_p/C_{p_I}$$

= equation (3.3.2.25)/ equation (3.3.2.27).

or with the above mentioned assumptions

ε_o = equation (3.3.2.26)/equation (3.3.2.28)

Forced Vortex Case

Consider the case when the tangential velocity is that of a forced vortex, i.e.

$$\frac{v}{R} = \text{constant}$$

then

$$\frac{v_1}{R_1} = \frac{v_2}{R_2}$$

thus for incompressible swirling flow with uniform velocity profile reduces to

$$C_{pI} = \cos^2\psi_1 \left[1 - 1/AR^2\right] - \sin^2\psi_1 \left[1 - RR^2\right] \qquad (3.3.2.6a)$$

similarly, when losses are included,

$$C_p = \cos^2\psi_1 \left[1 - 1/AR^2\right] - \sin^2\psi_1 \left[1 - RR^2\right] - \omega \qquad (3.3.2.8a)$$

When non-uniform flow is considered, C_{pI} and C_p are reduced by a distorted velocity profile, thus

$$C_p = \alpha_{s_1}\bar{u}_1^2/\bar{\bar{V}}^2 \left[1 - (\alpha_{s_2}\bar{u}_2^2/\alpha_{s_1}\bar{u}_1^2)\right] + \alpha_{s_1}\bar{v}_1^2/\bar{\bar{V}}^2\left[1 - (\alpha_{s_2}\bar{v}_2^2/\alpha_{s_1}\bar{v}_1^2)\right] - \bar{\omega} \qquad (3.3.2.25a)$$

Substituting continuity equation, conservation of angular momentum, neglecting the small effect of frictional dissipation, and forced vortex tangential velocity,

$$C_p = \alpha_{s_1}\cos^2\bar{\psi}_1 \left[1 - (\alpha_{s_2}/\alpha_{s_1}AR^2)\right] + \alpha_{s_1}\sin^2\bar{\psi}_1 \left[1 - (\alpha_{s_2}RR^2/\alpha_{s_1})\right] - \bar{\omega} \qquad (3.3.2.26a)$$

For ideal flow, $\bar{\omega} = 0$, the ideal pressure recovery coefficient for non-uniform flow will be

$$C_{pI} = \alpha_{s_1}\bar{u}_1^2/\bar{\bar{V}}^2 \left[1 - (\alpha_{s_2}\bar{u}_2^2/\alpha_{s_1}\bar{u}_1^2)\right] + \alpha_{s_1}\bar{v}_1^2/\bar{\bar{V}}^2 \left[1 - (\alpha_{s_2}\bar{v}_2^2/\alpha_{s_1}\bar{v}_1^2)\right] \qquad (3.3.2.27a)$$

again substituting continuity equation, conservation of angular momentum, neglecting the small effect of frictional dissipation and forced vortex tangential velocity yields

$$C_{p_I} = \alpha_{s_1}\cos^2\bar{\psi}_1\left[1 - (\alpha_{s_2}/\alpha_{s_1}AR^2)\right]$$

$$+ \alpha_{s_1}\sin^2\bar{\psi}_1\left[1 - (\alpha_{s_2}RR^2/\alpha_{s_1})\right] \qquad (3.3.2.28a)$$

Thus the overal diffuser effectiveness

ε_o = equation (3.3.2.25a) / equation (3.3.2.27a)

or with the above mentioned assumptions

ε_o = equation (3.3.2.26a)/ equation (3.3.2.28a)

3.4 TYLER AND WILLIAMSON'S MODEL

3.4.1 Introduction

In 1967 Tyler and Williamson (67) adopted a slightly different approach to non-uniformities. They used a distortion factor, DF, defined as a ratio of maximum to mean velocity for a given velocity profile. This approach has previously been used by Sovran and Klomp (9) but their result applied only to minimal build up of inlet boundary layer, although they did point out that the concept ought to be applicable to greater distortion. As a first approximation to finding diffuser efficiency, they related static pressures to the centre line conditions at diffusers inlet and exit, thus,

$$p_2 - p_1 = [\rho/_2\hat{u}_1^2 - \rho/_2\hat{u}_2^2] - [\hat{P}_1 - \hat{P}_2] \qquad (3.4.1.1)$$

where a circumflex denotes a maximum value. The pressure recovery coefficient, C_p

$$C_p = (p_2 - p_1)/(\rho/_2\bar{u}_1^2) \qquad (3.4.1.2)$$

$$= (\hat{u}_1^2/\bar{u}_1)^2 - (\hat{u}_2^2/\bar{u}_1)^2 - (\hat{P}_1 - \hat{P}_2)(\rho/_2\bar{u}_1^2) \qquad (3.4.1.3)$$

Inserting the continuity equation, $\bar{u}_1 A_1 = \bar{u}_2 A_2$, the above equation yields

$$C_p = (DF)_1^2 - (DF)_2^2/AR^2 - \hat{\omega} \qquad (3.4.1.4)$$

where $\hat{\omega} = (\hat{P}_1 - \hat{P}_2)/\rho/_2\bar{u}_1^2$, which accounts for the loss of total pressure in the diffuser.

They observed that conical diffusers exhibited marked differences in performance trends at high values of inlet blockage, B_1, $[= (1 - 1/DF)]$. This is illustrated by the pressure recovery coefficient of Fig.(3.4), taken from their results. Thus they felt that some insight into the behaviour of pressure recovery coefficient is afforded by energy consideration. This is briefly summarised in the next section.

3.4.2 Analysis

Considering the application of energy coefficient at diffuser inlet and outlet,

$$C_p = \alpha_1 - \alpha_2/AR^2 - W$$

where W represents the integrated pressure loss arising from energy dissipated in heat and disordered motion. The R.H.S. of the above equation represents the reduction in kinetic energy flux effected by the diffuser. For one-dimensional flow, $1 \leqslant \alpha \leqslant (DF)^2$ and the energy reduction can be referred to an ideal maximum value, $(DF)_1^2 - 1/AR^2$, to yield a diffusion factor, $\gamma \leqslant 1.0$. Thus.

$$C_p / \left[(DF)_1^2 - 1/(AR)^2 \right] + W / \left[(DF)_1^2 - 1/(AR)^2 \right]$$

$$= \left[\alpha_1 - \alpha_2/(AR)^2 \right] / \left[(DF)_1^2 - 1/(AR)^2 \right]$$

$$= \gamma \leqslant 1.0 \qquad (3.4.2.2)$$

The components of the L.H.S. of equation (3.4.2.2) can be regarded as modified effectiveness, $\bar{\eta}$, and modified loss coefficient, ξ, respectively. Since $\xi \geqslant 0$, then $\bar{\eta} \leqslant 1.0$. In addition, an energetic efficiency, η_e, can be defined relating useful pressure recovery to the reduction of kinetic energy flux. Thus,

$$\eta_e = C_p / \left[\alpha_1 - \alpha_2/(AR)^2 \right]$$

$$= \bar{\eta} / \gamma \qquad (3.4.2.3)$$

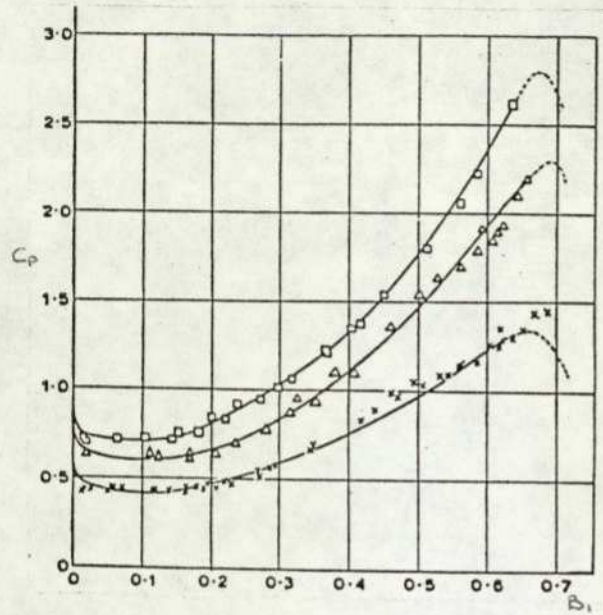

Symbol	L/R_1	AR
×	2	1.50
△	7	2.25
□	13	3.25

FIG.3.4 MEASURED DATA FOR C_p CONICAL TEST GEOMETRIES; TYLER & WILLIAMSON (67).

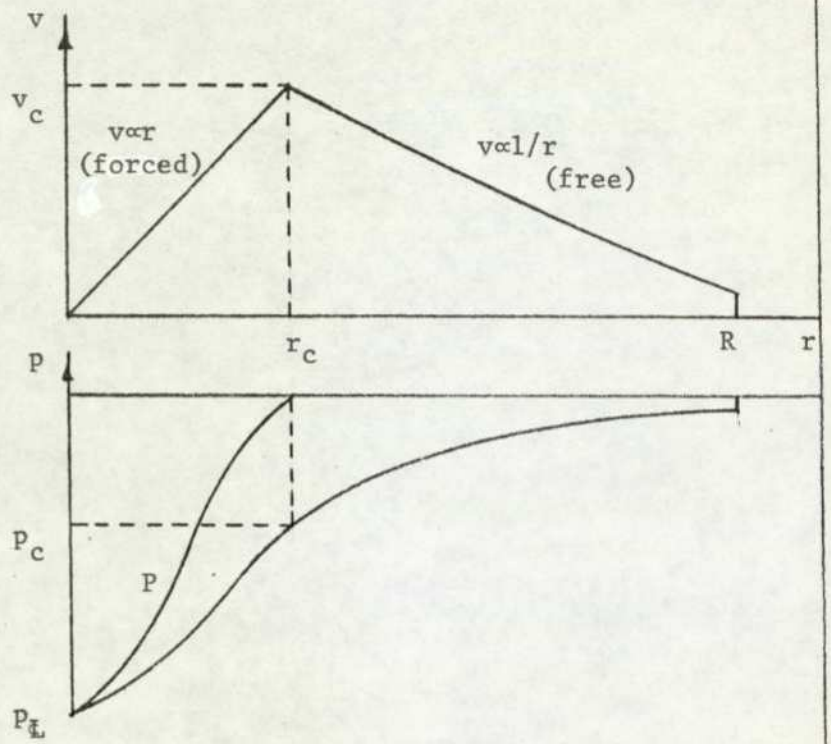

FIG.3.5 RELATIONSHIP BETWEEN TANGENTIAL VELOCITY AND PRESSURE DISTRIBUTION AT A SECTION.

3.5 EXTENSION OF PATTERSON'S EFFICIENCY EQUATION

3.5.1 Introduction

Patterson (5) suggested that the overall energy efficiency of a diffuser is defined as a ratio of the power transformed to the power supplied for transformation.

$$\eta_E = \frac{\int_2 pudA - \int_1 pudA}{\int_1 \tfrac{1}{2}\rho\tilde{V}^2 udA - \int_2 \tfrac{1}{2}\rho\tilde{V}^2 udA} \qquad (3.5.1.1)$$

For an inviscid, one-dimensional axial flow, $\tilde{V} = u$ and static pressure constant over a cross-section, equation (3.5.1.1) simplifies to

$$\eta_E = (p_2 - p_1)\ \bar{u}A/[\rho/2\int_{A_1} \bar{u}^3 dA - \rho/2 \int_{A_2} \bar{u}^3 dA] \qquad (3.5.1.2)$$

where $\bar{u}$ is the value of the (assumed) uniform velocity distribution at each section.

Using continuity equation, $\bar{u}_1 A_1 = \bar{u}_2 A_2$, equation further simplifies to

$$\eta = (p_2 - p_1)/\rho/2\bar{u}_1^2[1 - (A_1/A_2)^2] \qquad (3.5.1.3)$$

The above equation, known as pressure efficiency (thus suffix E is dropped) has been widely used, but in many practical cases the matter is complicated by presence of a non-uniform velocity profile at inlet and exit, and the flow being two-dimensional. Thus it is no longer applicable or justifiable and a modified version must be derived from equation (3.5.1.1). Neve (63) modified equation (3.5.1.1) to take account of solid-body rotation with the assumption that the inlet flow component of velocity is uniform. A brief summary of the analysis with and without the above assumption is presented in the next section. The analysis is further developed to take account of a Rankine vortex, without assuming uniform inlet flow component of velocity.

3.5.2 Theoretical Analysis of the Effect of Solid-Body Vortices

In swirling flow, the overall energy efficiency of a diffuser is still defined by equation (3.5.1.1) but now

$$\tilde{V}^2 = u^2 + v^2 \qquad (3.5.2.1)$$

and in a forced vortex, static pressure increases with radius according to the equation

$$p = p_{\text{ℓ}} + \rho/2v^2 \qquad (3.5.2.2)$$

and the relationship between v and r is

$$v = \text{constant} \quad r = v_1 r/R_1 \qquad (3.5.2.3)$$

Substituting equation (3.5.2.2) and (3.5.2.3) into numerator of equation (3.5.1.1)

$$\int_2 pudA - \int_1 pudA = \int_2 (p_{\text{ℓ}} + \rho/_2 v^2)udA - \int_1 (p_{\text{ℓ}} + \rho/_2 v^2)udA$$

$$= 2\pi \left[\int_0^{R_2} p_{\text{ℓ}} urdr + \int_0^{R_2} (\rho/2)(v_2^2/R_2^2)ur^3 dr \right.$$

$$\left. - \int_0^{R_1} p_{\text{ℓ}} urdr - \int_0^{R_1} (\rho/2)(v_1^2/R_1^2)ur^3 dr \right] \qquad (3.5.2.4)$$

If u is assumed to be constant over a cross-section, then the above equation reduces to

$$= \pi \left[p_{\text{ℓ}_2} R_2^2 u_2 + \rho v_2^2 R_2^2 u_2/4 - p_{\text{ℓ}_1} R_1^2 u_1 - \rho v_1^2 R_1^2 u_1/4 \right]$$

$$= Q \left[(p_{\text{ℓ}_2} - p_{\text{ℓ}_1}) + \rho/_4 (v_2^2 - v_1^2) \right] \qquad (3.5.2.5)$$

A more practical form of the equation (3.5.2.5) would be if the $p_{\text{ℓ}}$ is expressed in terms of wall static pressure.

$$\text{Numerator} = Q \left[(p_2 - \rho/2v_2^2 - p_1 + \rho/2v_1^2 + \rho/4v_2^2 - \rho/4v_1^2) \right]$$

$$= Q \left[(p_2 - p_1) + \rho/_4 (v_1^2 - v_2^2) \right] \qquad (3.5.2.6)$$

A relationship can be found between v_1 and v_2, if it is assumed that the shear stresses on the diffuser walls caused by swirl components are not sufficient to cause a major change in angular momentum as the fluid moves through the diffuser.

Consider an incremental ring dr wide in the plane normal to the diffuser axis. Then the angular momentum

$$M = \int_A \rho uvr dA$$

at entry section

$$M_1 = 2\pi\rho \int_0^{R_1} uvr^2 dr$$

for a forced vortex

$$M_1 = 2\pi\rho u_1 v_1 / R_1 \int_0^{R_1} r^3 dr$$

$$= \dot{m}(v_1 R_1/2)$$

where $\dot{m}$ is the mass flow rate. Thus if $\dot{m}$ is constant, the conservation of angular momentum would require that $v_1 R_1 = v_2 R_2$, so

$$(v_1/v_2)^2 = (R_2/R_1)^2 = (A_2/A_1) \qquad (3.5.2.7)$$

thus substituting into equation (3.5.2.6)

$$\text{Numerator} = Q\left[(p_2 - p_1) + \rho/4\ v_1^2(1 - A_1/A_2) \right]$$

Now consider the denominator of the overall energy efficiency equation (3.5.1.1)

$$\int_A \rho/2 \tilde{V}^2 u dA = \int_A \rho/2 (u^2 + v^2) u dA$$

$$= 2\pi\rho/2 \left[\int_0^R u^3 r dr + \int_0^R uv^2 r dr \right] \qquad (3.5.2.8)$$

Again, if u is assumed constant across a cross-section, and substituting equation (3.5.2.3)

$$\int_A \rho/2 \tilde{V}^2 u dA = \pi R^2 u \left[\rho u^2/2 + \rho v^2/4 \right]$$

$$= Q\left[\rho u^2/2 + \rho v^2/4\right]$$

thus

$$\text{Denominator} = Q\left[\rho u_1^2/2 + \rho v_1^2/4 - \rho u_2^2/2 - \rho v_2^2/4 \right]$$

Substituting continuity equation $u_1 A_1 = u_2 A_2$ and conservation of angular momentum, $v_1 R_1 = v_2 R_2$

$$\text{Denominator} = Q\left[\rho/_2 u_1^2 \left(1 - A_1^2/A_2^2\right) + \rho/_4 v_1^2 (1 - A_1/A_2)\right] \tag{3.5.2.9}$$

Thus the overall energy efficiency

$$\eta_E = \frac{(p_2 - p_1) + \rho/_4 v_1^2 (1 - A_1/A_2)}{\rho/_2 u_1^2 (1 - A_1^2/A_2^2) + \rho/_4 v_1^2 (1 - A_1/A_2)} \tag{3.5.2.10}$$

If u is not assumed to be constant across a cross-section, then

η_E equation (3.5.2.4)/equation (3.5.2.8) applied to inlet and exit station.

$$= \frac{\int_0^{R_2} p_{\text{℄}} u r dr + \int_0^{R_2} (\rho/2)(v_2^2/R_2^2) u r^3 dr - \int_0^{R_1} p_{\text{℄}} u r dr - \int_0^{R_1} (\rho/2)(v_1^2/R_1^2) u r^3 dr}{\rho/_2 \left[\int_0^{R_1} u^3 r dr + \int_0^{R_1} u v^2 r dr - \int_0^{R_2} u^3 r dr - \int_0^{R_2} u v r dr\right]} \tag{3.5.2.11}$$

3.5.3 Theoretical Analysis of the Effect of Rankine Vortex

Consider the tangential velocity profile to be that of a Rankine vortex. The overall energy efficiency of a diffuser is again defined by equation (3.5.1.1), but now the static pressure increases with radius according to the following equation; (refer to Fig.3.5)

For forced vortex core

$$p = p_{\text{℄}} + \rho v^2/2 \tag{3.5.3.1}$$

For free vortex outer region, H = constant

$$p_{\text{℄}} + \rho v_c^2 = p + \rho v^2/2$$

thus

$$p = p_{\text{℄}} + \rho v_c^2 - \rho v^2/2 \tag{3.5.3.2}$$

where v_c is the tangential velocity at vortex core.

Consider the numerator of equation (3.5.1.1)

$$\int pudA = 2\pi \int_o^R purdr$$

$$= 2\pi \int_o^{r_c} (p_{\text{ℓ}} + \rho v^2/2)urdr + 2\pi \int_{r_c}^R (p_{\text{ℓ}} + \rho v_c^2 - \rho v^2/2)urdr$$

$$= 2\pi p_{\text{ℓ}} \int_o^R urdr + \pi\rho \int_o^{r_c} v^2 urdr + 2\pi\rho v_c^2 \int_{r_c}^R urdr - \pi\rho \int_{r_c}^R v^2 urdr$$

$$= Qp_{\text{ℓ}} + \xi'$$

where $\xi' = \pi\rho \int_o^{r_c} v^2 urdr + 2\pi\rho v_c^2 \int_{r_c}^R urdr - \pi\rho \int_{r_c}^R v^2 urdr$

Thus Numerator $= \int_2 pudA - \int_1 pudA$

$$= Q(p_{\text{ℓ}_2} - p_{\text{ℓ}_1}) + \xi_2' - \xi_1' \qquad (3.5.3.3)$$

Let us now consider the denominator

$$\int_A \rho/2 \tilde{V}^2 udA = \int_A \rho/2 (u^2 + v^2)udA$$

$$= \pi\rho \left[\int_o^R u^3 rdr + \int_o^R uv^2 rdr \right]$$

$$= \gamma'$$

Thus

$$\text{Denominator} = \int_1 \rho/2 \tilde{V}^2 udA - \int_2 \rho/2 \tilde{V}^2 udA$$

$$= \gamma_1' - \gamma_2' \qquad (3.5.3.4)$$

Thus the overall energy efficiency

$$\eta_E = \frac{Q(p_{\text{ℓ}_2} - p_{\text{ℓ}_1}) + \xi_2' - \xi_1'}{\gamma_1' - \gamma_2'} \qquad (3.5.3.5)$$

3.6 CONCLUSIONS

From Cockrell and Markland's model, it is fairly easy to evaluate λ, and thus η, but the analysis is based on one-dimensional flow. One may ask a question, is it justifiable to apply the model to swirling flow, since λ is based only on p_1, p_2 and $\bar{u}$. Sovran and Klomp's approach is based on the effectiveness which relates the actual pressure rise to that achievable from the same geometry with ideal flow. It also takes account of the effect of non-uniformity on diffuser performance. The analysis is further developed to take account of two-dimensional flow, which makes it more complex. Tyler and Williamson's model adopts slightly different approach to non-uniformities. They used the concept of distortion factor, DF. Their approach is simpler, based on one-dimensional flow, and takes account of exit velocity profile. The next model is based on the expansion of Patterson's overall energy equation to accommodate the presence of non-uniform velocity profiles and effects of swirl.

It is worth noting that for swirling flow cases, investigators like Peters (6), Liepe (64) and Van Dewoestine (49) omitted the exit velocity profile details in evaluating performance owing to experimental difficulty.

The overall observation one could draw is that some degree of ambiguity exists in the estimation of diffuser performance; perhaps this being more serious when swirl is present. When swirling flow is being considered, there is probably no satisfactory way of defining diffuser efficiency. Thus it is intended to assess eventual experimental results against all of the theoretical models suggested, to see if

there is a trend to give a conclusion.

In concluding, the theoretical analysis forms a suitable foundation for evaluating conical diffuser performance for both one and two dimensional flow.

CHAPTER FOUR

EXPERIMENTAL EQUIPMENT

4.1 BASIC REQUIREMENTS

Swirling flow phenomena have very wide applications and this project was seen as one that would lay the foundation of a major research program in this field at this establishment. The test apparatus was designed to satisfy a more general requirement as oppose to the requirement of the present project.

The basic question of which medium to be used for studies was influenced by several factors, for example, flow measurements, flow visualization, newtonian and non-newtonian liquids. Thus the test-rig was design to handle liquids as well as air.

The scale of the test section depends on the experimental objectives. A small scale test section is ideal from a photographic point of view. In addition, lighting problems are minimised when the subject of interest is confined to a small area. If it is intended, to insert a probe into the flow-field, then a much larger scale is necessary to minimise local interference to flow. In light of the above considerations, a compromise was arrived at giving a 90 mm throat diameter and a 180 mm exit diameter.

4.2 GENERAL DESCRIPTION OF THE TEST RIG

The test rig consists of a recirculating system which enables the recovery of liquids other than water and also saves space. The general form and salient dimensions of the test rig are shown in Figs.(4.1), (4.2) and (4.3). The lower tier is the metal section which handles water. The top tier is the test section, which is common to both air and water applications. It consists of entry, diffuser and tail pipe, which are all made of perspex. In order to ensure smooth flow at entry, each

BLOCK DIAGRAM OF TEST-RIG

FIG. 4.1

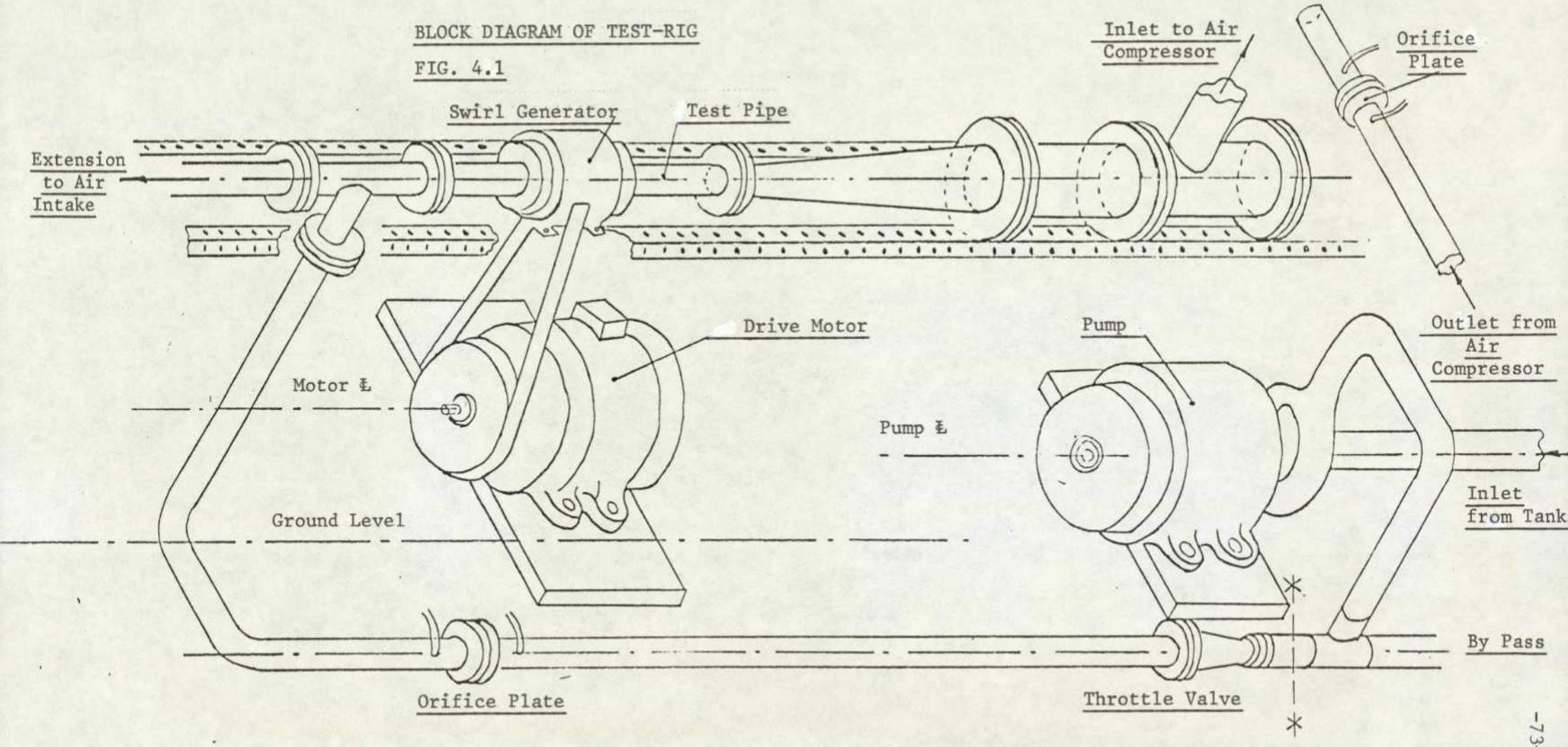

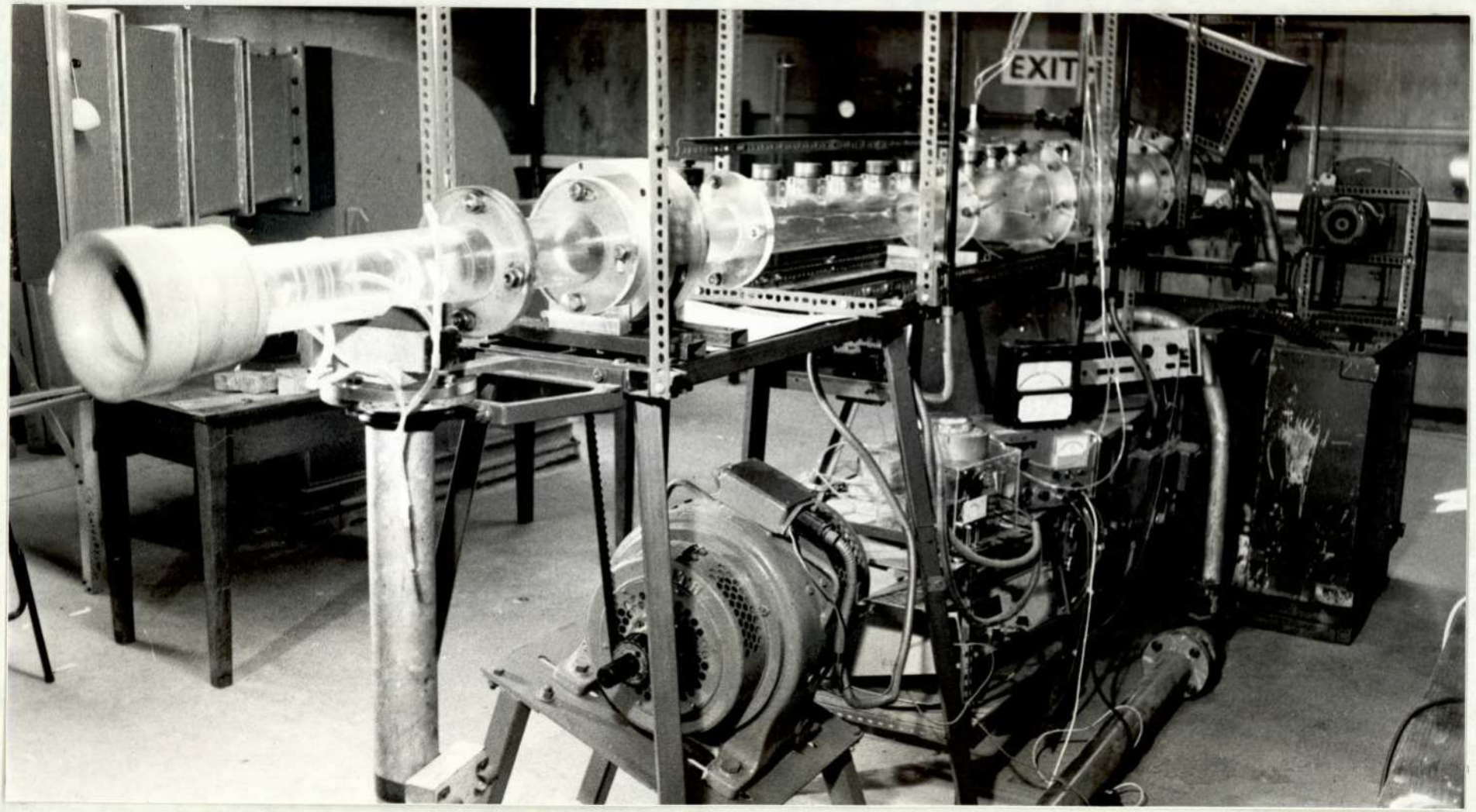

FIG. 4.2 LAYOUT OF TEST RIG

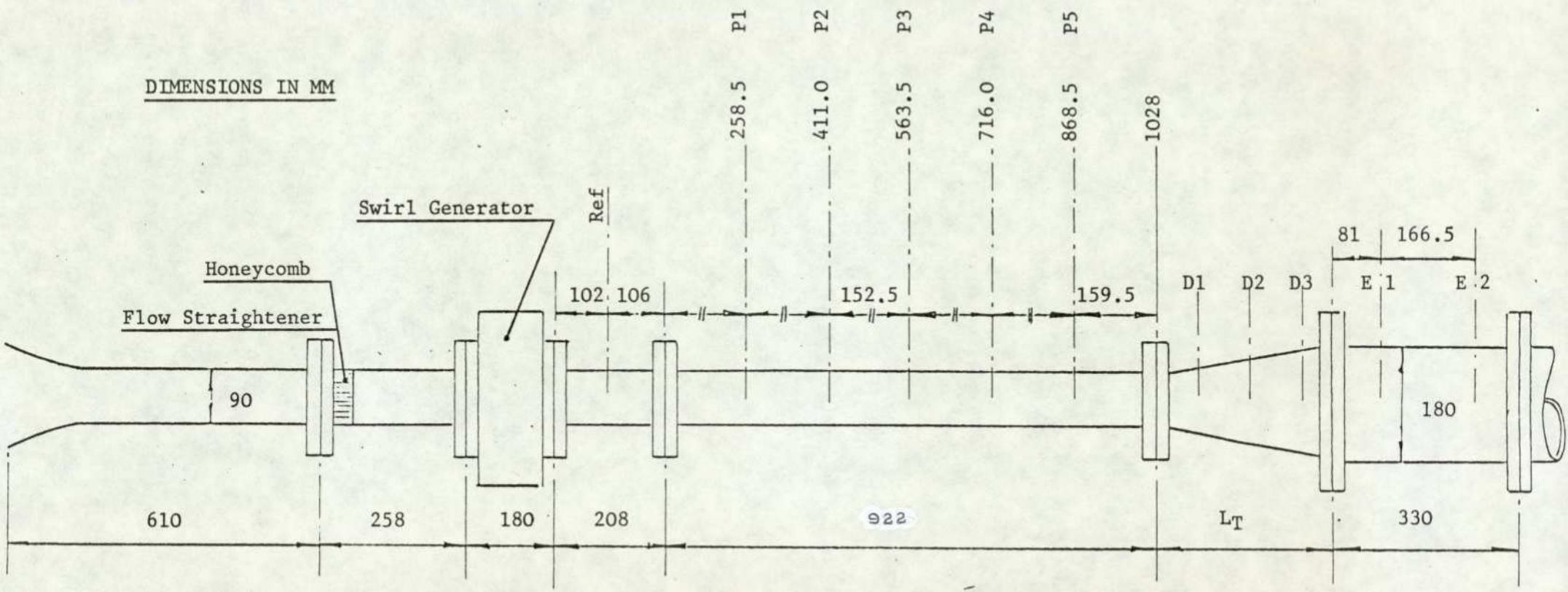

MAIN DIMENSIONS OF TEST AREA

FIG. 4.3

diffuser was dowelled at the throat and thick silicone grease was used to eliminate the need for a gasket which may disturb the flow. The tail pipe was mounted on rails so that it could be moved horizontally to accommodate the different axial lengths of the test diffusers. The downstream end was attached to an air tank which was itself connected to the suction side of a blower. The air flow was controlled and metered by a butterfly valve and orifice plate respectively. The salient dimensions and general features of diffusers used are shown in Fig.(4.4.a) and(4.4.b).

4.3 FLEXIBILITY OF TEST RIG

The test rig was designed by Wirasinghe (52); however additions were made and certain parts of the rig were modified; redesigned in some cases, to suit the purpose. Thus the flexibility of the rig is as follows:

1. The possibility of using air or water.
2. Diffuser with throat diameter 90 mm, an area ratio of 4.0 and double conical angle varying from 10^{o} to 30^{o}.
3. Pipes upstream and downstream of diffuser could be investigated.
4. Non-swirling and swirling studies can be conducted.
5. Photographic and flow visualization studies can be conducted since the test section is made from perspex.
6. Use of laser velocimeter.
7. Accommodation of five-hole spherical probe.
8. Auto and manual probe traverse mechanism to conduct detailed flow measurements.

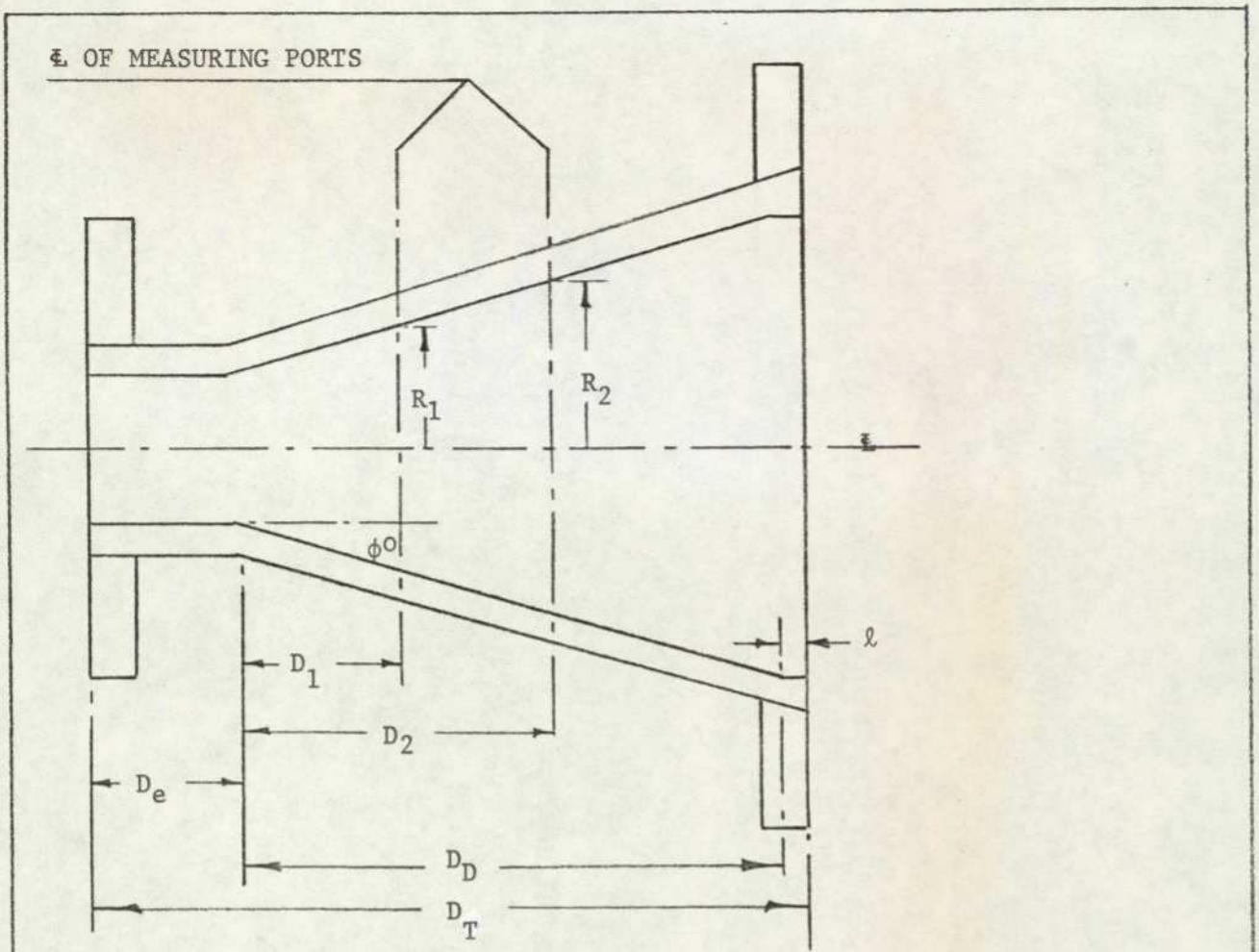

2ϕ	10°		20°		30°
D_T	517		291		223
D_D	500.3		245.2		168
D_e	10.7		39.8		44.04
ℓ	6		6		11
R_1 / D_1	48.75 / 42.80		48.03 / 17.21		46.33 / 4.96
R_2 / D_2	63.96 / 186.3		65.49 / 116.2		61.94 / 66.96
R_3 / D_3	75.35 / 326.3		82.95 / 215.2		79.55 / 129
R_4 / D_4	86.74 / 460.3				

FIG. 4.4a. DIMENSIONS OF DIFFUSERS USED IN EXPERIMENTS

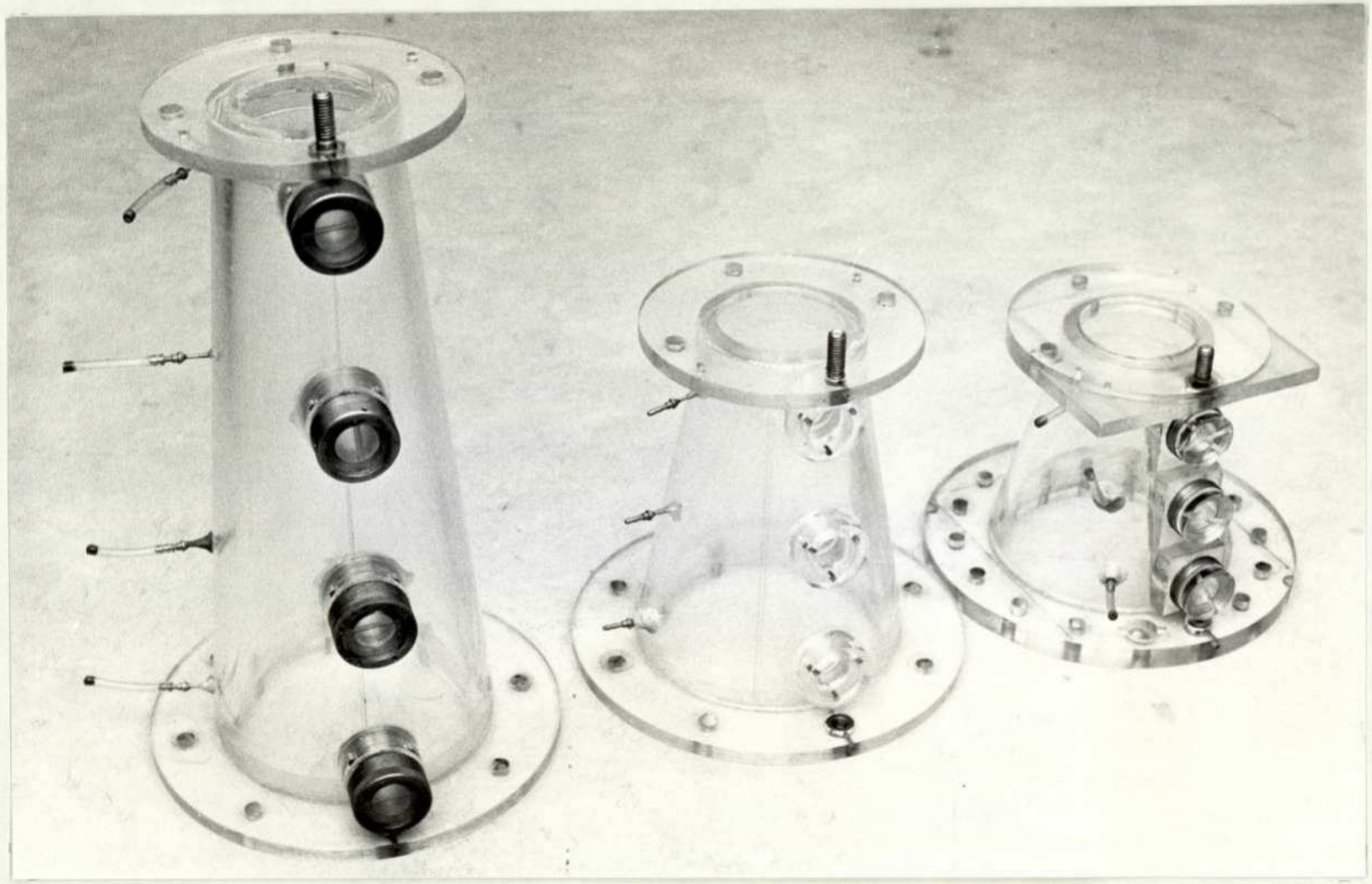

FIG. 4.4b LAYOUT OF DIFFUSERS USED IN EXPERIMENTS

9. Standard design feature permits the use of a DISA anemometer in place of the pitot-probe.
10. Various types of swirl generator may be employed (Rotating honeycomb, Rotating vanes, Fixed vanes, or a Fluidic vortex amplifier). At present rotating honeycomb (generating solid-body vortex) and fixed vane (generating Rankine vortex) are available.
11. For use with air, separate fan and bell-mouth entry is available.
12. The feed-back control system incorporated permits continuous increase or decrease of speed.
13. A wide range of Reynolds number and Rossby numbers are available.
14. Rapid static wall pressure measuring system is available.

4.4 USE WITH AIR

In this case only the top tier was required. The upstream end could be fitted with

(i) a bell-mouth for pure axial flow

(ii) a bell-mouth incorporating a solid-body swirl generator

(iii) a free vortex generator.

Fig.(4.5a), (4.5b) and (4.5c) shows the above arrangement quite clearly. The discharge tail-pipe was fitted to a settling chamber, which in turn was connected to the suction side of a blower fan. The discharge to atmosphere was via an orifice-plate. The flow rate was controlled with the aid of a butterfly valve, Fig.(4.6).

FAN UNIT: SECOMACK MODEL 152
SERVICE ELECTRIC COMPANY MOTOR
3 PHASE, 1.25 HP, 2850 R.P.M.

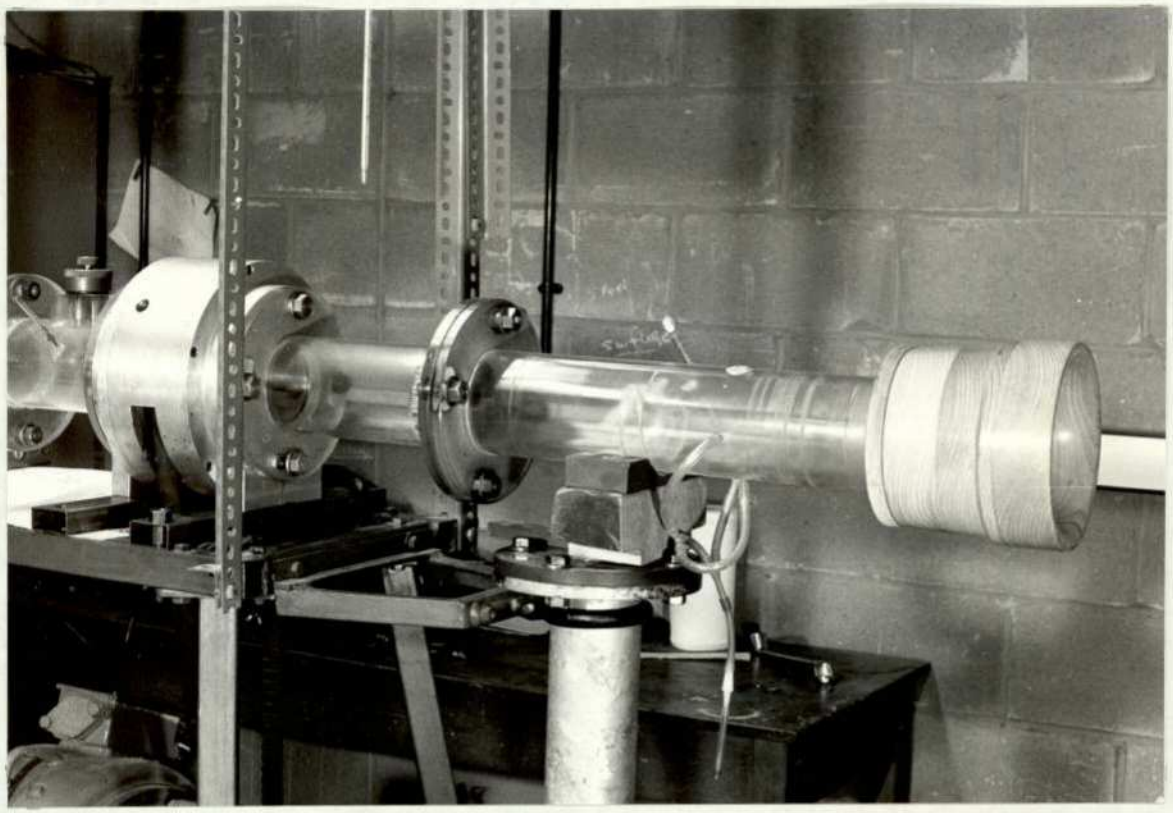

Stationary solid-body swirl generator

FIG. 4.5a AXIAL FLOW ENTRY

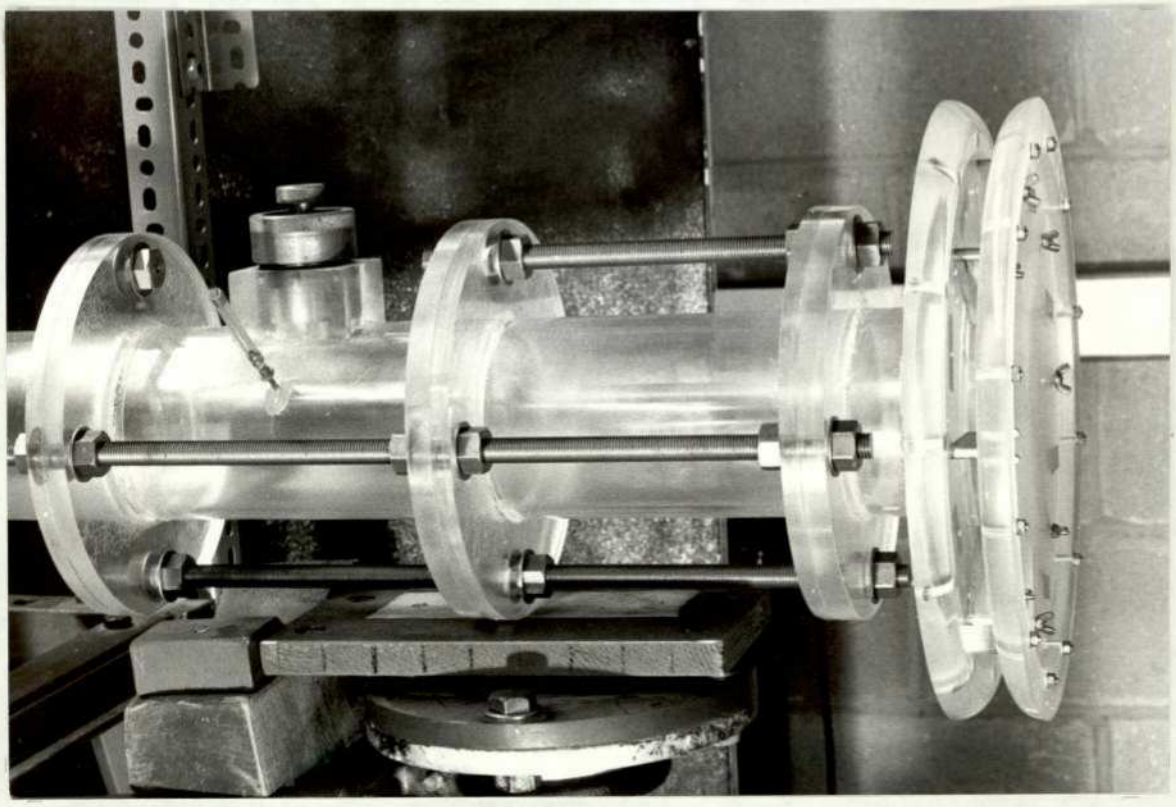

Blade angle of free vortex generator set at 0^{o}.

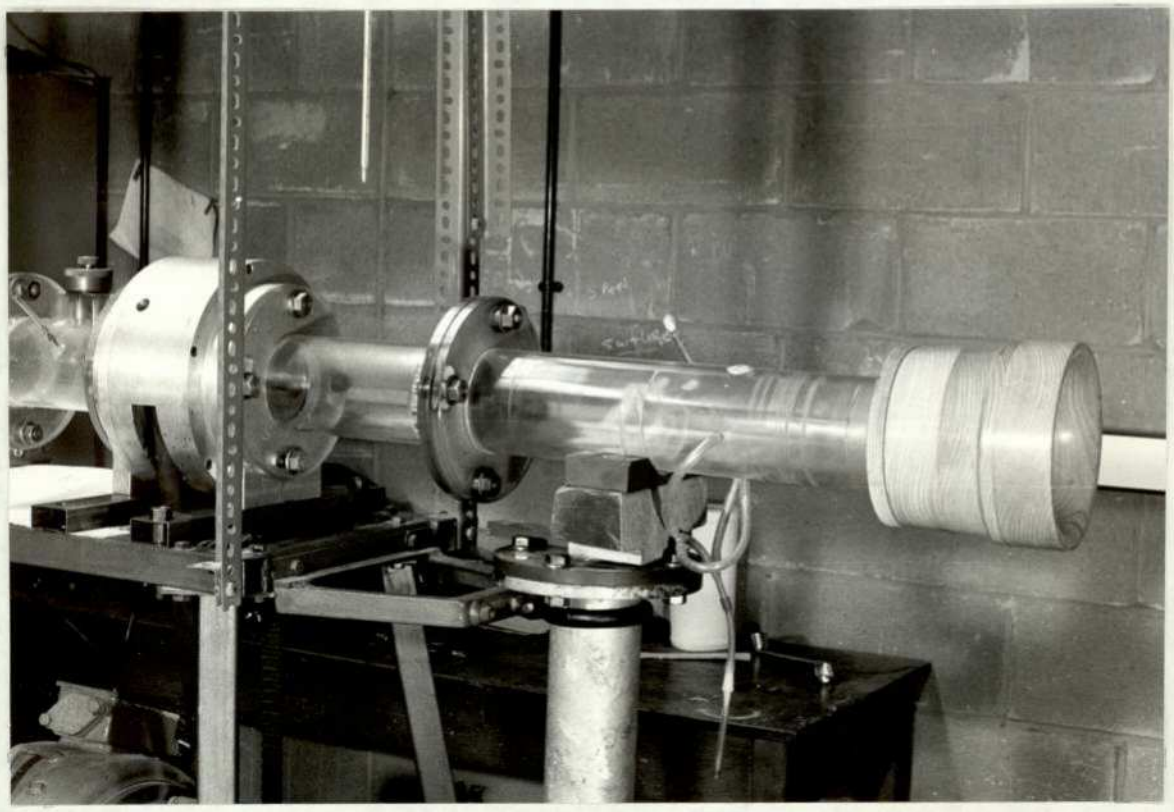

FIG. 4.5b SOLID-BODY SWIRLING FLOW ENTRY

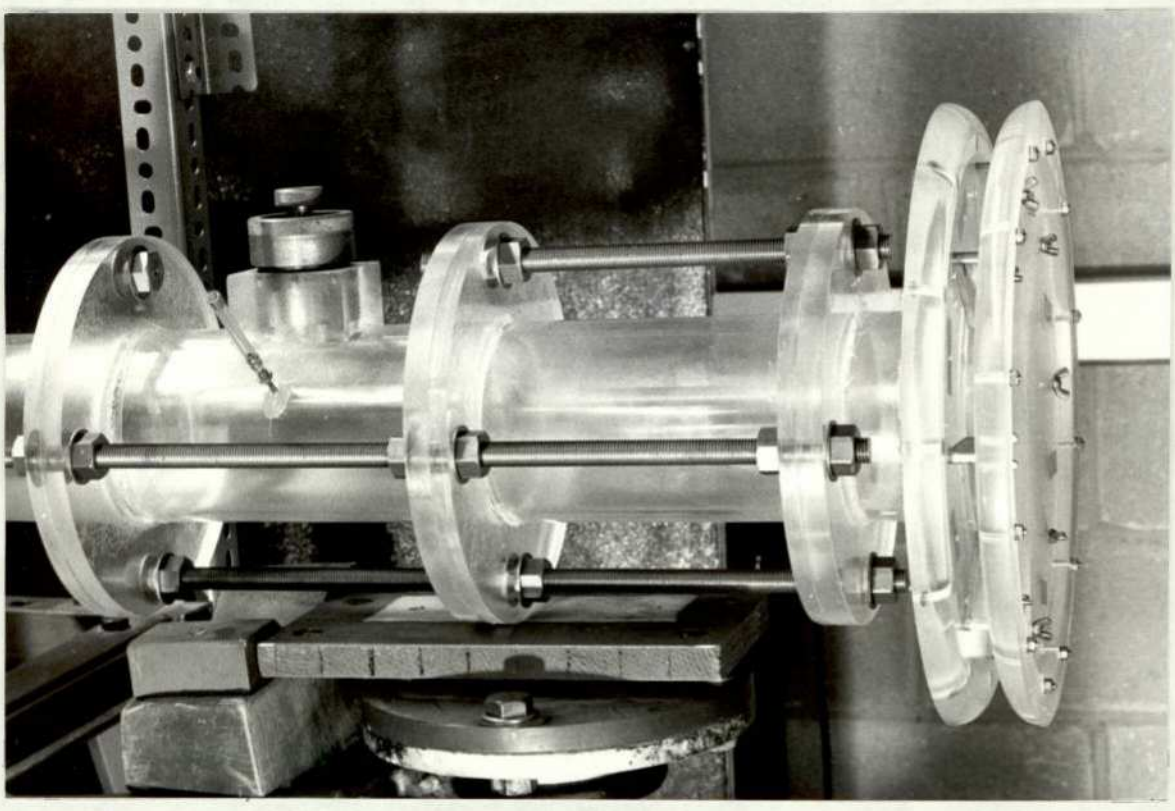

FIG. 4.5c RANKINE VORTEX FLOW ENTRY

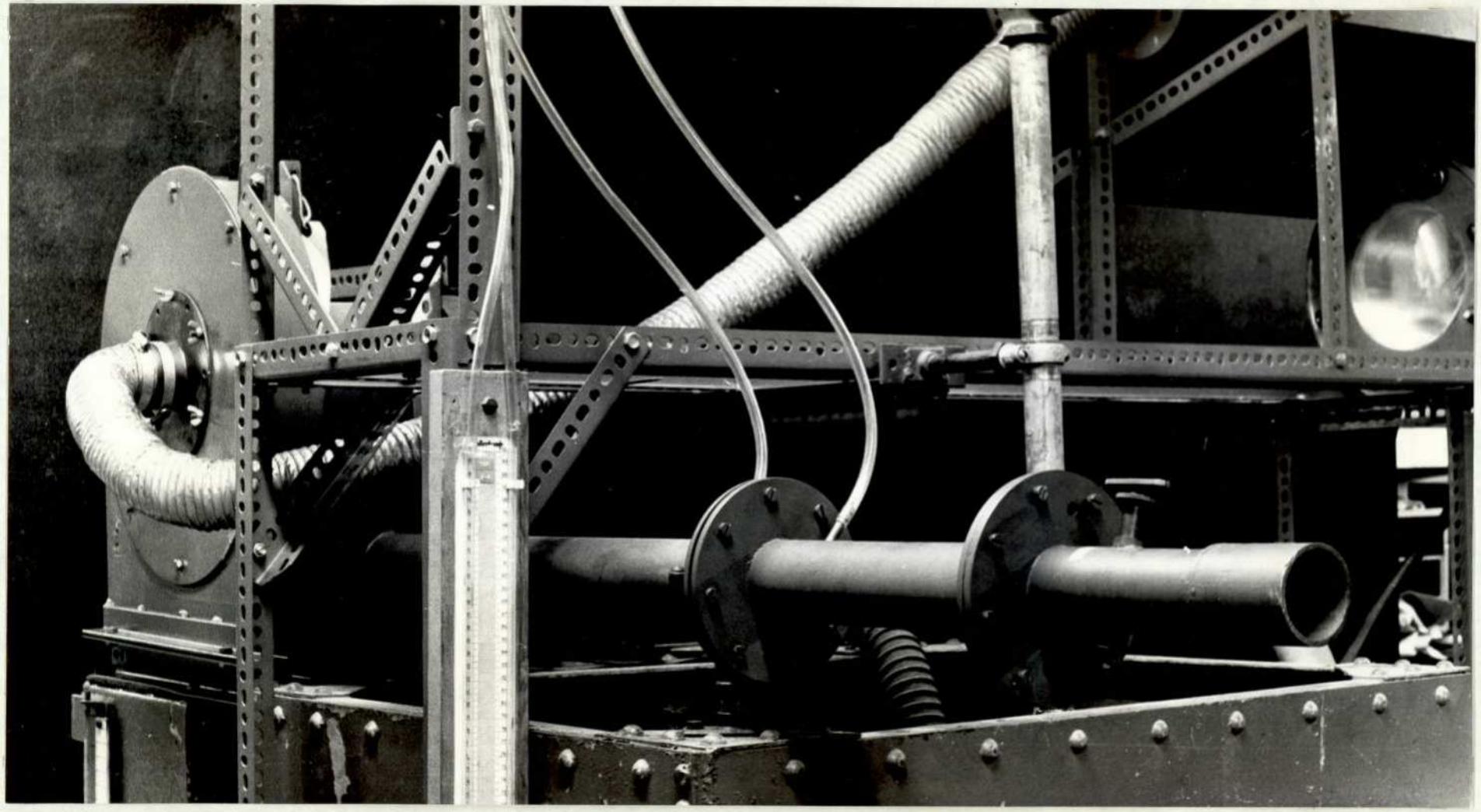

FIG. 4.6 BLOW FAN, ORIFICE PLATE AND BUTTERFLY VALVE

4.5 CHOICE OF FLUID

The rig was designed to handle liquids as well as air. Since flow visualization and detailed measurements are of primary interest, then air is preferred to liquids, because liquids tend to be sluggish in response. Also, the use of water would create sealing and corrosion problems, which in this case were thought to be serious. However, a detailed description and procedure of 'use of water' is given in (52).

4.6. SWIRL GENERATORS

4.6.1 Types of Swirl Generators

The figures below show different types of swirl generators and practical applications of swirling flow in diffusers.

TANGENTIAL INLET FIXED GUIDE VANES ROTATING GUIDES

TURBINE/DRAFT TUBE INSTALLATION

Swirl can be generated by one of three fundamental methods.

(a) Tangential inlet: A single jet (Fluidic Vortex Amplifier) or a series of jets discharging tangentially, in conjunction with an axial flow, to provide swirl. Research of this nature was carried out at University of Southampton.

(b) Fixed guide vane: Fluid is fed radially through the vanes and enters the test section axially. This type of generator has been used by Liepe (64), Harvey (32), Sarpkaya (43) and more recently by Senoo, Kawaguchi, Nagata (62).

(c) Rotating guides: The fluid enters the generator with zero swirl velocity and is carried round by the generator which imparts swirl to the fluid. Liepe (64), Van Dewoestine (49) and Wirasinghe (52) used this type of swirl generator.

In this project, it was decided to use a rotating honeycomb for solid-body vortex with a control system to obtain fine control of rotating speed. And also, a fixed guide vanes for Rankine vortex, where vanes can be set at a particular angle.

4.6.2 Rotating Honeycomb Solid-Body Swirl Generator

Solid-body type swirl was generated by a honeycomb swirl generator consisting of a honeycomb 50 mm long, 6 mm cell diameter, mounted on the same centre-line as the test section and rotated by an external motor via a tooth-belt drive. Figs.(4.7a) and (4.7b) show the main features of the generator. Sealing was a particular problem since the unit was intended to be rotated at up to 1000 revs/min. but the use of "GACO" knife edged spiro-seats proved satisfactory. In addition, the need to have an external drive necessitated to use of a "split system" design, particularly since it would be undesirable to remove the seals and bearings too often. The drive was provided by a direct

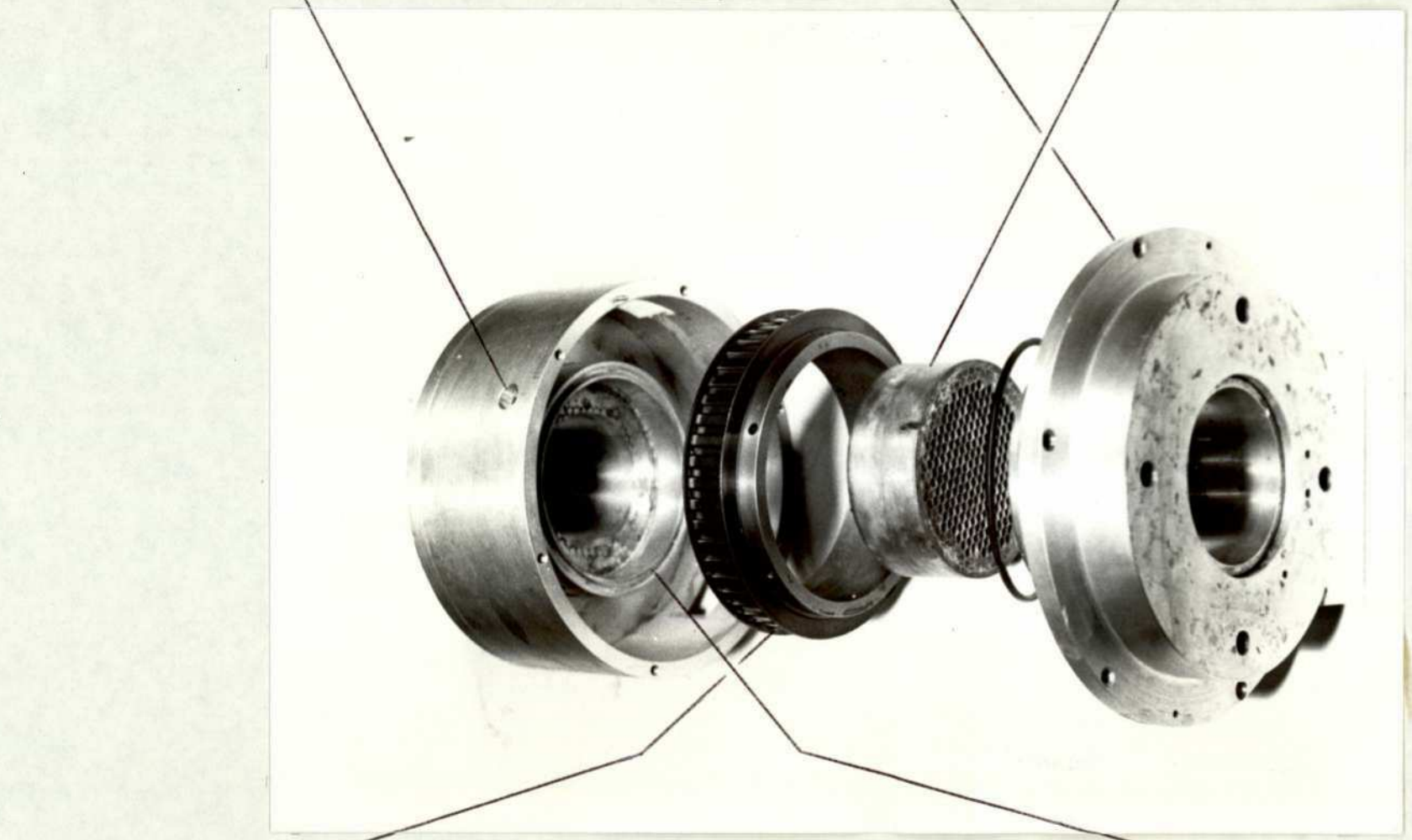

FIG. 4.7a EXPLODED VIEW OF SWIRL GENERATOR

FIG.4.7b. SWIRL GENERATOR ASSEMBLY

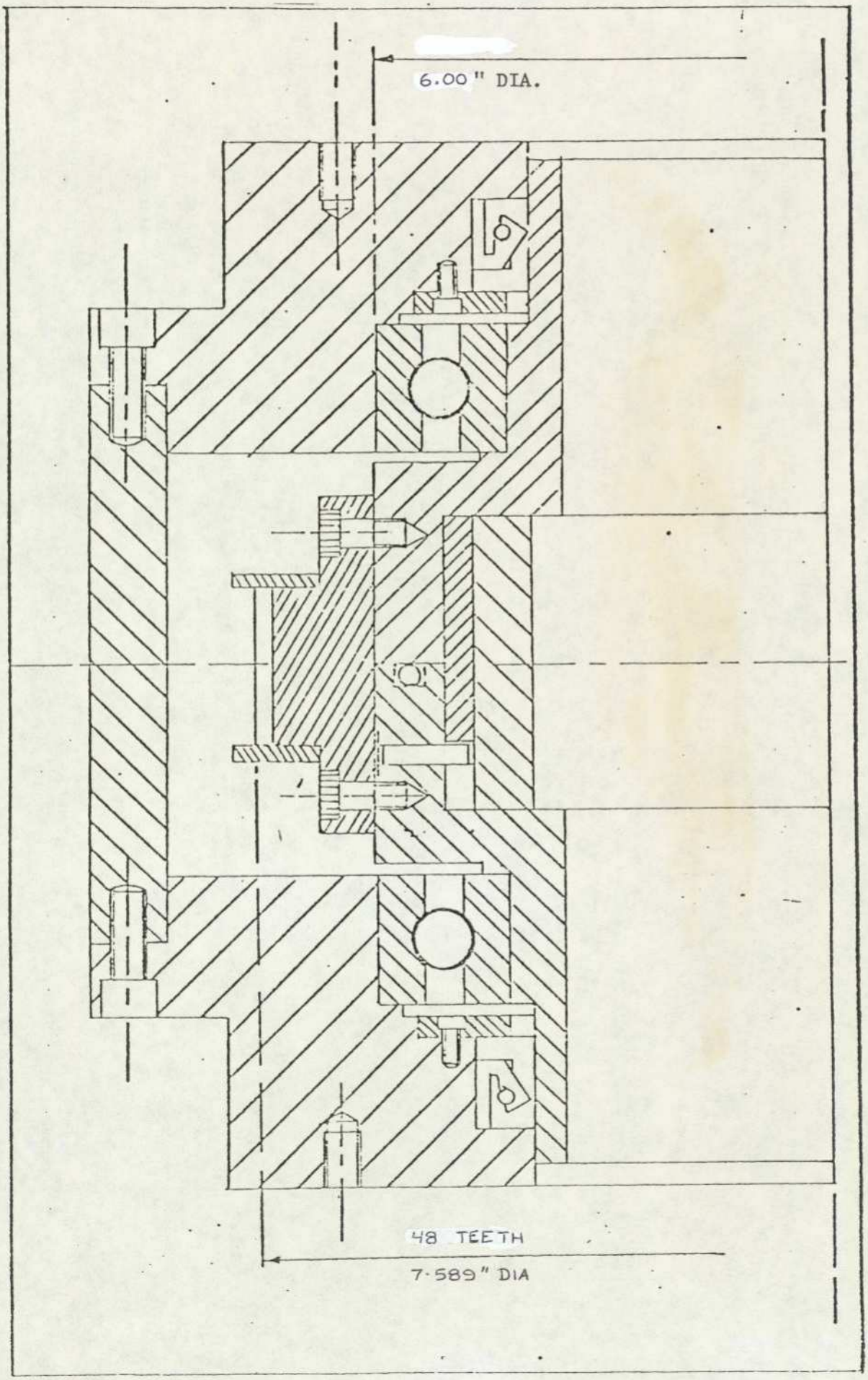

current shunt motor, equipped with a feedback control system providing a speed holding accuracy better than 1% at 1000 revs/min. A tooth-belt drive was employed since belt slip would be intolerable as would excessive tensioning against the "split system". The speed ratio between pinion of motor gear and gear of swirl generator provided were 2.4:1 (specified as DRIVE A) and 1:2 (specified as DRIVE B) with each having high and low range. The difference between centre distance was accommodated by the inclined bed of the table on which the motor was mounted. Details of the drive unit are as follows:-

DRIVE MOTOR: THOMPSON HOUSTON D.C. SHUNT MOTOR

220 V; 5 HP; 1000 R.P.M.

MOTOR SHAFT: 1.375" DIA.

KEYWAY: 0.375" x 0.125"

TRANSMISSION: ALL FENNER PRODUCTS

	DRIVE A (STEP DOWN)	DRIVE B (STEP UP)
DRIVE PULLEY	20 H 100; 20 T	96 H 100: 96 T
DRIVEN PULLEY	4B T; SPECIAL	
BELT	700 H	900 H
TAPER-LOCK BUSH	019E0106 (1310)	019M0106 (2517)
CENTRE-LINE DISTANCE	671 MM	679 MM
SEALS	GACO 'SPIROSEAL' DPSM 100 12012	
INCLINED TABLE	INCLINATION 20° TO HORIZONTAL LIMITS OF CENTRE DISTANCE - 655 MM to 715 MM.	

4.6.3. Fixed Guide Vane Swirl Generator

In this case, the swirl was generated by replacing the bell mouth with a free vortex generator, without change in the entry length to the diffuser. The free vortex generator is essentially a radial-to-axial intake. It is divided into two major sections, i.e. bell-mouth and blade section. The bell mouth assists in unification of the entry flow, while the blade section consists of 16 straight aero-foil section brass blades of 53.97 mm chord, 15.00 mm span and 6.35 mm thickness. The blades are pivoted 15.97 mm from the leading edge. Figs.(4.8) and (4.9) show the main features of the free vortex generator.

The blades are individually set by a special jig. The limitation of the jig is 0^{o} to 45^{o} in both clockwise and anti-clockwise direction. Fig.(4.10) shows the main feature of the jig.

4.7 PROBE TRAVERSING MECHANISM

4.7.1 Design Requirement

When radial distribution of velocities and pressure are required then the probe must be mounted on a reference face. Unlike in a pipe, in a diffuser the radius at each section is different from the next, which makes it necessary to traverse the probe over varying radii within the diffuser. Furthermore, when swirl is induced in the flow, it is necessary to rotate the probe about the centre sensing hole on the hemi-spherical cap. The dimensions needed to be so arranged, that a standard 'DISA' type anemometer probe holder can be used in place of the pitot probe with only a slight modification. Leakage of flow and vibration of probe cannot be tolerated. The diverging wall of a conical diffuser, unlike that of a pipe, does not permit it to be used as a reference datum. Thus the axis of the diffuser is regarded as the datum.

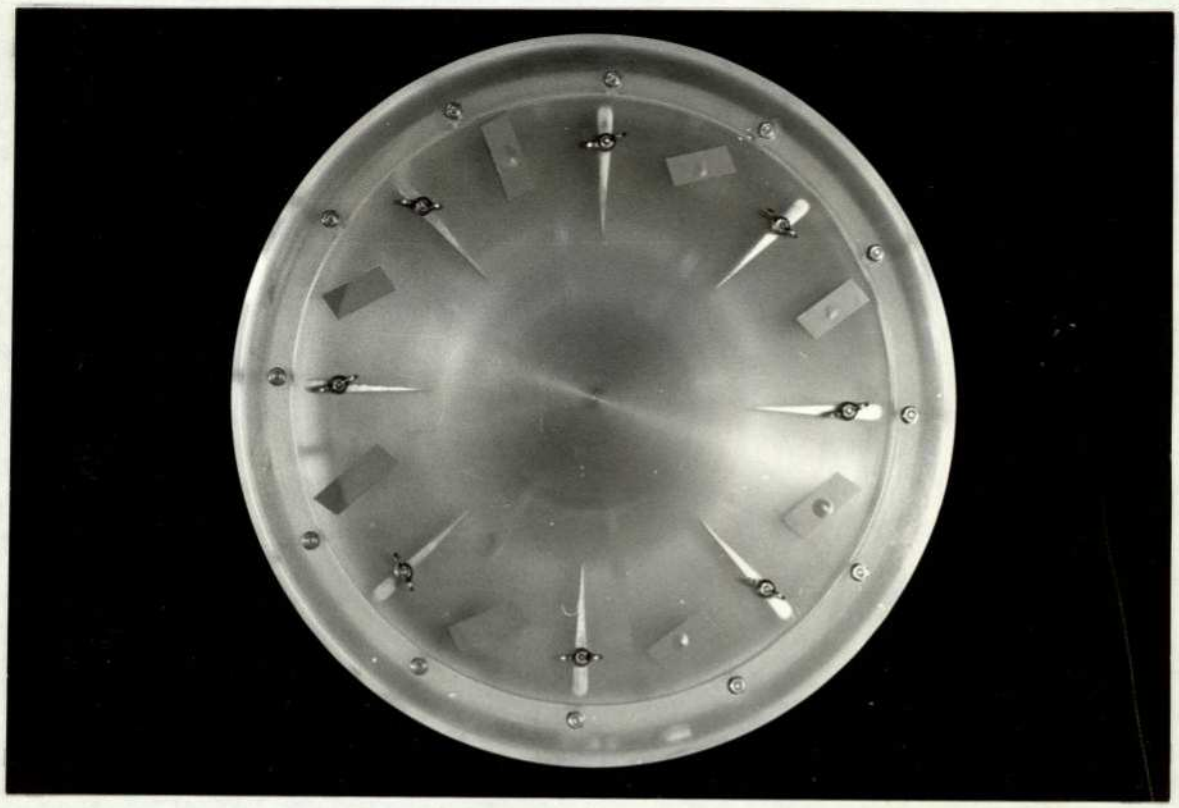

FIG. 4.8 LAYOUT OF FREE VORTEX GENERATOR

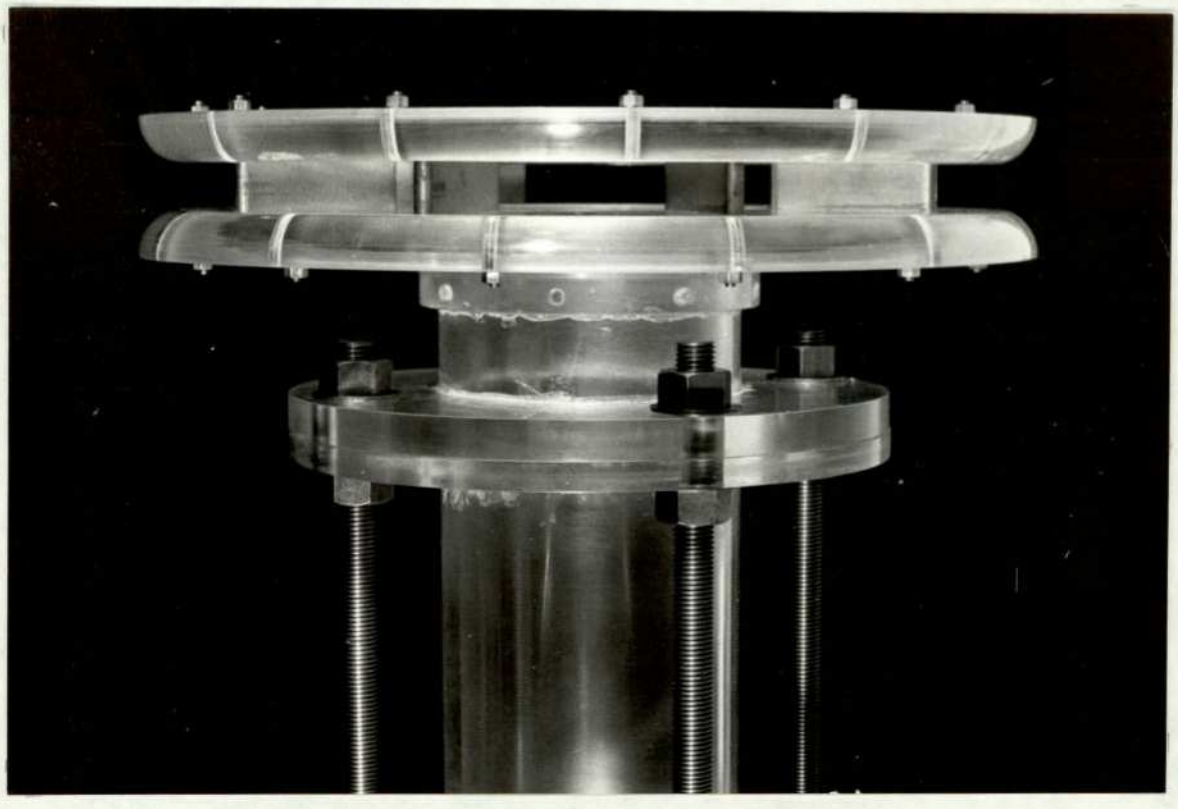

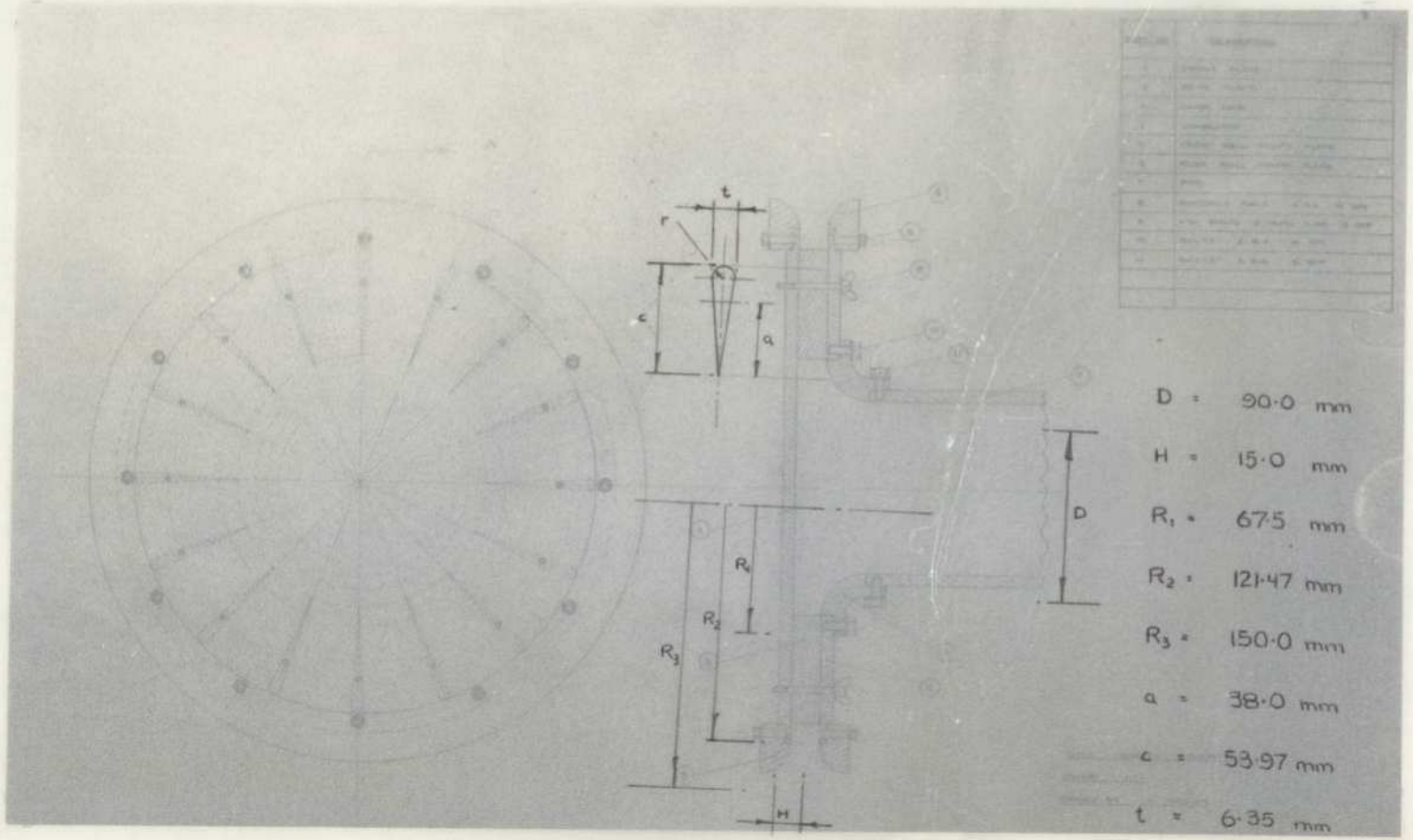

FIG. 4.9 FREE VORTEX GENERATOR ASSEMBLY

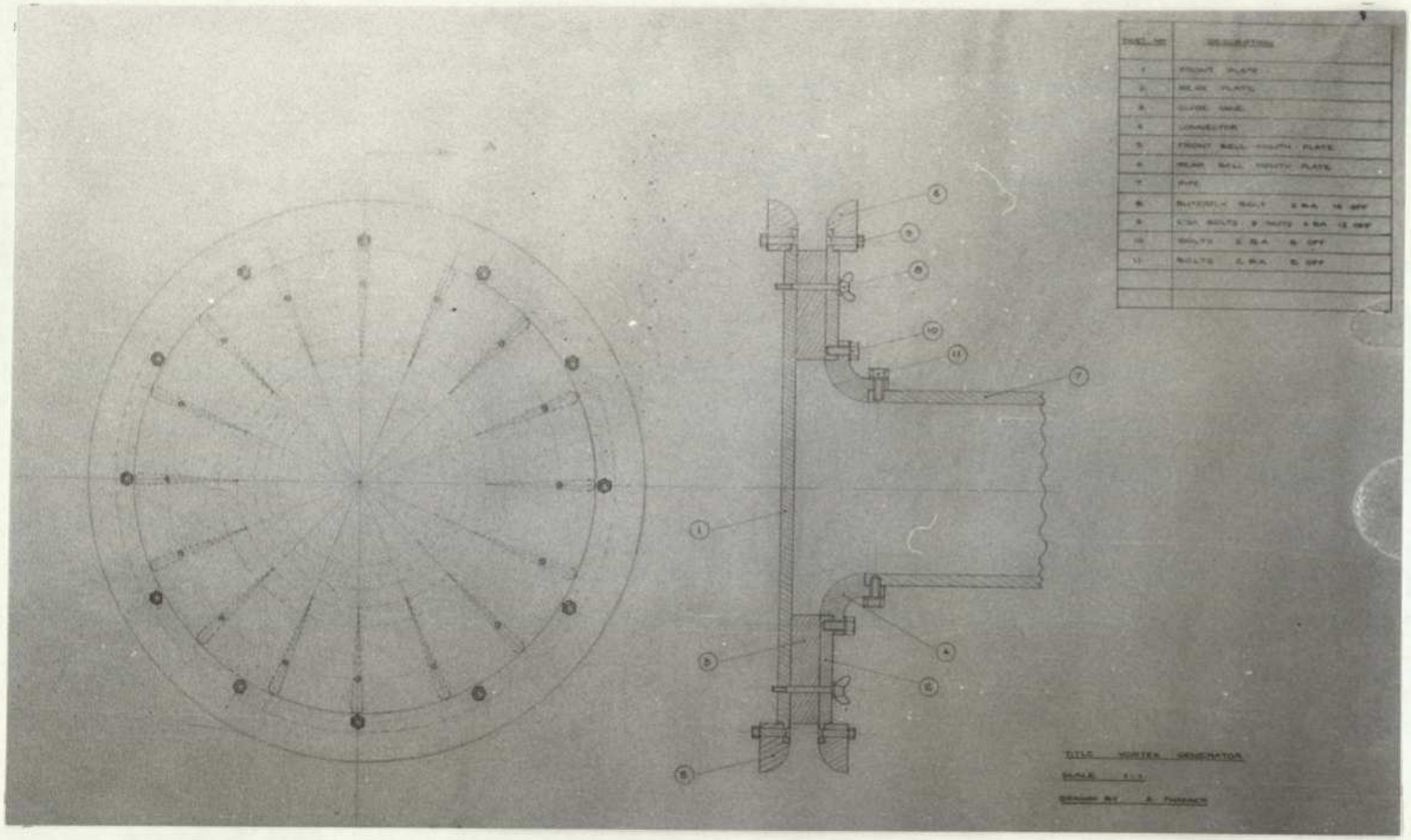

FIG. 4.9 FREE VORTEX GENERATOR ASSEMBLY

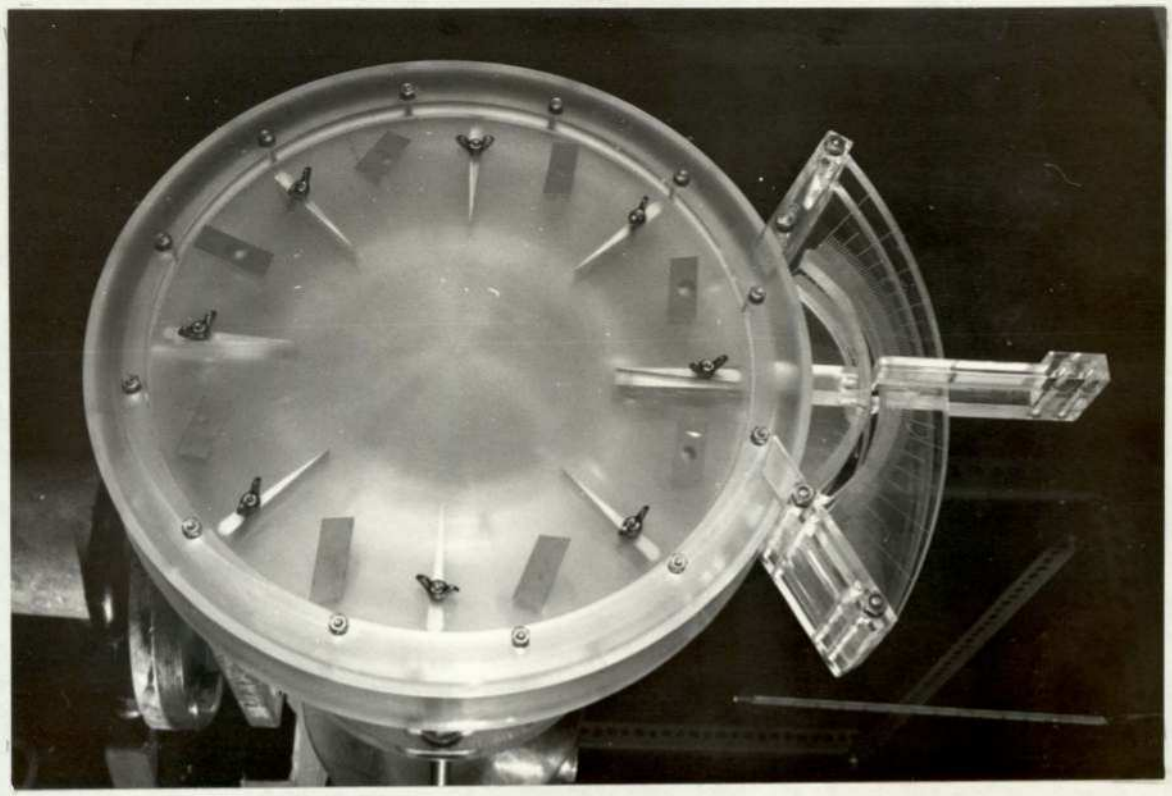

FIG. 4.10 BLADE SETTING JIG.

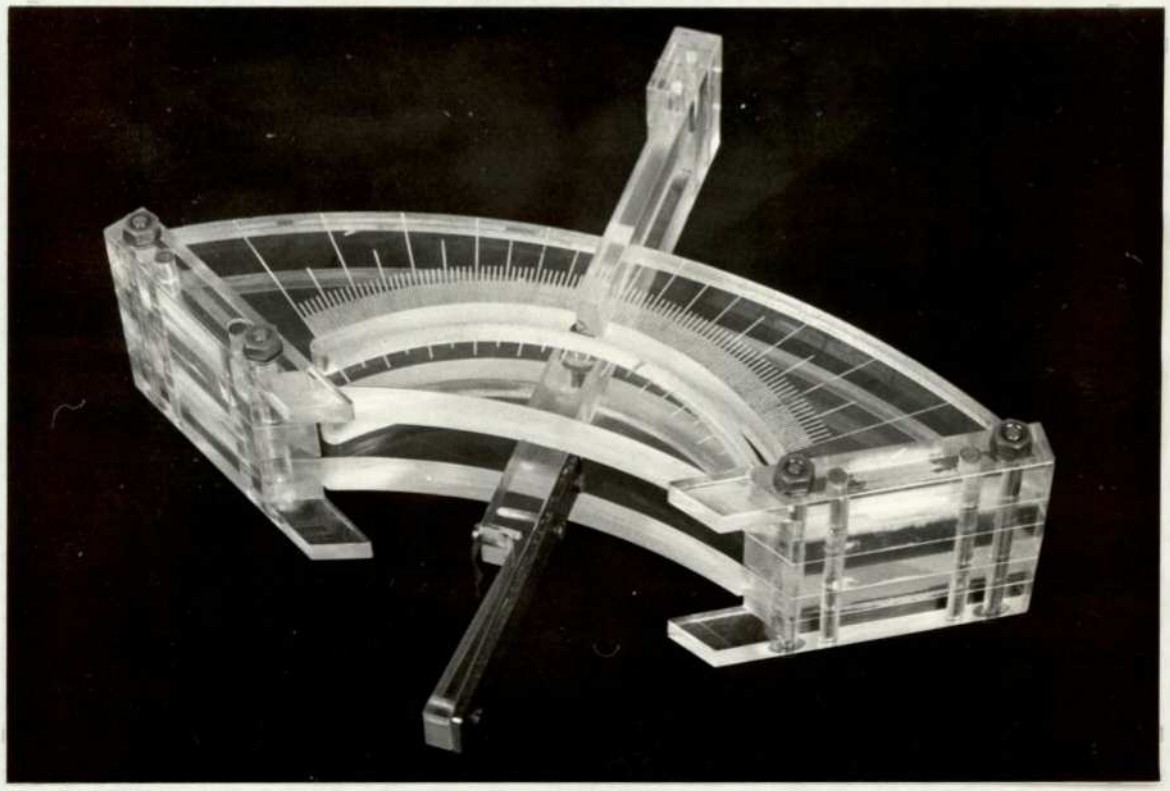

4.7.2 Probe Carrier

Two types of probe carrier were designed which satisfied the above requirement. They are specified as 'Probe Carrier A' and 'Probe Carrier B' Figs.(4.11a) and (4.11b) show the general features of the carriers.

(i) Probe Carrier A

The cross-sectional view of the probe carrier A is shown in Fig.(4.12) sitting on a perspex shoulder. The five hole hemi-spherical probe can be traversed linearly by placing slip gauges between U bracket and surface "A". Note the surface "A" and "B" were horizontally flat, that is within fabrication accuracy (0.002"). The U bracket can be fixed at a particular position along sleeve by help of cheese-head grub screw. For swirling flow measurements, a scale was used, where pointer, Fig.(4.11a) acted as a reference point for angle measurement. The handle assisted manual rotation of the probe carrier about the central sensing hole of the probe.

(ii) Probe Carrier B

This is essentially a modification of probe carrier A. The slip gauge traverse was replaced by accurate micrometer screw thread traverse. Fig.(4.11b) shows the general features of the carrier. Backlash was eliminated by turning the knob in one direction of rotation only.

4.8 FEED-BACK SPEED CONTROL SYSTEM

4.8.1 General Description

A direct current motor was used. Its speed was varied by varying the armature voltage. The block diagram associated with the mode of speed control is shown in Fig.(4.13). The thyristor triggered by an auxillary firing circuit, varies the armature voltage. At low speeds, under load, the speed is

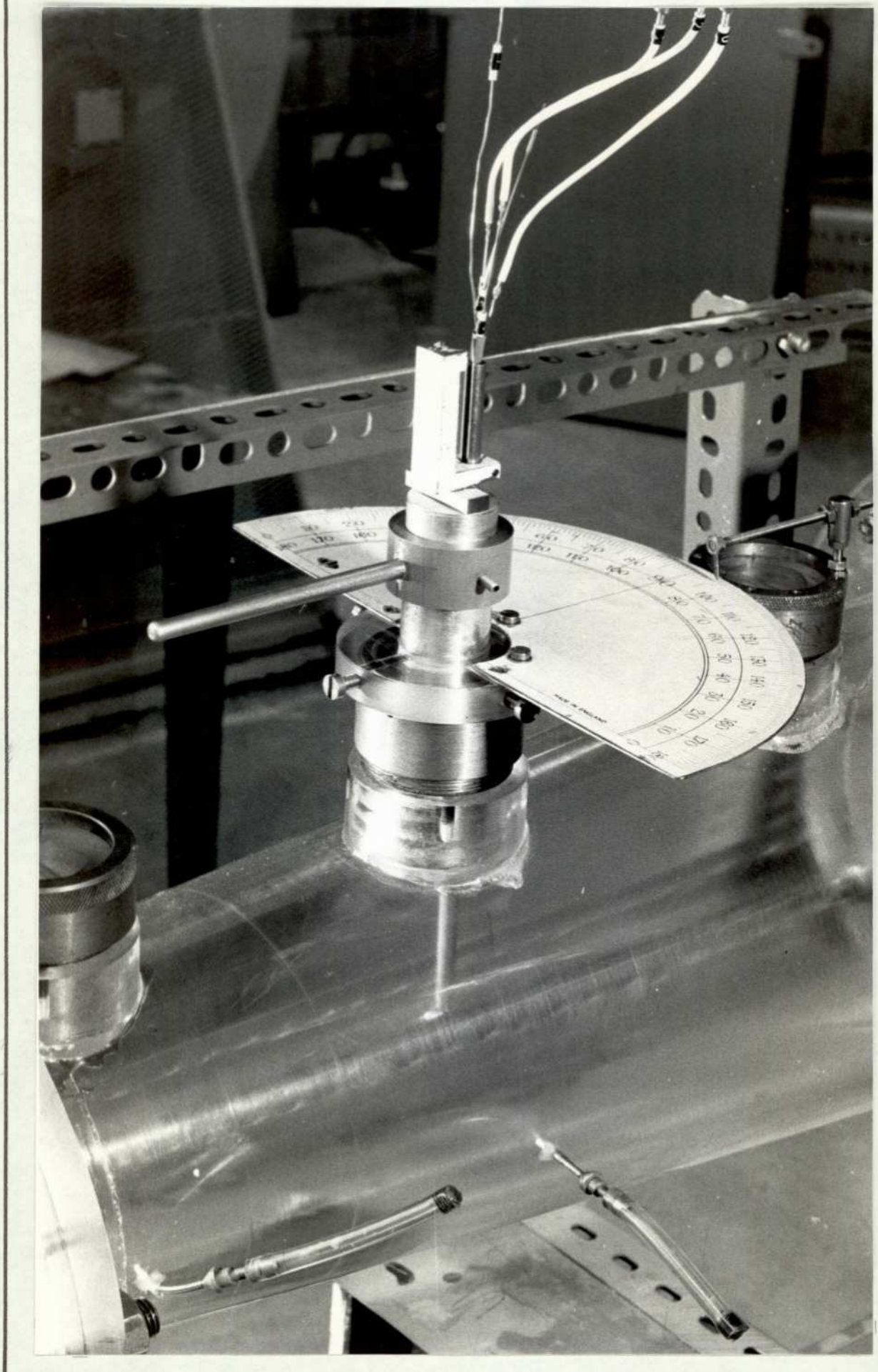

FIG. 4.11a PROBE CARRIER 'A'

FIG. 4.11 b PROBE CARRIER 'B'

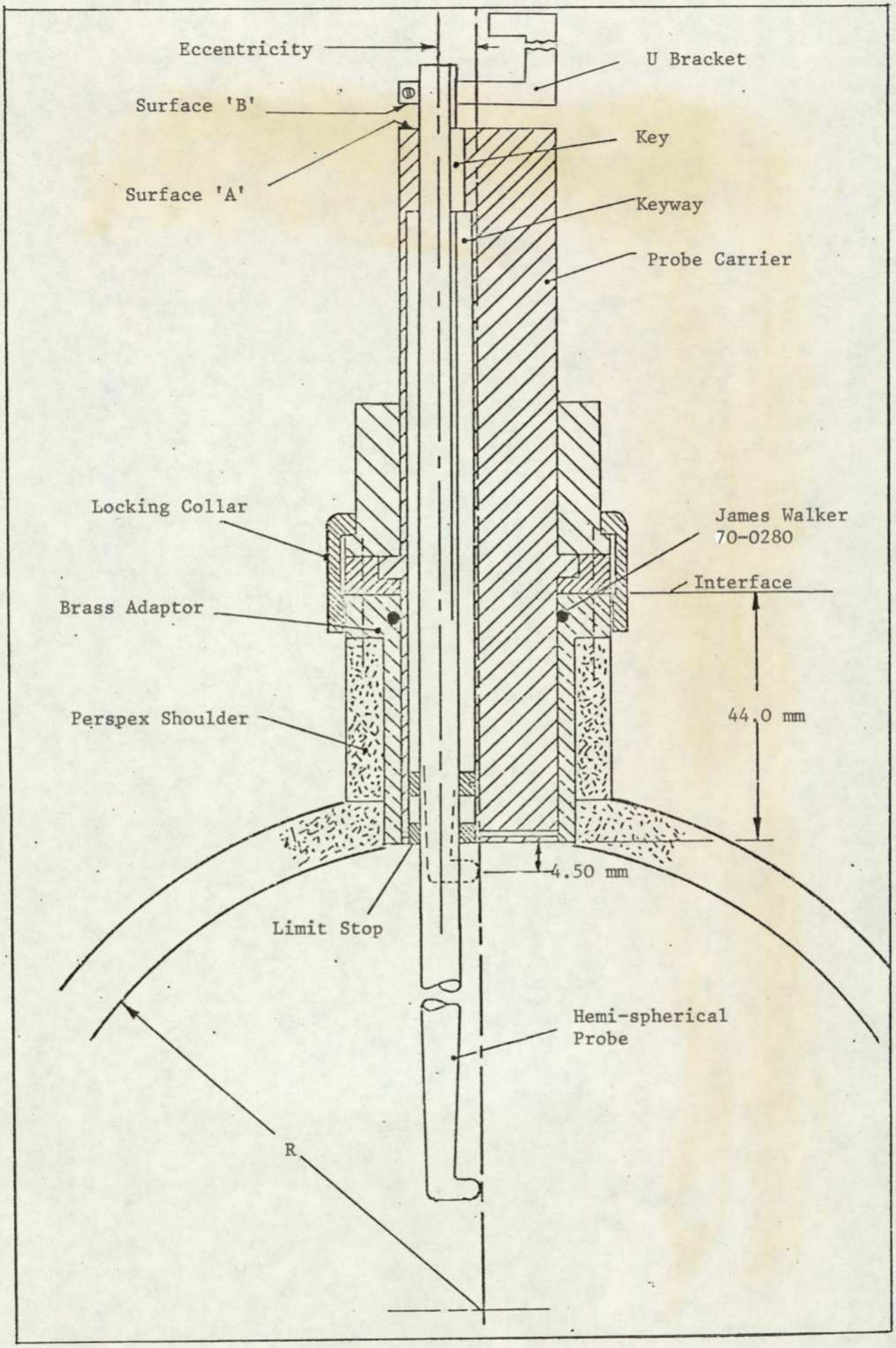

FIG. 4.12. COUPLING FOR PROBE HOLDER

likely to fluctuate and to compensate for this a tachogenerator, coupled to the motor shaft is used to obtain feed-back.

4.8.2 Description of the Control Circuit

A thyristor is employed to control the speed of the d.c. shunt motor. It is essentially a conventional rectifier with controllable firing position. When a pulse is supplied to its gate, it fires, where at this point it commences conducting and does so until the current drops to zero, at which point it effectively switches off. The effect of firing on an alternating current input is shown in Fig.(4.14) .

The pulse required to trigger the thyristor is obtained as follows: The d.c. voltage is obtained by rectifying a.c. mains. The Zener diode chops off voltage in excess of 18.0 volts, giving the "spiked" waveform, Fig.(4.15a). This waveform enters the capacitor C4, discharges it (which is charged by R4) and gives rise to a "saw tooth" waveform, Fig.(4.15b), which is superimposed on a constant d.c. voltage, is used to fire a Schmidt-trigger; thus the resulting output is a square wave form, Fig.(4.15c). This wave form is differentiated by R-C differentiator to obtain pulses, Fig.(4.15d). The diode eliminates the negative pulses. Firing of the thyristor is via a pulse transformer. Fig.(4.16) shows the modified circuit diagram.

The Schmidt-trigger (ST) fires at a certain voltage which is determined by R12, R13 and R14. The input to the ST consists of the saw toothed voltage superimposed on a d.c. voltage, the d.c. level, V_L. This d.c. level is the resultant of a d.c. control voltage, V_c and the feed-back voltage, V_f, from the techogenerator applied in opposition to each other.

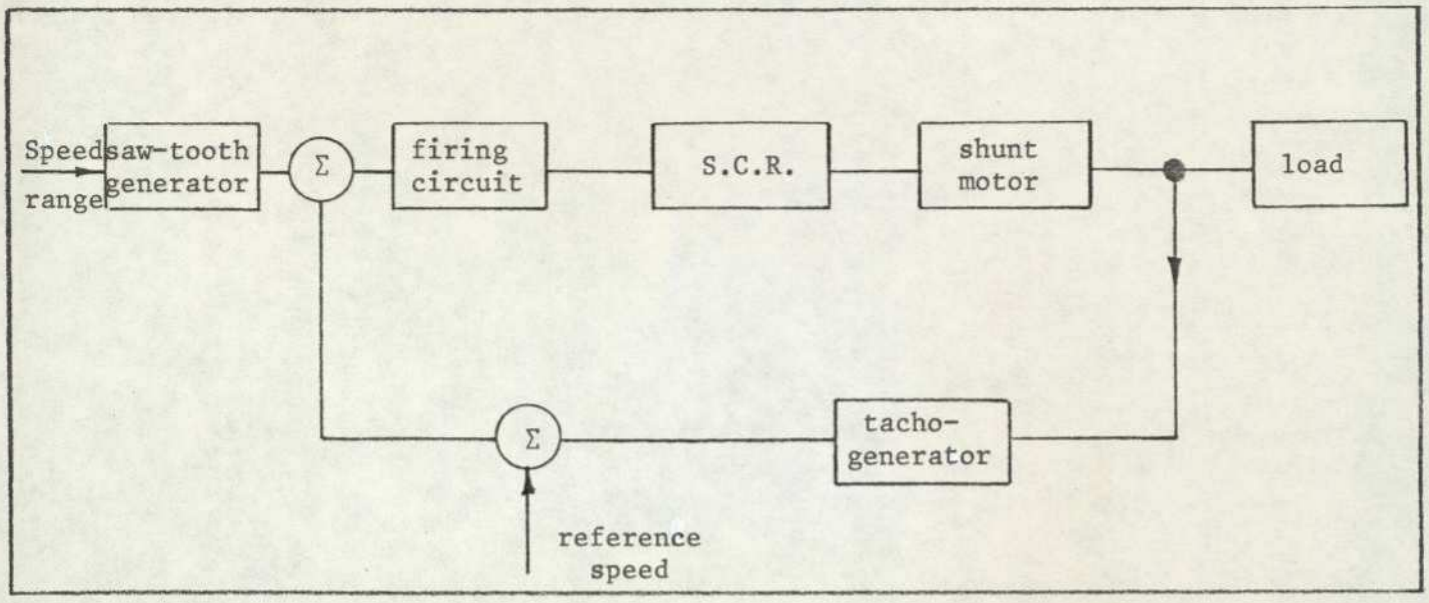

FIG. 4.13. CONTROL SYSTEM FOR SPEED VARIATION

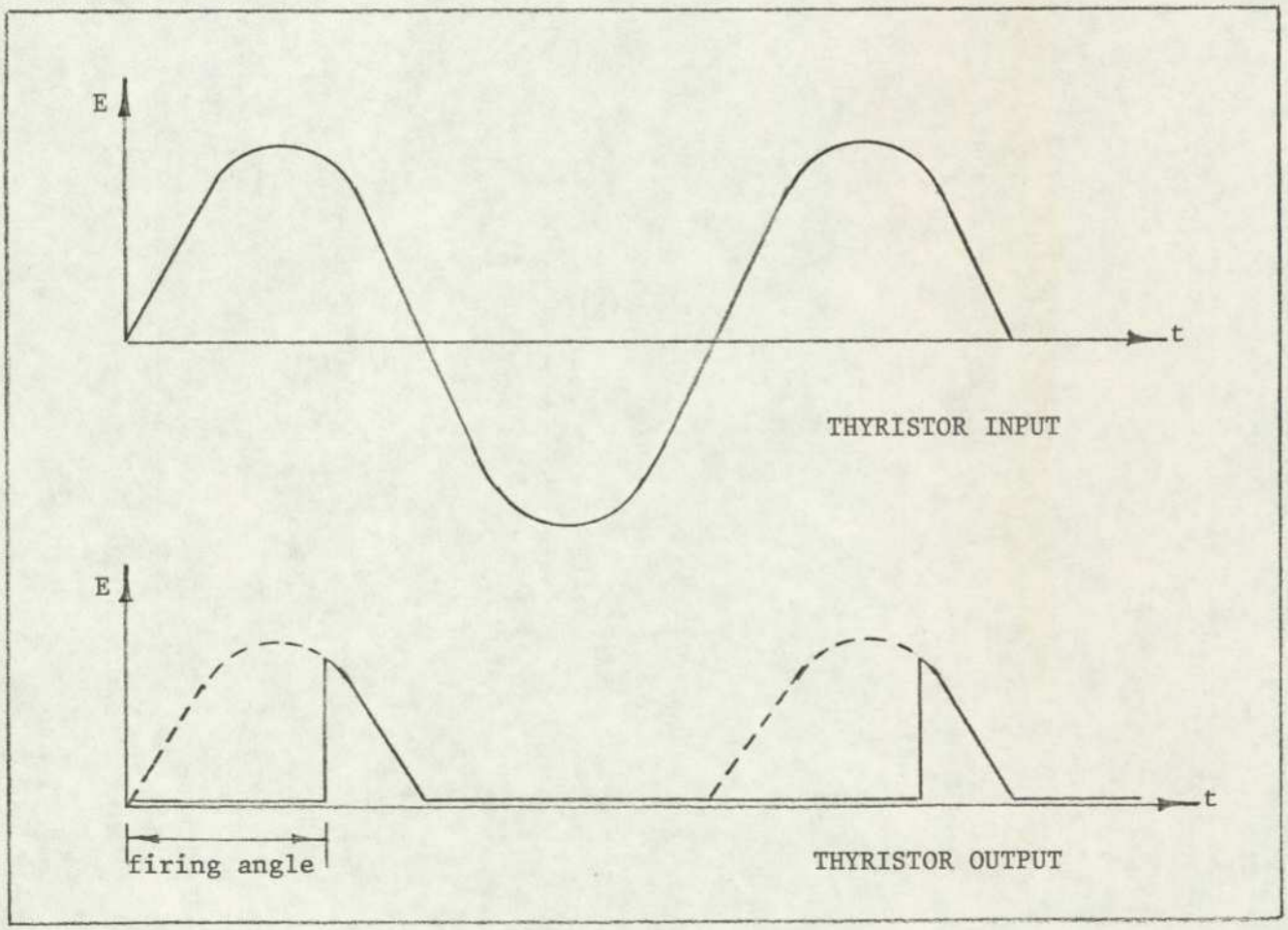

FIG.4.14. EFFECT OF THYRISTOR ON A.C. INPUT

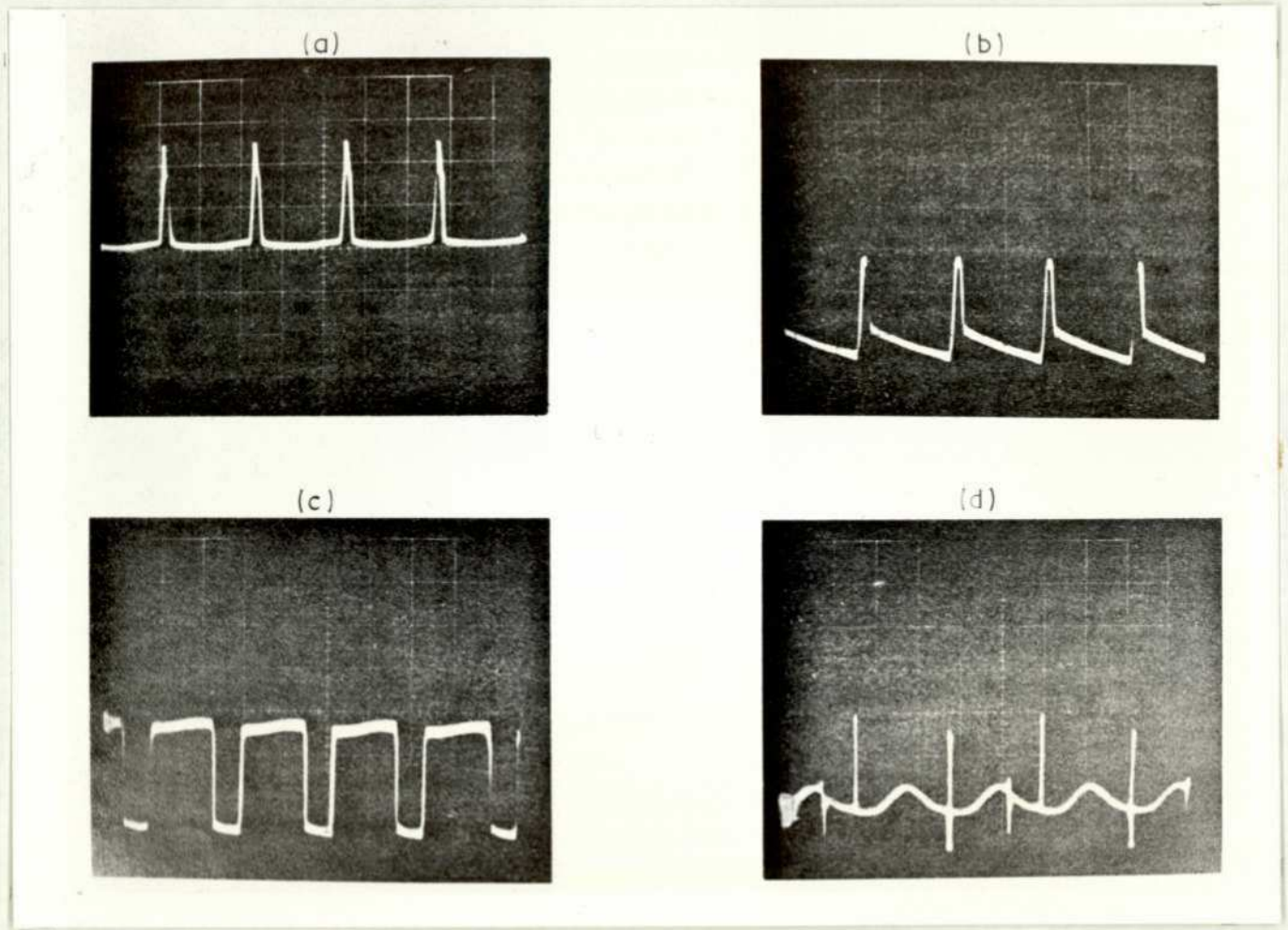

FIG. 4.15 METHOD OF OBTAINING PULSES

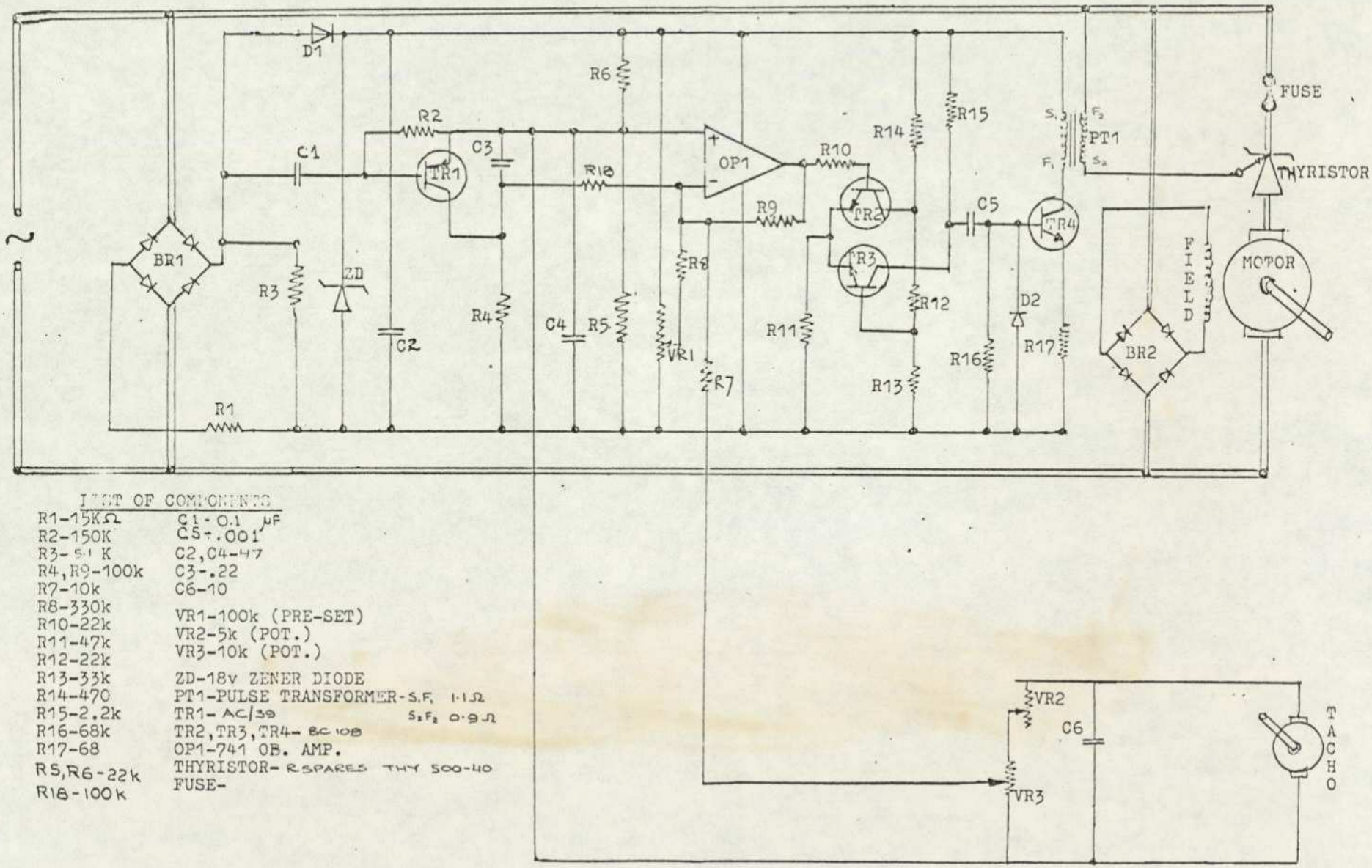

LIST OF COMPONENTS

R1-15KΩ	C1-0.1 μF
R2-150K	C5-.001
R3-5.1 K	C2,C4-47
R4,R9-100k	C3-.22
R7-10k	C6-10
R8-330k	VR1-100k (PRE-SET)
R10-22k	VR2-5k (POT.)
R11-47k	VR3-10k (POT.)
R12-22k	
R13-33k	ZD-18v ZENER DIODE
R14-470	PT1-PULSE TRANSFORMER-S.F. 1·1Ω
R15-2.2k	TR1-AC/39 S1F2 0·9Ω
R16-68k	TR2,TR3,TR4-BC 108
R17-68	OP1-741 OB. AMP.
R5,R6-22k	THYRISTOR-R SPARES THY 500-40
R18-100k	FUSE-

FIG.4.16. CIRCUIT USED IN SPEED CONTROL SYSTEM

The range of speed is governed by the magnitude of the controlled voltage which can be altered, using the pre-set potentiometer, to give any desired range. Fig.(4.17) shows the manner in which the speed control is achieved. By setting V_c, the system is initially set to the desired speed range. The feed-back voltage, V_f, is set using the potentiometer RP_1, to obtain the desired speed. The level V_L is now $V_c - V_f$. For a given speed range V_c is constant, $V_f = kV_T$ where V_T is the voltage developed by the tachogenerator and k is the fraction of this obtained from the potentiometer. If the motor speed increases, then V_T, hence V_f increases and V_L decreases. Thus the effective voltage supplied to the armature decreases and the effect is to slow down the motor countering the increase. The converse is true in the case of a decrease in speed. By reversing the field connections, the direction of rotation of the motor can be altered. The control system is independent of sense of rotation of the motor by presence of the bridge rectifier.

4.8.3 Precautionary measures

1. Multi-turn speed controls (fine and coarse) are non-linear.
2. Speed of the motor should be kept below 1370 R.P.M.
3. Do not earth control system.
4. Do not supply armature without first supplying field
5. Do not increase the speed of motor too rapidly.

NOTE: The system was originally designed by Chapman; however modification was required in order to optimise the system.

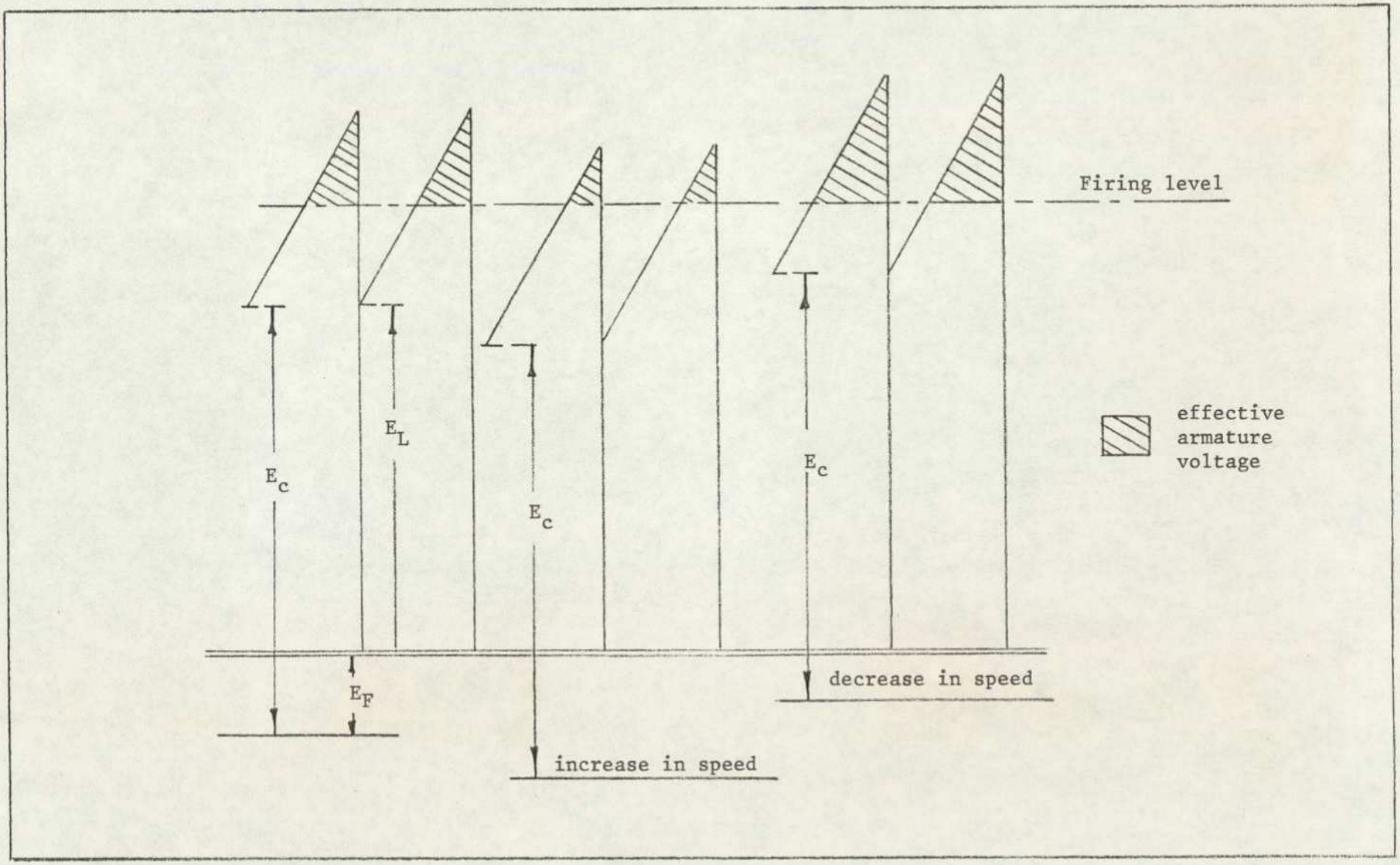

FIG.4.17 METHOD OF SPEED CONTROL VIA FEED-BACK

4.9 INSTRUMENTATION AND CALIBRATION

4.9.1 Five-Hole Hemi-Spherical Probe

A pressure probe provides a conveniently simple, mobile and robust tool for the quantitative exploration of most types of air flows. Coupled with an infrequent calibration requirement, these attributes account for its common use throughout a wide field of engineering and scientific activities involving the measurement of wind speed. A number of instruments are available for determining separately the static pressure and complete velocity vector at a point in a fluid stream. However, only the pitot-static probe, or any other form of it, is capable of determining both these parameters simultaneously. The choice of a particular instrument will no doubt depend on the nature of the application, information required and economic considerations.

A five-hole probe was designed and produced by Wirasinghe (52) following a comprehensive feasibility study. He also carried out a detailed calibration analysis, but the analysis was checked and verified as a precautionary measure.

The manufacturing precision of the probe is as follows:

1) Using a shadowgraphic enlarger with a magnification of 100 the probe contour was plotted. The profile error was estimated to be within 1.6% of radius.

2) The 'SIP UNIVERSAL' used with the Goniometer Head to measure the angle between the four side holes showed the error to be less than 1.5^{o}.

3) The relevant probe dimensions are as follows:

Radius of hemi-sphere	2.5 mm
Eccentricity of probe	6.7 mm
Hypodermic tubing	0.8 mm O.D. x 0.1 mm wall
Diameter of sensing hole	0.33 mm; each hole occupying 7.5^{o} of spherical cap.

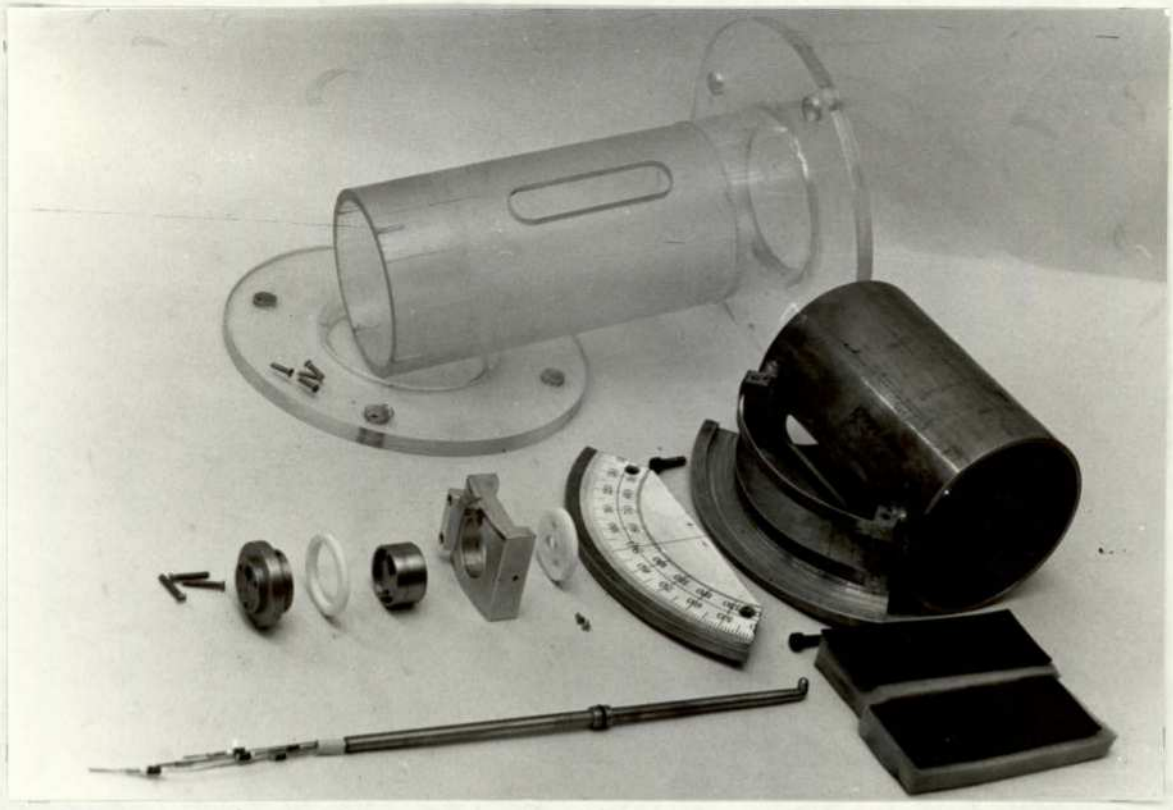

FIG. 4.18 THE CALIBRATION TUNNEL

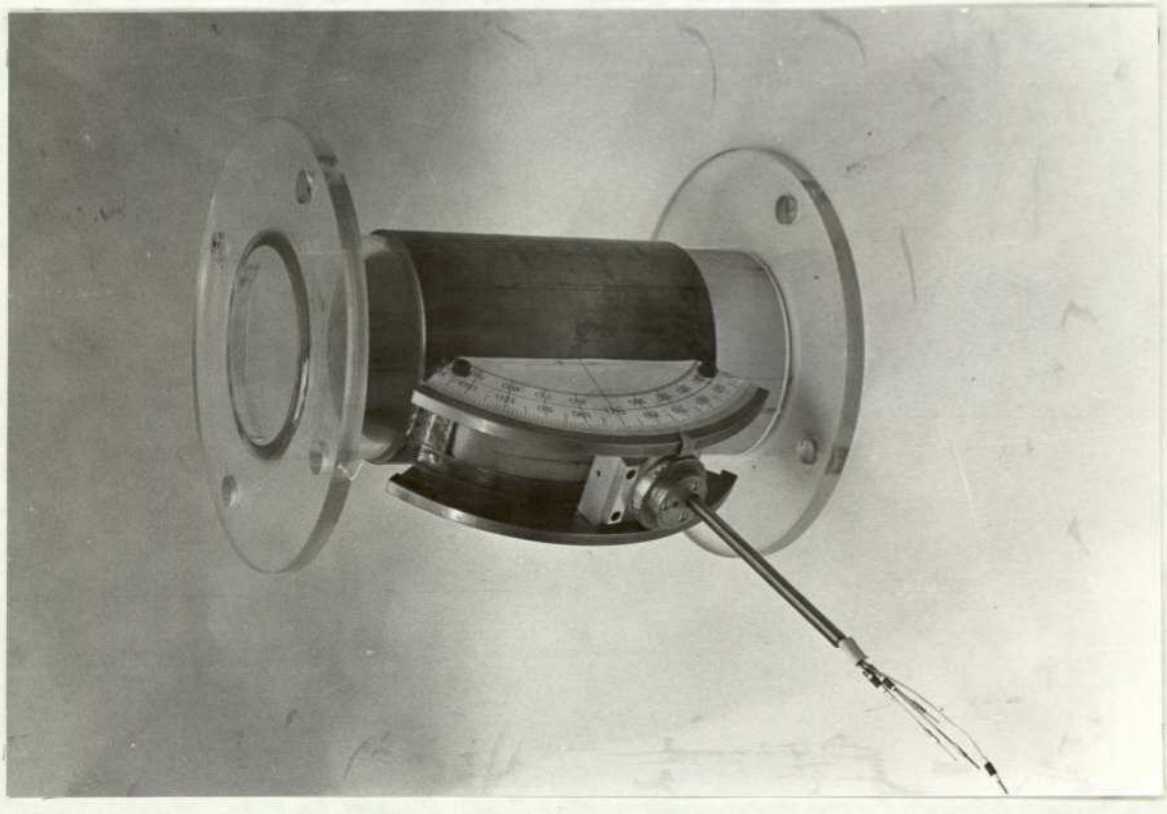

Calibration was carried out in a special calibration tunnel with facilities for yaw and pitch measurements. Fig.(4.18) shows the details of this along with the pitot-probe. A Furness Controls MDC type micrometer was used for pressure measurements, which uses a differential capacitance transducer with a highly stable bridge network and is capable of measuring pressure difference down to ± 0.0001 mm H_2O. The accuracy in any range is within 1% of full scale deflection. A time domain analyser (JM 1860) was used to find the mean of fluctuating readings.

4.9.2 Calibration and Analysis

The design limitations restricted the range to $\pm 30^{o}$ in yaw and in pitch. Using 5^{o} intervals, readings of the five sensing holes were obtained at each point. The above measurements were repeated for three different Reynolds numbers, the object being to obtain separate samples of the same population assuming that this parameter has no significance. Owing to the fluctation in readings, each measuring point required 5-10 minutes to obtain a steady value. The time domain analyser was used to obtain an approximate mean value. The raw-probe chacteristic curves are shown in Fig.(4.19), which reveals that the surface defined by the curves is uneven. Since simultaneous smoothing in pitch and yaw planes is required, the standard "least squares" method for obtaining the best fit is not suitable. Such a technique which is capable of identifying or replacing unacceptable rogue points was developed by Wirasinghe (52) (Appendix C) and use was made of it.

The method of analysis proposed by Wright (65) was not fully suitable, this was due to the effects of the stem. The above observation was made by Wirasinghe and was justified. However,

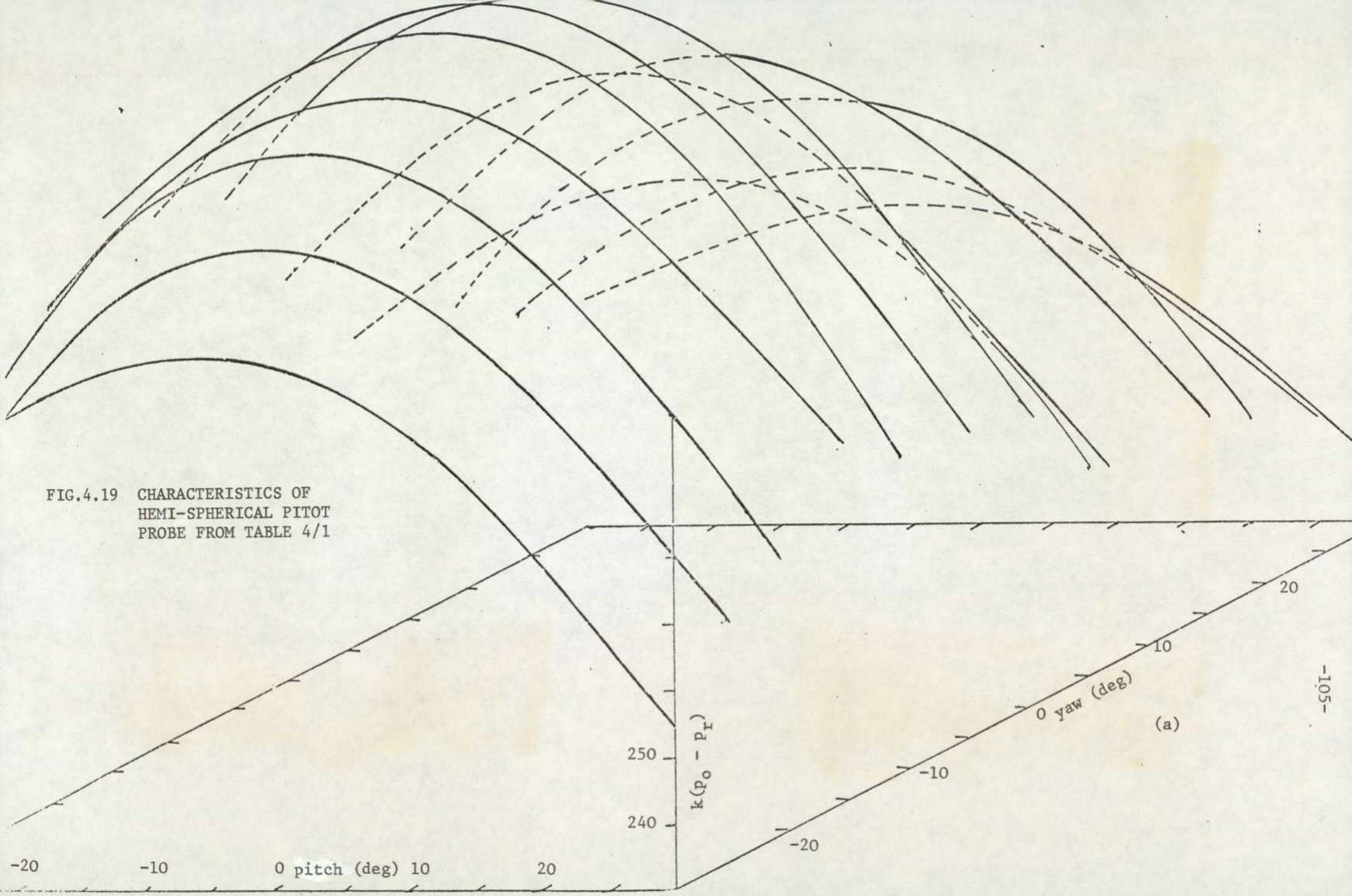

FIG.4.19 CHARACTERISTICS OF HEMI-SPHERICAL PITOT PROBE FROM TABLE 4/1

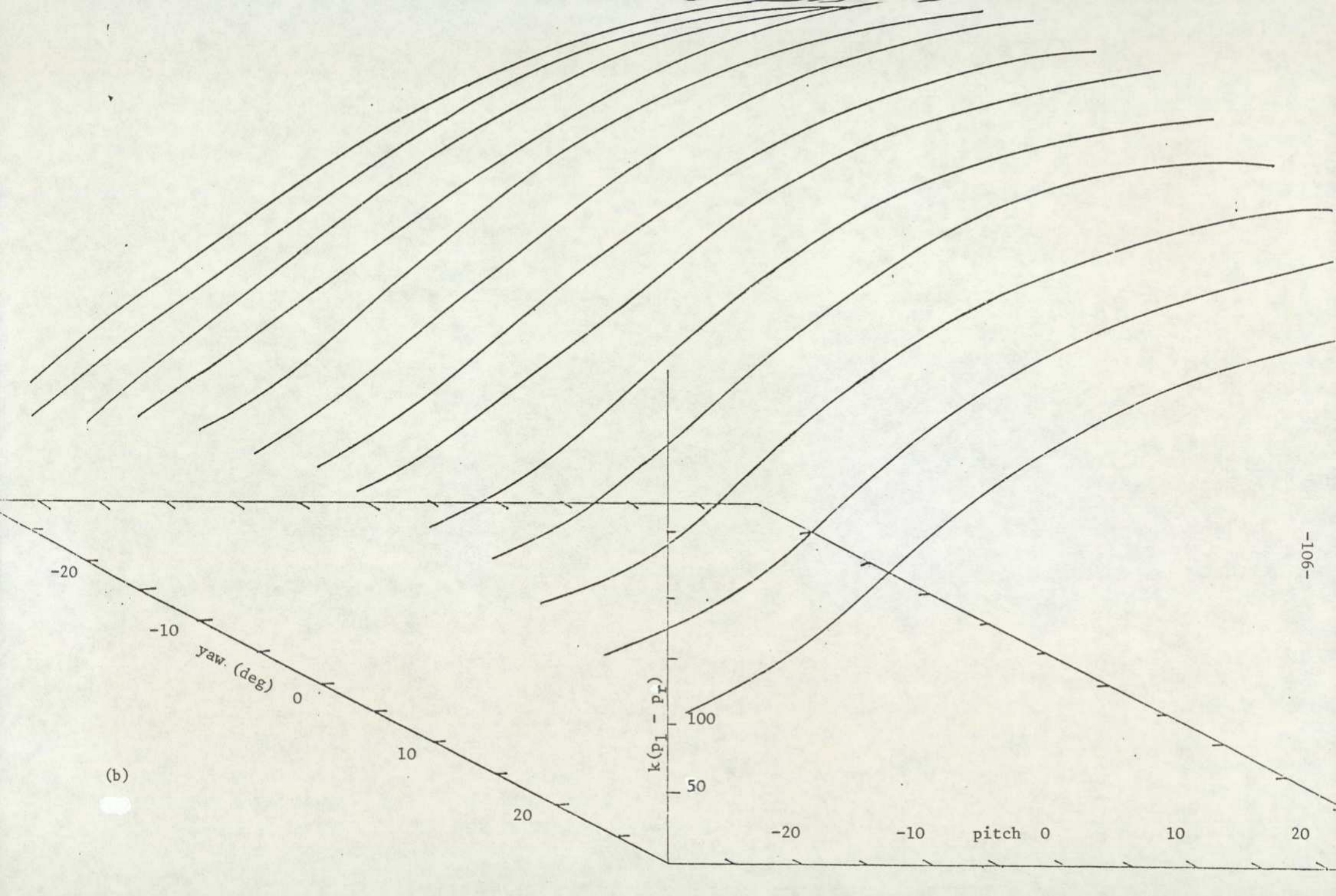
-20
-10
yaw (deg)
0
10
20
(b)
k(p1 - pr)
100
50
-20
-10
pitch 0
10
20

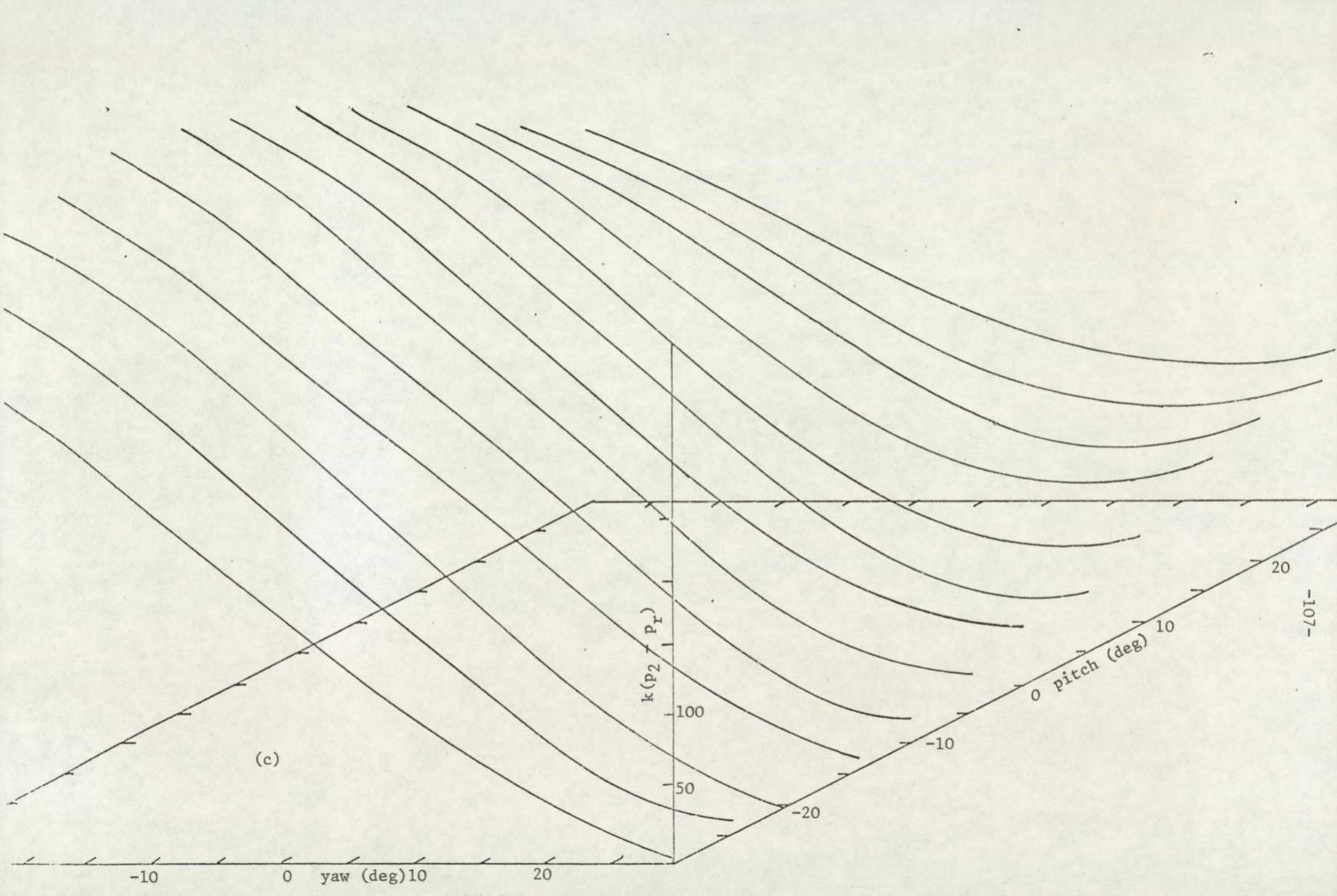
(c)
$k(p_2 - p_r)$
100
50
-10
0
yaw (deg)
10
20
-20
-10
0
pitch (deg)
10
20

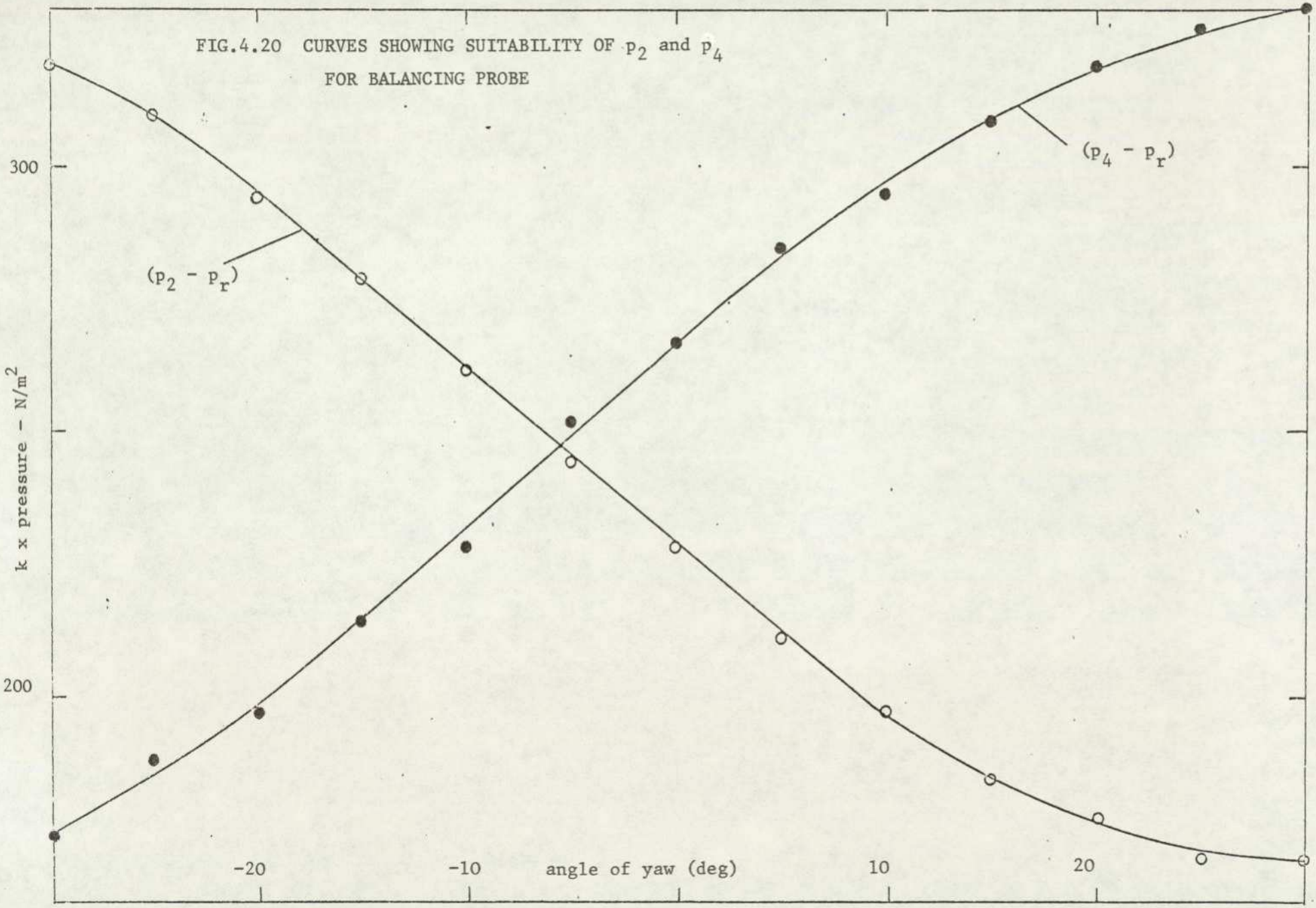
FIG.4.20 CURVES SHOWING SUITABILITY OF p_2 and p_4
FOR BALANCING PROBE
$(p_4 - p_r)$
$(p_2 - p_r)$
300
200
k x pressure - N/m^2
-20
-10
angle of yaw (deg)
10
20

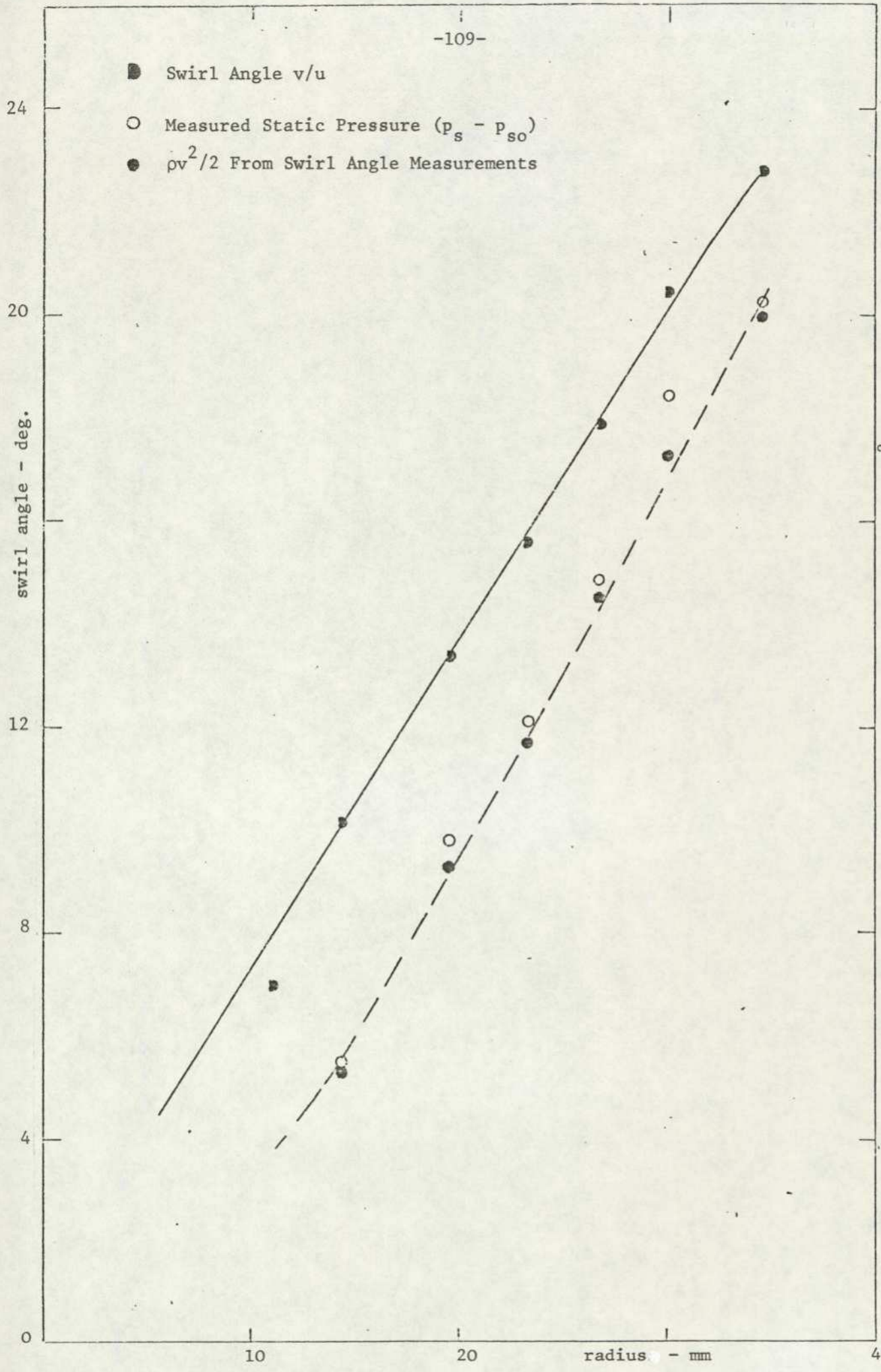

FIG.4.21 SWIRL ANGLE AND STATIC PRESSURE MEASUREMENT USING HEMI-SPHERICAL PROBE

it was much simpler to yaw the probe to obtain a null reading on the two side holes. Balance could be achieve and angle read (off a scale) to better than one degree in steady flow conditions. Fig.(4.20) shows the suitability of the characteristics to obtain this balance. The suitability of this method for static pressure measurement was verified and the results are seen clearly from Fig.(4.21). The centre sensing hole is insensitive to about 3^{o} when aligned in the flow direction. Thus velocity measurements are free from errors due to small misalignment and the neglecting of the radial velocity. In the present investigation the swirl angle was measured by obtaining a null-reading of two diagonally opposite sensing holes. The static pressure is obtained directly from the side sensing holes.

4.9.3 Calibration of Air Flow Rate

Air flow rate axis measured using an orifice plate, calibrated against a hot-wire anemometer traverse. The discharge coefficient quoted by Wirasinghe (52) was found to be in agreement. The anemometer was itself calibrated in a DISA calibration tunnel. The calibration curve is shown in Fig.(4.22). This also provided an ideal opportunity for checking the five-hole pitot-probe. Flow rates calibrated from velocity profiles thus obtained are also indicated in the figure.

4.9.4 Calibration of Solid-Body Swirl Generator Motor

Over a wide range giving 27 volts/1000 r.p.m., the tacho-generator has a linear characteristic. The output was measured satisfactorily using a standard moving coil voltmeter, but was simultaneously checked against a Solartron digital voltmeter. A stroboscope was used to measure the speed of the motor.

FIG.4.22 ORIFICE PLATE CALIBRATION CURVE - AIR

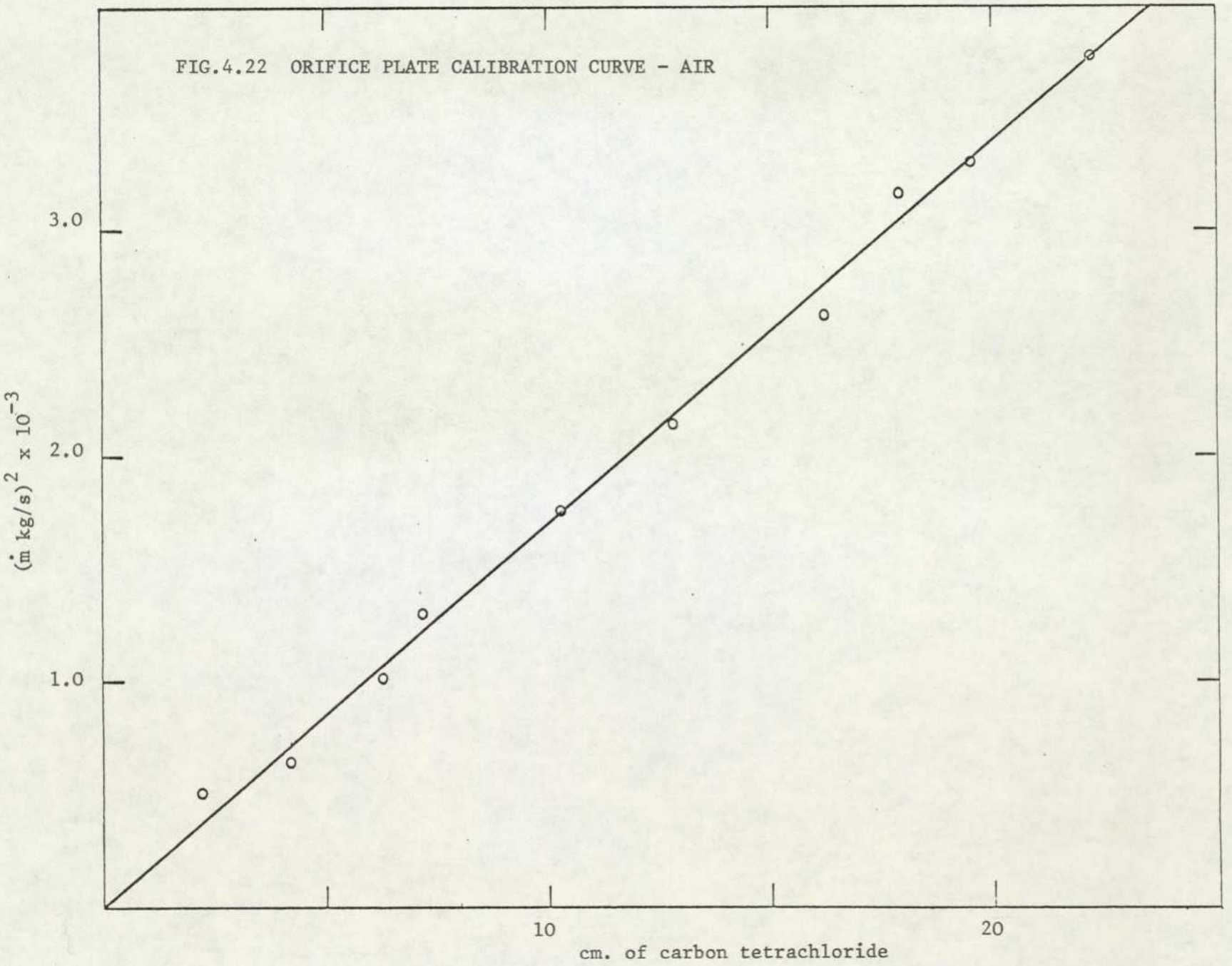

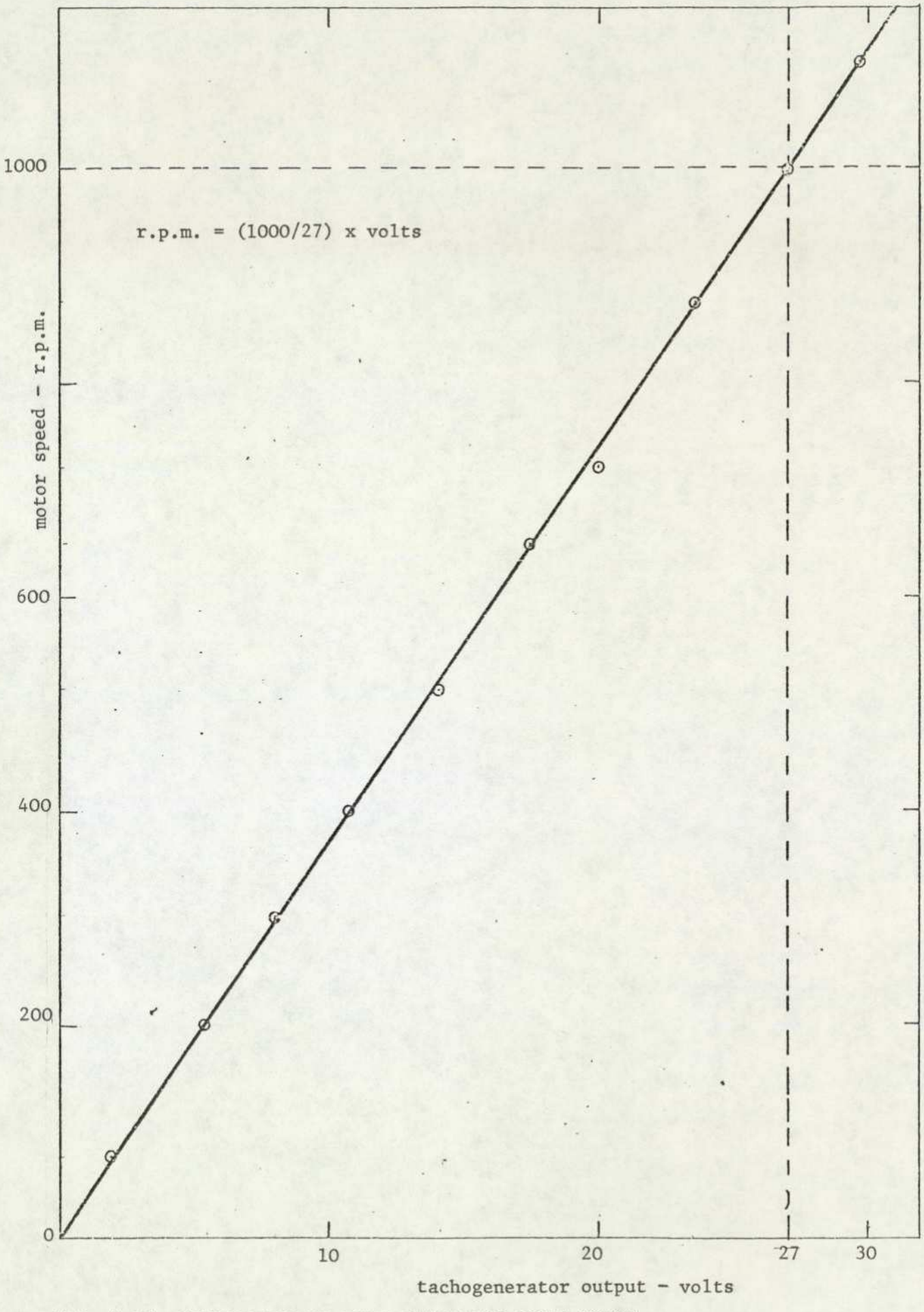

FIG. 4.23 CALIBRATION OF SWIRL GENERATOR DRIVE MOTOR

Fig.(4.23) shows the calibration curve. It was found that the speed could be held within 1% at 1000 r.p.m. This was seen as a very useful function in view of the need to control and reproduce inlet swirl accurately.

CHAPTER FIVE

FLOW VISUALIZATION TESTS - SOLID-BODY VORTEX

5.1 INTRODUCTION

Flow visualization is one of many available tools in experimental fluid mechanics. It differs from other experimental methods in that it renders certain properties of a flow field directly accessible to visual perception.

The great importance of many flow visualization techniques is that one can derive quantitative data from the obtained flow picture. Such techniques provide information about the complete flow field under study without physically interfering with the fluid flow. One could even say that visual sensation is the source of scientific evidence. The major disadvantage associated with observation studies is that it can only provide an instantaneous assessment of the behaviour and neither after-study nor close scrutiny is possible and furthermore it is subject to human error. The essential details of a survey of techniques of flow visualization is included for completeness, which is intended to be useful rather than exhaustive.

As far as the author is aware, the present project is the only one to attempt to investigate and photograph highly turbulent flows in pipes and wide angle conical diffusers with different degree and type of swirl. All experimental work was conducted at an entry Reynolds number of 28.4×10^3.

5.2 MAIN CLASSIFICATION OF FLOW VISUALIZATION TECHNIQUES

The method of flow visualization can be classified roughly into three groups. The first group comprises all techniques by which a foreign material is added to the flowing fluid that might be gaseous or liquid. The foreign material must be visible, and if the particles of which the material is composed are small enough, one may assume that the motion of these particles is the same as that of the fluid, in direction and magnitude of velocity. The technique is thus an indirect method, since one observes the motion of the foreign material instead of the fluid itself. The difference between the movement of the fluid and that of the foreign particles can be minimised,but not totally avoided, by using particles of a density almost coinciding with that of the fluid. The technique also fails to give precise results if the thermodynamic state of the fluid varies in the flow field (eg. temperature).

The second group comprises of an optical method displaying a variation of the fluid density. It is a purely non-disturbing test method. A quantitative evaluation of the obtained flow pictures is in many cases laborious, since the information of the density distribution is integrated along the path of the light rays in the object field.

The third group of visualization techniques is a combination of the above mentioned techniques. In this case, the foreign substance introduced into the flowing fluid is energy, e.g. in the form of heat or electric discharge. The fluid elements thus marked by their increased energy level sometimes need an optical visualization from the rest of the fluid. In other cases the energy released is so high that the marked

fluid elements become self-luminous and can be directly observed. These methods are often applied to flow with a low average density level. The method is not a non-disturbing method, since it affects, more or less, the original flow according to the amount of released energy.

In the present research programmes, only the first method was considered because it was felt that the method would yield a wealth of information, depending on the degree of sophistication of the technique employed. The necessary features of a good tracer-agent are as follows:

1. It must not cause any resistance to flow.
2. It must not alter the properties of the main fluid.
3. It must be immiscible in the main fluid.
4. If not recoverable it must be of relatively low cost.

Obviously it is impossible to obtain an agent satisfying every condition; the degree of tolerance exercised in the choice of a particular agent depends entirely on the application at hand.

The main fluid being air, smoke was used as a tracing-agent. It was produced by mixing Ondine oil with inert carbondioxide, giving a density of smoke very close to that of air. The smoke generated by this method was clean, dense and pure white in colour. The source was infinitely controllable, provided a constant output of consistent quantity and the smoke could also be piped for some distance from the generator.

5.3 EXPERIMENTAL APPARATUS

The rig is shown in Fig.(5.1). Air was used as the flow medium. The mean flow was measured using an orifice plate with a carbon tetrachloride manometer, Fig.(4.22). The

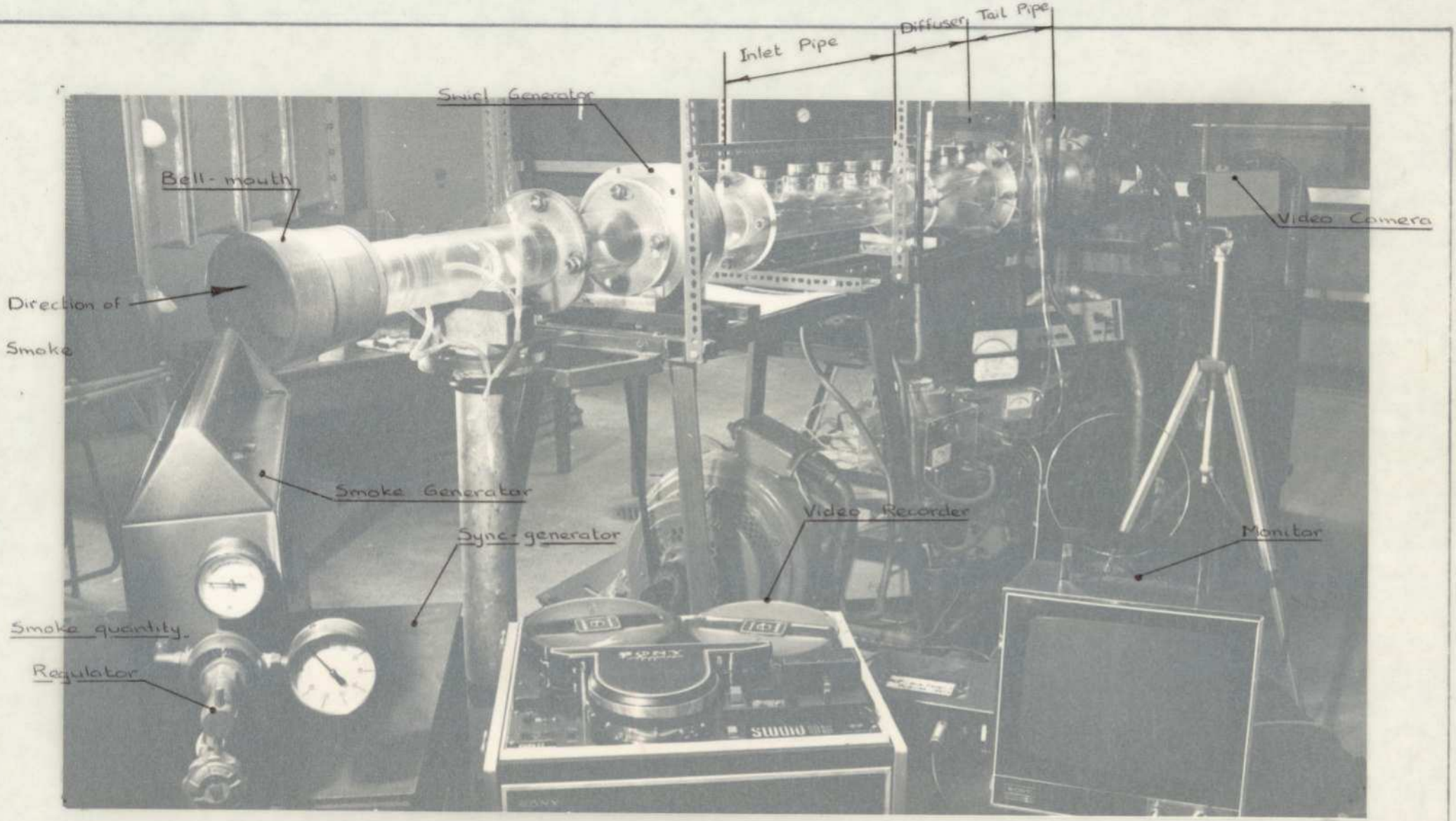

FIG.5.1 LAYOUT OF RIG, SOLID-BODY SWIRL GENERATOR, SMOKE GENERATOR and VIDEO SET UP

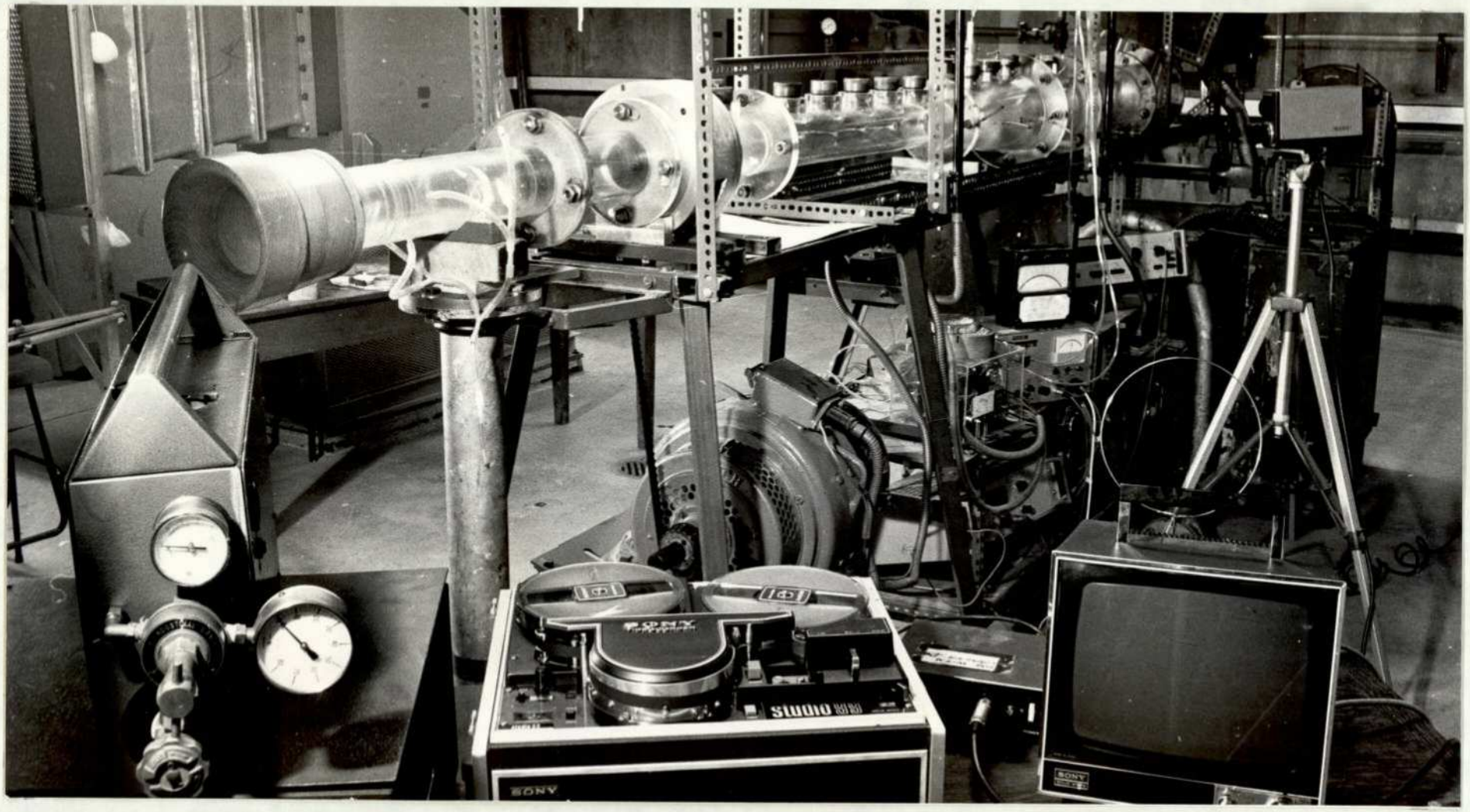

FIG.5.1 LAYOUT OF RIG, SOLID-BODY SWIRL GENERATOR, SMOKE GENERATOR and VIDEO SET UP

'step down' ratio was used in the swirl generator. Smoke was induced at the mid-section of the bell mouth. The smoke deposit in the working section was thoroughly cleaned at the end of each experiment.

5.4 EXPERIMENTAL WORK

The use of a camera for recording flow patterns was potentially difficult for the following reasons:

(i) light reflection from perspex wall

(ii) camera vibration

(iii) difficulty in capturing the picture of an instance in highly fluctuating turbulent flow.

Effort proved that the above problems could be overcome except (iii).

The ideal solution would have been to record on cine-film the behaviour of smoke particles in the pipe-diffuser combination. This too would have caused problems in the sense that the cost would be prohibitive and furthermore analysing such a large quantity of film would not have been an easy task. However, a compromise was made by recording on a video-tape. The video-recorder used had a facility of "still picture", thus a photograph can be taken of the still frame. A number of electronic signal problems was encountered when recording; the problem was one of age of the instrumentation, and matching electronically instruments made by different companies. However reasonale recording standards were achieved.

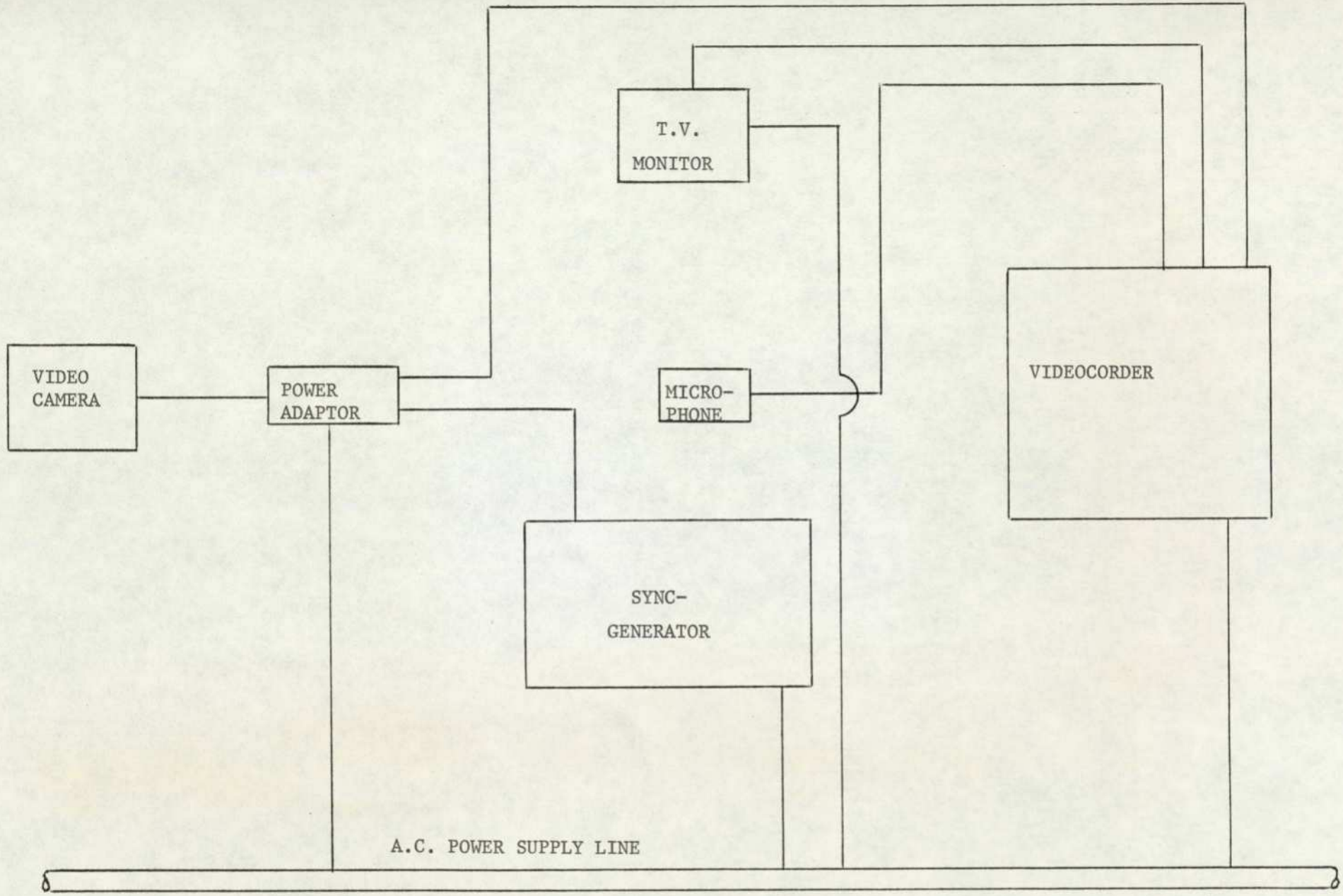

FIG. 5.2 BLOCK DIAGRAM SHOWING VIDEO SET UP

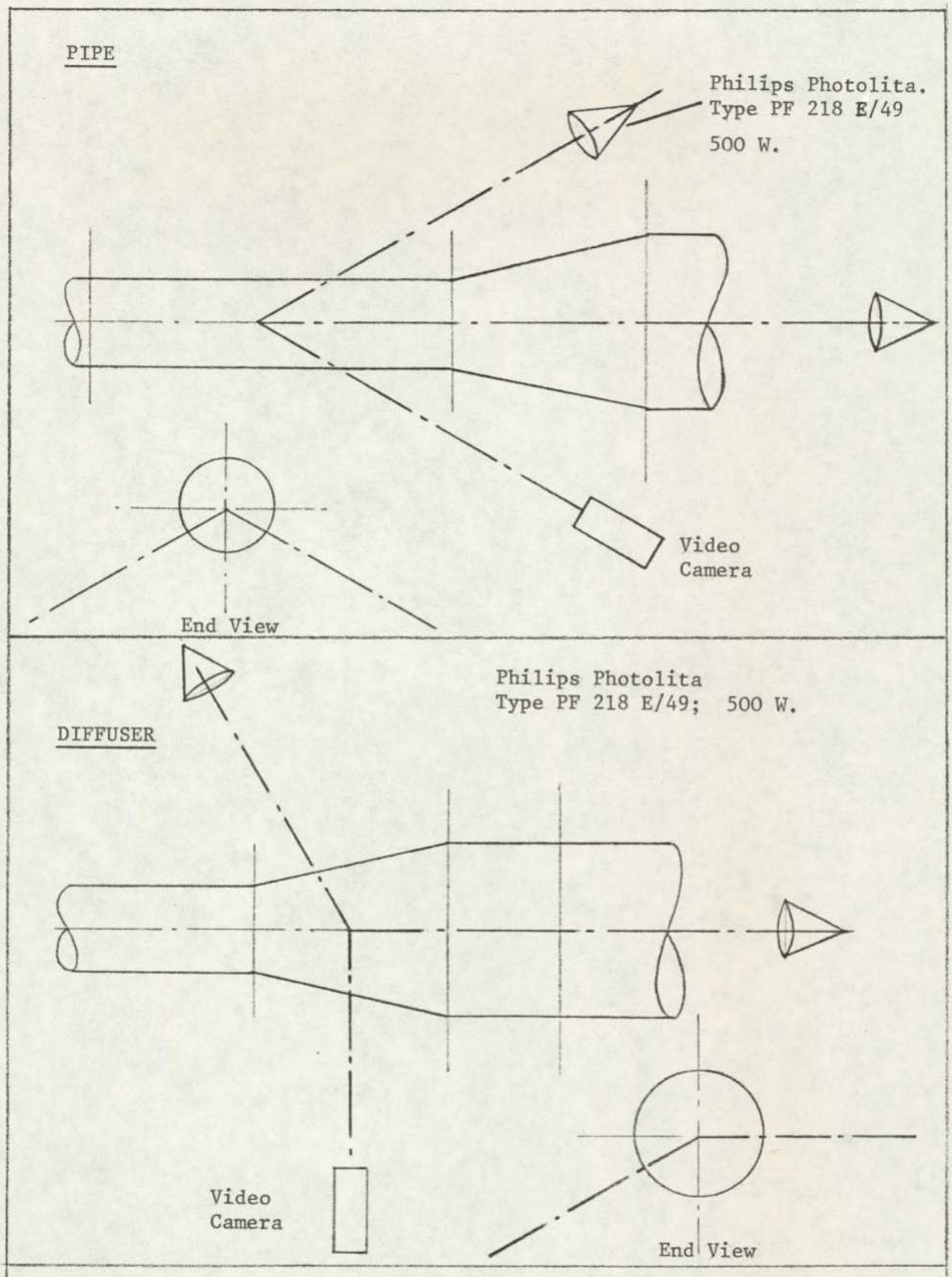

FIG. 5.3 ARRANGEMENT FOR PHOTOGRAPHY

The flow visualization tests were carried out in a pipe-diffuser combination. Three different conical diffusers were used: 10^{o}, 20^{o} and 30^{o}. Each test (i.e. a test per diffuser) was carried out in two parts. The first part relates to the behaviour of swirl in the pipe, while the second part relates to the diffuser and tail pipe. Three different flow conditions were generated: axial flow, swirl 2 and swirl 3 (classification of swirl is shown in the next chapter). For the purpose of studying the effect of swirl on the performance of the diffuser, a fixed flow rate was maintained. The smoke deposit on the wall of the test section, thus obscuring the view, prevented running the test rig for more than one-hour. The Figs.(5.2) and (5.3) show the video set up and lighting arrangement. Each of the above flow visualization tests were recorded on a 45 minute video-tape classified as FOV10, FOV20 and FOV30 for the 10^{o}, 20^{o}, and 30^{o} conical angle diffuser respectively.

5.5 VIDEO ANALYSIS

The video tapes were played back a number of times and analysed. The flow being highly fluctuating made the observation difficult. And since the smoke was not made to follow one particular stream line, the problem was worse when swirl was induced. Long hours had to be spent training the eye to pick-up as much detail as possible and recording the observation each time. This was attributed to human error as in observing an irregular occurrence and comparing it with a similar occurrence in the past; a loss of a certain degree of accuracy is inevitable. However, with a trained eye and a prior knowledge of the sequence, the task did seem less difficult.

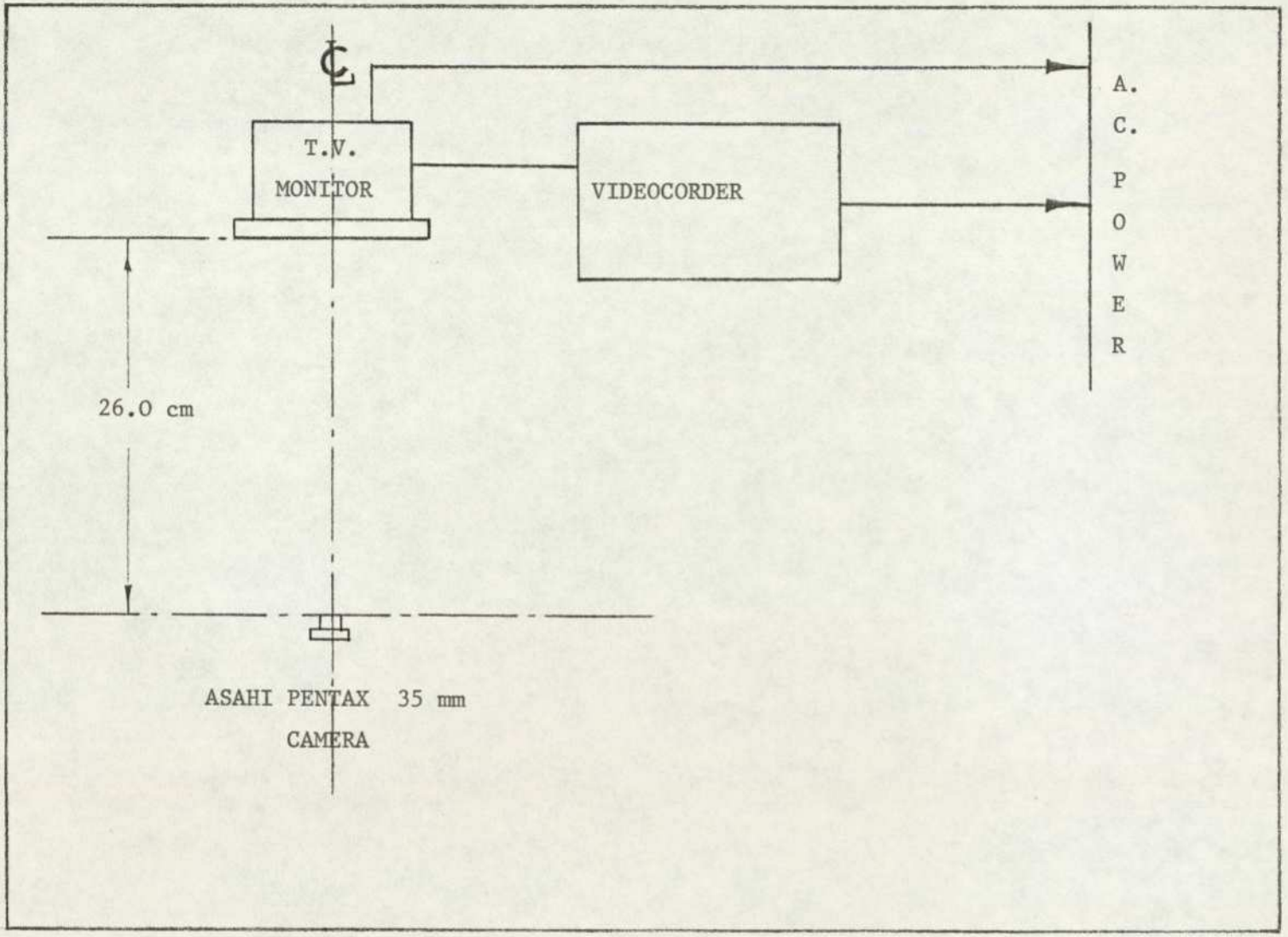

FIG. 5.4 ARRANGEMENT FOR PHOTOGRAPHY - T.V. MONITOR.

Owing to the feintness of the still frame, photographic work too required quite a lot of effort. An Asahi-Pentax 35 mm camera was used. The monitor and the camera were set up in a dark-room, the camera being 26 cm away from the monitor's screen and focused at its centre. Fig.(5.4) shows the arrangement used for photography. The photographic work was conducted for a long period with a day's break in between because of the hypnotic effect that developed when the same behaviour was observed continuously. More than 100 photographs were taken to obtain a photographic record, but only a few are included. However, the video-tapes are preserved as a future reference.

The photographic record is as follows:

DIFFUSER CONICAL ANGLE = 10 DEGREE

FLOW IN INLET PIPE

FIG. 5.5.
Flow condition:
Axial
Flow direction →

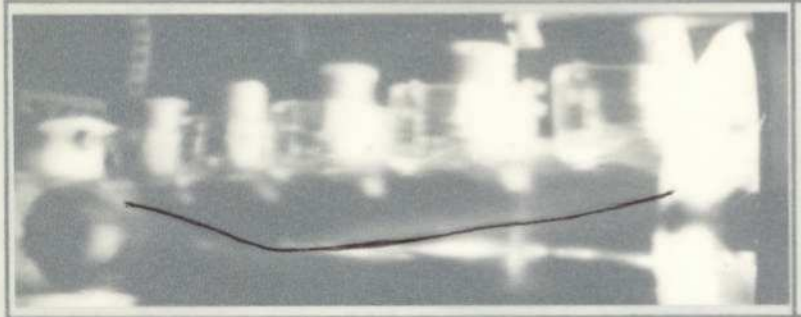

FIG. 5.6.
Flow condition:
Swirl 2 →

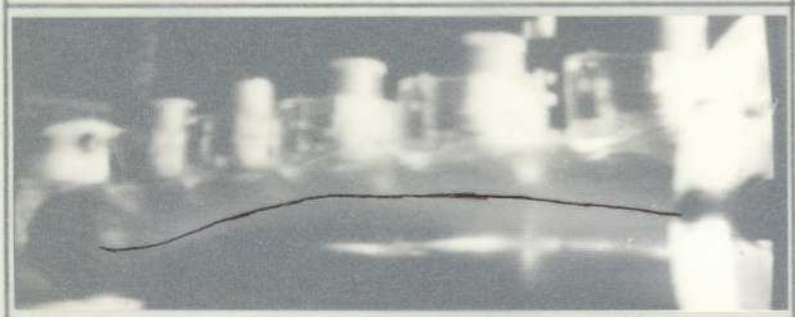

FIG. 5.7.
Flow condition:
Swirl 3 →

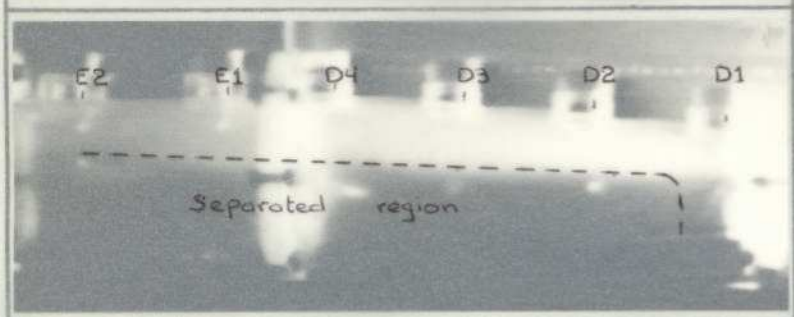

FLOW IN DIFFUSER AND TAIL-PIPE

FIG. 5.8.
Flow condition:
Axial ←

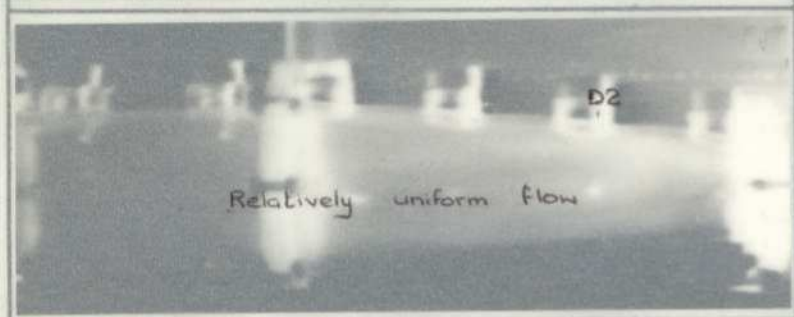

FIG. 5.9.
Flow condition:
Swirl 2 ←

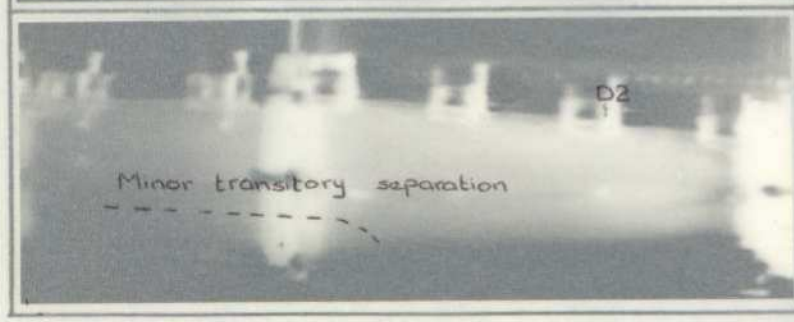

FIG. 5.10.
Flow condition:
Swirl 3 ←

DIFFUSER CONICAL ANGLE = 10 DEGREE

FLOW IN INLET PIPE

FIG. 5.5.
Flow condition:
Axial

FIG. 5.6.
Flow condition:
Swirl 2

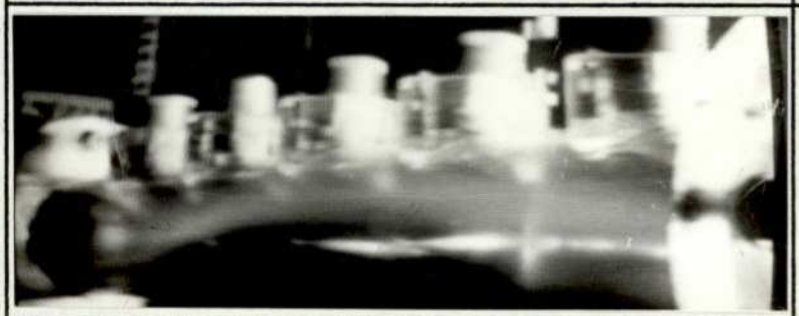

FIG. 5.7.
Flow condition:
Swirl 3

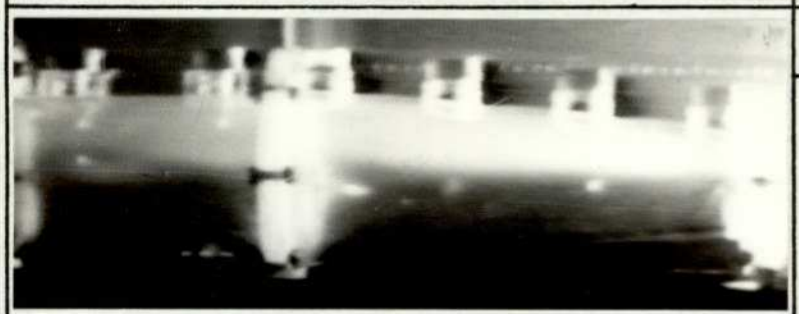

FLOW IN DIFFUSER AND TAIL-PIPE

FIG. 5.8.
Flow condition:
Axial

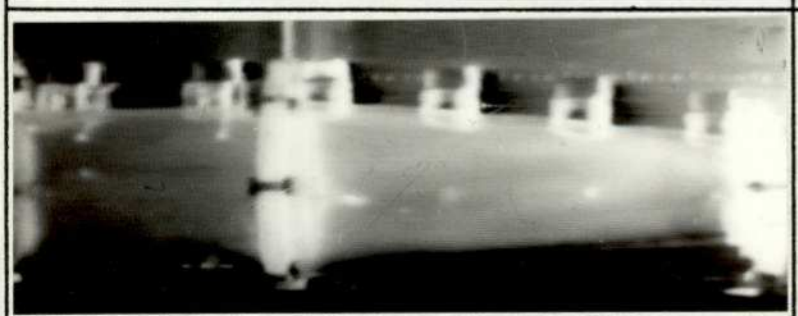

FIG. 5.9.
Flow condition:
Swirl 2

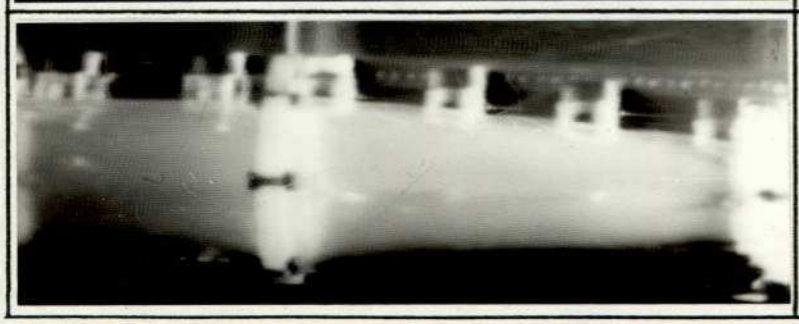

FIG. 5.10.
Flow condition:
Swirl 3

DIFFUSER CONICAL ANGLE = 20 DEGREE

FLOW IN INLET PIPE

FIG. 5.11.
Flow condition:
Axial
Flow direction

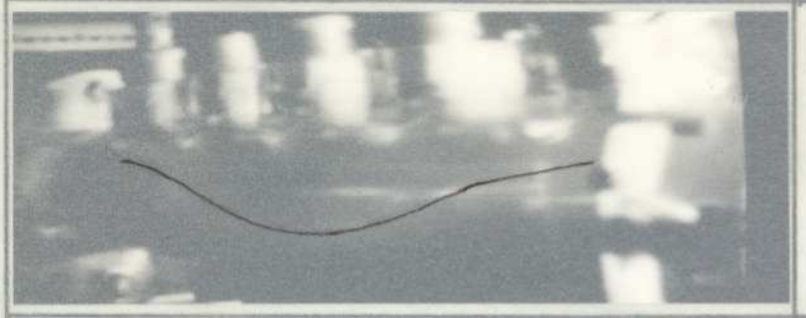

FIG. 5.12.
Flow condition:
Swirl 2

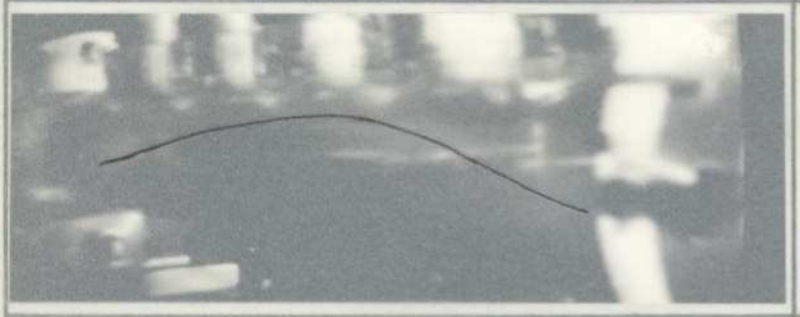

FIG. 5.13.
Flow condition:
Swirl 3

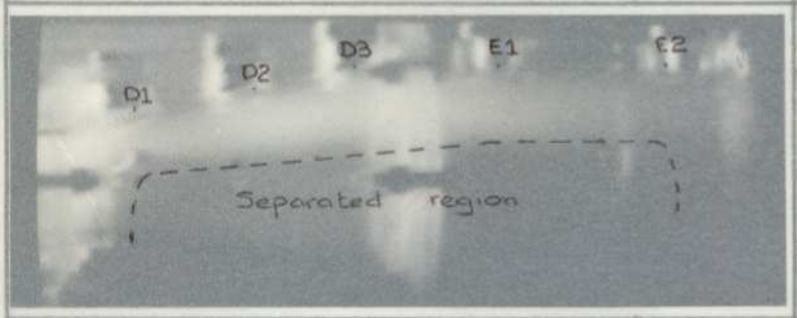

FLOW IN DIFFUSER AND TAIL-PIPE

FIG. 5.14.
Flow condition:
Axial

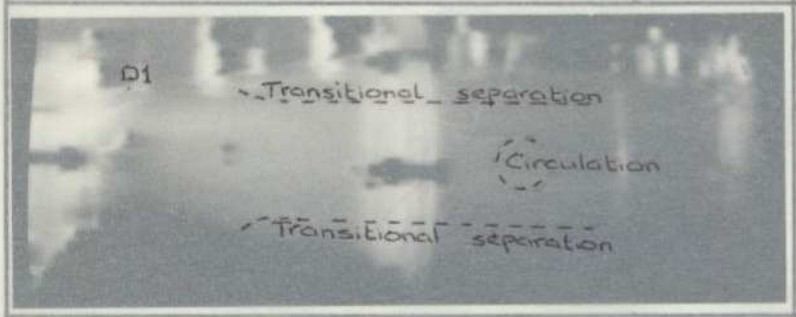

FIG. 5.15.
Flow condition:
Swirl 2

FIG. 5.16.
Flow condition:
Swirl 3

DIFFUSER CONICAL ANGLE = 20 DEGREE

FLOW IN INLET PIPE

FIG. 5.11.
Flow condition:
Axial

FIG. 5.12.
Flow condition:
Swirl 2

FIG. 5.13.
Flow condition:
Swirl 3

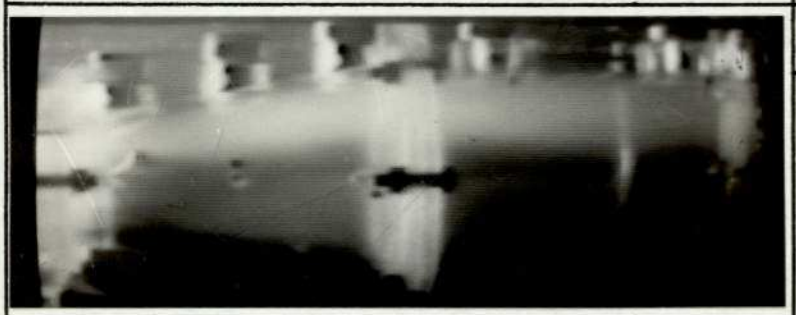

FLOW IN DIFFUSER AND TAIL-PIPE

FIG. 5.14.
Flow condition:
Axial

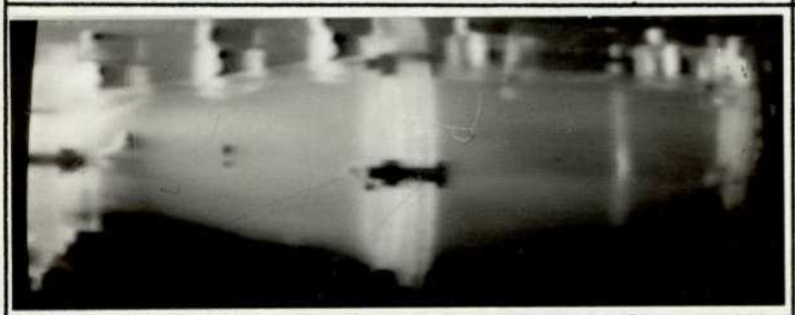

FIG. 5.15.
Flow condition:
Swirl 2

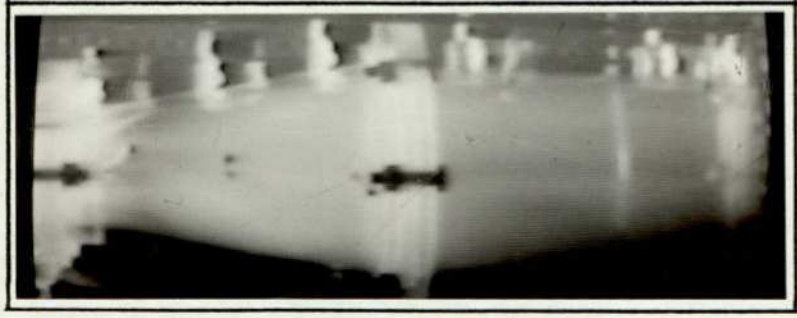

FIG. 5.16.
Flow condition:
Swirl 3

DIFFUSER CONICAL ANGLE = 30 DEGREE

FLOW IN INLET PIPE

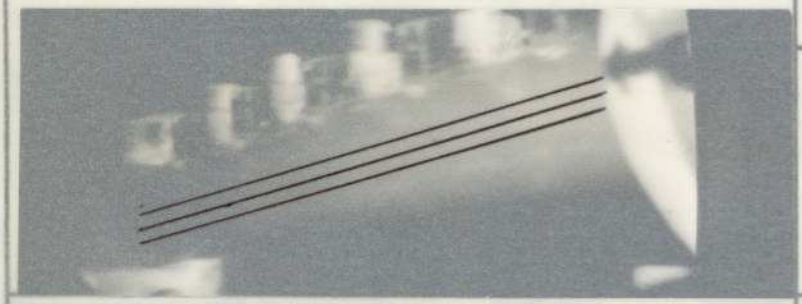

FIG. 5.17.
Flow condition:

Axial
Flow direction

FIG. 5.18.
Flow condition:

Swirl 2

FIG. 5.19.
Flow condition:

Swirl 3

FLOW IN DIFFUSER AND TAIL-PIPE

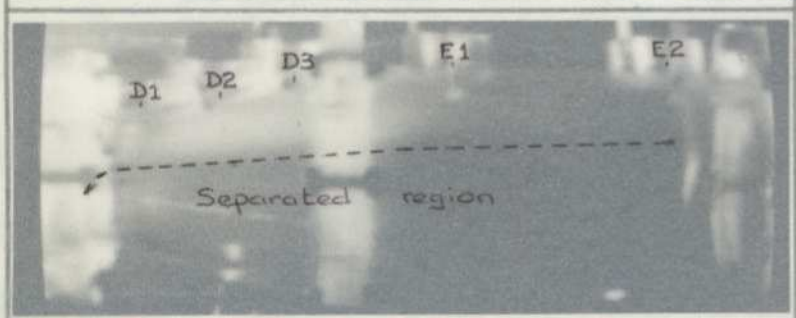

FIG. 5.20.
Flow condition:

Axial

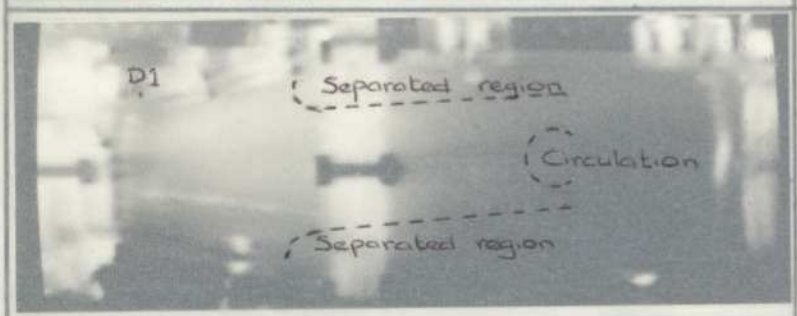

FIG. 5.21.
Flow condition:

Swirl 2

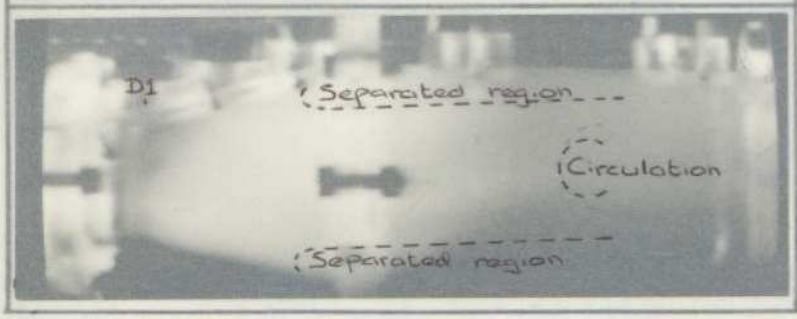

FIG. 5.22.
Flow condition:

Swirl 3

DIFFUSER CONICAL ANGLE = 30 DEGREE

FLOW IN INLET PIPE

FIG. 5.17.
Flow condition:
Axial

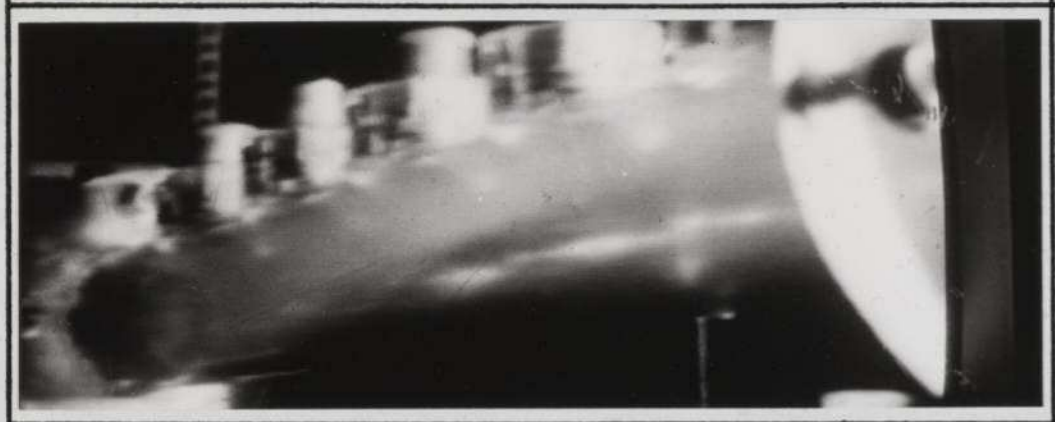

FIG. 5.18.
Flow condition:
Swirl 2

FIG. 5.19.
Flow condition:
Swirl 3

FLOW IN DIFFUSER AND TAIL-PIPE

FIG. 5.20.
Flow condition:
Axial

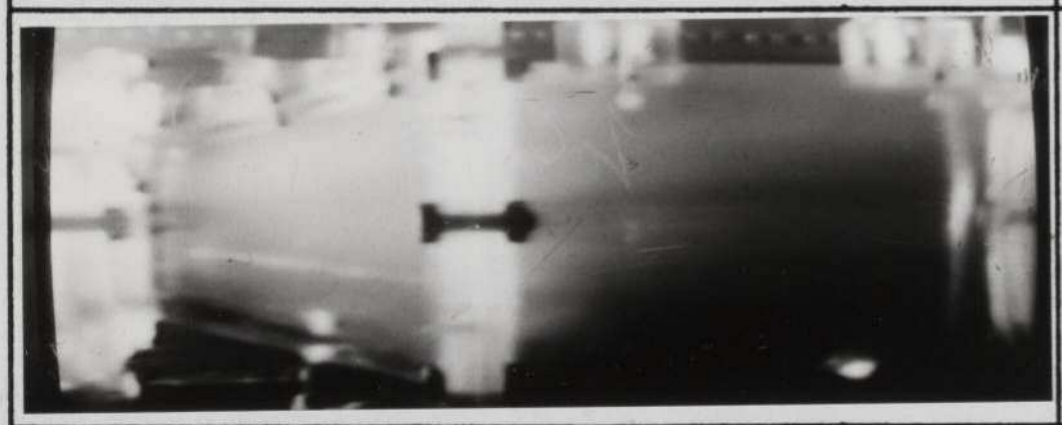

FIG. 5.21.
Flow condition:
Swirl 2

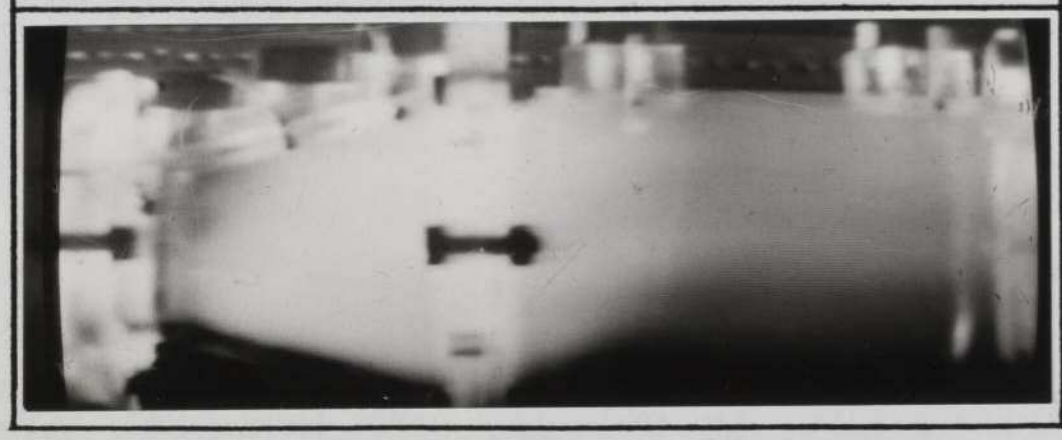

FIG. 5.22.
Flow condition:
Swirl 3

5.6 OBSERVATION

The observations were made from video-tapes FOV10, FOV20 and FOV30 and from the photographic record. It is important to note that the photographic record is intended as a guide only.

5.6.1 Flow in the 10^{o} Diffuser

For axial flow, the smoke enters the bell-mouth then passes through two honeycomb sections; this was intended to make the flow uniform. The flow in the pipe was highly turbulent, Fig.(5.5). The mass flux calculated at station P5 should compare well with values obtained at the orifice plate, which it does within experimental error (±2%). Flow in the diffuser, Fig.(5.8), shows a separation region at the lower surface before station D2 and extending to the tail pipe. Back flow was noticed at the region of separation. (see Figs.(4.3) and (4.4a))

Swirl 2 was induced by rotating the second honeycomb. A helical stream path was observed, Fig.(5.6), in the pipe section. The separation was eliminated in the diffuser and tail pipe, thus resulting in a more relatively uniform flow in the tail pipe Fig.(5.9). The diffusion was not completed at the end of the diffuser, but extended in the tail pipe. The spiral formation disintegrated near the exit of the diffuser.

When the swirl was increased,to swirl 3, the helical path changed its peak in the pipe, thus showing increased degree of swirl, Fig.(5.7). It was noted that there was zero separation or minor transitory separation in the diffuser, which disappeared a second or so after it appeared, Fig.(5.10). Again, the diffusion was extended in the tail pipe, but the spiral formation disintegrated at around station D2.

5.6.2 Flow in the 20° Diffuser

The flow pattern in the pipe was unchanged by increase in conical angle when the flow was purely axial, Fig.(5.11). A larger region of separation, at the lower surface occured in the diffuser. This region started after station D1 and ended around station E2, Fig.(5.14). When swirl 2 was induced, again a helical stream path was observed in the pipe, Fig.(5.12). The flow in the diffuser and tail pipe was highly complex, Fig.(5.15). Separation seems to occur at around station D2 and extending thereafter. Circulation was seen at station D3, at both upper and lower surfaces. Both the separation and circulation were transitional. Diffusion seems to be extended in the tail pipe. Large transitory circulation was seen around station E1. With swirl 3, the helical path changed its peak in the pipe, Fig.(5.13). Zero or very small transitory separation with back circulation was seen at both upper and lower surfaces in the diffuser, at around station D3, Fig.(5.16). Again the diffusion seems to extend into the tail pipe.

5.6.3 Flow in the 30° Diffuser

With axial flow, the flow in the pipe was highly turbulent, Fig.(5.17). A large separation region was seen in the diffuser, Fig.(5.20). However, when swirl 2 was introduced, a helical path was observed in the pipe, Fig.(5.18). Fig. (5.21) shows the flow in the diffuser. Separation seems to occur between station D2 and D3, on both surfaces. Circulation was seen in the tail pipe, between stations E1 and E2. And separation around station E1. The diffusion was seen to be extended into the tail pipe. With increase in degree of swirl,

swirl 3, the peak of the helical path changed in the pipe, Fig.(5.19). In the diffuser, separation occurred between stations D1 and D2, Fig.(5.22). Circulation was observed in the tail pipe, between stations E1 and E2, and diffusion was further carried out in the tail pipe.

5.7 CONCLUSION

The primary object of flow visualization tests was to investigate the influence of solid-body swirl on wide angle diffuser flow. This was successfully achieved, and without performing any quantitative analysis, major deductions are made. However, detailed experimental analysis is carried out in the next chapter in order to give detailed structure of flow in the wide angle diffuser. The above tests (observation study) also assisted in forming the strategy for the experimental analysis.

The 'experimental work' gives an account of problems associated with capturing flow patterns in highly turbulent flow. But this was half the battle, the other half being the obstacles which needed overcoming, in order to attain a photographic record, Fig.(5.5) to Fig.(5.22). The 'observation' deals with analysing flow in pipe and diffuser tail pipe combinations. The conclusions, based on the above studies, are as follows:

1. The solid-body swirl improves the diffusion process of wide angle diffusers. The degree of improvement depends on the double conical angle and the degree of swirl induced.
2. Swirl 2 had a more favourable influence on the flow in the 10^{o} diffuser than swirl 3 relative to axial flow.
3. For the 20^{o} diffuser, swirl 3 had a more favourable influence than swirl 2. However, separation was not eliminated

by the presence of swirl.

4. For the 30^{o} diffuser, both swirl 2 and swirl 3 had a favourable influence, but it was difficult to differentiate. Again, the separation was not eliminated.

5. From the formation of a spiral path in the pipe, wall static pressure in the pipe is also influenced by adverse pressure gradient downstream (i.e. effect of double conical angle of diffuser) and degree of swirl induced.

6. The above deductions confirm, quanlitatively, the past work of Van Dewoestine (49), McDonald and Fox (50) and Wirasinghe (52).

The degree of accuracy of the observations is arguable However, every care was taken to minimise the error. It is important to note that the observations are subject to the person who views the video-tapes, the number of times he views them and his experience in flow visualization. But the human error factor is inevitable. The flow pattern in the diffuser was highly complex, because of the number of flow processes taking place at the same time; for example, diffusion, mixing effect of swirl, flow problems like separation, back circulation, etc. Thus the observations in the diffuser flow are by no means conclusive.

CHAPTER SIX

MEASUREMENTS OF AXIAL AND SOLID-BODY SWIRLING FLOW IN DIFFUSERS

6.1 INTRODUCTION

It is evident that very little work has been done on flow in diffusers when flow at entry possesses swirl (solid-body). This chapter deals with the experimental investigation of the performance of conical diffusers having various cone angles and various degrees of imparted solid-body swirl, to see whether the latter could indeed improve performance. Improvement would be expected in diffusers which, with axial flow, would suffer from separation problems so that the addition of a solid-body type rotation would seem immediately attractive, since in this type total pressure increases with radius whereas in a free vortex it is constant. All experimental work was conducted at an entry Reynolds number of 28.4×10^3.

6.2 EXPERIMENTAL APPARATUS

The experimental arrangement is as shown in Fig.(4.2). Air was used as a flow medium. The five-hole pressure probe, with the associated instrumentation, was used for flow measurement.

6.3 EVALUATION OF FLOW PROPERTIES

It was necessary to consider the contribution of the errors due to experimental work and that due to analysis before launching into any discussion on the constancy or variation of the various flow properties. The experimental error would certainly affect the stability of α, which is a measure of the distortion of velocity profile. For a uniform profile, the deviation of this factor from unity is accentuated by the disturbances due to the experimental errors.

The two necessary measurements, at any point in a pipe or diffuser, are the total pressure and angle of yaw. From the design limitations of the five-hole probe and the insensitivity of each of the sensing holes, it may be concluded that most of the errors lay in the measurement of the angle of yaw. These errors were minimised by resorting to a longer stabilising time when obtaining the angle of yaw. The stabilising time per experimental point varied from 10 - 20 minutes according to the conical angle of the diffuser.

The flow properties were evaluated as follows:

mean axial velocity, $\bar{u}$, $= \int_A u dA/A$

mass flux, $\dot{m}$, $= \rho \bar{u} A$

kinetic energy factor, α $= \int_A u^3 dA/\bar{u}^3 A$

axial kinetic energy $= \dot{m}\bar{u}^2\alpha/2$

angular momentum flux, $\dot{M}$ $= \rho \int_A uvr dA$

A computer program called MASTER PROP was developed to calculate the flow properties. Fig.(6.1) shows the flow chart of the program. The numerical technique, Gill's and Miller's approach, employed for the evaluation of the integrals is based on the third order finite difference formulae (Refer Appendix A).

6.4 PERFORMANCE OF SOLID-BODY SWIRL GENERATOR

The honeycomb swirl generator was capable of producing a very good 'solid-body' type vortex as indicated by earlier studies, for example Van Dewoestine (49). A hot-wire anomometer was used to measure the mean turbulence which was approximately 3% with stationary swirl generator. The swirl measurements were made at the entry part of the 10° diffuser since there was no measurable decay in the inlet pipe between the generator and the diffuser.

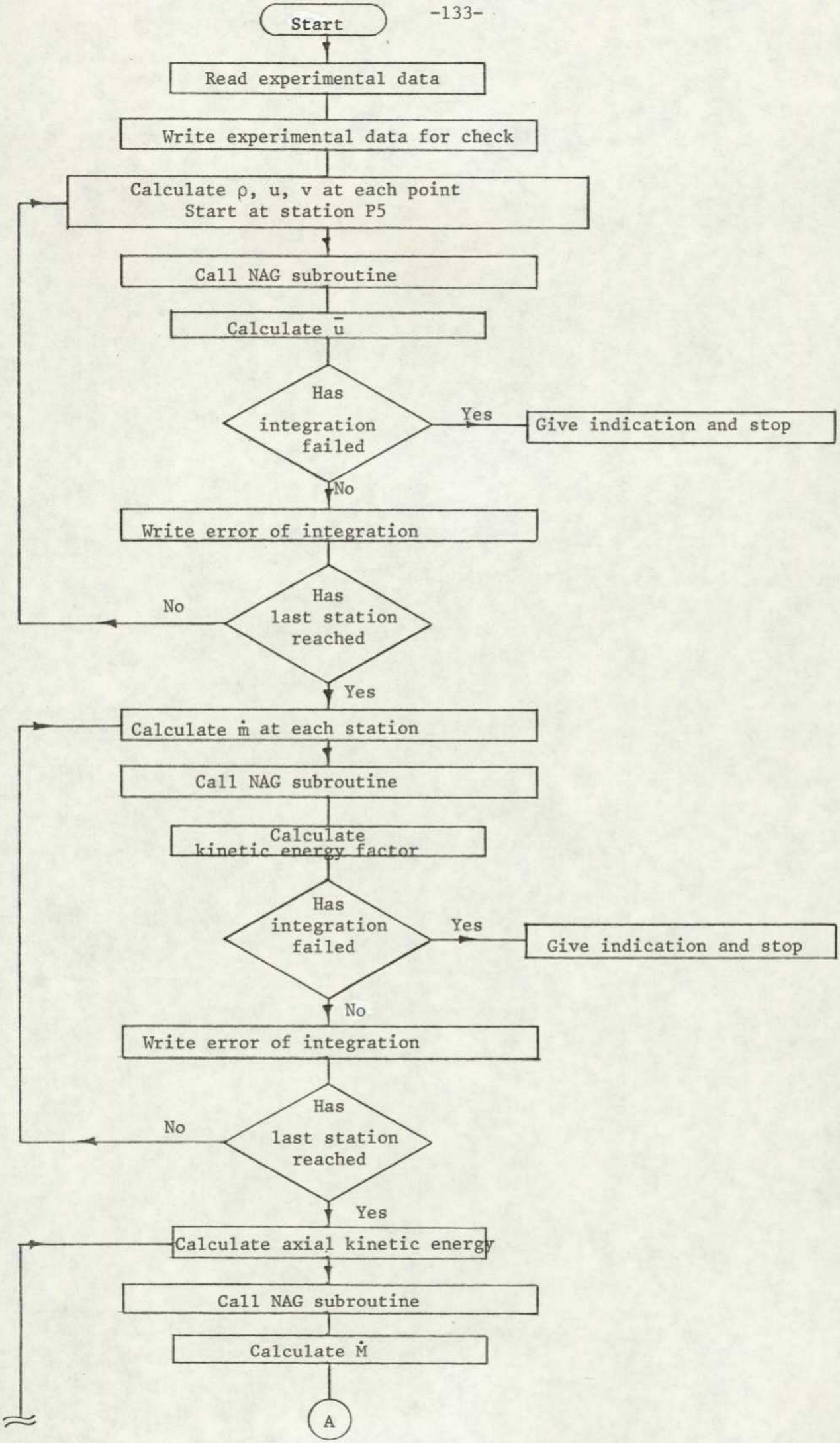
Start
Read experimental data
Write experimental data for check
Calculate ρ, u, v at each point
Start at station P5
Call NAG subroutine
Calculate ū
Has integration failed
Yes
Give indication and stop
No
Write error of integration
Has last station reached
No
Yes
Calculate ṁ at each station
Call NAG subroutine
Calculate kinetic energy factor
Has integration failed
Yes
Give indication and stop
No
Write error of integration
Has last station reached
No
Yes
Calculate axial kinetic energy
Call NAG subroutine
Calculate Ṁ
A

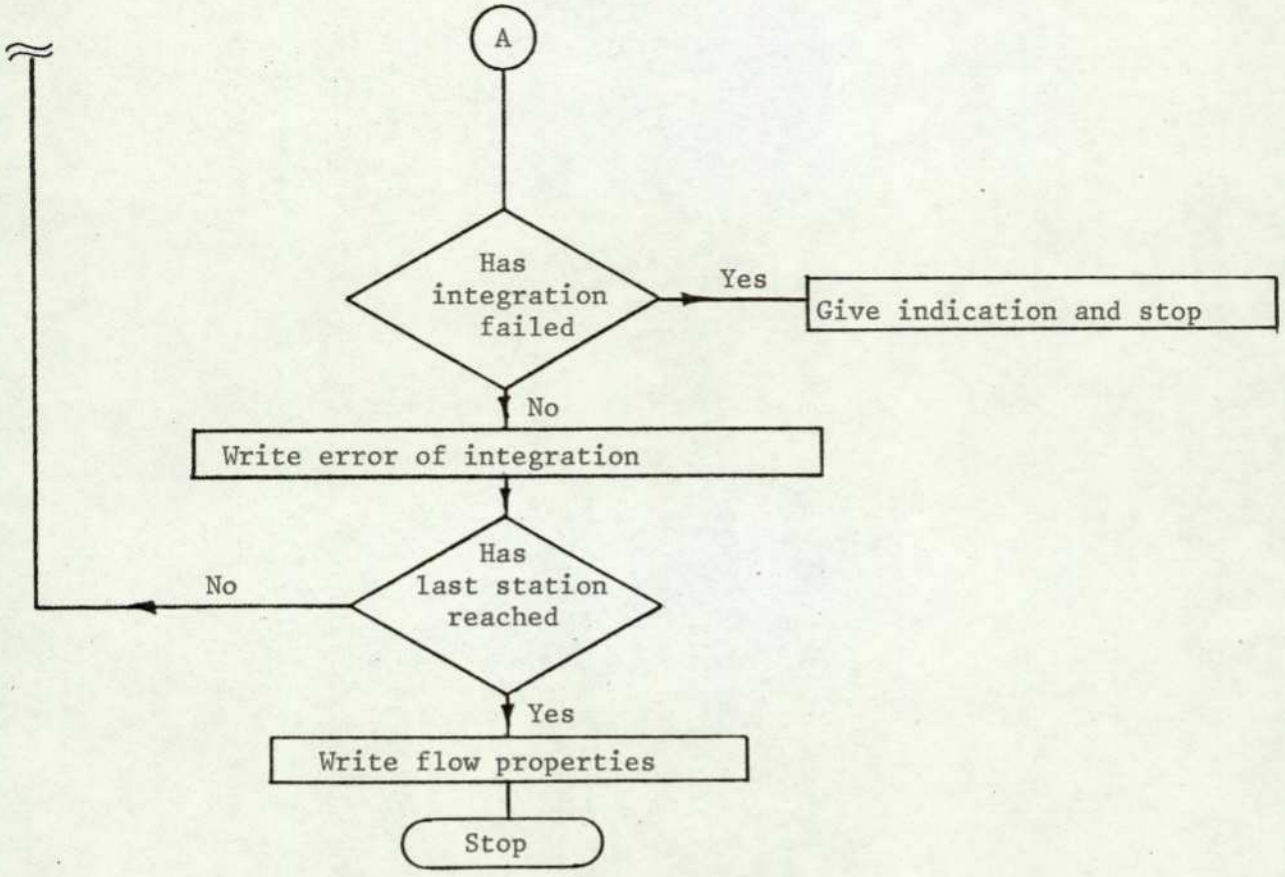

FIG. 6.1 FLOW CHART - MASTER 'PROP'.

FIG. 6.2 VARIATION OF TANGENTIAL VELOCITY WITH SPEED OF SWIRL GENERATOR

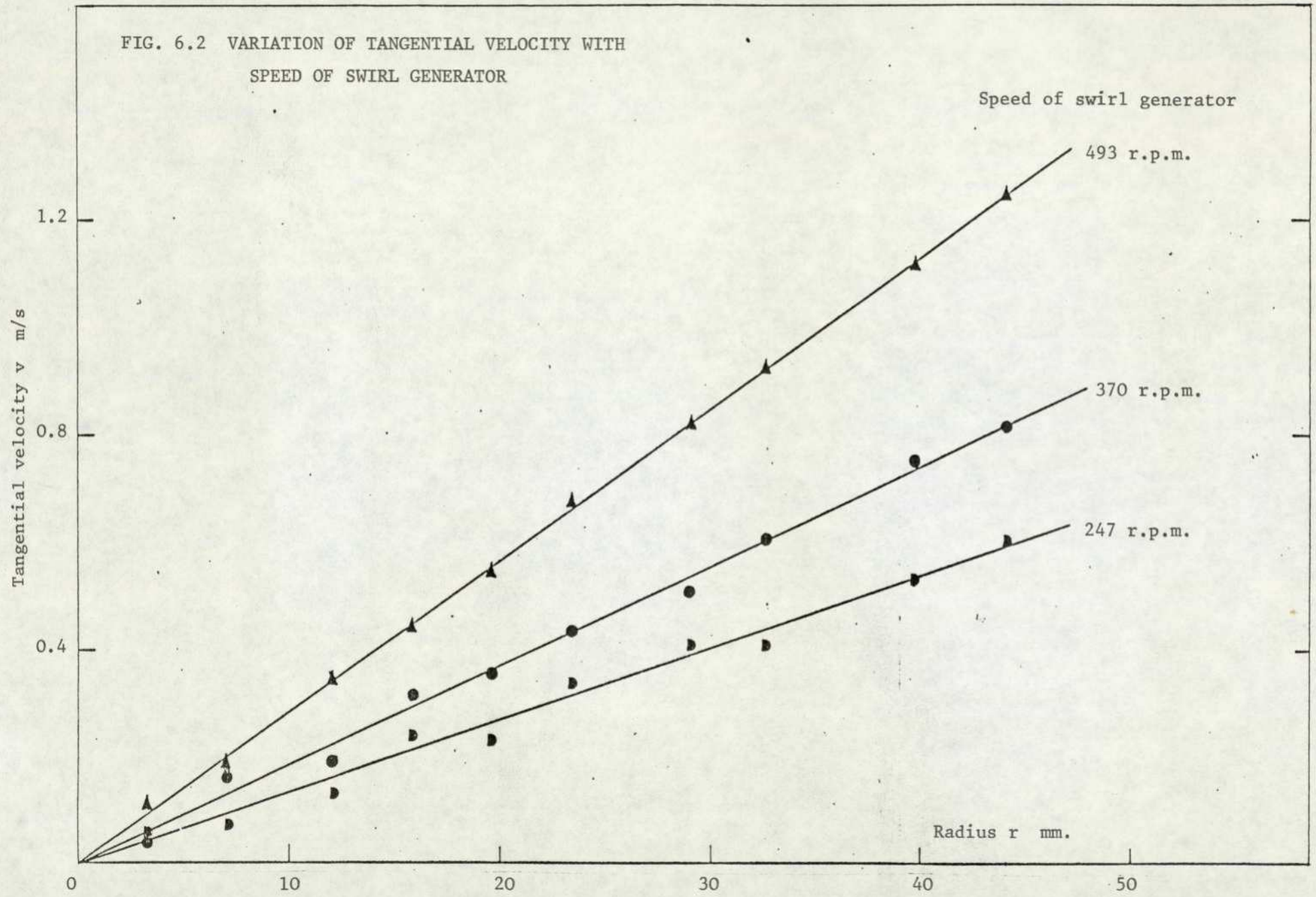

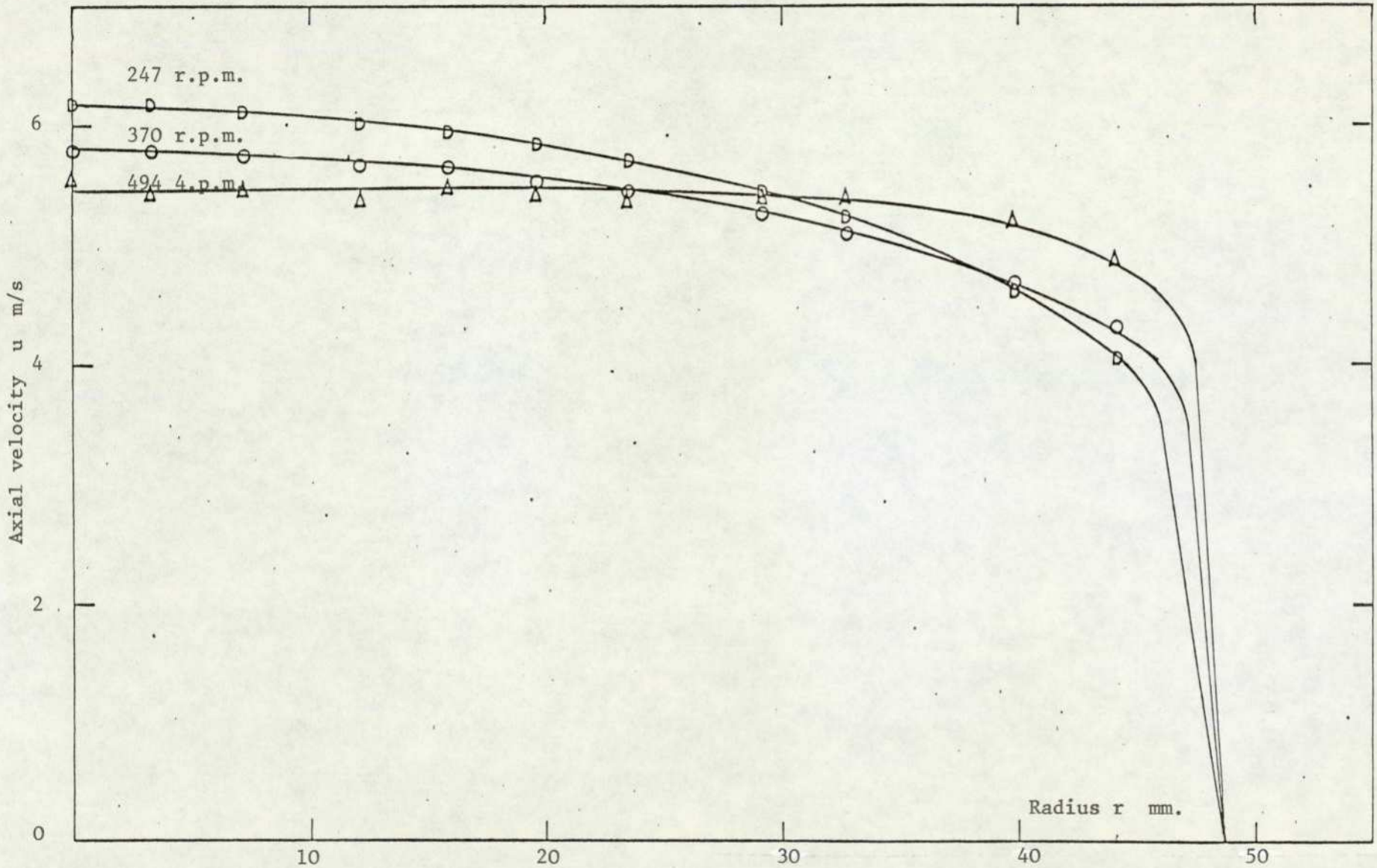

FIG. 6.3 VARIATION OF AXIAL VELOCITY WITH SPEED OF SWIRL GENERATOR

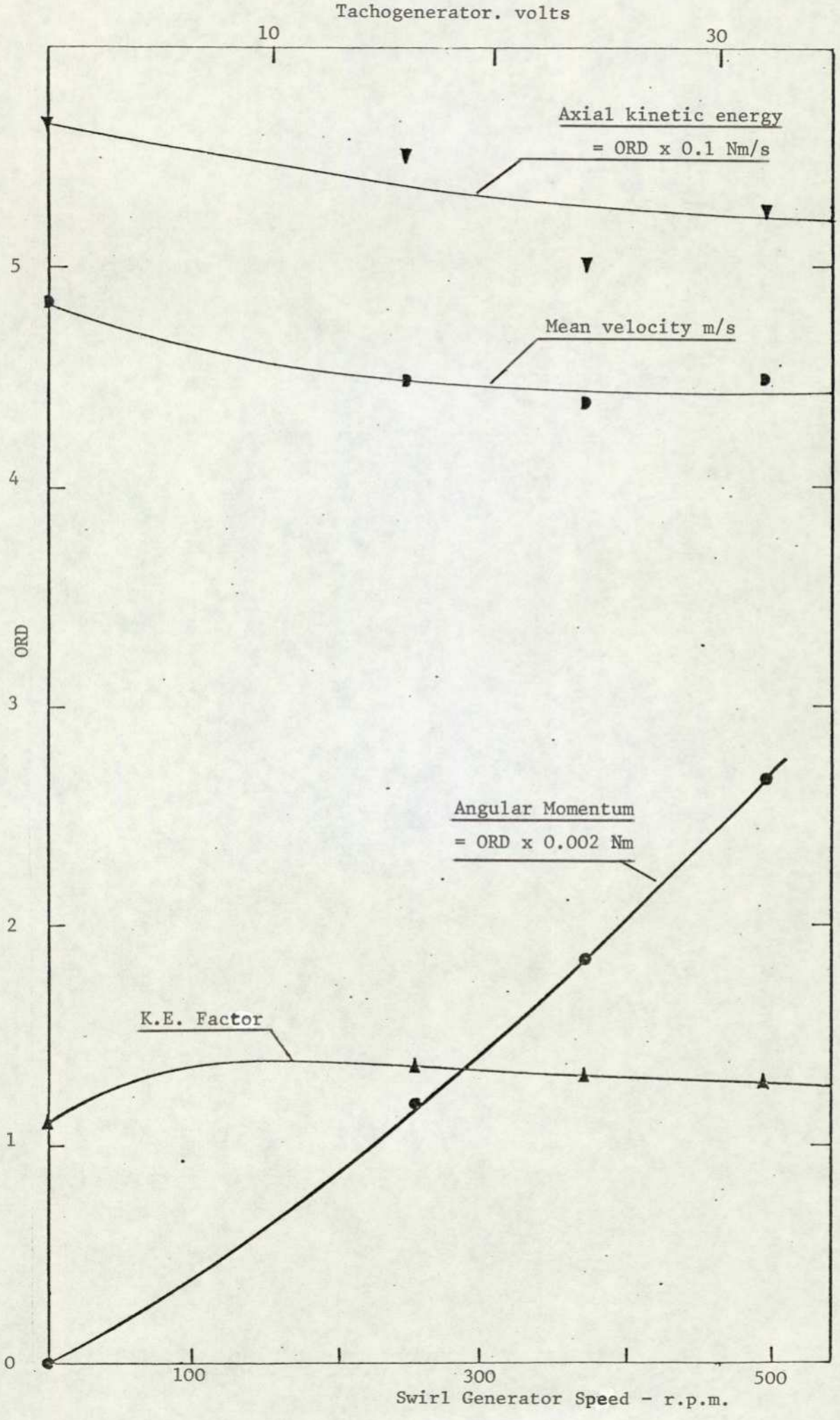

FIG. 6.4 VARIATION OF FLOW PROPERTIES WITH INCREASING SWIRL.

The relationship between tangential velocity and swirl generator speed for the three typical cases is shown in Fig. (6.2) Ref.(52).

	Tachogenerator Output (Volts)	Swirl generator Motor speed (R.P.M.)	Maximum swirl angle $\hat{\psi}$ at diffuser inlet (deg.)
Swirl 1	16	247	8.6
Swirl 2	24	370	10.9
Swirl 3	32	494	15.0

At lower speed, it was not possible to measure the swirl angle at each radial position, as the change in the swirl angle between two points was less than 1^{o}, thus outside the capabilities of the five-hole probe. However, such an error does not affect total velocity measurements as the probe is insensitive to such a change. This is reflected clearly in the data points in Fig.(6.3) which corresponds to axial velocity at inlet for swirl 1 to 3. It is seen that Fig.(6.3) displays a higher degree of consistency on comparison with Fig.(6.2). This confirms the comments made in the previous section on the causes of errors. It can also be seen, that with increasing swirl, the error in angular measurements decreases.

The flow properties are tabulated in Table (6/1) and shown in Fig.(6.4) are the variation of angular momentum, axial kinetic energy, kinetic energy factor, and mean velocity.

6.5 FLOW IN THE DIFFUSERS

Highly unstable flow was experienced in the diffusers. Time-variance of flow was observed, thus it was necessary to conduct long-time integration with the time-domain analyser (JM 1860), to obtain average values. Typically, these were

TABLE 'A'

FIGURE NUMBER	2φ (DEG)	FLOW CONDITIONS		GRAPH OF AXIAL VELOCITY DISTRIBUTION	GRAPH OF TANGENTIAL VELOCITY DISTRIBUTION	GRAPH OF FLOW PROPERTIES	RESULTS REPORTED IN TABLE NUMBER
6.5	10	AXIAL		*			
		SWIRL	2	*			
6.6		AXIAL		*			
		SWIRL	3	*			
6.7		SWIRL	2		*		
6.8		SWIRL	3		*		
6.9		AXIAL				*	6/2
6.10		SWIRL	2			*	6/3
6.11		SWIRL	3			*	6/4
6.12	20	AXIAL		*			
		SWIRL	2	*			
6.13		AXIAL		*			
		SWIRL	3	*			
6.14		SWIRL	2		*		
6.15		SWIRL	3		*		
6.16		AXIAL				*	6/5
6.17		SWIRL	2			*	6/6
6.18		SWIRL	3			*	6/7
6.19	30	AXIAL		*			
		SWIRL	2	*			
6.20		AXIAL		*			
		SWIRL	3	*			
6.21		SWIRL	2		*		
6.22		SWIRL	3		*		
6.23		AXIAL				*	6/8
6.24		SWIRL	2			*	6/9
6.25		SWIRL	3			*	6/10

of the order of 10 - 20 minutes for each measuring point. Time-variance of flow also caused problems in obtaining null readings for swirling flow measurements. Again, long-time integration was conducted;of the order of 15 - 45 minutes for each null readings.

Flow measurements in the 10 deg. diffuser, with axial flow and swirl 2 were made by Wirasinghe (52). The measurements were checked and were found to be within experimental error. The measurements were further extended to swirl 3 to find the effect of increased swirl on diffuser performance. Ref.(52) suggested that swirl 3 might further improve the diffuser performance.

The indexing of figures and tables for the 10 deg., 20 deg. and 30 deg. diffuser is shown in Table "A". Note, for the profiles of flow properties, the figures in parenthesis are the percentage deviations of the respective values from their mean.

6.6 WALL STATIC PRESSURE DISTRIBUTION

The wall static pressure measurements were found to be relatively straightforward. Unsteady readings were observed for wide angle diffusers. The time domain analyser averaged it out in about 6 minutes. The static pressure measurements were made with respect to a reference pressure. The measuring stations correspond to those in Fig.(4.3) and Fig.(4.4a). The observations are recorded in Table (6/11). The wall static pressures associated with diffusers are plotted in Figs.(6.26), (6.27) and (6.28).

It is evident that there is no appreciable variation in the pipe pressure drop up to about the third measuring station irrespective of the diffuser in position, Fig.(6.29). Note

that for pressure drop in the pipe, axial flow and swirl 3 cases only are plotted. The intermediate swirl cases were omitted for clarity.

6.7 DISCUSSION

The earlier section deals with improving experimental data and minimising errors. When calibrating the swirl generator, the velocity measurements were made at the inlet section of the 10^{o} diffuser. Since the variation of swirl angle between two stations was not measurable, a study of decay of swirl was not conducted. However, Hall (68) did solve the governing equations for swirling pipe flow and showed that swirl velocity decays to 0.33 of its initial value in about 100 radii of the downstream travel.

Detailed test for the diffusers establishes that by rotating the honeycomb, a solid-body vortex swirl velocity was successfully produced. This is shown in Fig.(6.7) where the profile for station D1 (see Figs. (4.3) and (4.4a)) clearly indicates that the tangential velocity is roughly proportional to radius. The swirl strength decays as it travels downstream. This rate is accelerated with increase in conical angle but decelerated with increase in swirl. The decay is not, in most cases, in accordance with a constancy of angular momentum at all stations. (Figs. (6.7a) and (6.8a)). The reason for this remains to be found. The outstanding feature of the profiles is the inflection point, which is also reported by Van Dewoestine (49) who suggested that it could not be caused by friction, but may be the result of pressure forces.

The effect of swirl on the diffuser flow is shown in the previous section. Consider the conditions at inlet for the 10^{o} diffuser, Fig. (6.5). The introduction of swirl 2 produces an even

less uniform profile but, however, with increase in swirl, Fig. (6.6) that is, swirl 3, there is an improvement in shape towards a more flat topped and therefore less separation prone profile. In the case of the 20° diffuser, Figs. (6.12) and (6.13), the introduction of both swirl 2 and swirl 3 produces an improvement in shape towards a more flat topped profile. However, for the 30° diffuser, swirl 2 seems to have a more marked affect than swirl 3. (Figs. (6.19) and (6.20))

From the exit axial velocity profile of the 10° diffuser, it can be seen that further downstream in the diffuser, the inflection associated with separation is developing. It is very encouraging to see the tremendous improvement with introduction of swirl 2 and swirl 3. Similar comments apply for the 20° and 30° diffuser.

The improvement in axial velocity profile shape is most readily seen in the graphs of variation of flow properties (Table 'A') in the 10°, 20° and 30° diffuser, with axial and swirling flow, bearing in mind that for perfectly uniform flow, the kinetic energy factor, α, is equal to unity. Fig.(6.30) shows the effect of swirl on kinetic energy factor which simplifies the observations made above and to follow.

For the 10° diffuser, it is evident that there is no improvement in the profile until after station D2 for addition of swirl 2. However, the difference due to swirl 2 addition is thereafter most marked. In particular, the improvement in the flow at station D4 is not only such that α has returned to very nearly its axial flow value at station D1, but Fig.(6.5) shows the profile has completely lost its inflection point. This inflection is usually a good indication of impending separation. Swirl 3 also has a favourable effect on the

improvement in the diffuser flow; not as favourable an effect as swirl 2, but certainly much better effect than for pure axial flow.

In the 20^{o} diffuser, the improvement in profile is immediate. It is also apparant that swirl 3 seems to have a much more favourable effect on the improvement than swirl 2; however, both swirls show marked favourable improvement compared with pure axial flow, Fig.(6.30). From the flow properties, it is evident that for swirl 3, the α value at station D3 is equal to that at station P5 for pure axial flow. This observation justifies the degree of improvement by induction of swirl 3 in the above diffuser.

For flow in the 30^{o} diffuser, again one could say that the improvement is immediate. Swirl 3 has a slightly more favourable effect than swirl 2, but both swirls show marked favourable improvement relative to pure axial flow.

From Fig.(6.30) it is evident that, for the diffuser tested, the beneficial results due to the induction of swirl do not occur until around station D2. Since the station D2, for any diffuser tested, has a value of area ratio relative to inlet of about two, it seems likely that any substantial improvements in diffuser performance resulting from swirl addition are restricted to area ratios greater than about two. The above deduction is also confirmed by the velocity profile of the diffusers tested.

From the mass flux values , computed from the experimental profiles, it is evident that for the diffuser with axial flow, the computed exit mass flux was higher than the inlet mass flux for zero swirl, swirl 2, and swirl 3. This indicates the presence of separation for pure axial flow. The separation

was also confirmed by flow visualization tests. The mass flux values at the exit moved closer to the inlet mass flux values by the induction of swirl. This shows that by inducing swirl, the degree of separation is reduced or in some cases even eliminated.

The variation of flow properties figures (Table 'A') also show that when swirl is induced, the axial kinetic energy decays more rapidly with downstream progress than for pure axial flow. This clearly indicates that the swirling flow improves the diffusion process.

The effect of the diffusers on velocity profile are interesting, but it is the effect of the swirl on pressure recovery that is of primary importance. However, one must treat static pressure recovery results with care since the values given are from wall tappings and in swirling flow these will not represent the pressure everywhere across a station. However, with maximum swirl angle not exceeding 15 degrees (i.e. swirl 3) the errors involved are small, especially at diffuser exit since the imposed vorticity will have decayed considerably by that time. (The error involved in using a wall value of static pressure compared with an area-averaged static pressure was 3.6%, 1.89%, 1.14% of dynamic pressure based on mean inlet velocity for swirl 3, swirl 2 and swirl 1 respectively).

Wall static pressures for the 10^{o}, 20^{o} and 30^{o} diffusers are shown in Figs.(6.26), (6.27) and (6.28) respectively. From the figures, it is evident that the presence of swirl modified the pressure drop in the pipe. It is also clear that the greater the divergence angle, the greater is the deviation. This in turn seems to indicate that the greater

the adverse pressure gradient, the greater is the effect on the flow in the pipe.

Results for the wall static pressure recovery for the 10^{o}, 20^{o} and 30^{o} diffusers is shown in Figs.(6.31),(6.32) and (6.33). These are typical of all the diffuser pressure plots. For completeness and qualitative comparison, the pressure recovery curve corresponding to inviscid, uniform flow is superimposed. It can be used for no more than this however since it is based on a mean inlet velocity whereas all the experimental curves correspond to inlet flow having α greater than unity. At high inlet distortion factor, therefore, experimental points could be obtained well above the "$C_{p_{ideal}}$" line. From the above figures, it is evident that reduction of separation due to swirl caused the performance to increase, the improvement still continuing at the maximum swirl angle used in this project. In 20^{o} and 30^{o} diffusers, C_p value falls well below the $C_{p_{ideal}}$ line. This implies that for the given inlet conditions, C_p is a strong function of something other than AR, i.e. it is affected by separation. The C_p line for any swirl case is above the C_p line for pure axial flow. This implies a large reduction in the dependence of performance on any variable other than area ratio.

It was observed that by introducing swirl, the wall static pressure in the pipe is modified. This presents a problem in assessing the diffuser performance since determination of any of the accepted efficiency criteria depends on p_1 and p_2 and the former has been artificially depressed by swirl addition. However, one could argue that the depressed value is not

artificial at all in the case of an industrial diffuser where swirl is present; for example, in the draught tube fitted to a hydraulic turbine running at an off-design condition.

One could measure the pressure recovery against the value at a station in the supply pipe sufficiently upstream to be unaffected (within experimental accuracy) by the problem at the pipe-diffuser join. Both results are plotted in Fig.(6.34) and by either method it is clear that swirl addition improves diffuser performance, purely in terms of C_p. Again, one confirms that the major improvement are for the wide angled diffusers which suffer from separation problems with axial flow. The figures also suggest that there is a prospect for further improvement for greater swirl angles. However, one should take into consideration the complication caused by vortex breakdown.

The inlet pipe, being 24.5 diameter long, gave a thick inlet boundary layer at the diffuser entry. The condition typical of many diffusers mounted in extensive pipe systems. A hot-wire traverse at the entry section showed θ/D to be about 4.1×10^{-2}.

A more realistic idea of diffuser efficiency may be obtained from the equation

$$\eta_e = (p_2 - p_1)/\rho/2\bar{u}_1^2\alpha_1 \ (1 - \alpha_2/\alpha_1 (AR)^2)$$

where η_e is diffuser energetic efficiency. The equation takes account of inlet and outlet non-uniformities in the denominator. Since the numerator still contains area-averaged static pressure terms and uniformity of axial velocity is assumed,the equation is open to objections.

Fig.(6.35) shows the effect of different swirl severity on diffuser energetic efficiency, based on the wall value of p_2 and the reference pressure in the inlet pipe. They are therefore pessimistic for the same reason as the C_p plots, but comparison can be made between diffusers for different swirl severity. For the 20^o and 30^o diffusers, the energetic efficiency increases with increasing swirl strength, but, for the 10^o diffuser, the performance drops markedly before regaining. The diffuser performance relative to zero swirl (i.e. pure axial flow) is shown in Fig.(6.36). From both these figures, it is evident that a poor result is obtained with the 10^o diffuser, which is a consequence of the increase in α, following the introduction of swirl. It is not obvious why only the 10^o diffuser is the one to suffer. They both also suggest that it might be possible to achieve greater improvement with increase in swirl.

The above approach is for comparative purpose only. A comprehensive study of the evaluation of diffuser performance is pursued in Chapter Ten.

6.8 CONCLUSIONS

1. The honeycomb swirl generator produced an excellent solid-body rotation superimposed on an axial flow.
2. The induction of swirl modified the pressure gradient in the inlet pipe immediately upstream of the diffuser.
3. The axial velocity profiles show that swirling flow produces a beneficial redistribution of axial velocity in the downstream section of the diffusers tested.
4. When swirl was induced, the axial kinetic energy decayed more rapidly with downstream progress than for pure axial flow, in all the diffusers tested. This clearly indicates that swirling flow improves the diffusion process.

5. Swirling inlet flow had a beneficial effect on separation tendencies in the diffusers tested.

6. The results show that swirling inlet flow increases the static pressure recovery for diffusers up to 30^{o} double conical angle. The improvements are not complete at the highest swirl angle (15 degrees) used in this project.

7. The results confirm McDonald, Fox and Van Dewoestine's (50) suggestions that in some cases designers might consider adding swirl to improve the overall performance of a complete flow system. The geometry of the optimum diffuser will be different for swirling inflow than for axial flow.

8. The conclusions regarding the influence of swirling flow arrived at on qualitative bases (Flow visualization tests) agree with those made on quantitative bases.

9. Circulation Γ is in general not conserved with downstream travel in the diffusers.

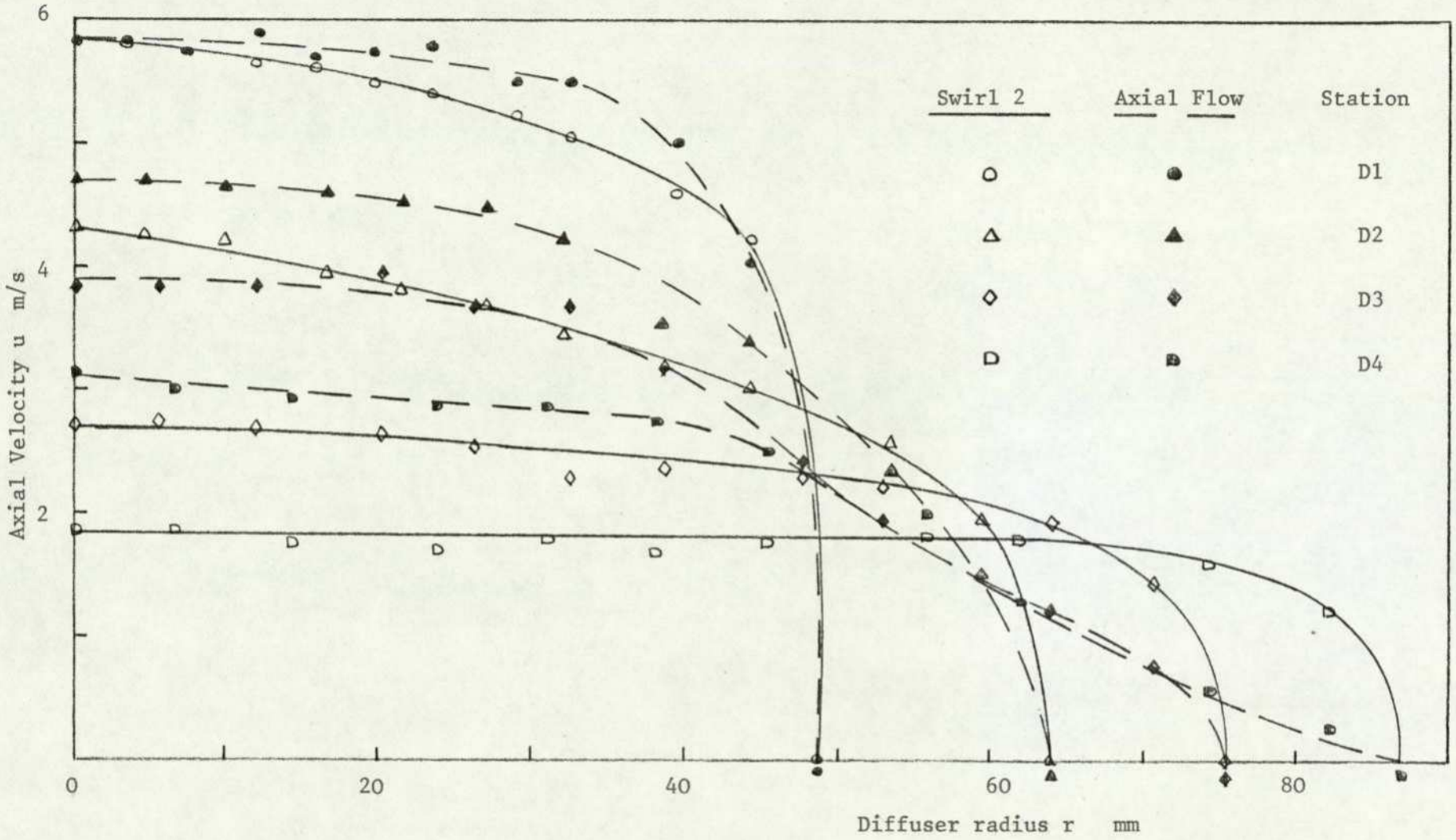

FIG. 6.5 AXIAL VELOCITY DISTRIBUTION IN 10 DEGREE DIFFUSER WITH SWIRL 2

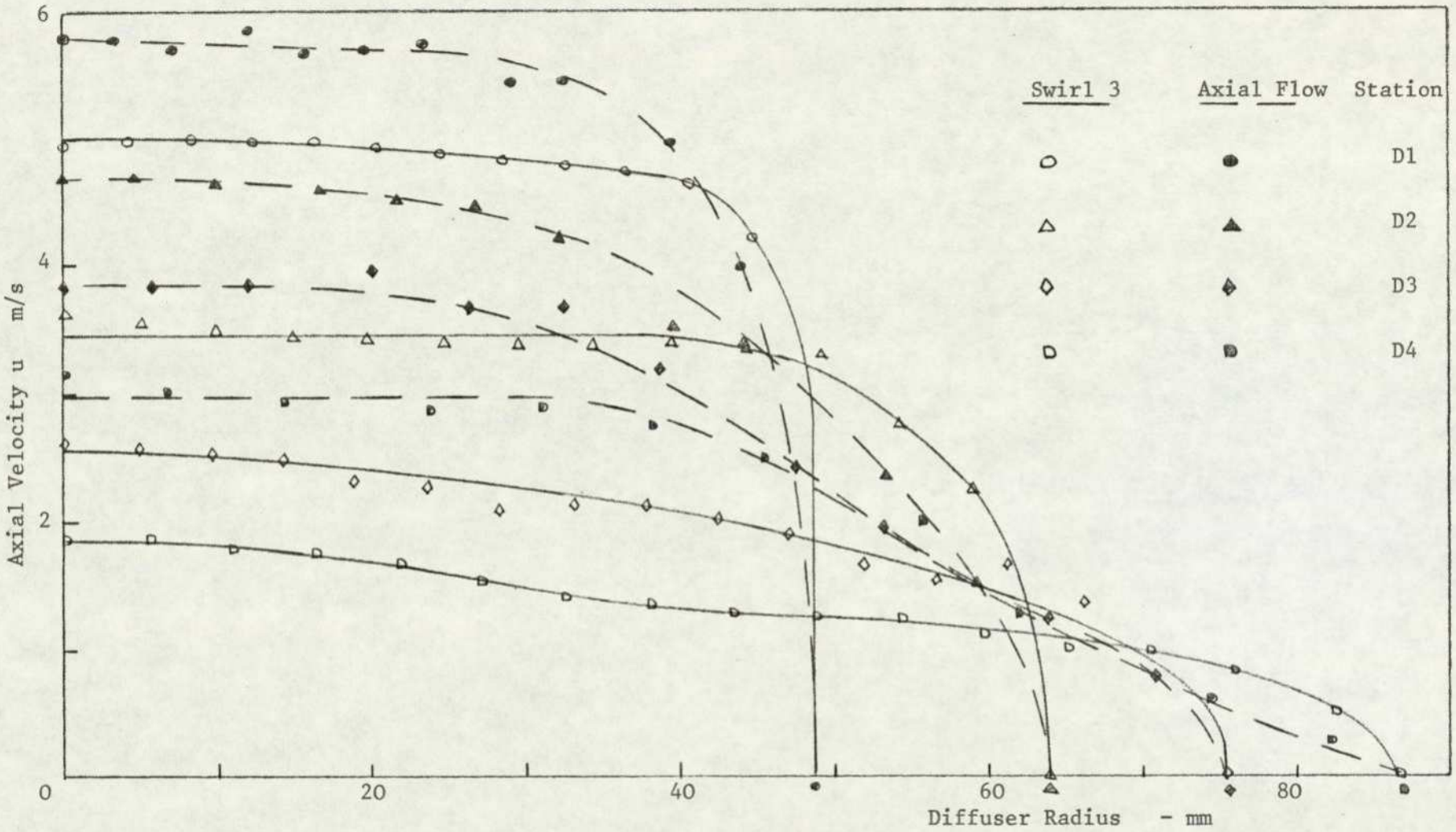

FIG. 6.6 AXIAL VELOCITY DISTRIBUTION IN 10 DEGREE DIFFUSER WITH SWIRL 3.

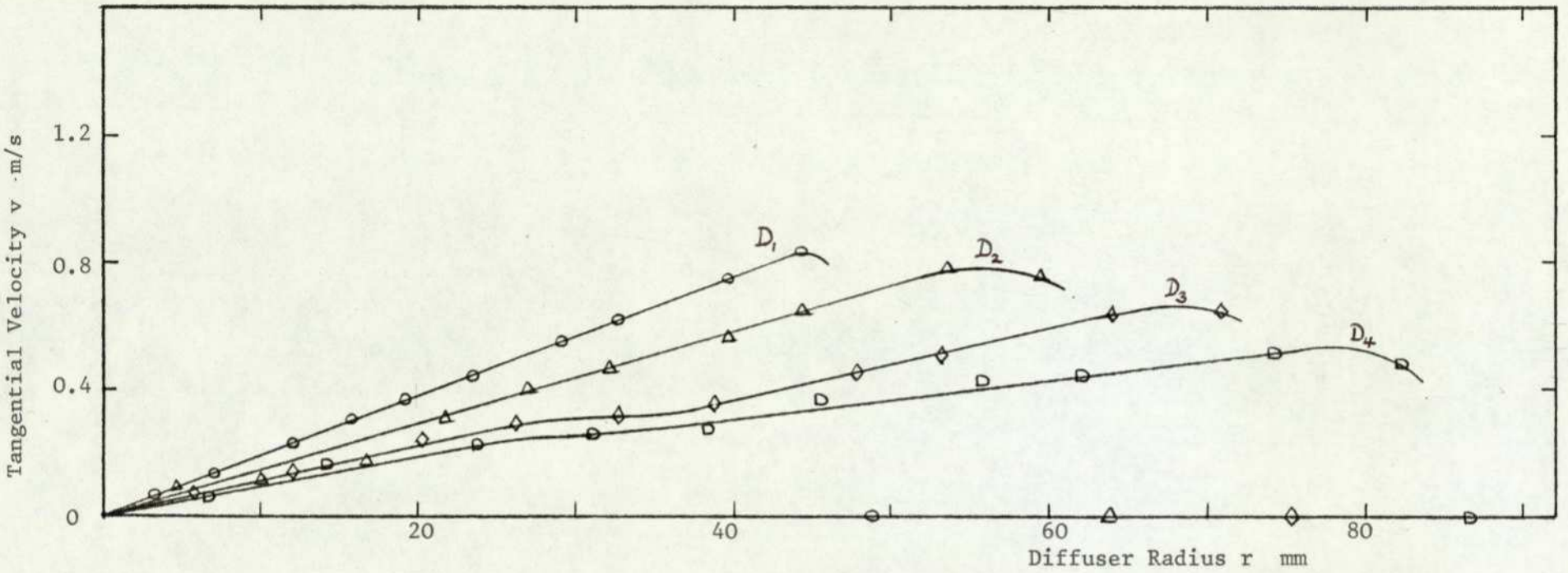

FIG. 6.7 TANGENTIAL VELOCITY DISTRIBUTION IN 10 DEGREE DIFFUSER WITH SWIRL 2.

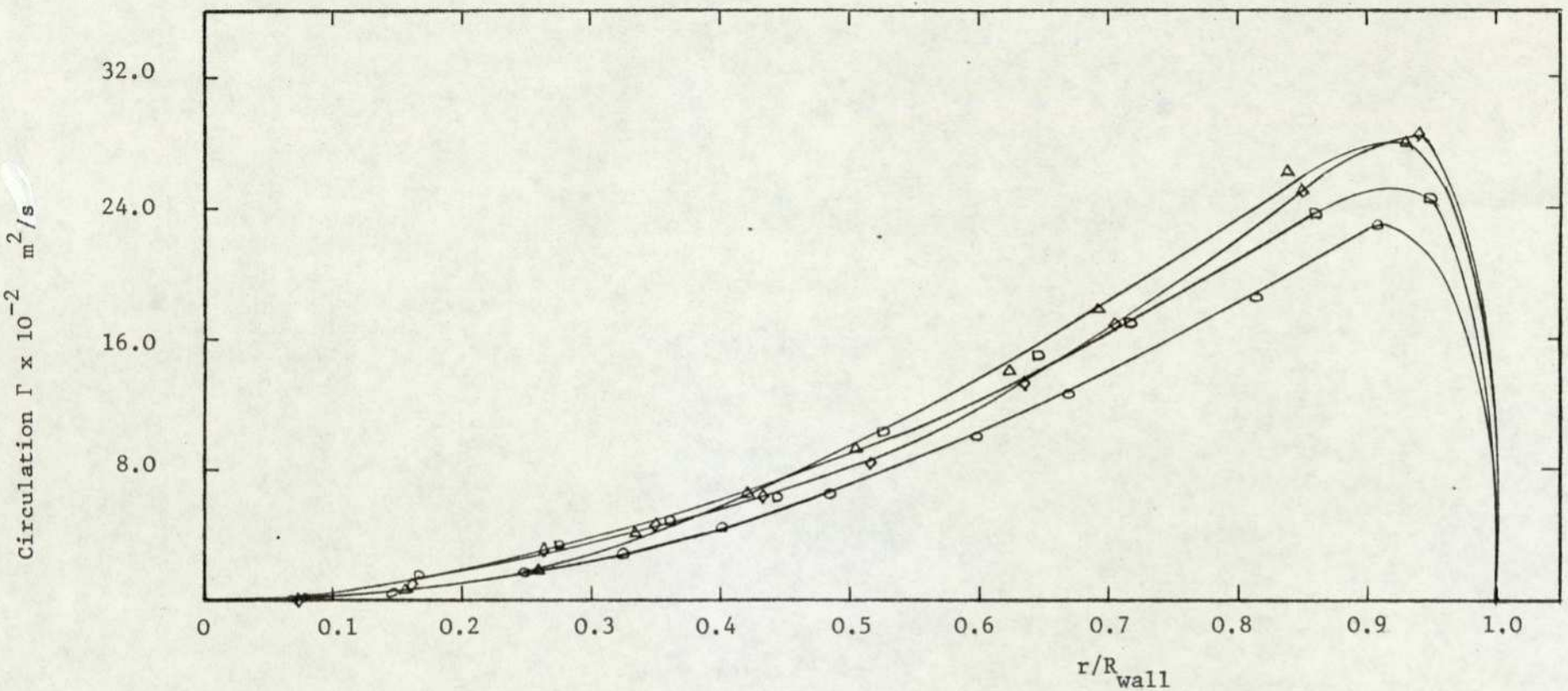

FIG. 6.7a DISTRIBUTION OF CIRCULATION Γ IN 10 DEGREE DIFFUSER WITH SWIRL 2.

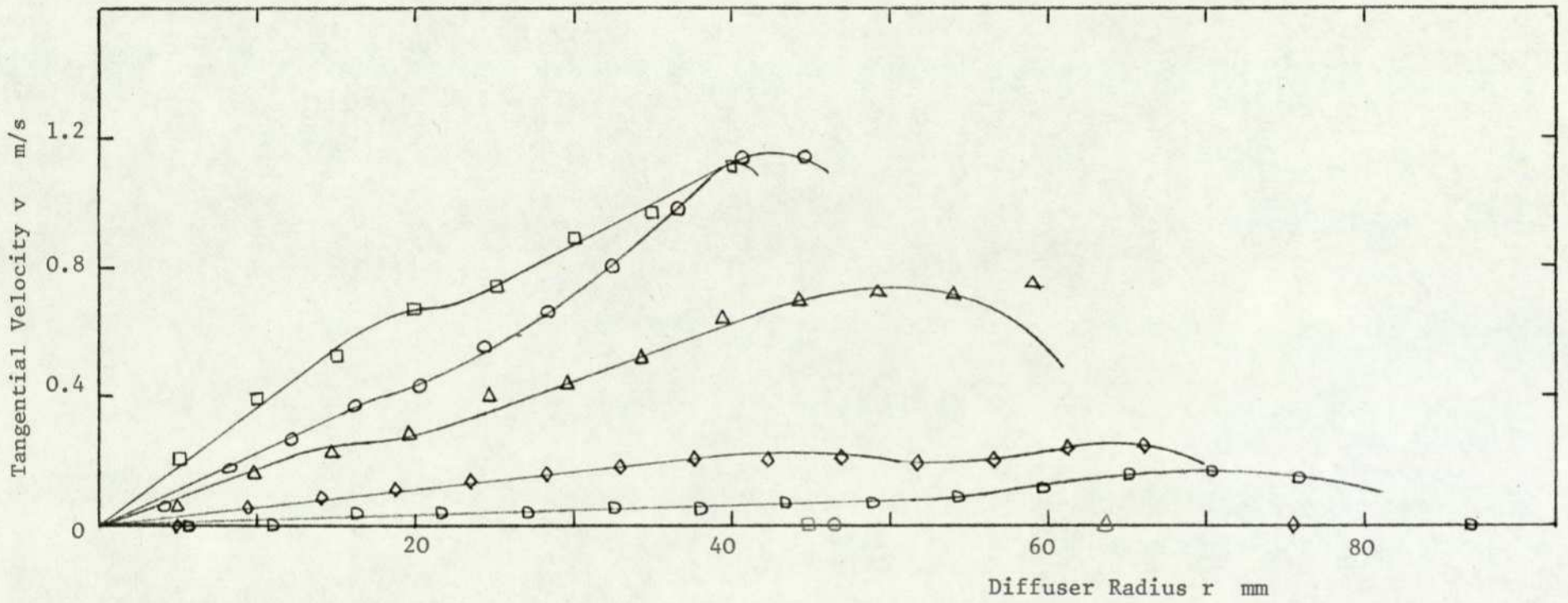

FIG. 6.8 TANGENTIAL VELOCITY DISTRIBUTION IN 10 DEGREE DIFFUSER WITH SWIRL 3.

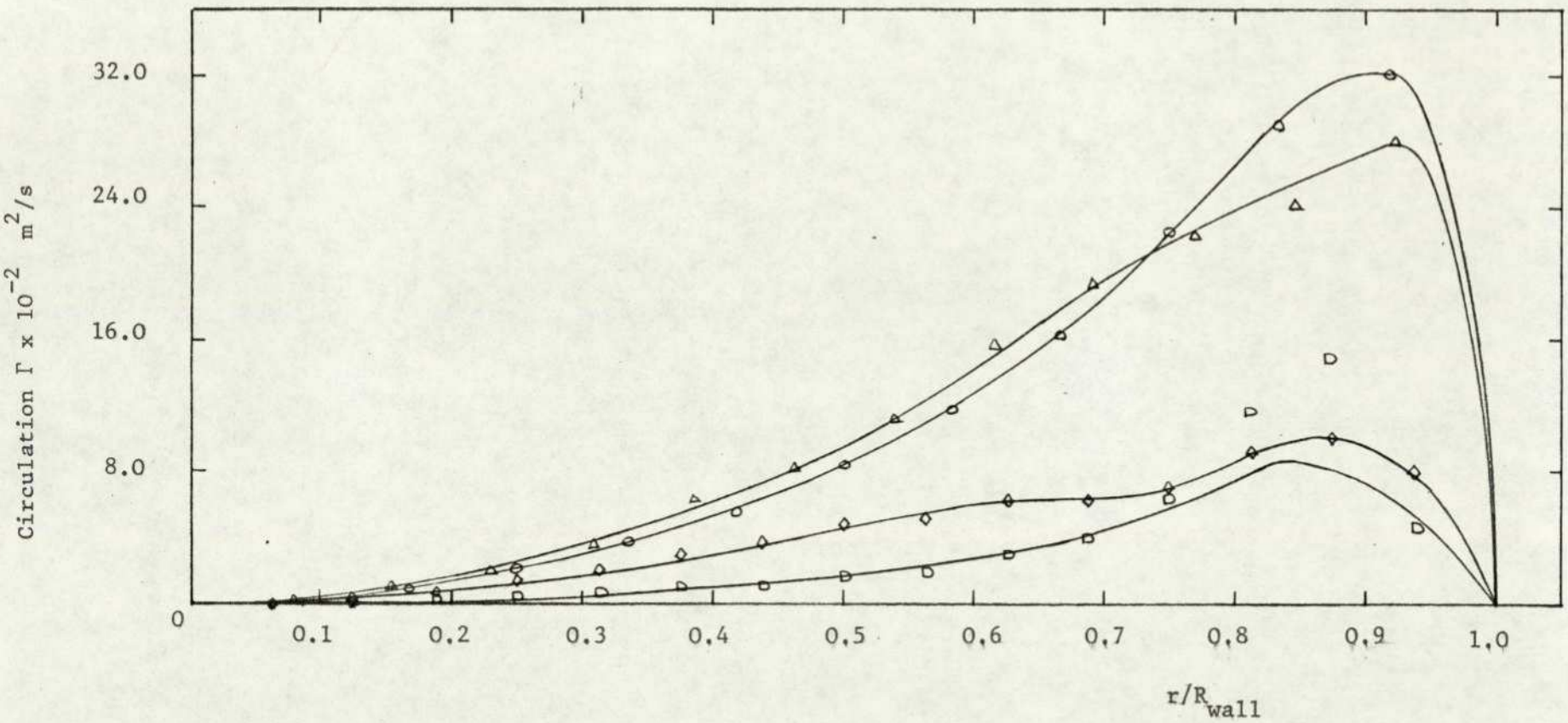

FIG.6.8a. DISTRIBUTION OF CIRCULATION Γ IN 10 DEGREE DIFFUSER WITH SWIRL 3.

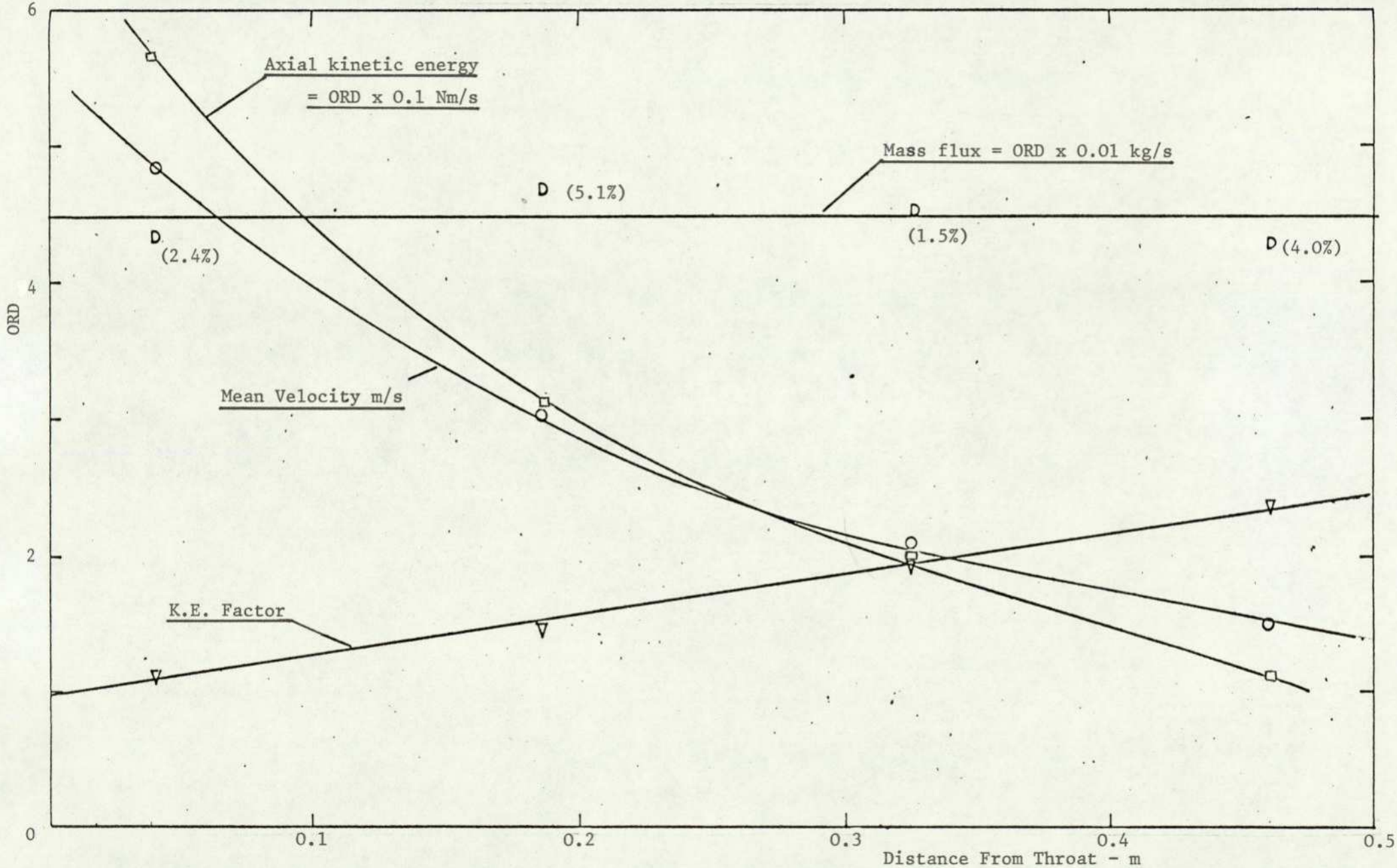

FIG. 6.9 VARIATION OF FLOW PROPERTIES IN 10 DEGREE DIFFUSER WITH AXIAL FLOW

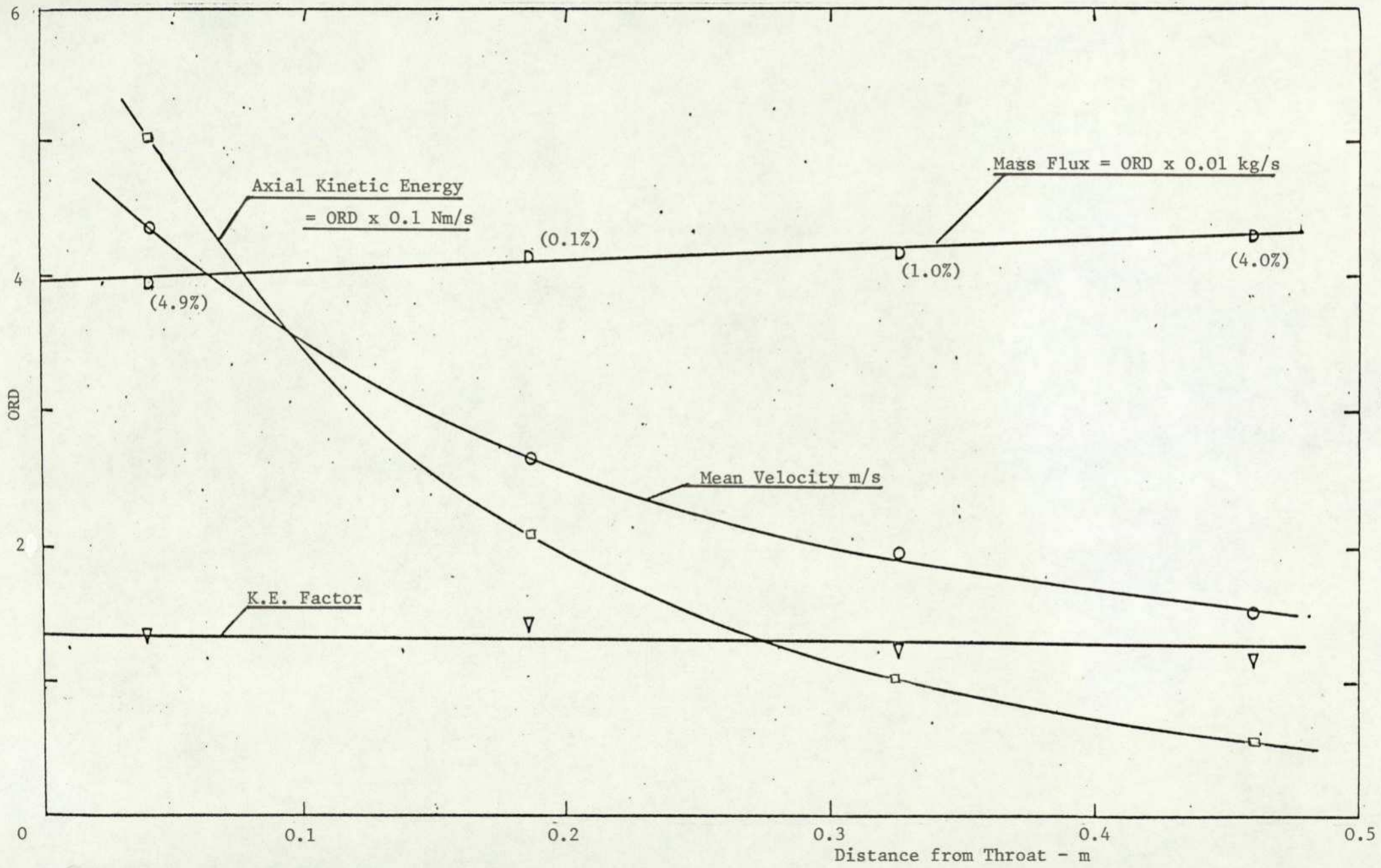

FIG. 6.10 VARIATION OF FLOW PROPERTIES IN 10 DEGREE DIFFUSER WITH SWIRL 2.

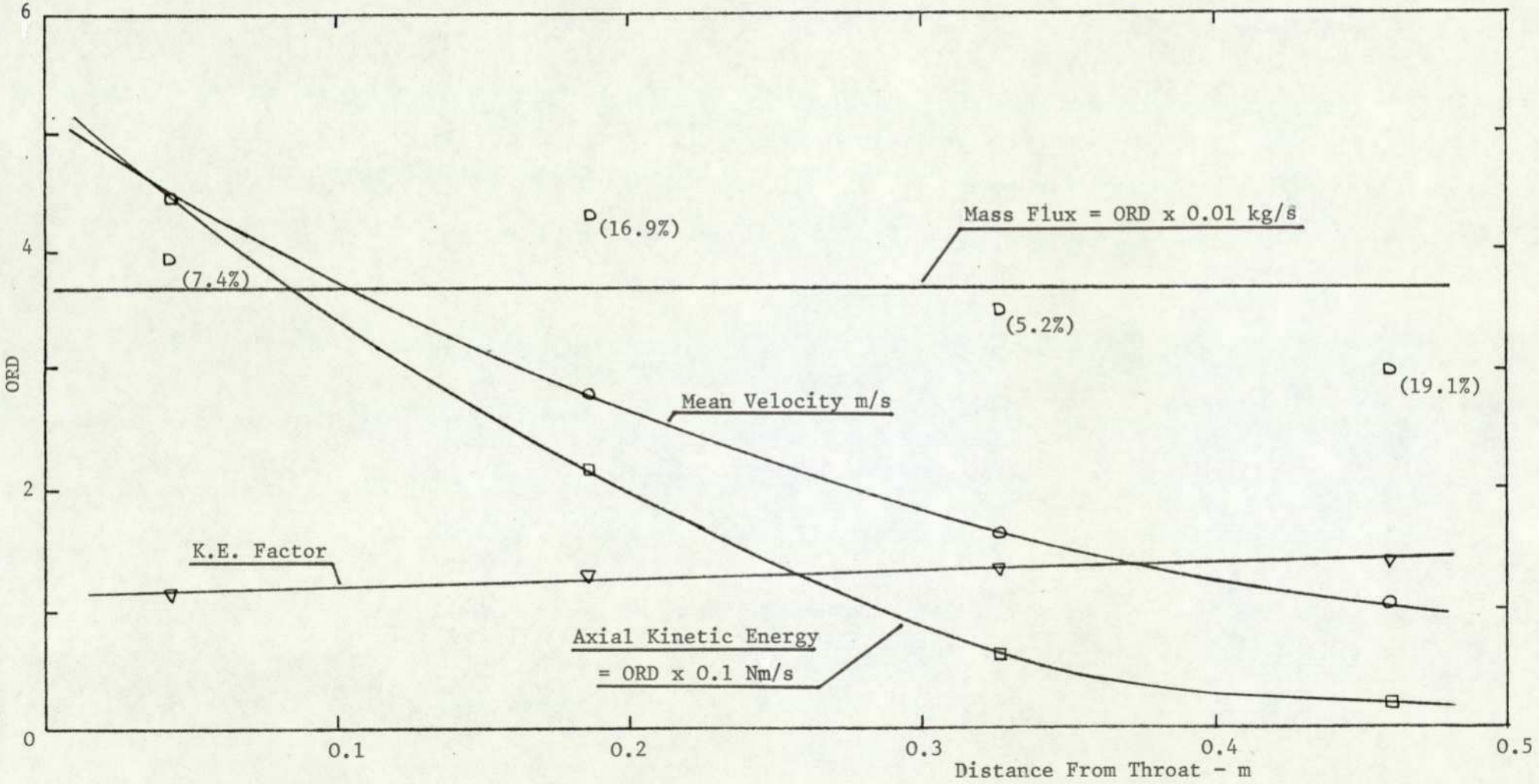

FIG. 6.11 VARIATION OF FLOW PROPERTIES IN 10 DEGREE DIFFUSER WITH SWIRL 3.

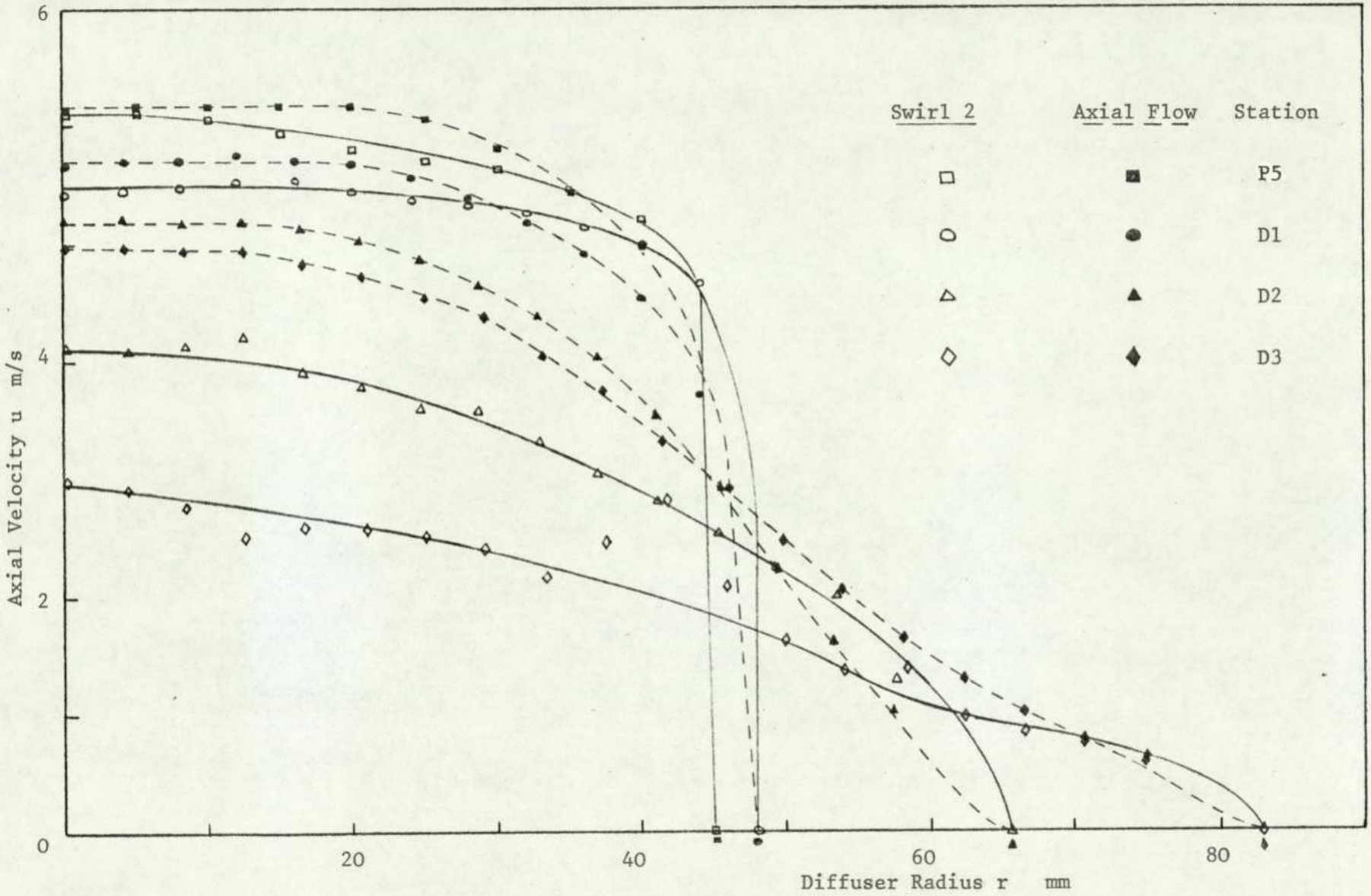

FIG. 6.12 AXIAL VELOCITY DISTRIBUTION IN 20 DEGREE DIFFUSER WITH SWIRL 2.

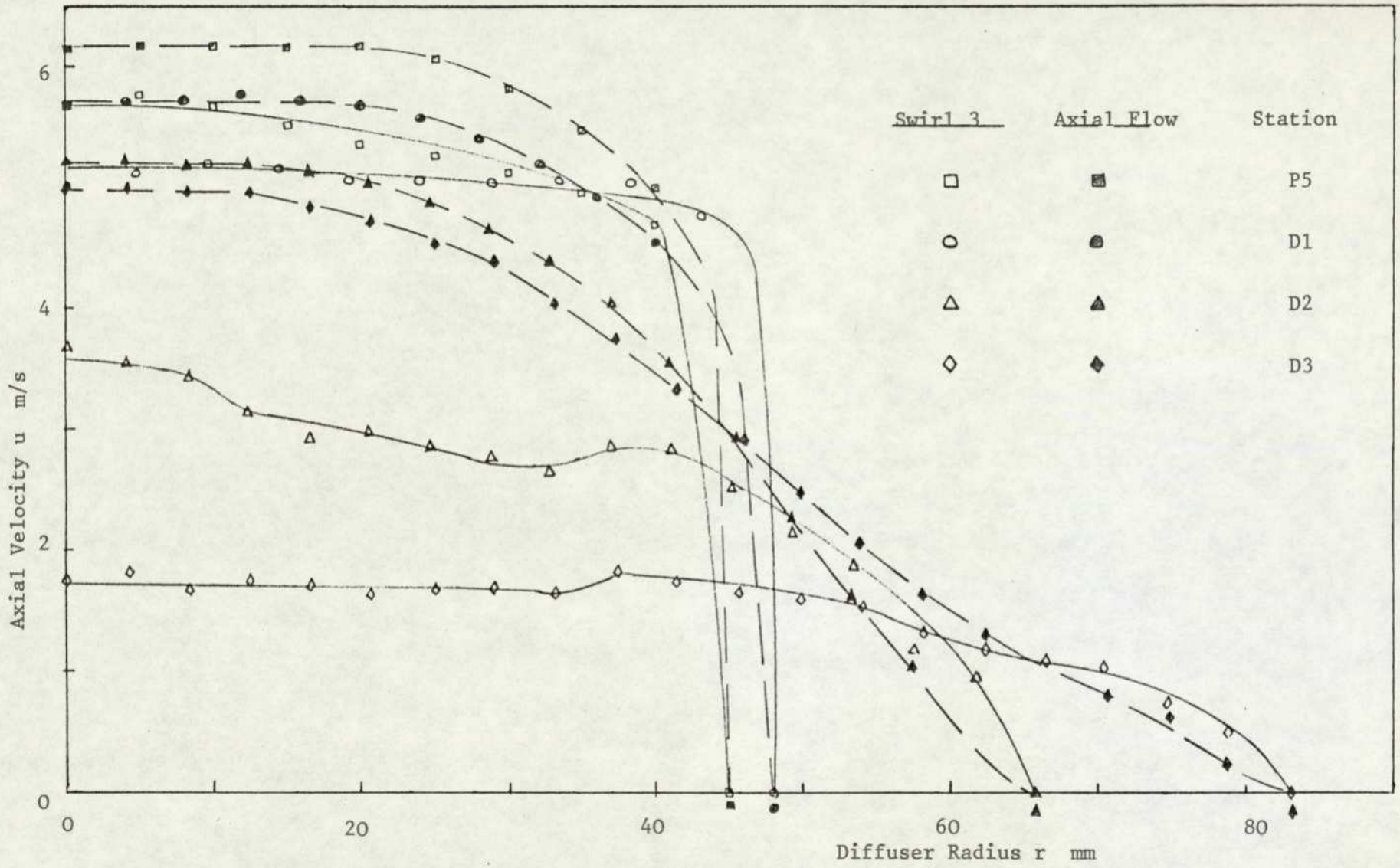

FIG. 6.13 AXIAL VELOCITY DISTRIBUTION IN 20 DEGREE DIFFUSER WITH SWIRL 3.

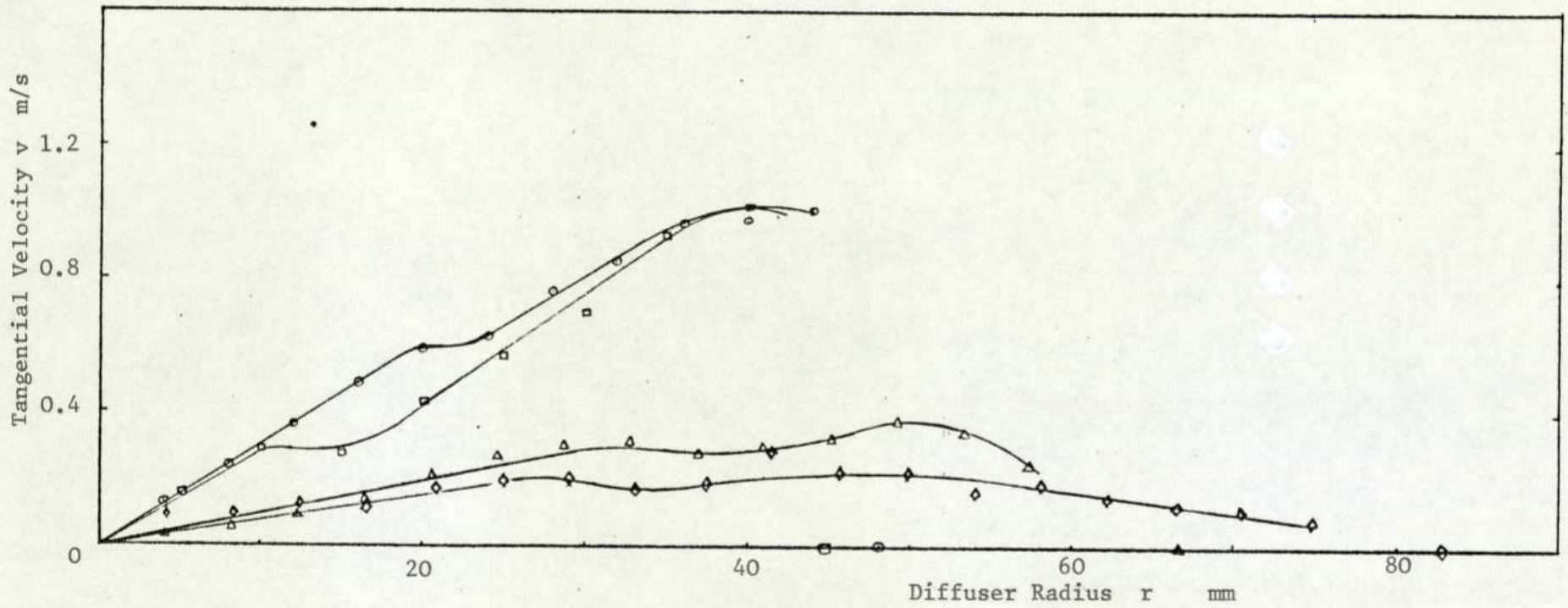

FIG. 6.14 TANGENTIAL VELOCITY DISTRIBUTION IN 20 DEGREE DIFFUSER WITH SWIRL 2.

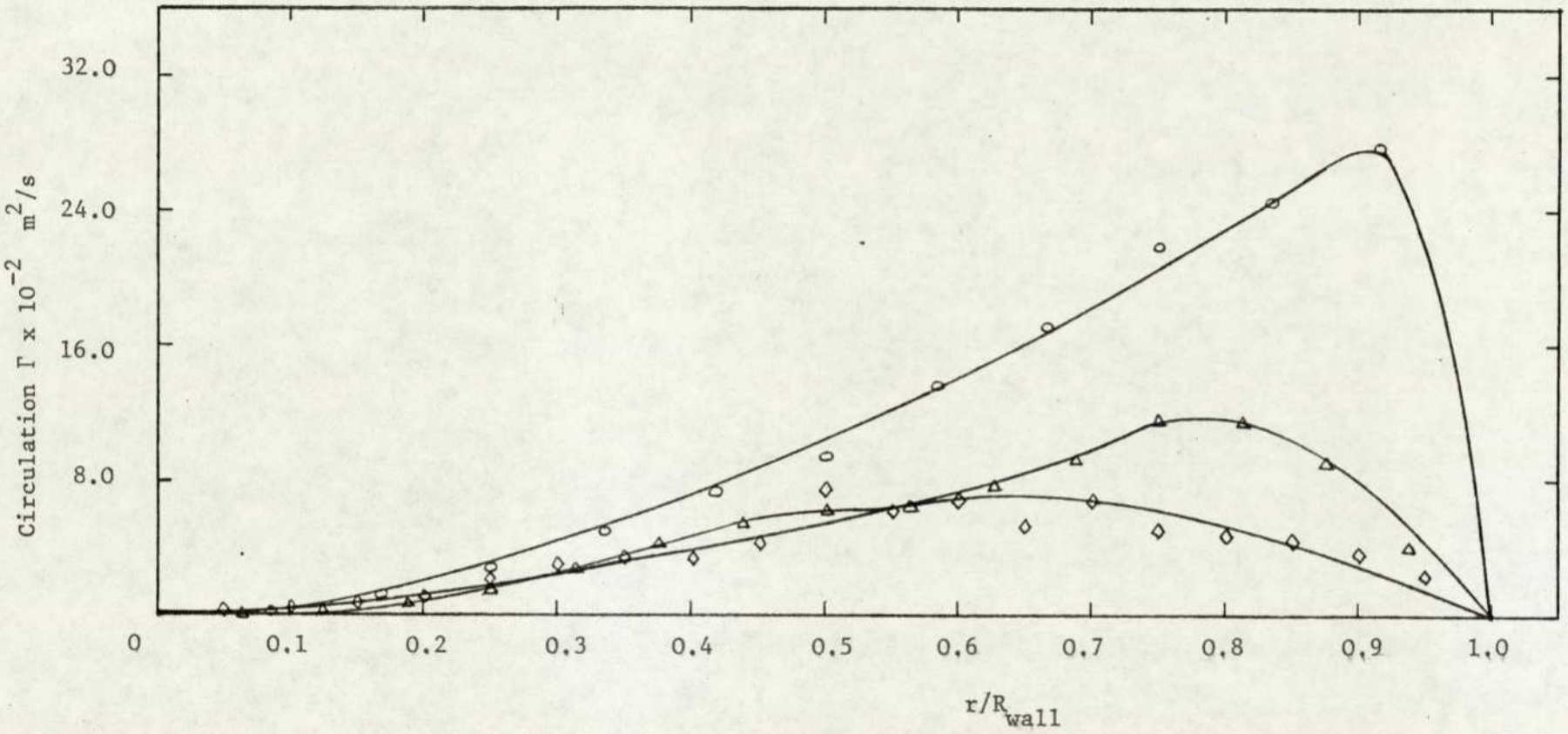

FIG.6.14a. DISTRIBUTION OF CIRCULATION Γ IN 20 DEGREE DIFFUSER WITH SWIRL 2.

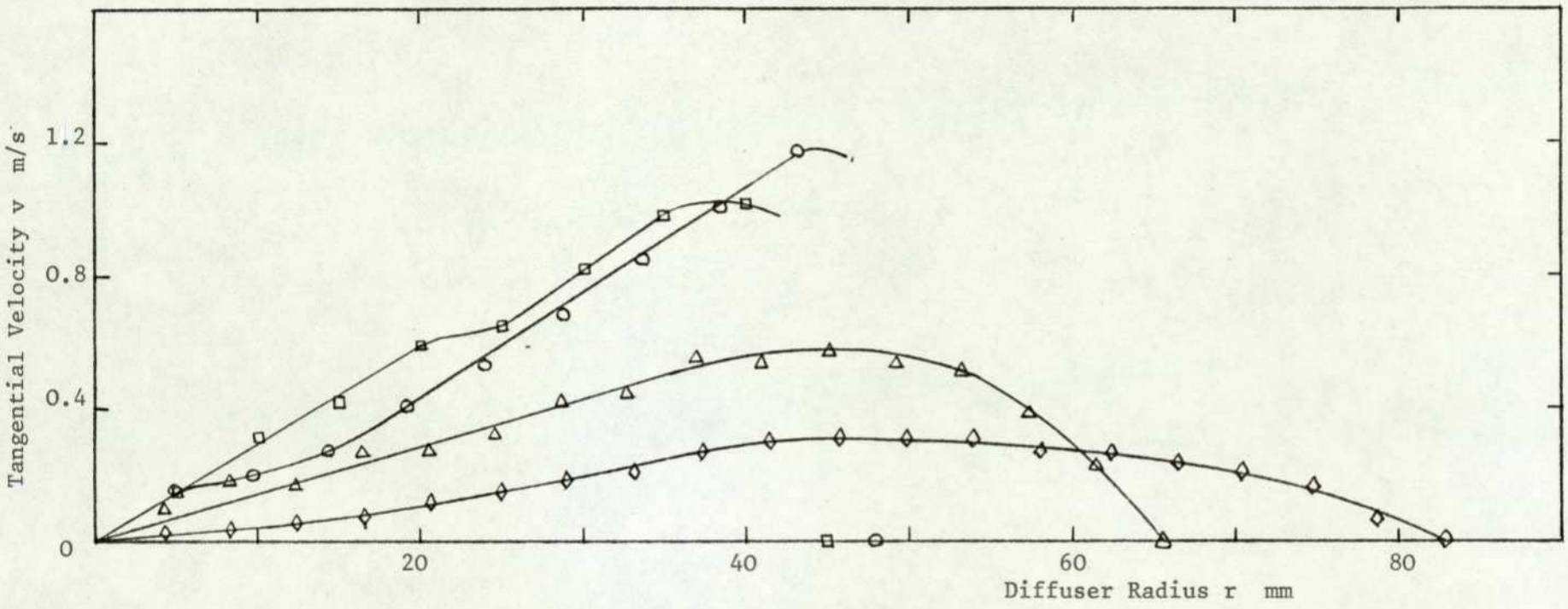

FIG. 6.15 TANGENTIAL VELOCITY DISTRIBUTION IN 20 DEGREE DIFFUSER WITH SWIRL 3

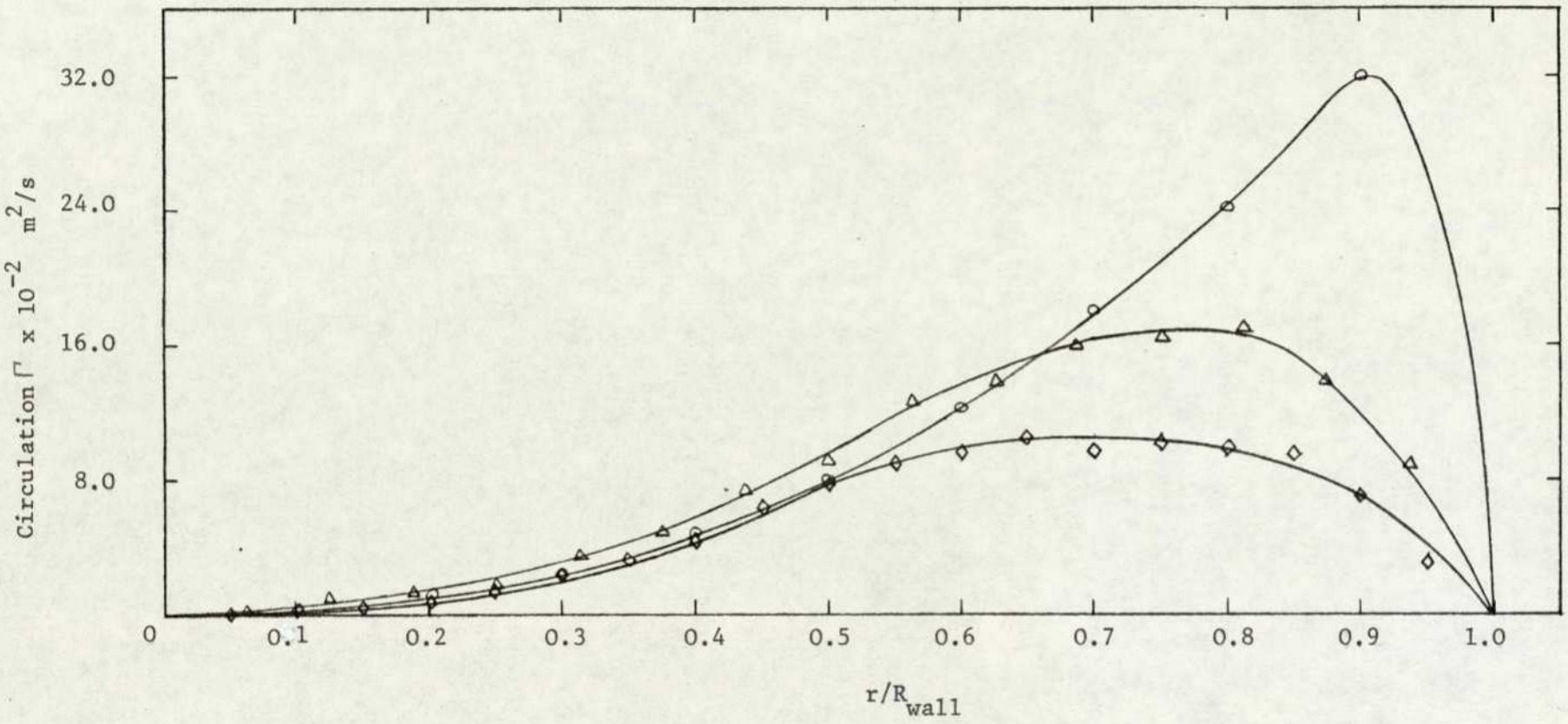

FIG.6.15a. DISTRIBUTION OF CIRCULATION Γ IN 20 DEGREE DIFFUSER WITH SWIRL 3.

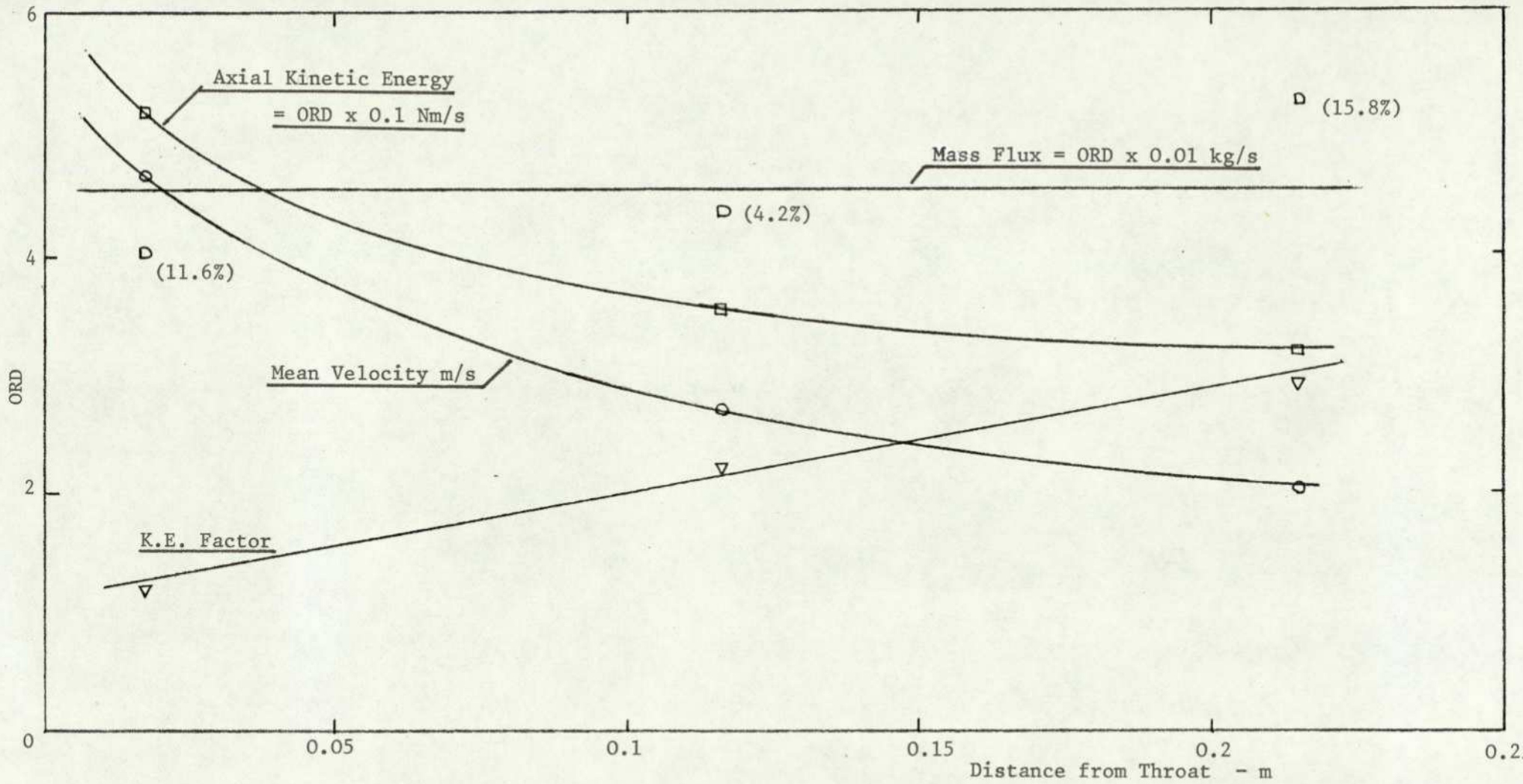

FIG. 6.16 VARIATION OF FLOW PROPERTIES IN 20 DEGREE DIFFUSER WITH AXIAL FLOW

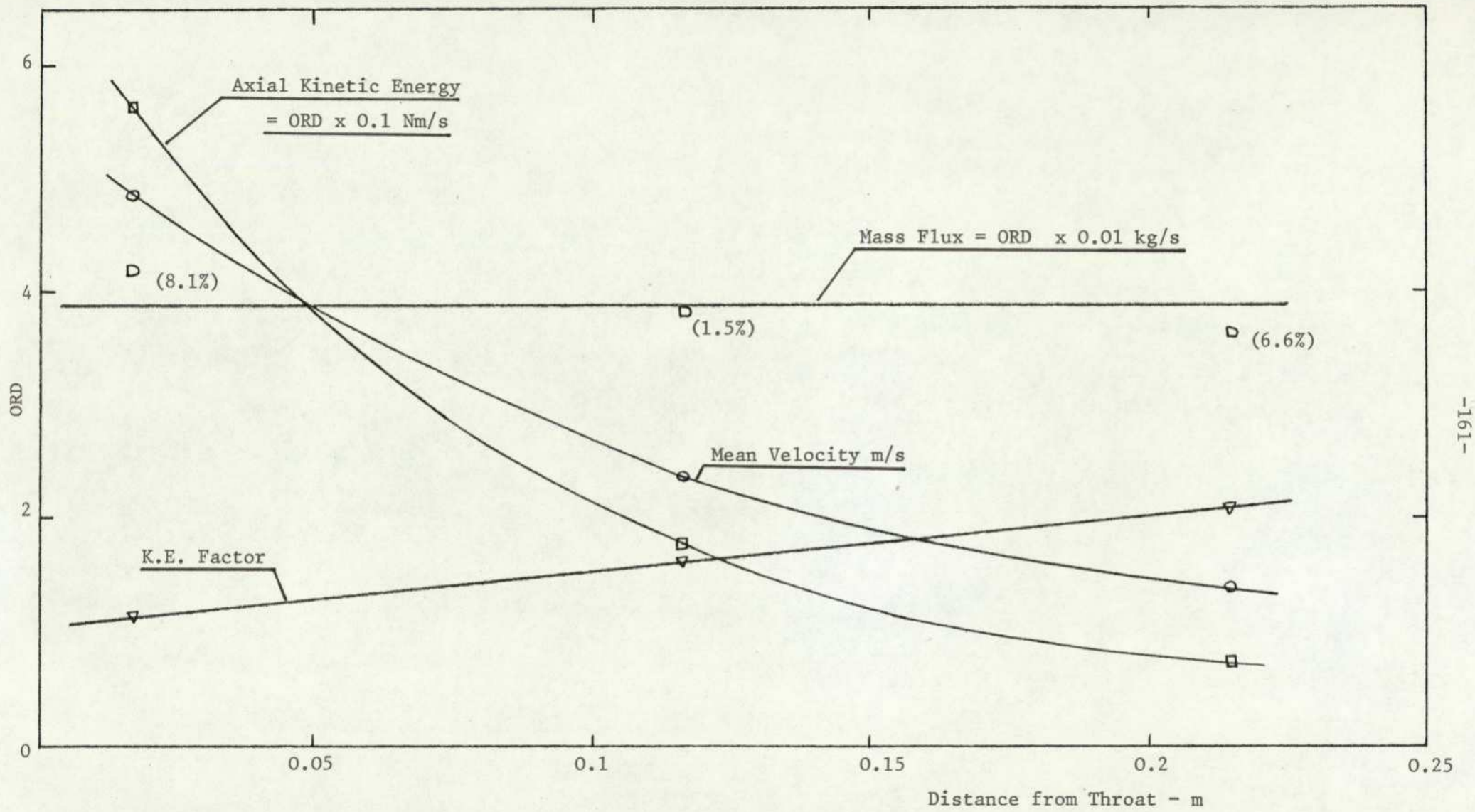

FIG. 6.17 VARIATION OF FLOW PROPERTIES IN 20 DEGREE DIFFUSER WITH SWIRL 2.

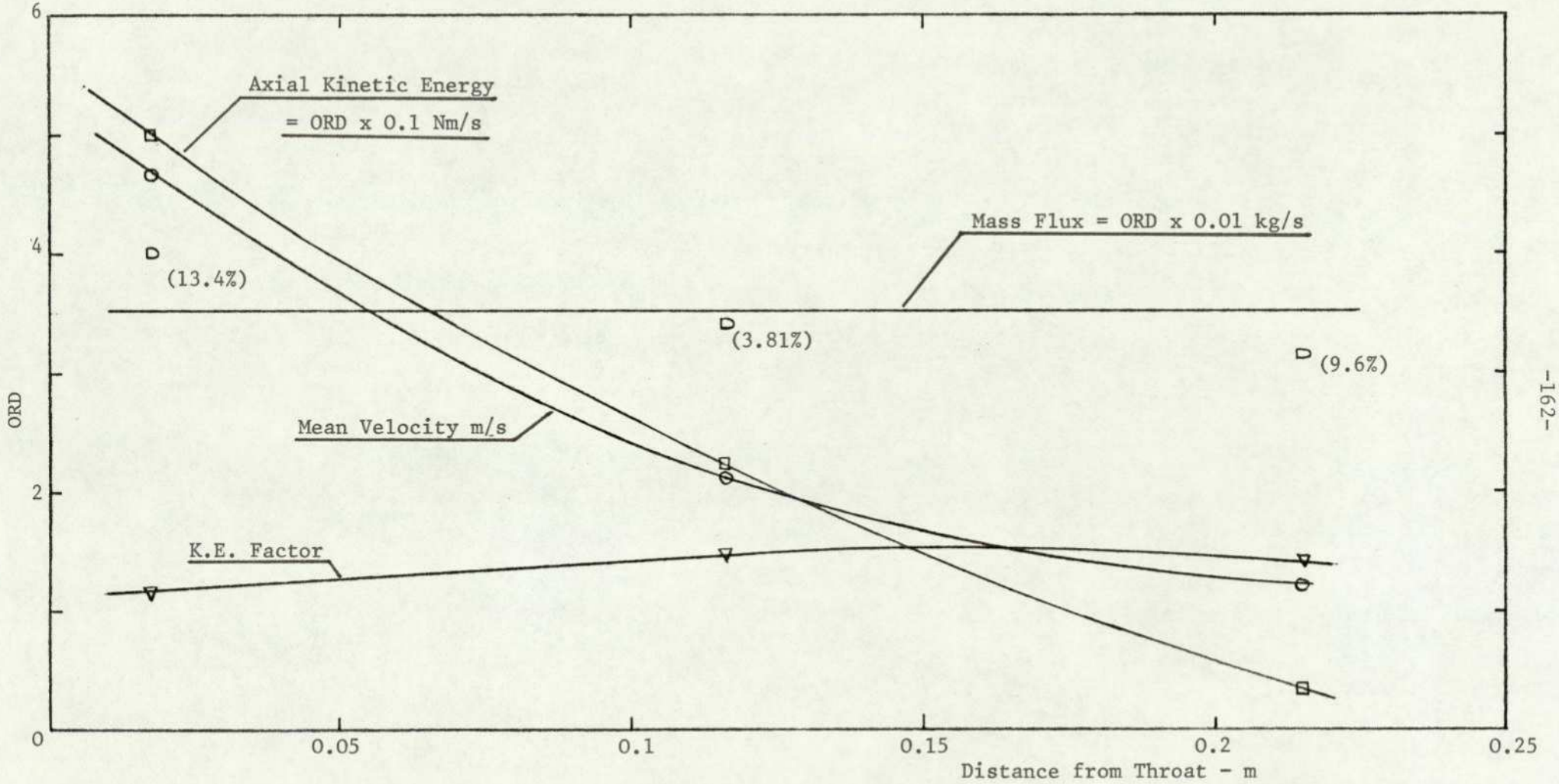

FIG. 6.18 VARIATION OF FLOW PROPERTIES IN 20 DEGREE DIFFUSER WITH SWIRL 3.

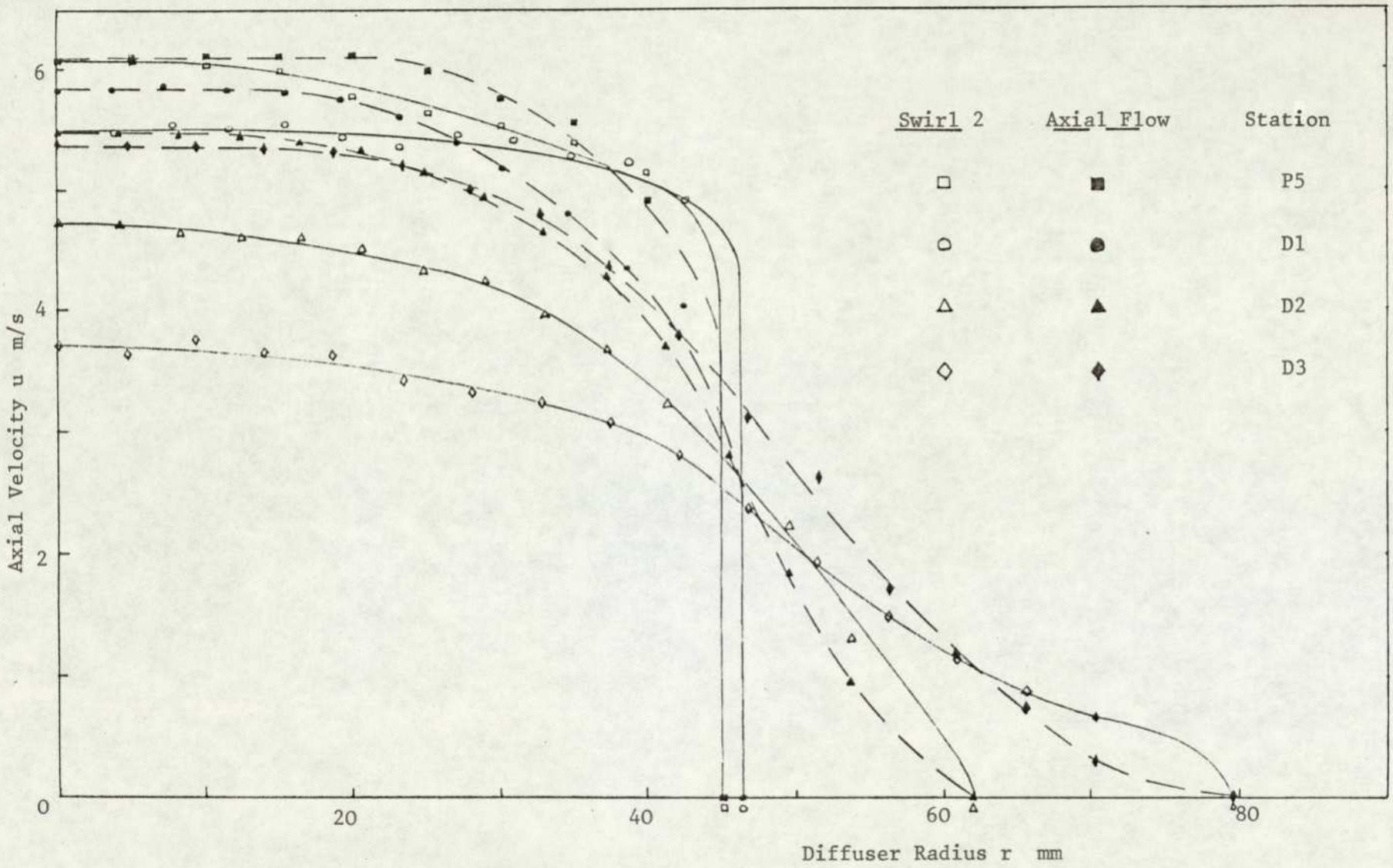

FIG. 6.19 AXIAL VELOCITY DISTRIBUTION IN 30 DEGREE DIFFUSER WITH SWIRL 2.

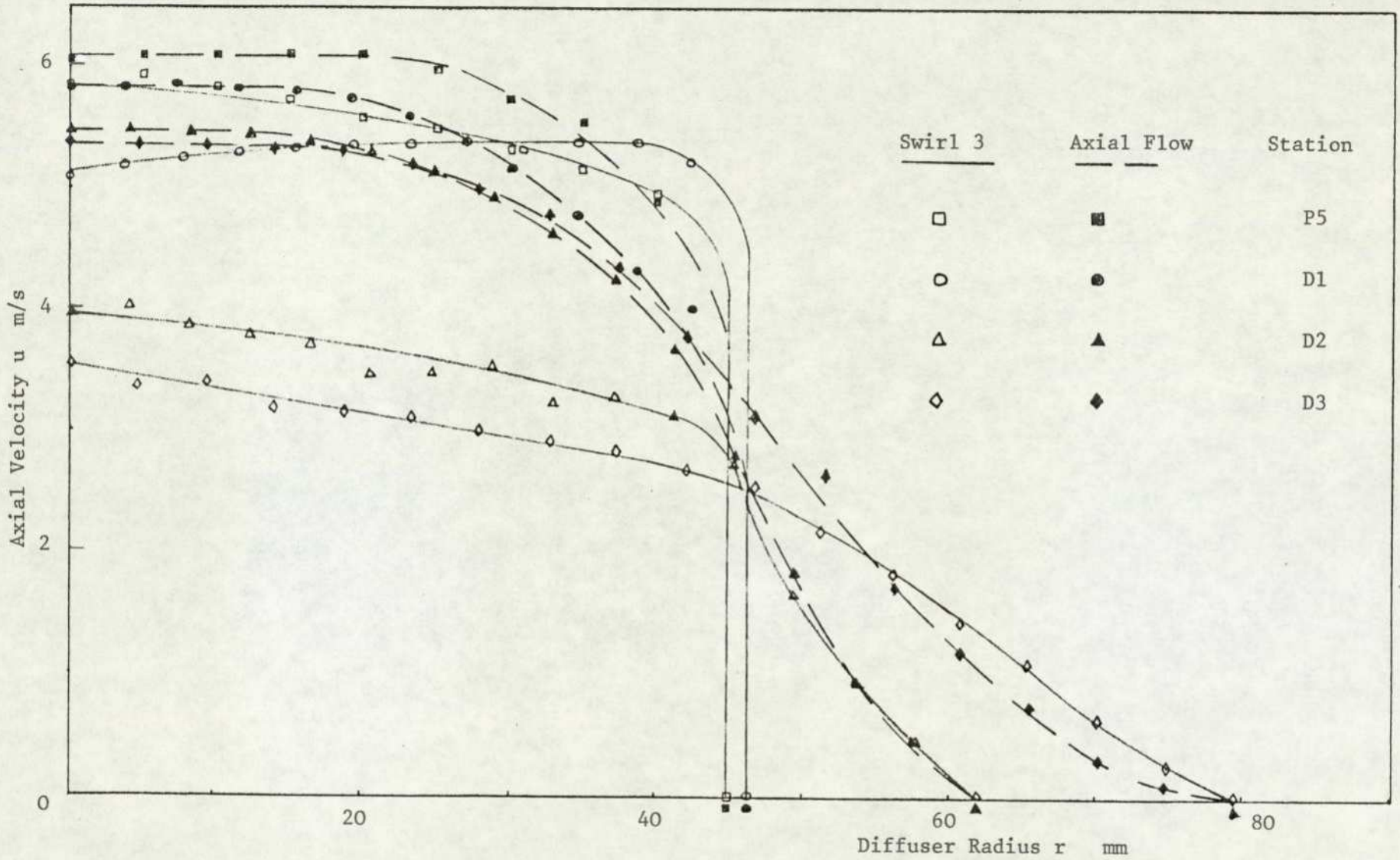

FIG. 6.20 AXIAL VELOCITY DISTRIBUTION IN 30 DEGREE DIFFUSER WITH SWIRL 3.

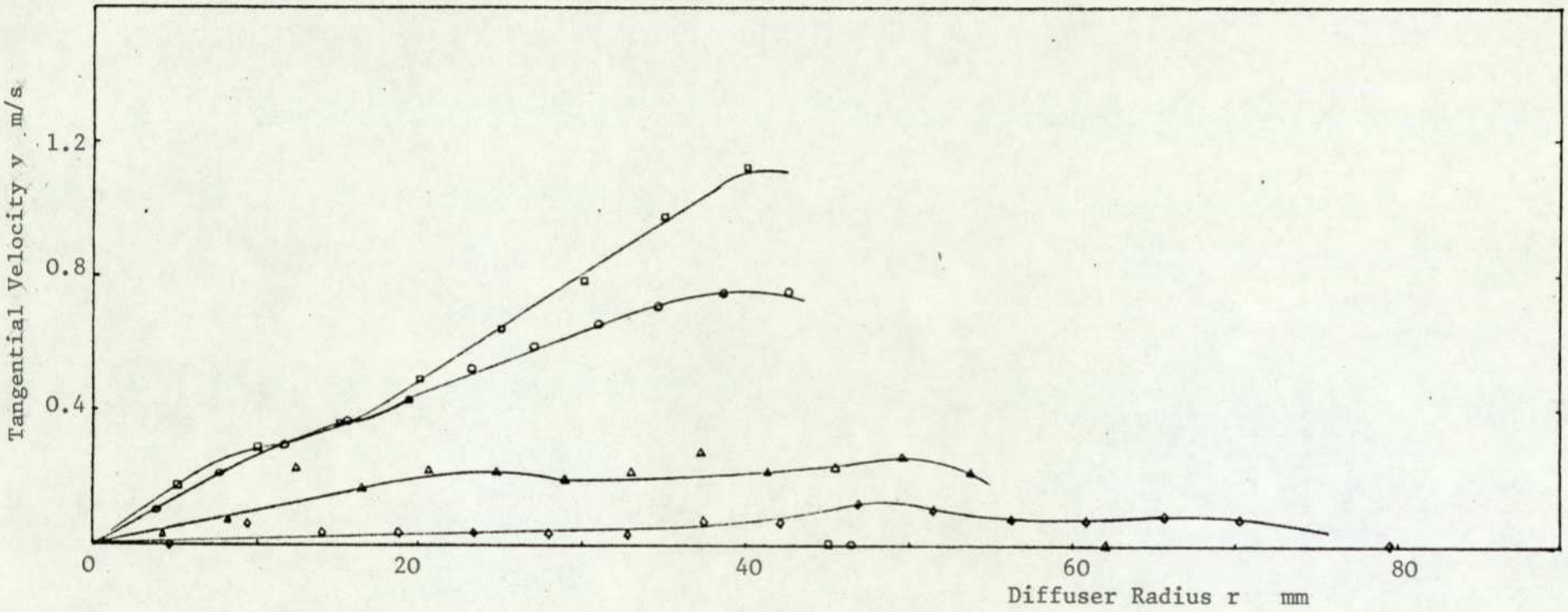

FIG. 6.21 TANGENTIAL VELOCITY DISTRIBUTION IN 30 DEGREE DIFFUSER WITH SWIRL 2.

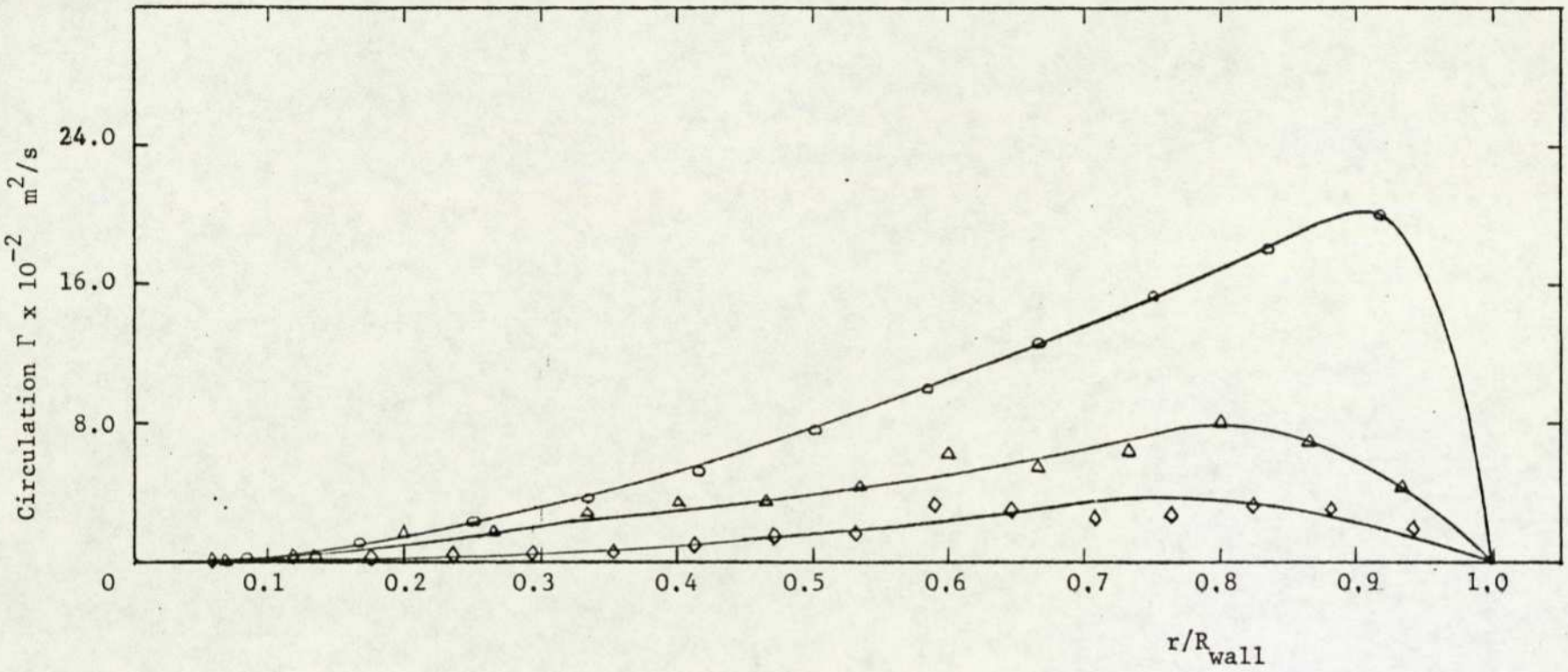

FIG.6.21a. DISTRIBUTION OF CIRCULATION Γ IN 30 DEGREE DIFFUSER WITH SWIRL 2.

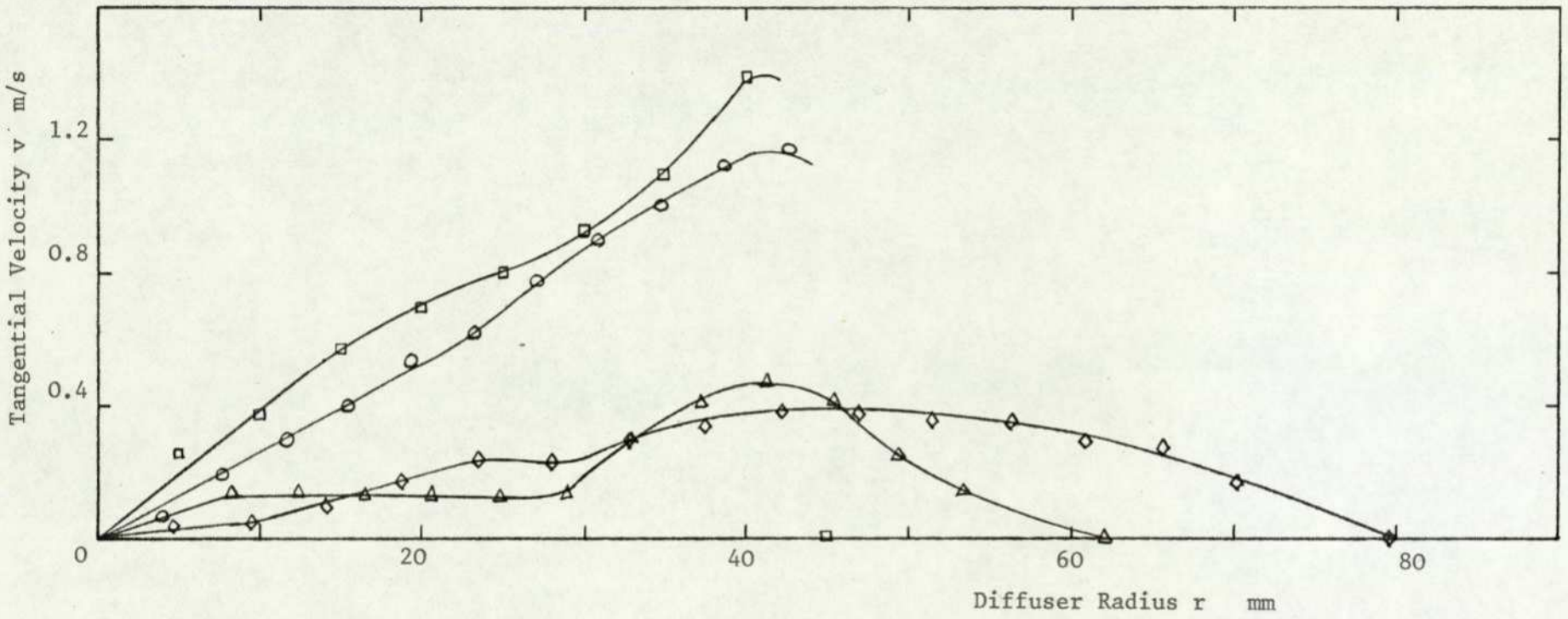

FIG. 6.22 TANGENTIAL VELOCITY DISTRIBUTION IN 30 DEGREE DIFFUSER WITH SWIRL 3.

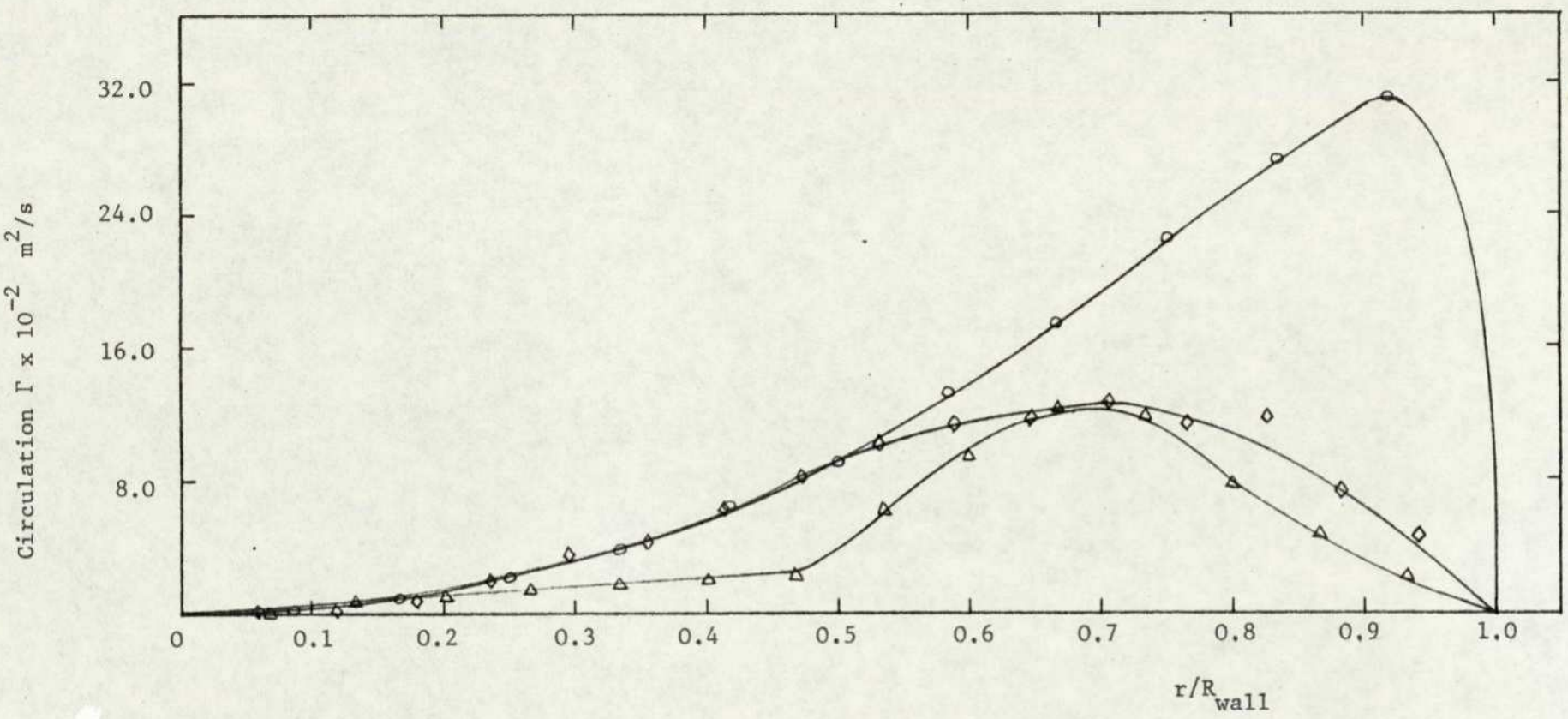

FIG.6.22a. DISTRIBUTION OF CIRCULATION Γ IN 30 DEGREE DIFFUSER WITH SWIRL 3.

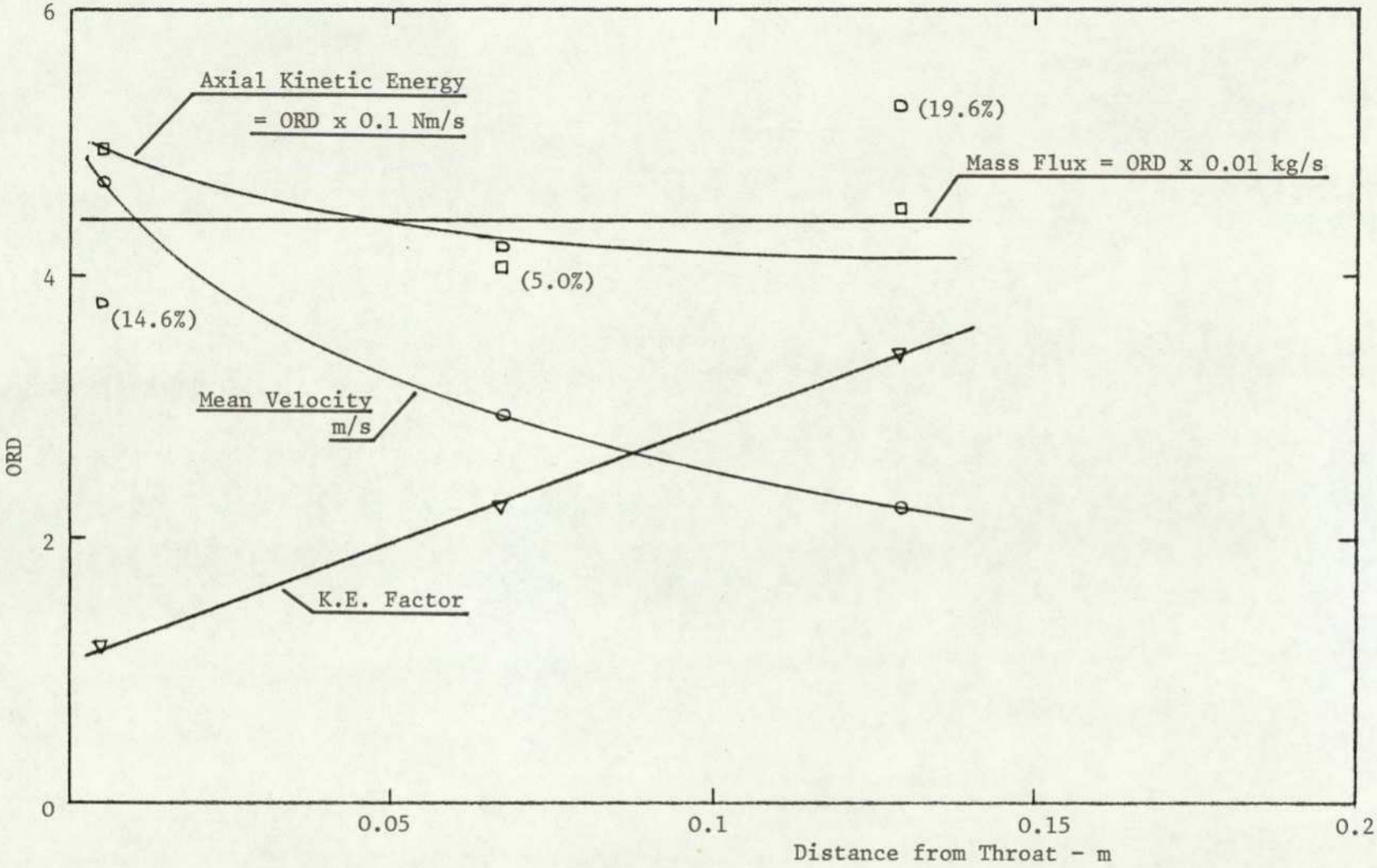

FIG. 6.23 VARIATION OF FLOW PROPERTIES IN 30 DEGREE DIFFUSER WITH AXIAL FLOW

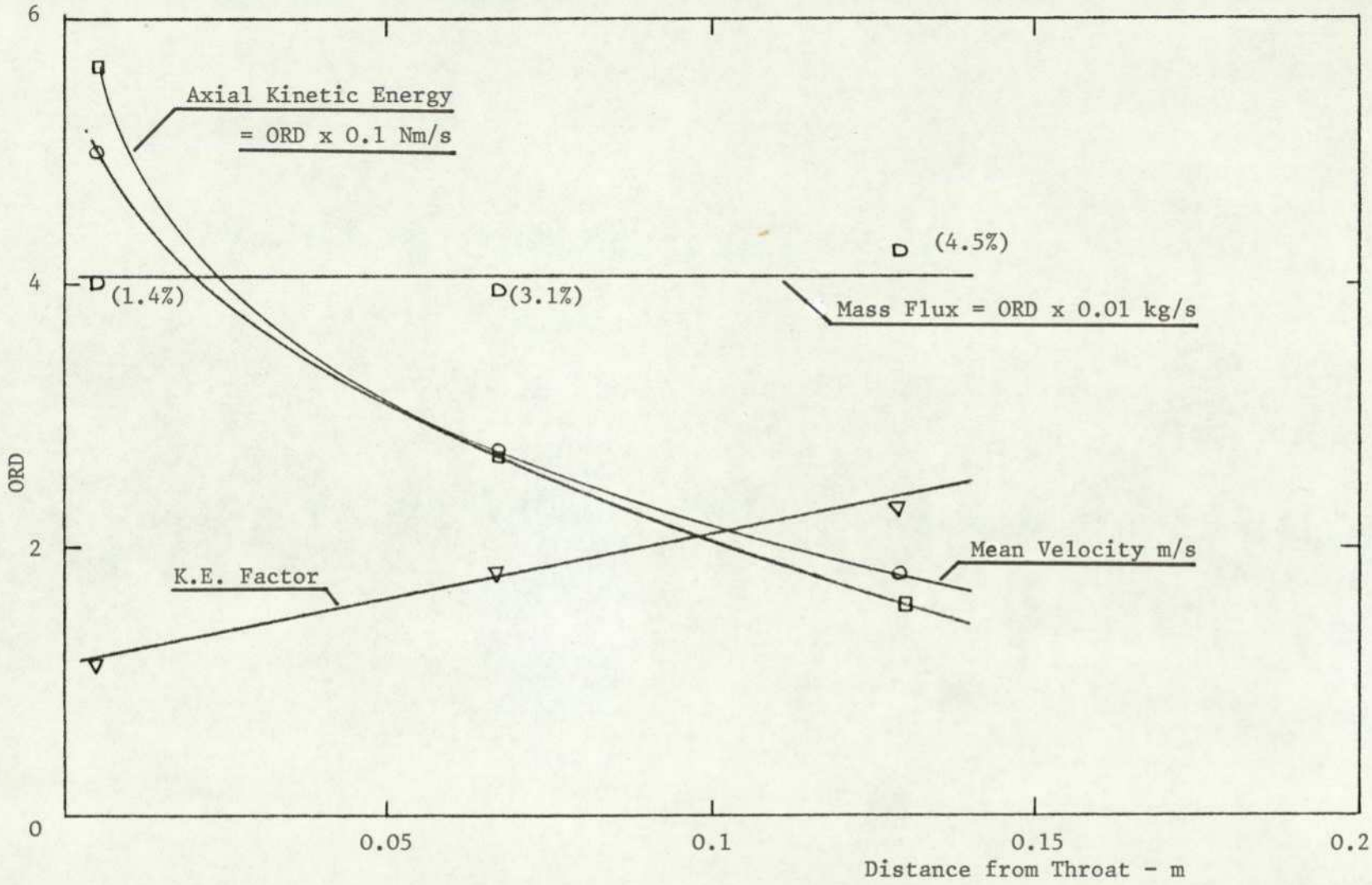

FIG. 6.24 VARIATION OF FLOW PROPERTIES IN 30 DEGREE DIFFUSER WITH SWIRL 2.

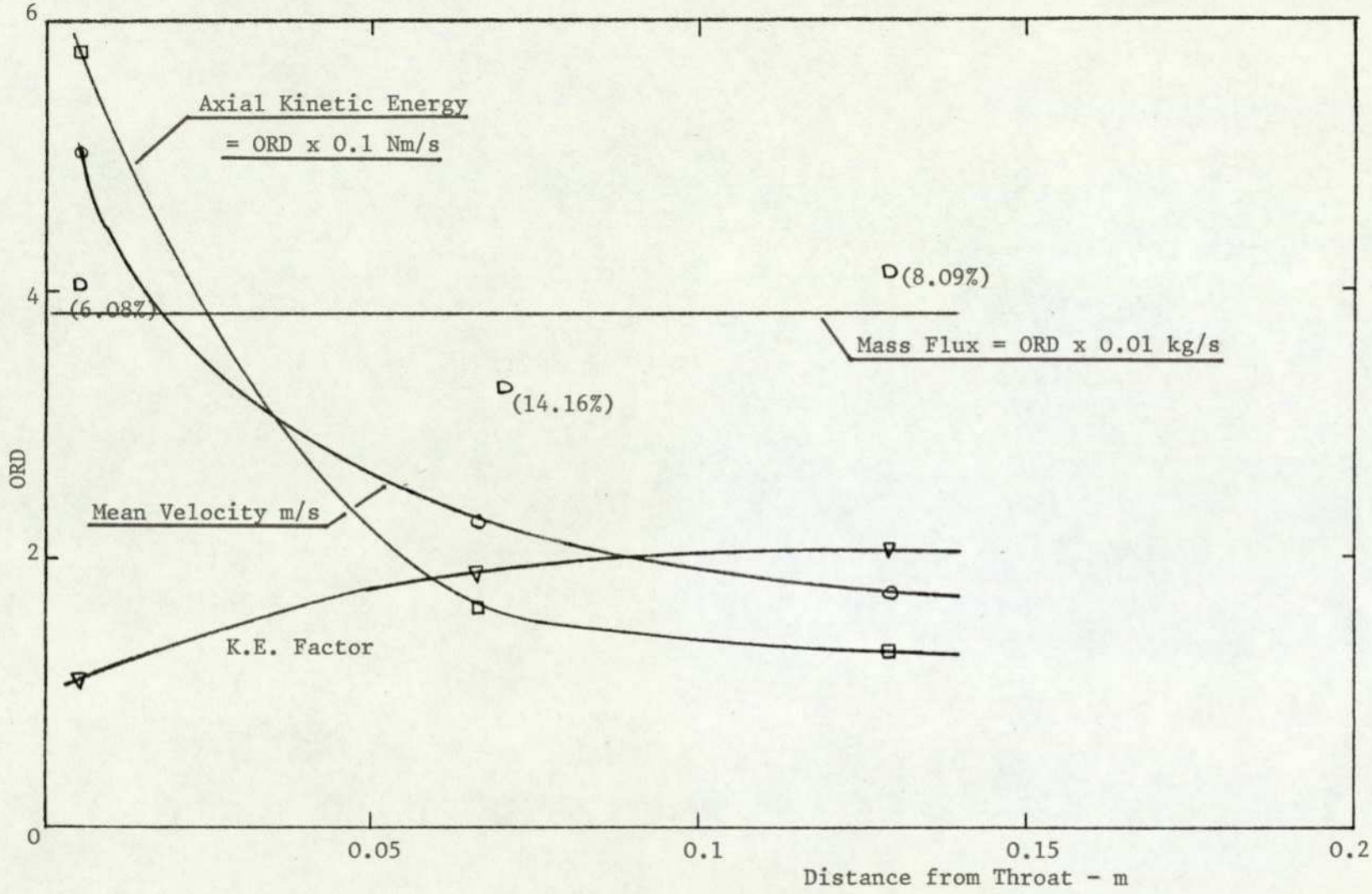

FIG. 6.25 VARIATION OF FLOW PROPERTIES IN 30 DEGREE DIFFUSER WITH SWIRL 3.

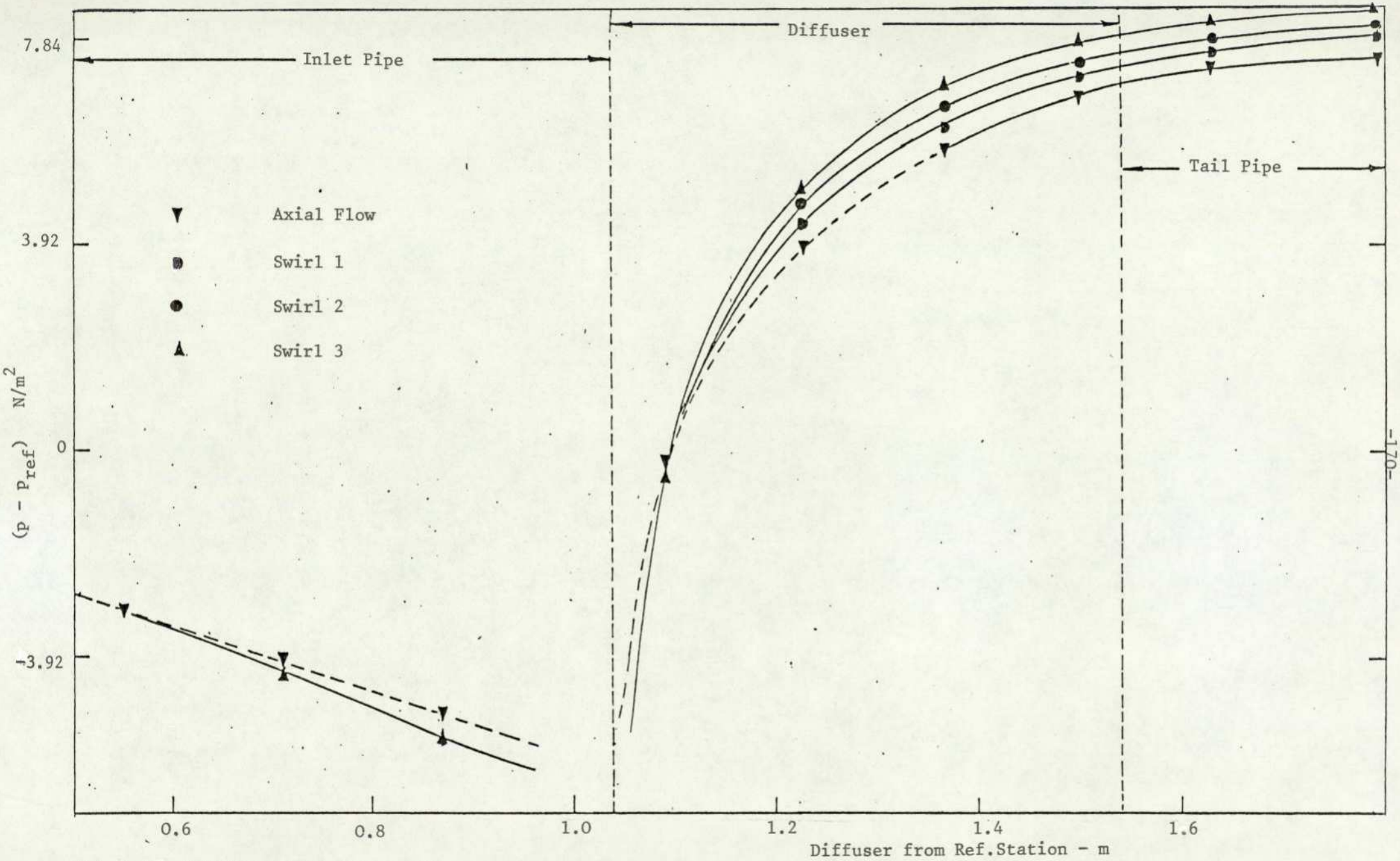

FIG. 6.26 PRESSURE VARIATION IN 10° DIFFUSER-PIPE COMBINATION

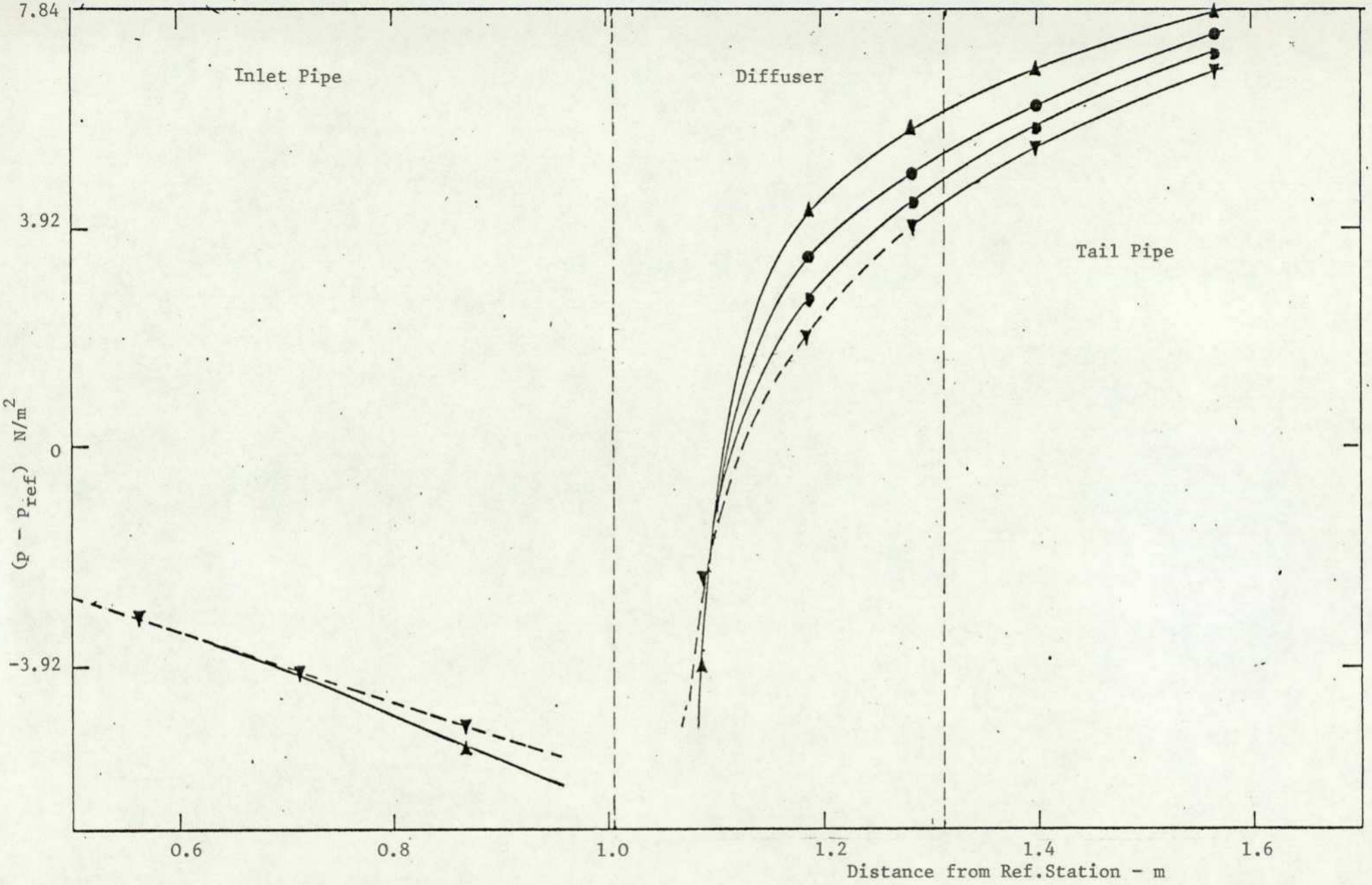

FIG. 6.27 PRESSURE VARIATION IN 20° DIFFUSER-PIPE COMBINATION

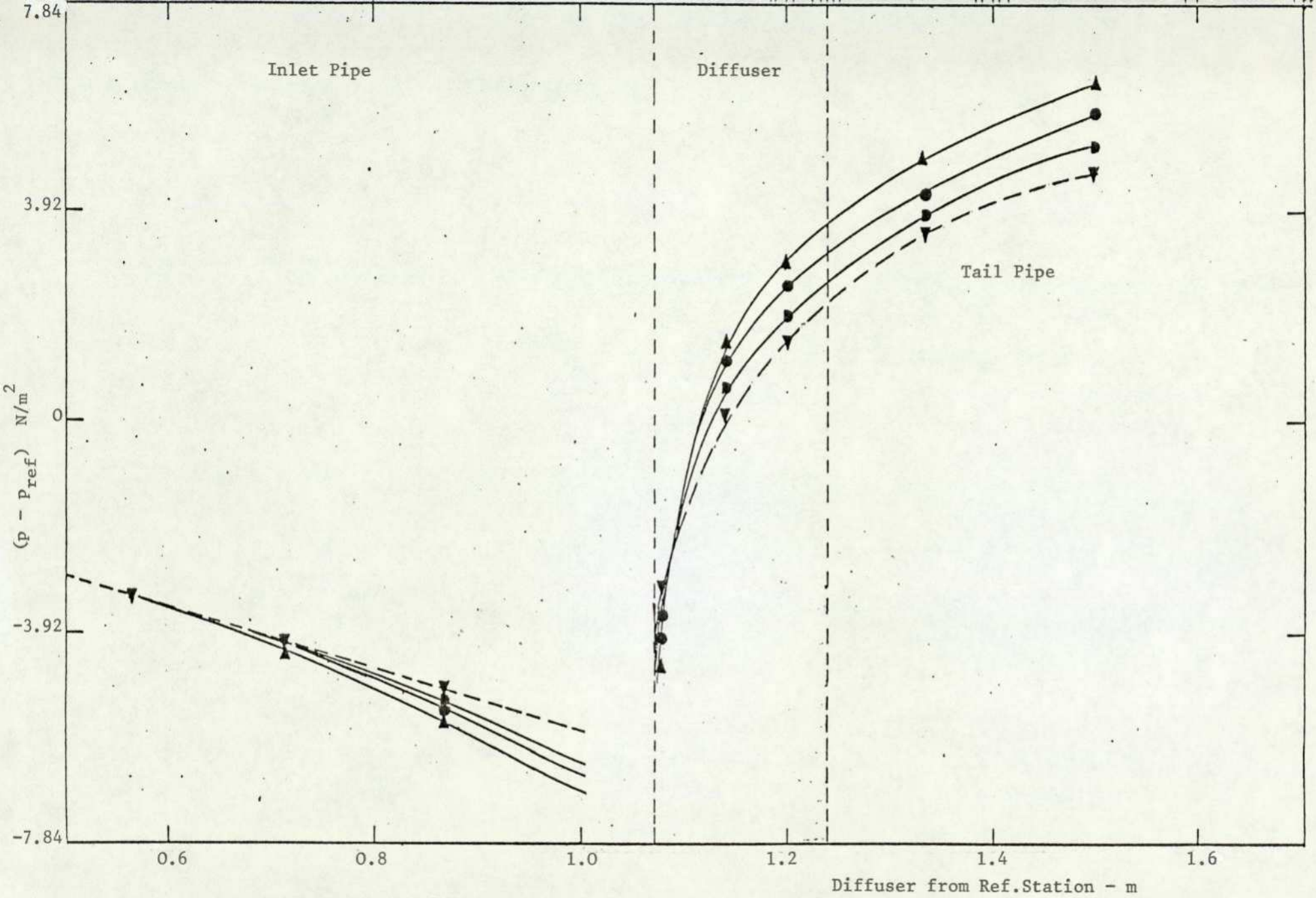

FIG. 6.28 PRESSURE VARIATION IN 30° DIFFUSER-PIPE COMBINATION

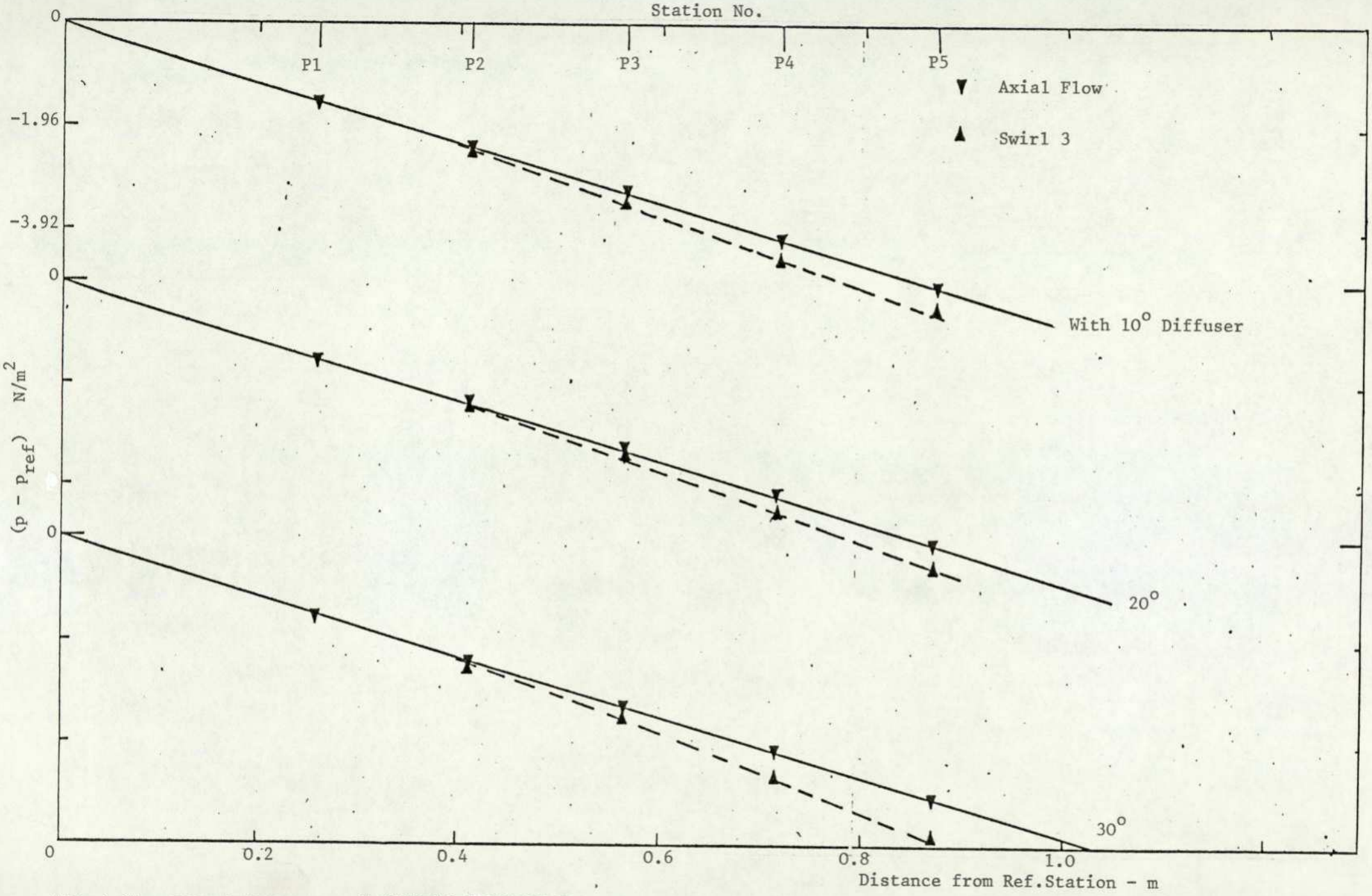

FIG. 6.29 WALL STATIC PRESSURE DROP IN INLET PIPE

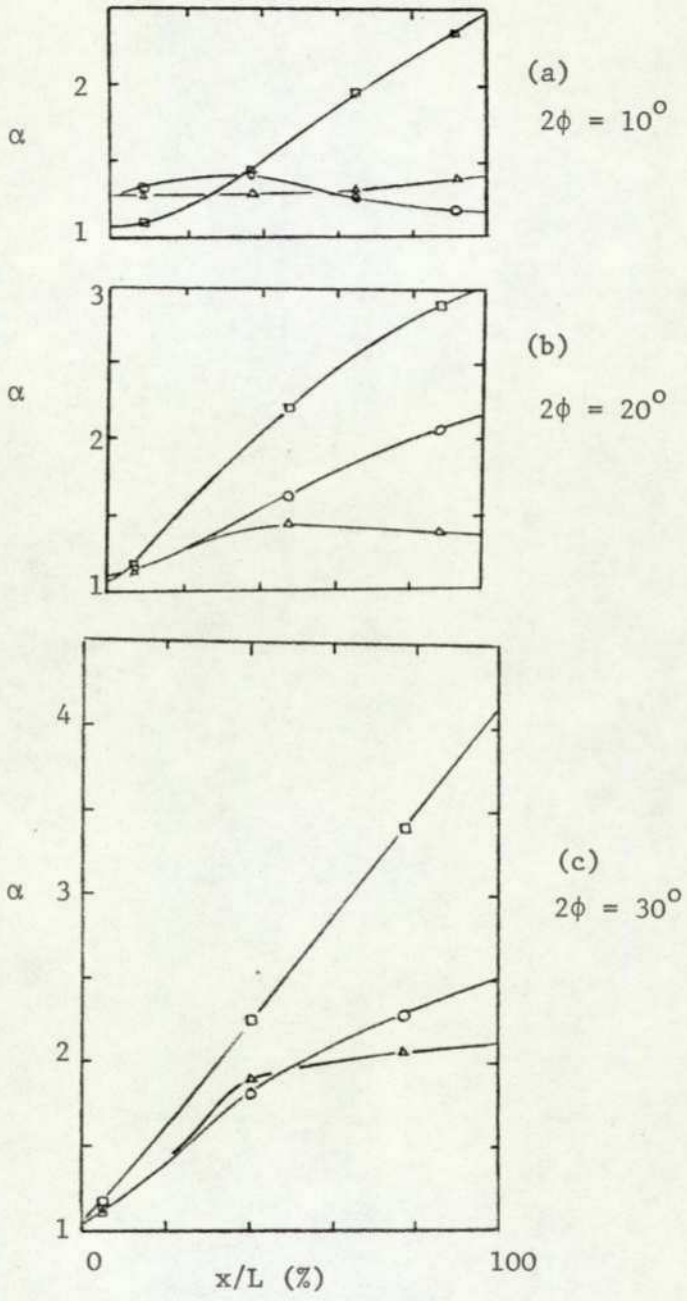

FIG. 6.30 EFFECT OF SOLID-BODY SWIRL ON KINETIC ENERGY FACTOR

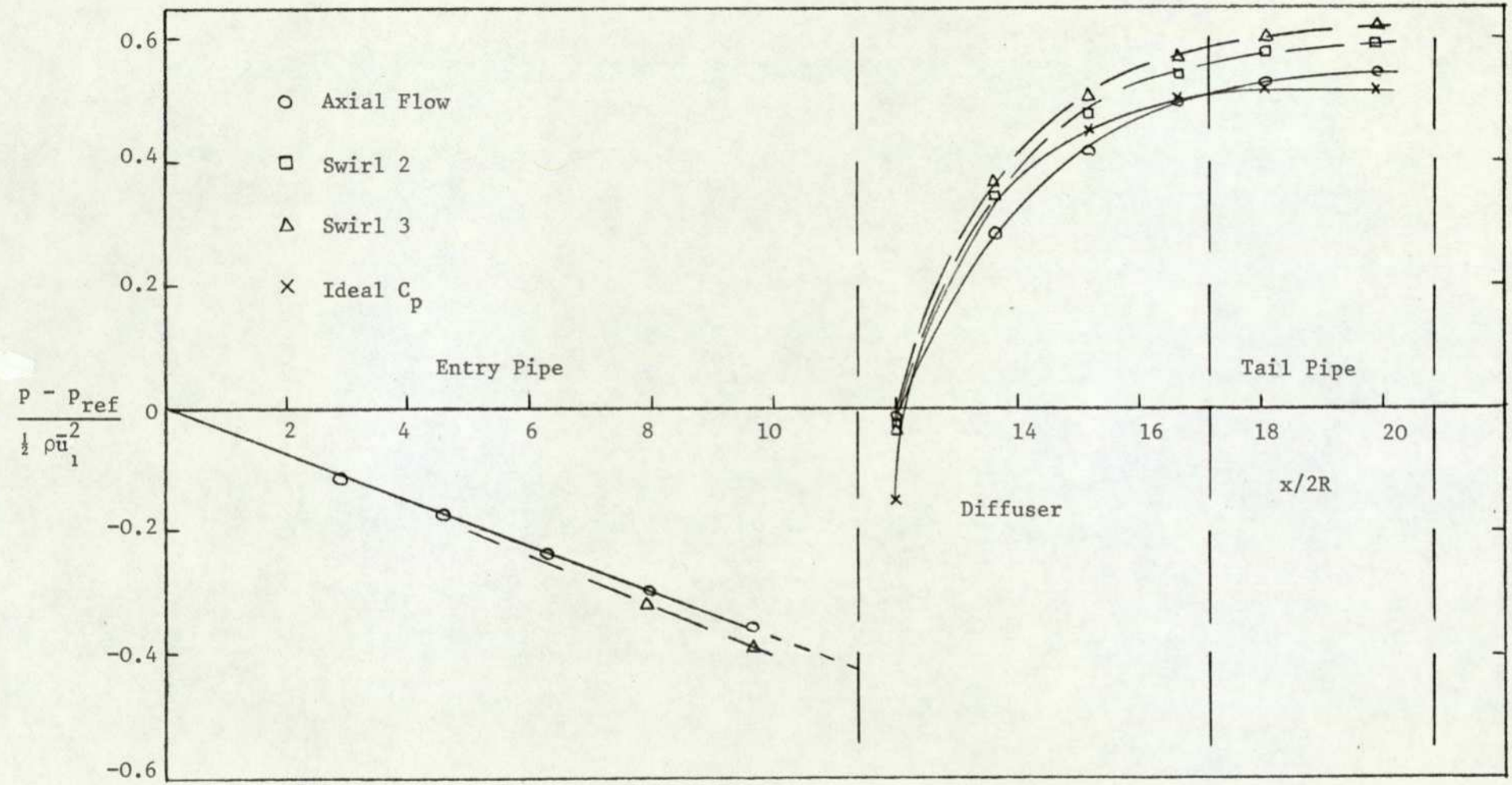

FIG. 6.31 VARIATION OF PRESSURE RECOVERY COEFFICIENT IN 10^{o} DIFFUSER-PIPE COMBINATION.

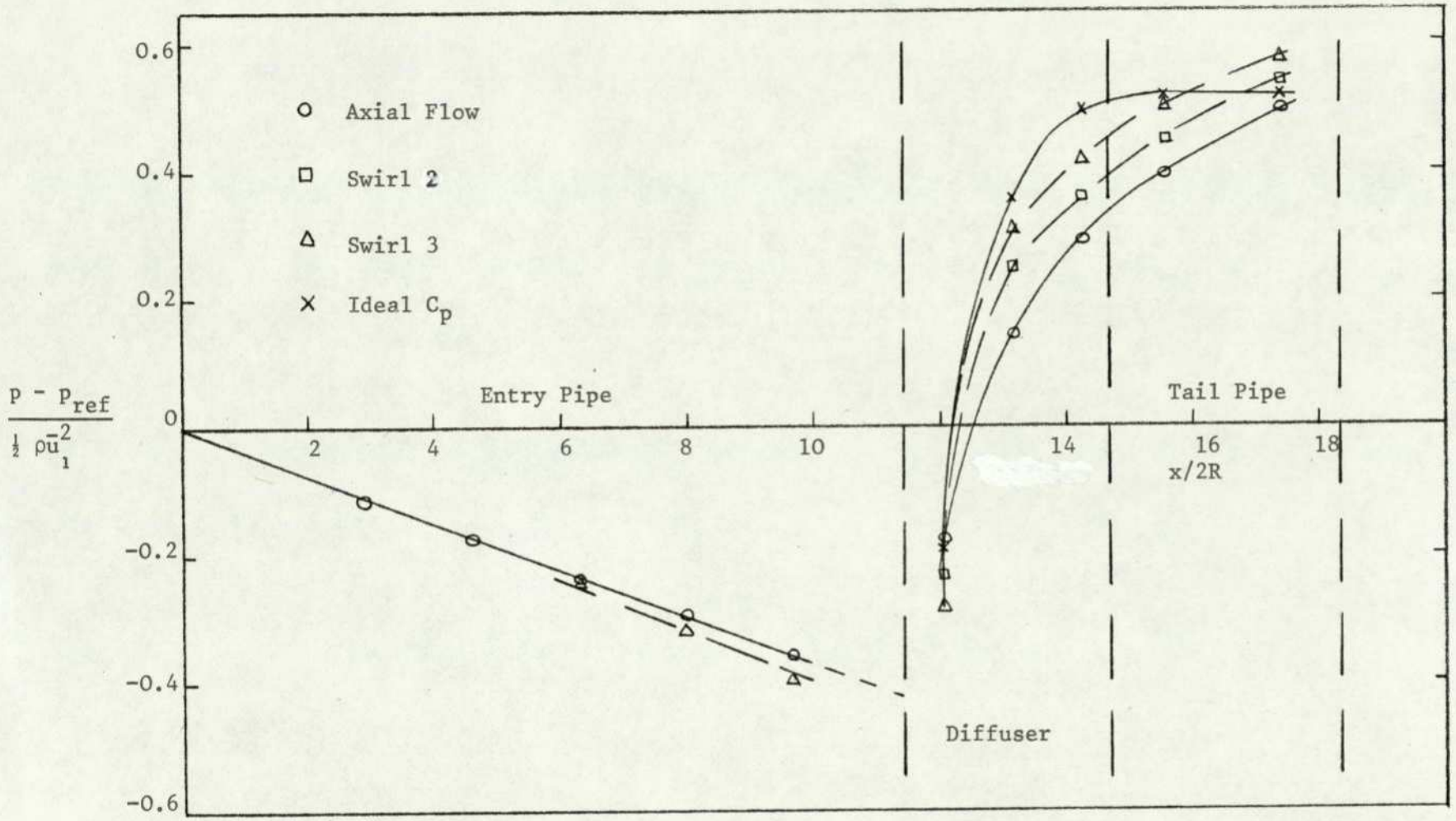

FIG. 6.32 VARIATION OF PRESSURE RECOVERY COEFFICIENT IN 20° DIFFUSER-PIPE COMBINATION

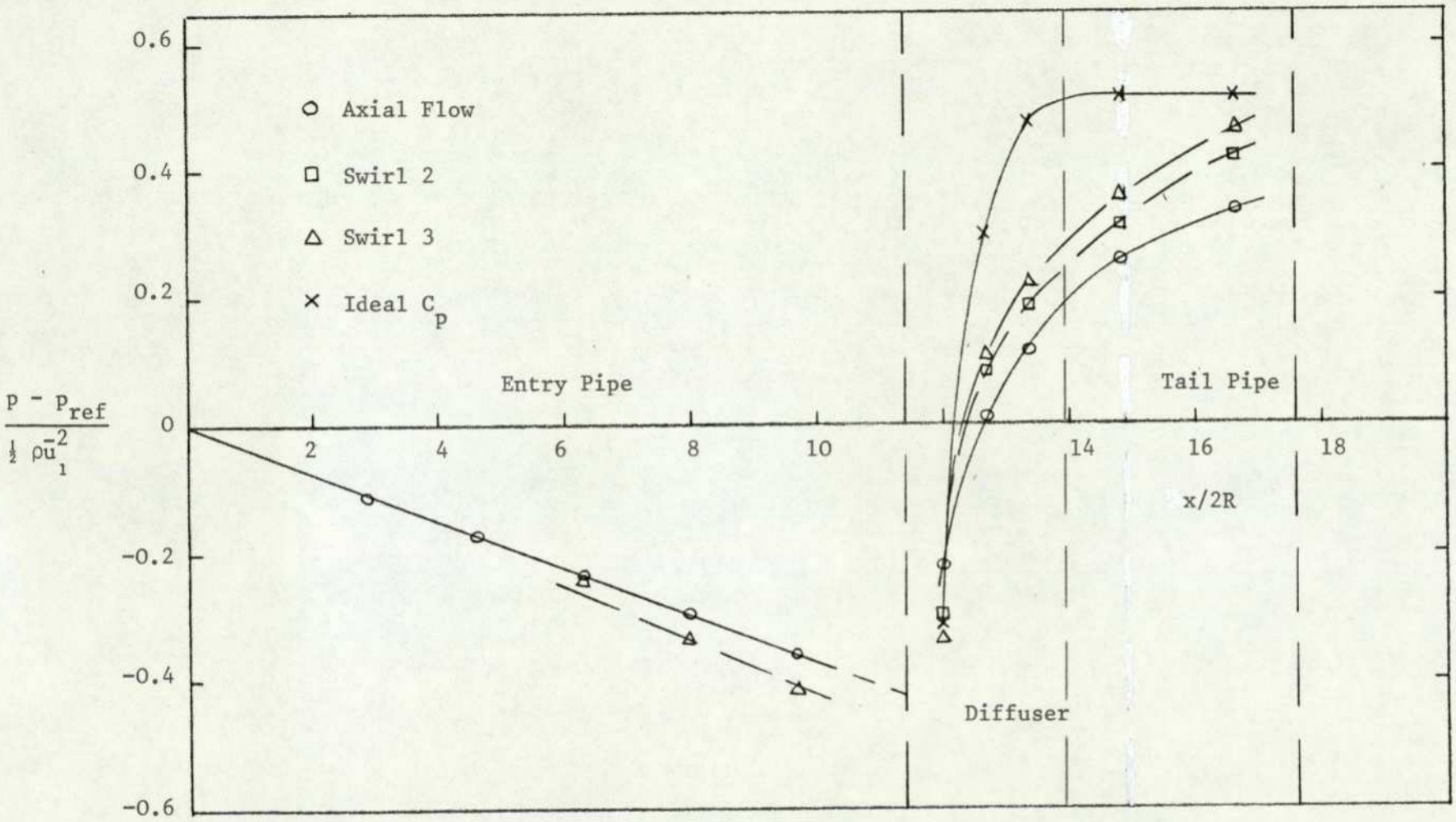

FIG. 6.33 VARIATION OF PRESSURE RECOVERY COEFFICIENT IN 30° DIFFUSER-PIPE COMBINATION.

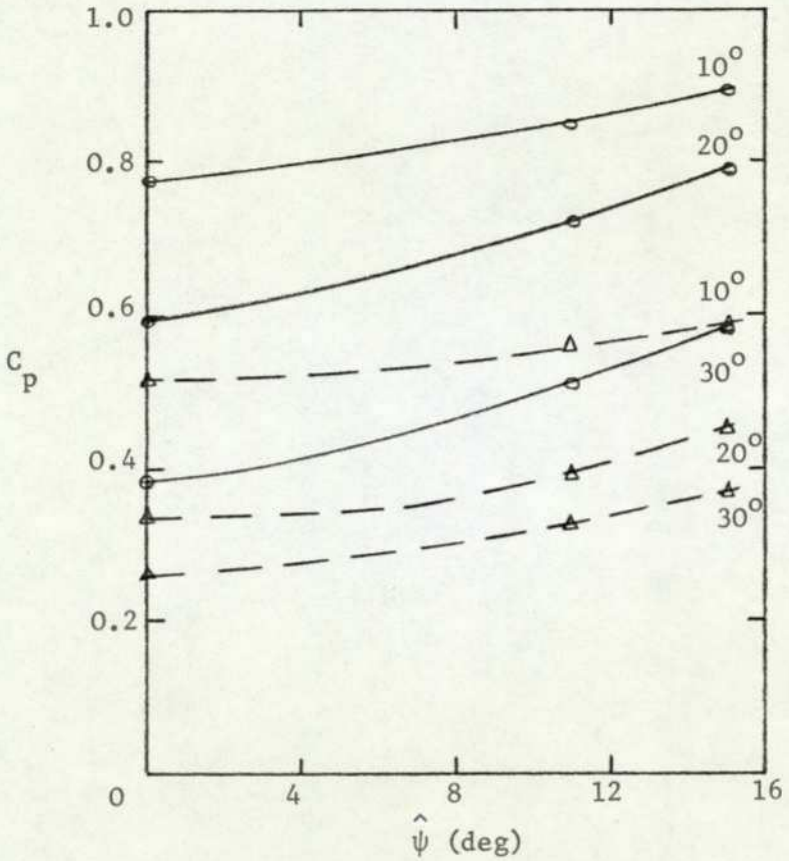

$$C_p = \frac{p_2 - p_1}{\frac{1}{2}\rho\bar{u}_1^2} \qquad C_p = \frac{p_2 - p_{ref}}{\frac{1}{2}\rho\bar{u}_1^2}$$

FIG. 6.34 EFFECT OF SOLID-BODY SWIRL ON DIFFUSER PERFORMANCE.

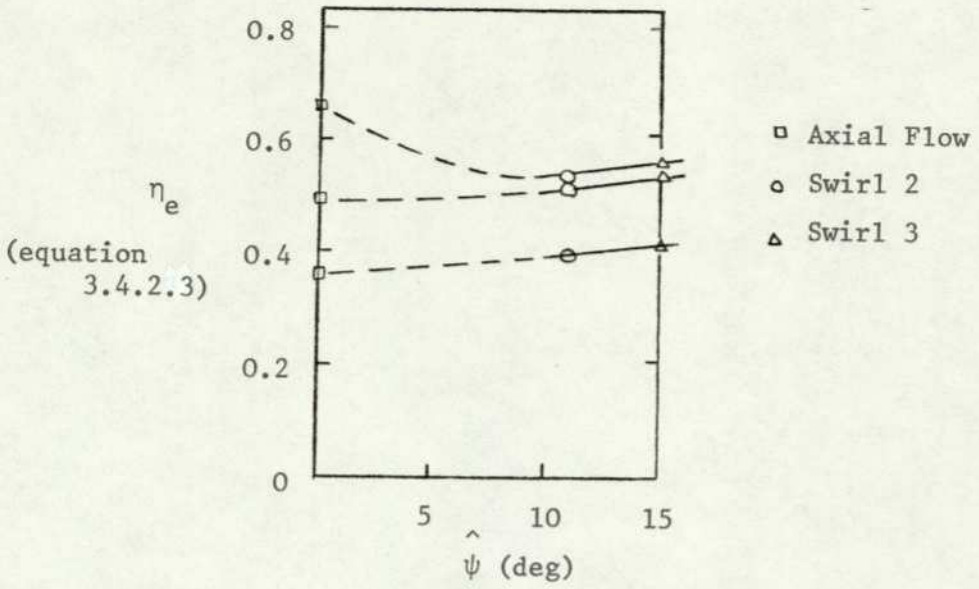

FIG. 6.35 EFFECT OF SOLID-BODY SWIRL ON EFFICIENCY (EQUATION 3.4.2.3)

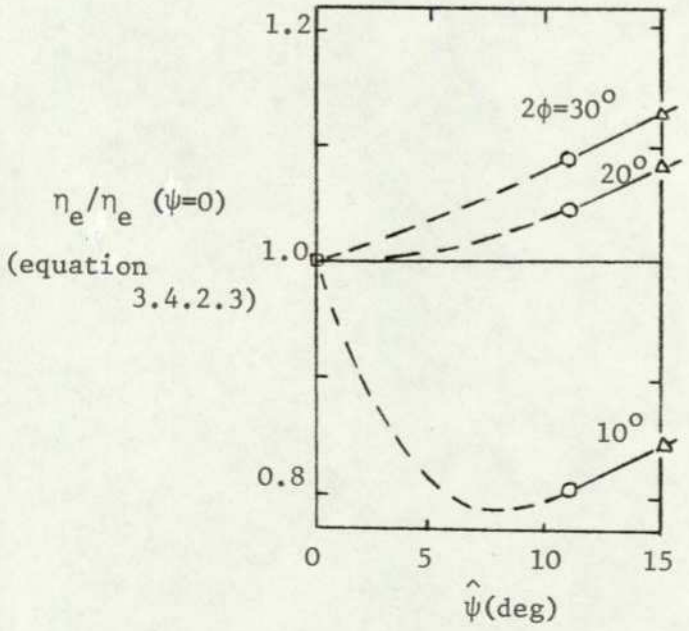

FIG. 6.36 EFFECT OF SOLID-BODY SWIRL ON EFFICIENCY (EQUATION 3.4.2.3)

CHAPTER SEVEN

PERFORMANCE OF FREE VORTEX GENERATOR

7.1 INTRODUCTION

Preliminary studies were conducted to investigate the possibility of designing a free vortex generator. This was to take the form of a radial-to-axial intake. Specialists were consulted and some exploratory calculations were made. Chapter Four, section (4.6) gives details of design parameters of the free vortex generator. Figs.(4.8) and (4.9) show the main features of the generator.

Having designed and manufactured the free vortex generator, great task lay ahead. Its performance needed to be evaluated and information regarding how the configuration with respect to number of blades, blade angle would affect the generation of tangential velocity profile and the flow in pipe-diffuser combination needed to be found.

The above evaluation would be necessary in setting suitable guide lines for the experimental work to follow in relation to the time scale and the limitations imposed by various factors.

The next sections deal with how the above objectives were achieved. All the experimental work was conducted at an entry Reynolds number of 28.4×10^3.

7.2 DESCRIPTION OF THE EXPERIMENTAL APPARATUS

The arrangement shown in Fig.(4.5c) was used for all the experiments with air as the flow medium. The five-hole pressure probe, with associated instrumentation was used for flow measurements. A detailed description of the free vortex generator is provided in Chapter Four, section (4.6.3). The bell-mouth section of the rig was replaced by the free vortex generator, without change in the entry length to the diffusers.

The honeycomb flow straightener was removed since this would no longer serve the purpose. The blades of the generator were individually set by a special blade jig, Fig.(4.10). Mean flow rate (constant) was measured using an orifice plate with carbon tetrachloride manometer, Fig.(4.22).

7.3 WALL STATIC PRESSURE MEASUREMENTS AND TANGENTIAL VELOCITY PROFILES

From the previous chapter, it is evident that wall static pressure measurements played a key part in assessing diffuser performance. This idea can be used to evaluate the performance of the free vortex generator and to find the geometrical configuration of the generator which has an optimum favourable effect on the 10^{o} to 30^{o} diffuser. This section is devoted to achieve the above objectives.

The wall static pressure measurements were found to be relatively straight forward. Unsteady readings were observed, but the time domain analyser averaged it out in about 6 minutes. The static pressure measurements were made with respect to a reference pressure. The measuring stations correspond to those in Fig.(4.3). There was no measurable decay of swirl in the pipe between the generator and the diffuser; hence swirl measurements were made at entry to the 10^{o} diffuser.

From Figs.(7.1a) and (7.1b) it is evident that, for 16 blades of the vortex generator, the blade angle of 6^{o} (radial direction) has the strongest effect on the 10^{o} diffuser-pipe combination. The flow in the diffuser deteriorates with further increase in the blade angle. It is also evident from Figs.(7.2a) and (7.2b) that for 8 blades, a blade angle of 6^{o} has the strongest effect too, relative to 0^{o} blade angle on the 10^{o} diffuser-pipe.

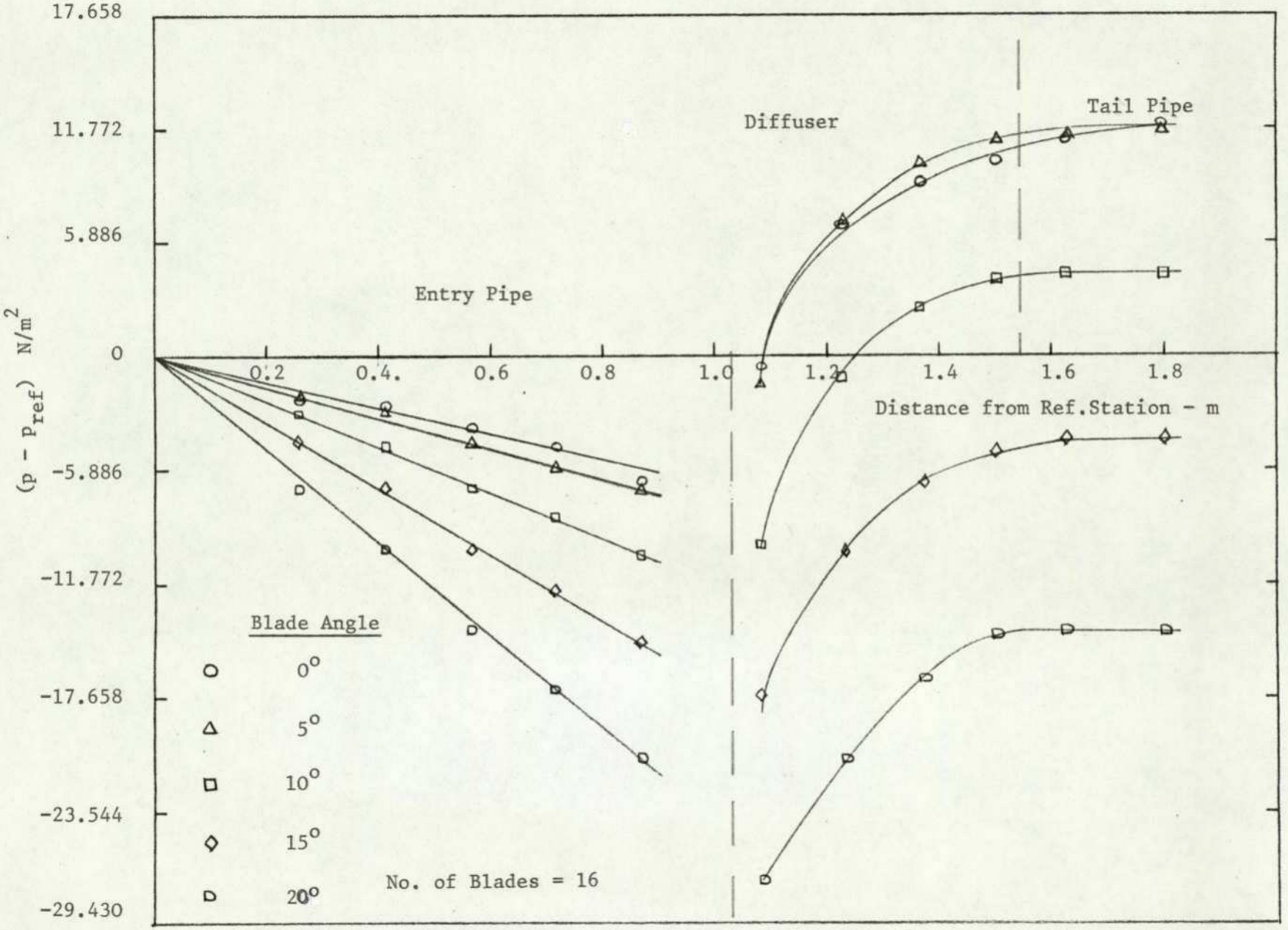

FIG. 7.1a VARIATION OF PRESSURE IN 10° DIFFUSER-PIPE COMBINATION

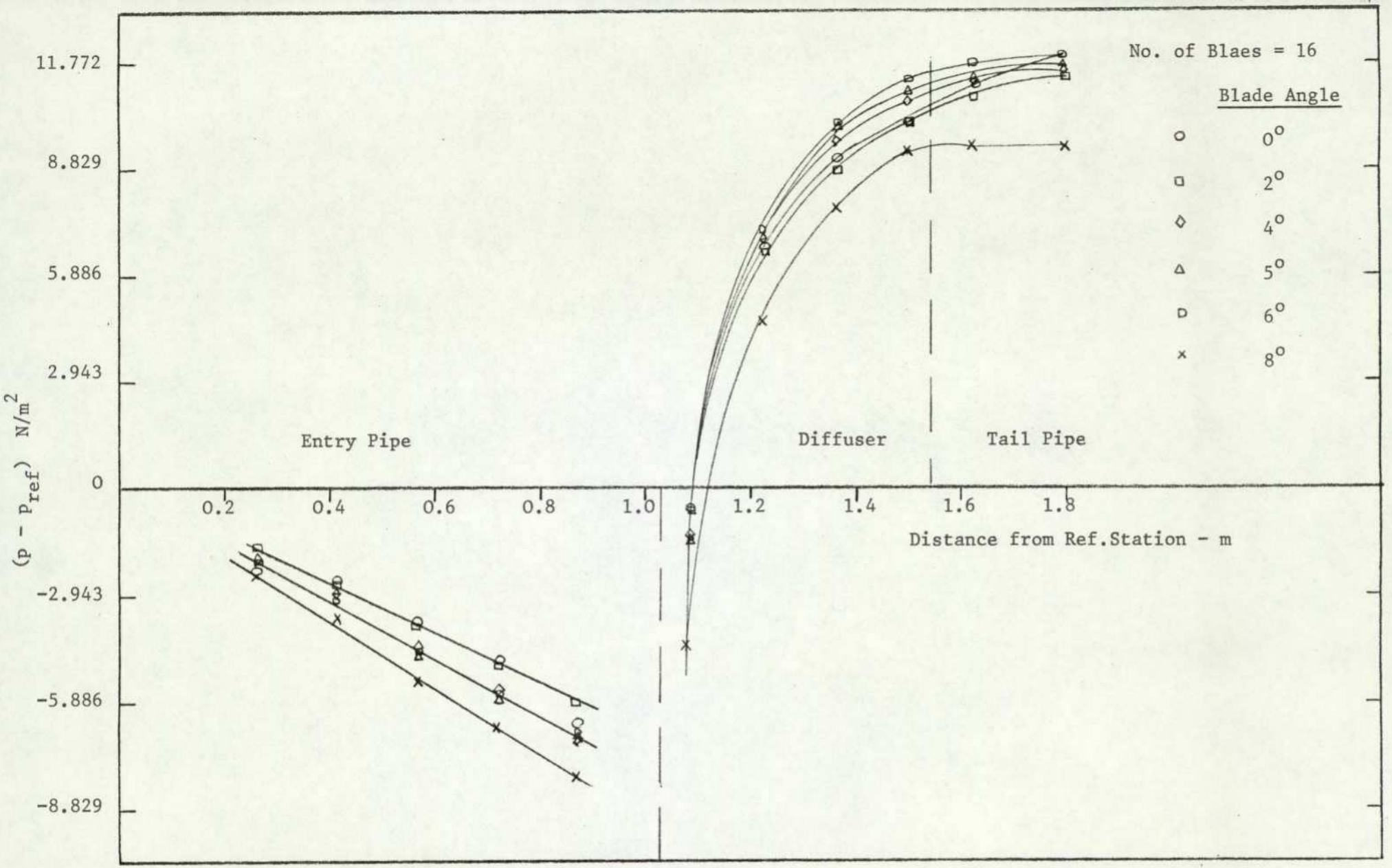

FIG. 7.1b VARIATION OF PRESSURE IN 10° DIFFUSER-PIPE COMBINATION

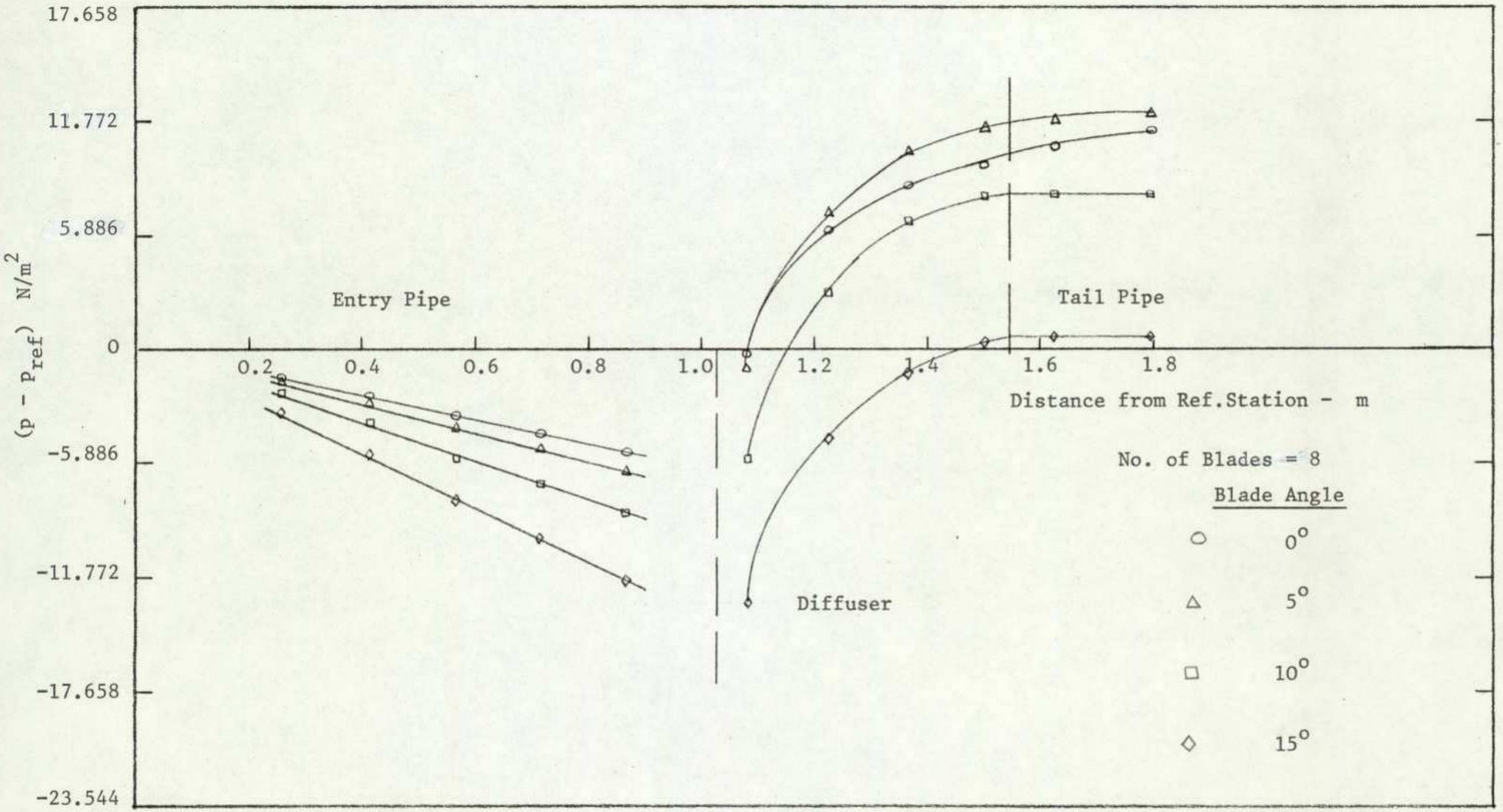

FIG. 7.2a VARIATION OF PRESSURE IN 10° DIFFUSER-PIPE COMBINATION

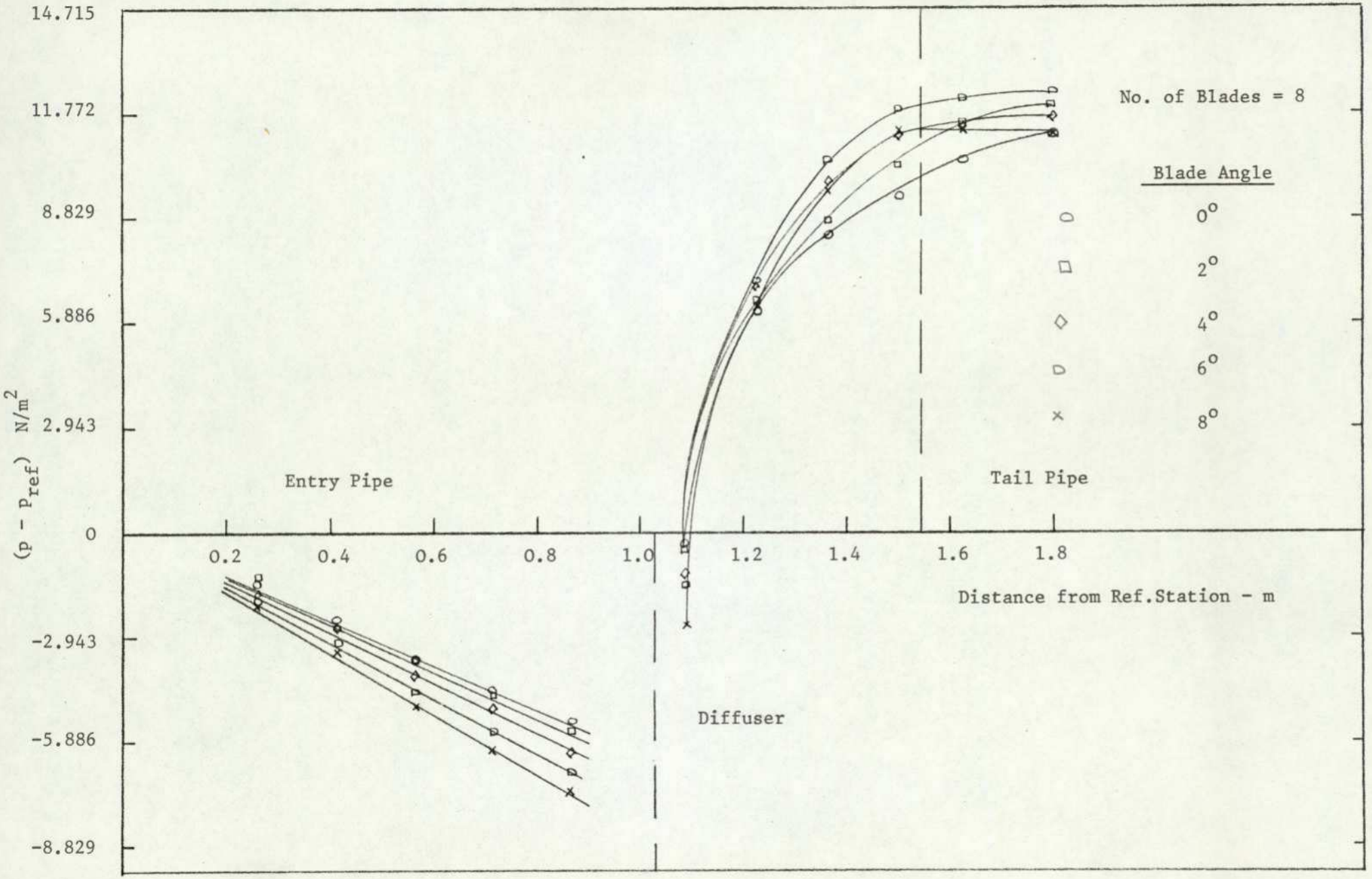

FIG. 7.2b VARIATION OF PRESSURE IN 10° DIFFUSER-PIPE COMBINATION

As a consequence of above analysis, an interesting question develops: Which of the above two configurations produced the most favourable effect on the diffuser? In terms of C_p, the use of eight blades is considered better than sixteen, Fig.(7.3).

Fig.(7.4) and Fig.(7.5) show the tangential velocity distribution at the 10^o diffuser inlet, for 6^o blade angle and 16 and 8 blades respectively. It is absolutely clear that 8 blades generate a better Rankine vortex tangential velocity profile than 16 blades. Fig.(7.4) shows that tangential velocity distribution is considerably weaker at the wall, thus defeating the object of the vortex generator. Further reduction in number of blades could not be made because of design limitations.

The pressure distribution in the 20^o and 30^o diffuser-pipe combinations for different blade angles of the vortex generator (number of blades being 8) is shown in Fig.(7.6) and Fig.(7.7). The measurements are recorded in Table (7/1) to Table (7/4).

7.4 DISCUSSION

In finding the performance of the free vortex generator, velocity measurements were conducted at the inlet section of the 10^o diffuser. A study of the decay of the Rankine vortex swirl in the inlet pipe was not pursued as variation between two stations was not measurable. The governing equation for swirling pipe flow was solved by Hall (68), numerically, and showed that swirl velocity decays to 0.33 of its initial value in about 100 radii. From the analysis, it was evident that an 8 blade vortex generator, generates a better Rankine vortex swirl velocity distribution than 16 blades.

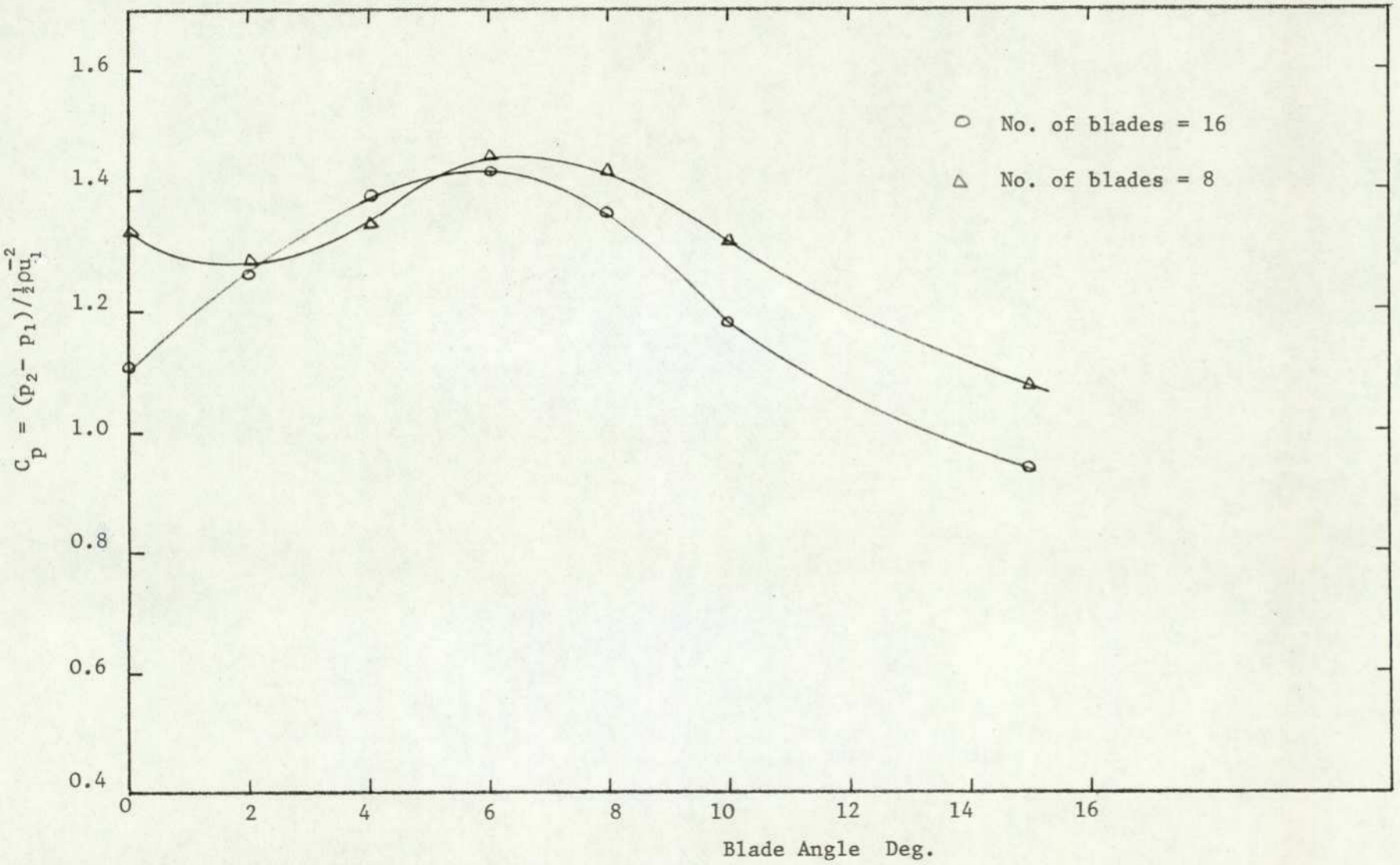

FIG. 7.3 EFFECT OF C_p ON NUMBER OF BLADES OF FREE VORTEX GENERATOR

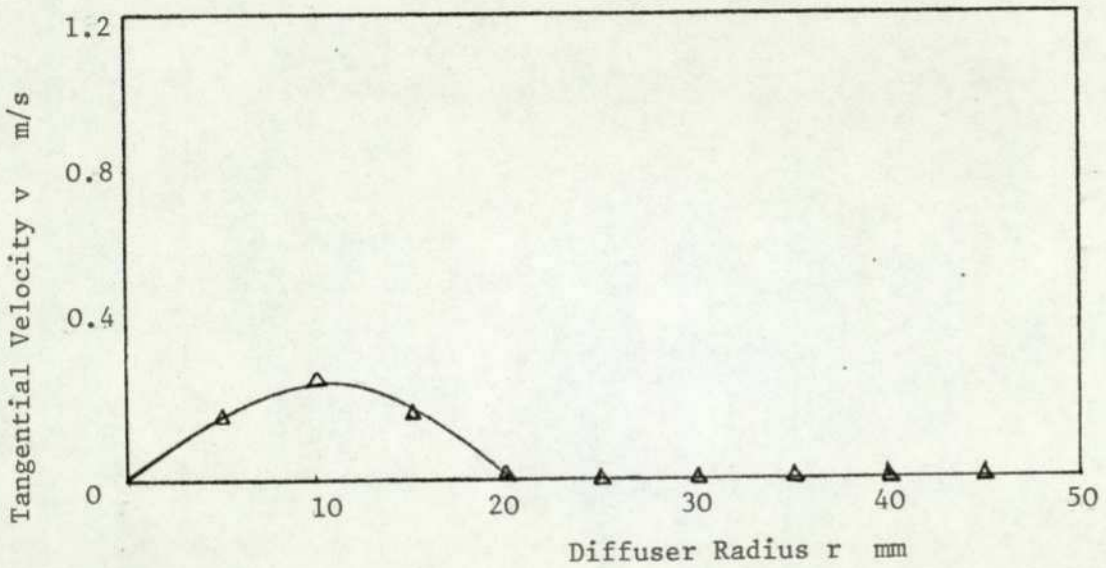

No. of blades = 16

Blade angle = 6^{o}

Measuring station P5

$\bar{u}$ = 5·054 m/s

FIG. 7.4 EFFECT OF 16 BLADES OF FREE VORTEX GENERATION ON TANGENTIAL VELOCITY DISTRIBUTION

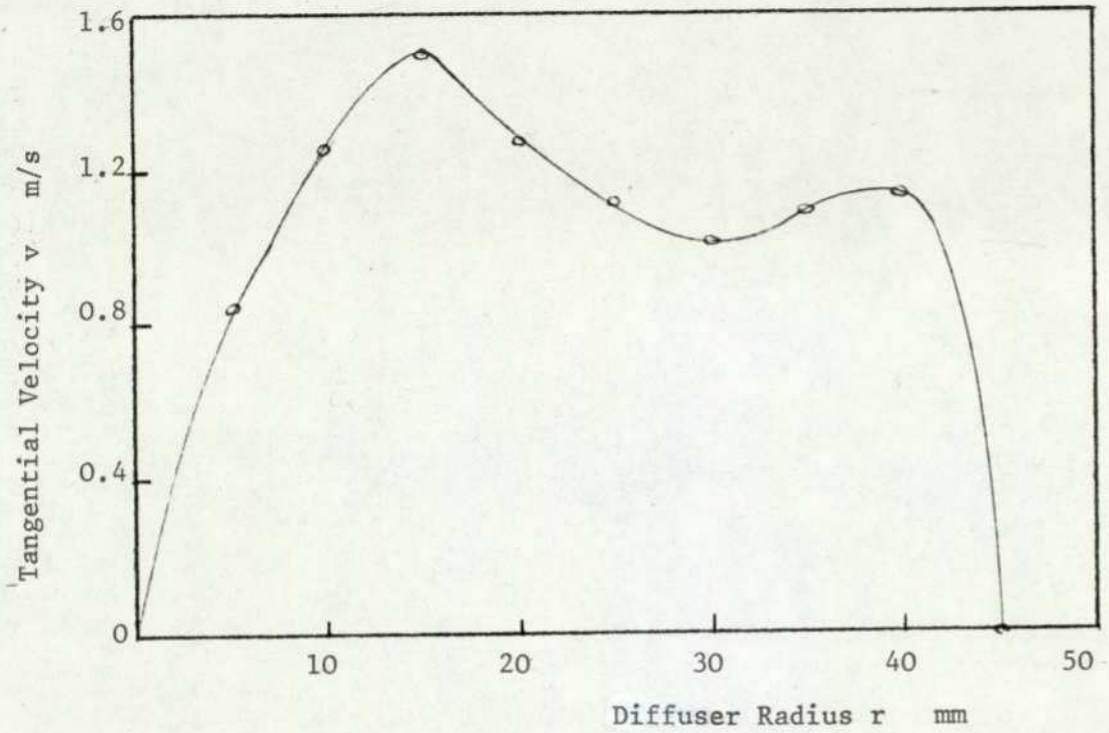

No. of blades = 8

Blade angle = 6^{o}

Measuring station P5

$\bar{c}$ = 4·912 m/s

FIG. 7.5 EFFECT OF 8 BLADES OF FREE VORTEX GENERATOR ON TANGENTIAL VELOCITY DISTRIBUTION

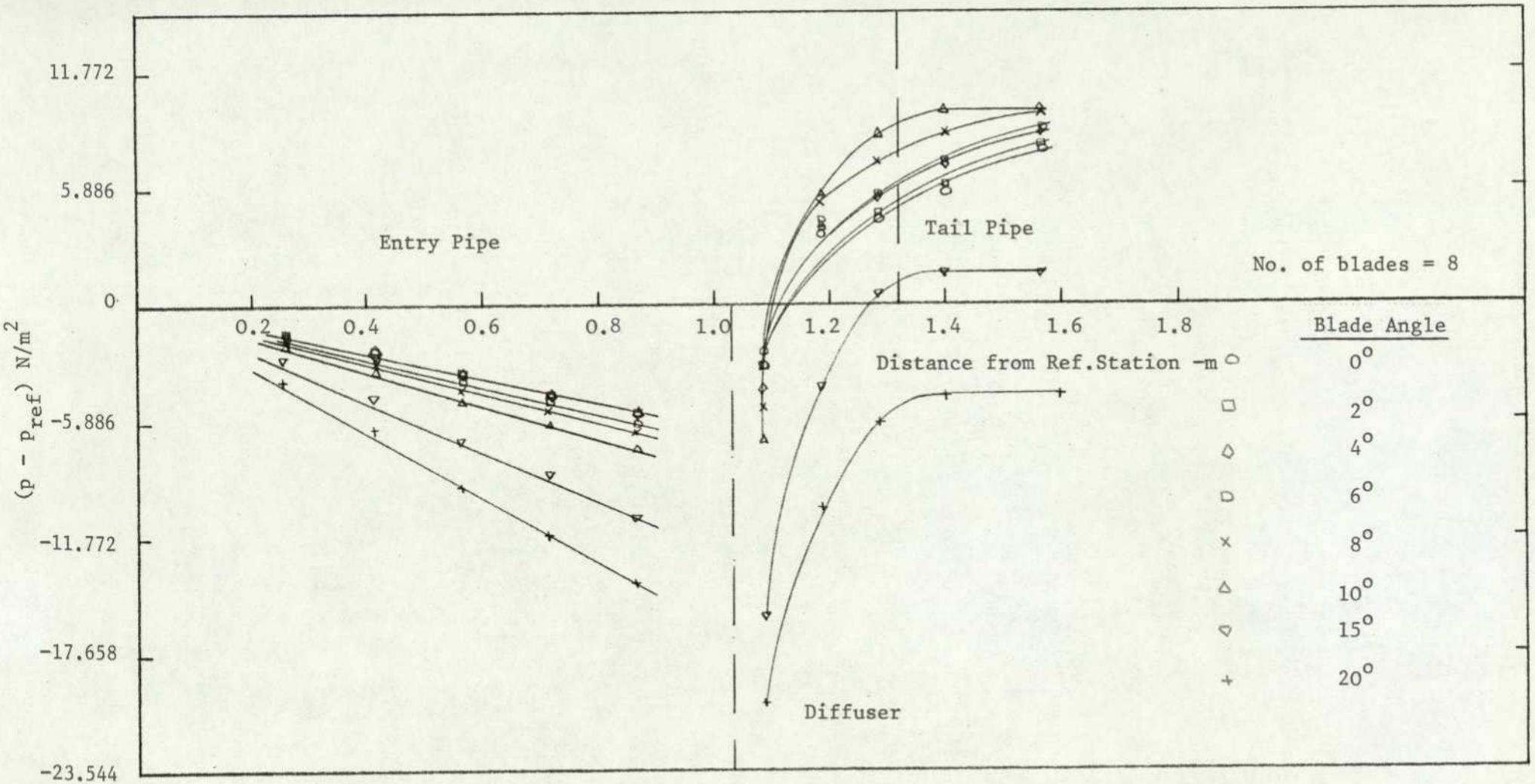

FIG. 7.6 VARIATION OF PRESSURE IN 20° DIFFUSER-PIPE COMBINATION

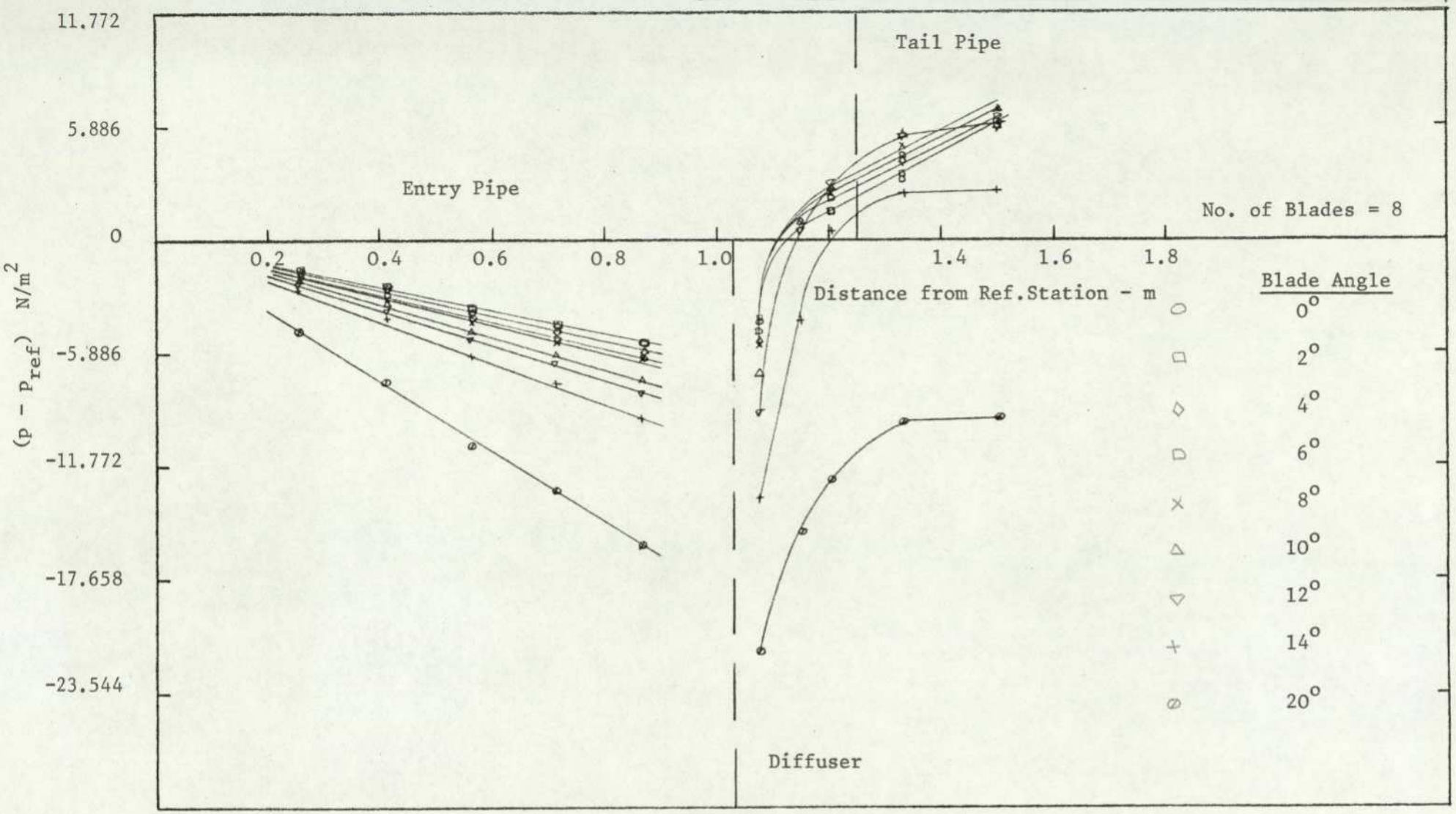

FIG. 7.7 VARIATION OF PRESSURE IN 30° DIFFUSER-PIPE COMBINATION

From the curves of wall static pressure variation along the test section, it was seen that the presence of Rankine vortex swirl modified the pressure drop in the pipe. It also indicates that for the diffusers tested, there is an optimum blade angle setting in the vortex generator, which has the most favourable effect on diffuser flow. When the blade angle is set above the optimum angle, the flow in the diffuser deteriorates. The optimum blade angle was found to be 6^{o} for the 10^{o} diffuser and 10^{o} for both the 20^{o} and 30^{o} diffusers.

7.5 CONCLUSIONS

The primary object was to evaluate the performance of the free vortex generator and to set suitable guide lines for the experimental work to follow. The analysis satisfies the objectives set out.

The analysis indicates that the optimum blade angle of the vortex generator, which optimises diffuser performance are as follows:

For the 10^{o} diffuser, the blade angle was 6^{o}
For the 20^{o} diffuser, the blade angle was 10^{o}
For the 30^{o} diffuser, the blade angle was 10^{o}

see page 273a for suggested vortex strength

The flow in the diffuser deteriorates when the blade angle of the vortex generator was set above its respective optimum angle.

The static pressure distribution in the pipe was modified by the presence of Rankine vortex swirl velocity distribution superimposed on axial flow.

CHAPTER EIGHT

FLOW VISUALIZATION TEST - RANKINE VORTEX

8.1 INTRODUCTION

Chapter Seven formulated suitable guide lines for the experimental work. The object of this programme is to execute them from a flow visualization point of view and to arrive at qualitative deductions as to the effect of Rankine vortex swirl on wide angle diffuser flows.

The flow visualization analysis has advantages and disadvantages, which are very well defined in Chapter Five, but it is important to note that the observation studies can only provide an instantaneous assessment of the behaviour and neither after-study nor close scrutiny is possible and furthermore it is subject to human error. The main classification of flow visualization techniques are included in Chapter Five, section (5.2) for completeness. The technique used in this programme is the same as that of Chapter Five.

To gain a broader understanding, it was necessary to divide the tests into a number of parts, i.e. flow in the vortex generator, flow in the entry pipe and extend the investigation to study the effect of an adverse pressure gradient on the flow. In the main, deductions were made purely from observations and photographs are provided to supplement the discussions.

As far as the author is aware, the present study is the only one to attempt to investigate and photograph highly turbulent flow in pipes and wide angle diffusers with different degrees of Rankine vortex type swirl.

All the tests were carried out at an entry Reynolds number of 28.4×10^3.

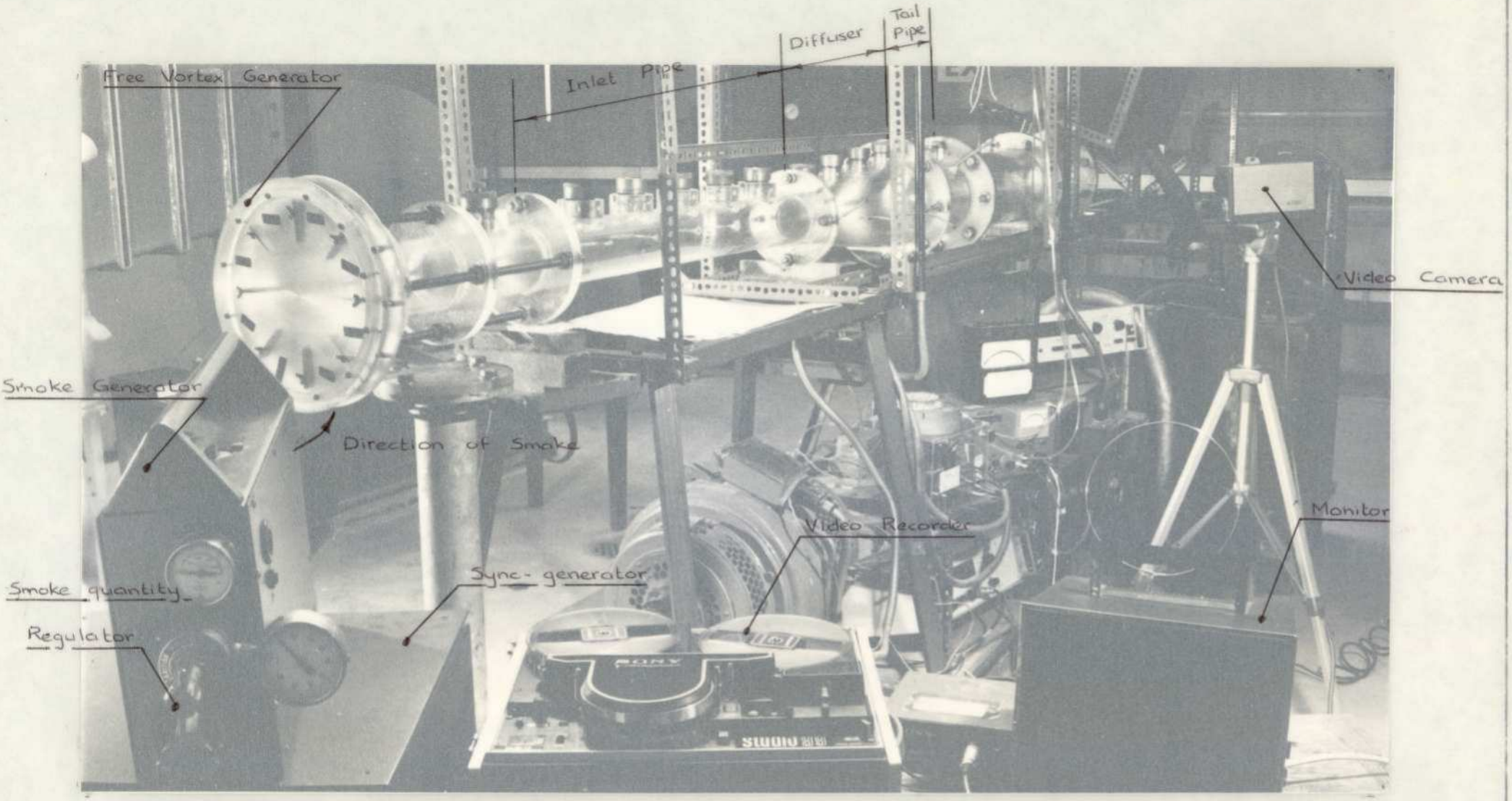

FIG. 8.1 LAYOUT OF RIG WITH FREE VORTEX GENERATOR, SMOKE GENERATOR AND VIDEO SET UP

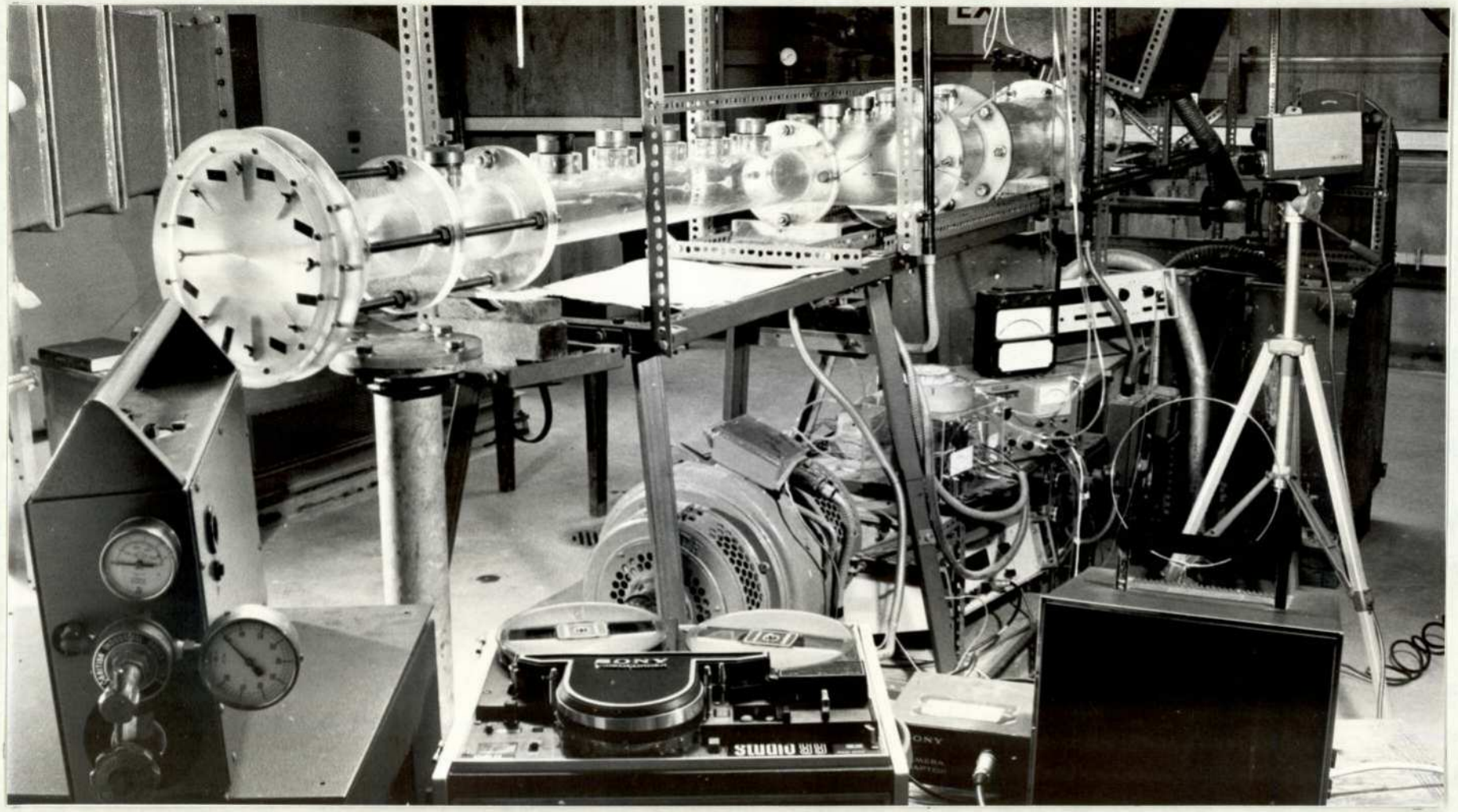

FIG. 8.1 LAYOUT OF RIG WITH FREE VORTEX GENERATOR, SMOKE GENERATOR AND VIDEO SET UP

8.2 EXPERIMENTAL APPARATUS

The arrangement shown in Fig.(8.1) was used for all the experiments with air as the flow medium. The mean flow rate was measured using an orifice plate with a carbon tetrachloride manometer, Fig(4.22). The Rankine vortex was generated by the vortex generator (8 blades). The jig shown in Fig.(4.10) was used to set the blade angles of the generator. The smoke was induced through the vortex generator, and its deposit in the working section was thoroughly cleaned at the end of each test.

8.3 EXPERIMENTAL WORK

The observations of the tests were recorded on a video-tape recorder. With its still picture facility, photographs of instances were taken. The electronic signal processing problems were already solved (Chapter Five), thus the task of recording flow visualization tests was straight-forward.

The flow visualization tests were carried out in pipe-diffuser combinations. Three different conical diffusers were used: 10^{o}, 20^{o} and 30^{o}. Each test (i.e. a test per diffuser) was carried out in three parts. The first and second part relates to the behaviour of Rankine vortex swirl in pipe, while the third part relates to diffuser and tail pipe. Different Rankine vortex swirl strengths were generated by altering the blade angle of the vortex generator. For the purpose of studying the effect of swirl on the performance of the diffuser, a fixed flow rate was maintained. The smoke deposit on the walls of the test-section thus obscuring the view prevented running the test rig for more than 45 minutes.

FIG. 8.2 ARRANGEMENT OF PHOTOGRAPHY

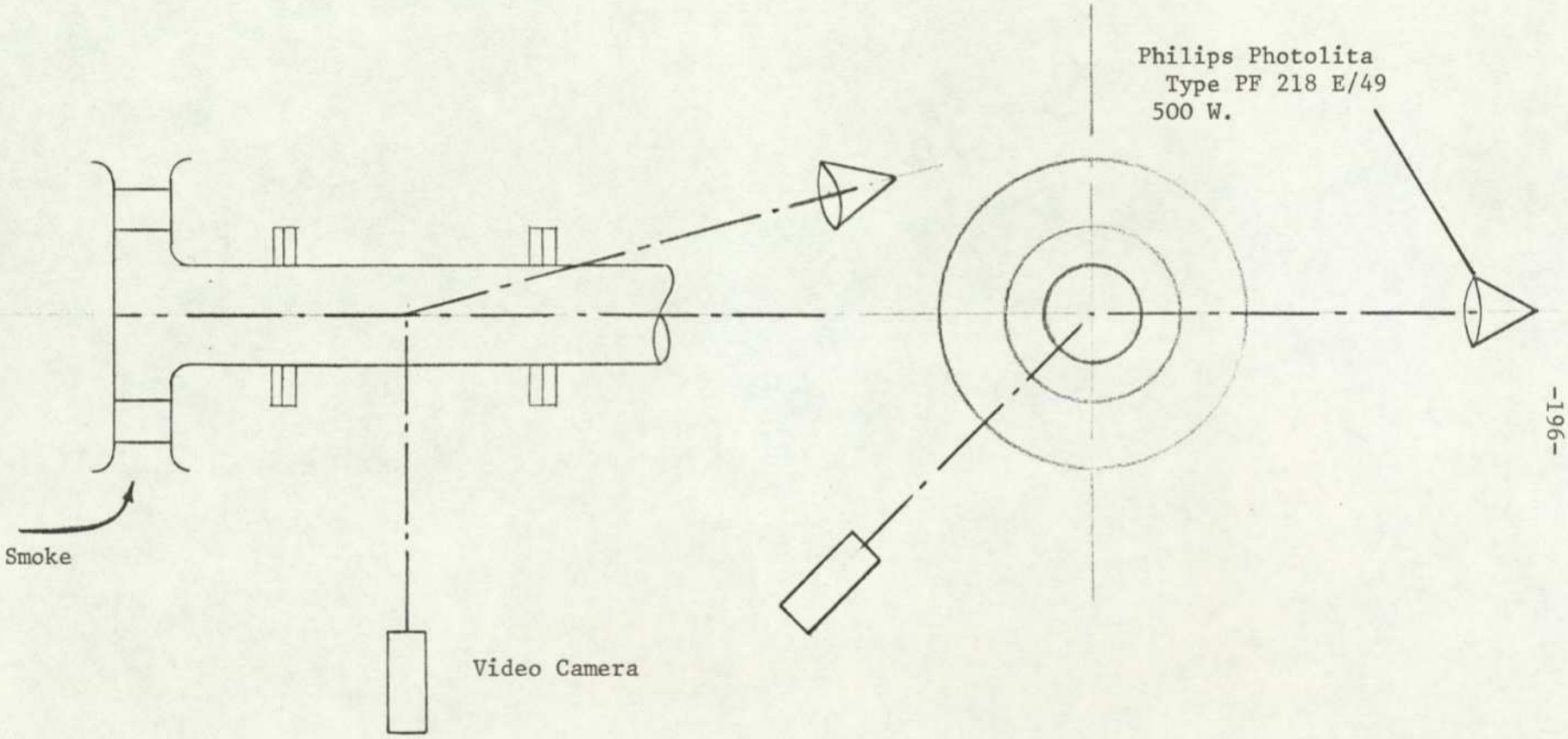

The video set up was the same as that reported in Chapter Five, shown in Fig.(5.2). The lighting for the vortex generator is shown in Fig.(8.2), while the set up for pipe and diffuser was the same as that reported in Chapter Five Fig.(5.3). Each of the above tests was recorded on 45 minute video-tape classified as FRV10, FRV20, FRV30 for the 10^{o}, 20^{o} and 30^{o} conical angle diffusers respectively.

8.4 VIDEO ANALYSIS

The video tapes were played a number of times and analysed. The problems encountered in analysing the video tapes were no different from those mentioned in Chapter Five, section (5.5).

Asahi-Pentax, 35 mm camera was used to photograph still frames as shown in Fig.(5.4). Again, the photographic work was conducted for a long period with a day's break in between because of the hypnotic effect that developed when the same behaviour was observed continuously. More than 200 photographs were taken to obtain a photographic record, but only few are included. The video-tapes are preserved as a future reference. The photographic record is as follows:

DIFFUSER CONICAL ANGLE = 10 DEGREE

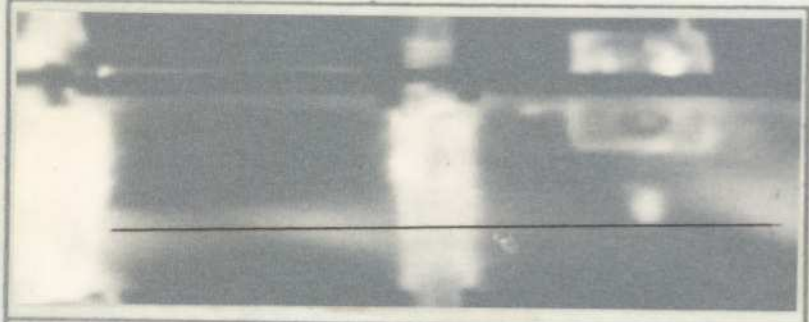

FIG. 8.3

Flow in entry section

Blade angle = 0°

Flow direction →

FIG. 8.4

Flow in pipe section

Blade angle = 0°

→

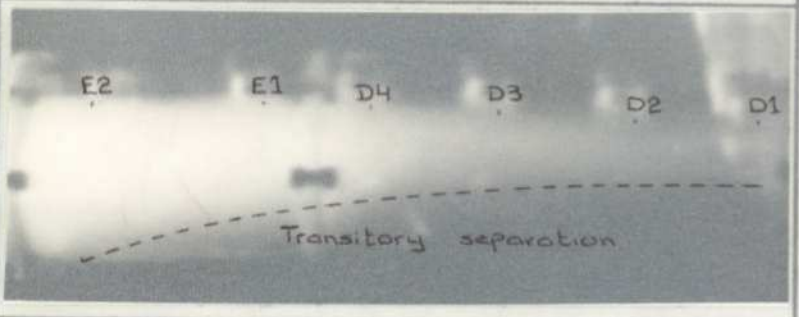

FIG. 8.5

Flow in diffuser-tail pipe

Blade angle = 0°

←

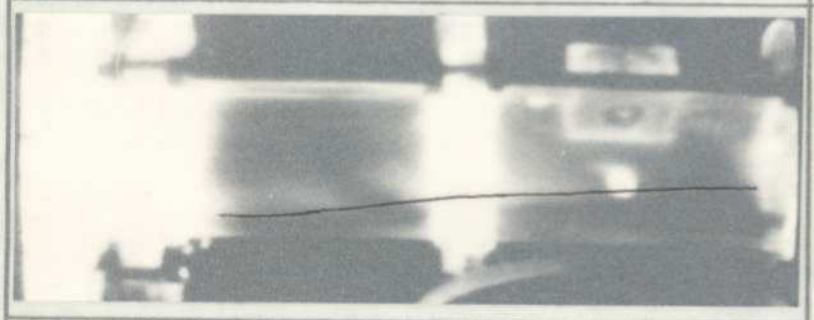

FIG. 8.6

Flow in entry section

Blade angle = 2°

→

FIG. 8.7

Flow in pipe section

Blade angle = 2°

→

FIG. 8.8

Flow in diffuser-tail pipe

Blade angle = 2°

←

DIFFUSER CONICAL ANGLE = 10 DEGREE

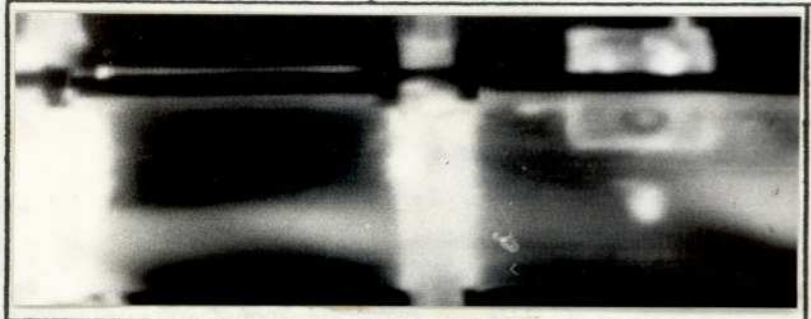

FIG. 8.3

Flow in entry section

Blade angle = 0^{o}

FIG. 8.4

Flow in pipe section

Blade angle = 0^{o}

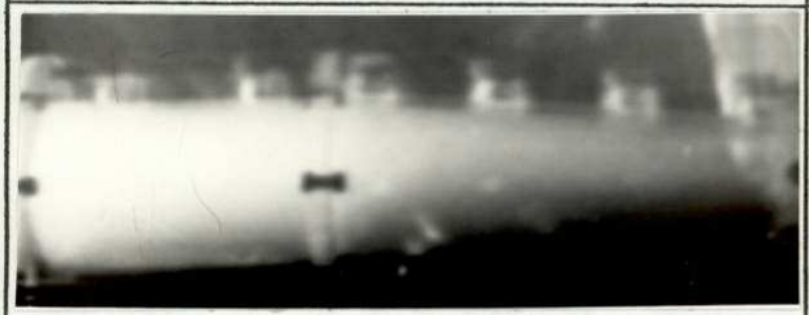

FIG. 8.5

Flow in diffuser-tail pipe

Blade angle = 0^{o}

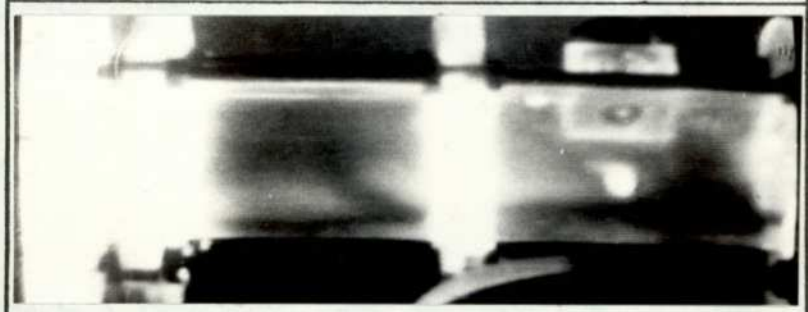

FIG. 8.6

Flow in entry section

Blade angle = 2^{o}

FIG. 8.7

Flow in pipe section

Blade angle = 2^{o}

FIG. 8.8

Flow in diffuser-tail pipe

Blade angle = 2^{o}

DIFFUSER CONICAL ANGLE = 10 DEGREE

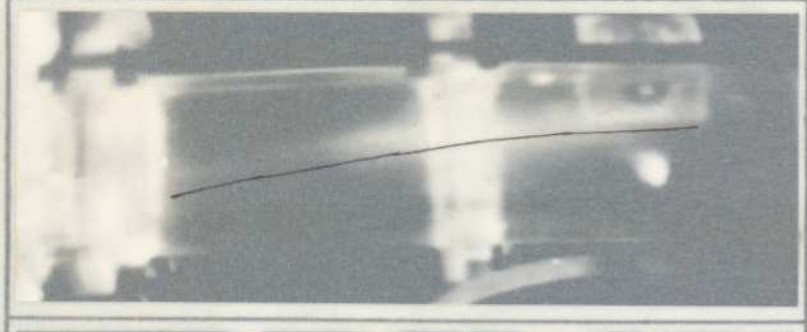

FIG. 8.9

Flow in entry section

Blade angle = 4^{o}

Flow direction →

FIG. 8.10

Flow in pipe section

Blade angle = 4^{o}

→

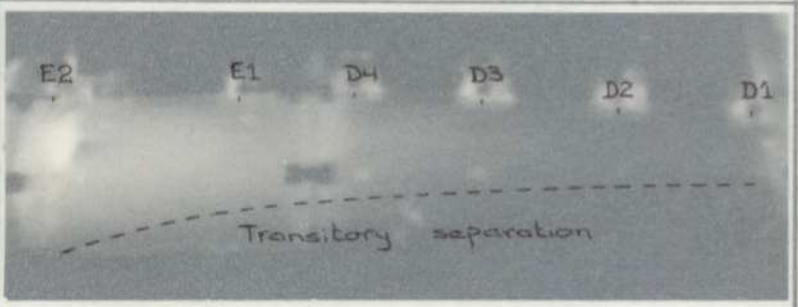

FIG. 8.11

Flow in diffuser-tail pipe

Blade angle = 4^{o}

←

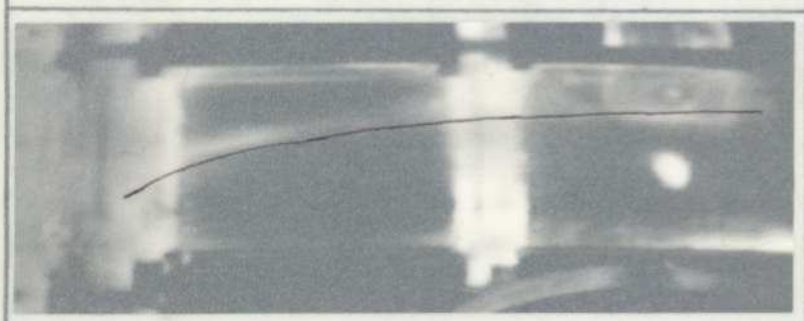

EIG. 8.12

Flow in entry section

Blade angle = 6^{o}

→

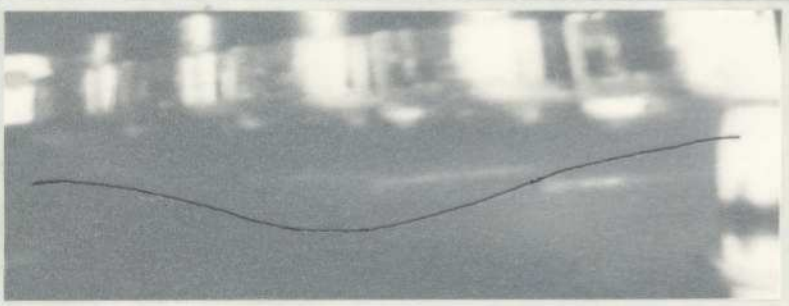

FIG. 8.13

Flow in pipe section

Blade angle = 6^{o}

→

FIG. 8.14

Flow in diffuser-tail pipe

Blade angle = 6^{o}

←

DIFFUSER CONICAL ANGLE = 10 DEGREE

FIG. 8.9

Flow in entry section

Blade angle = 4^{o}

FIG. 8.10

Flow in pipe section

Blade angle = 4^{o}

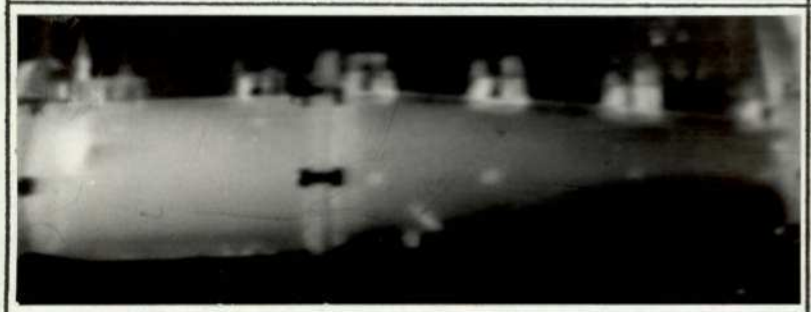

FIG. 8.11

Flow in diffuser-tail pipe

Blade angle = 4^{o}

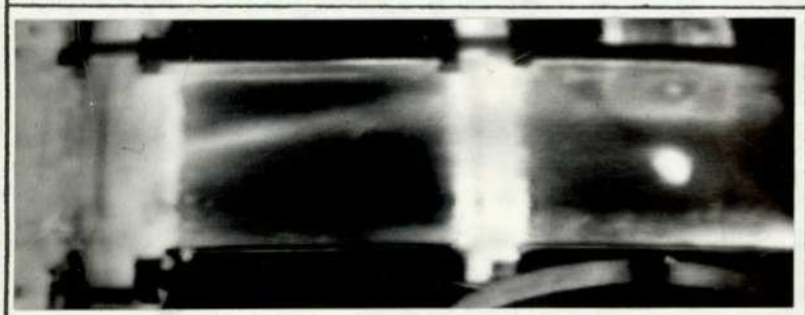

FIG. 8.12

Flow in entry section

Blade angle = 6^{o}

FIG. 8.13

Flow in pipe section

Blade angle = 6^{o}

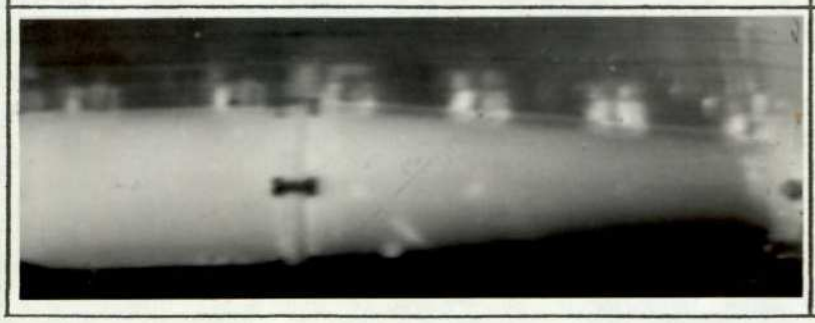

FIG. 8.14

Flow in diffuser-tail pipe

Blade angle = 6^{o}

DIFFUSER CONICAL ANGLE = 10 DEGREE

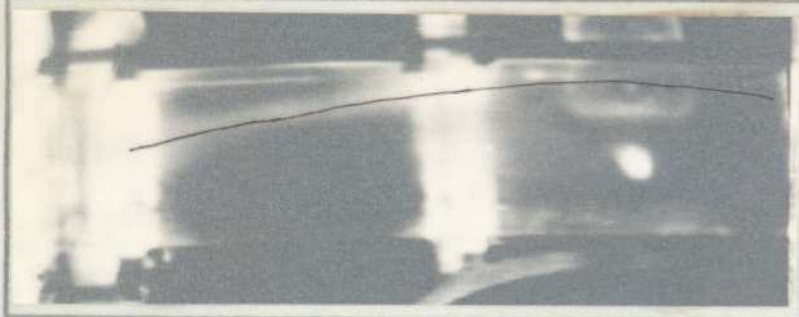

FIG. 8.15

Flow in entry section

Blade angle = 10°

Flow direction →

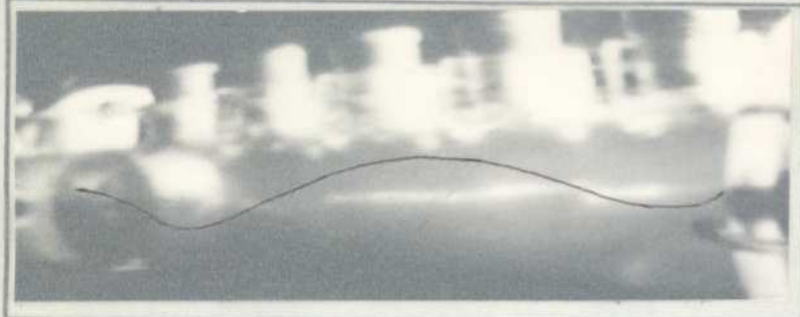

FIG. 8.16

Flow in pipe section

Blade angle = 10°

→

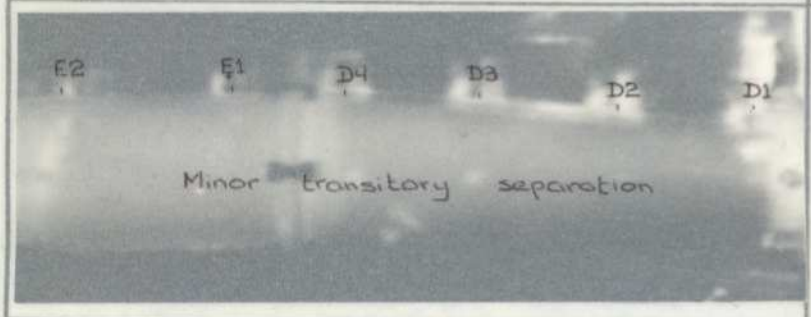

FIG. 8.17

Flow in diffuser-tail pipe

Blade angle = 10°

←

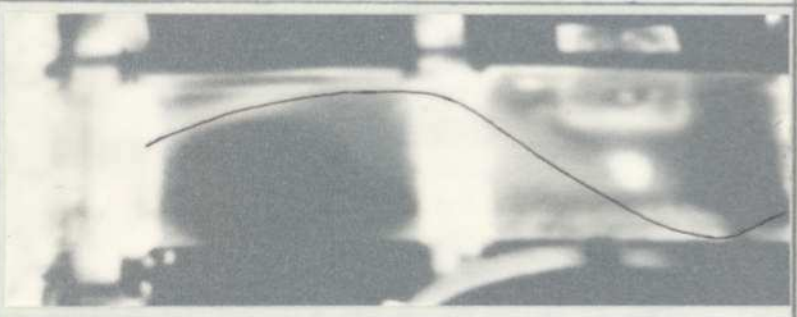

FIG. 8.18

Flow in entry section

Blade angle = 15°

→

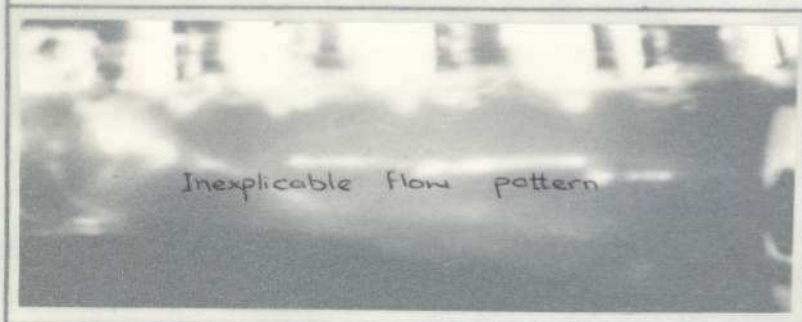

FIG. 8.19

Flow in pipe section

Blade angle = 15°

→

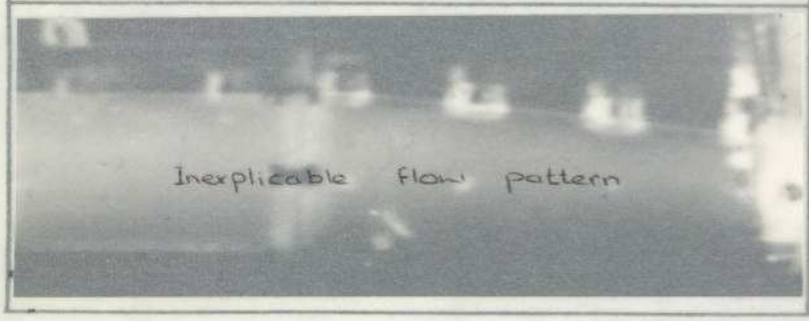

FIG. 8.20

Flow in diffuser-tail pipe

Blade angle = 15°

←

DIFFUSER CONICAL ANGLE = 10 DEGREE

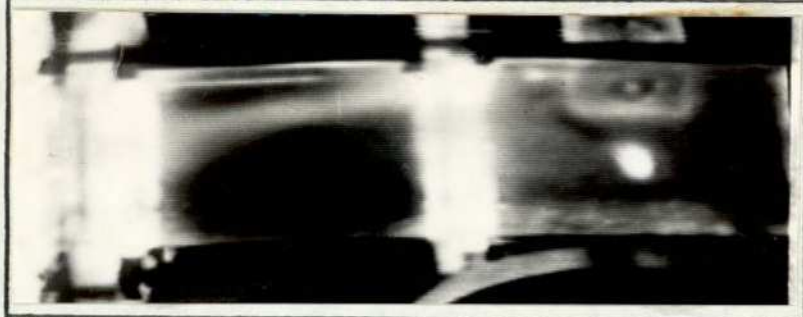

FIG. 8.15

Flow in entry section

Blade angle = 10^{o}

FIG. 8.16

Flow in pipe section

Blade angle = 10^{o}

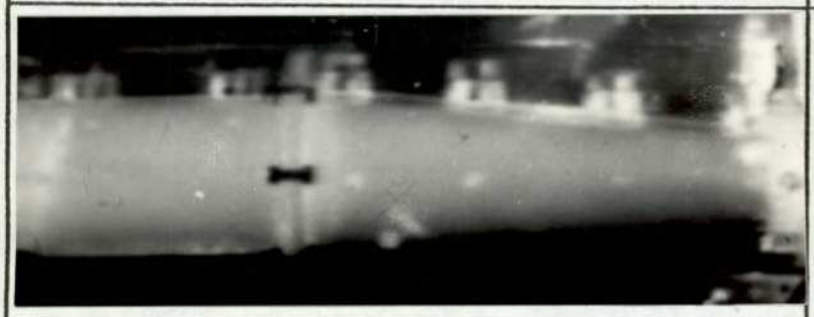

FIG. 8.17

Flow in diffuser-tail pipe

Blade angle = 10^{o}

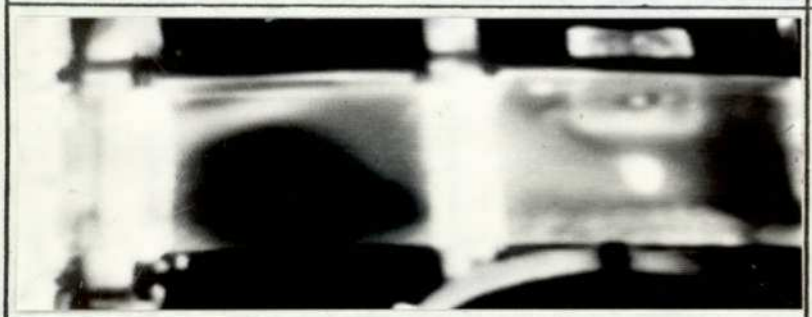

FIG. 8.18

Flow in entry section

Blade angle = 15^{o}

FIG. 8.19

Flow in pipe section

Blade angle = 15^{o}

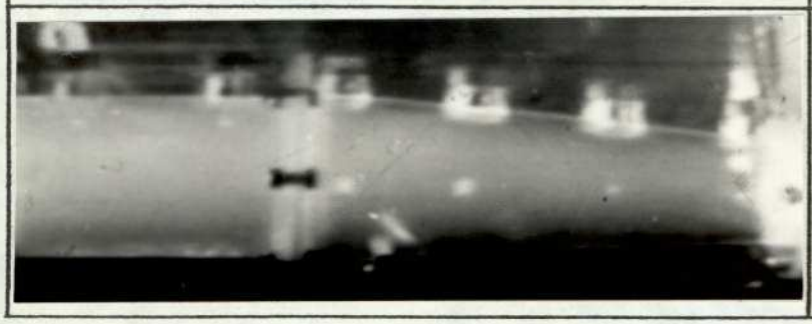

FIG. 8.20

Flow in diffuser-tail pipe

Blade angle = 15^{o}

DIFFUSER CONICAL ANGLE = 10 DEGREE

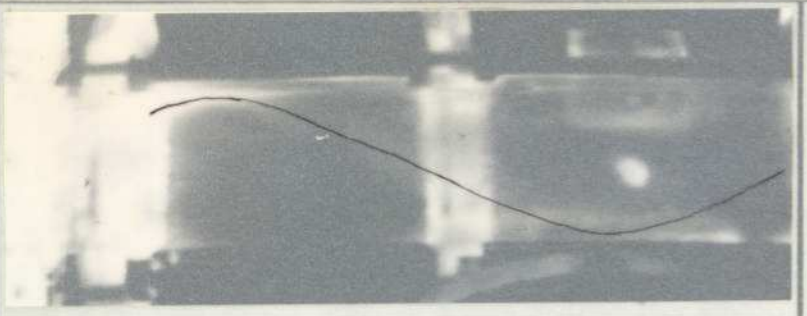

FIG. 8.21

Flow in entry section

Blade angle = 20°

Flow direction →

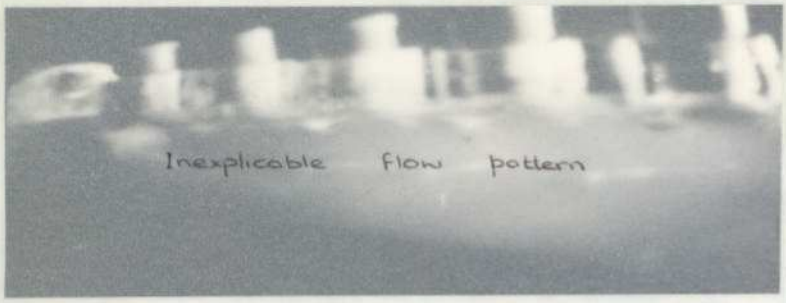

FIG. 8.22

Flow in pipe section

Blade angle = 20°

→

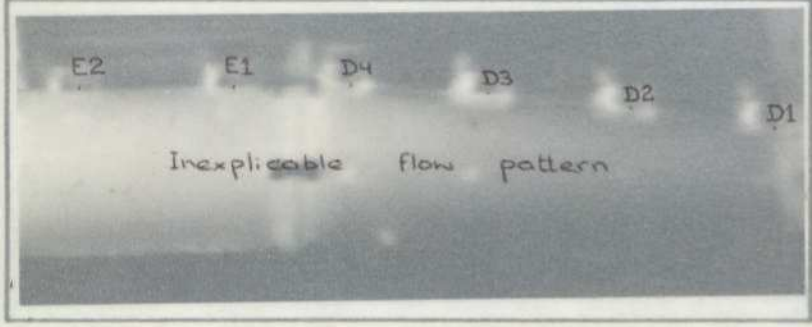

FIG. 8.23

Flow in diffuser-tail pipe

Blade angle = 20°

←

DIFFUSER CONICAL ANGLE = 10 DEGREE

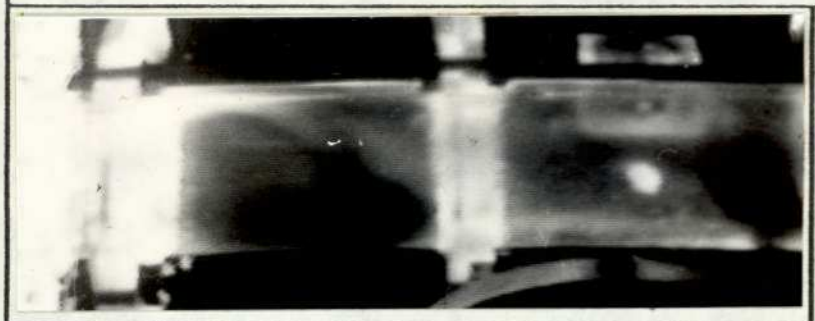

FIG. 8.21

Flow in entry section

Blade angle = 20^{o}

FIG. 8.22

Flow in pipe section

Blade angle = 20^{o}

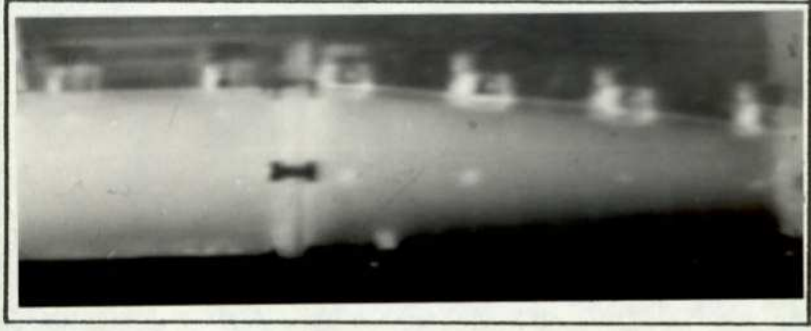

FIG. 8.23

Flow in diffuser-tail pipe

Blade angle = 20^{o}

DIFFUSER CONICAL ANGLE = 20 DEGREE

FIG. 8.24

Flow in entry section

Blade angle = 0°
Flow direction →

FIG. 8.25

Flow in pipe section

Blade angle = 0°
→

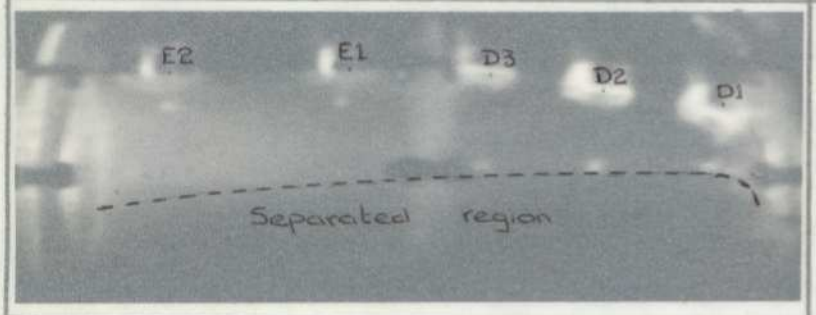

FIG. 8.26

Flow in diffuser-tail pipe

Blade angle = 0°
←

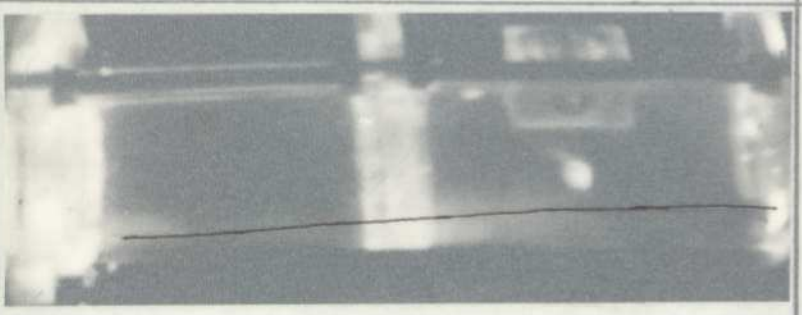

FIG. 8.27

Flow in entry section

Blade angle = 2°
→

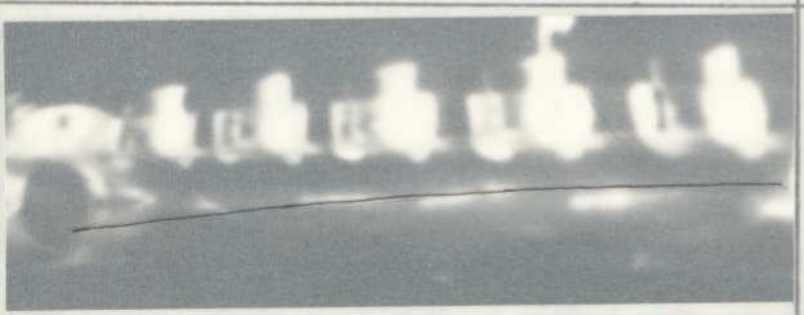

FIG. 8.28

Flow in pipe section

Blade angle = 2°
→

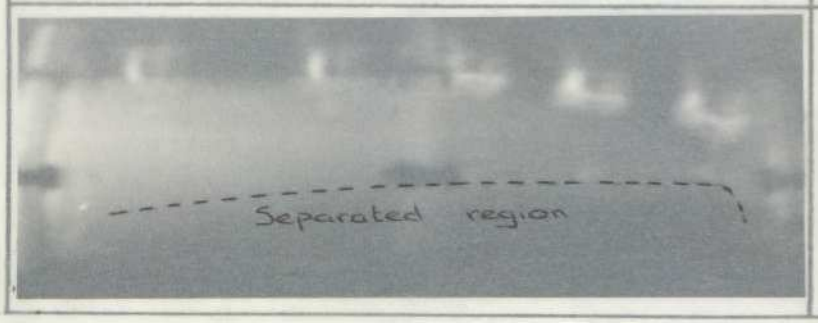

FIG. 8.29

Flow in diffuser-tail pipe

Blade angle = 2°
←

DIFFUSER CONICAL ANGLE = 20 DEGREE

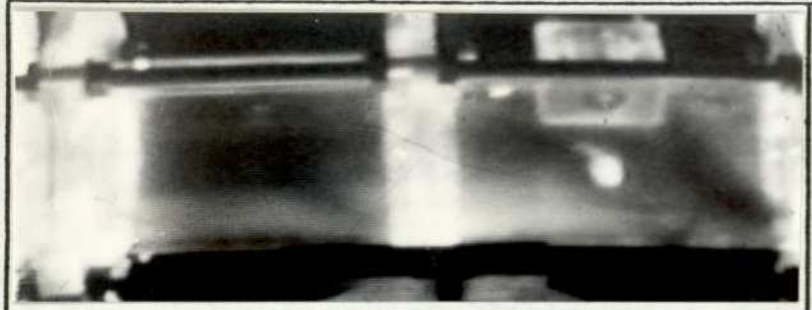

FIG. 8.24

Flow in entry section

Blade angle = 0^{o}

FIG. 8.25

Flow in pipe section

Blade angle = 0^{o}

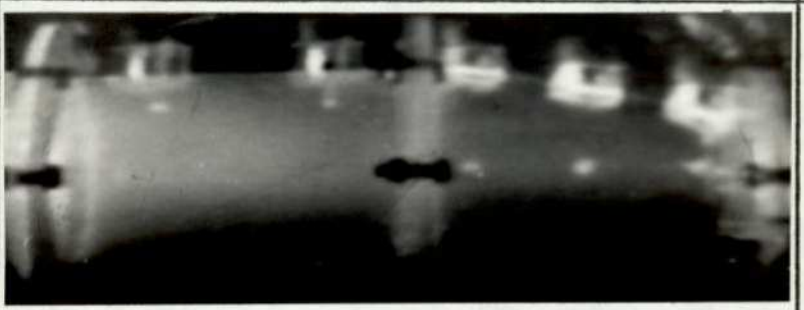

FIG. 8.26

Flow in diffuser-tail pipe

Blade angle = 0^{o}

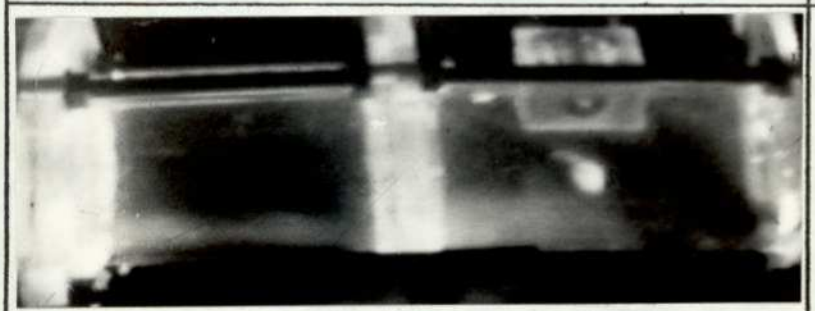

FIG. 8.27

Flow in entry section

Blade angle = 2^{o}

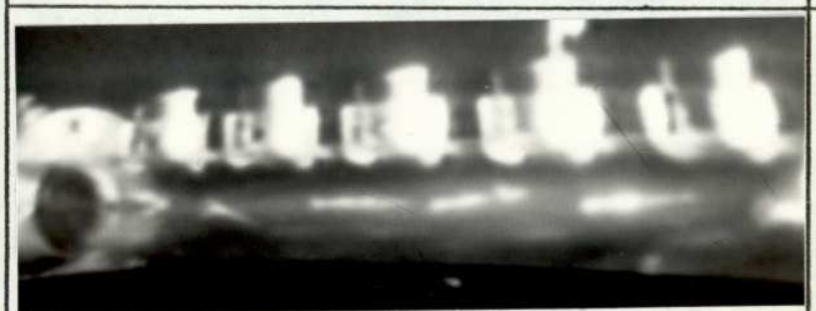

FIG. 8.28

Flow in pipe section

Blade angle = 2^{o}

FIG. 8.29

Flow in diffuser-tail pipe

Blade angle = 2^{o}

DIFFUSER CONICAL ANGLE = 20 DEGREE

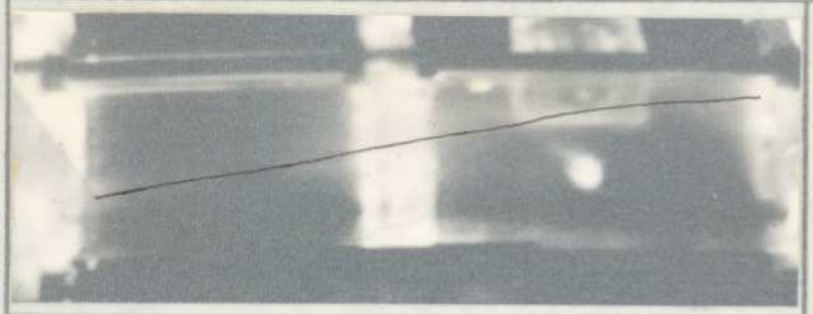

FIG. 8.30

Flow in entry section

Blade angle = 4°

Flow direction →

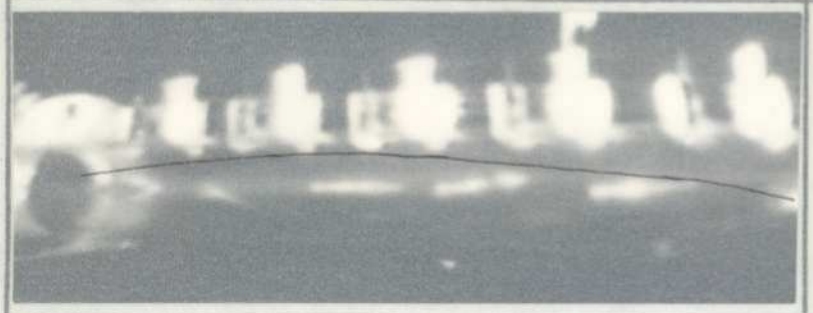

FIG. 8.31

Flow in pipe section

Blade angle = 4° →

FIG. 8.32

Flow in diffuser-tail pipe

Blade angle = 4° ←

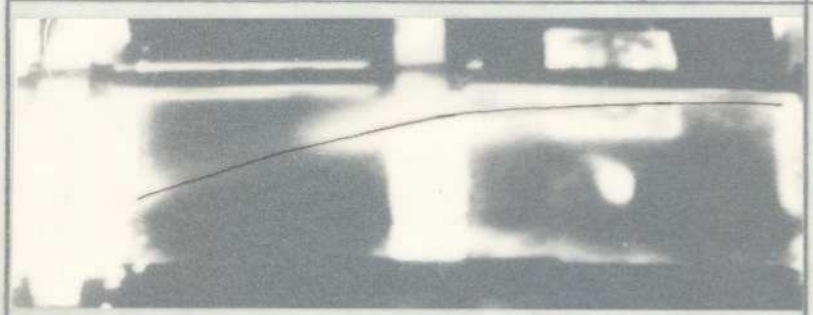

FIG. 8.33

Flow in entry section

Blade angle = 6° →

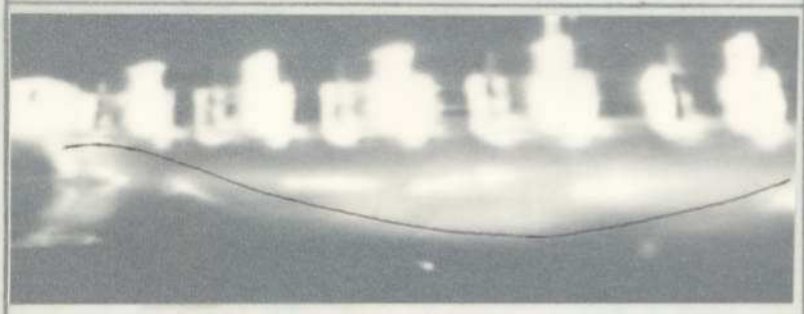

FIG. 8.34

Flow in pipe section

Blade angle = 6° →

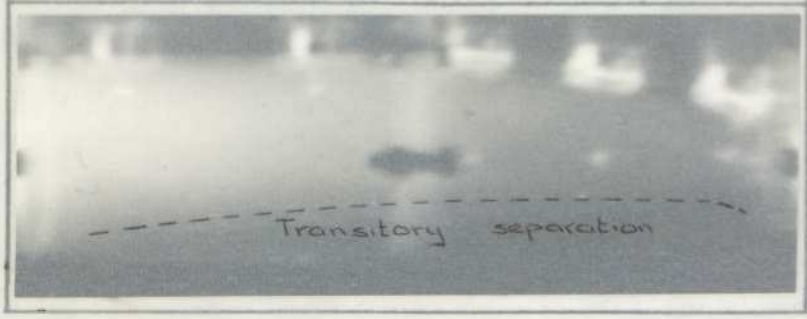

FIG. 8.35

Flow in diffuser-tail pipe

Blade angle = 6° ←

DIFFUSER CONICAL ANGLE = 20 DEGREE

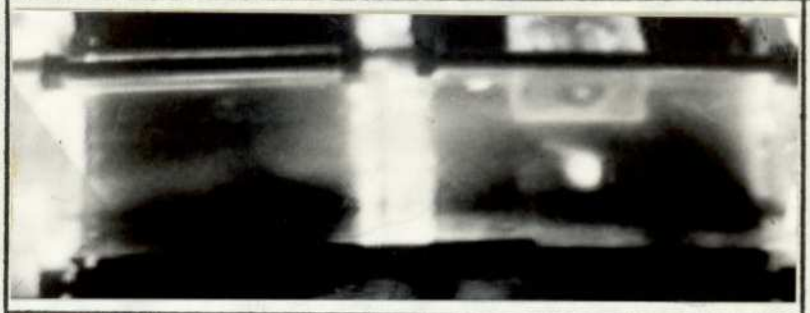

FIG. 8.30

Flow in entry section

Blade angle = 4^{o}

FIG. 8.31

Flow in pipe section

Blade angle = 4^{o}

FIG. 8.32

Flow in diffuser-tail pipe

Blade angle = 4^{o}

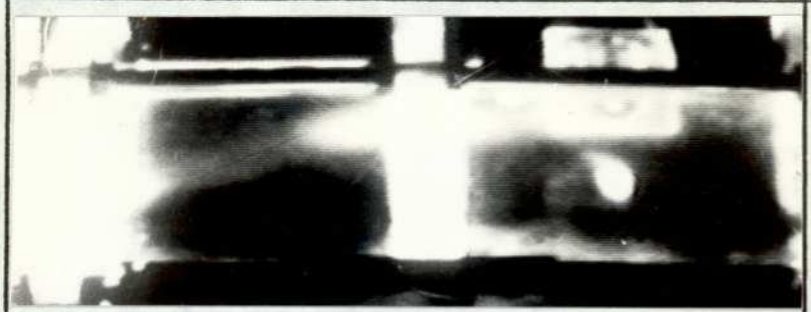

FIG. 8.33

Flow in entry section

Blade angle = 6^{o}

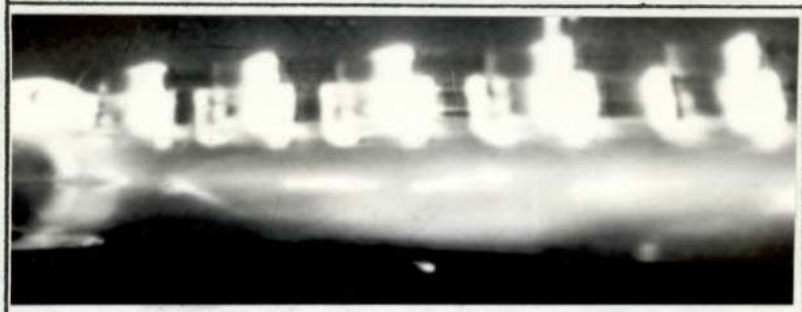

FIG. 8.34

Flow in pipe section

Blade angle = 6^{o}

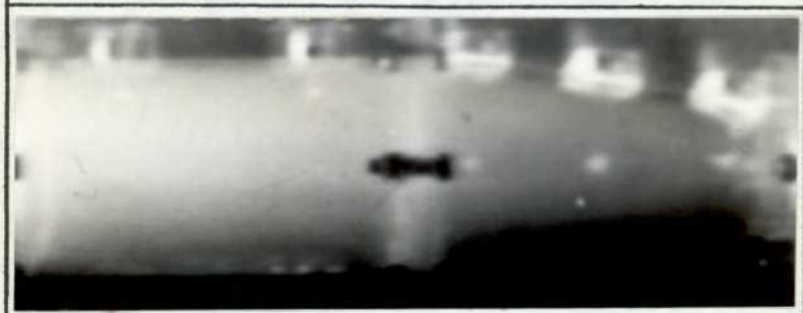

FIG. 8.35

Flow in diffuser-tail pipe

Blade angle = 6^{o}

DIFFUSER CONICAL ANGLE = 20 DEGREE

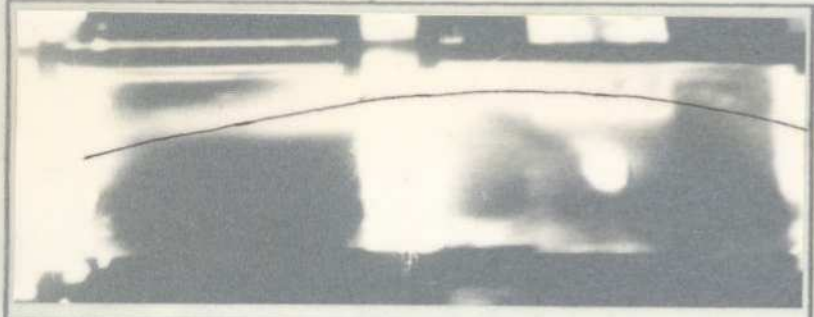

FIG. 8.36

Flow in entry section

Blade angle = 10°

Flow direction →

FIG. 8.37

Flow in pipe section

Blade angle = 10°

→

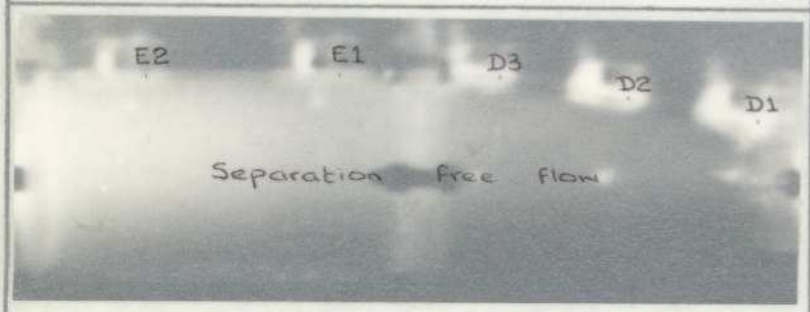

FIG. 8.38

Flow in diffuser-tail pipe

Blade angle = 10°

←

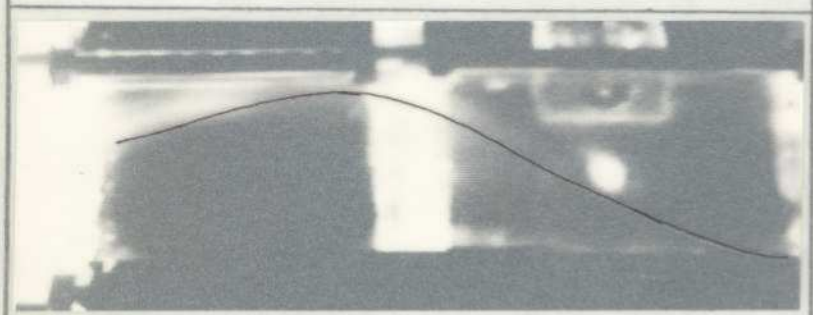

FIG. 8.39

Flow in entry section

Blade angle = 15°

→

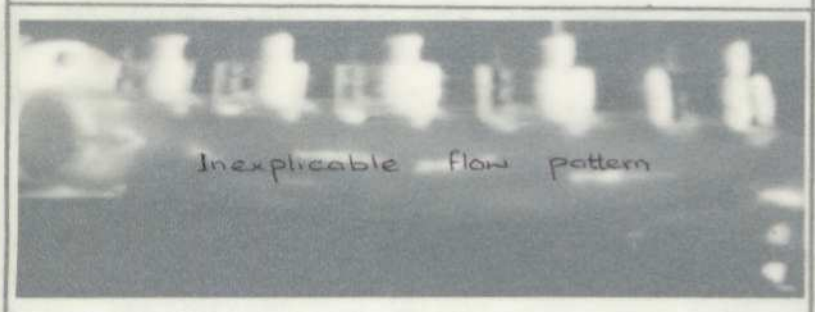

FIG. 8.40

Flow in pipe section

Blade angle = 15°

→

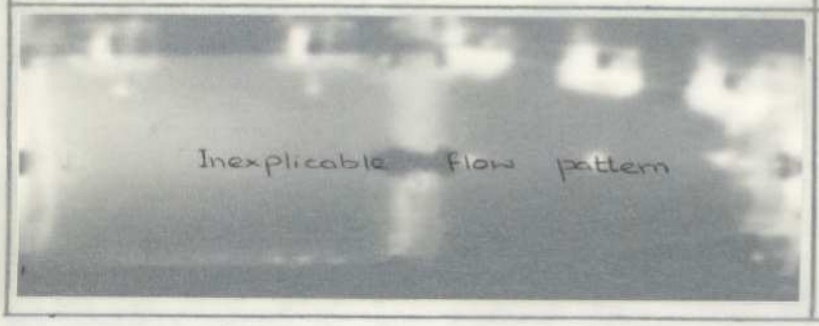

FIG. 8.41

Flow in diffuser-tail pipe

Blade angle = 15°

←

DIFFUSER CONICAL ANGLE = 20 DEGREE

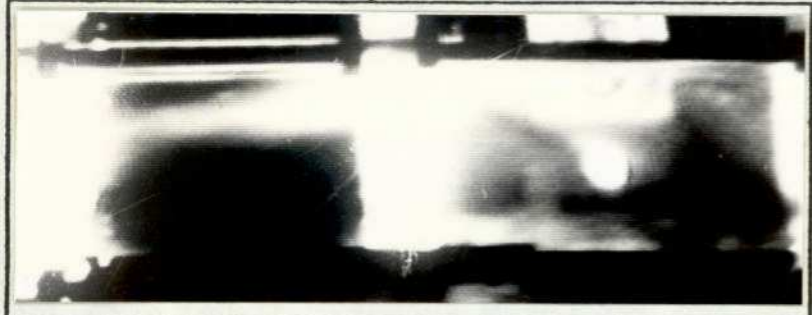

FIG. 8.36

Flow in entry section

Blade angle = 10°

FIG. 8.37

Flow in pipe section

Blade angle = 10°

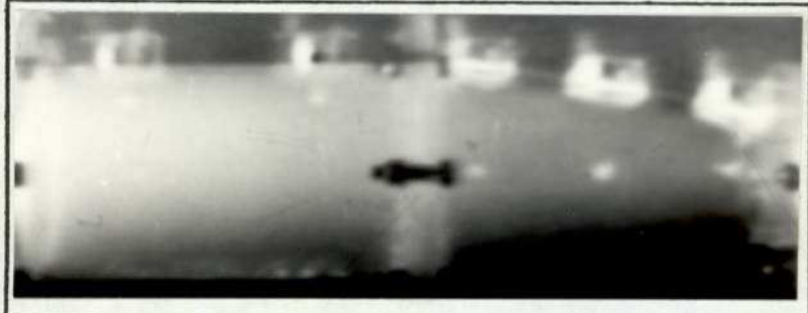

FIG. 8.38

Flow in diffuser-tail pipe

Blade angle = 10°

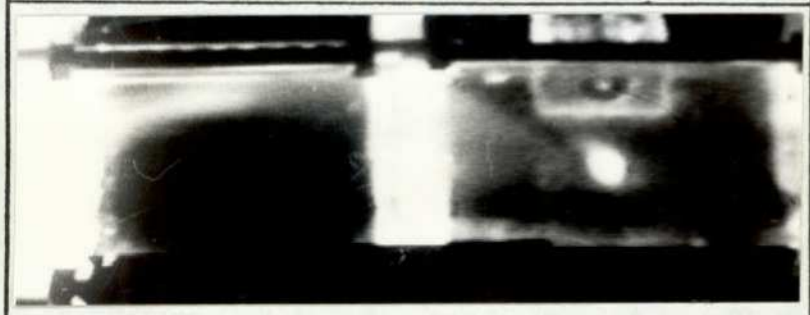

FIG. 8.39

Flow in entry section

Blade angle = 15°

FIG. 8.40

Flow in pipe section

Blade angle = 15°

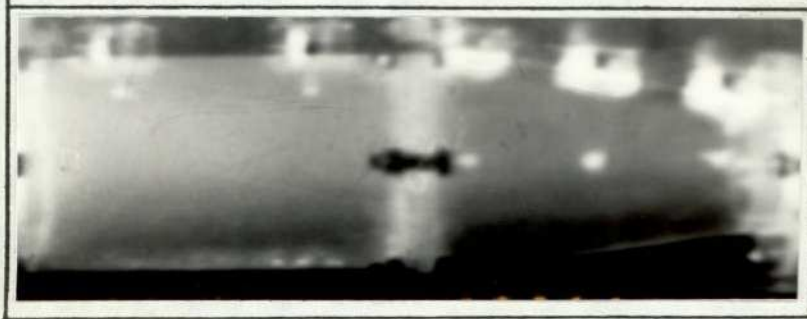

FIG. 8.41

Flow in diffuser-tail pipe

Blade angle = 15°

DIFFUSER CONICAL ANGLE = 20 DEGREE

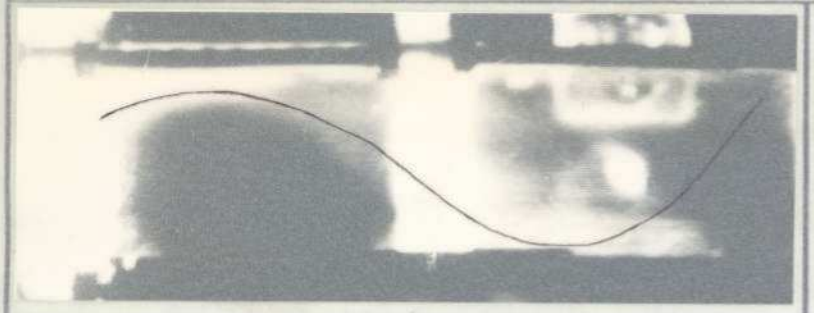

FIG. 8.42

Flow in entry section

Blade angle = 20°

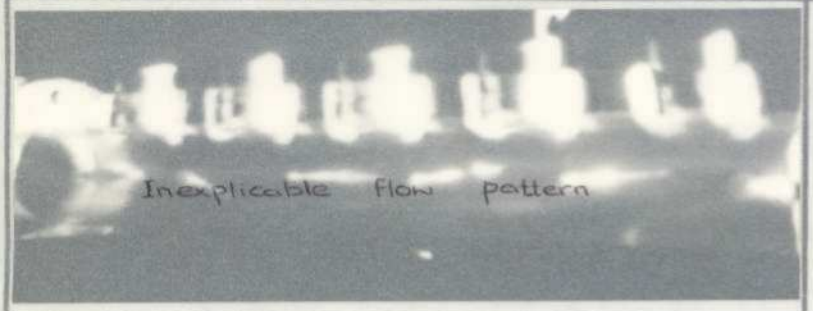

FIG. 8.43

Flow in pipe section

Blade angle = 20°

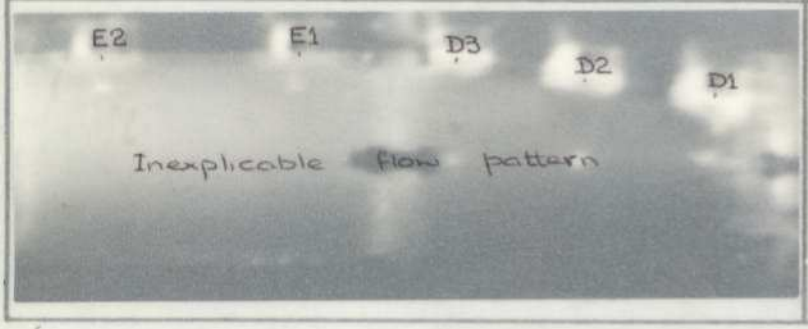

FIG. 8.44

Flow in diffuser-tail pipe

Blade angle = 20°

DIFFUSER CONICAL ANGLE = 20 DEGREE

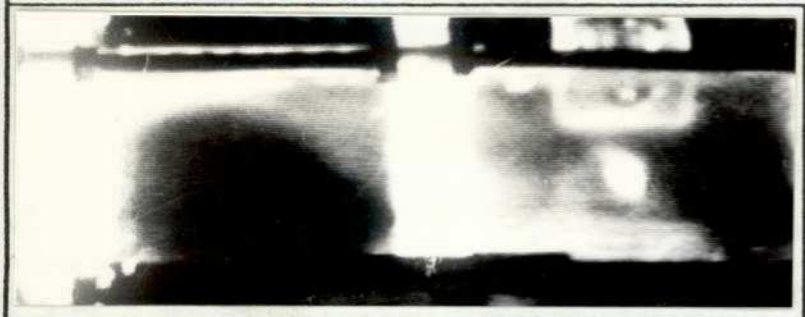

FIG. 8.42

Flow in entry section

Blade angle = 20^{o}

FIG. 8.43

Flow in pipe section

Blade angle = 20^{o}

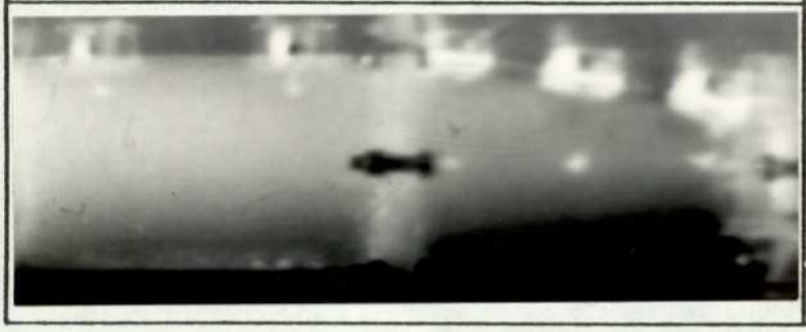

FIG. 8.44

Flow in diffuser-tail pipe

Blade angle = 20^{o}

DIFFUSER CONICAL ANGLE = 30 DEGREE

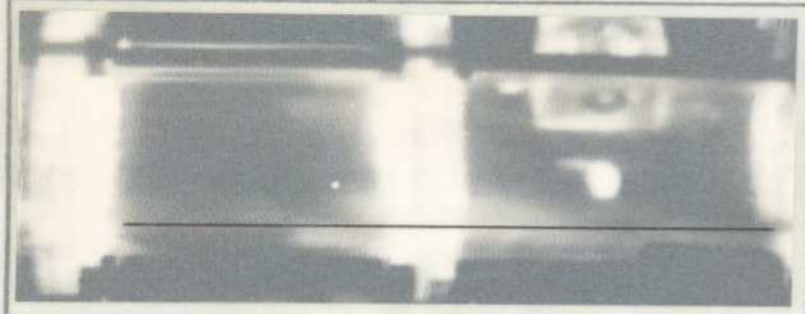

FIG. 8.45

Flow in entry section

Blade angle = 0^{o}

Flow direction →

FIG. 8.46

Flow in pipe section

Blade angle = 0^{o} →

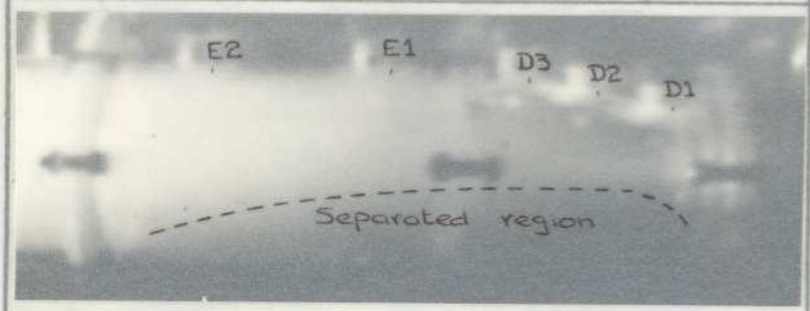

FIG. 8.47

Flow in diffuser-tail pipe

Blade angle = 0^{o} ←

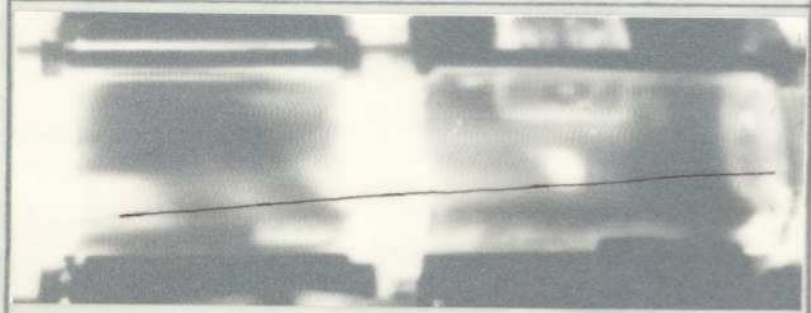

FIG. 8.48

Flow in entry section

Blade angle = 2^{o} →

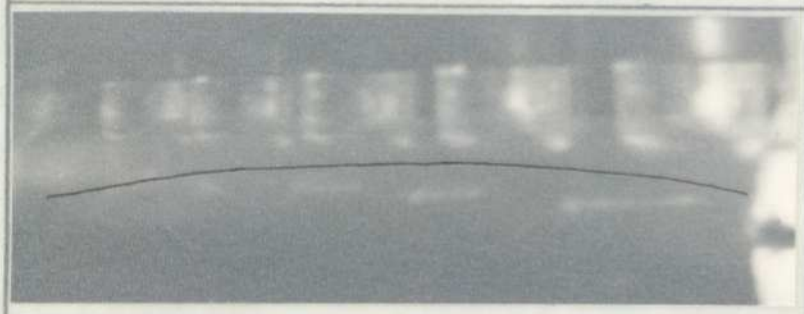

FIG. 8.49

Flow in pipe section

Blade angle = 2^{o} →

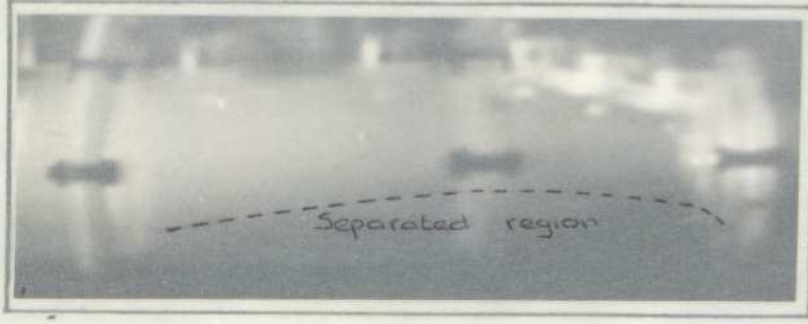

FIG. 8.50

Flow in diffuser-tail pipe

Blade angle = 2^{o} ←

DIFFUSER CONICAL ANGLE = 30 DEGREE

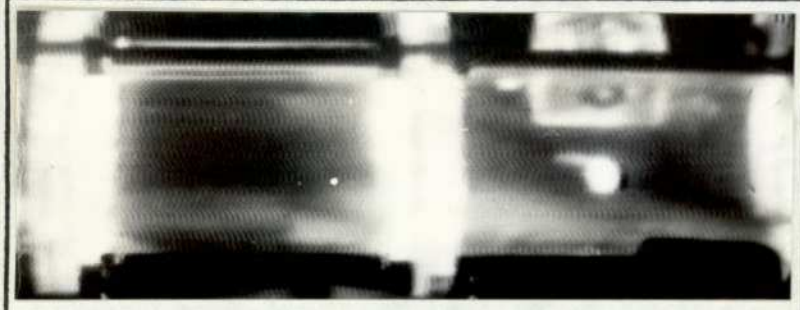

FIG. 8.45

Flow in entry section

Blade angle = 0^{o}

FIG. 8.46

Flow in pipe section

Blade angle = 0^{o}

FIG. 8.47

Flow in diffuser-tail pipe

Blade angle = 0^{o}

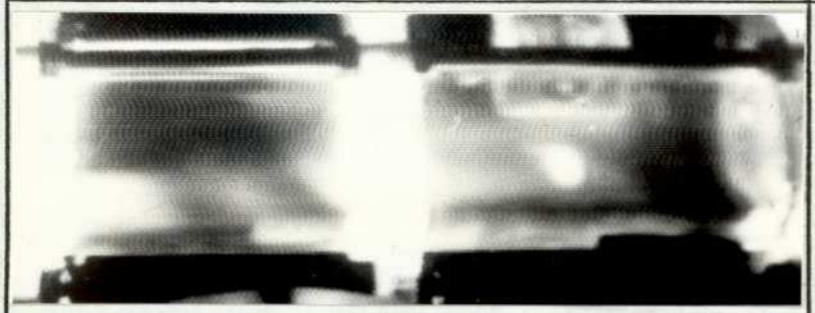

FIG. 8.48

Flow in entry section

Blade angle = 2^{o}

FIG. 8.49

Flow in pipe section

Blade angle = 2^{o}

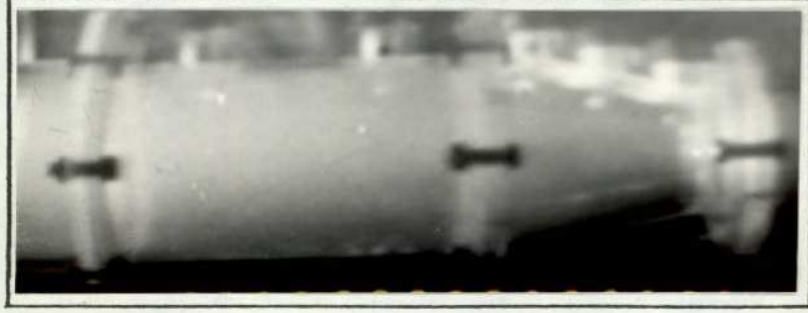

FIG. 8.50

Flow in diffuser-tail pipe

Blade angle = 2^{o}

DIFFUSER CONICAL ANGLE = 30 DEGREE

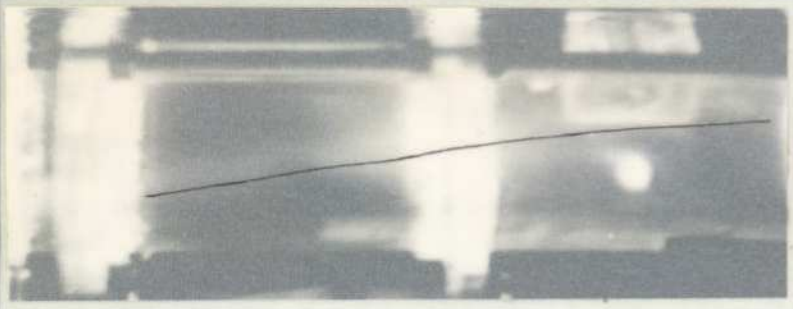

FIG. 8.51

Flow in entry section

Blade angle = 4°

Flow direction →

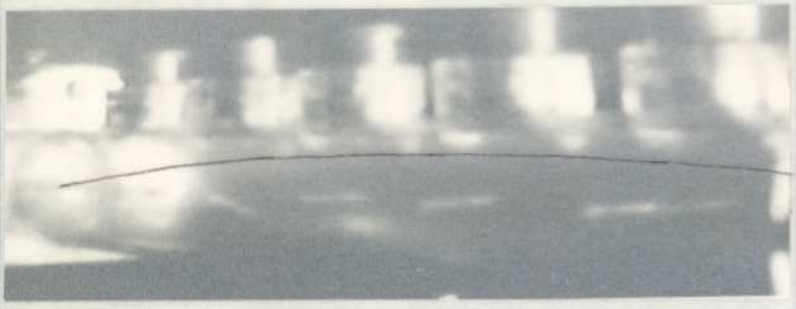

FIG. 8.52

Flow in pipe section

Blade angle = 4°

→

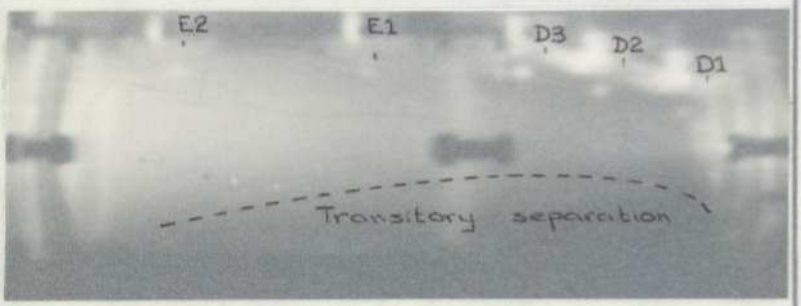

FIG. 8.53

Flow in diffuser-tail pipe

Blade angle = 4°

←

FIG. 8.54

Flow in entry section

Blade angle = 6°

→

FIG. 8.55

Flow in pipe section

Blade angle = 6°

→

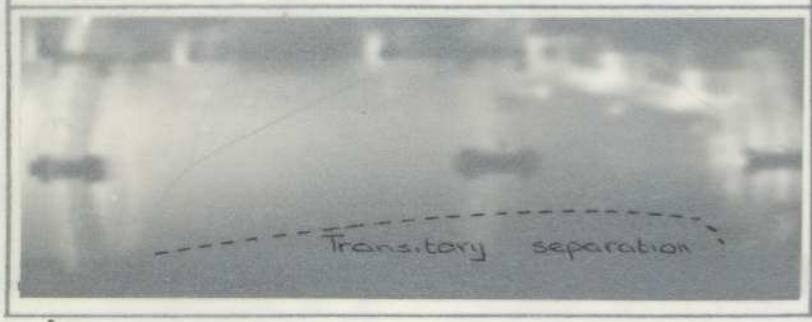

FIG. 8.56

Flow in diffuser-tail pipe

Blade angle = 6°

←

DIFFUSER CONICAL ANGLE = 30 DEGREE

FIG. 8.51

Flow in entry section

Blade angle = 4^{o}

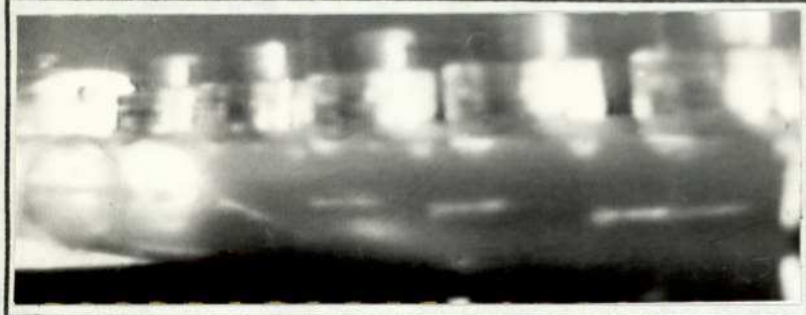

FIG. 8.52

Flow in pipe section

Blade angle = 4^{o}

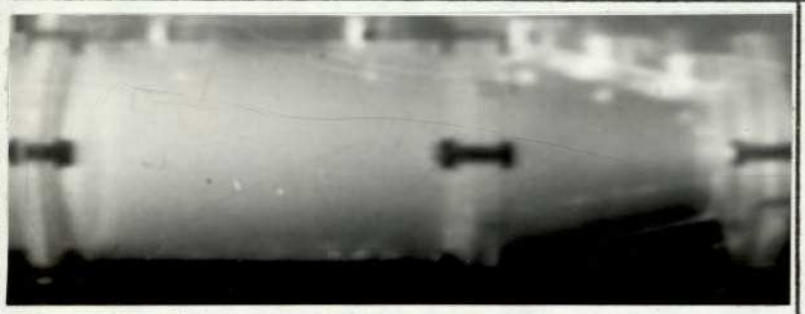

FIG. 8.53

Flow in diffuser-tail pipe

Blade angle = 4^{o}

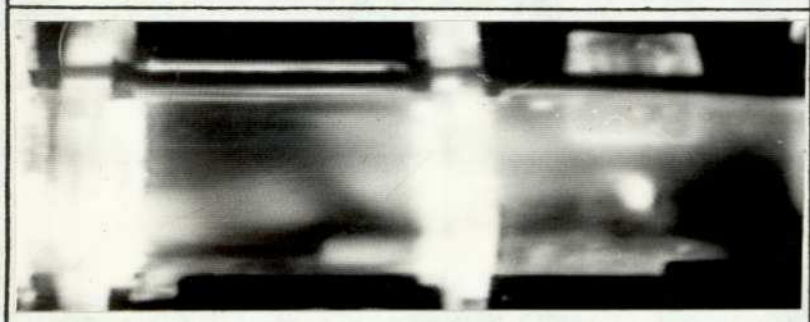

FIG. 8.54

Flow in entry section

Blade angle = 6^{o}

FIG. 8.55

Flow in pipe section

Blade angle = 6^{o}

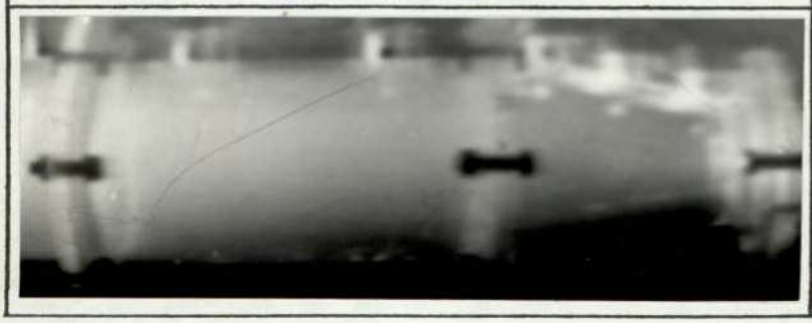

FIG. 8.56

Flow in diffuser-tail pipe

Blade angle = 6^{o}

DIFFUSER CONICAL ANGLE = 30 DEGREE

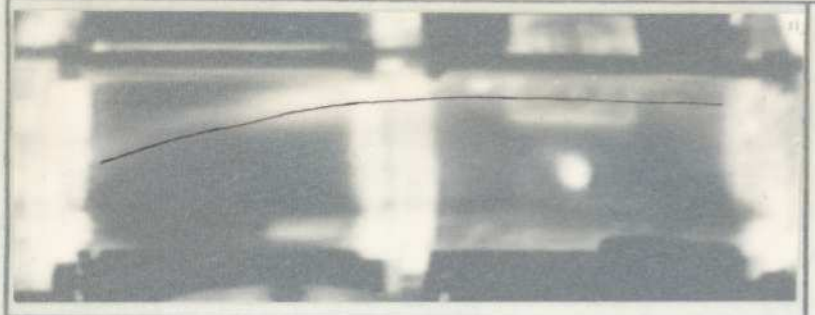

FIG. 8.57

Flow in entry section

Blade angle = 10°

Flow direction →

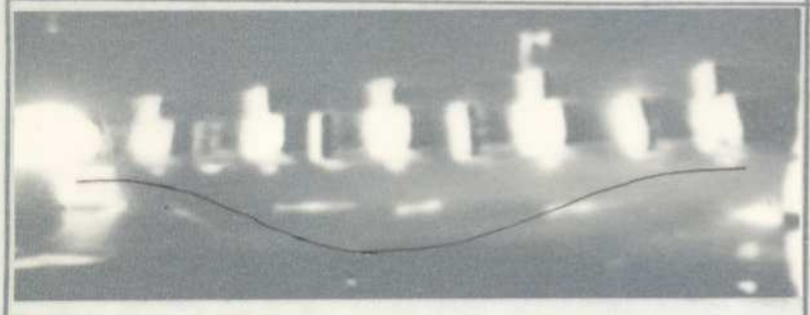

FIG. 8.58

Flow in pipe section

Blade angle = 10°

→

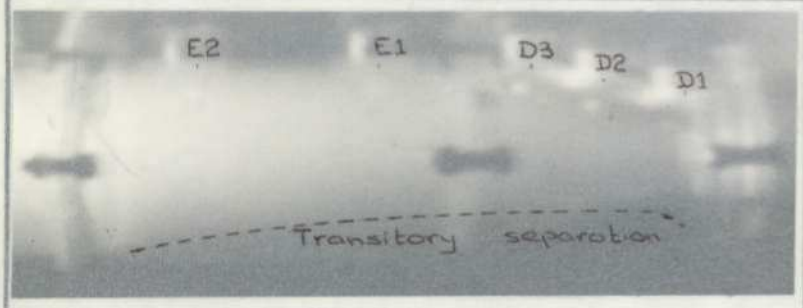

FIG. 8.59

Flow in diffuser-tail pipe

Blade angle = 10°

←

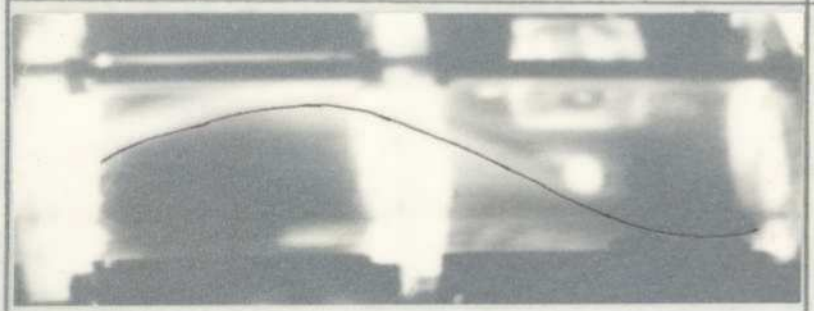

FIG. 8.60

Flow in entry section

Blade angle = 15°

→

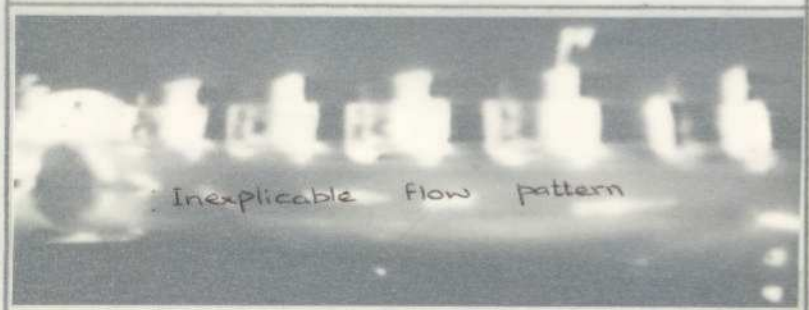

FIG. 8.61

Flow in pipe section

Blade angle = 15°

→

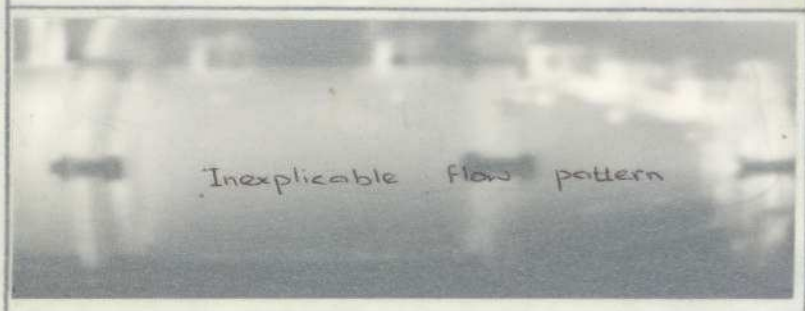

FIG. 8.62

Flow in diffuser-tail pipe

Blade angle = 15°

←

DIFFUSER CONICAL ANGLE = 30 DEGREE

FIG. 8.57

Flow in entry section

Blade angle = 10^{o}

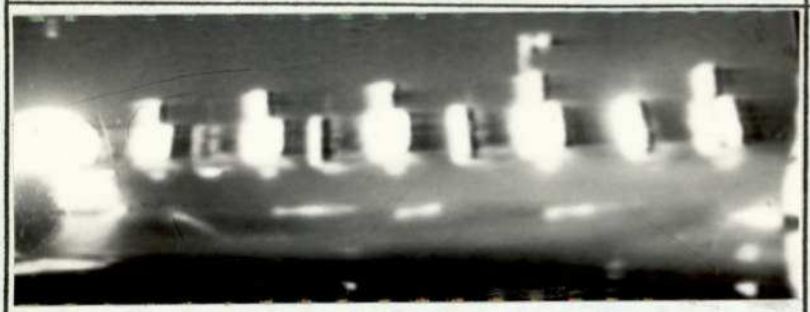

FIG. 8.58

Flow in pipe section

Blade angle = 10^{o}

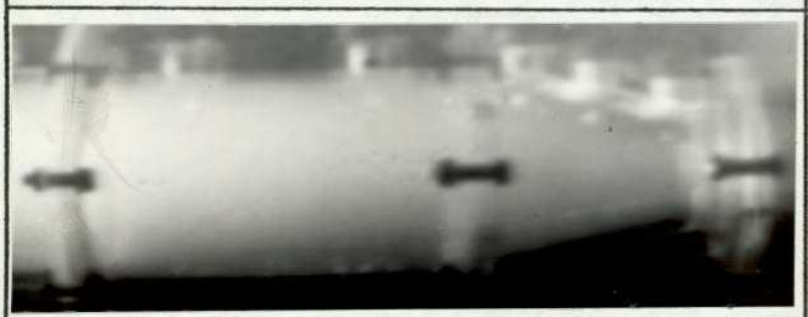

FIG. 8.59

Flow in diffuser-tail pipe

Blade angle = 10^{o}

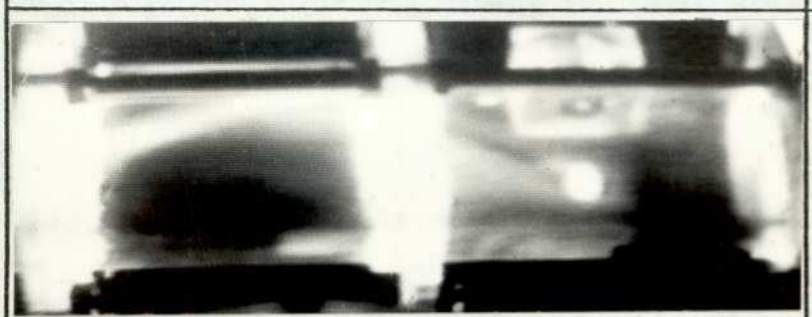

FIG. 8.60

Flow in entry section

Blade angle = 15^{o}

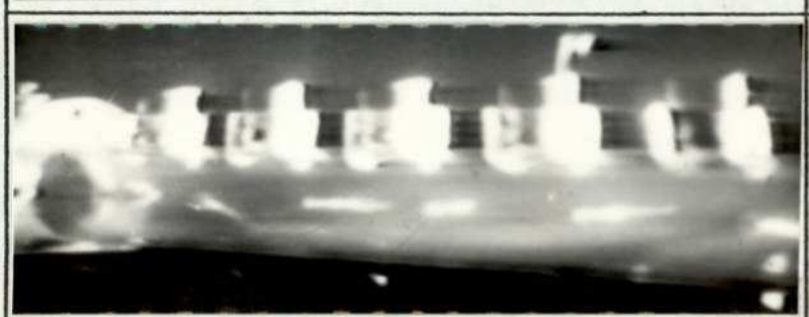

FIG. 8.61

Flow in pipe section

Blade angle = 15^{o}

FIG. 8.62

Flow in diffuser-tail pipe

Blade angle = 15^{o}

DIFFUSER CONICAL ANGLE = 30 DEGREE

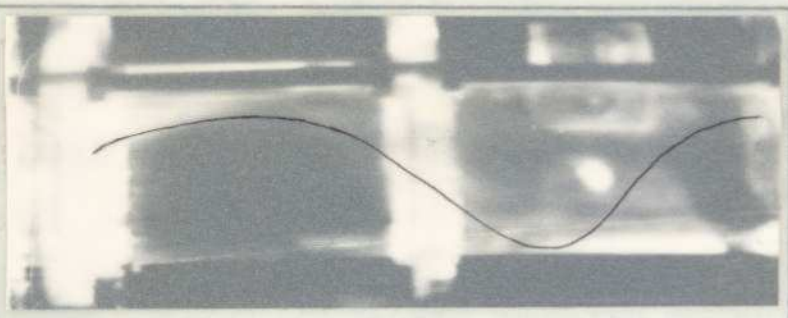

FIG. 8.63

Flow in entry section

Blade angle = 20°

Flow direction →

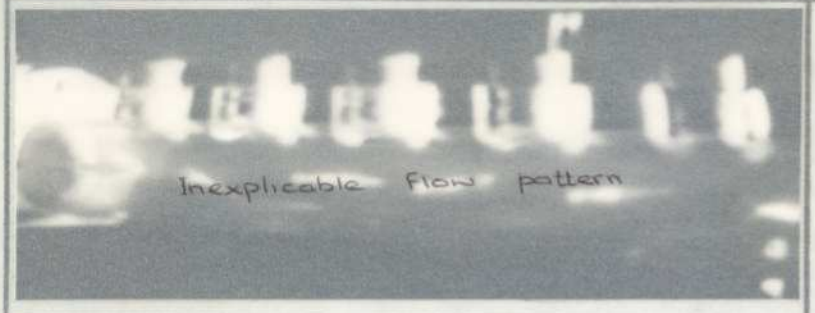

FIG. 8.64

Flow in pipe section

Blade angle = 20°

→

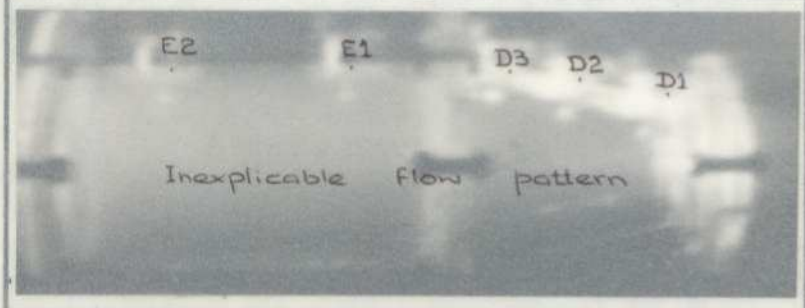

FIG. 8.65

Flow in diffuser-tail pipe

Blade angle = 20°

←

DIFFUSER CONICAL ANGLE = 30 DEGREE

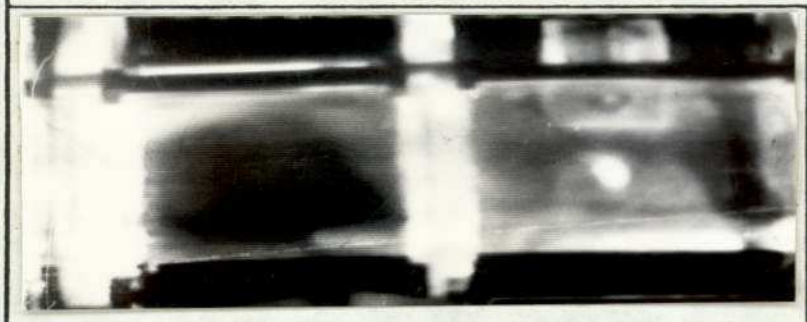

FIG. 8.63

Flow in entry section

Blade angle = 20^{o}

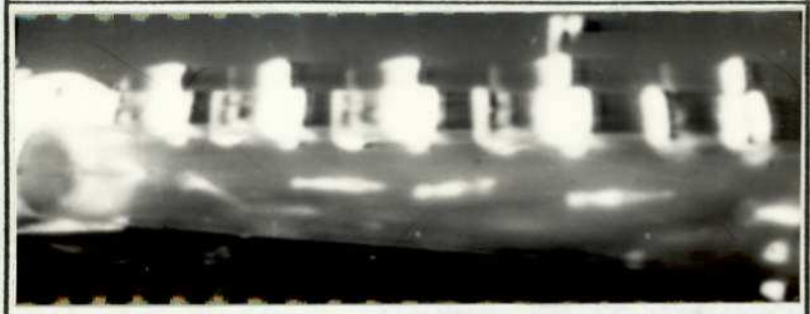

FIG. 8.64

Flow in pipe section

Blade angle = 20^{o}

FIG. 8.65

Flow in diffuser-tail pipe

Blade angle = 20^{o}

8.5 OBSERVATIONS

The observations were made from video-tapes FRV10, FRV20, FRV30 and from the photographic record. It is important to note that the photographic record is intended as a guide only.

8.5.1 Flow in the 10° Diffuser

For axial flow, the blade angle of the vortex generator was zero. The smoke entered through the vortex generator. From Figs.(8.3) and (8.4) it is evident that the flow in both entry and pipe section was highly turbulent. Thus the mass flux calculated at P5 should compare well with value at the orifice plate (Fig.(4.3)). This was found to be true within experimental error (±2%). Transitory separation was observed at the lower surface of the diffuser as shown in Fig.(8.5). By increasing the blade angle, the swirl strength is increased as seen from the photgraphs of entry and pipe section, thus causing the helical stream path to get closer. The flow in the diffuser appears to be getting more stable from the separation point of view, with increase in blade angle up to 6°. When the blade angle was 6°, the flow in the diffuser exhibited zero separation and the diffusion process was further carried in the tail pipe. At higher blade angles, there was always a small region of transitory separation present at the lower surface of the diffuser. The flow pattern in the pipe and thus flow situation in the diffuser was inexplicable for the blade angles greater than 15°. Because of the complexity of the flow pattern within the test section, it was not evident whether this was due to vortex breakdown.

8.5.2 Flow in the 20° Diffuser

For axial flow, the flow pattern in the entry and pipe section remained unchanged with increase in conical angle. A large region of separation, at the lower surface of the diffuser, was observed. The separation bubble started around station D1 and ended in the tail pipe, station E2. Again, by changing the blade angle, the swirl strength was increased, causing the helical path line of the swirl to come closer, in the entry and pipe section. The flow in the diffuser is also affected, in the sense that it gets more stable until the blade angle was 10°, where the separation was mild transitory and the diffusion process was further carried out in the tail pipe. With blade angle 15° and above, the flow pattern in the test section was inexplicable.

8.5.3 Flow in the 30° Diffuser

In this case, the swirl had a similar effect on the diffuser as on the 20° one. When the blade angle was 10°, the flow in the diffuser separated as a transitory stall.

8.6 CONCLUSIONS

Having formed the strategy of the experimental work from the previous chapter, the object of the flow visualization tests, to find the effect of Rankine vortex swirl on the wide angle diffusers was successfully achieved. The difficulties encountered with recording flow visualization patterns were solved in Chapter Five, thus the task of recording was straight-forward.

All the deductions are based on the observation studies, which are as follows:

1. The Rankine vortex swirl improves the diffusion process of the wide angle diffusers tested. The degree of improvement depends on the double conical angle and the degree of swirl induced.
2. Above a particular optimum blade angle of the vortex generator, the swirl does not seem to have a beneficial affect on diffuser flow and the flow patterns within the test section get highly complex. This optimum blade angle is different for each diffuser tested.
3. The optimum blade angle of the vortex generator found agrees with the analysis carried out in Chapter Seven.
4. The variation of wall static pressure observed quantitatively in Chapter Seven is confirmed qualitatively by the change in helical path line of the swirl, in entry and pipe sections, with change in blade angle of the vortex generator.

The degree of accuracy of the observations is subject to human error.

CHAPTER NINE

AXIAL AND RANKINE VORTEX SWIRLING FLOW MEASUREMENTS IN DIFFUSERS

9.1 INTRODUCTION

From the discussions presented in the previous chapters, it is evident that Rankine vortex swirl has a marked effect on flow in the wide angle diffusers. This is quite clearly shown qualitatively in Chapter Eight and to a certain extent quantitatively in Chapter Seven. The object of the programme is to investigate experimentally the performance of conical diffusers having various cone angles and the optimum degree of imparted Rankine vortex swirl.

Chapter Two shows that very little work has been done on flows in diffusers when flow at entry possesses Rankine vortex swirl. Suitable guide lines for the experimental work were set and justified by the previous two chapters. On the strength of this it was decided to conduct comprehensive flow measurements for the 10^{o}, 20^{o} and 30^{o} diffusers with the blade angles of the vortex generator set at the optimum blade angle, being 6 deg, 10 deg and 10 deg, respectively. All the experimental work was conducted at an entry Reynolds number of 28.4×10^{3}.

9.2 EXPERIMENTAL APPARATUS

The arrangement shown in Fig.(4.5c) was used for all the experiments with air as the flow medium. The five-hole pressure probe, with associated instruments was used for flow measurements. The blade angle of the vortex generator was set by special jig, Fig.(4.10). The flow rate was measured using an orifice plate with a carbon tetrachloride manometer, Fig.(4.22).

TABLE 'B'

FIGURE NUMBER	2ϕ (DEG)	FLOW CONDITIONS	GRAPH OF AXIAL VELOCITY DISTRIBUTION	GRAPH OF TANGENTIAL VELOCITY DISTRIBUTION	GRAPH OF FLOW PROPERTIES	RESULTS REPORTED IN TABLE NUMBER
9.1	10	AXIAL	*			
		OPT. SWIRL	*			
9.2		OPT. SWIRL		*		
9.3		AXIAL			*	9/1
9.4		OPT. SWIRL			*	9/2
9.5	20	AXIAL	*			
		OPT. SWIRL	*			
9.6		OPT. SWIRL		*		
9.7		AXIAL			*	9/3
9.8		OPT. SWIRL			*	9/4
9.9	30	AXIAL	*			
		OPT. SWIRL	*			
9.10		OPT. SWIRL		*		
9.11		AXIAL			*	9/5
9.12		OPT. SWIRL			*	9/6

9.3 EVALUATION OF FLOW PROPERTIES

The method of evaluation of flow properties was the same as that used in Chapter Six. Experimental errors were potentially the same as in Chapter Six and the same measures were taken to minimise these. The computer program, 'MASTER PROP', Fig.(6.1) was used to evaluate the flow properties.

9.4 FLOW IN THE DIFFUSERS

Highly unstable flow was experienced in all the diffusers tested. Time-variance was also observed; thus it was necessary to conduct long-time integration in the time domain analyser to obtain average values. Typically these were of the order of 10-20 minutes for each point. Time-variance of the flow also caused problems in obtaining null readings for Rankine vortex swirling measurements. Again long-time integration was conducted of the order of 15-45 minutes for each null reading.

The indexing of figures and tables for the 10^{o}, 20^{o} and 30^{o} diffuser is shown in Table 'B'. Note, for axial flow, the blade angle of the vortex generator was set at zero deg. Also, for the profiles of flow properties, the figures in parentheses are the percentage deviations of the respective values from their mean.

9.5 DISCUSSION

From the experimental results, it is established that the vortex generator produced a reasonable approximation to Rankine vortex swirl, as shown in the tangential velocity profiles of the diffusers tested. The swirl strength decays as it travels downstream, as would be expected, (having greater forced vortex core at downstream stations). The

decay is not in accordance with a constancy of angular momentum at all stations. (Fig. (9.2a)). The reason for this remains to be found. It is felt that perhaps this discrepancy is largely the result of lack of information on the structure of turbulent flow.

The axial velocity profiles for the 10^{o} diffuser show outstanding features. The effect of swirl is marked. For axial flow, the separation tendencies are clearly evident at downstream stations of the diffuser. When the optimum swirl is induced, the axial velocity profiles, outside the boundary layer are more uniform across the cross-section, at downstream stations, thus stabilising the diffuser flow. There is a trend for the axial velocity to dip at the diffuser axis for upstream stations. The above features are clearly shown in Fig.(9.1). It is important that the diffuser axis velocity must not drop below zero in magnitude. This to avoid reversible (vortex breakdown bubble) flow at diffuser axis, which would not improve the diffuser flow.

For the flow in the 20^{o} diffuser, the change in axial velocity due to optimum swirl is very marked, Fig.(9.5). For axial flow, it is evident that separation is present at downstream stations. It is felt that the profile at station D3 should be analysed with caution, because it is thought that the flow was asymmetric. When optimum swirl is induced, the velocity at the diffuser axis, at all axial positions, has dropped considerably. The bulk fluid has moved from the diffuser axis to the diffuser wall. This has a very favourable effect by suppressing separation tendencies, thus improving the diffuser flow. The trend

is also more clearly exhibited in the 30^{o} diffuser. The above trend was explained by Senoo, Kawaguchi and Nagata (62) as follows. At the inlet section of the diffuser, the radius of the forced vortex core is small. Since the maximum tangential velocity is inversely proportional to the radius, there is a steep pressure gradient in the radial direction and pressure near the centre is much lower than the pressure at the wall. At a downstream section, the radius of the solid vortex core increases more than the ratio of change of the radius of the diffuser wall, and the free vortex zone is limited to a region of large radii. Consequently the tangential velocity and the radial pressure gradient are small and the pressure near the centre is not so different from the pressure at the wall. Comparing the radial pressure distribution (from the axial velocity profiles) at the inlet section with that at a downstream section, it is clear that the axial pressure gradient near the centre is much larger than that near the wall. The pressure force acting on the core may be balanced by the shear force which in turn severely reduces the axial velocity of the layer of the fluid just outside of the core, and the layer is now involved in the core. In this way the radius of the solid vortex core increases quickly in the axial direction.

From Fig.(9.5) and Fig.(9.9) it is evident that the strength of swirl above the optimum angle would not improve the diffuser flow. From the above figures, a deduction can be made as to what would happen to the axial profiles of the diffuser flow if the swirl strength was to be increased.

If the swirl is increased, new phenomena would occur. First, the diffuser upstream axis velocity would attain a noticeable negative value, indicating that the flow has reversed itself and is moving upstream around the axis. According to So (34), this reversal phenomenon is another characteristic of vortex breakdown flow. As the vortex moves downstream in the diffuser, the pressure near the axis recovers, and the fluid near the axis tends to be pushed back upstream towards the centre of the end wall. So (34) even goes further, to analyse the flow situation for extremely strong swirl, and puts forward a cocoon-like flow pattern structure, positioned on diffuser axes. From the above analysis, it seems that greater swirl induction doesn't improve the diffuser flow, because the favourable effect of increased stability at the wall is unbalanced by the undesirable effect at the diffuser axis. This fact is justified from the flow visualization tests reported in Chapter Eight, where it is evident that the flow for greater blade angles of the vortex generator like 15^{o} and 20^{o}, is more stable at the diffuser wall. It is quite possible that this obscured the view as to what was happening to the diffuser flow at its axis.

The improvement in axial velocity profiles shapes is readily seen from the graphs of variation of flow properties in the 10^{o}, 20^{o} and 30^{o} diffusers. Fig.(9.13) shows the effect of swirl on kinetic energy factor, bearing in mind that for perfectly uniform flow α is equal to unity. For the flow in the 10^{o} diffuser, it is evident that the effect of swirl on the profile is nearly immediate. The improvement

in the flow at downstream station, D4, is such that the α value at station D4 is very nearly equal to the α value at diffuser inlet for pure axial flow, thus confirming the comments regarding separation tendencies. For the 20^{o} diffuser, the effect of swirl is after station D1. The value of α for optimum swirl drops with progress downstream. The overall effect on α seems to be one of consistent improvement. Similar comment apply for the 30^{o} diffuser.

For all the diffusers tested, for axial flow, the mass flux calculated from the axial component of velocity at downstream stations was greater than the mass flux measured at orifice plate. The discrepancy was greater for wide angle diffusers. It is expected that the discrepancy of flow rate is due to asymmetric nature of flow in the diffusers and due to the unsteadiness such as separation, etc. The above mass flux figures moved much closer to the measured value when the optimum swirl was induced. This is another indication that swirl reduces or even eliminates the degree of separation.

The variation of flow properties for the diffusers tested shows that when optimum swirl was induced, the axial kinetic energy decays more rapidly with downstream progress, than pure axial flow. Thus indicating that the optimum swirl improves the diffusion process.

The effect of swirl on the static pressure distribution of the diffusers tested is clearly shown in Chapter Seven. A step further was achieved by evaluating the effect of optimum swirl on pressure recovery, as shown in Figs.(9.14), (9.15) and (9.16) for the 10^{o}, 20^{o} and 30^{o} diffusers

respectively. One must treat static pressure recovery results with care since the values given are from the wall tappings and in swirling flow these will not represent the pressure everywhere across a station. However, comparison can be made between diffusers for different (optimum) swirl severity. For completeness and qualitative comparison, the pressure recovery curve corresponding to inviscid, uniform flow is superimposed. It can be used for no more than this, however, since it is based on a mean inlet velocity whereas all the experimental curves correspond to inlet flow having α greater than unity. At high inlet distortion factors, therefore, experimental points could be obtained well above the C_p ideal line. From the above figures, it is evident that reduction of separation due to optimum swirl caused the performance to increase. The increase in the performance is much more marked in the 10^o and 20^o diffusers than in the 30^o diffuser.

The difficulties encountered in assessing the diffuser performance were no different from those of Chapter Six. The problem is explicitly explained in the chapter mentioned. The above pressure recovery is measured against the value at a station in the supply pipe sufficiently upstream to be un-affected (within experimental accuracy) by the problem at the pipe-diffuser join.

The static pressure distribution in the diffusers tested Figs.(7.2),(7.6) and (7.7) clearly indicates that above the optimum swirl angles, there is no prospect for

further improvement. Perhaps this is so because the turbulence in the boundary layer along the diffuser wall becomes stronger due to swirl, and the displacement thickness of boundary layer with respect to the axial velocity component does not develop quickly for the axial pressure gradient. Consequently an optimum swirl improves the pressure recovery coefficient of the diffuser but if the swirl is strong, a large forced vortex core is developed at the centre where the axial velocity is very low. That is, the effective cross-sectional area of the section is reduced by a strong swirl and a low pressure recovery coefficient results.

The inlet pipe, being 24.5 diameter long, gave a thick inlet boundary layer at the diffuser entry. The condition is typical of many diffusers mounted in extensive pipe system. A hot-wire traverse at the entry section showed θ/D to be about 4.0×10^{-2}

9.6 CONCLUSIONS

1. The tangential component of swirling flow was represented closely by a Rankine vortex. The axial velocity at the centre of vortex was low. For the 20^{o} and 30^{o} diffuser the forced vortex core of Rankine vortex approximately coincided with the displacement area of axial velocity at the centre.

2. In all the diffusers tested, by adding optimum swirl, the axial velocity distribution across the section was improved; as a result, separation tendencies were either minimised or eliminated and the pressure recovery coefficient was increased.

3. The presence of optimum Rankine vortex swirl permits diffusers of relatively high double conical angle and area ratio to be designed with yet better performance.

4. In all the diffusers tested, the presence of Rankine vortex swirl caused the decay of axial kinetic energy more rapidly with downstream progress than pure axial flow, thus indicating improvement in the diffusion process.

5. The results agree with Hoadley (53), Senoo, Kawaguchi and Nagata (62) and Shaalan and Shabaka (55) in that the improvement due to the presence of Rankine vortex swirl in the diffusers tested is subject to an optimum intensity of swirl, above which it deteriorates.

6. The conclusions regarding the influence of Rankine vortex swirl arrived at by the qualitative analysis (flow visualization tests) agree with those of the quantitative analysis.

7. As in the case of forced vortex addition (Chapter 6), the circulation Γ is not conserved with downstream travel in the diffuser. Plots of tangential velocity show that the Rankine vortex core expands with downstream motion.

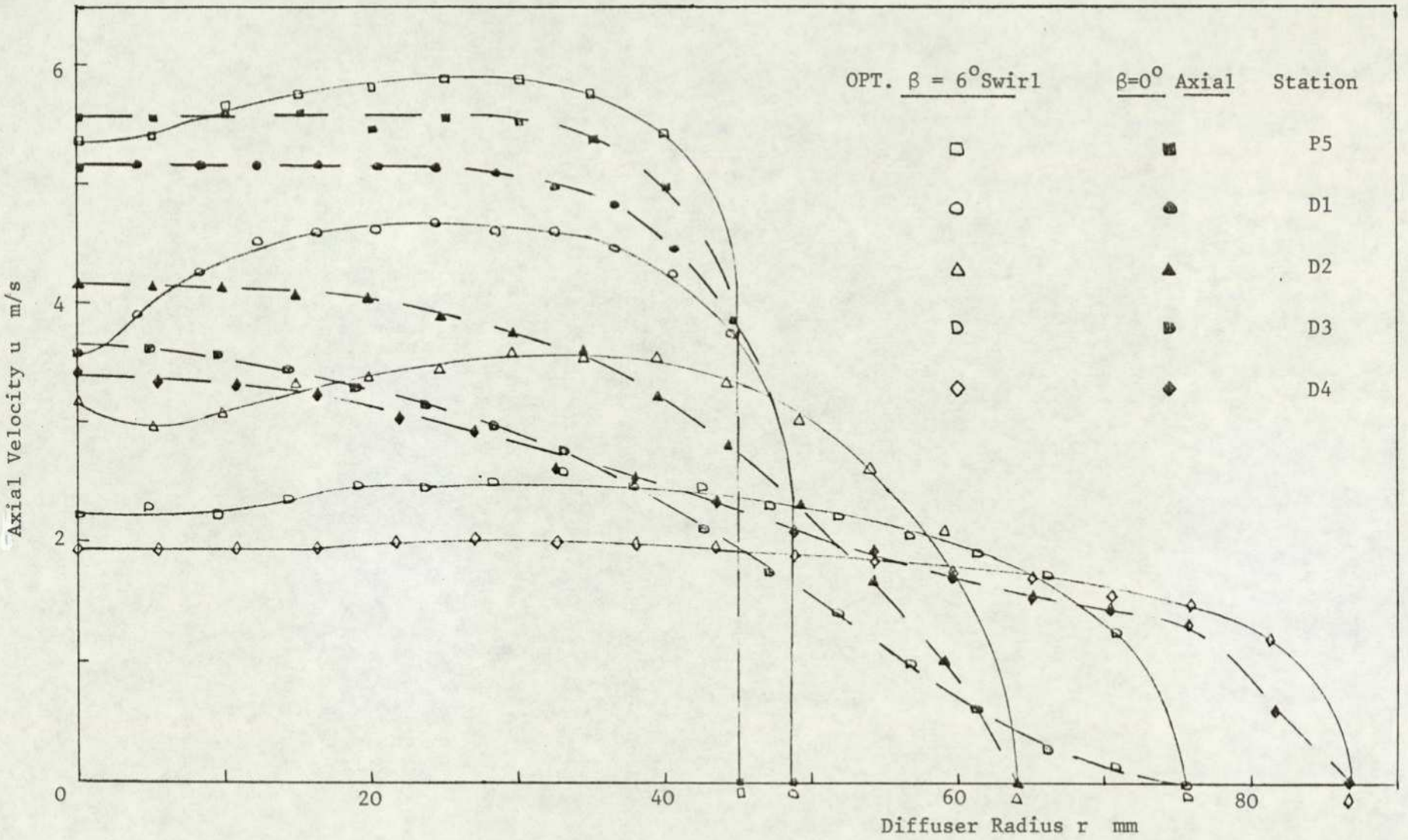

FIG. 9.1 AXIAL VELOCITY DISTRIBUTION IN 10 DEGREE DIFFUSER WITH OPT.RANKINE VORTEX SWIRL.

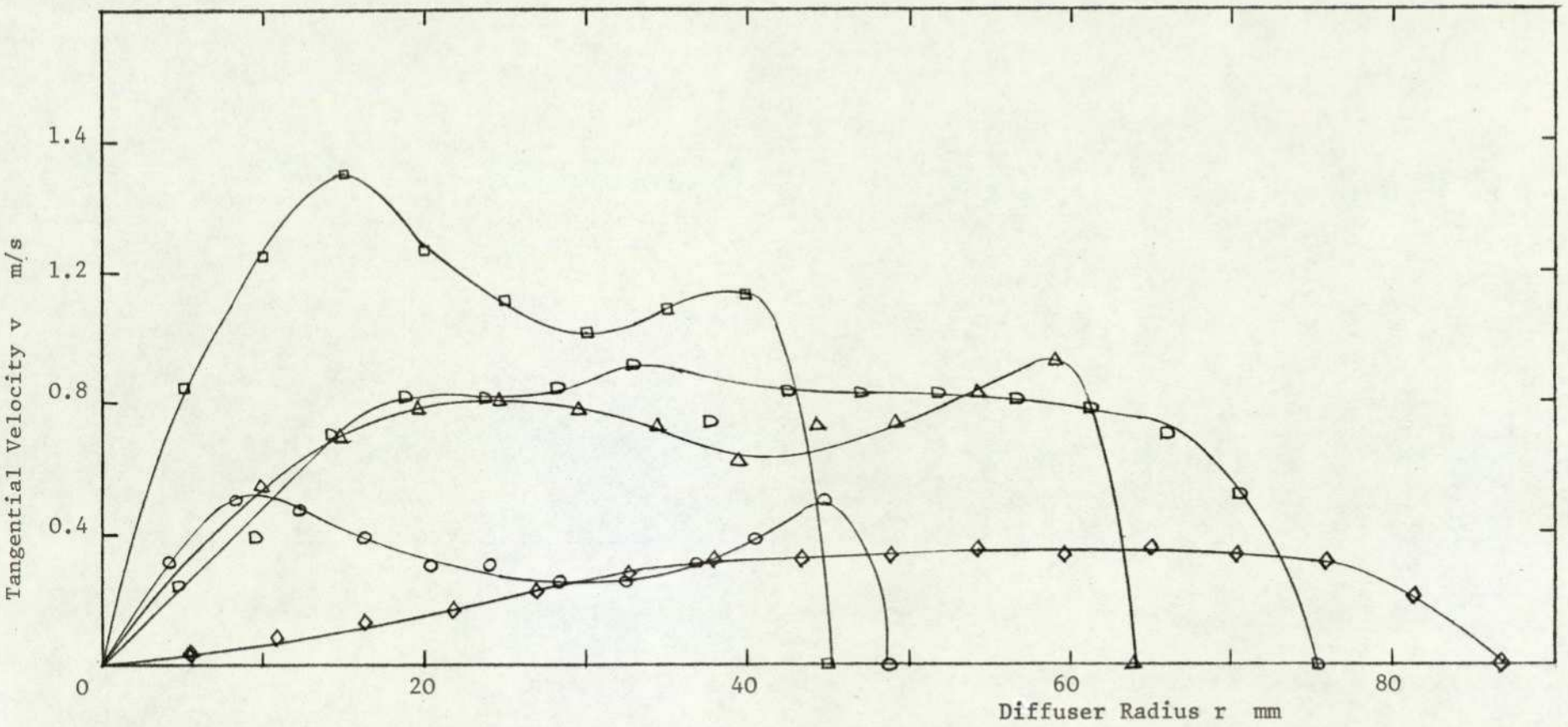

FIG. 9.2 TANGENTIAL VELOCITY DISTRIBUTION IN 10 DEGREE DIFFUSER WITH OPT. RANKINE VORTEX SWIRL.

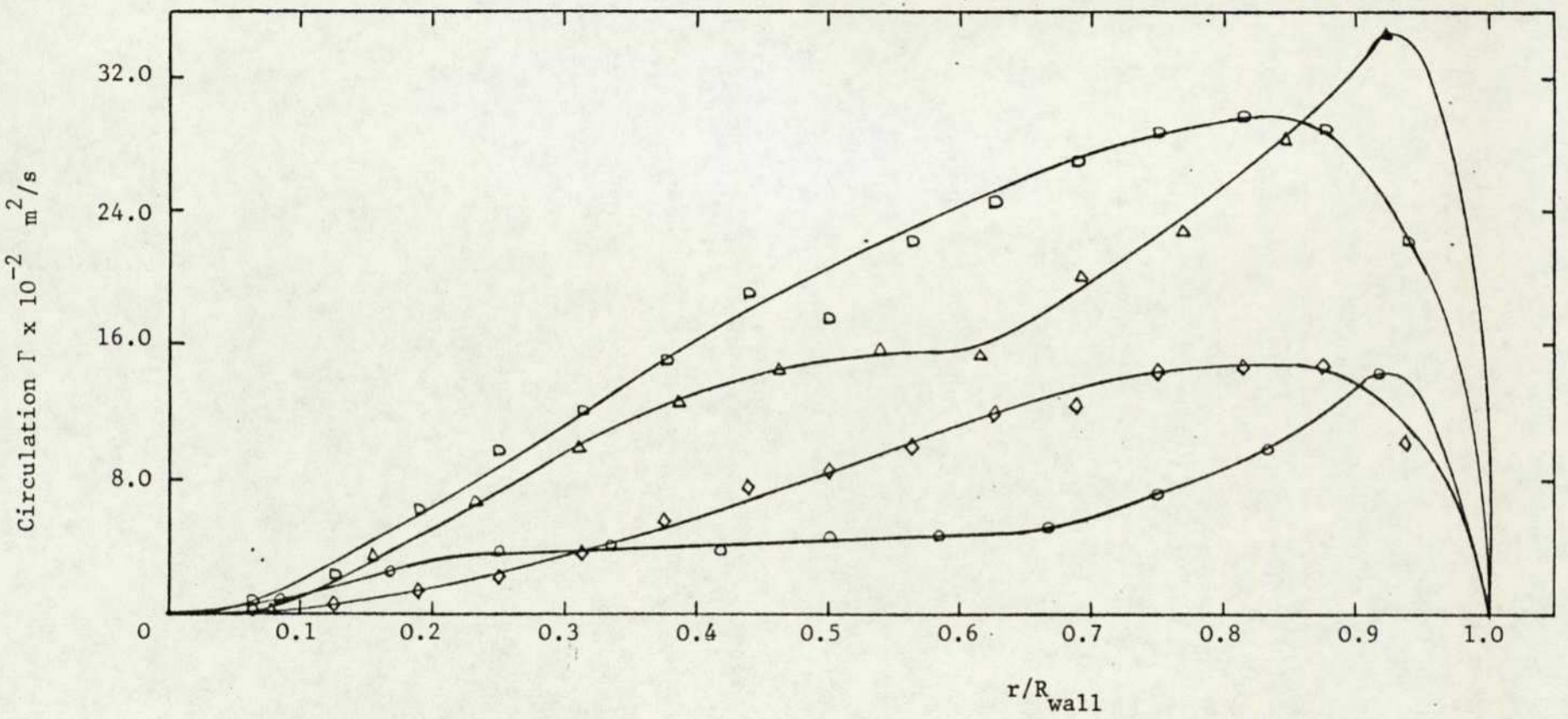

FIG.9.2a. DISTRIBUTION OF CIRCULATION IN 10 DEGREE DIFFUSER WITH OPT.RANKINE VORTEX SWIRL.

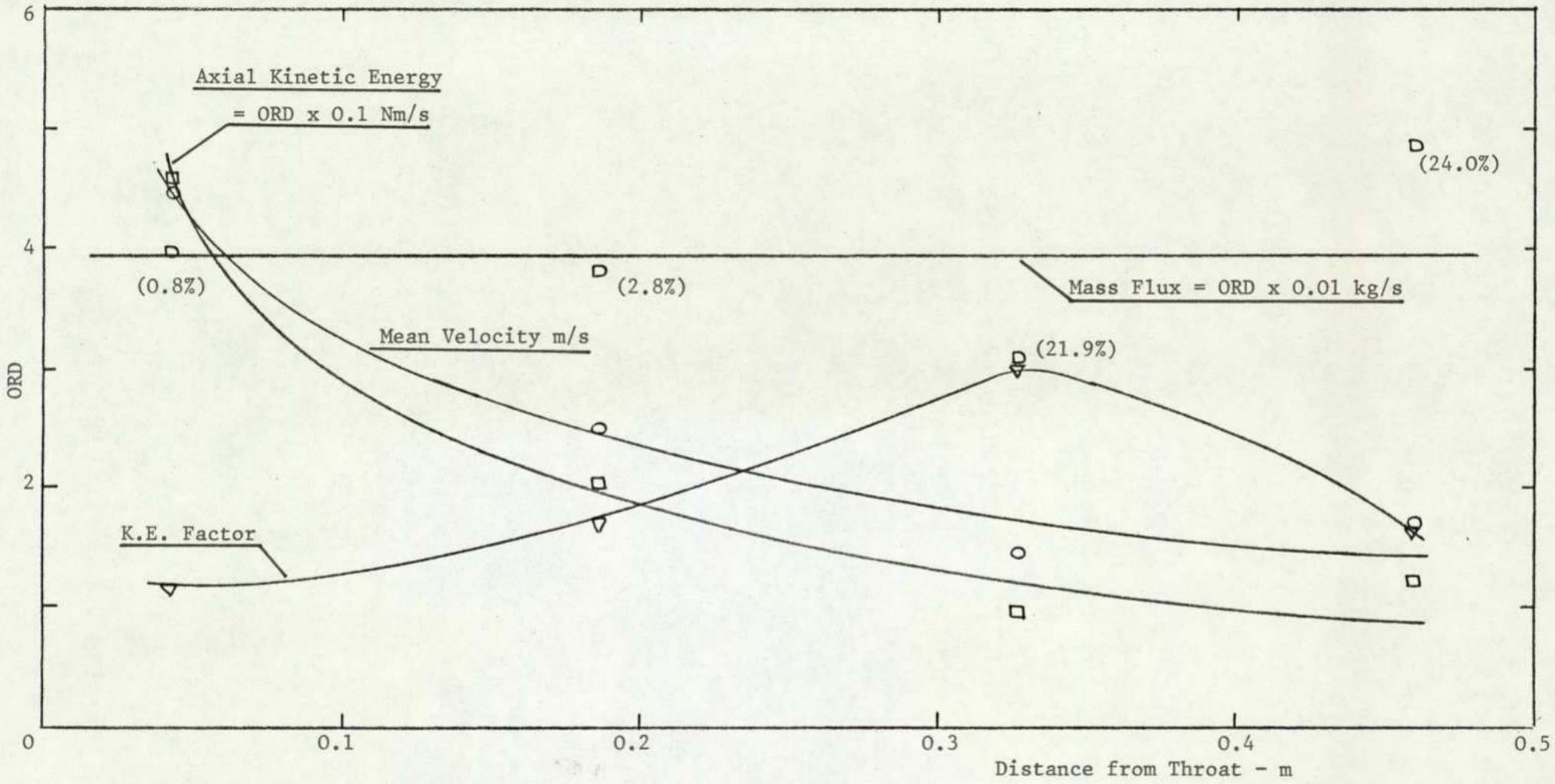

FIG. 9.3 VARIATION OF FLOW PROPERTIES IN 10 DEGREE DIFFUSER WITH AXIAL FLOW ($\beta=0^{o}$)

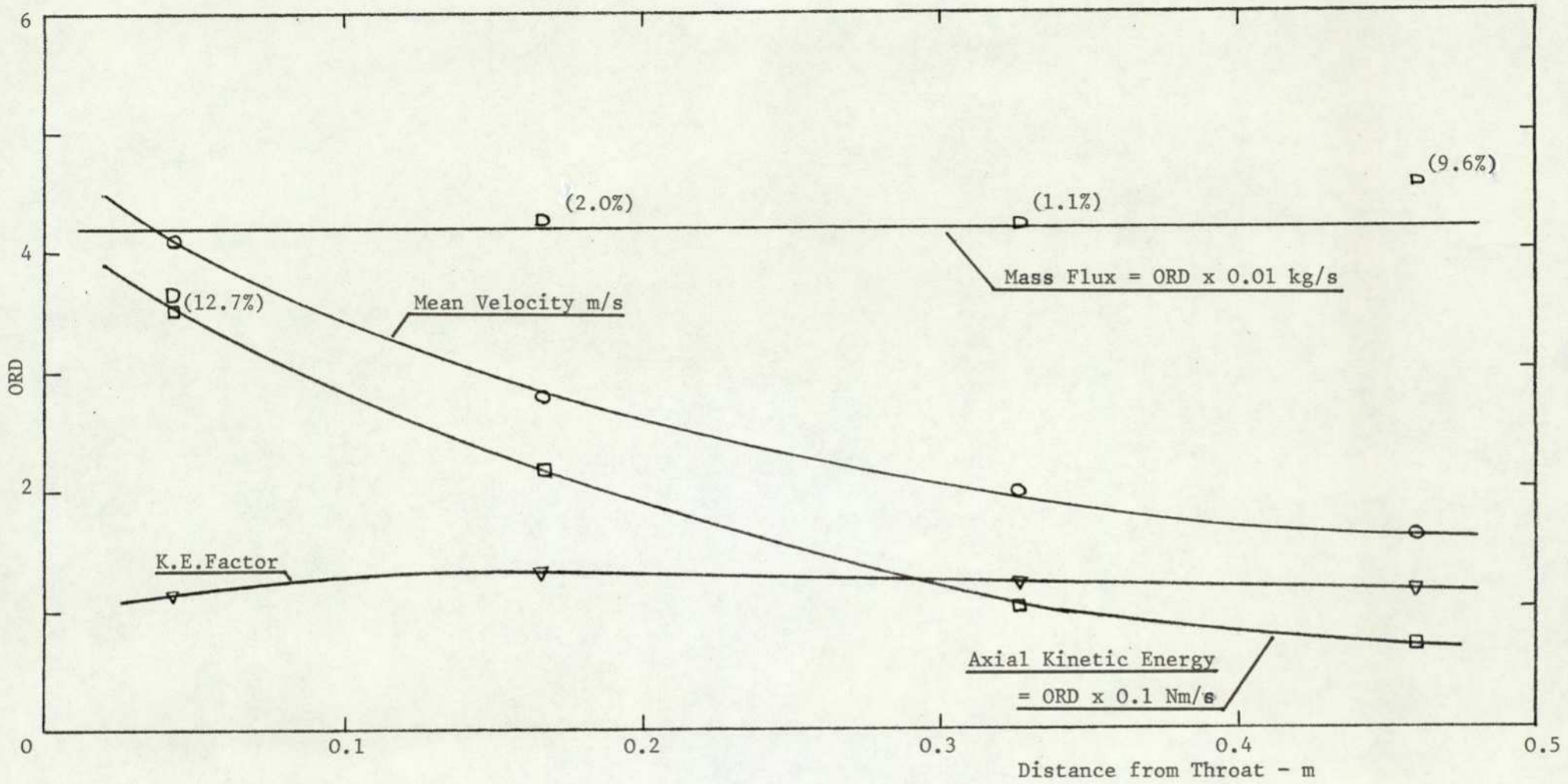

FIG. 9.4 VARIATION OF FLOW PROPERTIES IN 10 DEGREE DIFFUSER WITH OPT. RANKINE VORTEX SWIRL.

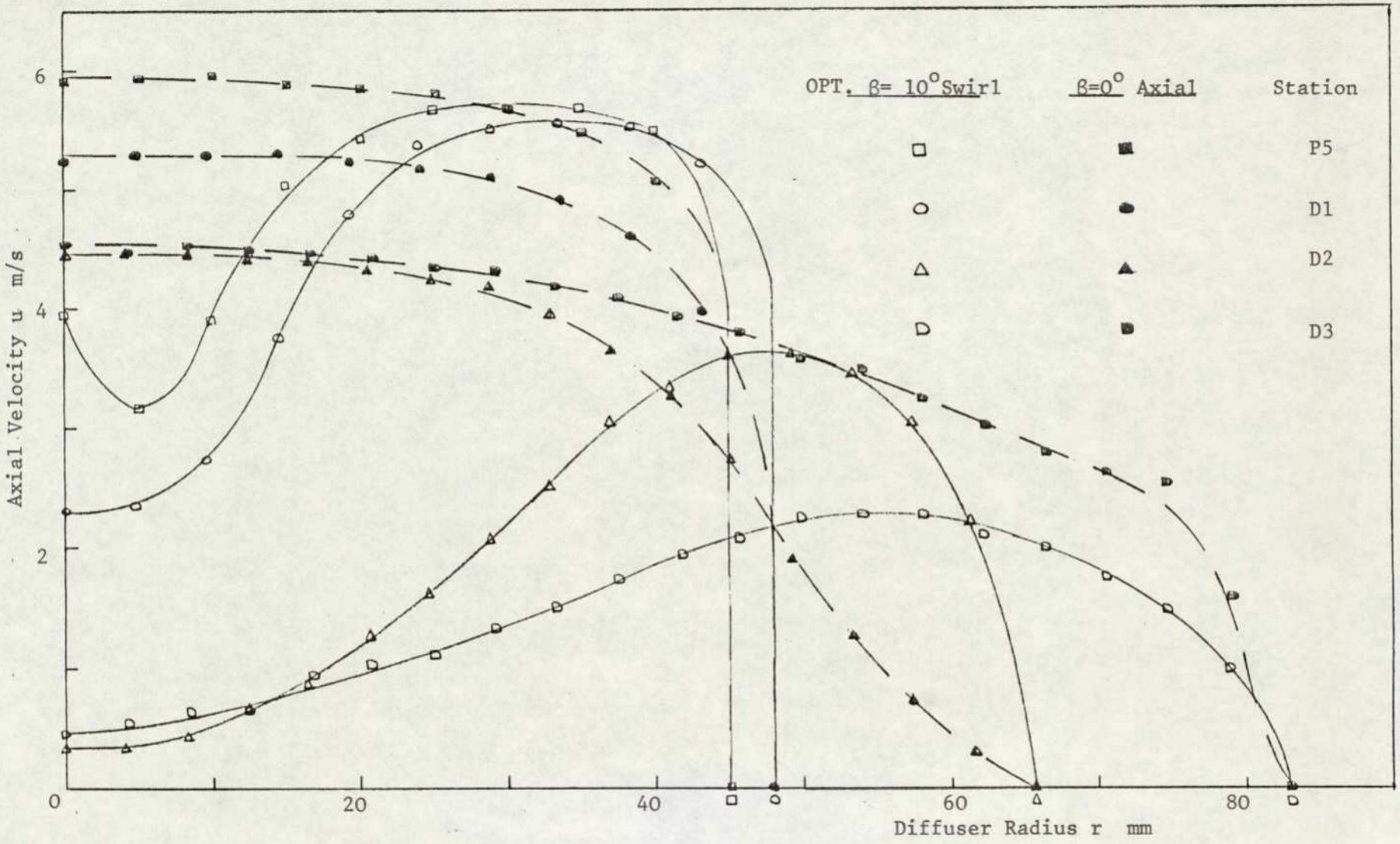

FIG. 9.5 AXIAL VELOCITY DISTRIBUTION IN 20 DEGREE DIFFUSER WITH OPT. RANKINE VORTEX SWIRL.

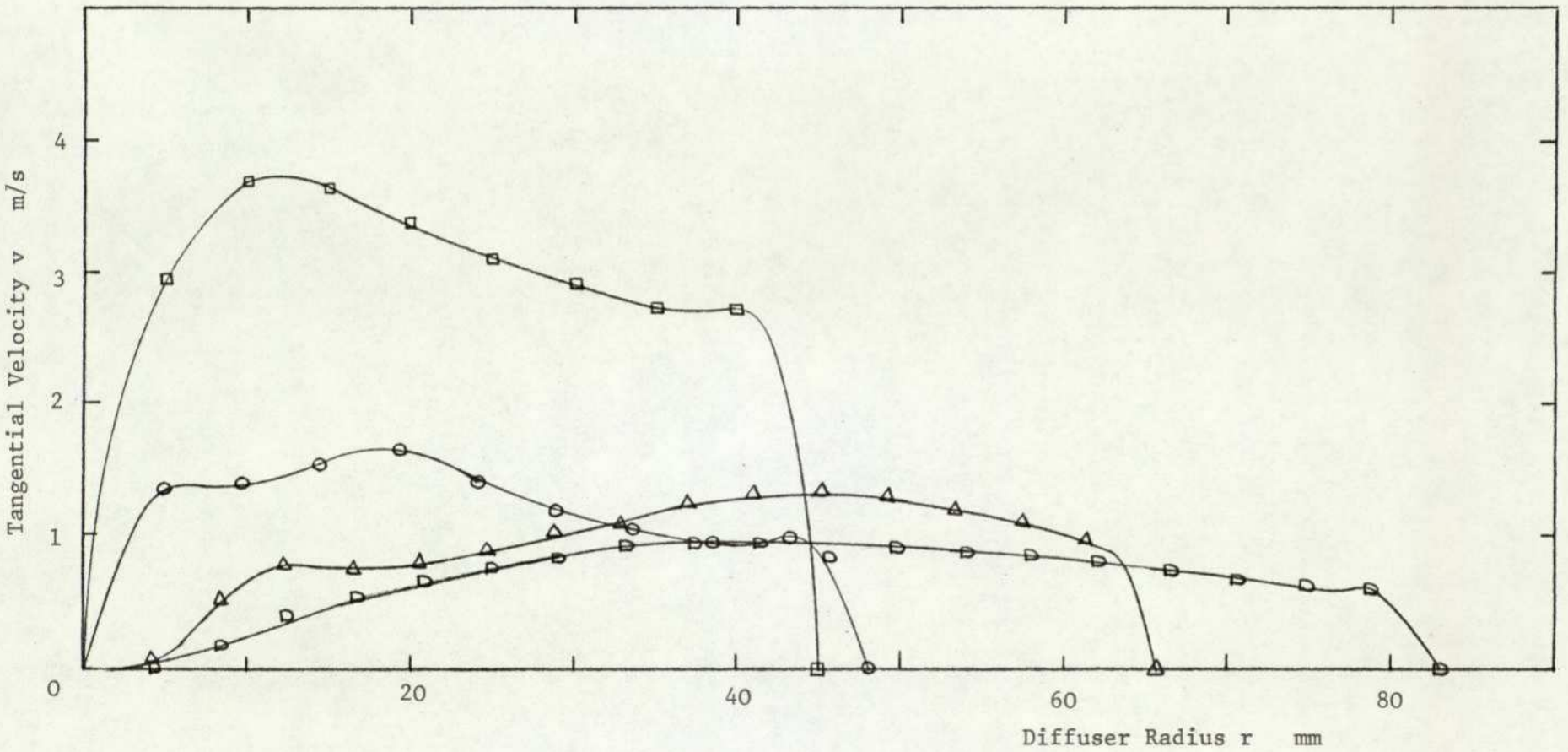

FIG. 9.6 TANGENTIAL VELOCITY DISTRIBUTION IN 20 DEGREE DIFFUSER WITH OPT. RANKINE VORTEX SWIRL.

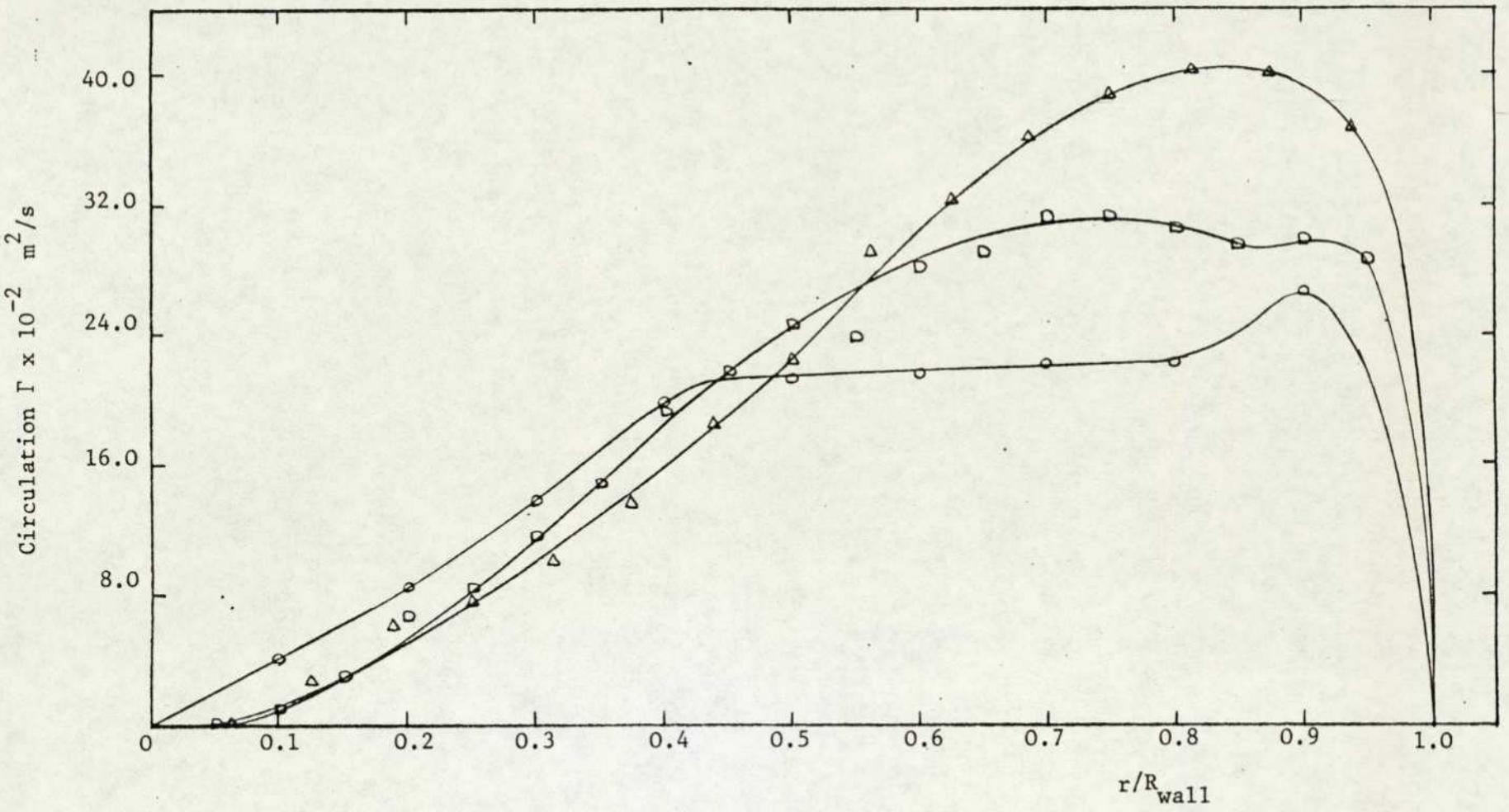

FIG.9.6a. DISTRIBUTION OF CIRCULATION IN 20 DEGREE DIFFUSER WITH OPT.RANKINE VORTEX SWIRL.

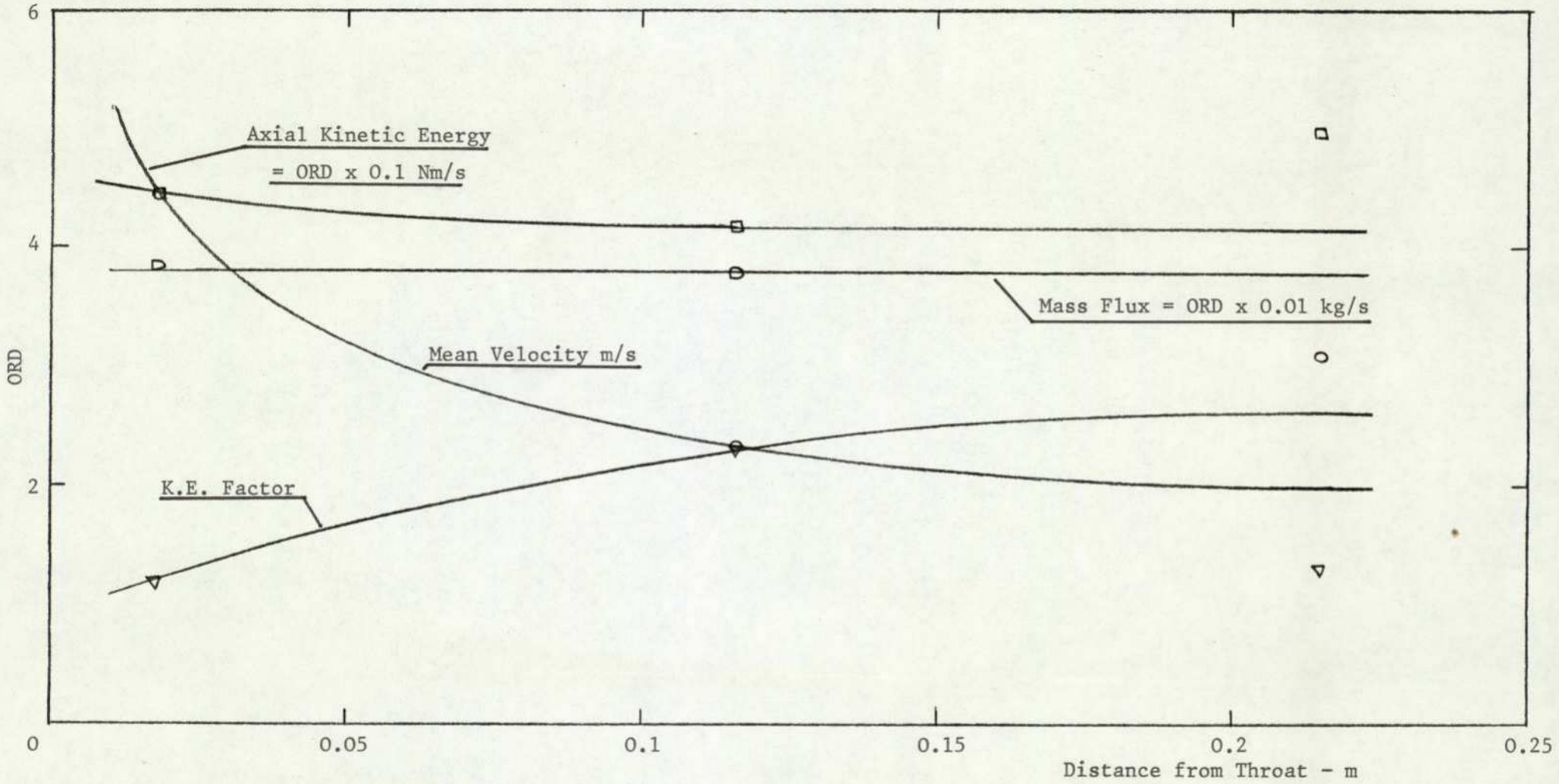

FIG. 9.7 VARIATION OF FLOW PROPERTIES IN 20 DEGREE DIFFUSER WITH AXIAL FLOW ($\beta = 0^{o}$).

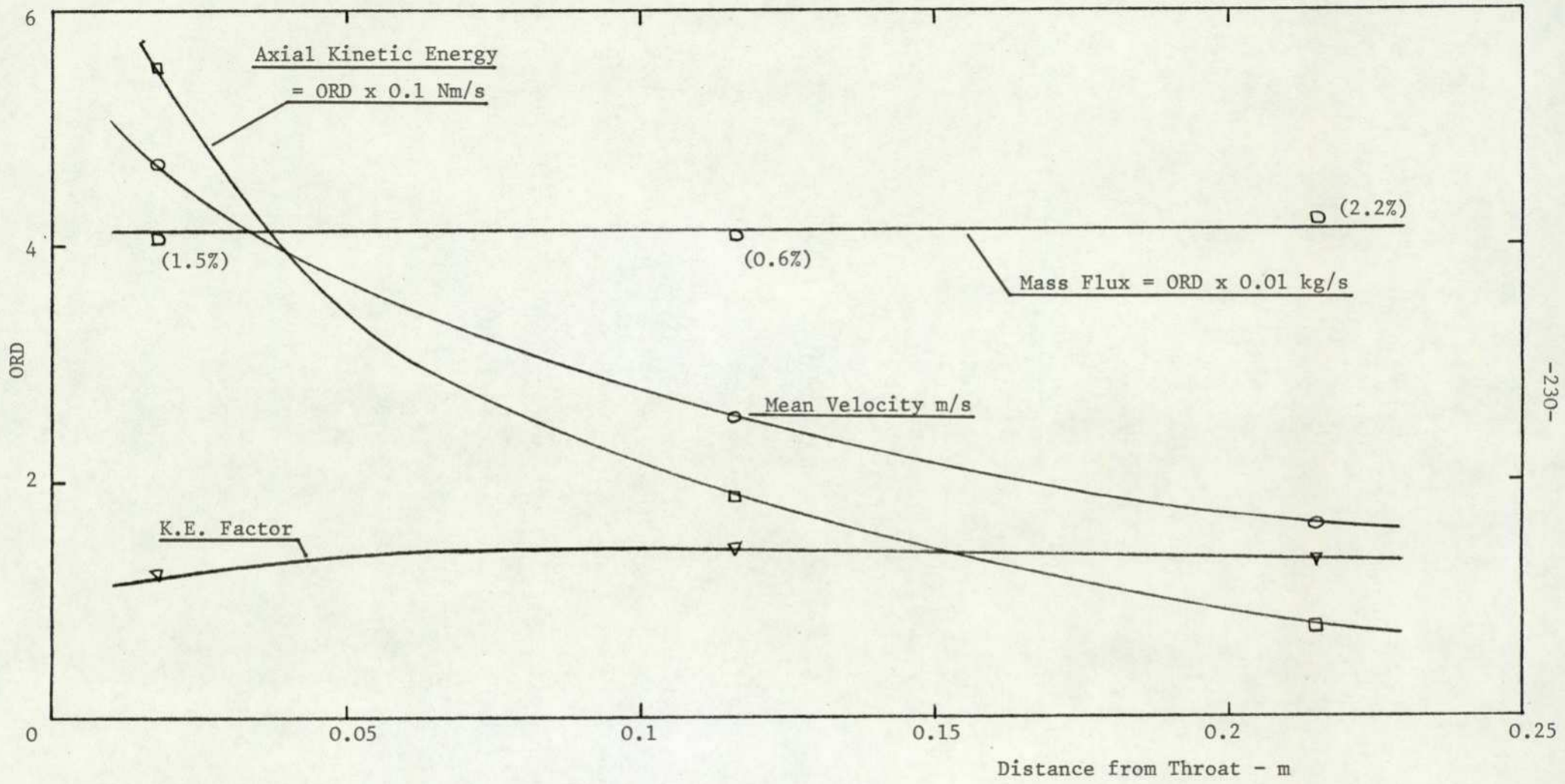

FIG. 9.8 VARIATION OF FLOW PROPERTIES IN 20 DEGREE DIFFUSER WITH OPT. RANKINE VORTEX SWIRL.

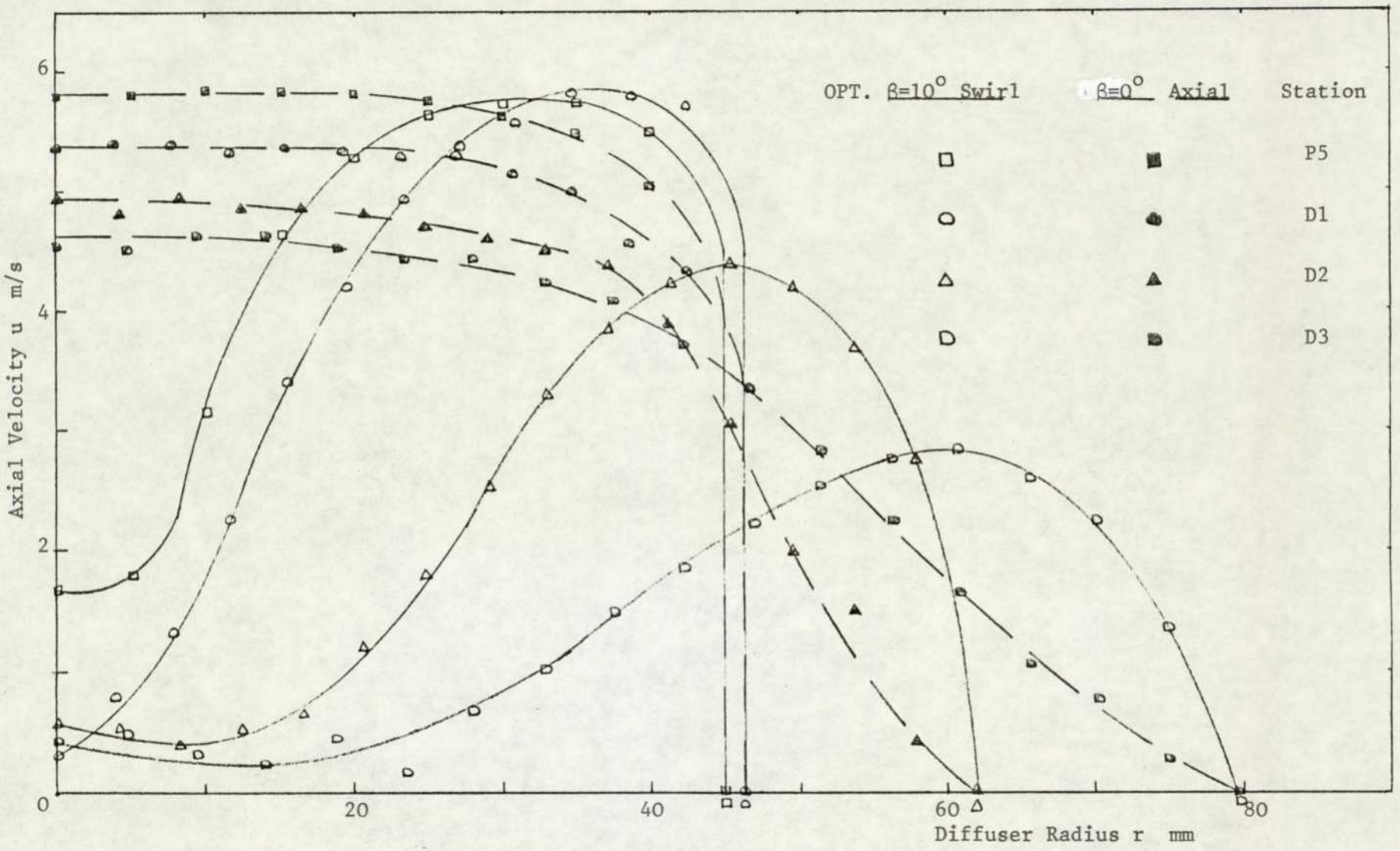

FIG. 9.9 AXIAL VELOCITY DISTRIBUTION IN 30 DEGREE DIFFUSER WITH OPT. RANKINE VORTEX SWIRL.

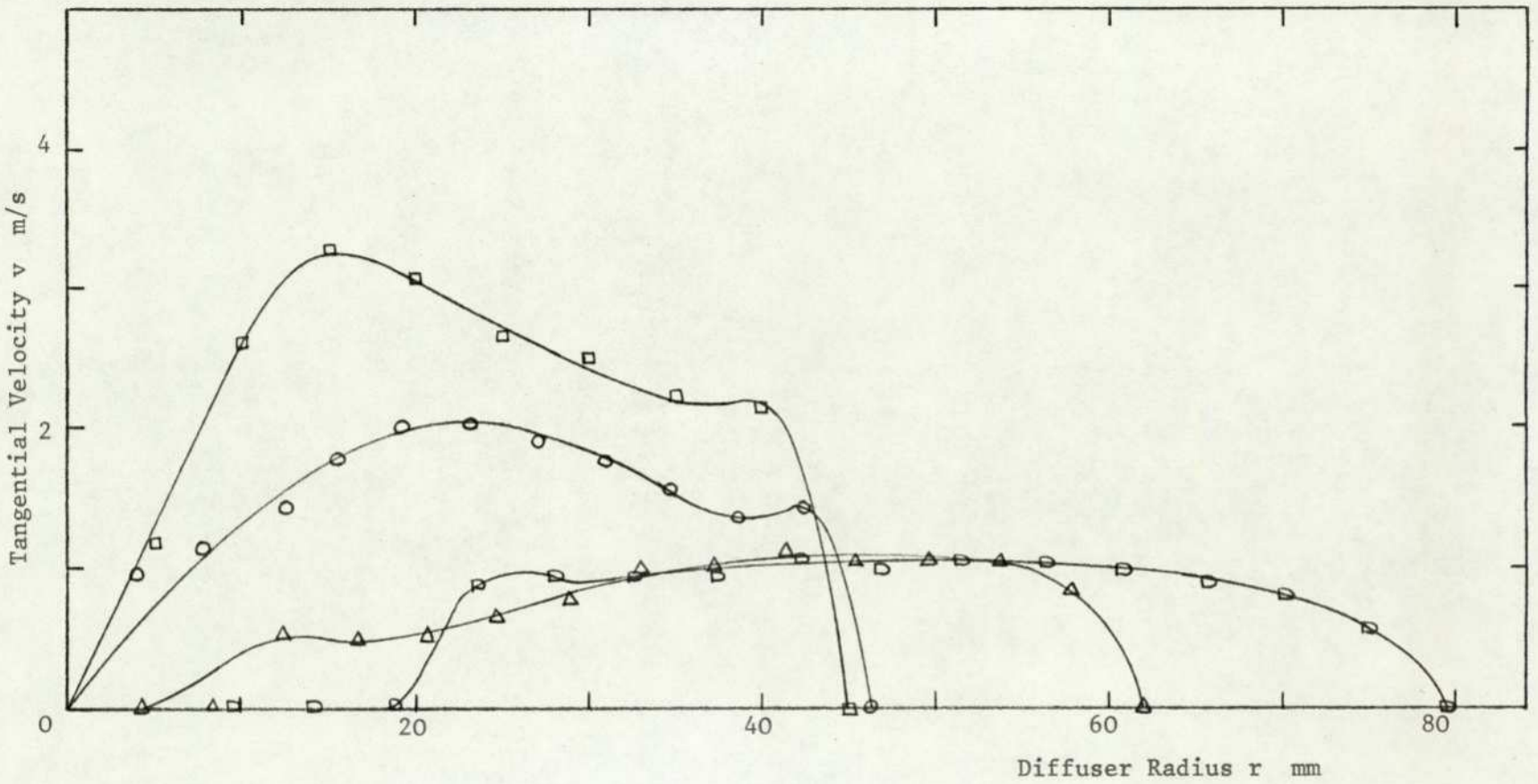

FIG. 9.10 TANGENTIAL VELOCITY DISTRIBUTION IN 30 DEGREE DIFFUSER WITH OPT. RANKINE VORTEX SWIRL.

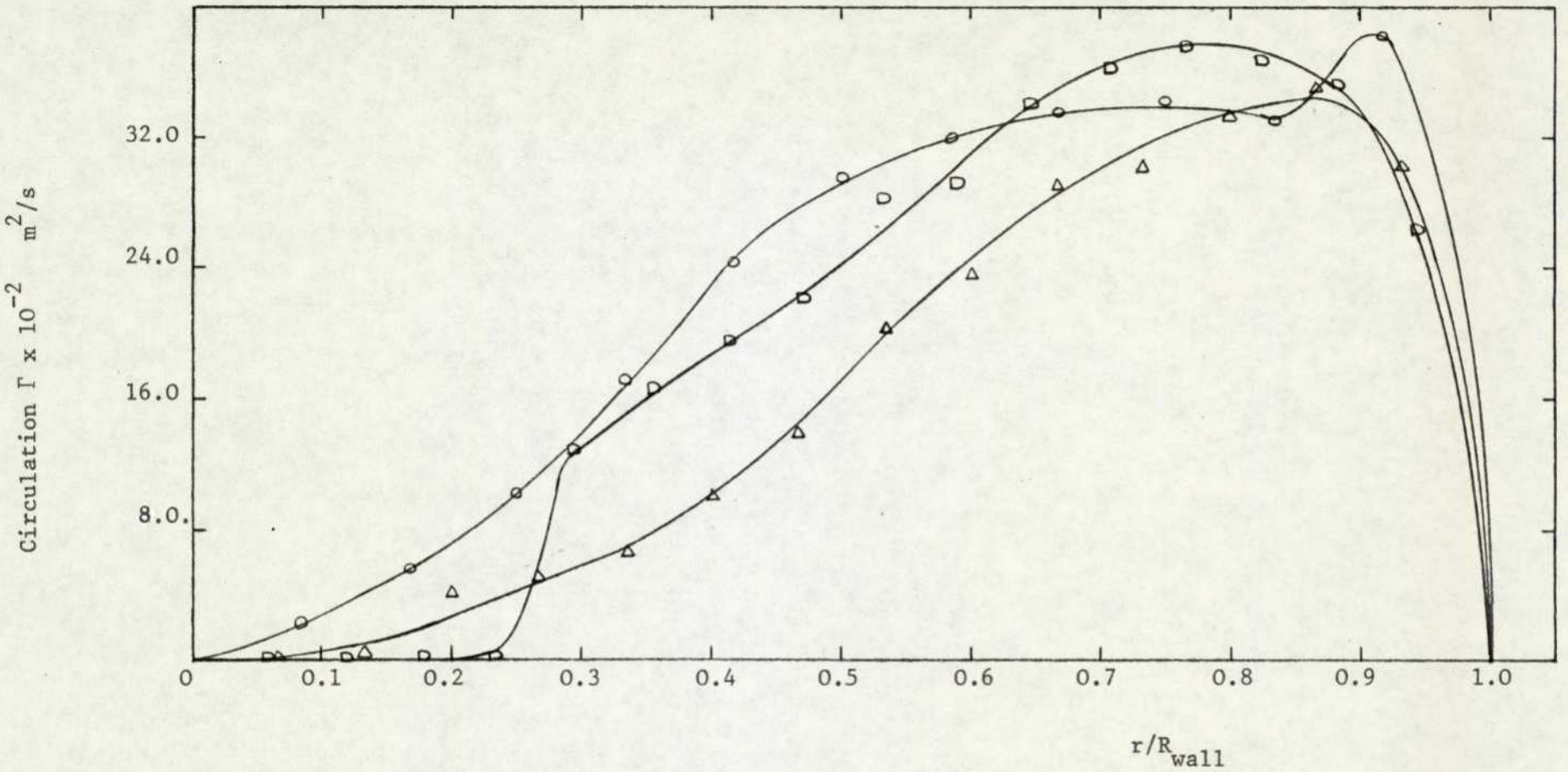

FIG.9.10a. DISTRIBUTION OF CIRCULATION IN 30 DEGREE DIFFUSER WITH OPT.RANKINE VORTEX SWIRL.

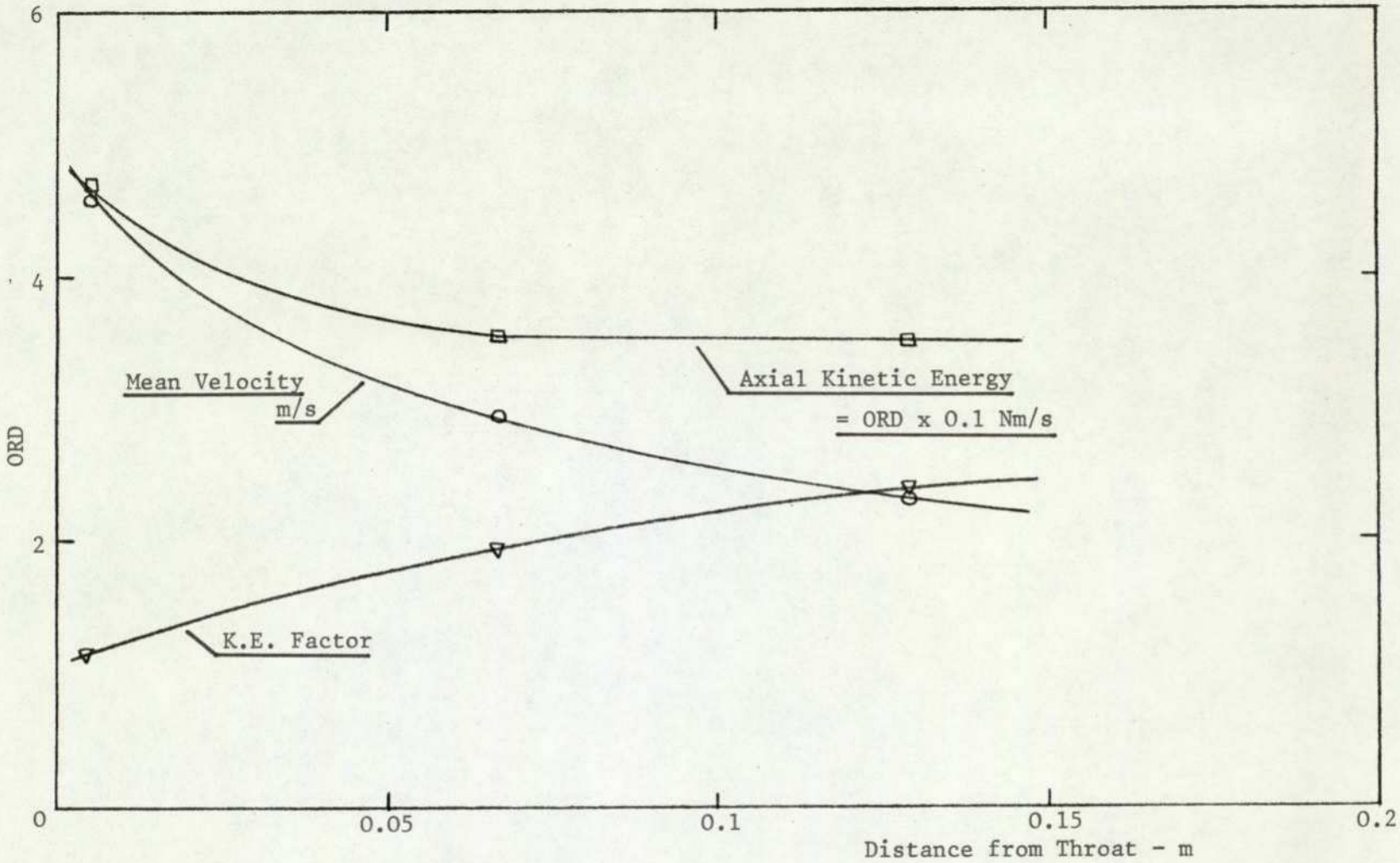

FIG. 9.11 VARIATION OF FLOW PROPERTIES IN 30 DEGREE DIFFUSER WITH AXIAL FLOW ($\beta = 0^{o}$).

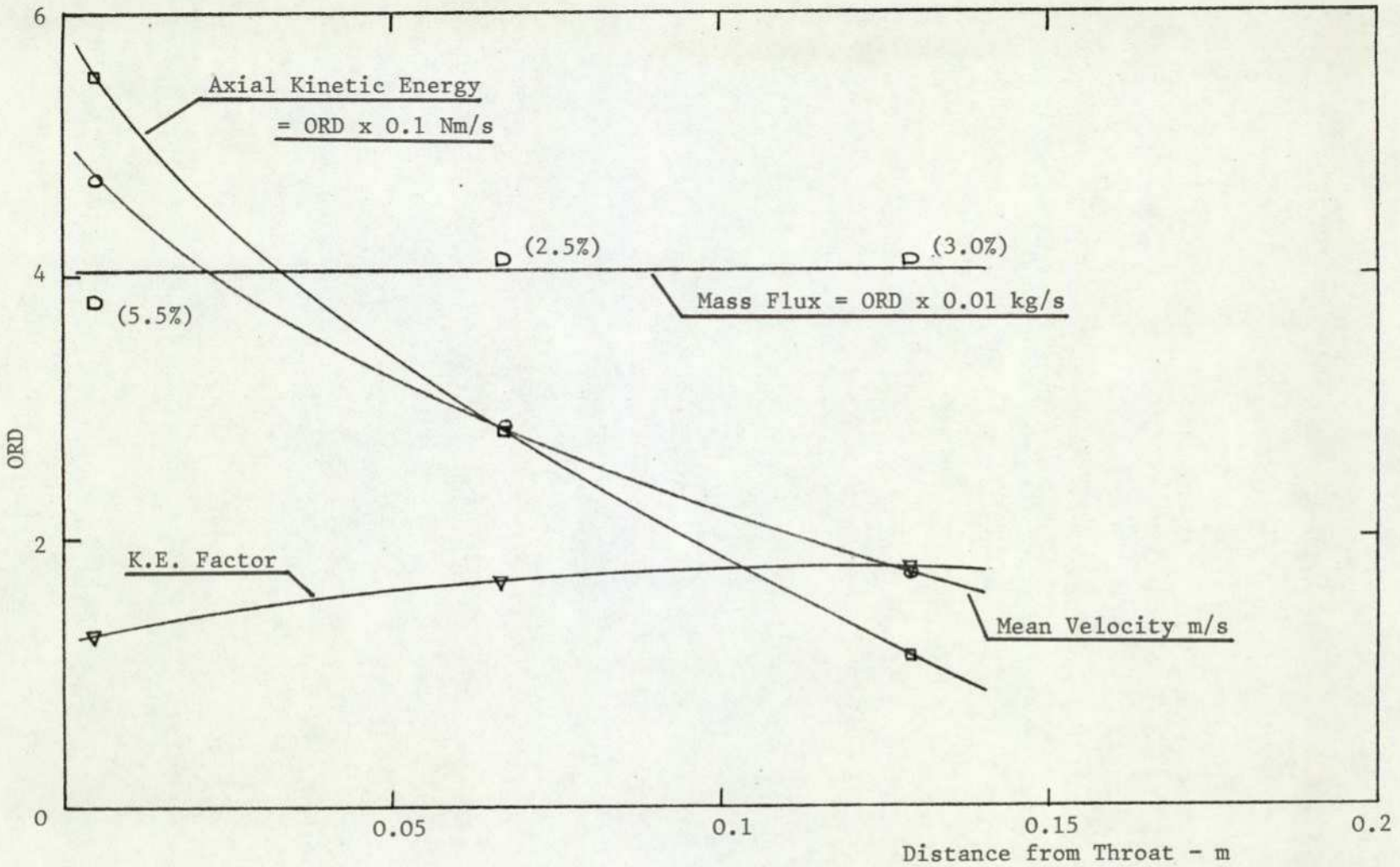

FIG. 9.12 VARIATION OF FLOW PROPERTIES IN 30 DEGREE DIFFUSER WITH OPT. RANKINE VORTEX SWIRL.

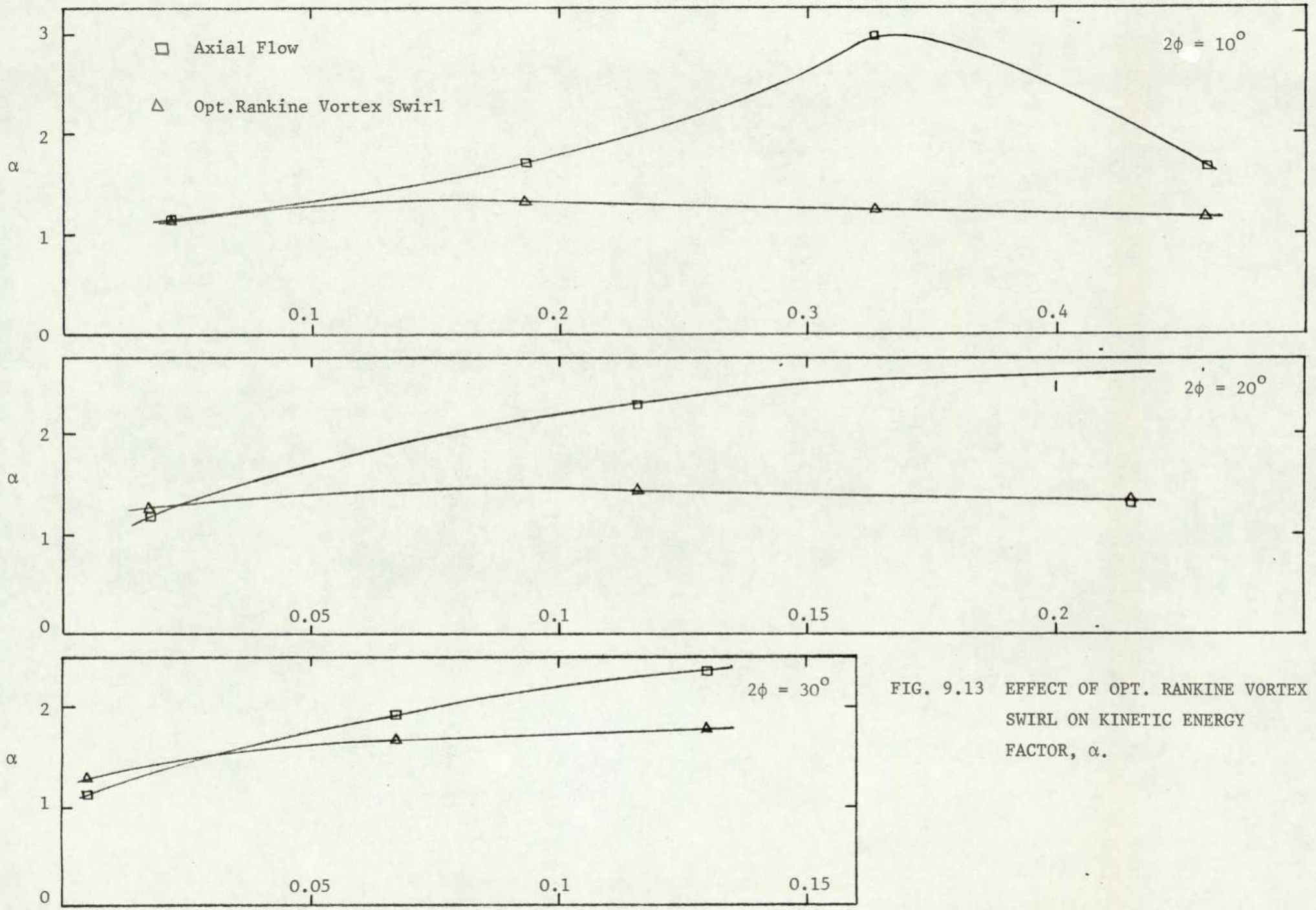

FIG. 9.13 EFFECT OF OPT. RANKINE VORTEX SWIRL ON KINETIC ENERGY FACTOR, α.

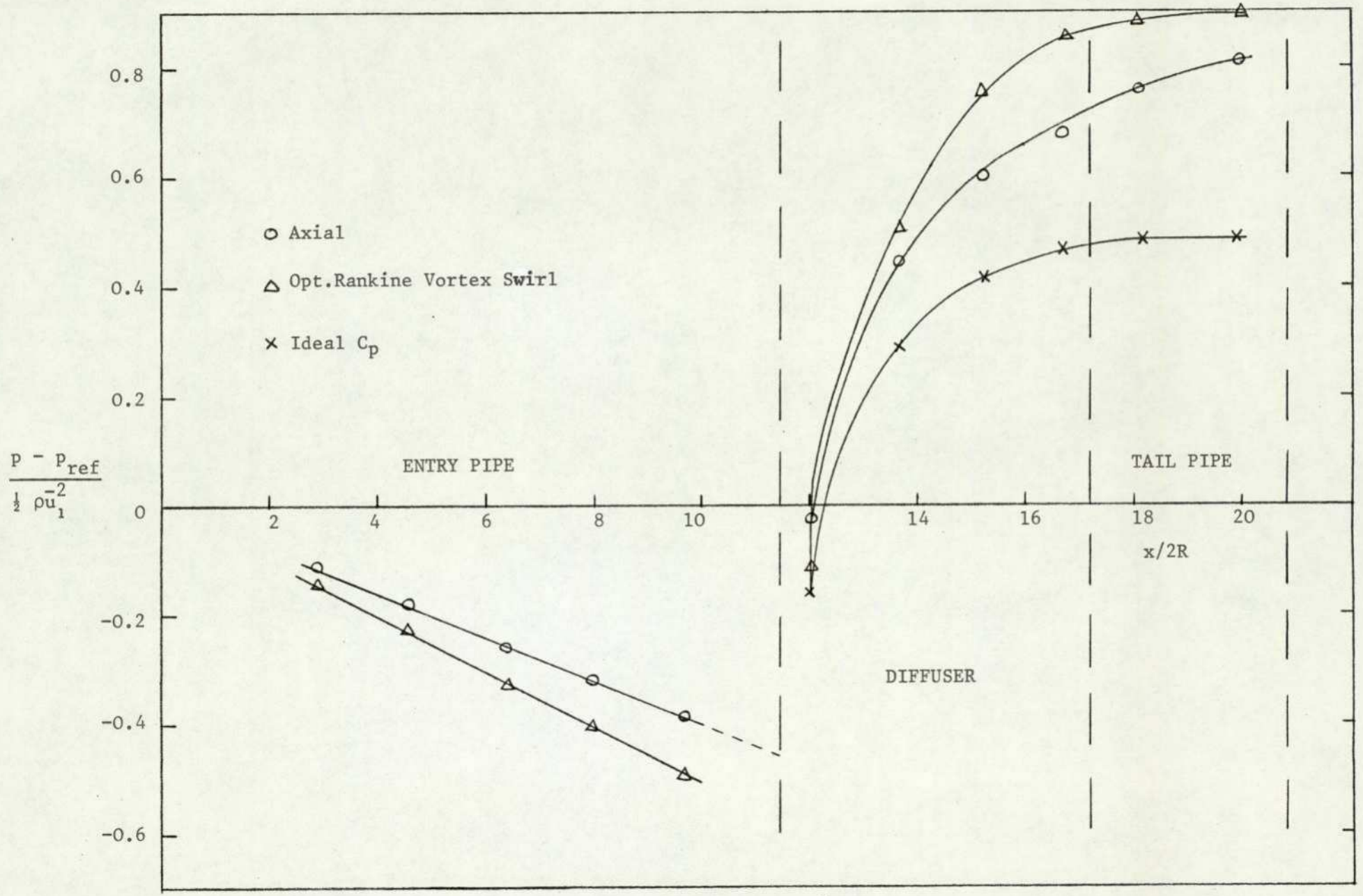

FIG. 9.14 VARIATION OF PRESSURE RECOVERY COEFFICIENT IN 10^{o} DIFFUSER-PIPE COMBINATION.

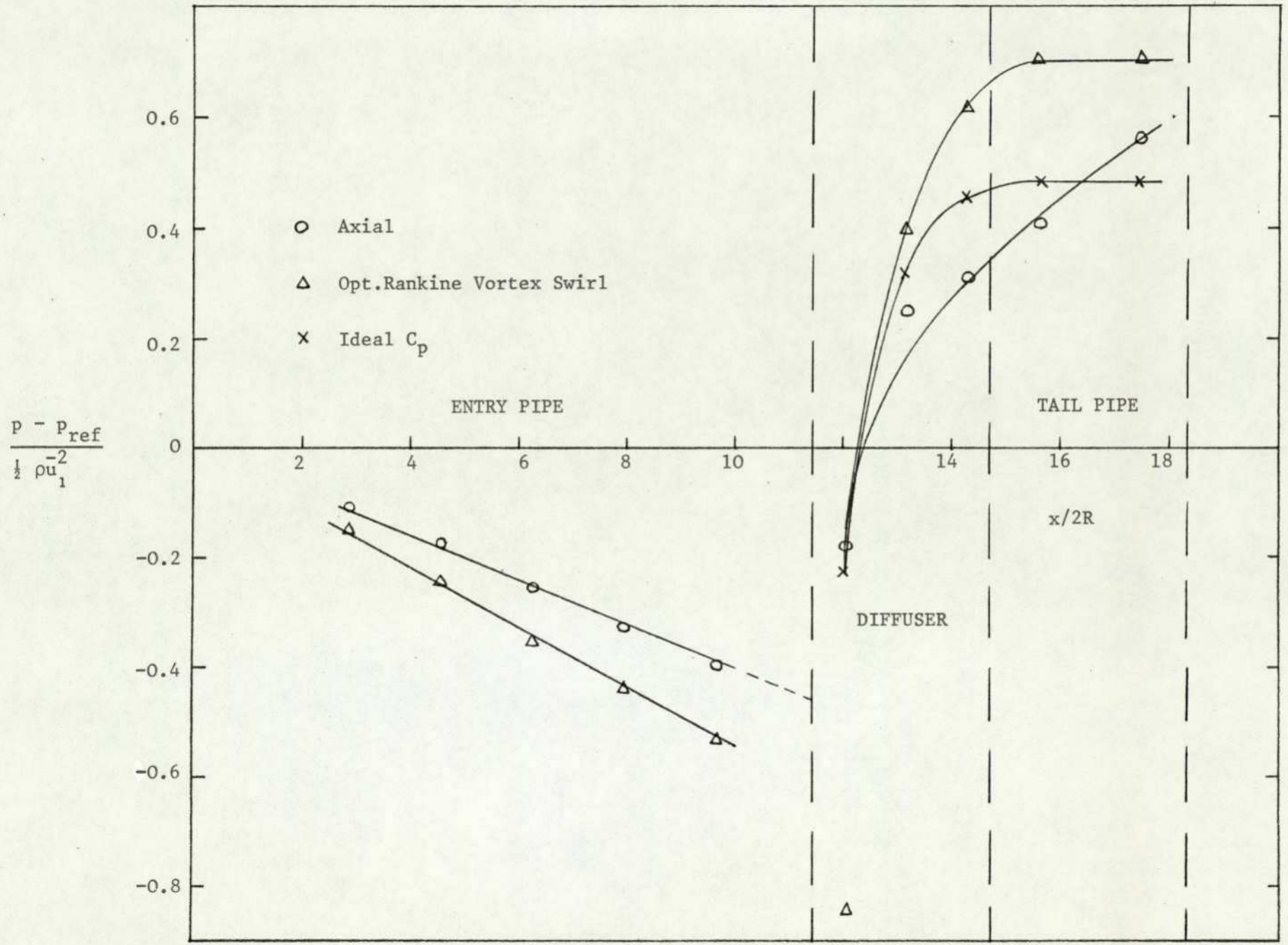

FIG. 9.15 VARIATION OF PRESSURE RECOVERY COEFFICIENT IN 20° DIFFUSER-PIPE COMBINATION.

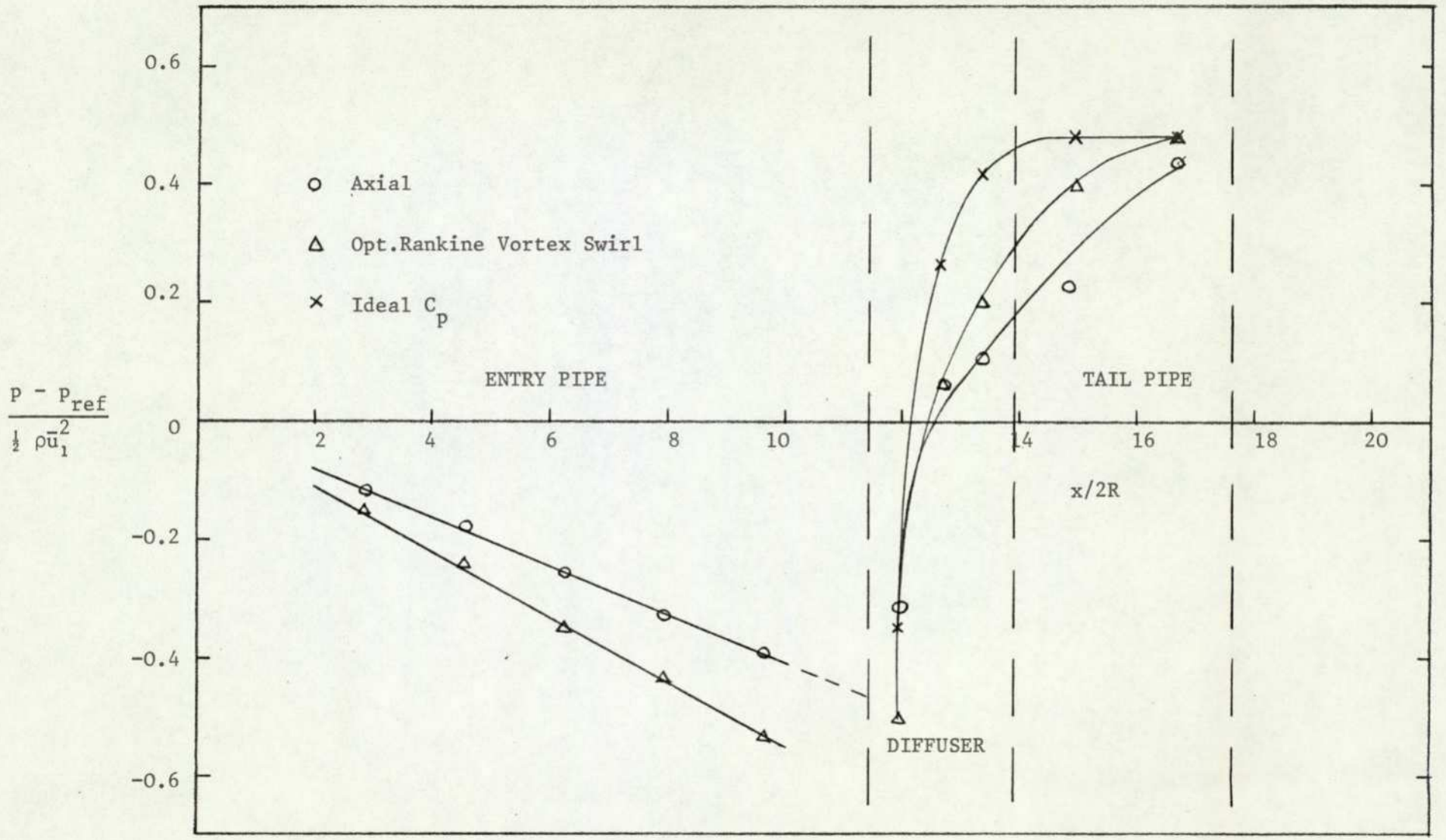

FIG. 9.16 VARIATION OF PRESSURE RECOVERY COEFFICIENT IN 30° DIFFUSER-PIPE COMBINATION.

CHAPTER TEN

EVALUATION OF DIFFUSER PERFORMANCE

10.1 INTRODUCTION

Chapter Three lays down the foundation for the presentation of relevant theories for expressing diffuser performance in a logical manner. The analysis was also concentrated on developing a suitable basis for presenting such information when the flow at entry of the diffuser possesses a swirl component of velocity.

The limitations of each of the analyses were presented and it was observed that some degree of ambiguity exists in the estimation of diffuser performance, perhaps this being more serious when swirl is present. It would be unreasonable to hope to achieve the same numerical answer from each theoretical model for a particular flow situation, because the models presented were all based on different assumptions, but the general trend of the overall picture of diffuser performance ought to be consistent irrespective of the model used.

The object of the Chapter is, having got the necessary experimental data, to use the data in the theoretical analysis put forward and to observe how the overall picture of the diffuser performance is affected by the presence of swirl.

10.2 ENGINEERING SCIENCES DATA UNIT

The Data Item 76027 provides a comprehensive survey of diffuser performance which gives good background information and enables one to assess the effects of geometrical and flow variables on diffuser performance. It deals with the following items:

(a) parameters used in defining diffuser performance

(b) analytical performance prediction methods

(c) principal features of performance trends with overall diffuser geometry together with comments on the effects of cross-sectional shape and surface finish.

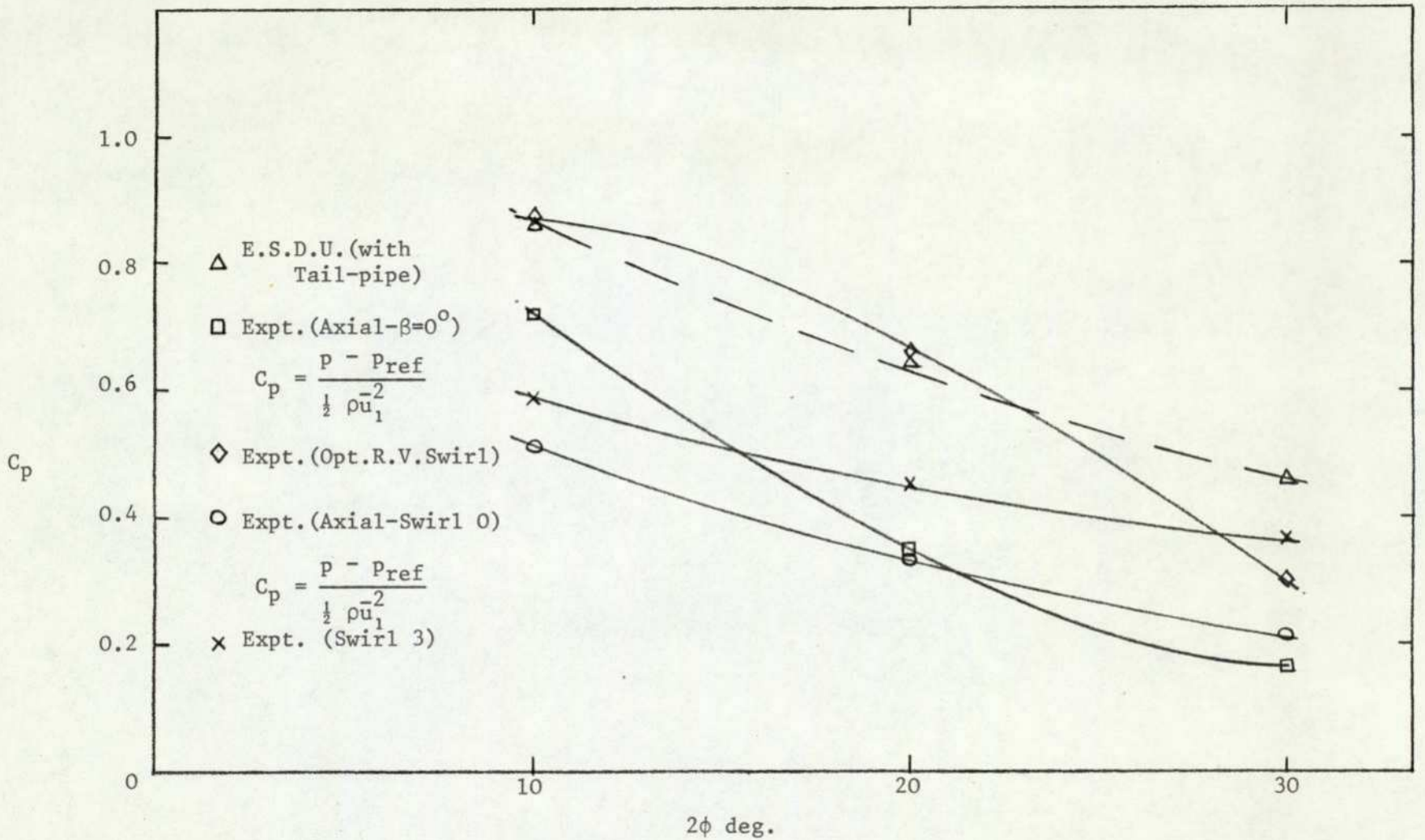

FIG. 10.1 COMPARISON OF PRESSURE RECOVERY COEFFICIENT WITH E.S.D.U.

(d) effect of inlet flow conditions on performance

(e) some methods that have been suggested for improving diffuser performance.

Preliminary calculations were conducted, based on AR and L/R_1 for the 10^o, 20^o and 30^o diffusers. From the pressure recovery map given by the Item, the corresponding values for C_p [= $(p_2 - p_1/\frac{1}{2}\rho\bar{u}^2)$] and ϕ were obtained, Fig.(10.1). The values are reported in Table (10/1). Note, the above values of C_p could only be used as a guide line. Fig.(10.1) also shows the calculated C_p based on experimental results for different kind and severity of swirl.

10.3 APPLICATION OF COCKRELL AND MARKLAND'S MODEL

It is thought that a brief outline of the model may be beneficial for the discussion to follow.

The pressure loss coefficient, λ , is

$$\lambda = 1 - C_p/(1 - A_1^2/A_2^2) \qquad (3.2.2.6)$$

If the axial velocity distribution is uniform at inlet and final station, then Patterson's energy equation reduces to

$$\eta = 1 - \lambda \qquad (3.3.2.13)$$

Detailed calculations were conducted to evaluate λ and η for the 10^o, 20^o and 30^o diffusers for different kinds and severity of swirl. For Rankine vortex swirl Figs.(10.2) (10.3) and (10.4) show the effect of axial flow and optimum swirl on η and λ with downstream progress for the diffusers tested. The effect of swirl on η with respect to the double conical angle of the diffuser is shown in Fig.(10.5). The calculated results are tabulated in Tables (10/2), (10/3) and (10/4).

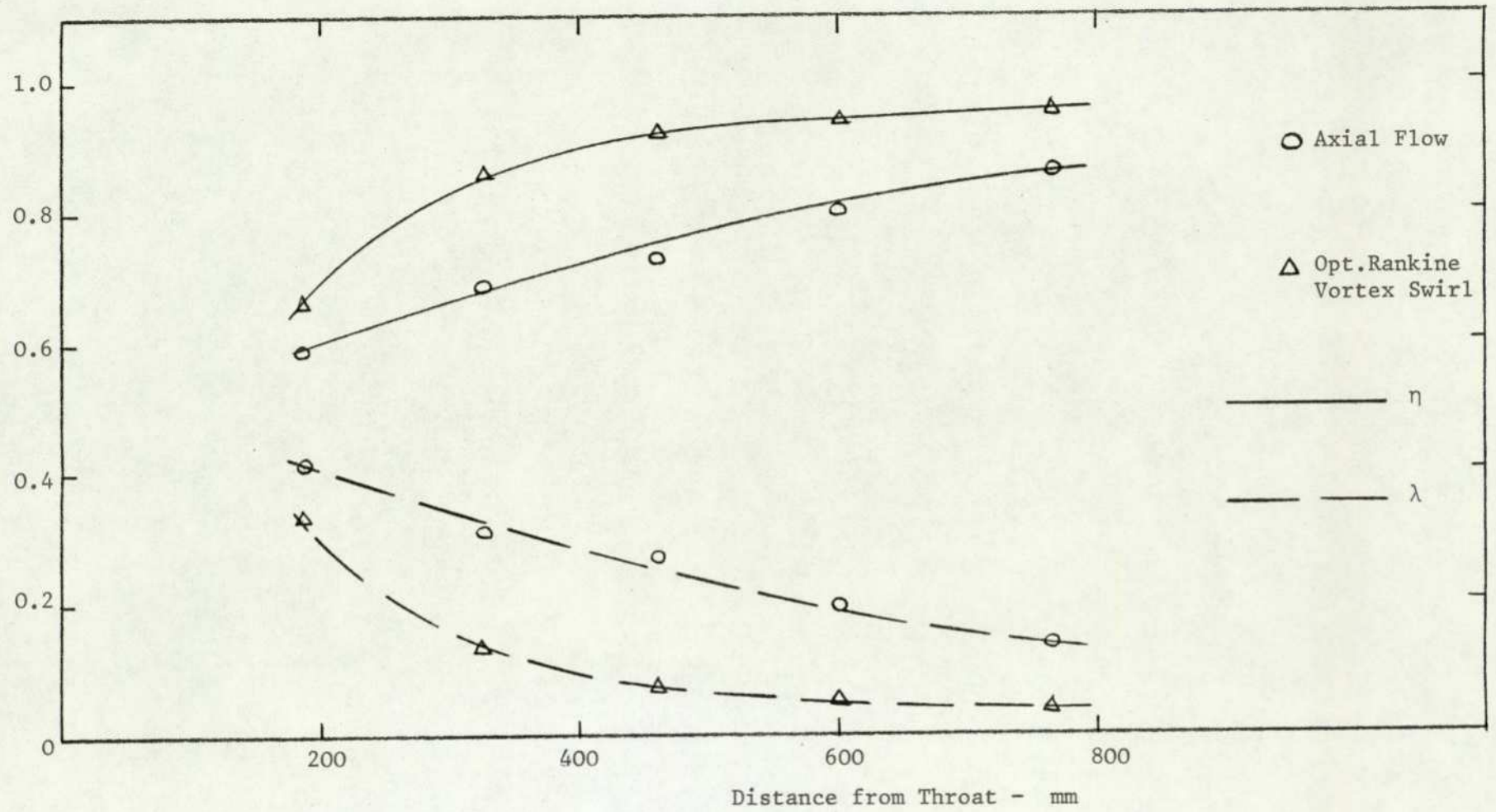

FIG. 10.2 VARIATION OF η AND λ IN 10^{o} DIFFUSER WITH OPT. RANKINE VORTEX SWIRL.

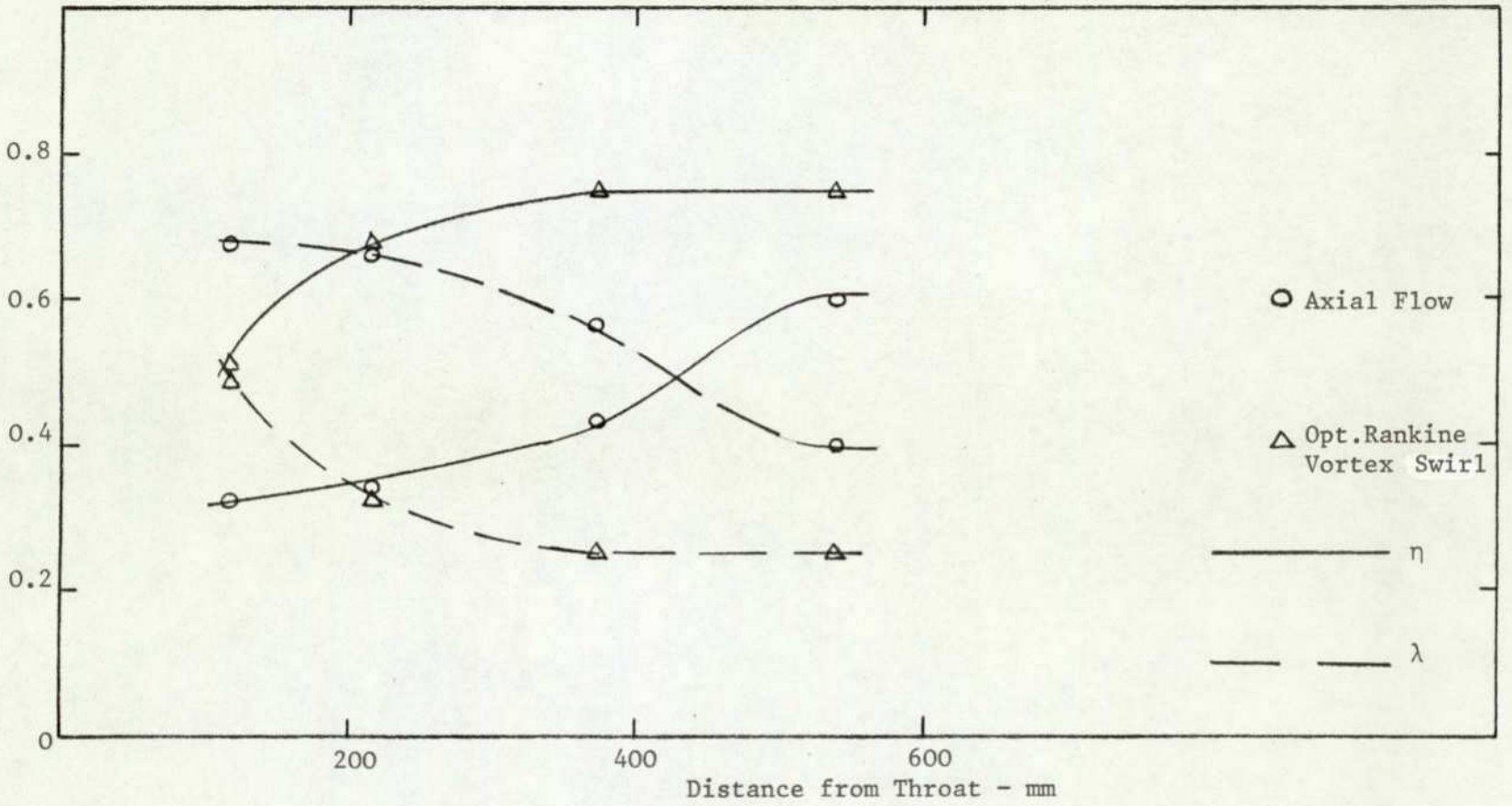

FIG. 10.3 VARIATION OF η AND λ IN 20^{o} DIFFUSER WITH OPT. RANKINE VORTEX SWIRL.

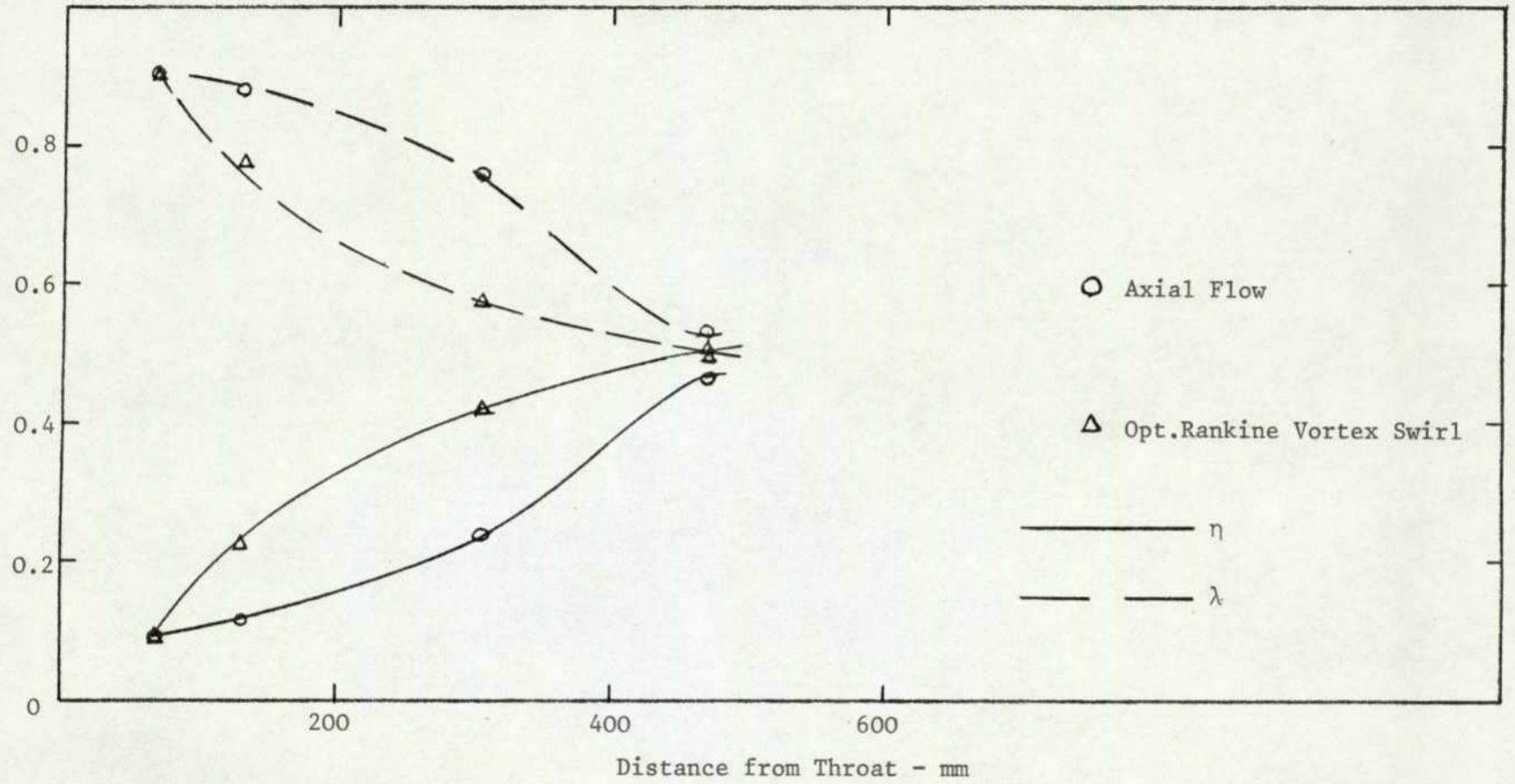

FIG. 10.4 VARIATION OF η AND λ IN 30° DIFFUSER WITH OPT.RANKINE VORTEX SWIRL.

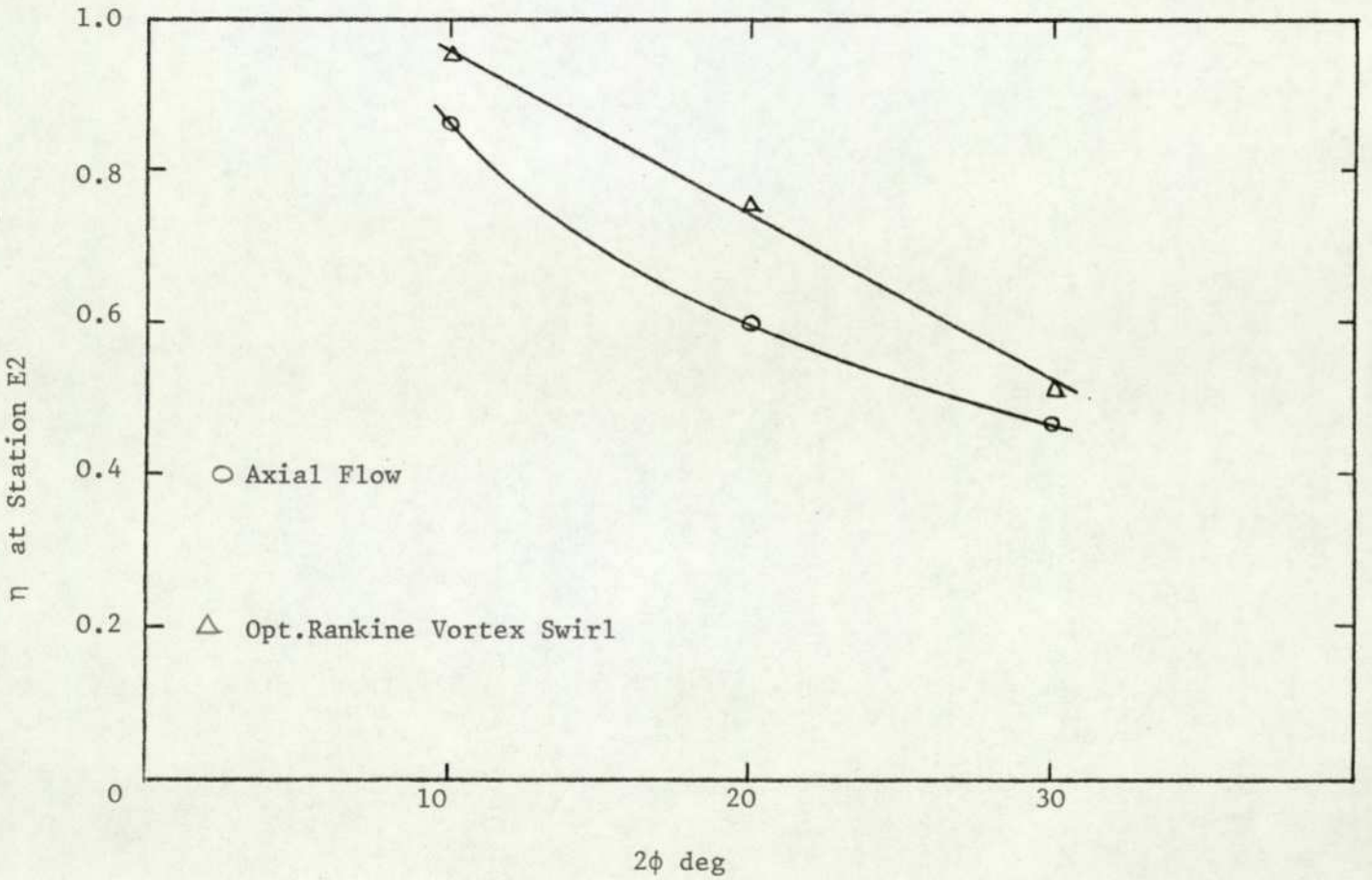

FIG. 10.5 EFFECT OF 2ϕ ON η - OPT.RANKINE VORTEX SWIRL.

The corresponding evaluation of λ and η for solid-body swirl is shown in Figs.(10.6), (10.7),(10.8) and (10.9), and the calculated results are tabulated in Tables (10/5), (10/6) and (10/7).

10.4 APPLICATION OF SOVRAN AND KLOMP'S MODEL

A brief outline of the model is as follows. Sovran and Klomp suggested that the overall diffuser effectiveness relates the actual pressure rise to that achievable from the same geometry with ideal, one dimensional flow at the same flow rate, i.e.

$$\varepsilon_o = C_p / C_{p_{ideal}}$$

Since C_p is strongly influenced by inlet flow, they presented a procedure based upon kinetic energy profile to assess the effect of non-uniformities of inlet velocity profile on diffuser performance, i.e.

$$\varepsilon_o = \frac{\alpha_1 \left[1 - \frac{\alpha_2/\alpha_1}{AR^2}\right]}{\left[1 - \frac{1}{AR^2}\right]} - \frac{\bar{\omega}}{\left[1 - \frac{1}{AR^2}\right]} \qquad (3.3.1.3)$$

The analysis was further developed to accommodate the effect of free vortex swirl, for both uniform and non-uniform flow. For isentropic, incompressible free vortex swirling flow with uniform velocity profile

$$C_{p_{ideal}} = \cos^2\psi_1 \left[1 - 1/AR^2\right] - \sin^2\psi_1 \left[1 - 1/RR^2\right] \quad (3.3.2.6)$$

and when losses are included

$$C_p = \cos^2\psi_1 \left[1 - 1/AR^2\right] - \sin^2\psi_1 \left[1 - 1/RR^2\right] - \omega \quad (3.2.2.8)$$

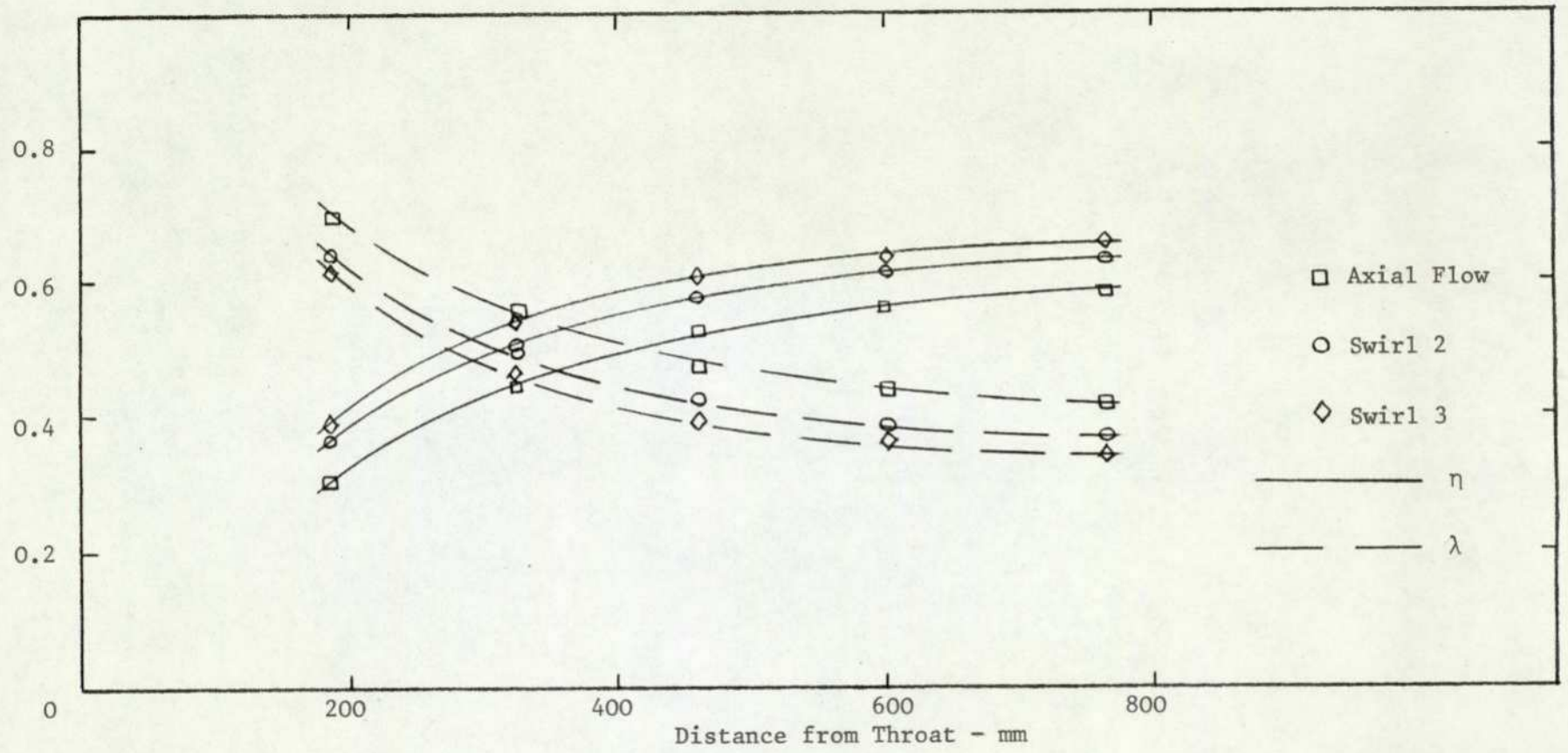

FIG. 10.6 VARIATION OF η AND λ IN 10^{o} DIFFUSER WITH SOLID-BODY SWIRL.

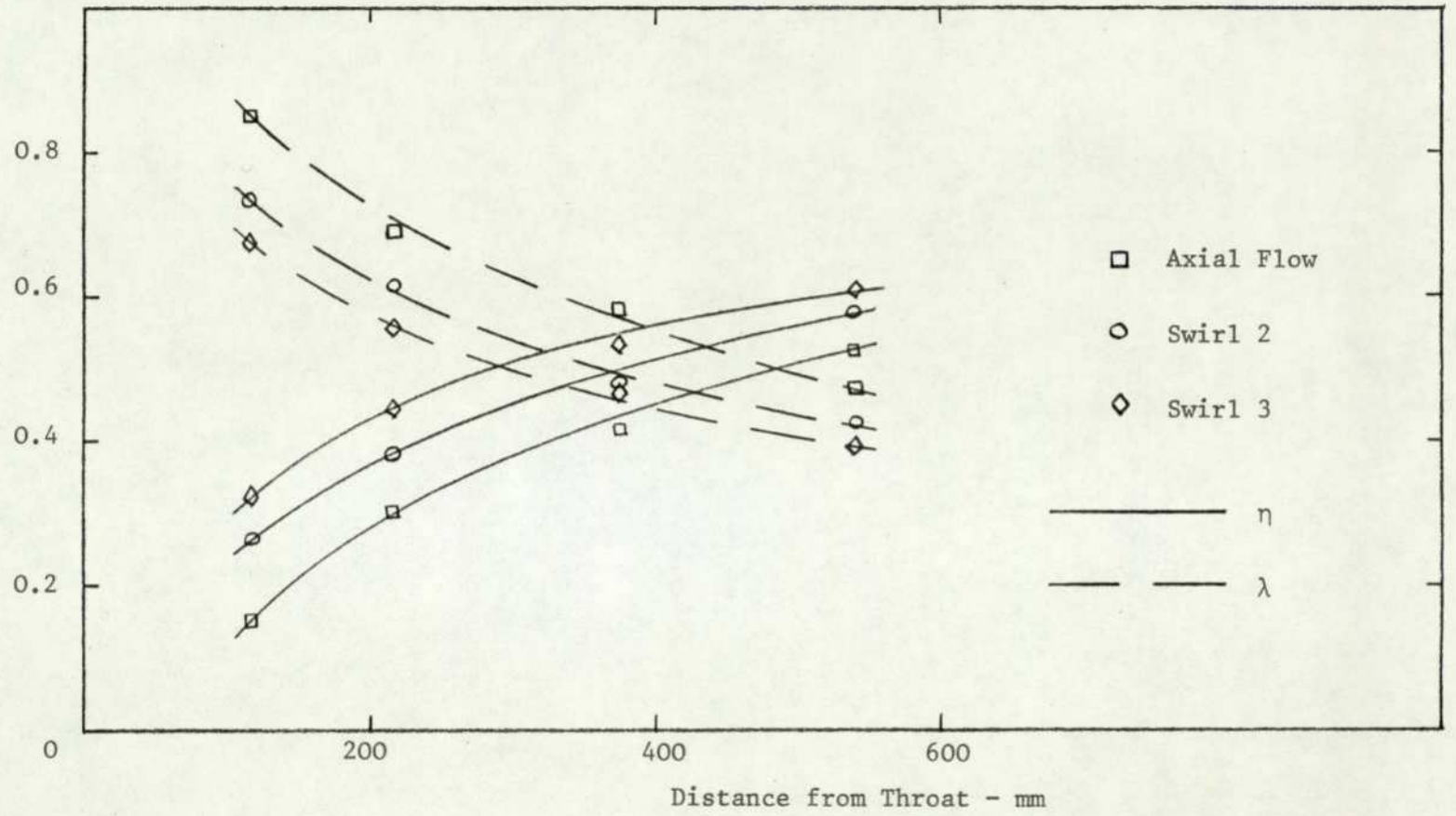

FIG. 10.7 VARIATION OF η AND λ IN 20° DIFFUSER WITH SOLID-BODY SWIRL.

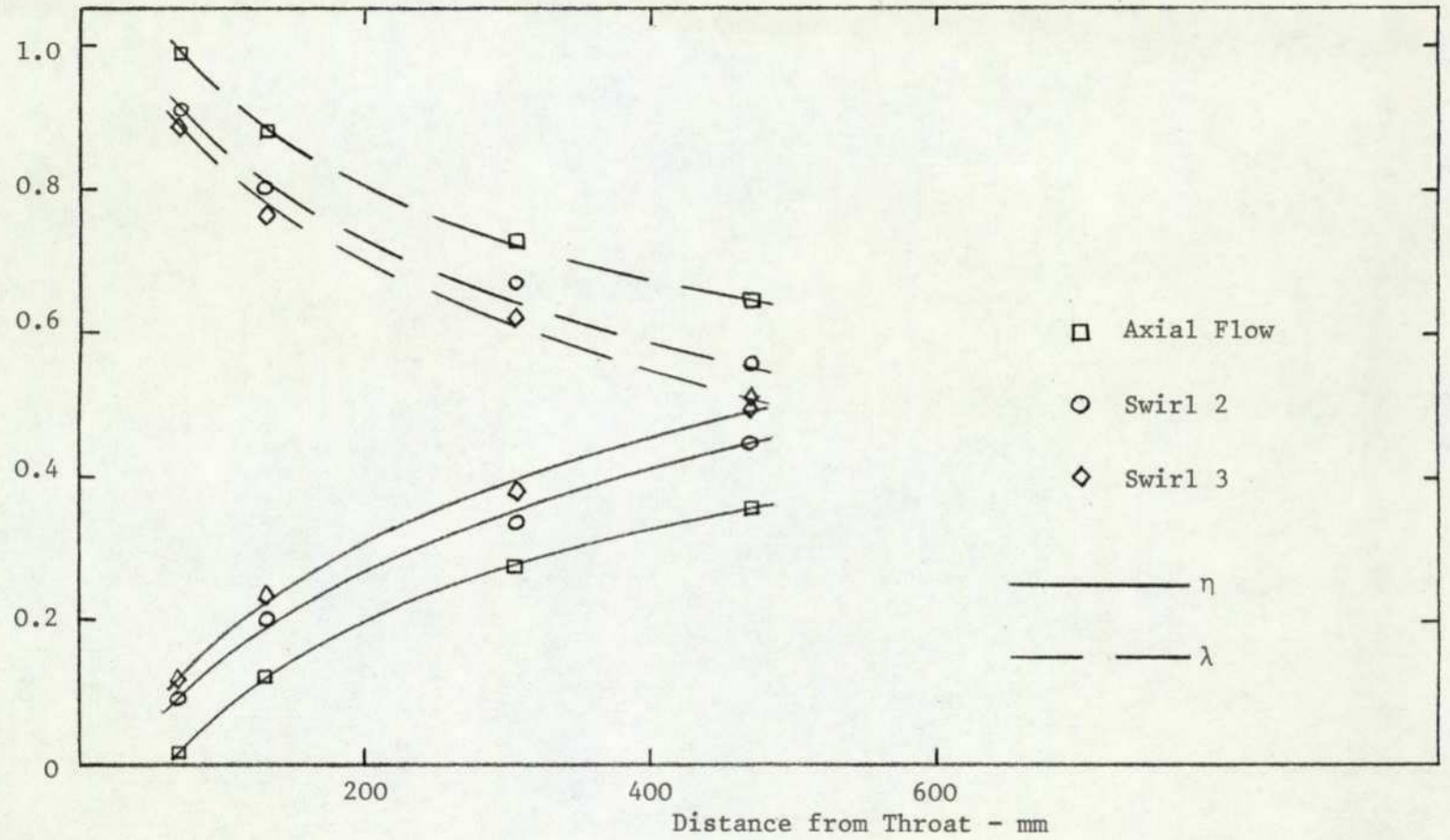

FIG. 10.8 VARIATION OF η AND λ IN 30° DIFFUSER WITH SOLID-BODY SWIRL.

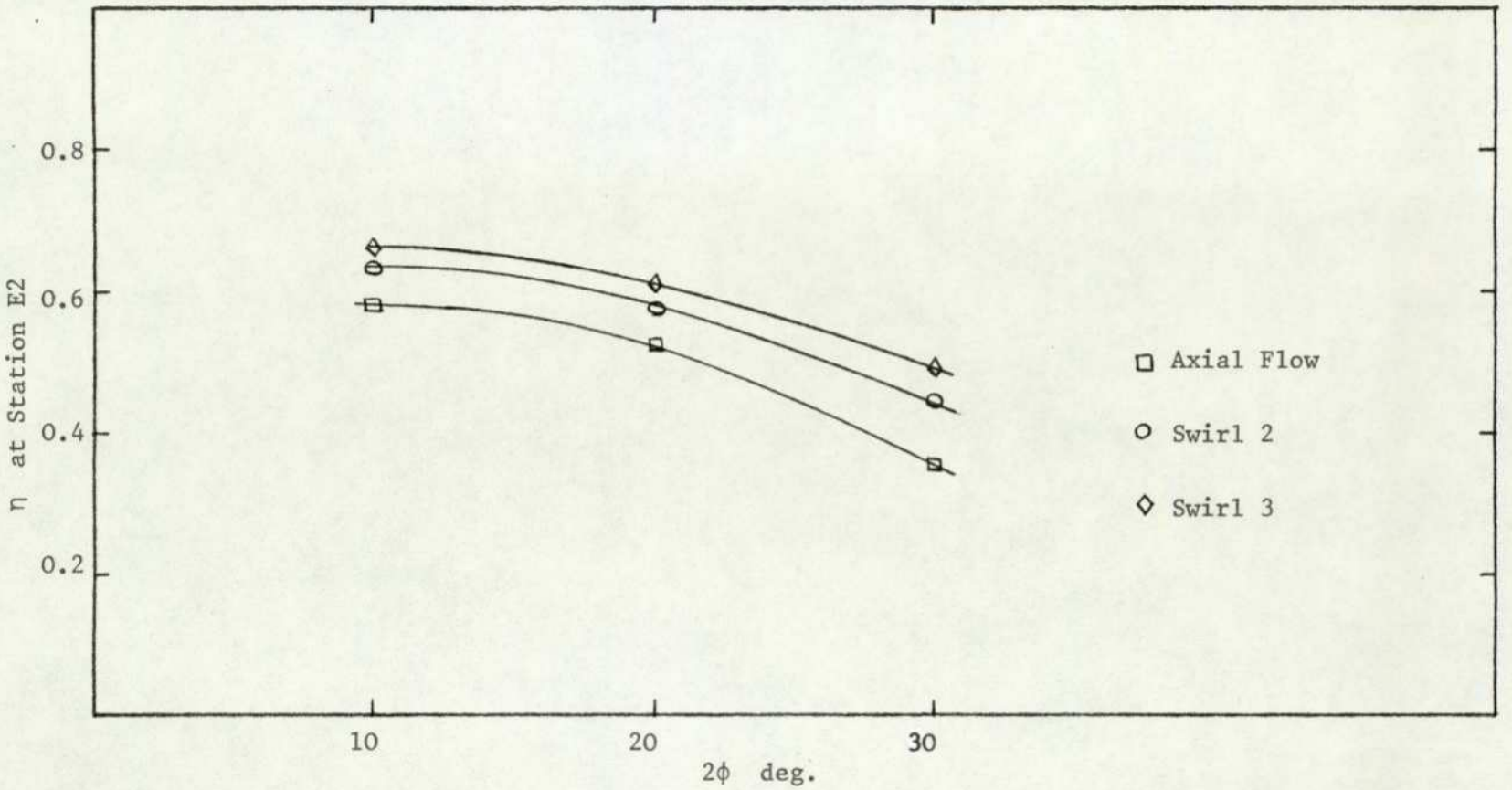

FIG. 10.9 EFFECT OF η ON 2ϕ - SOLID-BODY SWIRL.

Thus the diffuser effectiveness for free vortex swirl, incompressible, and uniform flow,

$$\varepsilon_o = \text{equation (3.2.2.8)/equation (3.2.2.6)}$$

To accommodate the effect of non-uniform velocity profile

$$C_{pideal} = \alpha_{s1}\bar{u}_1^2/\bar{\bar{V}}_1^2 \left[1 - (\alpha_{s2}\bar{u}_2^2/\alpha_{s1}\bar{u}_1^2)\right] + \alpha_{s1}\bar{v}_1^2/\bar{\bar{V}}_1^2\left[1 - (\alpha_{s2}\bar{v}_2^2/\alpha_{s1}\bar{v}_1^2)\right] \quad (3.3.2.27)$$

and

$$C_p = \alpha_{s1}\bar{u}_1^2/\bar{\bar{V}}_1^2 \left[1 - (\alpha_{s2}\bar{u}_2^2/\alpha_{s1}\bar{u}_1^2)\right] + \alpha_{s1}\bar{v}_1^2/\bar{\bar{V}}_1^2\left[1 - (\alpha_{s2}\bar{v}_2^2/\alpha_{s1}\bar{v}_1^2)\right] - \bar{\omega} \quad (3.3.2.25)$$

Thus the ε_o for free vortex swirl, non-uniform flow

$$\varepsilon_o = \text{equation (3.3.2.25)/equation (3.3.2.27)}$$

If the equation (3.3.2.25) and (3.3.2.27) were subjected to the following assumptions

(1) conservation of angular momentum

(2) neglecting the small effect of frictional dissipation

(3) $R_1\bar{v}_1 = R_2\bar{v}_2$

then they reduce to

$$C_{pideal} = \alpha_{s_1}\cos^2\bar{\psi}_1 \left[1 - (\alpha_{s_2}/\alpha_{s_1}AR^2)\right] + \alpha_{s_1}\sin^2\bar{\psi}_1 \left[1 - (\alpha_{s_2}/\alpha_{s_1}RR^2)\right] \quad (3.3.2.28)$$

and

$$C_p = \alpha_{s_1}\cos^2\bar{\psi}_1 \left[1 - (\alpha_{s_2}/\alpha_{s_1}AR^2)\right] + \alpha_{s_1}\sin^2\bar{\psi}_1 \left[1 - (\alpha_{s_2}/\alpha_{s_1}RR^2)\right] - \bar{\omega} \quad (3.3.2.26)$$

and

$$\varepsilon_o = \text{equation (3.3.2.26)/equation (3.3.2.28)}$$

The above analysis was further extended to take account of the effect of forced vortex swirl, for both uniform and non-uniform flow.

For incompressible, forced vortex swirling flow with uniform velocity profile

$$C_{p_{ideal}} = \cos^2\psi_1 \left[1 - 1/AR^2\right] - \sin^2\psi_1 \left[1 - RR^2\right] \quad (3.3.2.6a)$$

and when losses are included

$$C_p = \cos^2\psi_1 \left[1 - 1/AR^2\right] - \sin^2\psi_1 \left[1 - RR^2\right] - \omega \quad (3.3.2.8a)$$

Thus the ε_o for forced vortex incompressible and uniform flow

ε_o = equation (3.3.2.8a)/equation (3.3.2.6a)

To accommodate the effect of non-uniform velocity profile

$$C_{p_{ideal}} = \alpha_{s_1}\bar{u}_1^2/\bar{\bar{V}}_1^2\left[1 - (\alpha_{s_2}\bar{u}_2^2/\alpha_{s_1}\bar{u}_1^2)\right] + \alpha_{s_1}\bar{v}_1^2/\bar{\bar{V}}_1^2\left[1 - (\alpha_{s_2}\bar{v}_2^2/\alpha_{s_1}\bar{v}_1^2)\right] \quad (3.3.2.27a)$$

and

$$C_p = \alpha_{s_1}\bar{u}_1^2/\bar{\bar{V}}_1^2\left[1 - (\alpha_{s_2}\bar{u}_2^2/\alpha_{s_1}\bar{u}_1^2)\right] + \alpha_{s_1}\bar{v}_1^2/\bar{\bar{V}}_1^2\left[1 - (\alpha_{s_2}\bar{v}_2^2/\alpha_{s_1}\bar{v}_1^2)\right] - \bar{\omega} \quad (3.3.2.25a)$$

Thus the ε_o for forced vortex swirl, non-uniform flow

ε_o = equation (3.3.2.25a)/equation (3.3.2.27a)

Again if the following assumptions were made

(1) conservation of angular momentum

(2) neglecting the small effect of frictional dissipation

(3) forced vortex tangential velocity profile

i.e. $\bar{v}_1 R_2 = \bar{v}_2 R_1$

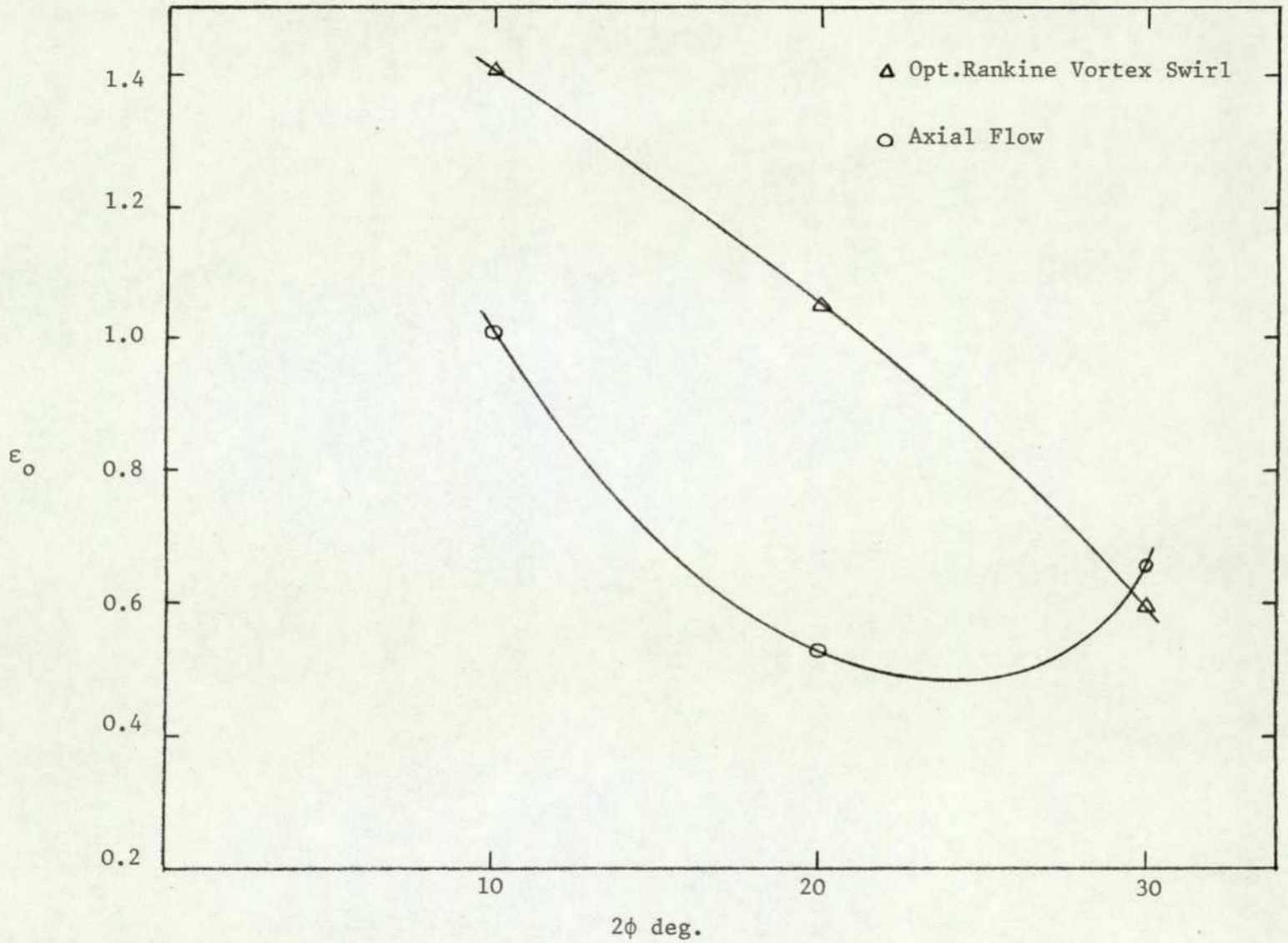

FIG. 10.10 EFFECT OF 2ϕ ON ε_o - OPT.RANKINE VORTEX SWIRL.

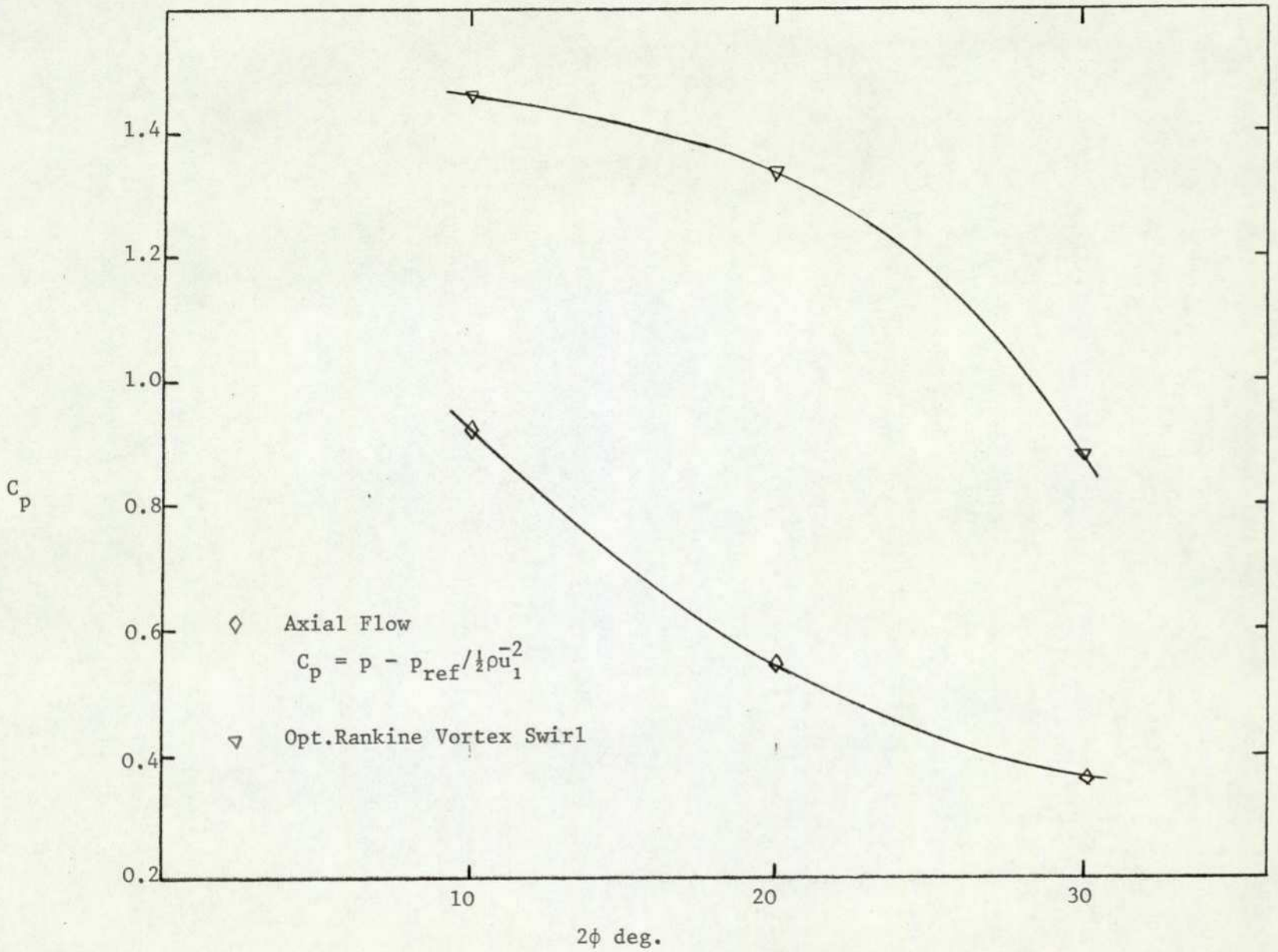

FIG. 10.11 EFFECT OF 2ϕ ON C_p - OPT. RANKINE VORTEX SWIRL.

then equation (3.3.2.25a) and equation (3.3.2.27a) reduce to

$$C_{p_{ideal}} = \alpha_{s_1}\cos^2\bar{\psi}_1\left[1 - (\alpha_{s_2}/\alpha_{s_1}AR^2)\right] + \alpha_{s_1}\sin^2\bar{\psi}_1\left[1 - (\alpha_{s_2}RR^2/\alpha_{s_1})\right] \quad (3.3.2.28a)$$

and

$$C_p = \alpha_{s_1}\cos^2\bar{\psi}_1\left[1 - (\alpha_{s_2}/\alpha_{s_1}AR^2)\right] + \alpha_{s_1}\sin^2\bar{\psi}_1\left[1 - (\alpha_{s_2}RR^2/\alpha_{s_1})\right] - \bar{\omega} \quad (3.3.2.26a)$$

and ε_o = equation (3.3.2.26a)/equation (3.3.2.28a)

A computer program called 'MASTER KET' was developed to conduct a detailed calculation for non-uniform flow to evaluate C_p, $C_{p_{ideal}}$, and thus ε_o, for the 10^o, 20^o and 30^o diffuser for different kind and severity of swirl. (Appendix B).

For optimum Rankine vortex swirl, equation (3.3.2.25) and (3.3.2.27) were used to evaluate C_p, $C_{p_{ideal}}$ and thus ε_o. For axial flow, equation (3.3.1.3) was used to evaluate ε_o. Fig. (10.10) and Fig.(10.11) show the effect of optimum Rankine vortex swirl and axial flow on ε_o and C_p with respect to the double conical angles of the diffusers tested. The calculated results are tabulated in Table (10/8).

For solid-body vortex swirl, equations (3.3.2.25a) and (3.3.2.27a) were used to calculate C_p, $C_{p_{ideal}}$ and thus ε_o. Again for axial flow equation (3.3.1.3) was used. Fig.(10.12) and Fig.(10.13) show the effect of swirl 0, swirl 2 and swirl 3 on ε_o and C_p with respect to the double conical angles of the diffusers tested. The calculated results are tabulated in Table (10/9).

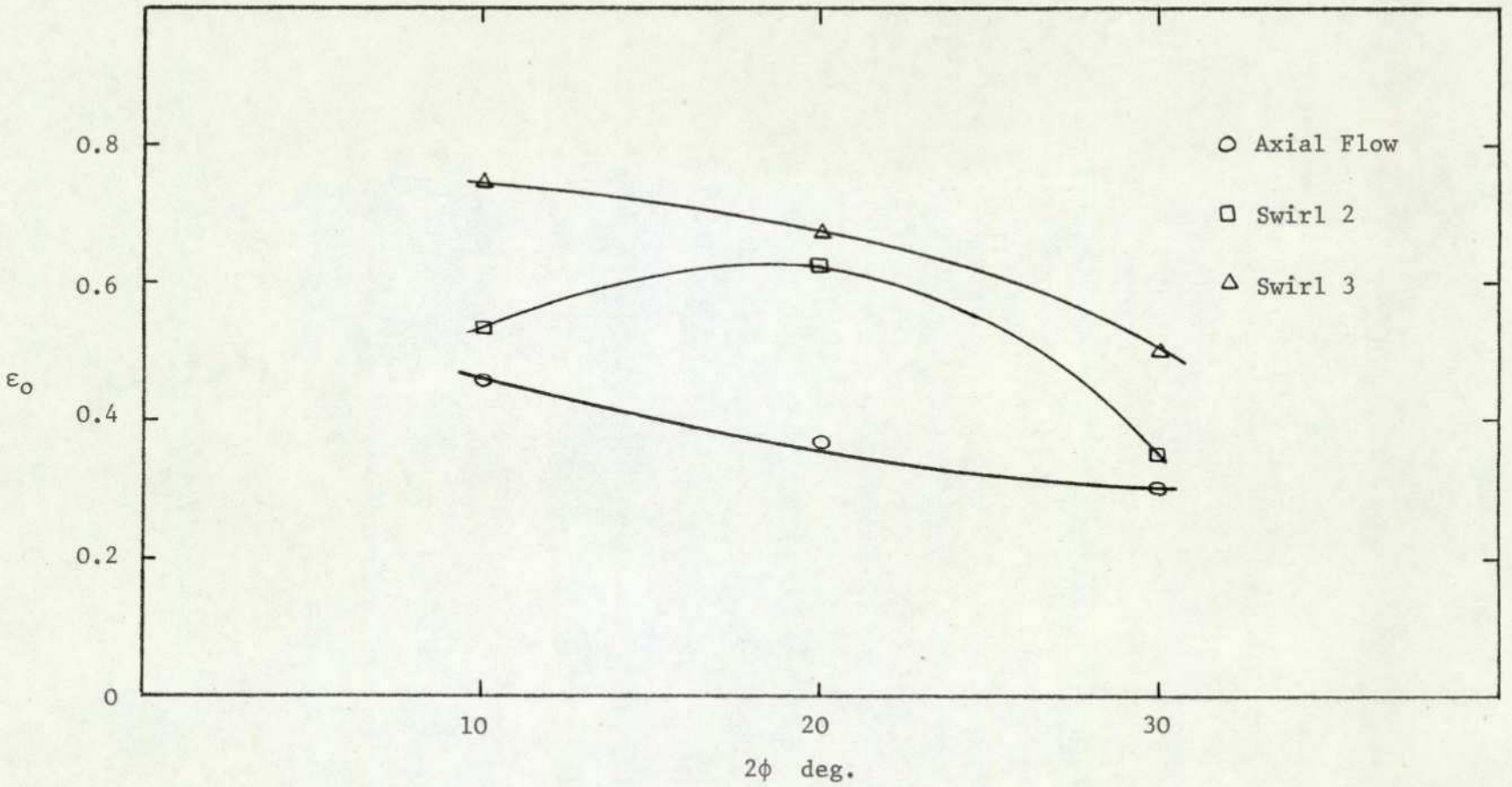

FIG. 10.12 EFFECT OF 2ϕ ON ε_o - SOLID-BODY SWIRL.

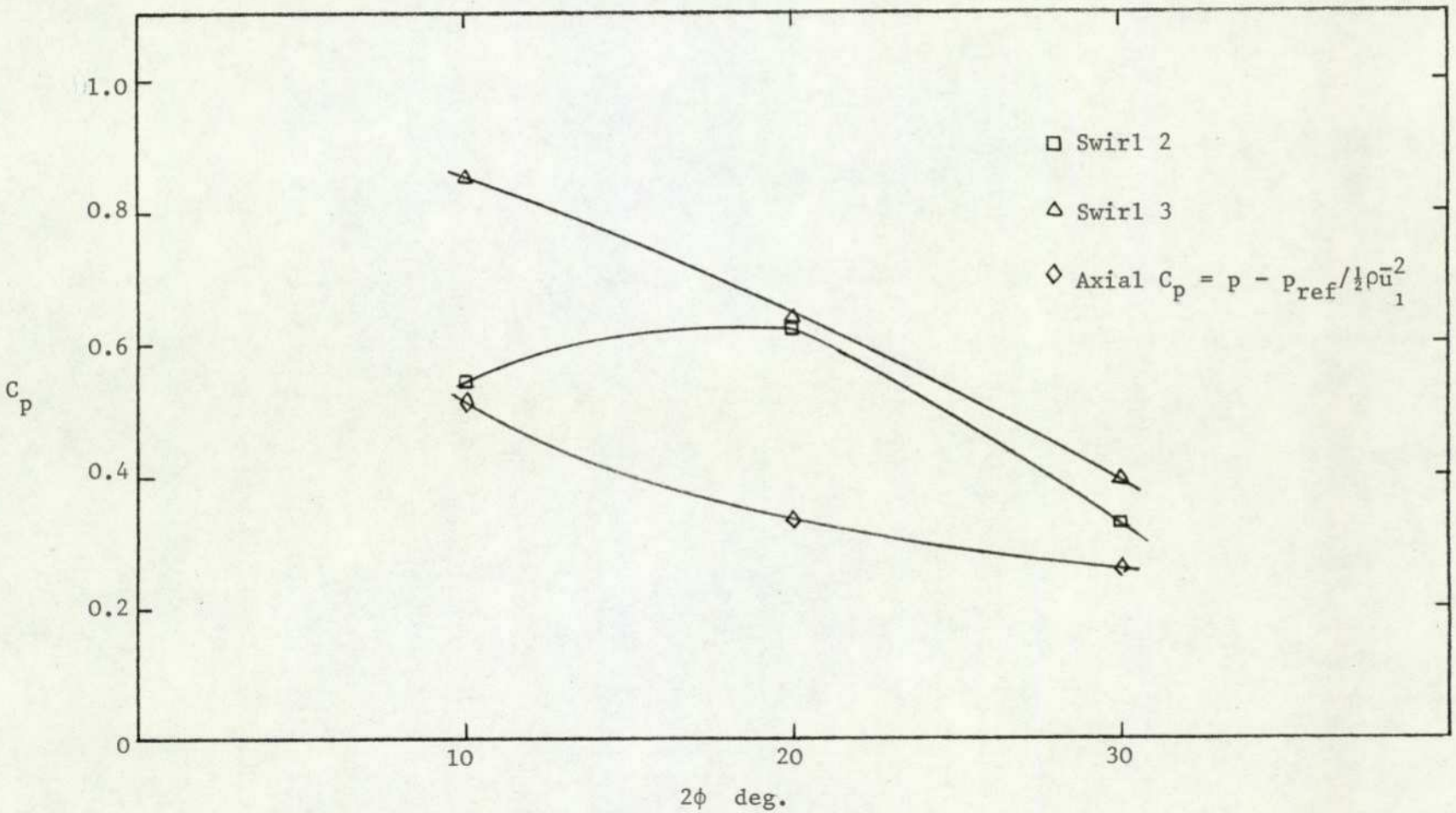

FIG. 10.13 EFFECT OF 2ϕ ON C_p - SOLID-BODY SWIRL.

10.5. APPLICATION OF TYLER AND WILLIAMSON'S MODEL

These authors adopted a slightly different approach to non-uniformities by using distortion factors. Their approach has previously been used by Sovran and Klomp. A brief outline of their model is as follows:

$$\eta_e = C_p / [\alpha_1 - \alpha_2/(AR)^2] \qquad (3.4.2.3)$$

The above equation was applied to the 10^o, 20^o and 30^o diffusers for different kinds and severity of swirl.

Fig.(10.14) shows the effect of optimum vortex swirl and axial flow with respect to the double conical angles of the diffusers tested. The calculated results are tabulated in Table (10/10).

The effect of solid-body swirl, i.e. swirl 0, swirl 2 and swirl 3, with respect to the double conical angle of the diffusers tested in shown in Fig.(10.15). The calculated results are tabulated in Table (10/11).

10.6 APPLICATION OF EXTENSION OF PATTERSON'S EFFICIENCY EQUATION

The experimental results were applied to the analysis which is developed fully in section (3.5). Unsatisfactory results were obtained, though it is not obvious why this was so.

10.7 DISCUSSION

10.7.1 Cockrell and Markland's Model

In arriving at an expression for λ and η, a number of assumptions were made; that is, the velocity distribution at inlet and exit being uniform, the flow being symmetrical and an effective total pressure loss takes account of both the total pressure loss and the effect of redistribution of velocities. Furthermore, since p_1 has been depressed by addition of swirl at inlet, a reference value was taken

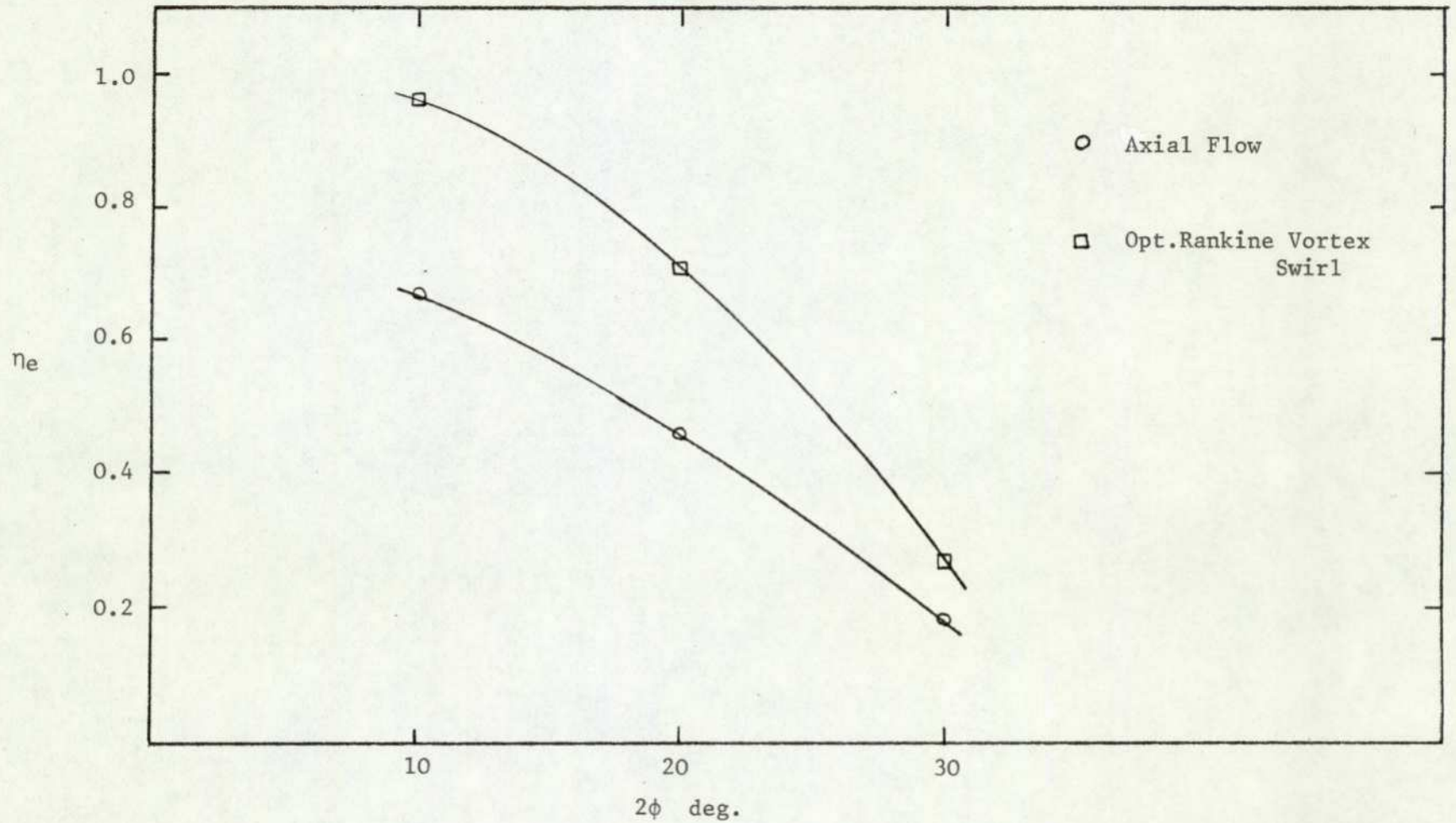

FIG. 10.14 EFFECT OF 2ϕ ON η_e - OPT.RANKINE VORTEX SWIRL.

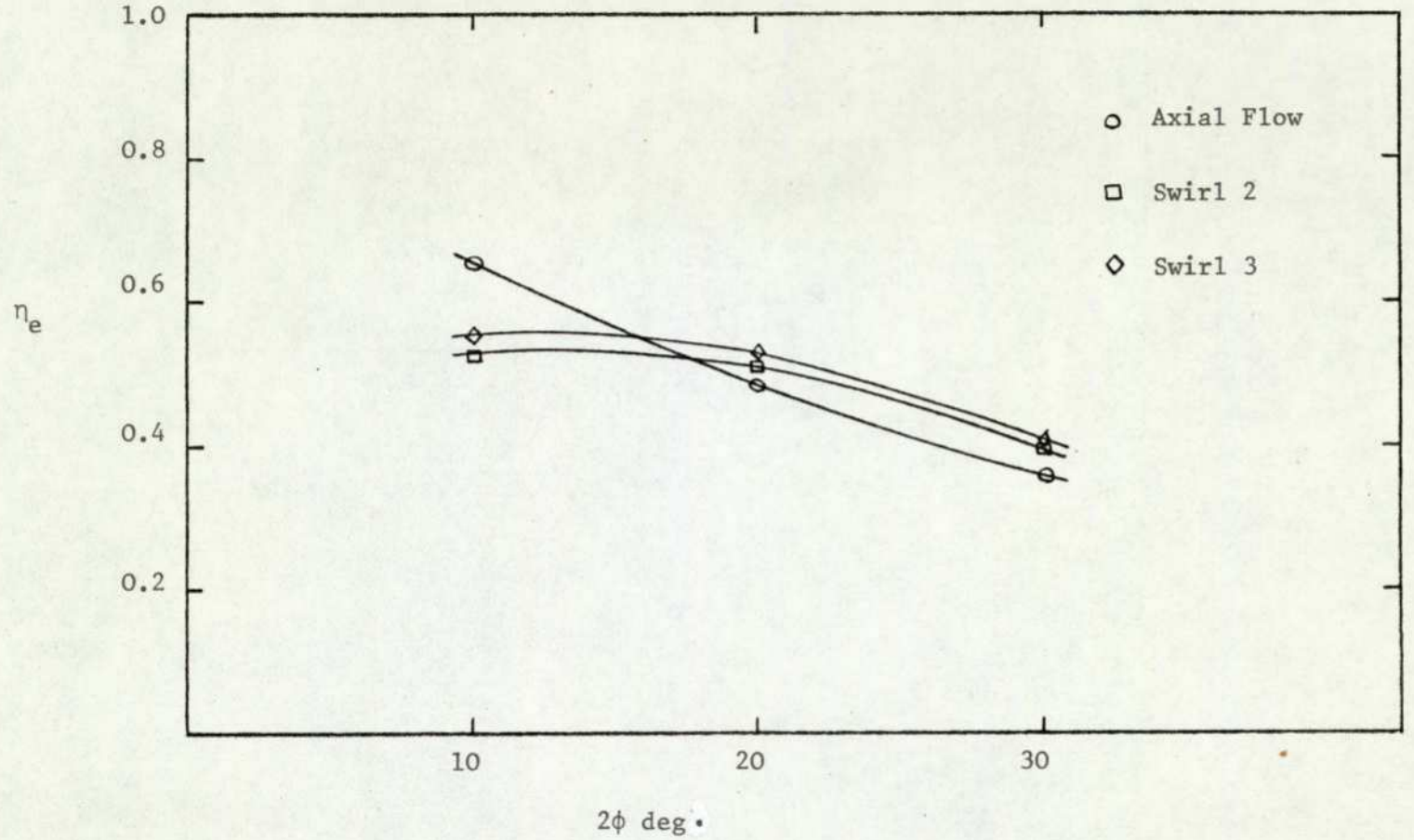

FIG. 10.15 EFFECT OF 2ϕ ON η_e - SOLID-BODY SWIRL

at a station sufficiently upstream to be unaffected by the problem at the pipe-diffuser join.

When optimum Rankine vortex swirl was present in the diffusers tested, it is evident that swirl had a marked effect on both reduction in diffuser λ and increase in η with downstream progress. This is clearly shown in Figs.(10.2), (10.3) and (10.4). However, the 10^{o} and 20^{o} diffusers experience a more favourable effect than the 30^{o} diffuser. It seems that it takes about 0.3 of the total length of the diffuser, for the swirl to have a distinct favourable effect on diffuser flow. The influence of the swirl in all the diffusers is more positive in the middle of the diffuser. This is not surprising, because it is known that it is around the middle of the diffusers that separation occurs. It is questionable without experimental evidence whether the two curves, for axial flow and for optimum swirl, meet at a point downstream from the tail pipe. It is felt that they would not meet because of the higher pressure drop for case of axial flow than swirling flow after the tail pipe. Fig.(10.5) shows the effect of η on 2ϕ of the diffusers tested. The trend of improvement of diffuser performance by the presence of Rankine vortex swirl is consistent in all three diffusers tested. It also confirms the comment made earlier that the 10^{o} and 20^{o} diffuser had a more favourable effect from swirl than the 30^{o} diffuser. Again, it is questionable whether the

optimum swirl would have a beneficial effect for diffusers less than 10^{o} and greater than 30^{o}. The curves seem to indicate otherwise. However, experimental evidence is required to answer the question.

The presence of solid-body swirl, that is swirl 2 and swirl 3, again has a marked effect on λ and η as shown by Figs.(10.6), (10.7) and (10.8). In all the diffusers tested, swirl 3 experiences a more favourable effect on the improvement in diffuser flow than swirl 2, relative to pure axial flow. The influence of swirl is positive from the diffusers entry. However, for 10^{o} and 20^{o}, the influence is more distinct near the middle, but in the case of 30^{o} diffuser, this is near the exit of the tail pipe. From Fig.(10.9), it is evident that the trend of improvement of diffuser performance by the presence of solid-body swirl is consistent in all three diffusers tested. It also indicates the prospect for further improvement with increase in swirl.

It is clear from Fig.(10.5) and Fig.(10.9) that the optimum Rankine vortex swirl experiences a more favourable effect on diffuser performance than the maximum solid-body swirl (swirl 3). It is important to note that swirl 3 was not the optimum solid-body swirl, but one should also take into consideration the complication caused by vortex breakdown due to increase in swirl. The axial flow due to swirl 0 and β=0 does not give the same values of η and λ for the diffusers tested. This is possible due to the change in entry condition of the diffusers.

10.7.2 Sovran and Klomp's Model

The theory is essentially an extension of Sovran and Klomp's model to take account of non-uniformities and the two-dimensional flow (swirling flow).

The expression for C_p, $C_{p_{ideal}}$, and ε_o takes account of non-uniformities within the flow and the effect of two dimensional flow. When evaluating the flow properties of the swirling flow, an assumption was made, that

$$\bar{P}_o = p + \alpha_s \rho \bar{V}^2/2$$

Thus this implies that the static pressure was assumed to be constant across the fluid stream. The validity of the above equation for one-dimensional flow is justified by Sovran and Klomp.

Fig.(10.10) shows that the diffuser performance improvement based on ε_o due to the presence of optimum Rankine vortex swirl is more marked for the 10^o and 20^o diffusers. It also indicated that, based on this model, the diffuser performance would not improve further by the presence of optimum Rankine vortex swirl for 2ϕ greater than about 30^o. The performance improvement for 2ϕ less than 10^o appears to be poor, but is subject to experimental evidence. The above deductions are also confirmed by Fig.(10.11) which shows the effect on C_p of the double conical angle.

The effect of solid-body swirl on the diffuser performance is shown by Fig.(10.12). The trend of improvement is consistent in all the diffusers tested. Swirl 3 experiences a more beneficial effect on diffuser performance than swirl 2. This being more true for the

10^{o} and 30^{o} diffuser. The above figure also indicates the prospect for further improvement due to increase in swirl. Based on this model, it is questionable whether the swirl would have beneficial effect for diffuser greater than 30^{o}. The curves seem to indicate that the prospect is perhaps poor for diffusers greater than about 33^{o}. The above deductions are also confirmed by Fig.(10.13).

From Figs.(10.10) and (10.12), one confirms the deduction made, based on Cockrell and Markland's model that the optimum Rankine vortex has more beneficial effect on diffuser performance than the maximum solid-body swirl.

10.7.3 Tyler and Williamson's Model

The expression for η_e takes account of non-uniformities at inlet and exit. Again, the value of inlet static pressure is taken at a station sufficiently upstream to be unaffected by the problem at the pipe-diffuser join. The expression is open to some objection on the grounds that the numerator still contains area-averaged static pressure terms and uniformity of axial velocity is assumed.

Fig.(10.14) shows that the improvement due to the presence of optimum Rankine vortex swirl relative to pure axial flow is consistent with all the diffusers tested. The 10^{o} and 20^{o} diffusers experienced more benefit than the 30^{o} diffuser. It raises the same question regarding the possibility of improvement for diffusers less than 10^{o} and greater than 30^{o}, as raised by Cockrell and Markland's model. The figure indicates that the probability of further improvement is low, but experimental evidence is required for justification.

Fig.(10.15) shows the effect of solid-body swirl (swirl 2 and swirl 3) on the diffuser performance relative to swirl 0 (axial flow). It is evident that for the 20^{o} and 30^{o} diffuser, η_e increases slightly with swirl 3, but for the 10^{o} diffuser, the performance drops markedly. It may be assumed that the poor results obtained with the 10^{o} diffuser was a consequence of the increase in α, due to the introduction of swirl 3 though it is not obvious why the 10^{o} diffuser is the only one to suffer in this respect. The figure also indicates that there is some prospect of further improvement with (a) increase in severity of solid-body swirl, since swirl 3 was not the optimum solid-body swirl (b) increase in the double conical angle of the diffuser.

The axial flow due to swirl 0 and $\beta=0$ gives nearly the same value of η_e except for the 30^{o} diffuser. For the 10^{o} and 20^{o} diffuser, the optimum Rankine vortex swirl has favourable effect than the maximum solid-body swirl tested except for the 30^{o} diffuser. It appears from Fig.(10.14) and (10.15) that around $2\phi = 25^{o}$ is the demarcation point between the two kinds of swirl tested with respect to the favourable effect on diffuser performance.

Fig.(10.16) shows the improvement relative to pure axial flow based on all three models considered. Irrespective of the model considered, the figure indicates that optimum Rankine vortex swirl improves diffuser performance more than maximum solid-body swirl for the 10^{o} and 20^{o} diffusers, and vice versa for the 30^{o} diffuser. It is questionable whether

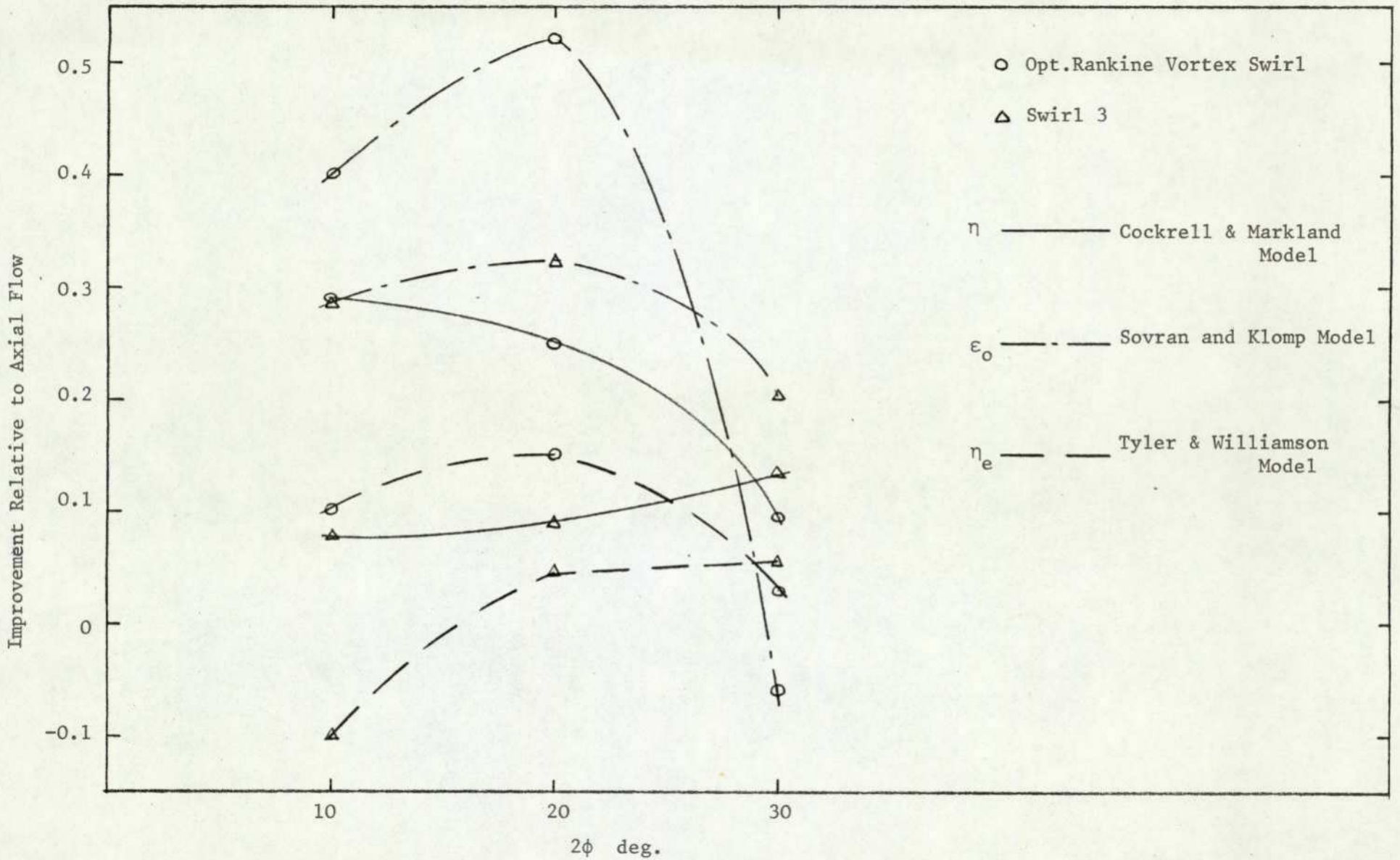

FIG. 10.16 COMPARISON OF DIFFUSER PERFORMANCE WITH VARIOUS THEORETICAL MODELS.

the effect of optimum solid-body swirl on diffuser performance would overtake the improvement due to optimum Rankine vortex swirl for the 10° and 20° diffuser. The curves indicate that the prospect is perhaps poor. However, experimental evidence is required to answer the question. The figure also indicates that around $2\phi = 26^{\circ}$ is a demarcation point between the two kinds of swirl tested with respect to the favourable effect on diffuser performance.

From the experimental curves of Fig.(10.1) it is evident that both swirls have a marked effect on diffuser performance relative to axial flow. The trend of improvement is consistent in all three diffusers tested using both types of swirl. The figure poses the question whether the optimum Rankine vortex swirl would have a beneficial effect for diffusers less than 10° and greater than 30°. However, there is a prospect for further improvement due to increase in solid-body swirl. The optimum Rankine vortex swirl has a more beneficial effect on diffuser performance than maximum solid-body swirl for the 10° and 20° diffusers and vice versa for the 30° diffuser.

10.8 CONCLUSION

1. From all the models used to evaluate the diffuser performance by the presence of optimum Rankine vortex swirl, the trend is consistent; that is, for all the diffusers tested, the Rankine vortex swirl has a favourable effect on diffuser performance. However, the 10° and the 20° diffusers benefit more than the 30° diffuser.

2. All the models predict that the improvement due to optimum Rankine vortex swirl is limited to $2\phi = 10^{\circ}$ to $2\phi = 30^{\circ}$. Outside this band, the improvement would be either small or zero.

3. For solid-body swirl, Cockrell and Markland's model and Sovran and Klomp's model suggest that in all the diffusers tested, swirl 3 produces a favourable effect on diffuser performance. Tyler and Williamson's model suggests that the above trend is consistent, except for the 10^{o} diffuser.

4. All the models suggest that there is a prospect for further improvement with

   (a) increase in solid-body swirl

   (b) for $2\phi < 10^{o}$ and $2\phi > 30^{o}$.

5. For 10^{o} and 20^{o} diffusers, optimum Rankine vortex swirl is seen to be best whereas for the 30^{o} diffuser, best improvements result from "solid-body" swirl 3.

CHAPTER ELEVEN

CONCLUDING COMMENTS

11.1 THE OBJECT OF THE INVESTIGATION

A number of researchers have expressed the view that the performance of conical diffusers may be improved by imparting swirl to the fluid at entry. In addition to this, in fluid-handling devices such as turbines, pumps, vortex amplifiers, etc., swirling flow is an inherent feature and as such diffuser performance data are required in these instances.

The object of the programme was to investigate the performance of the conical diffusers with solid-body type and Rankine vortex type swirling flow, having varying severities of swirl and, where necessary, contribute to the existing knowledge of performance with axial flow.

The strategy of the current project was pursued in four main stages. Stage one would survey the present state of the subject. Stage two was concerned with theoretical analysis associated with the evaluation of diffuser performance. Stage three was primarily concerned with the qualitative and quantitative experimental work. Stage four was concerned with marrying stage two and stage three and thus had a secondary function of steering future research.

11.2 RESULTS

The results were presented in each chapter and they concluded with a discussion. The associated assumptions and the limitations were included in the discussion.

Here it suffices to present the results in a concise form. The discussion that follows is both qualitative and quantitative in nature.

A comprehensive survey of previous experimental and theoretical work associated with swirling flow was conducted, with particular emphasis on areas not covered previously. It served two purposes. First, it presented the present state of the subject, and secondly, it would permit future investigators to proceed with their work without major individual surveys.

As a vast number of definitions have been used in the past to define diffuser performance with axial flow, it was necessary to review the definitions. On this basis, a theoretical analysis for presenting performance data with swirling flow was developed. It was seen that some degree of ambiguity exists in the estimation of diffuser performance and probably there is no satisfactory way of defining diffuser efficiency. Thus it was intended to assess experimental results against the theoretical models to see if there was a trend to give a conclusion.

The characteristics of the hemi-spherical five hole probe and the performance of the solid-body swirl generator was investigated to examine Wirasinghe's analysis. It was experimentally justified.

The effects of the presence of various severities of solid-body swirl on the 10°, 20° and 30° diffusers were recorded on video tapes and photographed quite successfully. It was observed that solid-body swirl improves the diffusion process of the wide angle diffusers. The degree of improvement depends on 2ϕ and the degree of swirl induced.

The study confirmed qualitatively, the work of Van Dewoestine, McDonald and Fox (50) and Wirasinghe (52).

It was seen that honeycomb swirl generator produced an excellent solid-body rotation superimposed on an axial flow. The solid-body swirling flow had a marked influence on the flow in the following manner:

1. modified the pressure drop in the inlet pipe
2. benefited the redistribution of axial velocity in the downstream sections of the diffusers tested
3. improved the diffusion process
4. eliminated the separation tendencies completely or partly
5. improved the pressure recovery coefficient for the diffusers tested
6. showed that there is a prospect of further improvement with higher swirl severity.

It was also observed that the conclusions regarding the influence of solid-body swirling flow arrived at on qualitative bases agreed with those arrived at on quantitative bases.

The characteristics of the performance of the free vortex generator were evaluated. It was found that the configuration of the generator that had an optimum influence of Rankine vortex swirl on the 10^{o}, 20^{o} and 30^{o} diffuser was as follows:

1. number of blades equals 8
2. the optimum blade angle of the generator was 6 deg, 10 deg and 10 deg, for the 10^{o}, 20^{o} and 30^{o} diffusers respectively.

The flow in the diffuser deteriorated when the blade angle was increased above its appropriate optimum angle. The static pressure distribution in the pipe was modified by the presence of the Rankine vortex swirl. The evaluation of the vortex generator served two purposes. First, it set suitable guide lines for the experimental work and secondly it saved considerable time.

The effect of various degrees of Rankine vortex swirl on the 10^{o}, 20^{o} and 30^{o} diffusers were recorded on video tapes and photographed quite successfully. It was found that

1. Rankine vortex swirl improved the diffusion process of the diffusers tested. The degree of improvement depended on 2ϕ and the degree of swirl imparted.
2. the conclusions made in Chapter Seven were confirmed qualitatively.

From a detailed experimental analysis as to the effect of optimum degree of imparted Rankine vortex swirl on diffusers, it was seen that the free vortex generator produced a swirl very much like a Rankine vortex superimposed on an axial flow. It was also found that the optimum Rankine vortex swirl had a marked influence on diffusers tested in the following manner:

1. it eliminated the separation tendencies completely or partly
2. the axial velocity at the centre of vortex was low and, for the 20^{o} and 30^{o} diffusers, the solid vortex core of the Rankine vortex approximately coincided with the displacement area of axial velocity at the centre.

3. it improved the diffusion process and the pressure recovery coefficient of the diffusers tested
4. the results confirmed those of Senoo, Kawaguchi, and Nagata (62), and Shaalan and Shabaka (55) who deduced that the improvement due to the presence of Rankine vortex swirl in the diffusers tested was subject to the optimum swirl intensity and deteriorated thereafter.
5. the conclusions of Chapter Seven and Chapter Eight were confirmed.

The experimental data for axial flow, Rankine vortex and solid-body rotation swirling flows were applied in the theoretical analysis put forward in Chapter Three. Since each model is based on different assumptions, it would be unreasonable to expect the same numerical answer for each theoretical model for a particular flow situation. The following deductions were made:

1. Both the optimum Rankine vortex swirl and solid-body swirl had a distinct effect on diffuser performance predicted by all three of the theoretical models.
2. The analysis suggests that the improvement due to the optimum Rankine vortex swirl is limited to $2\phi = 10^{o}$ to $2\phi = 30^{o}$.
3. There is a prospect of further improvement for (a) increase in solid-body swirl severity
   (b) $2\phi < 10^{o}$ and $2\phi > 30^{o}$ with imparted solid-body swirl.
4. The best swirl relative to pure axial flow was optimum Rankine vortex for the 10^{o} and 20^{o} diffusers and solid-body swirl 3 for the 30^{o} diffuser.

In connection with this last conclusion, it is necessary to be able to give a more generally applicable recommendation since the strengths of the two types of vortex mentioned here are peculiar to the rig used in this investigation only.

For a 30 deg. diffuser, there seems little doubt that the addition of a forced vortex gives a better improvement than a Rankine one. A forced vortex occupying the whole radial extent of the supply pipe is easily defined merely in terms of its rotation rate. For swirl 2, this was about 19 rad/s and for swirl 3 about 28 rad/s. These correspond to peak value of circulation Γ (close to the pipe wall) of about 0.22 and 0.35 m^2/s respectively.

In the case of 10 deg. and 20 deg. diffusers, Rankine vortex addition seemed better than adding a forced one. For the 10 deg. diffuser, peak performance was achieved by imposing a Rankine vortex having a core rotating at about 102 rad/s and occupying about one third of the radial extent of the compound vortex. For the 20 deg.diffuser, a core rotation rate of just under 285 rad/s was best, occupying about one third of the supply pipe radius. It is interesting to note that the peak circulations (core edge) represented by these figures are 0.14 and 0.36 m^2/s respectively, the latter being of the same order as for the forced vortices, though at a quite different radius,of course.

11.3 GUIDE LINES FOR FUTURE RESEARCH

It is well known that the associated characteristics of axial flow in diffusers are not fully understood, although the research in this field has been in progress for nearly a century. A single project would not be able to do more than scratch the surface of the subject of swirling flow in diffusers. As each chapter was self-contained, the discussion that follows will treat each area in the same manner.

The theoretical analysis associated with extension of Patterson's expression for diffuser efficiency, to take account of swirl, needs more refinement. When those experimental data were evaluated, an efficiency greater than 1.0 was obtained, yet the reason why this was so remains to be found.

There is plenty of scope for work in the area of flow visualization in diffusers. In the present project, it was possible to visualise the effect of both solid-body type and Rankine vortex type swirl in the pipe and diffuser-tail-pipe combinations. There is a prospect of visualising and recording the structure of vortex breakdown and its influence on diffuser performance. It is also possible to conduct quantitative measurements within the structure of vortex breakdown regions using a laser-doppler velocimeter.

The experimental analysis of flow in the wide angle diffusers was conducted and it was established that angular momentum was not conserved for both types of swirl induced with different severity of swirl. Further analysis is required to find why this was so. It is felt that this discrepancy is largely the result of lack of information on the structure of turbulent flow. In the experimental

analysis with presence of solid-body type swirl, optimum swirl angle was not found although it is felt that this would not be very far off swirl 3. However, it would be advantageous to find the optimum swirl thus enabling quantitative comparison with optimum Rankine vortex swirl. To understand the effect of swirling flow on the structure of turbulent flow, especially in diffusers, better knowledge of Reynolds stresses is required.

Neve and Wirasinghe (58) put forward a method which accurately predicts turbulent boundary layer growth in diffusers, knowing only the diffuser geometry and flow properties at the inlet section, together with some empirical data from Ross (56) and Fraser (57). Their predictions agree closely with published data by Fraser and give justification for the use of the model for the turbulent boundary layer in a diffuser, provided the diffuser is not too long and the inlet boundary layer is not thicker than $\theta/R_1 = 0.04$. The experimental results presented in the present project enable a test of the model, although it is felt that an extension of the model would be required to take account of the thicker inlet boundary layer.

REFERENCES

1. EIFFEL, G. — PARIS LIBRAIRIE AERONAUTIQUE; 1919.

2. WARNER, E.P. NORTON, F.H. & HEBBERT, C.M. — NACA TECH.REP. 73; 1919.

3. GIBSON, A.H. — PROC. ROY.SOC., Vol.83; A 563; 1910

4. GIBSON, A.H. — TRANS. ROY.SOC. (EDIN) Vol.48; I.5; 1911.

5. PATTERSON, G.N. — Modern diffuser design; AIRCRAFT ENGINEERING: Vol.10; p.267; 1938.

6. PETERS, H. — Conversion of energy in cross-sectional divergences under different conditions of inflow; NACA TM 737, 1934.

7. McDONALD, A.T. & FOX, R.W. — An experimental investigation of incompressible flow in conical diffusers; INT.J.MECH.SCI; Vol.8; p.125; 1966

8. COCKRELL, D.J. & MARKLAND, E. — Effects of inlet conditions on incompressible flow through conical diffusers; J.ROY.AERO.SOC; Vol.66; No.613; p.51; 1962.

9. SOVRAN, G.& KLOMP, E.D. — Experimentally determined optimum geometries for rectilinear diffusers with rectangular, conical or annular cross-section. FLUID MECHANICS OF INTERNAL FLOW; ed.by G.SOVRAN; Elsevier Publishing Company, Amsterdam; pp.270-319; 1967.

10. WOLF, S. & JOHNSTON, J.P. — Effect of non-uniform inlet velocity profiles on flow regimes and performance in two-dimensional diffuser; ASME PAPER NO.68-WA/FE-25; 1968.

11. MIGAY, V.K. — Effect of initial turbulence on the efficiency of diffuser flows; TEPLOENERGATIKA No.2; 1966.

12. LIVESEY, J.L. & TURNER, J.T. — The dependence of diffuser performance upon inlet flow conditions; J.ROY.AERO.SOC; Vol.69; 1965.

13. WILLIAMS, G.J. & STEVENS, S.J. — The influence of initial turbulence on the performance of an annular diffuser; LOUGHBOROUGH UNIV.OF TECH. Rep.No.TT 7101; 1971.

14. NICOLL, W.B. & RAMAPRIAN, B.R. — Performance of conical diffusers with annular injection at inlet; ASME, Pap.No.70-FE-18; 1970.

15. DUGGINS, R.K. — Conical diffusers with annular injection; J.MECH.ENG.SCI; Vol.17; p.237; 1975.

16. FIEDLER, R.A. & GESSNER, F.B. — Influence of tangential fluid injection on the performance of two-dimensional diffusers; ASME J.BASIC ENG; Vol.94; p.666; 1972.

17. RAO, D.M. — A method of flow stabilization with high pressure recovery in short, conical diffuser; AERO.J.ROY.AERO.SOC; Vol.75, p.335; 1971.

18. KRASINSKI, J.S. & AZIZ, A. — A study of the efficiency on a radial diffuser with boundary layer control at the throat; 5th AUSTRIAN CONF.ON HYDRAULICS AND FLUID MECHANICS; Dec.1974.

19. VYAS, B.D. SAMBA SIVA RAO,P.& RAGHUNATHAN, S. — Effect of straight vane system on the Performance of conical diffusers, INDIAN J TECH; Vol.9; p.194; 1975.

20. JOHNSTON, J.P. & POWARS, C.P. — TRANS.AM.SOC.MECH.ENGRN; Vol.91 D; p.551; 1969.

21. PECK, D.F. — Unpublished senior project. Carnegie Mellon Univ.Pittsburgh, Pa.

22. BEAL, G.F. — Unpublished research, Carnegie Mellon Univ.Pittsburgh, Pa. (1962).

23. NUTTAL, J.B. — Axial flow in a Vortex; NATURE; Vol.172; p.582; Septe.1953.

24. BINNIE, A.M. — QUART.J.MECH.APPL.MATH.; Vol.30, No.3; p.276; 1957.

25. TALBOT, L. — Laminar swirling pipe flow; J.APP.MECH; Vol.21; No.1; p.1; 1954.

26. BRESAN, V.P. & TROY, N.Y. — Ph.D. thesis; Rensselaer Polytechnic Inst; N.Y.; 1960.

27. NISSAN, A.F. & BRESAN, V.P. — Swirling flow in cylinders; A.I.CHEM.E.JOURNAL; Vol.7; p.535; 1961.

28. KING, M.K. ROTHFUS, R.R. & KERMODE, R.I. — Static pressure and velocity profile in swirling incompressible tube flow; A.I.CHEM. E.JOURNAL; Vol.15; p.837; 1969.

29. MENIS, M. — Effect of vortex decay on pipe flow; M.I.T. GAS TURBINE LAB.REP. 61; Nov.1960.

30. PRANDTL, L. — The mechanics of viscous fluids in aerodynamic theory; A general review of progress by W.F. DURRAND; Vol.III; p.68.

31. KREITH, F. & SONJU, O.K. — J.FLUID MECH.; Vol.22; p.257; 1961.

32. HARVEY, J.K. — Some observations of the vortex breakdown pehnomenon; J.FLUID MECH; Vol.14, p.585; 1962.

33. YOUSSEF, T.E.A. — Some investigations of the rotating flow with a recirculation core in straight pipes; ASME PAP.No. 66-WA/FE-36; 1966.

34. SO, K.L. — Vortex phenomenon in a conical diffuser; A.I.A.A.; Vol.5, p.1072; 1967.

35. KIRKPATRICK, D.L.T. — Experimental investigation of the breakdown of a vortex in a tube; ARC C.P. 821; May 1964.

36. GORE, R.W. & RANZ, W.E. — Backflow in rotating fluids moving axially through expanding cross-section; A.I.CHEM. JOURNAL; Vol.10; p.83; 1964.

37. LAVAN, Z. NIELSEN, & FUJER, A.A. — Separation and flow reversal in swirling flow in circular ducts; THE PHYSICS OF FLUIDS; Vol.12; No.9; p.1747; 1969.

38. WESKA, D.R. & STUROV, G. Ye. — Experimental study of turbulent swirled flow in a cylindrical tube. FLUID MECH. SOVIET RES; Vol.3; No.1; p.77; 1974.

39. BELLAMY-KNIGHT,P.G. — A note on vortex breakdown in a cylindrical tube; ASME J.FLUID ENG; Vol.98, p.322; 1976.

40. ANDERS, K. — GERMAN PUBLICATION V.D.I.; P.76; 1909.

41. VULLERS, H. — ZEITSCHRIFT DES VEREINES DEUTSCHER INGENIEURE; Vol.77; No.31; 1933.

42. SARPKAYA,T. — On stationary and travelling vortex breakdown; J.FLUID MECH; Vol.45; Pt.73; p.545; 1971.

43. SARPKAYA, T. — Vortex breakdown in swirling conical flow; A.I.A.A.; Vol.9; p.1792; 1971.

44. BOSSEL, H.H. — Swirling flows in stream tube of variable cross-section; A.I.A.A.; Vol.11; p.1161; 1973.

45. BINNIE, A.M. HOOKINGS, & KAMAL, — The flow of swirling water through a convergent-divergent nozzle; J.FLUID MECH; Dec.1957.

46. SPRENGER, H. — Experimentelle Untersuchungen an geraden und gekrümmten diffusoren; MITTEILUNG AUS DEM INSTITÜT FÜR AERODYNAMIK AN DER; E.T.H. ZÜRICH; No.27; 1959.

47. VELENTINE, E.F. & CARROLL, R.D. — Effect of several arrangements of rectangular vortex generators on the static-pressure rise through a short 2:1 diffuser; NACA RM L 50L04; 1951.

48. SENOO, Y. & NISHI, M. — Improvement of the performance of conical diffuser by vortex generators; ASME J.FLUID ENG; Vol.96; p.4; 1974.

49. VAN DEWOESTINE, R.V. — Swirling flow in conical diffusers; Ph.D. Thesis;PURDUE UNIV; 1969.

50. McDONALD, A.T. FOX, R.W. & VAN DEWOESTINE, R.V. — Effect of swirling inlet flow on pressure recovery in conical diffusers; A.I.A.A. PAP.No.71-84; 1971.

51. SAMBA SIVA RAO, P., VYAS, B.D. & RAGHUNATHAN, S. — Effect of inlet circulation on the performance of subsonic straight conical diffuser; INDIAN J.TECH; Vol.9; p.135; 1971.

52. WIRASINGHE, N.E.A. — Swirling and non-swirling flow in a conical diffuser; Ph.D. Thesis; CITY UNIV.; 1975.

53. HOADLEY, D. & HUGHES, D.W. — Swirling flow in an annular diffuser; CUED/A-TURBO/TR5, ENGINEERING DEPT. CAMBRIDGE UNIV; 1969.

54. HONAMI, S. ET AL — Investigation concerning the fluid flow in mixed flow diffusers; ASME Pap.No. 71-Gt-40; 1971.

55. SHAALAN, M.R.A. & SHABAKA, I.M.M. — An experimental investigation of the swirling flow performance in an annular diffuser at low speed; ASME Pap.No. 75-WA/FE-17; 1975.

56. ROSS, D. — A physical approach to turbulent boundary layers; TRANS.A.S. CIVIL ENG; Vol.21; p.1219; 1956.

57. FRASER. H.R. — The turbulent boundary layer in a conical diffuser; J.HYDRAULICS DIV.PROC.A.S. CIVIL ENG; Paper 1684; 1958.

58. WIRASINGHE, N.E.A. & NEVE, R.S. — The prediction of turbulent boundary layer parameters in conical diffuser flows; AERO. QUART; Vol.25; p.199; 1974.

59. CEBECI, T. — Eddy-viscosity distribution in thick axisymmetric turbulent boundary layer; ASME J. FLUID ENG; Vol.95; p.319, 1973.

60. PATEL, V.C. — A simple integral method for the calculation of thick axisymmetric turbulent boundary layers; AERO.QUART; Vol.25; p.47; 1974.

61. DOMKUNDWAR, V.M. SRIRAMULU, V & GUPTA, M.C. — Analysis of swirling recirculating turbulent jets passing through diffusers; COMB.FLAME; Vol.33; p.241; 1978.

62. SENOO, Y., KAWAGUCH, N. & NAGATA, T. — Swirling flow in conical diffusers; Bull J.S.M.E.; Vol.21; No.151; p.112; 1978.

63. NEVE, R.S. — An investigation of factors influencing the static and dynamic performance of fluidic vortex amplifiers; Ph.D. Thesis; CITY UNIV.(London); 1971.

64. LIEPE, F. — Investigation into the conditions of swirling flow in conical diffusers; MACHINENBAUTECHNIK; Vol.XII; No.3; p.137-147; 1963.

65. WRIGHT, M.A. — The evaluation of a simplified form of presentation for five-hole spherical and hemi-spherical pitometer calibration data; J.PHYS.; Vol.5; p.356; 1970.

66. WALLACE, F.J. WHITEFIELD, A.& BARBOTIC, D. — Experimental and theoretical evaluation of flow patterns in curved annular diffusers; Unpublished research; BATH UNIV; 1979.

67. TYLER, R.A. & WILLIAMSON, R.G. — Diffuser performance with distorted inflow; PROC.I.MECH.ENG.; Vol.182; Pt.3D; p.115-126; 1967.

68. HALL, M.G. — A numerical method for solving the equation for a vortex core; A.R.C. R & M 3467; HMSO (London); 1967.

69. THAKKER, A. — Conical diffuser performance; Part 1 : A review of the problem; M.E.D. Res.Memo. ML 94; CITY UNIV.(London); 1977.

ANGLE OF PITCH =	-30.00											
-30.	-25.	-20.	-15.	-10.	-5.	0.	5.	10.	15.	20.	25.	30.
287.	294.	301.	306.	309.	308.	311.	304.	295.	288.	282.	271.	254.
200.	208.	215.	215.	218.	220.	216.	212.	209.	204.	193.	186.	179.
307.	298.	286.	272.	259.	246.	224.	210.	202.	184.	169.	160.	155.
294.	306.	309.	312.	323.	320.	315.	318.	312.	305.	295.	291.	284.
174.	180.	198.	210.	225.	238.	252.	267.	275.	291.	295.	302.	309.
ANGLE OF PITCH =	-25.00											
-30.	-25.	-20.	-15.	-10.	-5.	0.	5.	10.	15.	20.	25.	30.
285.	299.	305.	313.	320.	322.	317.	316.	306.	303.	286.	281.	266.
204.	218.	222.	222.	228.	252.	228.	223.	219.	220.	214.	202.	185.
311.	304.	291.	278.	263.	242.	234.	211.	198.	182.	168.	162.	145.
281.	290.	300.	301.	304.	306.	302.	299.	303.	288.	281.	282.	260.
164.	179.	196.	208.	231.	240.	258.	275.	289.	300.	308.	315.	314.
ANGLE OF PITCH =	-20.00											
-30.	-25.	-20.	-15.	-10.	-5.	0.	5.	10.	15.	20.	25.	30.
295.	309.	319.	328.	327.	331.	328.	324.	318.	309.	297.	283.	272.
219.	222.	254.	241.	240.	249.	246.	242.	237.	227.	220.	215.	203.
320.	309.	301.	284.	267.	248.	233.	217.	199.	180.	168.	156.	150.
263.	277.	276.	285.	292.	298.	291.	285.	286.	280.	266.	262.	250.
162.	180.	190.	212.	232.	245.	263.	282.	295.	307.	320.	327.	331.
ANGLE OF PITCH =	-15.00											
-30.	-25.	-20.	-15.	-10.	-5.	0.	5.	10.	15.	20.	25.	30.
303.	314.	327.	330.	333.	335.	331.	331.	323.	314.	305.	290.	284.
233.	240.	248.	253.	259.	262.	261.	261.	253.	246.	243.	235.	226.
324.	314.	300.	285.	271.	247.	233.	218.	203.	189.	177.	173.	168.
252.	254.	258.	260.	267.	274.	269.	267.	262.	259.	256.	245.	238.
169.	182.	194.	211.	229.	246.	265.	284.	297.	314.	325.	330.	334.
ANGLE OF PITCH =	-10.00											
-30.	-25.	-20.	-15.	-10.	-5.	0.	5.	10.	15.	20.	25.	30.
313.	318.	330.	335.	337.	340.	339.	330.	332.	317.	306.	291.	277.
253.	259.	260.	271.	279.	275.	271.	272.	268.	262.	252.	241.	224.
326.	317.	299.	285.	273.	253.	233.	217.	201.	184.	169.	160.	158.
230.	239.	243.	250.	256.	253.	252.	252.	251.	247.	241.	228.	226.
171.	185.	199.	217.	231.	253.	270.	289.	304.	319.	326.	332.	340.
ANGLE OF PITCH =	-5.00											
-30.	-25.	-20.	-15.	-10.	-5.	0.	5.	10.	15.	20.	25.	30.
309.	321.	330.	334.	341.	341.	336.	332.	325.	317.	302.	291.	276.
267.	278.	281.	287.	290.	292.	290.	283.	284.	272.	273.	255.	246.
327.	317.	299.	284.	267.	251.	228.	218.	199.	182.	175.	168.	168.
215.	225.	234.	231.	234.	236.	236.	235.	230.	224.	222.	217.	207.
175.	188.	196.	216.	232.	250.	270.	287.	302.	314.	324.	334.	338.
ANGLE OF PITCH =	0.00											
-30.	-25.	-20.	-15.	-10.	-5.	0.	5.	10.	15.	20.	25.	30.
306.	318.	325.	333.	336.	337.	333.	331.	325.	315.	302.	285.	277.
272.	284.	294.	296.	301.	306.	298.	298.	295.	285.	273.	261.	255.
320.	310.	299.	279.	265.	252.	229.	211.	200.	184.	177.	169.	168.
197.	206.	206.	205.	213.	226.	217.	215.	218.	210.	212.	200.	196.
173.	188.	197.	214.	228.	244.	267.	285.	295.	309.	319.	326.	332.
ANGLE OF PITCH =	5.00											
-30.	-25.	-20.	-15.	-10.	-5.	0.	5.	10.	15.	20.	25.	30.
301.	307.	316.	324.	326.	328.	328.	325.	312.	309.	298.	281.	266.
289.	296.	306.	306.	310.	311.	311.	310.	304.	296.	288.	275.	261.
315.	295.	289.	271.	258.	241.	223.	207.	187.	182.	171.	165.	166.
189.	190.	193.	192.	195.	195.	199.	197.	192.	190.	191.	188.	182.
174.	182.	192.	206.	226.	241.	258.	273.	285.	296.	312.	318.	319.
ANGLE OF PITCH =	10.00											
-30.	-25.	-20.	-15.	-10.	-5.	0.	5.	10.	15.	20.	25.	30.
294.	299.	312.	314.	317.	321.	317.	310.	308.	304.	299.	285.	266.
295.	299.	312.	315.	321.	322.	319.	322.	314.	306.	300.	284.	275.
304.	292.	281.	269.	245.	234.	214.	200.	190.	183.	175.	172.	175.
184.	185.	183.	182.	180.	181.	180.	179.	185.	181.	183.	181.	182.
178.	184.	189.	204.	214.	231.	248.	266.	279.	293.	305.	311.	316.
ANGLE OF PITCH =	15.00											
-30.	-25.	-20.	-15.	-10.	-5.	0.	5.	10.	15.	20.	25.	30.
285.	289.	300.	311.	314.	315.	306.	306.	301.	296.	282.	273.	260.
298.	307.	318.	329.	329.	330.	331.	325.	322.	313.	307.	293.	285.
296.	280.	272.	263.	240.	228.	212.	200.	191.	185.	182.	183.	188.
181.	178.	183.	178.	177.	177.	177.	178.	182.	181.	184.	184.	183.
177.	182.	189.	205.	215.	226.	246.	258.	274.	290.	297.	301.	305.
ANGLE OF PITCH =	20.00											
-30.	-25.	-20.	-15.	-10.	-5.	0.	5.	10.	15.	20.	25.	30.
273.	287.	285.	300.	301.	302.	300.	300.	288.	291.	278.	266.	253.
305.	317.	312.	331.	331.	334.	333.	333.	328.	322.	311.	303.	287.
279.	275.	272.	248.	257.	223.	208.	202.	190.	186.	181.	187.	191.
182.	179.	179.	176.	177.	175.	175.	182.	182.	184.	184.	184.	188.
183.	187.	190.	197.	215.	219.	233.	250.	262.	271.	281.	289.	296.
ANGLE OF PITCH =	25.00											
-30.	-25.	-20.	-15.	-10.	-5.	0.	5.	10.	15.	20.	25.	30.
268.	271.	279.	286.	287.	289.	286.	284.	278.	274.	266.	259.	248.
311.	322.	326.	333.	336.	336.	335.	335.	329.	323.	315.	304.	293.
272.	264.	255.	258.	232.	218.	207.	200.	191.	189.	188.	188.	195.
194.	185.	182.	181.	181.	182.	185.	185.	187.	189.	187.	192.	191.
187.	190.	191.	199.	205.	217.	232.	240.	252.	262.	273.	279.	282.
ANGLE OF PITCH =	30.00											
-30.	-25.	-20.	-15.	-10.	-5.	0.	5.	10.	15.	20.	25.	30.
267.	266.	269.	275.	277.	277.	277.	274.	272.	263.	258.	246.	238.
322.	326.	328.	333.	337.	342.	339.	337.	332.	327.	317.	305.	296.
262.	256.	244.	233.	225.	215.	205.	199.	194.	191.	190.	193.	196.
203.	198.	195.	191.	194.	192.	194.	195.	195.	196.	197.	199.	201.
189.	192.	196.	201.	206.	213.	223.	233.	239.	249.	258.	267.	269.

TABLE 4/1 PROBE CHARACTERISTIC DATA (FIG. 4.19).

TABLE 6/1

FLOW PROPERTIES FOR INCREASING SOLID-BODY SWIRL

SOLID-BODY SWIRL 1

RADIUS (M)

0.00000	0.00331	0.00718	0.01211	0.01580
0.01964	0.02353	0.02916	0.03263	0.03965
0.04425	0.04875			

YAW (DEGREES)

0.00000	0.41400	0.90600	1.55800	2.05700
2.60500	3.19100	4.19000	4.83000	6.61700
8.38700	0.00000			

AXIAL VELOCITY (M/S)

6.19300	6.18500	6.12900	6.01400	5.93900
5.82800	5.69800	5.37400	5.21300	4.61500
4.05200	0.00000			

TANGENTIAL VELOCITY (M/S)

0.00000	0.04500	0.09700	0.16400	0.21300
0.26500	0.31800	0.39400	0.44000	0.53500
0.59700	0.00000			

MEAN VELOCITY	=	4.497900 M/S
MASS FLUX	=	0.040300 KG/S
K. E. FACTOR	=	1.360500
AXIAL KINECTIC ENERGY	=	0.554600 NM/S
ANGULAR MOMENTUM FLUX	=	0.5942E-03 NM

SOLID-BODY SWIRL 2

RADIUS (M)

0.00000	0.00314	0.00718	0.01211	0.01580
0.01964	0.02353	0.02916	0.03263	0.03965
0.04425	0.04875			

YAW (DEGREES)

0.00000	0.61100	1.33600	2.29500	3.00700
3.82500	4.65200	5.99400	6.88700	9.16800
11.0890	0.00000			

AXIAL VELOCITY (M/S)

5.80100	5.80000	5.74800	5.64200	5.61300
5.48500	5.39800	5.18400	5.04300	4.58600
4.21400	0.00000			

TANGENTIAL VELOCITY (M/S)

0.00000	0.06200	0.13400	0.22600	0.29500
0.36700	0.43900	0.54400	0.60900	0.74000
0.82600	0.00000			

MEAN VELOCITY	=	4.386600 M/S
MASS FLUX	=	0.039300 KG/S
K. E. FACTOR	=	1.325500
AXIAL KINETIC ENERGY	=	0.501200 NM/S
ANGULAR MOMENTUM FLUX	=	0.9250E-03 NM

SOLID-BODY SWIRL 3

RADIUS (M)

0.00000	0.00331	0.00718	0.01211	0.01580
0.01964	0.02353	0.02916	0.03263	0.03965
0.04425	0.04875			

YAW (DEGREES)

0.00000	1.00300	2.15100	3.76400	4.85900
6.13200	7.27300	9.05900	10.1110	12.4520
15.0010	0.00000			

AXIAL VELOCITY (M/S)

5.55900	5.39700	5.44800	5.24800	5.29600
5.21100	5.25400	5.21200	5.21500	5.11800
4.70600	0.00000			

TANGENTIAL VELOCITY (M/S)

0.00000	0.09400	0.20500	0.34500	0.45000
0.56000	0.67100	0.83100	0.93000	1.13000
1.26100	0.00000			

MEAN VELOCITY	=	4.495100 M/S
MASS FLUX	=	0.040270 KG/S
K. E. FACTOR	=	1.288200
AXIAL KINETIC ENERGY	=	0.524100 NM/S
ANGULAR MOMENTUM FLUX	=	0.1343E-02 NM

TABLE 6/2

10 DEGREE DIFFUSER FLOW PROPERTIES

AXIAL FLOW (SWIRL = 0)

STATION 2

RADIUS (M)

0.00000	0.00331	0.00718	0.01211	0.01580
0.01944	0.02353	0.02916	0.03263	0.03965
0.04425	0.04875			

YAW (RADIANS)

0.00000	0.00000	0.00000	0.00000	0.00000
0.00000	0.00000	0.00000	0.00000	0.00000
0.00000	0.00000			

AXIAL VELOCITY (M/S)

5.84300	5.82600	5.74100	5.89300	5.69000
5.73300	5.78400	5.48800	5.49700	4.99200
4.02300	0.00000			

TANGENTIAL VELOCITY (M/S)

0.00000	0.00000	0.00000	0.00000	0.00000
0.00000	0.00000	0.00000	0.00000	0.00000
0.00000	0.00000			

MEAN VELOCITY	=	4.854100 M/S
MASS FLUX	=	0.043900 KG/S
K. E. FACTOR	=	1.109700
AXIAL KINETIC ENERGY	=	0.568600 NM/S
ANGULAR MOMENTUM FLUX	=	0.0000E 00 NM

STATION 3

RADIUS (M)

0.00000	0.00459	0.00992	0.01669	0.02171
0.02693	0.03217	0.03970	0.04429	0.05351
0.05946	0.06396			

YAW (RADIANS)

0.00000	0.00000	0.00000	0.00000	0.00000
0.00000	0.00000	0.00000	0.00000	0.00000
0.00000	0.00000			

AXIAL VELOCITY (M/S)

4.69800	4.69800	4.64600	4.59300	4.51700
4.47400	4.20200	3.51600	3.37300	2.34400
1.50200	0.00000			

TANGENTIAL VELOCITY (M/S)

0.00000	0.00000	0.00000	0.00000	0.00000
0.00000	0.00000	0.00000	0.00000	0.00000
0.00000	0.00000			

MEAN VELOCITY	=	3.043500 M/S
MASS FLUX	=	0.046940 KG/S
K. E. FACTOR	=	1.446600
AXIAL KINETIC ENERGY	=	0.314500 NM/S
ANGULAR MOMENTUM FLUX	=	0.0000E 00 NM

STATION 4

RADIUS (M)

0.00000	0.00558	0.01205	0.02023	0.02627
0.03253	0.03879	0.04773	0.05315	0.06394
0.07085	0.07535			

YAW (RADIANS)

0.00000	0.00000	0.00000	0.00000	0.00000
0.00000	0.00000	0.00000	0.00000	0.00000
0.00000	0.00000			

AXIAL VELOCITY (M/S)

3.82300	3.83600	3.83600	3.94900	3.66600
3.67900	3.17900	2.40600	1.93100	1.21300
0.76700	0.00000			

TANGENTIAL VELOCITY (M/S)

0.00000	0.00000	0.00000	0.00000	0.00000
0.00000	0.00000	0.00000	0.00000	0.00000
0.00000	0.00000			

MEAN VELOCITY = 2.117000 M/S
MASS FLUX = 0.045310 KG/S
K. E. FACTOR = 1.953500
AXIAL KINETIC ENERGY = 0.198400 NM/S
ANGULAR MOMENTUM FLUX = 0.0000E 00 NM

STATION 5

RADIUS (M)

0.00000	0.00660	0.01426	0.02386	0.03094
0.03825	0.04553	0.05587	0.06211	0.07443
0.08224	0.08674			

YAW (RADIANS)

0.00000	0.00000	0.00000	0.00000	0.00000
0.00000	0.00000	0.00000	0.00000	0.00000
0.00000	0.00000			

AXIAL VELOCITY (M/S)

3.13700	2.98800	2.91600	2.85900	2.86500
2.73600	2.49300	1.98100	1.27900	0.57200
0.25600	0.00000			

TANGENTIAL VELOCITY (M/S)

0.00000	0.00000	0.00000	0.00000	0.00000
0.00000	0.00000	0.00000	0.00000	0.00000
0.00000	0.00000			

MEAN VELOCITY = 1.510600 M/S
MASS FLUX = 0.042850 KG/S
K. E. FACTOR = 2.375000
AXIAL KINETIC ENERGY = 0.116100 NM/S
ANGULAR MOMENTUM FLUX = 0.0000E 00 NM

TABLE 6/3

10 DEGREE DIFFUSER FLOW PROPERTIES

SOLID-BODY SWIRL (SWIRL 2)

STATION 2

RADIUS (M)

0.00000	0.00331	0.00718	0.01211	0.01580
0.01964	0.02353	0.02916	0.03263	0.03965
0.04425	0.04875			

YAW (RADIANS)

0.00000	0.01047	0.02269	0.04015	0.05237
0.06633	0.08117	0.10473	0.12044	0.16059
0.19376	0.00000			

AXIAL VELOCITY (M/S)

5.80100	5.80000	5.74800	5.64200	5.61300
5.48500	5.39800	5.18400	5.04300	4.58600
4.21400	0.00000			

TANGENTIAL VELOCITY (M/S)

0.00000	0.06100	0.13000	0.22700	0.02940
0.36400	0.43900	0.54500	0.61000	0.74300
0.82700	0.00000			

MEAN VELOCITY = 4.386500 M/S
MASS FLUX = 0.039300 KG/S
K. E. FACTOR = 1.325500
AXIAL KINETIC ENERGY = 0.501200 NM/S
ANGULAR MOMENTUM FLUX = 0.9250E-03 NM

STATION 3

RADIUS (M)

0.00000	0.00459	0.00992	0.01669	0.02171
0.02693	0.03217	0.03970	0.04429	0.05351
0.05946	0.06396			

YAW (RADIANS)

0.00000	0.02159	0.02849	0.04229	0.07935
0.10648	0.13312	0.17457	0.20968	0.29580
0.36784	0.00000			

AXIAL VELOCITY (M/S)

4.30600	4.25900	4.21200	3.94600	3.81100
3.65900	3.44300	3.17600	3.01700	2.56000
1.93900	0.00000			

TANGENTIAL VELOCITY (M/S)

0.00000	0.09200	0.12000	0.16700	0.30300
0.39100	0.46100	0.56000	0.64200	0.78000
0.74700	0.00000			

MEAN VELOCITY = 2.704300 M/S
MASS FLUX = 0.041710 KG/S
K. E. FACTOR = 1.410900
AXIAL KINETIC ENERGY = 0.215200 NM/S
ANGULAR MOMENTUM FLUX = 0.9810E-03 NM

STATION 4

RADIUS (M)

0.00000	0.00558	0.01205	0.02023	0.02627
0.03253	0.03879	0.04773	0.05315	0.06394
0.07085	0.07535			

YAW (RADIANS)

0.00000	0.02444	0.05062	0.08902	0.11172
0.13615	0.14663	0.19201	0.22518	0.31245
0.40497	0.00000			

AXIAL VELOCITY (M/S)

2.69900	2.74400	2.68400	2.62900	2.52700
2.28900	2.35200	2.28100	2.21200	1.93700
1.49300	0.00000			

TANGENTIAL VELOCITY (M/S)

0.00000	0.06700	0.13600	0.23500	0.28300
0.31400	0.34700	0.44300	0.50700	0.62600
0.64000	0.00000			

MEAN VELOCITY	=	1.948800 M/S
MASS FLUX	=	0.041700 KG/S
K. E. FACTOR	=	1.272100
AXIAL KINETIC ENERGY	=	0.100000 NM/S
ANGULAR MOMENTUM FLUX	=	0.1008E-02 NM

STATION 5

RADIUS (M)

0.00000	0.00660	0.01423	0.02386	0.03094
0.03825	0.04553	0.05587	0.06211	0.07443
0.08224	0.08674			

YAW (RADIANS)

0.00000	0.03142	0.09251	0.12743	0.13964
0.15710	0.20248	0.23216	0.24089	0.31071
0.37529	0.00000			

AXIAL VELOCITY (M/S)

1.85000	1.86400	1.75000	1.68000	1.78700
1.67300	1.75200	1.80000	1.78200	1.58200
1.21700	0.00000			

TANGENTIAL VELOCITY (M/S)

0.00000	0.05900	0.16200	0.21500	0.25100
0.26500	0.36000	0.42600	0.43800	0.50800
0.47900	0.00000			

MEAN VELOCITY	=	1.514200 M/S
MASS FLUX	=	0.042950 KG/S
K. E. FACTOR	=	1.184300
AXIAL KINETIC ENERGY	=	0.058310 NM/S
ANGULAR MOMENTUM FLUX	=	0.1042E-02 NM

TABLE 6/4

10 DEGREE DIFFUSER FLOW PROPERTIES

SOLID-BODY SWIRL (SWIRL 3)

STATION 1

RADIUS (M)

0.00000	0.00500	0.01000	0.01500	0.02000
0.02500	0.03000	0.03500	0.04000	0.04500

YAW (RADIANS)

0.00000	0.03491	0.06720	0.09251	0.12044
0.13615	0.16757	0.18765	0.22518	0.00000

AXIAL VELOCITY (M/S)

5.84052	5.89571	5.79779	5.64063	5.48829
5.37462	5.21271	5.07817	4.88262	0.00000

TANGENTIAL VELOCITY (M/S)

0.00000	0.20591	0.39022	0.52333	0.66424
0.73633	0.88178	0.96425	1.11842	0.00000

MEAN VELOCITY = 4.852314 M/S
MASS FLUX = 0.036863 KG/S
K. E. FACTOR = 1.176102
AXIAL KINETIC ENERGY = 0.510396 NM/S
ANGULAR MOMENTUM FLUX = 0.9566E-03 NM

STATION 2

RADIUS (M)

0.00000	0.00406	0.00812	0.01218	0.01624
0.02030	0.02436	0.02842	0.03248	0.03654
0.04060	0.04466	0.04872		

YAW (RADIANS)

0.00000	0.01047	0.03404	0.05324	0.07331
0.08641	0.11172	0.13528	0.16583	0.20248
0.23914	0.26358	0.00000		

AXIAL VELOCITY (M/S)

4.94968	5.00880	5.01600	5.00689	4.99071
4.94607	4.89402	4.83989	4.79756	4.76491
4.66641	4.22231	0.00000		

TANGENTIAL VELOCITY (M/S)

0.00000	0.05246	0.17080	0.26682	0.36654
0.42843	0.54902	0.65877	0.80294	0.97823
1.13770	1.13942	0.00000		

MEAN VELOCITY = 4.450393 M/S
MASS FLUX = 0.039631 KG/S
K. E. FACTOR = 1.130710
AXIAL KINETIC ENERGY = 0.443763 NM/S
ANGULAR MOMENTUM FLUX = 0.1097E-02 NM

STATION 3

RADIUS (M)

0.00000	0.00492	0.00984	0.01476	0.01968
0.02460	0.02952	0.03444	0.03936	0.04428
0.04920	0.05412	0.05904	0.06396	

YAW (RADIANS)

0.00000	0.01746	0.04538	0.06459	0.08204
0.11870	0.12830	0.15186	0.18416	0.20510
0.22343	0.25311	0.32293	0.00000	

AXIAL VELOCITY (M/S)

3.63468	3.55183	3.49283	3.44667	3.42085
3.38679	3.37558	3.36438	3.39547	3.33930
3.15978	2.74429	2.24803	0.00000	

TANGENTIAL VELOCITY (M/S)

0.00000	0.06201	0.15863	0.22292	0.28128
0.40390	0.43547	0.51489	0.63246	0.69467
0.71798	0.70982	0.75228	0.00000	

MEAN VELOCITY = 2.909237 M/S
MASS FLUX = 0.044649 KG/S
K. E. FACTOR = 1.178670
AXIAL KINETIC ENERGY = 0.222709 NM/S
ANGULAR MOMENTUM FLUX = 0.1136E-02 NM

STATION 4

RADIUS (M)

0.00000	0.00471	0.00942	0.01413	0.01884
0.02355	0.02826	0.03297	0.03768	0.04239
0.04710	0.05181	0.05652	0.06123	0.06594
0.07065	0.07536			

YAW (RADIANS)

0.00000	0.00000	0.02269	0.03491	0.04800
0.05935	0.07506	0.08204	0.09601	0.09601
0.10910	0.11346	0.12743	0.14314	0.17456
0.20283	0.00000			

AXIAL VELOCITY (M/S)

2.61762	2.56050	2.53080	2.48078	2.30468
2.27106	2.07690	2.12241	2.11977	2.00125
1.89856	1.65079	1.52575	1.65910	1.36547
0.87477	0.00000			

TANGENTIAL VELOCITY (M/S)

0.00000	0.00000	0.05744	0.08664	0.11072
0.13494	0.15618	0.17452	0.20414	0.19272
0.20795	0.18811	0.19548	0.23911	0.24080
0.17991	0.00000			

MEAN VELOCITY = 1.632817 M/S
MASS FLUX = 0.034789 KG/S
K. E. FACTOR = 1.325912
AXIAL KINETIC ENERGY = 0.061489 NM/S
ANGULAR MOMENTUM FLUX = 0.3075E-03 NM

STATION 5

RADIUS (M)

0.00000	0.00542	0.01084	0.01626	0.02168
0.02710	0.03252	0.03794	0.04336	0.04878
0.05420	0.05962	0.06504	0.07046	0.07588
0.08130	0.08672			

YAW (RADIANS)

0.00000	0.00000	0.00000	0.02182	0.02182
0.02182	0.03491	0.03491	0.05062	0.05062
0.06982	0.09601	0.15535	0.16059	0.16932
0.14890	0.00000			

AXIAL VELOCITY (M/S)

1.87080	1.88393	1.79001	1.74780	1.66108
1.52175	1.40334	1.36781	1.27379	1.25434
1.23316	1.12689	1.00519	1.00435	0.81886
0.59970	0.00000			

TANGENTIAL VELOCITY (M/S)

0.00000	0.00000	0.00000	0.03814	0.03625
0.03321	0.04901	0.04777	0.06454	0.06355
0.08624	0.10852	0.15743	0.16269	0.13999
0.08996	0.00000			

MEAN VELOCITY	=	1.064259 M/S
MASS FLUX	=	0.030027 KG/S
K. E. FACTOR	=	1.366170
AXIAL KINETIC ENERGY	=	0.023231 NM/S
ANGULAR MOMENTUM FLUX	=	0.1574E-03 NM

TABLE 6/5

20 DEGRE DIFFUSER FLOW PROPERTIES

AXIAL FLOW (SWIRL 0)

STATION 1

RADIUS (M)

0.00000	0.00500	0.01000	0.01500	0.02000
0.02500	0.03000	0.03500	0.04000	0.04500

YAW (RADIANS)

0.00000	0.00000	0.00000	0.00000	0.00000
0.00000	0.00000	0.00000	0.00000	0.00000

AXIAL VELOCITY (M/S)

6.13594	6.15201	6.16002	6.16403	6.17602
6.05499	5.80536	5.46834	4.97704	0.00000

TANGENTIAL VELOCITY (M/S)

0.00000	0.00000	0.00000	0.00000	0.00000
0.00000	0.00000	0.00000	0.00000	0.00000

MEAN VELOCITY = 5.239198 M/S
MASS FLUX = 0.039762 KG/S
K. E. FACTOR = 1.189276
AXIAL KINETIC ENERGY = 0.649011 NM/S
ANGULAR MOMENTUM FLUX = 0.0000E 00 NM

STATION 2

RADIUS (M)

0.00000	0.00400	0.00800	0.01200	0.01600
0.02000	0.02400	0.02800	0.03200	0.03600
0.04000	0.04400	0.04800		

YAW (RADIANS)

0.00000	0.00000	0.00000	0.00000	0.00000
0.00000	0.00000	0.00000	0.00000	0.00000
0.00000	0.00000	0.00000		

AXIAL VELOCITY (M/S)

5.66774	5.70245	5.70678	5.75842	5.71110
5.67643	5.56228	5.39109	5.17629	4.91217
4.53615	3.71705	0.00000		

TANGENTIAL VELOCITY (M/S)

0.00000	0.00000	0.00000	0.00000	0.00000
0.00000	0.00000	0.00000	0.00000	0.00000
0.00000	0.00000	0.00000		

MEAN VELOCITY = 4.657323 M/S
MASS FLUX = 0.040216 KG/S
K. E. FACTOR = 1.190800
AXIAL KINETIC ENERGY = 0.519374 NM/S
ANGULAR MOMENTUM FLUX = 0.0000E 00 NM

STATION 3

RADIUS (M)

0.00000	0.00410	0.00820	0.01230	0.01640
0.02050	0.02460	0.02870	0.03280	0.03690
0.04100	0.04510	0.04920	0.05330	0.05740
0.06150	0.06560			

YAW (RADIANS)

0.00000	0.00000	0.00000	0.00000	0.00000
0.00000	0.00000	0.00000	0.00000	0.00000
0.00000	0.00000	0.00000	0.00000	0.00000
0.00000	0.00000			

AXIAL VELOCITY (M/S)

5.20007	5.21429	5.18106	5.18106	5.11878
5.02145	4.85661	4.68597	4.38121	4.03530
3.54027	2.92174	2.25443	1.61717	1.04191
0.37959	0.00000			

TANGENTIAL VELOCITY (M/S)

0.00000	0.00000	0.00000	0.00000	0.00000
0.00000	0.00000	0.00000	0.00000	0.00000
0.00000	0.00000	0.00000	0.00000	0.00000
0.00000	0.00000			

MEAN VELOCITY = 2.706283 M/S
MASS FLUX = 0.043648 KG/S
K. E. FACTOR = 2.214406
AXIAL KINETIC ENERGY = 0.353944 NM/S
ANGULAR MOMENTUM FLUX = 0.0000E 00 NM

STATION 4

RADIUS (M)

0.00000	0.00415	0.00830	0.01245	0.01660
0.02075	0.02490	0.02905	0.03320	0.03735
0.04150	0.04565	0.04980	0.05395	0.05810
0.06225	0.06640	0.07055	0.07470	0.07885
0.08300				

YAW (RADIANS)

0.00000	0.00000	0.00000	0.00000	0.00000
0.00000	0.00000	0.00000	0.00000	0.00000
0.00000	0.00000	0.00000	0.00000	0.00000
0.00000	0.00000	0.00000	0.00000	0.00000
0.00000				

AXIAL VELOCITY (M/S)

4.95219	4.97208	4.93722	4.93222	4.82092
4.71222	4.54701	4.38684	4.04141	3.75666
3.33944	2.90481	2.48356	2.06001	1.63236
1.31417	1.04191	0.80092	0.62830	0.23509
0.00000				

TANGENTIAL VELOCITY (M/S)

0.00000	0.00000	0.00000	0.00000	0.00000
0.00000	0.00000	0.00000	0.00000	0.00000
0.00000	0.00000	0.00000	0.00000	0.00000
0.00000	0.00000	0.00000	0.00000	0.00000
0.00000				

MEAN VELOCITY = 2.037345 M/S
MASS FLUX = 0.052602 KG/S
K. E. FACTOR = 2.916125
AXIAL KINETIC ENERGY = 0.318350 NM/S
ANGULAR MOMENTUM FLUX = 0.0000E 00 NM

TABLE 6/6

20 DEGREE DIFFUSER FLOW PROPERTIES

SOLID-BODY SWIRL (SWIRL 2)

STATION 1

RADIUS (M)

0.00000	0.00500	0.01000	0.01500	0.02000
0.02500	0.03000	0.03500	0.04000	0.04500

YAW (RADIANS)

0.00000	0.02531	0.04800	0.04713	0.07419
0.09862	0.12393	0.16932	0.21121	0.00000

AXIAL VELOCITY (M/S)

6.10773	6.10578	6.06427	5.94564	5.80210
5.71336	5.62858	5.43002	5.20826	0.00000

TANGENTIAL VELOCITY (M/S)

0.00000	0.15457	0.29133	0.28043	0.43123
0.56531	0.70117	0.92829	1.11670	0.00000

MEAN VELOCITY = 5.165030 M/S
MASS FLUX = 0.039199 KG/S
K. E. FACTOR = 1.173588
AXIAL KINETIC ENERGY = 0.613633 NM/S
ANGULAR MOMENTUM FLUX = 0.9175E-03 NM

STATION 2

RADIUS (M)

0.00000	0.00400	0.00800	0.01200	0.01600
0.02000	0.02400	0.02800	0.03200	0.03600
0.04000	0.04400	0.04800		

YAW (RADIANS)

0.00000	0.02444	0.04451	0.06633	0.08728
0.10648	0.11608	0.14314	0.16059	0.18677
0.19376	0.21121	0.00000		

AXIAL VELOCITY (M/S)

5.42303	5.46219	5.48990	5.52343	5.54111
5.44185	5.35936	5.32235	5.26723	5.12360
4.96591	4.67862	0.00000		

TANGENTIAL VELOCITY (M/S)

0.00000	0.13351	0.24453	0.36691	0.48485
0.58164	0.62492	0.76706	0.85322	0.96824
0.97440	1.00314	0.00000		

MEAN VELOCITY = 4.867188 M/S
MASS FLUX = 0.042028 KG/S
K. E. FACTOR = 1.130553
AXIAL KINETIC ENERGY = 0.562804 NM/S
ANGULAR MOMENTUM FLUX = 0.1110E-02 NM

STATION 3

RADIUS (M)

0.00000	0.00400	0.00800	0.01200	0.01600
0.02100	0.02500	0.02900	0.03300	0.03700
0.04100	0.04500	0.04900	0.05300	0.05700
0.06100	0.06600			

YAW (RADIANS)

0.00000	0.00785	0.01309	0.01920	0.03491
0.05586	0.07506	0.08379	0.09077	0.09077
0.10473	0.12655	0.16583	0.16845	0.19201
0.13266	0.00000			

AXIAL VELOCITY (M/S)

4.10802	4.07775	4.13758	4.20224	3.88343
3.77694	3.60593	3.57613	3.31094	3.04129
2.81184	2.53174	2.23428	2.00710	1.29002
0.74992	0.00000			

TANGENTIAL VELOCITY (M/S)

0.00000	0.03203	0.05417	0.08070	0.13563
0.21119	0.27117	0.30034	0.30136	0.27682
0.29557	0.32212	0.37394	0.34132	0.25079
0.10007	0.00000			

MEAN VELOCITY = 2.329473 M/S
MASS FLUX = 0.037570 KG/S
K. E. FACTOR = 1.708219
AXIAL KINETIC ENERGY = 0.174130 NM/S
ANGULAR MOMENTUM FLUX = 0.3799E-03 NM

STATION 4

RADIUS (M)

0.00000	0.00400	0.00800	0.01200	0.01700
0.02100	0.02500	0.02900	0.03300	0.03700
0.04100	0.04600	0.05000	0.05400	0.05800
0.06200	0.06600	0.07100	0.07500	0.07900
0.08300				

YAW (RADIANS)

0.00000	0.02967	0.03055	0.04015	0.04015
0.06633	0.07855	0.07855	0.07419	0.07331
0.10124	0.10124	0.11521	0.11521	0.13266
0.13266	0.13266	0.13266	0.13266	0.11067
0.00000				

AXIAL VELOCITY (M/S)

2.97198	2.90353	2.76428	2.51116	2.58844
2.56576	2.51520	2.39536	2.15916	2.45699
2.81285	2.09658	1.88535	1.36026	1.39257
0.98469	0.85277	0.76274	0.58255	0.45030
0.00000				

TANGENTIAL VELOCITY (M/S)

0.00000	0.08619	0.08447	0.10087	0.10398
0.17044	0.19798	0.18854	0.16047	0.18045
0.28576	0.21299	0.21817	0.15741	0.18583
0.13140	0.11380	0.10178	0.07774	0.05004
0.00000				

MEAN VELOCITY = 1.421623 M/S
MASS FLUX = 0.036705 KG/S
K. E. FACTOR = 2.085201
AXIAL KINETIC ENERGY = 0.077341 NM/S
ANGULAR MOMENTUM FLUX = 0.2689E-03 NM

TABLE 6/7

20 DEGREE DIFFUSER FLOW PROPERTIES

SOLID-BODY SWIRL (SWIRL 3)

STATION 1

RADIUS (M)

0.00000	0.00500	0.01000	0.01500	0.02000
0.02500	0.03000	0.03500	0.04000	0.04500

YAW (RADIANS)

0.00000	0.02618	0.05586	0.07593	0.10910
0.12219	0.15885	0.19550	0.23129	0.00000

AXIAL VELOCITY (M/S)

5.65902	5.75217	5.65890	5.49739	5.35449
5.23611	5.11113	4.94023	4.68756	0.00000

TANGENTIAL VELOCITY (M/S)

0.00000	0.15065	0.31642	0.41823	0.58649
0.64300	0.81878	0.97832	1.10392	0.00000

MEAN VELOCITY = 4.715197 M/S
MASS FLUX = 0.035785 KG/S
K. E. FACTOR = 1.178324
AXIAL KINETIC ENERGY = 0.468747 NM/S
ANGULAR MOMENTUM FLUX = 0.8866E-03 NM

STATION 2

RADIUS (M)

0.00000	0.00480	0.00960	0.01440	0.01920
0.02400	0.02880	0.03360	0.03840	0.04320
0.04800				

YAW (RADIANS)

0.00000	0.02531	0.03840	0.05237	0.07855
0.10473	0.13441	0.16757	0.19637	0.24263
0.00000				

AXIAL VELOCITY (M/S)

4.99189	5.11232	5.18200	5.16444	5.06441
5.04257	5.03425	5.05183	5.02040	4.75853
0.00000				

TANGENTIAL VELOCITY (M/S)

0.00000	0.12942	0.19910	0.27069	0.39863
0.53006	0.68075	0.85457	0.99875	1.17778
0.00000				

MEAN VELOCITY = 4.655983 M/S
MASS FLUX = 0.040204 KG/S
K. E. FACTOR = 1.148885
AXIAL KINETIC ENERGY = 0.500660 NM/S
ANGULAR MOMENTUM FLUX = 0.1091E-02 NM

STATION 3

RADIUS (M)

0.00000	0.00410	0.00820	0.01230	0.01640
0.02050	0.02460	0.02870	0.03280	0.03690
0.04100	0.04510	0.04920	0.05330	0.05740
0.06150	0.06560			

YAW (RADIANS)

0.00000	0.02618	0.05237	0.05237	0.09251
0.09251	0.11084	0.15012	0.16583	0.18852
0.18852	0.21994	0.24438	0.26620	0.31420
0.23757	0.00000			

AXIAL VELOCITY (M/S)

3.68371	3.54601	3.42225	3.12932	2.93437
2.98396	2.85301	2.76080	2.65631	2.87826
2.84499	2.51881	2.13370	1.86833	1.17625
0.94995	0.00000			

TANGENTIAL VELOCITY (M/S)

0.00000	0.09287	0.17938	0.16402	0.27225
0.27685	0.31754	0.41759	0.44457	0.54913
0.54278	0.56310	0.53206	0.50943	0.38224
0.23002	0.00000			

MEAN VELOCITY = 2.107692 M/S
MASS FLUX = 0.033993 KG/S
K. E. FACTOR = 1.462744
AXIAL KINETIC ENERGY = 0.110445 NM/S
ANGULAR MOMENTUM FLUX = 0.5835E-03 NM

STATION 4

RADIUS (M)

0.00000	0.00415	0.00830	0.01245	0.01660
0.02075	0.02490	0.02905	0.03320	0.03735
0.04150	0.04565	0.04980	0.05395	0.05810
0.06225	0.06640	0.07055	0.07470	0.07885
0.08300				

YAW (RADIANS)

0.00000	0.01396	0.02269	0.03142	0.04189
0.06982	0.08902	0.10473	0.12655	0.14837
0.17019	0.18852	0.18852	0.20074	0.20074
0.20947	0.20947	0.20947	0.20947	0.11940
0.00000				

AXIAL VELOCITY (M/S)

1.77709	1.83160	1.67666	1.73408	1.69025
1.62838	1.67045	1.68247	1.63423	1.82493
1.73768	1.64738	1.60344	1.53920	1.30605
1.22912	1.10792	0.94710	0.72064	0.50003
0.00000				

TANGENTIAL VELOCITY (M/S)

0.00000	0.02558	0.03805	0.05450	0.07085
0.11388	0.14910	0.17686	0.20793	0.27277
0.29863	0.31430	0.30591	0.31320	0.26575
0.26129	0.23553	0.20134	0.15320	0.05999
0.00000				

MEAN VELOCITY = 1.229428 M/S
MASS FLUX = 0.031742 KG/S
K. E. FACTOR = 1.418421
AXIAL KINETIC ENERGY = 0.034027 NM/S
ANGULAR MOMENTUM FLUX = 0.3580E-03 NM

TABLE 6/8

30 DEGREE DIFFUSER FLOW PROPERTIES

AXIAL FLOW (SWIRL 0)

STATION 1

RADIUS (M)

0.00000	0.00500	0.01000	0.01500	0.02000
0.02500	0.03000	0.03500	0.04000	0.04500

YAW (RADIANS)

0.00000	0.00000	0.00000	0.00000	0.00000
0.00000	0.00000	0.00000	0.00000	0.00000

AXIAL VELOCITY (M/S)

6.05499	6.09560	6.11581	6.10773	6.11581
5.98944	5.74985	5.57114	4.90212	0.00000

TANGENTIAL VELOCITY (M/S)

0.00000	0.00000	0.00000	0.00000	0.00000
0.00000	0.00000	0.00000	0.00000	0.00000

MEAN VELOCITY = 5.202332 M/S
MASS FLUX = 0.039482 KG/S
K. E. FACTOR = 1.189646
AXIAL KINETIC ENERGY = 0.635604 NM/S
ANGULAR MOMENTUM FLUX = 0.0000E 00 NM

STATION 2

RADIUS (M)

0.00000	0.00386	0.00772	0.01156	0.01544
0.01930	0.02316	0.02702	0.03088	0.03474
0.03860	0.04246	0.04632		

YAW (RADIANS)

0.00000	0.00000	0.00000	0.00000	0.00000
0.00000	0.00000	0.00000	0.00000	0.00000
0.00000	0.00000	0.00000		

AXIAL VELOCITY (M/S)

5.81810	5.84349	5.86035	5.82657	5.80111
5.75414	5.61086	5.40937	5.17629	4.80554
4.34729	4.02306	0.00000		

TANGENTIAL VELOCITY (M/S)

0.00000	0.00000	0.00000	0.00000	0.00000
0.00000	0.00000	0.00000	0.00000	0.00000
0.00000	0.00000	0.00000		

MEAN VELOCITY = 4.709389 M/S
MASS FLUX = 0.037869 KG/S
K. E. FACTOR = 1.180441
AXIAL KINETIC ENERGY = 0.495707 NM/S
ANGULAR MOMENTUM FLUX = 0.0000E 00 NM

STATION 3

RADIUS (M)

0.00000	0.00413	0.00826	0.01239	0.01652
0.02065	0.02478	0.02891	0.03304	0.03717
0.04130	0.04543	0.04956	0.05369	0.05782
0.06195				

YAW (RADIANS)

0.00000	0.00000	0.00000	0.00000	0.00000
0.00000	0.00000	0.00000	0.00000	0.00000
0.00000	0.00000	0.00000	0.00000	0.00000
0.00000				

AXIAL VELOCITY (M/S)

5.48636	5.47735	5.46834	5.43666	5.38193
5.32664	5.14282	4.93222	4.64896	4.27287
3.69040	2.80103	1.84520	0.94244	0.37959
0.00000				

TANGENTIAL VELOCITY (M/S)

0.00000	0.00000	0.00000	0.00000	0.00000
0.00000	0.00000	0.00000	0.00000	0.00000
0.00000	0.00000	0.00000	0.00000	0.00000
0.00000				

MEAN VELOCITY = 2.936068 M/S
MASS FLUX = 0.042231 KG/S
K. E. FACTOR = 2.233745
AXIAL KINETIC ENERGY = 0.406597 NM/S
ANGULAR MOMENTUM FLUX = 0.0000E 00 NM

STATION 4

RADIUS (M)

0.00000	0.00468	0.00936	0.01404	0.01872
0.02340	0.02808	0.03276	0.03744	0.04212
0.04680	0.05148	0.05616	0.06084	0.06552
0.07020	0.07488	0.07956		

YAW (RADIANS)

0.00000	0.00000	0.00000	0.00000	0.00000
0.00000	0.00000	0.00000	0.00000	0.00000
0.00000	0.00000	0.00000	0.00000	0.00000
0.00000	0.00000	0.00000		

AXIAL VELOCITY (M/S)

5.39109	5.37734	5.38193	5.34513	5.33127
5.22374	5.05085	4.80040	4.35862	3.78936
3.10990	2.39248	1.72066	1.19624	0.73674
0.31415	0.09934	0.00000		

TANGENTIAL VELOCITY (M/S)

0.00000	0.00000	0.00000	0.00000	0.00000
0.00000	0.00000	0.00000	0.00000	0.00000
0.00000	0.00000	0.00000	0.00000	0.00000
0.00000	0.00000	0.00000		

MEAN VELOCITY = 2.237627 M/S
MASS FLUX = 0.053083 KG/S
K. E. FACTOR = 3.395409
AXIAL KINETIC ENERGY = 0.451226 NM/S
ANGULAR MOMENTUM FLUX = 0.0000E 00 NM

TABLE 6/9

30 DEGREE DIFFUSER FLOW PROPERTIES

SOLID-BODY SWIRL (SWIRL 2)

STATION 1

RADIUS (M)

0.00000	0.00500	0.01000	0.01500	0.02000
0.02500	0.03000	0.03500	0.04000	0.04500

YAW (RADIANS)

0.00000	0.02880	0.04713	0.06022	0.08466
0.11259	0.13964	0.17805	0.21470	0.00000

AXIAL VELOCITY (M/S)

6.08345	6.07687	6.03196	5.94973	5.78034
5.64050	5.52130	5.39077	5.14517	0.00000

TANGENTIAL VELOCITY (M/S)

0.00000	0.17507	0.28450	0.35874	0.49053
0.63775	0.77607	0.97008	1.12198	0.00000

MEAN VELOCITY = 5.113091 M/S
MASS FLUX = 0.038805 KG/S
K. E. FACTOR = 1.174691
AXIAL KINETIC ENERGY = 0.595867 NM/S
ANGULAR MOMENTUM FLUX = 0.9509E-03 NM

STATION 2

RADIUS (M)

0.00000	0.00386	0.00772	0.01156	0.01544
0.01930	0.02316	0.02702	0.03088	0.03474
0.03860	0.04246	0.04632		

YAW (RADIANS)

0.00000	0.01833	0.03840	0.05411	0.06633
0.07855	0.09775	0.10648	0.11957	0.13266
0.14139	0.15186	0.00000		

AXIAL VELOCITY (M/S)

5.49085	5.49891	5.55818	5.52750	5.55447
5.44698	5.36080	5.46868	5.41584	5.28901
5.23667	4.90503	0.00000		

TANGENTIAL VELOCITY (M/S)

0.00000	0.10080	0.21355	0.29940	0.36898
0.42874	0.52570	0.58451	0.65068	0.70580
0.74539	0.75067	0.00000		

MEAN VELOCITY = 4.998431 M/S
MASS FLUX = 0.040193 KG/S
K. E. FACTOR = 1.125502
AXIAL KINETIC ENERGY = 0.565111 NM/S
ANGULAR MOMENTUM FLUX = 0.7809E-03 NM

STATION 3

RADIUS (M)

0.00000	0.00413	0.00826	0.01239	0.01652
0.02065	0.02478	0.02891	0.03304	0.03717
0.04130	0.04543	0.04956	0.05369	0.05782
0.06195				

YAW (RADIANS)

0.00000	0.00524	0.01396	0.04888	0.03491
0.04800	0.04888	0.04364	0.05237	0.07331
0.06546	0.07593	0.11608	0.15710	0.14366
0.00000				

AXIAL VELOCITY (M/S)

4.74873	4.72261	4.66440	4.61683	4.60885
4.50914	4.34776	4.25146	3.97444	3.66713
3.23503	2.92173	2.23926	1.31640	0.83020
0.00000				

TANGENTIAL VELOCITY (M/S)

0.00000	0.02473	0.06514	0.22583	0.16097
0.21662	0.21267	0.18565	0.20832	0.26933
0.21206	0.22228	0.26111	0.20853	0.12009
0.00000				

MEAN VELOCITY = 2.772274 M/S
MASS FLUX = 0.039875 KG/S
K. E. FACTOR = 1.764378
AXIAL KINETIC ENERGY = 0.270354 NM/S
ANGULAR MOMENTUM FLUX = 0.2916E-03 NM

STATION 4

RADIUS (M)

0.00000	0.00468	0.00936	0.01404	0.01872
0.02340	0.02808	0.03276	0.03744	0.04212
0.04680	0.05148	0.05616	0.06084	0.06552
0.07020	0.07488	0.07956		

YAW (RADIANS)

0.00000	0.00000	0.01658	0.00960	0.00960
0.00960	0.00960	0.00960	0.02182	0.02182
0.04800	0.04800	0.04800	0.06109	0.08902
0.10648	0.08641	0.00000		

AXIAL VELOCITY (M/S)

3.71705	3.64330	3.75615	3.65665	3.62957
3.42679	3.32447	3.24942	3.07727	2.80915
2.36903	1.94699	1.48842	1.15210	0.88503
0.66263	0.51995	0.00000		

TANGENTIAL VELOCITY (M/S)

0.00000	0.00000	0.06229	0.03511	0.03485
0.03290	0.03192	0.03120	0.06716	0.06130
0.11381	0.09353	0.07150	0.07047	0.07900
0.07082	0.04504	0.00000		

MEAN VELOCITY = 1.775413 M/S
MASS FLUX = 0.042118 KG/S
K. E. FACTOR = 2.323657
AXIAL KINETIC ENERGY = 0.154244 NM/S
ANGULAR MOMENTUM FLUX = 0.1165E-03 NM

TABLE 6/10

30 DEGREE DIFFUSER FLOW PROPERTIES

SOLID-BODY SWIRL (SWIRL 3)

STATION 1

RADIUS (M)

0.00000	0.00500	0.01000	0.01500	0.02000
0.02500	0.03000	0.03500	0.04000	0.04500

YAW (RADIANS)

0.00000	0.04364	0.06459	0.09950	0.12568
0.14488	0.17281	0.22692	0.27231	0.00000

AXIAL VELOCITY (M/S)

5.86877	5.94244	5.83972	5.72995	5.59272
5.49961	5.33778	5.17652	4.97177	0.00000

TANGENTIAL VELOCITY (M/S)

0.00000	0.25949	0.37769	0.57200	0.70662
0.80241	0.93171	1.19525	1.38833	0.00000

MEAN VELOCITY = 4.944675 M/S
MASS FLUX = 0.037527 KG/S
K. E. FACTOR = 1.175350
AXIAL KINETIC ENERGY = 0.539207 NM/S
ANGULAR MOMENTUM FLUX = 0.1147E-02 NM

STATION 2

RADIUS (M)

0.00000	0.00386	0.00772	0.01158	0.01544
0.01930	0.02316	0.02702	0.03088	0.03474
0.03860	0.04246	0.04632		

YAW (RADIANS)

0.00000	0.01222	0.03666	0.05586	0.07331
0.10037	0.11433	0.14314	0.16670	0.18852
0.20510	0.21907	0.00000		

AXIAL VELOCITY (M/S)

5.09946	5.19019	5.25317	5.30907	5.34915
5.36396	5.37405	5.40348	5.34786	5.39798
5.39771	5.24883	0.00000		

TANGENTIAL VELOCITY (M/S)

0.00000	0.06342	0.19265	0.29686	0.39287
0.54019	0.61713	0.77876	0.89984	1.02986
1.12288	1.16860	0.00000		

MEAN VELOCITY = 5.048165 M/S
MASS FLUX = 0.040593 KG/S
K. E. FACTOR = 1.120188
AXIAL KINETIC ENERGY = 0.579400 NM/S
ANGULAR MOMENTUM FLUX = 0.1161E-02 NM

STATION 3

RADIUS (M)

0.00000	0.00413	0.00826	0.01239	0.01652
0.02065	0.02478	0.02891	0.03304	0.03717
0.04130	0.04543	0.04956	0.05369	0.05782
0.06195				

YAW (RADIANS)

0.00000	0.00000	0.03578	0.03578	0.03578
0.03578	0.03578	0.03578	0.09251	0.12219
0.14925	0.14925	0.14925	0.14925	0.14925
0.13266				

AXIAL VELOCITY (M/S)

3.97989	4.04751	3.85784	3.78042	3.70803
3.47475	3.48184	3.54496	3.24323	3.29247
3.13747	2.73483	1.65845	0.93197	0.44911
0.00000				

TANGENTIAL VELOCITY (M/S)

0.00000	0.00000	0.13811	0.13534	0.13274
0.12439	0.12465	0.12691	0.30090	0.40432
0.47176	0.41122	0.24937	0.14013	0.06753
0.00000				

MEAN VELOCITY = 2.287737 M/S
MASS FLUX = 0.032905 KG/S
K. E. FACTOR = 1.872973
AXIAL KINETIC ENERGY = 0.161280 NM/S
ANGULAR MOMENTUM FLUX = 0.3195E-03 NM

STATION 4

RADIUS (M)

0.00000	0.00468	0.00936	0.01404	0.01872
0.02340	0.02808	0.03276	0.03744	0.04212
0.04680	0.05148	0.05616	0.06084	0.06552
0.07020	0.07488	0.07956		

YAW (RADIANS)

0.00000	0.00785	0.01309	0.03055	0.05586
0.07855	0.07855	0.10473	0.12044	0.14314
0.14925	0.16583	0.19201	0.20598	0.25485
0.25485	0.38053	0.00000		

AXIAL VELOCITY (M/S)

3.50525	3.37607	3.40499	3.18676	3.14441
3.10821	3.02019	2.91412	2.85835	2.67477
2.56173	2.17991	1.83735	1.42585	1.09609
0.64488	0.24921	0.00000		

TANGENTIAL VELOCITY (M/S)

0.00000	0.02652	0.04458	0.09738	0.17582
0.24465	0.23773	0.30633	0.34594	0.38549
0.38519	0.36484	0.35719	0.29792	0.28555
0.16800	0.09969	0.00000		

MEAN VELOCITY = 1.750653 M/S
MASS FLUX = 0.041531 KG/S
K. E. FACTOR = 2.070461
AXIAL KINETIC ENERGY = 0.131767 NM/S
ANGULAR MOMENTUM FLUX = 0.5396E-03 NM

TABLE 6/11

WALL STATIC PRESSURE DISTRIBUTION IN DIFFUSER-PIPE COMBINATION (M. VOLTS)
PRESSURE. (N/M^2) = 0. 01962 * M. VOLTS

AXIAL SOLID-BODY SWIRL 3	SOLID-BODY SWIRL 2			
STATION	P1	P2	P3	P4	P5
DIFFUSER					
10	-79	-120	-166	-208	-252
			-166 -166	-224 -218	-275 -267
20	-79	-120	-166	-207	-252
			-166 -168	-225 -219	-280 -270
30	-79	-120	-165	-209	-252
			-168 -166	-234 -225	-292 -277

STATION	D1	D2	D3	D4
DIFFUSER				
10	-13	200	293	348
	-28 -20	255 240	355 335	400 380
20	-125	100	203	
	-203 -164	215 175	293 253	
30	-155	8	80	
	-235 -210	75 60	155 133	

STATION	E1	E2
DIFFUSER		
10	370	383
	420 405	435 415
20	275	348
	350 315	403 380
30	180	235
	250 220	325 295

TABLE 7/1

WALL STATIC PRESSURE DISTRIBUTION IN DIFFUSER-PIPE COMBINATION (M. VOLTS)

PRESSURE (N/M^2) = 0.05886 * (M. VOLTS)

10 DEGREE DIFFUSER

NUMBER OF BLADES = 16

	BLADE ANGLES (DEGREES)								
STATION	0	2	4	5	6	8	10	15	20
P1	-38	-28	-34	-33	-35	-41	-52	-77	-118
P2	-43	-44	-49	-51	-52	-61	-80	-116	-170
P3	-63	-64	-74	-78	-76	-90	-116	-171	-240
P4	-80	-82	-94	-98	-95	-112	-141	-207	-294
P5	-110	-100	-115	-117	-114	-136	-176	-252	-353
D1	-9	-11	-22	-25	-24	-73	-166	-300	-461
D2	113	112	120	117	120	78	-18	-172	-355
D3	154	149	163	169	172	137	42	-111	-283
D4	172	172	182	188	192	158	67	-84	-247
E1	191	184	191	193	200	161	72	-75	-242
E2	203	193	196	198	202	159	71	-74	-244

TABLE 7/2

WALL STATIC PRESSURE DISTRIBUTION IN DIFFUSER-PIPE COMBINATION (M. VOLTS)

PRESSURE (N/M^2) = 0.05886 * (M. VOLTS)

10 DEGREE DIFFUSER

NUMBER OF BLADES = 8

	BLADE ANGLES (DEGREES)							
STATION	0	2	4	5	6	8	10	15
P1	-26	-22	-30	-30	-33	-35	-39	-57
P2	-42	-41	-46	-48	-53	-57	-66	-93
P3	-61	-61	-68	-71	-77	-83	-97	-134
P4	-75	-78	-85	-89	-96	-104	-119	-166
P5	-91	-95	-106	-108	-116	-124	-145	-203
D1	-5	-8	-20	-18	-26	-44	-98	-224
D2	104	109	116	120	118	108	49	-79
D3	141	148	167	172	177	167	113	-22
D4	159	174	188	193	201	190	134	6
E1	177	194	193	200	207	192	135	10
E2	190	203	198	206	210	189	135	10

TABLE 7/3

WALL STATIC PRESSURE DISTRIBUTION IN DIFFUSER-PIPE

CIMBINATION (M. VOLTS)

PRESSURE (N/M^2) = 0.05886 * (M. VOLTS)

20 DEGREE DIFFUSER

NUMBER OF BLADES = 8

	BLADE ANGLES (DEGREES)								
STATION	0	2	4	6	8	10	12	15	20
P1	-25	-25	-26	-27	-30	-35	-40	-47	-66
P2	-40	-40	-41	-45	-50	-57	-65	-79	-107
P3	-60	-60	-62	-67	-73	-83	-96	-119	-158
P4	-77	-76	-78	-84	-91	-103	-119	-147	-198
P5	-93	-93	-97	-103	-109	-125	-146	-183	-238
D1	-42	-54	-72	-54	-89	-119	-197	-269	-342
D2	59	63	67	69	88	93	17	-71	-175
D3	73	77	91	93	121	145	89	9	-102
E1	96	101	119	122	146	165	106	25	-80
E2	132	137	147	149	163	165	105	24	-78

TABLE 7/4

WALL STATIC PRESSURE DISTRIBUTION IN DIFFUSER-PIPE COMBINATION (M. VOLTS)

PRESSURE (N/M^2) = 0.05886 * (M. VOLTS)

30 DEGREE DIFFUSER

NUMBER OF BLADES = 8

	BLADE ANGLES (DEGREES)								
STATION	0	2	4	6	8	10	12	14	20
P1	-26	-25	-27	-29	-31	-35	-38	-44	-82
P2	-41	-40	-43	-48	-50	-56	-62	-70	-126
P3	-60	-69	-64	-70	-73	-82	-89	-104	-184
P4	-76	-76	-81	-88	-90	-102	-110	-128	-223
P5	-91	-92	-99	-106	-109	-125	-137	-158	-270
D1	-73	-70	-91	-82	-93	-118	-153	-230	-366
D2	16	18	19	19	17	16	9	-71	-259
D3	25	25	36	34	40	47	49	7	-213
E1	53	59	69	73	81	93	90	41	-161
E2	103	106	103	106	112	112	100	43	-158

TABLE 9/1

10 DEGREE DIFFUSER FLOW PROPERTIES

AXIAL FLOW VORTEX GENERATOR BLADE ANGLE = 0

STATION 1

RADIUS (M)

0.00000	0.00500	0.01000	0.01500	0.02000
0.02500	0.03000	0.03500	0.04000	0.04500

YAW (RADIANS)

0.00000	0.00000	0.00000	0.00000	0.00000
0.00000	0.00000	0.00000	0.00000	0.00000

AXIAL VELOCITY (M/S)

5.55340	5.56228	5.58441	5.59324	5.50880
5.56671	5.52221	5.37275	4.97208	0.00000

TANGENTIAL VELOCITY (M/S)

0.00000	0.00000	0.00000	0.00000	0.00000
0.00000	0.00000	0.00000	0.00000	0.00000

MEAN VELOCITY = 4.967631 M/S
MASS FLUX = 0.037701 KG/S
K. E. FACTOR = 1.172049
AXIAL KINETIC ENERGY = 0.545216 NM/S
ANGULAR MOMENTUM FLUX = 0.0000E 00 NM

STATION 2

RADIUS (M)

0.00000	0.00406	0.00812	0.01218	0.01624
0.02030	0.02436	0.02842	0.03248	0.03654
0.04060	0.04466	0.04872		

YAW (RADIANS)

0.00000	0.00000	0.00000	0.00000	0.00000
0.00000	0.00000	0.00000	0.00000	0.00000
0.00000	0.00000	0.00000		

AXIAL VELOCITY (M/S)

5.14762	5.17153	5.17629	5.14762	5.15241
5.13802	5.13802	5.08493	4.98199	4.82092
4.46488	3.84109	0.00000		

TANGENTIAL VELOCITY (M/S)

0.00000	0.00000	0.00000	0.00000	0.00000
0.00000	0.00000	0.00000	0.00000	0.00000
0.00000	0.00000	0.00000		

MEAN VELOCITY = 4.458983 M/S
MASS FLUX = 0.039667 KG/S
K. E. FACTOR = 1.156533
AXIAL KINETIC ENERGY = 0.456068 NM/S
ANGULAR MOMENTUM FLUX = 0.0000E 00 NM

STATION 3

RADIUS (M)

0.00000	0.00492	0.00984	0.01476	0.01968
0.02460	0.02952	0.03444	0.03936	0.04428
0.04920	0.05412	0.05902	0.06396	

YAW (RADIANS)

0.00000	0.00000	0.00000	0.00000	0.00000
0.00000	0.00000	0.00000	0.00000	0.00000
0.00000	0.00000	0.00000	0.00000	

AXIAL VELOCITY (M/S)

4.15579	4.13197	4.12001	4.05360	4.02306
3.87307	3.73691	3.59559	3.19598	2.79221
2.30851	1.66231	1.01796	0.00000	

TANGENTIAL VELOCITY (M/S)

0.00000	0.00000	0.00000	0.00000	0.00000
0.00000	0.00000	0.00000	0.00000	0.00000
0.00000	0.00000	0.00000	0.00000	

MEAN VELOCITY = 2.528678 M/S
MASS FLUX = 0.038769 KG/S
K. E. FACTOR = 1.646306
AXIAL KINETIC ENERGY = 0.204060 NM/S
ANGULAR MOMENTUM FLUX = 0.0000E 00 NM

STATION 4

RADIUS (M)

0.00000	0.00471	0.00942	0.01413	0.01884
0.02355	0.02826	0.03297	0.03768	0.04239
0.04710	0.05181	0.05652	0.06123	0.06594
0.07065	0.07536			

YAW (RADIANS)

0.00000	0.00000	0.00000	0.00000	0.00000
0.00000	0.00000	0.00000	0.00000	0.00000
0.00000	0.00000	0.00000	0.00000	0.00000
0.00000	0.00000			

AXIAL VELOCITY (M/S)

3.57494	3.61611	3.56111	3.43414	3.29481
3.14148	2.96366	2.75664	2.45357	2.11904
1.74910	1.40491	0.99342	0.62039	0.32037
0.12167	0.00000			

TANGENTIAL VELOCITY (M/S)

0.00000	0.00000	0.00000	0.00000	0.00000
0.00000	0.00000	0.00000	0.00000	0.00000
0.00000	0.00000	0.00000	0.00000	0.00000
0.00000	0.00000			

MEAN VELOCITY = 1.448251 M/S
MASS FLUX = 0.030825 KG/S
K. E. FACTOR = 3.001204
AXIAL KINETIC ENERGY = 0.097019 NM/S
ANGULAR MOMENTUM FLUX = 0.0000E 00 NM

STATION 5

RADIUS (M)

0.00000	0.00542	0.01084	0.01626	0.02168
0.02710	0.03252	0.03794	0.04336	0.04878
0.05420	0.05962	0.06504	0.07046	0.07588
0.08130	0.08672			

YAW (RADIANS)

0.00000	0.00000	0.00000	0.00000	0.00000
0.00000	0.00000	0.00000	0.00000	0.00000
0.00000	0.00000	0.00000	0.00000	0.00000
0.00000	0.00000			

AXIAL VELOCITY (M/S)

3.42695	3.33944	3.31720	3.23435	3.02953
2.91329	2.61895	2.54246	2.32978	2.08382
1.91089	1.70626	1.53900	1.43961	1.31417
0.65971	0.00000			

TANGENTIAL VELOCITY (M/S)

0.00000	0.00000	0.00000	0.00000	0.00000
0.00000	0.00000	0.00000	0.00000	0.00000
0.00000	0.00000	0.00000	0.00000	0.00000
0.00000	0.00000			

MEAN VELOCITY = 1.729162 M/S
MASS FLUX = 0.048736 KG/S
K. E. FACTOR = 1.654994
AXIAL KINETIC ENERGY = 0.120585 NM/S
ANGULAR MOMENTUM FLUX = 0.0000E 00 NM

TABLE 9/2

10 DEGREE DIFFUSER FLOW PROPERTIES

OPTIMUM RANKINE VORTEX SWIRL

STATION 1

RADIUS (M)

0.00000	0.00500	0.01000	0.01500	0.02000
0.02500	0.03000	0.03500	0.04000	0.04500

YAW (RADIANS)

0.00000	0.15535	0.21819	0.25485	0.21383
0.18765	0.17106	0.18765	0.20510	0.00000

AXIAL VELOCITY (M/S)

5.38651	5.42916	5.67187	5.77202	5.82479
5.88835	5.88169	5.76574	5.43700	0.00000

TANGENTIAL VELOCITY (M/S)

0.00000	0.85030	1.25759	1.50370	1.26485
1.11809	1.01608	1.09481	1.13105	0.00000

MEAN VELOCITY = 5.282804 M/S
MASS FLUX = 0.040093 KG/S
K. E. FACTOR = 1.168223
AXIAL KINETIC ENERGY = 0.653573 NM/S
ANGULAR MOMENTUM FLUX = 0.1298E-02 NM

STATION 2

RADIUS (M)

0.00000	0.00406	0.00812	0.01218	0.01624
0.02030	0.02436	0.02842	0.03248	0.03654
0.04060	0.04466	0.04872		

YAW (RADIANS)

0.00000	0.08030	0.11782	0.10473	0.08553
0.06459	0.06459	0.05586	0.05586	0.06982
0.09077	0.13615	0.00000		

AXIAL VELOCITY (M/S)

3.59559	3.91106	4.27182	4.53826	4.60013
4.62867	4.68145	4.62047	4.61514	4.46501
4.24953	3.74136	0.00000		

TANGENTIAL VELOCITY (M/S)

0.00000	0.31472	0.50567	0.47705	0.39442
0.29936	0.30277	0.25836	0.25806	0.31226
0.38679	0.51257	0.00000		

MEAN VELOCITY = 4.107901 M/S
MASS FLUX = 0.036544 KG/S
K. E. FACTOR = 1.140971
AXIAL KINETIC ENERGY = 0.351802 NM/S
ANGULAR MOMENTUM FLUX = 0.4184E-03 NM

STATION 3

RADIUS (M)

0.00000	0.00492	0.00984	0.01476	0.01968
0.02460	0.02952	0.03444	0.03936	0.04428
0.04920	0.05412	0.05904	0.06396	

YAW (RADIANS)

0.00000	0.02182	0.17805	0.20772	0.23041
0.23041	0.21383	0.20248	0.17281	0.21470
0.23914	0.30722	0.41893	0.00000	

AXIAL VELOCITY (M/S)

3.18825	2.95462	3.08408	3.33208	3.37124
3.44670	3.58670	3.54224	3.54203	3.34122
3.02910	2.61902	2.09909	0.00000	

TANGENTIAL VELOCITY (M/S)

0.00000	0.06448	0.55499	0.70227	0.79082
0.80853	0.77885	0.72721	0.61827	0.72860
0.73851	0.83092	0.93471	0.00000	

MEAN VELOCITY = 2.875574 M/S
MASS FLUX = 0.044088 KG/S
K. E. FACTOR = 1.211158
AXIAL KINETIC ENERGY = 0.220770 NM/S
ANGULAR MOMENTUM FLUX = 0.1359E-02 NM

STATION 4

RADIUS (M)

0.00000	0.00471	0.00942	0.01413	0.01884
0.02355	0.02826	0.03297	0.03768	0.04239
0.04710	0.05181	0.05652	0.06123	0.06594
0.07065	0.07536			

YAW (RADIANS)

0.00000	0.10473	0.17456	0.28976	0.31944
0.31944	0.32467	0.33602	0.29063	0.32642
0.34387	0.35784	0.37529	0.38402	0.38402
0.39450	0.00000			

AXIAL VELOCITY (M/S)

2.23244	2.30646	2.23093	2.36090	2.47750
2.45948	2.50876	2.61931	2.48189	2.46275
2.31938	2.22153	2.05639	1.90997	1.73542
1.25011	0.00000			

TANGENTIAL VELOCITY (M/S)

0.00000	0.24245	0.39342	0.70391	0.81947
0.81351	0.84441	0.91483	0.74234	0.83371
0.83057	0.83071	0.81015	0.77179	0.70126
0.52045	0.00000			

MEAN VELOCITY = 1.986590 M/S
MASS FLUX = 0.042283 KG/S
K. E. FACTOR = 1.226048
AXIAL KINETIC ENERGY = 0.102297 NM/S
ANGULAR MOMENTUM FLUX = 0.1474E-02 NM

STATION 5

RADIUS (M)

0.00000	0.00542	0.01084	0.01626	0.02168
0.02710	0.03252	0.03794	0.04336	0.04878
0.05420	0.05962	0.06504	0.07046	0.07588
0.08130	0.08672			

YAW (RADIANS)

0.00000	0.02182	0.04189	0.06459	0.08204
0.10997	0.13615	0.16059	0.16059	0.17019
0.18677	0.18677	0.20423	0.20772	0.20772
0.16513	0.00000			

AXIAL VELOCITY (M/S)

1.94924	1.94877	1.94753	1.95776	2.00476
2.04756	1.99291	1.97350	1.94898	1.88328
1.85211	1.75977	1.69888	1.56741	1.47421
1.19934	0.00000			

TANGENTIAL VELOCITY (M/S)

0.00000	0.04253	0.08164	0.12662	0.16484
0.22608	0.27303	0.31968	0.31571	0.32365
0.35001	0.33256	0.35187	0.33035	0.31071
0.19987	0.00000			

MEAN VELOCITY = 1.627806 M/S
MASS FLUX = 0.045880 KG/S
K. E. FACTOR = 1.170075
AXIAL KINETIC ENERGY = 0.071123 NM/S
ANGULAR MOMENTUM FLUX = 0.7347E-03 NM

TABLE 9/3

20 DEGREE DIFFUSER FLOW PROPERTIES

AXIAL FLOW - VORTEX GENERATOR BLADE ANGLE = 0

STATION 1

RADIUS (M)

0.00000	0.00500	0.01000	0.01500	0.02000
0.02500	0.03000	0.03500	0.04000	0.04500

YAW (RADIANS)

0.00000	0.00000	0.00000	0.00000	0.00000
0.00000	0.00000	0.00000	0.00000	0.00000

AXIAL VELOCITY (M/S)

5.89812	5.93565	5.95225	5.92317	5.85193
5.80961	5.66774	5.45479	5.06061	0.00000

TANGENTIAL VELOCITY (M/S)

0.00000	0.00000	0.00000	0.00000	0.00000
0.00000	0.00000	0.00000	0.00000	0.00000

MEAN VELOCITY = 5.141042 M/S
MASS FLUX = 0.039017 KG/S
K. E. FACTOR = 1.177234
AXIAL KINETIC ENERGY = 0.607003 NM/S
ANGULAR MOMENTUM FLUX = 0.0000E 00 NM

STATION 2

RADIUS (M)

0.00000	0.00480	0.00960	0.01440	0.01920
0.02400	0.02880	0.03360	0.03840	0.04320
0.04800				

YAW (RADIANS)

0.00000	0.00000	0.00000	0.00000	0.00000
0.00000	0.00000	0.00000	0.00000	0.00000
0.00000				

AXIAL VELOCITY (M/S)

5.23318	5.28478	5.27544	5.29411	5.21902
5.15241	5.09946	4.90212	4.57945	3.95502
0.00000				

TANGENTIAL VELOCITY (M/S)

0.00000	0.00000	0.00000	0.00000	0.00000
0.00000	0.00000	0.00000	0.00000	0.00000
0.00000				

MEAN VELOCITY = 4.434565 M/S
MASS FLUX = 0.038292 KG/S
K. E. FACTOR = 1.184677
AXIAL KINETIC ENERGY = 0.446052 NM/S
ANGULAR MOMENTUM FLUX = 0.0000E 00 NM

STATION 3

RADIUS (M)

0.00000	0.00410	0.00820	0.01230	0.01640
0.02050	0.02460	0.02870	0.03280	0.03690
0.04100	0.04510	0.04920	0.05330	0.05740
0.06150	0.06560			

YAW (RADIANS)

0.00000	0.00000	0.00000	0.00000	0.00000
0.00000	0.00000	0.00000	0.00000	0.00000
0.00000	0.00000	0.00000	0.00000	0.00000
0.00000	0.00000			

AXIAL VELOCITY (M/S)

4.44827	4.45381	4.43716	4.39807	4.37557
4.29591	4.22059	4.16172	3.94878	3.62293
3.24957	2.72965	1.89793	1.25659	0.72527
0.29968	0.00000			

TANGENTIAL VELOCITY (M/S)

0.00000	-0.00000	0.00000	0.00000	0.00000
0.00000	0.00000	0.00000	0.00000	0.00000
0.00000	0.00000	0.00000	0.00000	0.00000
0.00000	0.00000			

MEAN VELOCITY = 2.352406 M/S
MASS FLUX = 0.037940 KG/S
K. E. FACTOR = 2.288683
AXIAL KINETIC ENERGY = 0.240259 NM/S
ANGULAR MOMENTUM FLUX = 0.0000E 00 NM

STATION 4

RADIUS (M)

0.00000	0.00415	0.00830	0.01245	0.01660
0.02075	0.02490	0.02905	0.03320	0.03735
0.04150	0.04565	0.04980	0.05395	0.05810
0.06225	0.06640	0.07055	0.07470	0.07885
0.08300				

YAW (RADIANS)

0.00000	0.00000	0.00000	0.00000	0.00000
0.00000	0.00000	0.00000	0.00000	0.00000
0.00000	0.00000	0.00000	0.00000	0.00000
0.00000	0.00000	0.00000	0.00000	0.00000
0.00000				

AXIAL VELOCITY (M/S)

4.52526	4.46488	4.51434	4.47592	4.45381
4.41487	4.33592	4.30165	4.16764	4.07182
3.92371	3.78284	3.56111	3.48407	3.24197
3.02138	2.80982	2.62835	2.54246	1.60000
0.00000				

TANGENTIAL VELOCITY (M/S)

0.00000	0.00000	0.00000	0.00000	0.00000
0.00000	0.00000	0.00000	0.00000	0.00000
0.00000	0.00000	0.00000	0.00000	0.00000
0.00000	0.00000	0.00000	0.00000	0.00000
0.00000				

MEAN VELOCITY = 3.107135 M/S
MASS FLUX = 0.080222 KG/S
K. E. FACTOR = 1.294249
AXIAL KINETIC ENERGY = 0.501192 NM/S
ANGULAR MOMENTUM FLUX = 0.0000E 00 NM

TABLE 9/4

20 DEGREE DIFFUSER FLOW PROPERTIES

OPTIMUM RANKINE VORTEX SWIRL

STATION 1

RADIUS (M)

0.00000	0.00500	0.01000	0.01500	0.02000
0.02500	0.03000	0.03500	0.04000	0.04500

YAW (RADIANS)

0.00000	0.75233	0.75932	0.62840	0.55858
0.50097	0.47479	0.44861	0.46257	0.00000

AXIAL VELOCITY (M/S)

3.92999	3.15732	3.89023	5.02200	5.41390
5.66375	5.66775	5.66834	5.47669	0.00000

TANGENTIAL VELOCITY (M/S)

0.00000	2.95514	3.69242	3.64932	3.38352
3.10129	2.91327	2.72839	2.73099	0.00000

MEAN VELOCITY	=	4.975579 M/S
MASS FLUX	=	0.037761 KG/S
K. E. FACTOR	=	1.198890
AXIAL KINETIC ENERGY	=	0.560383 NM/S
ANGULAR MOMENTUM FLUX	=	0.3239E-02 NM

STATION 2

RADIUS (M)

0.00000	0.00480	0.00960	0.01440	0.01920
0.02400	0.02880	0.03360	0.03840	0.04320
0.04800				

YAW (RADIANS)

0.00000	0.52192	0.47305	0.38402	0.33166
0.25660	0.21296	0.18765	0.16932	0.18677
0.00000				

AXIAL VELOCITY (M/S)

2.30851	2.35051	2.73285	3.74706	4.77560
5.36298	5.48411	5.53823	5.50456	5.19287
0.00000				

TANGENTIAL VELOCITY (M/S)

0.00000	1.35182	1.39868	1.51413	1.64460
1.40714	1.18587	1.05160	0.94104	0.98133
0.00000				

MEAN VELOCITY	=	4.714249 M/S
MASS FLUX	=	0.040708 KG/S
K. E. FACTOR	=	1.219679
AXIAL KINETIC ENERGY	=	0.551715 NM/S
ANGULAR MOMENTUM FLUX	=	0.1432E-02 NM

STATION 3

RADIUS (M)

0.00000	0.00410	0.00820	0.01230	0.01640
0.02050	0.02460	0.02870	0.03280	0.03690
0.04100	0.04500	0.04920	0.05330	0.05740
0.06160	0.06560			

YAW (RADIANS)

0.00000	0.06982	0.86929	0.86929	0.70259
0.55160	0.49923	0.46432	0.41021	0.38839
0.36308	0.34213	0.33602	0.33602	0.35260
0.40445	0.00000			

AXIAL VELOCITY (M/S)

0.31415	0.31338	0.43008	0.65696	0.86443
1.26913	1.60822	2.05452	2.50320	3.05634
3.30947	3.57586	3.58971	3.43315	3.02101
2.22021	0.00000			

TANGENTIAL VELOCITY (M/S)

0.00000	0.02192	0.50905	0.77758	0.73193
0.78090	0.87696	1.02898	1.08858	1.25056
1.25733	1.27349	1.25376	1.19908	1.11167
0.95035	0.00000			

MEAN VELOCITY = 2.542745 M/S
MASS FLUX = 0.041010 KG/S
K. E. FACTOR = 1.422382
AXIAL KINETIC ENERGY = 0.188574 NM/S
ANGULAR MOMENTUM FLUX = 0.2166E-02 NM

STATION 4

RADIUS (M)

0.00000	0.00415	0.00830	0.01245	0.01660
0.02075	0.02490	0.02905	0.03320	0.03735
0.04150	0.04565	0.04980	0.05395	0.05810
0.06225	0.06640	0.07055	0.07470	0.07885
0.08300				

YAW (RADIANS)

0.00000	0.00000	0.26358	0.51930	0.51930
0.55421	0.59000	0.55160	0.55160	0.48876
0.45035	0.38053	0.38053	0.36133	0.36133
0.36133	0.35435	0.36308	0.40497	0.52559
0.00000				

AXIAL VELOCITY (M/S)

0.49671	0.54412	0.64339	0.63961	0.94477
1.03457	1.10749	1.32434	1.50166	1.74322
1.94924	2.08298	2.24988	2.26674	2.26674
2.10886	1.97644	1.74973	1.48637	0.99994
0.00000				

TANGENTIAL VELOCITY (M/S)

0.00000	0.00000	0.17362	0.36563	0.54007
0.64031	0.74152	0.81487	0.92397	0.92703
0.94244	0.83325	0.90002	0.85665	0.85665
0.79698	0.73121	0.66475	0.63715	0.57997
0.00000				

MEAN VELOCITY = 1.639769 M/S
MASS FLUX = 0.042337 KG/S
K. E. FACTOR = 1.323086
AXIAL KINETIC ENERGY = 0.075308 NM/S
ANGULAR MOMENTUM FLUX = 0.1793E-02 NM

TABLE 9/5

30 DEGREE DIFFUSER FLOW PROPERTIES

AXIAL FLOW - VORTEX GENERATOR BLADE ANGLE = 0

STATION 1

RADIUS (M)

0.00000	0.00500	0.01000	0.01500	0.02000
0.02500	0.03000	0.03500	0.04000	0.04500

YAW (RADIANS)

0.00000	0.00000	0.00000	0.00000	0.00000
0.00000	0.00000	0.00000	0.00000	0.00000

AXIAL VELOCITY (M/S)

5.78407	5.80111	5.83504	5.82657	5.79260
5.75414	5.61965	5.47735	5.03127	0.00000

TANGENTIAL VELOCITY (M/S)

0.00000	0.00000	0.00000	0.00000	0.00000
0.00000	0.00000	0.00000	0.00000	0.00000

MEAN VELOCITY = 5.099356 M/S
MASS FLUX = 0.038701 KG/S
K. E. FACTOR = 1.175747
AXIAL KINETIC ENERGY = 0.591609 NM/S
ANGULAR MOMENTUM FLUX = 0.0000E 00 NM

STATION 2

RADIUS (M)

0.00000	0.00386	0.00772	0.01158	0.01544
0.01930	0.02316	0.02702	0.03088	0.03474
0.03860	0.04246	0.04632		

YAW (RADIANS)

0.00000	0.00000	0.00000	0.00000	0.00000
0.00000	0.00000	0.00000	0.00000	0.00000
0.00000	0.00000	0.00000		

AXIAL VELOCITY (M/S)

5.36356	5.40024	5.39109	5.32200	5.36816
5.32200	5.28011	5.28011	5.13802	4.97704
4.56866	4.34729	0.00000		

TANGENTIAL VELOCITY (M/S)

0.00000	0.00000	0.00000	0.00000	0.00000
0.00000	0.00000	0.00000	0.00000	0.00000
0.00000	0.00000	0.00000		

MEAN VELOCITY = 4.682815 M/S
MASS FLUX = 0.037655 KG/S
K. E. FACTOR = 1.140525
AXIAL KINETIC ENERGY = 0.470883 NM/S
ANGULAR MOMENTUM FLUX = 0.0000E 00 NM

STATION 3

RADIUS (M)

0.00000	0.00413	0.00826	0.01239	0.01652
0.02065	0.02478	0.02891	0.03304	0.03717
0.04130	0.04543	0.04956	0.05369	0.05782
0.06195				

YAW (RADIANS)

0.00000	0.00000	0.00000	0.00000	0.00000
0.00000	0.00000	0.00000	0.00000	0.00000
0.00000	0.00000	0.00000	0.00000	0.00000
0.00000				

AXIAL VELOCITY (M/S)

4.93222	4.81067	4.94720	4.85152	4.84134
4.81067	4.69123	4.60095	4.51434	4.37557
3.87944	3.04578	1.98685	1.49013	0.42030
0.00000				

TANGENTIAL VELOCITY (M/S)

0.00000	0.00000	0.00000	0.00000	0.00000
0.00000	0.00000	0.00000	0.00000	0.00000
0.00000	0.00000	0.00000	0.00000	0.00000
0.00000				

MEAN VELOCITY = 2.928245 M/S
MASS FLUX = 0.042118 KG/S
K. E. FACTOR = 1.957750
AXIAL KINETIC ENERGY = 0.353518 NM/S
ANGULAR MOMENTUM FLUX = 0.0000E 00 NM

STATION 4

RADIUS (M)

0.00000	0.00468	0.00936	0.01404	0.01872
0.02340	0.02808	0.03276	0.03744	0.04212
0.04680	0.05148	0.05616	0.06084	0.06552
0.07020	0.07488	0.07956		

YAW (RADIANS)

0.00000	0.00000	0.00000	0.00000	0.00000
0.00000	0.00000	0.00000	0.00000	0.00000
0.00000	0.00000	0.00000	0.00000	0.00000
0.00000	0.00000	0.00000		

AXIAL VELOCITY (M/S)

4.54158	4.50339	4.64365	4.62235	4.53070
4.42603	4.44272	4.23226	4.07788	3.73030
3.34682	2.81859	2.24346	1.63236	1.06533
0.76950	0.26095	0.00000		

TANGENTIAL VELOCITY (M/S)

0.00000	0.00000	0.00000	0.00000	0.00000
0.00000	0.00000	0.00000	0.00000	0.00000
0.00000	0.00000	0.00000	0.00000	0.00000
0.00000	0.00000	0.00000		

MEAN VELOCITY = 2.309622 M/S
MASS FLUX = 0.054791 KG/S
K. E. FACTOR = 2.416435
AXIAL KINETIC ENERGY = 0.353132 NM/S
ANGULAR MOMENTUM FLUX = 0.0000E 00 NM

TABLE 9/6

30 DEGREE DIFFUSER FLOW PROPERTIES

OPTIMUM RANKINE VORTEX SWIRL

STATION 1

RADIUS (M)

0.00000	0.00500	0.01000	0.01500	0.02000
0.02500	0.03000	0.03500	0.04000	0.04500

YAW (RADIANS)

0.00000	0.58476	0.69473	0.61444	0.52890
0.43988	0.41457	0.37268	0.37268	0.00000

AXIAL VELOCITY (M/S)

1.67709	1.80537	3.14664	4.65593	5.28711
5.63846	5.70743	5.72223	5.50493	0.00000

TANGENTIAL VELOCITY (M/S)

0.00000	1.19514	2.62216	3.28495	3.09002
2.65365	2.51170	2.23708	2.15212	0.00000

MEAN VELOCITY = 4.879103 M/S
MASS FLUX = 0.037029 KG/S
K. E. FACTOR = 1.242649
AXIAL KINETIC ENERGY = 0.547701 NM/S
ANGULAR MOMENTUM FLUX = 0.2674E-02 NM

STATION 2

RADIUS (M)

0.00000	0.00386	0.00772	0.01158	0.01544
0.01930	0.02316	0.02702	0.03088	0.03474
0.03860	0.04246	0.04632		

YAW (RADIANS)

0.00000	0.89372	0.71393	0.56207	0.48003
0.44337	0.38926	0.33689	0.30198	0.26358
0.23216	0.24612	0.00000		

AXIAL VELOCITY (M/S)

0.31415	0.78727	1.33258	2.25554	3.40698
4.20425	4.93672	5.37373	5.56696	5.80640
5.78449	5.71632	0.00000		

TANGENTIAL VELOCITY (M/S)

0.00000	0.97940	1.15453	1.42062	1.77383
1.99662	2.02499	1.88212	1.73415	1.56690
1.36758	1.43603	0.00000		

MEAN VELOCITY = 4.733660 M/S
MASS FLUX = 0.038064 KG/S
K. E. FACTOR = 1.292343
AXIAL KINETIC ENERGY = 0.551132 NM/S
ANGULAR MOMENTUM FLUX = 0.1955E-02 NM

STATION 3

RADIUS (M)

0.00000	0.00413	0.00826	0.01239	0.01652
0.02065	0.02478	0.02891	0.03304	0.03717
0.04130	0.04543	0.04956	0.05369	0.05782
0.06195				

YAW (RADIANS)

0.00000	0.00873	0.00873	0.78899	0.63713
0.39711	0.34562	0.29500	0.28802	0.25747
0.25747	0.23565	0.24961	0.27580	0.29308
0.00000				

AXIAL VELOCITY (M/S)

0.58772	0.54410	0.38474	0.51908	0.64379
1.21191	1.78570	2.51481	3.31329	3.83670
4.23134	4.39489	4.18497	3.67734	2.75020
0.00000				

TANGENTIAL VELOCITY (M/S)

0.00000	0.00475	0.00336	0.52282	0.47646
0.50827	0.64298	0.76416	0.98157	1.01026
1.11417	1.05526	1.06688	1.04072	0.82992
0.00000				

MEAN VELOCITY = 2.964740 M/S
MASS FLUX = 0.042643 KG/S
K. E. FACTOR = 1.527577
AXIAL KINETIC ENERGY = 0.286283 NM/S
ANGULAR MOMENTUM FLUX = 0.1847E-02 NM

STATION 4

RADIUS (M)

0.00000	0.00468	0.00936	0.01404	0.01872
0.02340	0.02808	0.03276	0.03744	0.04212
0.04680	0.05148	0.05616	0.06084	0.06552
0.07020	0.07488	0.07956		

YAW (RADIANS)

0.00000	0.00000	0.00000	0.01571	0.04364
0.39644	0.96006	0.74710	0.56381	0.52367
0.41719	0.39799	0.35784	0.33340	0.33340
0.34387	0.39327	0.00000		

AXIAL VELOCITY (M/S)

0.44427	0.49671	0.31415	0.22211	0.54360
0.15414	0.66193	1.01777	1.47838	1.84513
2.22467	2.54119	2.75244	2.82397	2.57934
2.23291	1.35013	0.00000		

TANGENTIAL VELOCITY (M/S)

0.00000	0.00000	0.00000	0.00349	0.02374
0.87507	0.94559	0.94265	0.93474	1.06545
0.98598	1.06837	1.02924	0.97802	0.89330
0.79961	0.56015	0.00000		

MEAN VELOCITY = 1.782289 M/S
MASS FLUX = 0.042281 KG/S
K. E. FACTOR = 1.668717
AXIAL KINETIC ENERGY = 0.112061 NM/S
ANGULAR MOMENTUM FLUX = 0.2148E-02 NM

TABLE 10/1

CALCULATED RESULTS FROM ENGINEERING SCIENCES
DATA UNIT (76027)

20	L/R	AR	C_p
10	11.12	4.0	0.86
20	5.45	4.0	0.64
30	3.73	4.0	0.46

TABLE 10/2

CALCULATED RESULTS FROM COCKRELL AND MARKLAND'S MODEL
10 DEGREE DIFFUSER

	VORTEX GENERATOR BLADE ANGLE = 0 DEG		VORTEX GENERATOR BLADE ANGLE = 6 DEG	
STATION	λ	η	λ	η
D2	0.412	0.588	0.334	0.666
D3	0.311	0.689	0.135	0.865
D4	0.271	0.729	0.076	0.924
E1	0.195	0.805	0.058	0.942
E2	0.136	0.864	0.044	0.956

TABLE 10/3

CALCULATED RESULTS FROM COCKRELL AND MARKLAND'S MODEL
20 DEGREE DIFFUSER

	VORTEX GENERATOR BLADE ANGLE = 0 DEG		VORTEX GENERATOR BLADE ANGLE = 10 DEG	
STATION	λ	η	λ	η
D2	0.676	0.324	0.489	0.511
D3	0.660	0.340	0.323	0.677
E1	0.564	0.436	0.249	0.751
E2	0.399	0.601	0.249	0.751

TABLE 10/4

CALCULATED RESULTS FROM COCKRELL AND MARKLAND'S MODEL
30 DEGREE DIFFUSER

	VORTEX GENERATOR BLADE ANGLE = 0 DEG		VORTEX GENERATOR BLADE ANGLE = 10 DEG	
STATION	λ	η	λ	η
D2	0.906	0.094	0.906	0.094
D3	0.881	0.119	0.777	0.223
E1	0.759	0.241	0.577	0.423
E2	0.532	0.468	0.490	0.510

TABLE 10/5

10 DEGREE DIFFUSER
CALCULATED RESULTS FROM COCKRELL AND MARKLAND'S MODEL

	AXIAL FLOW		SOLID - BODY SWIRL 2		SOLID - BODY SWIRL 3	
STATION	λ	η	λ	η	λ	η
D2	0.697	0.303	0.636	0.364	0.613	0.387
D3	0.556	0.444	0.492	0.508	0.461	0.539
D4	0.473	0.527	0.424	0.576	0.393	0.607
E1	0.439	0.561	0.386	0.614	0.363	0.637
E2	0.419	0.581	0.371	0.629	0.341	0.659

TABLE 10/6

20 DEGREE DIFFUSER
CALCULATED RESULTS FROM COCKRELL AND MARKLAND'S MODEL

	AXIAL FLOW		SOLID - BODY SWIRL 2		SOLID - BODY SWIRL 3	
STATION	λ	η	λ	η	λ	η
D2	0.849	0.151	0.734	0.266	0.674	0.326
D3	0.693	0.307	0.617	0.383	0.556	0.444
E1	0.583	0.417	0.522	0.478	0.469	0.531
E2	0.473	0.527	0.424	0.576	0.390	0.610

TABLE 10/7

30 DEGREE DIFFUSER
CALCULATED RESULTS FROM COCKRELL AND MARKLAND'S MODEL

	AXIAL FLOW		SOLID - BODY SWIRL 2		SOLID - BODY SWIRL 3	
STATION	λ	η	λ	η	λ	η
D2	0.988	0.012	0.909	0.091	0.886	0.114
D3	0.878	0.122	0.799	0.201	0.765	0.235
E1	0.727	0.273	0.666	0.334	0.621	0.379
E2	0.644	0.356	0.553	0.447	0.507	0.493

TABLE 10/8

CALCULATED RESULTS FROM SOVRAN AND KLOMP'S MODEL

20	FLOW CONDITION	C_p	ε_o
10	AXIAL	0.720	1.011
	OPT. RANKINE VORTEX SWIEL	1.262	1.412
20	AXIAL	0.350	0.528
	OPT. RANKINE VORTEX SWIRL	1.137	1.049
30	AXIAL	0.165	0.656
	OPT. RANKINE VORTEX SWIRL	0.678	0.594

TABLE 10/9

CALCULATED RESULTS FROM SOVRAN AND KLOMP'S MODEL

20	FLOW CONDITION	C_p	ε_o
10	AXIAL	0.510	0.458
	SWIRL 2	0.544	0.533
	SWIRL 3	0.851	0.741
20	AXIAL	0.334	0.367
	SWIRL 2	0.622	0.625
	SWIRL 3	0.636	0.673
30	AXIAL	0.260	0.301
	SWIRL 2	0.328	0.350
	SWIRL 3	0.394	0.498

TABLE 10/10

CALCULATED RESULTS FROM TYLER AND WILLIAMSON'S MODEL

2ϕ	FLOW CONDITION	η_e
10	AXIAL	0.669
	OPT. RANKINE VORTEX SWIRL	0.962
20	AXIAL	0.460
	OPT. RANKINE VORTEX SWIRL	0.708
30	AXIAL	0.181
	OPT. RANKINE VORTEX SWIRL	0.271

TABLE 10/11

CALCULATED RESULTS FROM TYLER AND WILLIAMSON'S MODEL

2ϕ	FLOW CONDITION	η_e
10	AXIAL	0.655
	SWIRL 2	0.526
	SWIRL 3	0.553
20	AXIAL	0.487
	SWIRL 2	0.509
	SWIRL 3	0.527
30	AXIAL	0.359
	SWIRL 2	0.391
	SWIRL 3	0.405

APPENDIX A

```
      MASTER PROP
C     PROGRAM TO CALCULATE FLOW PROPERTIES OF PIPE + DIFFUSER
C     GILL'S AND MILLER'S APPROACH IS USED TO CALCULATE THE
C     INTEGRALES (BASED ON THIRD ORDER FINITE DIFFERENCE FORMULE)
C     THE SUBROUTINE D01GAF (STANDARD NAG SUBROUTINE) INTEGRATES
C     A FUNCTION (Y) SPECIFIED NUMERICALLY AT N POINTS (X),
C     WHERE N IS AT LEAST 4, OVER THE RANGE X(1) TO X(N). THE
C     POINTS NEED NOT BE EQUALLY SPACED, BUT SHOULD BE DISTINCT
C     AND ASCENDING OR DESCENDING ORDER. AN ERROR ESTIMATE IS
C     RETURNED.
C
C           U     =  AXIAL  VELOCITY
C           UM    =  MEAN  AXIAL  VELOCITY
C           YAW   =  SWIRL  ANGLE
C           P02   =  P0  -  P2
C           P04   =  P0  -  P4
C           RAD   =  RADIUS
C           RR    =  WALL  RADIUS
C           TA    =  ATMOSPHERIC  TEMPERATURE
C           PA    =  ATMOSPHERIC  PRESSURE
C           SF    =  SCALE  FACTOR
C           MASF  =  MASS  FLUX
C           EKF   =  KINETIC  ENERGY  FACTOR
C           AKE   =  AXIAL  KINETIC  ENERGY
C           AMM   =  ANGULAR  MOMENTUM
C           DENS  =  AIR  DENSITY
C
      DIMENSION U(5,21), V(5,21), YAW(5,21), P02(5,21),
     1P04(5,21), RAD(5,21), TA(5), PA(5), SF(5), RR(5), UM(5),
     2MASF(5), EKF(5), AKE(5), AMM(5), X(21), Y(21), W(21),
     3Z(21), ERA(5), ERB(5), ERC(5), DENS(5)
      INTEGER IFAIL, N
      REAL MASF
C
C     READ EXPERIMENTAL DATA
C
      NI=5
      NJ=21
      DO 1 I=1,NI
      READ(1,10)(YAW(I,J),J=1,NJ)
 1    CONTINUE
      DO 2 I=1,NI
      READ(1,10)(P02(I,J),J=1,NJ)
 2    CONTINUE
      DO 3 I=1,NI
      READ(1,10)(P04(I,J),J=1,NJ)
 3    CONTINUE
      DO 4 I=1,NI
      READ(1,9)(RAD(I,J),J=1,NJ)
 4    CONTINUE
      READ(1,11)(TA(I), I=1,NI)
```

```
      READ(1,11)(PA(I), I=1,NI)
      READ(1,11)(SF(I), I=1,NI)
      READ(1,11)(RR(I), I=1,NI)
      READ(1,12) R
 9    FORMAT(9F0.0)
 10   FORMAT(14F0.0)
 11   FORMAT (5F0.0)
 12   FORMAT(1F0.0)
 13   FORMAT(4I0)
C
C     WRITE EXPERIMENTAL DATA FOR CHECK
C
      DO 5 I=1,NI
      WRITE(2,110)(YAW(I,J),J=1,NJ)
 5    CONTINUE
      DO 6 I=1,NI
      WRITE(2,110)(PO2(I,J),J=1,NJ)
 6    CONTINUE
      DO 7 I=1,NI
      WRITE(2,110)(PO4(I,J),J=1,NJ)
 7    CONTINUE
      DO 8 I=1,NI
      WRITE(2,109)(RAD(I,J),J=1,NJ)
 8    CONTINUE
      WRITE(2,111)(TA(I),I=1,NI)
      WRITE(2,111)(PA(I),I=1,NI)
      WRITE(2,111)(SF(I),I=1,NI)
      WRITE(2,111)(RR(I),I=1,NI)
      WRITE(2,112) R
 109  FORMAT(5F12.6)
 110  FORMAT(5F12.6)
 111  FORMAT(4F14.3)
 112  FORMAT(F7.2)
C
C     CALCULATE DENSITY, AXL. VELOCITY,
C     TAN. VELOCITY.  NOTE  TAKES ACCOUNT
C     OF VARIATION OF MEASURING POINTS AT
C     EACH STATION, OTHERWISE, GILL'S AND
C     MILLER'S INTEGRATION METHOD WILL FAIL
C
      NJ=10
      DO 60 I=1,NI
      DENS(I) = PA(I)/(R*TA(I))
      DO 50 J=1,NJ
      C=((PO2(I,J) + PO4(I,J)) *9.81)/(DENS(I) * SF(I))
      YAW(I,J)=YAW(I,J)*(3.142/180.0)
      D=1.0+(1.0-(COS(2.0*YAW(I,J))))/(1.0+(COS(2.0*YAW(I,J))))
      U(I,J) = (C/D)**0.5
      V(I,J) = U(I,J)*(SIN(YAW(I,J))/COS(YAW(I,J)))
      X(J) =RAD(I,J)
      Y(J) = (2.0*U(I,J)*RAD(I,J))/(RR(I)**2.0)
 50   CONTINUE
      IFAIL = 0
      N=NJ
C
C     CALCULATION OF MEAN VELOCITY
```

```
C
      CALL D01GAF(X,Y,N,ANS,ER,IFAIL)
      UM(I) = ANS
      ERA(I) = ER
      NJ1=3
      IF(I.EQ.2)NJ1=NJ1-2
      IF(I.EQ.4)NJ1=0
      NJ=NJ+NJ1
 60   CONTINUE
C
C     CALCULATION OF MASS FLUX, K. E. FACTOR
C     MOMENTUM FACTOR, AXIAL KINETIC ENERGY
C     AND ANGULAR MOMENTUM.
C
      NJ=10
      DO 70 I=1,NI
      MASF(I)=DENS(I)*3.142*(RR(I)**2.0)*UM(I)
      DO 80 J=1,NJ
      W(J)=2.0*(U(I,J)**3.0)*RAD(I,J)/(UM(I)**3.0*RR(I)**2.0)
      X(J) = RAD(I,J)
 80   CONTINUE
      IFAIL = 0
      N=NJ
      CALL D01GAF(X,W,N,ANS,ER,IFAIL)
      EKF(I)=ANS
      ERB(I) = ER
      NJ1=3
      IF(I.EQ.2)NJ1=NJ1-2
      IF(I.EQ.4)NJ1=0
      NJ=NJ+NJ1
 70   CONTINUE
      NJ=10
      DO 75 I=1,NI
      AKE(I)=(MASF(I)*(UM(I)**2.0)*EKF(I))*0.5
      DO 85 J=1,NJ
      Z(J)=2.0*3.142*DENS(I)*U(I,J)*V(I,J)*(RAD(I,J)**2.0)
      X(J)=RAD(I,J)
 85   CONTINUE
      IFAIL = 0
      N=NJ
      CALL D01GAF(X,Z,N,ANS,ER,IFAIL)
      AMM(I)=ANS
      ERC(I) = ER
      NJ1=3
      IF(I.EQ.2)NJ1=NJ1-2
      IF(I.EQ.4)NJ1=0
      NJ=NJ+NJ1
 75   CONTINUE
      NJ=21
C
C     WRITE DENSITY, (U, Y, FOR CHECK NOT
C     NECESSARY ) AND ERROR OF INTEGRATION
C
      WRITE(2,14)(DENS(I),I=1,NI)
 14   FORMAT(4F7.4)
      DO 21 I=1,NI
      WRITE(2,22)(U(I,J), J=1,NJ)
 22   FORMAT(5F12.6)
```

```
 21   CONTINUE
      DO 23 I=1,NI
      WRITE(2,24)(V(I,J), J=1,NJ)
 24   FORMAT(5F12.6)
 23   CONTINUE
      WRITE(2,17)(ERA(I),I=1,NI)
      WRITE(2,18)(ERB(I),I=1,NI)
      WRITE(2,19)(ERC(I),I=1,NI)
 17   FORMAT(' ERA '/(4(5X,E12.4)))
 18   FORMAT(' ERB '/(4(5X,E12.4)))
 19   FORMAT(' ERC '/(4(5X,E12.4)))
C
C     WRITE THE FLOW PROPERTIES
C
      WRITE(2,100)
 100  FORMAT(10X,' 10 DEGREE DIFFUSER FLOW PROPERTIES ',///)
      NJ=10
      DO 40 I=1,NI
      WRITE(2,61) I
      WRITE(2,62)(RAD(I,J),J=1,NJ)
      WRITE(2,63)(YAW(I,J),J=1,NJ)
      WRITE(2,64)(U(I,J),J=1,NJ)
      WRITE(2,65)(V(I,J),J=1,NJ)
 61   FORMAT(10X,' STATION ',I2//)
 62   FORMAT(10X,' RADIUS  (M) '/(10X,5F12.5))
 63   FORMAT(10X,' YAW  (RADIANS) '/(10X,5F12.5))
 64   FORMAT(10X,' AXIAL VELOCITY  (M/S) '/(10X,5F12.5))
 65   FORMAT(10X,' TANGENTIAL VELOCITY  (M/S)'/(10X,5F
     112.5))
      WRITE(2,106) UM(I)
      WRITE(2,107) MASF(I)
      WRITE(2,108) EKF(I)
      WRITE(2,114) AKE(I)
      WRITE(2,115) AMM(I)
 115  FORMAT(10X,' ANGULAR MOMENTUM FLUX = ',E12.4,' NM' ///)
 114  FORMAT(10X,' AXIAL KINETIC ENERGY  = ',F12.6,' NM/S')
 108  FORMAT(10X,' K.   E.   FACTOR      = ',F12.6)
 107  FORMAT(10X,' MASS  FLUX            = ',F12.6,' KG/S')
 106  FORMAT(//10X,' MEAN  VELOCITY        = ',F12.6,' M/S')
      NJ1=3
      IF(I.EQ.2)NJ1=NJ1-2
      IF(I.EQ.4)NJ1=0
      NJ=NJ+NJ1
 40   CONTINUE
      STOP
      END
      FINISH
```

APPENDIX B

```
      MASTER KET
C     APPLICATION OF KINETIC ENERGY THEORY TO CONICAL DIFFUSERS.
C     THE THEORY IS AN EXTENSION OF SOVRAN AND KLOMPS APPROACH
C     TO TAKE ACCOUNT OF 2-D FLOW.  THE PROGRAM EVALUATES THE
C     PARAMETERS REQUIRED TO CALCULATE:
C           (1)  MEAN PRESSURE RECOVERY COEFFICIENT
C           (2)  DIFFUSER EFFECTIVENESS
C     GILL'S AND MILLER'S APPROACH IS USED TO CALCULATE THE
C     INTEGRALS  (STANDARD NAG SUBROUTINE D01GAF)
C           U      =  AXIAL  VELOCITY
C           UM     =  MEAN  AXIAL  VELOCITY
C           VM     =  MEAN  TANGENTIAL  VELOCITY
C           YAW    =  SWIRL  ANGLE
C           P02    =  P0  -  P2
C           P04    =  P0  -  P4
C           EPSM   =  MEAN  SWIRL  ANGLE
C           ALFK   =  KINETIC  ENERGY  FLUX  VELOCITY
C                     PROFILE  PARAMETER
C           RAD    =  RADIUS
C           RR     =  WALL  RADIUS
C
      DIMENSION U(4,21), RAD(4,21), YAW(4,21), P02(4,21), P04(4,21),
     1UM(4), RR(4), X(21), Y(21), ERA(4), E(4,21), F(4,21), G(4,21),
     2H(4,21),P(21),PP(4),ERB(4),PPP(4),EPSM(4),
     3A(4),VM(4),YA(4),Q(4,21),R(4,21),S(21),ALFK(4),SS(4),
     4ERC(4),YW(4,21),W(4),Z(4)
C
C     READ EXPERIMENTAL DATA
C
      NI=4
      NJ=21
      DO 1 I=1,NI
      READ (1,10)(YAW(I,J),J=1,NJ)
1     CONTINUE
      DO 2 I=1,NI
      READ (1,10)(P02(I,J),J=1,NJ)
2     CONTINUE
      DO 3 I=1,NI
      READ (1,10)(P04(I,J),J=1,NJ)
3     CONTINUE
      DO 4 I=1,NI
      READ(1,9)(RAD(I,J),J=1,NJ)
4     CONTINUE
      READ (1,11)(RR(I),I=1,NI)
10    FORMAT (14F0.0)
9     FORMAT (9F0.0)
11    FORMAT (4F0.0)
C
C     WRITE EXPERIMENTAL DATA
C
```

```
      DO 5 I=1,NI
      WRITE (2,110)(YAW(I,J),J=1,NJ)
5     CONTINUE
      DO 6 I=1,NI
      WRITE (2,110)(PO2(I,J),J=1,NJ)
6     CONTINUE
      DO 7 I=1,NI
      WRITE (2,110)(PO4(I,J),J=1,NJ)
7     CONTINUE
      DO 8 I=1,NI
      WRITE (2,110)(RAD(I,J),J=1,NJ)
8     CONTINUE
      WRITE (2,111)(RR(I),I=1,NI)
110   FORMAT (5F12.6)
111   FORMAT (4F14.3)
C
C     CALCULATE AXIAL VELOCITY
C
      NJ = 10
      DO 60 I=1,NI
      DO 50 J=1,NJ
      C=((PO2(I,J)+PO4(I,J))*9.81)/(1.1928*166.67)
      YAW(I,J) = YAW(I,J) * (3.142 / 180.0)
      D = 1.0 + (1.0 - (COS(2.0*YAW(I,J))))/(1.0+(COS(2.0*YAW(I,J))))
      U(I,J) = (C/D)**0.5
      X(J) = RAD(I,J)
      Y(J) = (2.0 * U(I,J) * RAD(I,J))/(RR(I)**2.0)
50    CONTINUE
      IFAIL = 0
      N = NJ
      CALL D01GAF (X,Y,N,ANS,ER,IFAIL)
      UM(I) = ANS
      ERA(I) = ER
      NJ1=4
      IF(I.EQ.1)NJ1=NJ1-1
      NJ = NJ + NJ1
60    CONTINUE
C
C     CALCULATION OF MEAN EPSI AND MEAN TANGENTIAL VELOCITY
C
      NJ = 10
      DO 61 I=1,NI
      DO 51 J=1,NJ
      E(I,J) = U(I,J) / UM(I)
      F(I,J) = SIN(YAW(I,J))
      G(I,J) = COS(YAW(I,J))
      WRITE(2,14) E(I,J), F(I,J), G(I,J)
14    FORMAT(10X,F10.6,10X,F10.6,10X,F10.6)
      H(I,J) = F(I,J) / G(I,J)
      P(J)=(E(I,J)**2.0)*H(I,J)*(RAD(I,J)**2.0)
      WRITE(2,15) H(I,J), P(J)
15    FORMAT(10X,F10.6,10X,E12.6)
      X(J) = RAD(I,J)
51    CONTINUE
      IFAIL=0
      N=NJ
```

```
      CALL D01GAF (X,P,N,ANS,ER,IFAIL)
      PP(I) = ANS
      ERB(I) = ER
      WRITE(2,12)PP(I)
      PPP(I) = (PP(I) * 2.0 )/( RR(I)**3.0 )
      WRITE(2,13)PPP(I)
12    FORMAT(10X,' INT.  FOR  EPSI  IS  ',E12.6)
13    FORMAT(10X, ' TAN  EPSI  IS  ',E12.6)
      EPSM(I) = ATAN(PPP(I))
      W(I) = SIN(EPSM(I))
      A(I) = COS(EPSM(I))
      Z(I) = W(I)/A(I)
      VM(I) = UM(I) * Z(I)
      NJ1=4
      IF(I.EQ.1)NJ1=NJ1-1
      NJ = NJ+NJ1
61    CONTINUE
C
C     CALCULATION OF ALFK, THE KINETIC ENERGY FLUX VELOCITY
C     PROLILE PARAMETER
C
      NJ = 10
      DO 70 I=1,NI
      DO 80 J = 1,NJ
      YW(I,J) = 1.0 + (COS(2.0*YAW(I,J)))
      YA(I) = 1.0 + (COS(2.0*EPSM(I)))
      Q(I,J) = YA(I)/YW(I,J)
      R(I,J) = (U(I,J)/UM(I))**3.0
      S(J)=R(I,J)*Q(I,J)*RAD(I,J)
      WRITE(2,16) S(J)
16    FORMAT(20X,E12.6)
      X(J) = RAD(I,J)
80    CONTINUE
      IFAIL = 0
      N = NJ
      CALL D01GAF (X,S,N,ANS,ER,IFAIL)
      SS(I)=ANS
      ERC(I) = ER
      ALFK(I)=(2.0*SS(I))/(RR(I)**2.0)
      WRITE(2,17) SS(I),ALFK(I)
17    FORMAT(10X,' INTIGRAND IS ',E12.6,'ALFK IS ',F12.8)
      NJ1=4
      IF(I.EQ.1)NJ1=NJ1-1
      NJ = NJ + NJ1
70    CONTINUE
C
C     WRITE THE FLOW PROPERTIES
C
      WRITE(2,100)
100   FORMAT(10X,' 20 DEGREE DIFFUSER FLOW PROPERTIES ',//)
      NJ = 10
      DO 40 I=1,NI
      EPSM(I) = EPSM(I) * (180.0/3.142)
      WRITE(2,91) I
      WRITE (2,62) (RAD(I,J),J=1,NJ)
      WRITE (2,63) (YAW(I,J),J=1,NJ)
```

```
      WRITE (2,64) (U(I,J),J=1,NJ)
91    FORMAT(10X,' STATION ',I2//)
62    FORMAT(10X,' RADIUS  (M) '/(10X,5F12.5))
63    FORMAT(10X,' YAW  (RADIANS) '/(10X,5F12.5))
64    FORMAT(10X,' AXIAL VELOCITY  (M/S) '/(10X,5F12.5))
      WRITE (2,106) UM(I)
      WRITE (2,107) EPSM(I)
      WRITE (2,108) VM(I)
      WRITE (2,105) ALFK(I)
106   FORMAT(10X,' MEAN  AXIAL  VELOCITY        =',F12.6,'M/S')
107   FORMAT(10X,' MEAN  SWIRL  ANGLE     =',F8.4,'DEG')
108   FORMAT(10X,' MEAN  TANGENTIAL  VELOCITY  =',F12.6,'M/S')
105   FORMAT(10X,' K. E. V. P. PARAMETER        =',F12.8)
      NJ1=4
      IF(I.EQ.1)NJ1=NJ1-1
      NJ=NJ+NJ1
40    CONTINUE
      STOP
      END
      FINISH
```

APPENDIX C

LEAST SQUARE FIT APPLIED TO SURFACE SMOOTHING

It is assumed that the variation of the function with respect to yaw (α) and pitch (β) can be represented by polynomials.

Consider a general β, suppose

$$v_{ij} = a_1 + a_2\alpha_i + a_3\alpha_i^2 \text{ --------} + a_n\alpha_i^{n-1} \qquad (C.1)$$

where i and j are the indices associated with yaw and pitch respectively and n is the degree of the polynomial representing the variation of the function with respect to the yaw angle. N and M are the limiting values of i and j respectively.

Using the method of least square, the coefficients of equation (C.1) are given by

$$\begin{bmatrix} a \\ a \\ \vdots \\ a_n \end{bmatrix} = (\underline{A}^r\underline{A})^{-1} \cdot \underline{A}^r \begin{bmatrix} v_{ij} \\ v_j \\ \vdots \\ v_{Nj} \end{bmatrix} \qquad (C.2)$$

where

$$\underline{A} = \begin{bmatrix} 1 & \alpha_1 & \alpha_1^2 \text{------} \alpha_1^{n-1} \\ 1 & \alpha_2 & \alpha_2^2 \text{------} \alpha_2^{n-1} \\ \vdots & \vdots & \vdots \\ 1 & \alpha_N & \alpha_N^2 \text{------} \alpha_N^{n-1} \end{bmatrix}$$

If the above procedure is applied to all the j values

then

$$\underline{a} = \begin{bmatrix} a_1 \\ a_2 \\ \\ \\ a_n \end{bmatrix}_j$$

Now considering the variation of a w.r.t. β,

let

$$a_j = \underline{\alpha}_1 + \underline{\alpha}_2\beta_j^2 \text{ ----------} + \underline{\alpha}_m\beta_j^{m-1} \qquad \text{(C.3)}$$

where m is the degree of the polynomial.

Then, as before

$$\begin{bmatrix} \alpha_{11} \\ \alpha_{21} \\ \\ \\ \alpha_{m1} \end{bmatrix} = (\underline{B}^r\underline{B})^{-1}\underline{B}^r \begin{bmatrix} a_{11} \\ a_{12} \\ \\ \\ a_{1M} \end{bmatrix}$$

and similarly for j = 2, 3 - - m.

where

$$\underline{B} = \begin{bmatrix} 1 & \beta_1 & \beta_1^2 - - - - \beta_1^{m-1} \\ 1 & \beta_2 & \beta_2^2 - - - - \beta_2^{m-1} \\ \vdots & \vdots & \vdots \\ 1 & \beta_M & \beta_M^2 - - - - \beta_M^{m-1} \end{bmatrix}$$

But

$$v_{ij} = (1\ \alpha_i\ \alpha_i^2 \text{ ---------} \alpha_i^{n-1}) \begin{bmatrix} a_1 \\ a_2 \\ \\ \\ a_n \end{bmatrix}$$

$$v_{ij} = (1\ \alpha_i\ \alpha_i^2 \text{ --------} \alpha_i^{n-1}) \begin{bmatrix} \underline{\alpha}_1 & \underline{\alpha}_2 & \text{-------} & \underline{\alpha}_m \end{bmatrix} \begin{bmatrix} 1 \\ \beta_j \\ \beta_j^2 \\ \\ \beta_j^{m-1} \end{bmatrix}$$

The matrix $\underline{\alpha}$ is given by

$$\begin{bmatrix} \alpha_{11} & \alpha_{12} \text{----} \alpha_{1n} \\ \alpha_{21} & \alpha_{22} \text{----} \alpha_{2n} \\ \vdots & \vdots \\ \alpha_{m1} & \alpha_{m2} \text{----} \alpha_{mn} \end{bmatrix} = (\underline{B}^r\underline{B})^{-1}.\underline{B}^r \begin{bmatrix} a_{11} & a_{12} \text{----} a_{n1} \\ a_{12} & a_{22} \text{----} a_{n2} \\ \vdots & \vdots \\ a_{1M} & a_{2M} \text{----} a_{nM} \end{bmatrix}$$

i.e. $$\alpha = (B^rB)^{-1}.\ B^r\ a^r \qquad (C.4)$$

Using equation (C.2) to eliminate a from equation (C.4) yields

$$\underline{\alpha} = (\underline{B}^r\underline{B})^{-1}.\underline{B}^r \begin{bmatrix} v_{11} & v_{21} \text{----} v_{N1} \\ v_{12} & v_{22} \text{----} v_{N2} \\ \vdots & \vdots \\ v_{1M} & v_{2M} \text{----} v_{NM} \end{bmatrix} \underline{A}.(\underline{A}^r\underline{A})^{-1}$$

and finally

$$\underline{v}_{ij} = (1\ \alpha_i\ \alpha_i^2 \text{ -----} \alpha_i^{n-1}).(\underline{A}^r\underline{A})^{-1}.\underline{A}^r\underline{V}.\underline{B}.(\underline{B}^r\underline{B})^{-1} \begin{bmatrix} 1 \\ \beta_j \\ \beta_j^2 \\ \vdots \\ \beta_j^{m-1} \end{bmatrix}$$

where $\underline{v}$ and $\underline{V}$ are the calculated and experimental values of the function respectively.

or

$$\underline{v}_{ij} = \underline{\alpha}^{r} . \underline{M} . \underline{\beta}$$

where M is calculated from experimental information.

Now it is possible to obtain a smooth set of values for v_{ij}. However, as always there are unacceptable "rogue" points in the raw data. The test for their existence is as follows:

Let v and v* be the experimental and fitted values of the population, then the variance is given by

$$S = \sum_{i=1}^{N} \sum_{j=1}^{M} (v_{ij} - v^{*}_{ij})^2$$

and the standard deviation is

$$\sigma = \sqrt{S/(NxM - nxm)}$$

If at any point $|(v_{ij} - v^{*}_{ij})| > 2\sigma$ then that point is a "rogue" point.

This 'rogue' point is replaced by a new point estimated on the following basis;

Consider c to be a 'rogue' point. It may be replaced by an estimate based on the points surrounding it provided suitable weightings are introduced.

From Taylor's series the value at any point is

$$v(x,y) = v_c + h(\partial v_c/\partial x + \partial v_c/\partial y) + [h^2/2!] (\partial^2 v_c/\partial x^2 + \partial^2 v_c/\partial x \partial y + \partial^2 v_c/\partial y^2) + \text{------}$$

$$= v_c \exp (hD_x + hD_y)$$

where $D_x = \frac{\partial}{\partial x}$ and $D_y = \frac{\partial}{\partial y}$

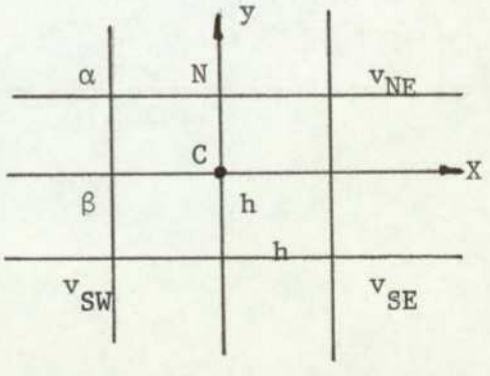

From the figure

$$v_{sw} + v_{ne} = \left[\exp(-hD_x - hD_y) + \exp(hD_x + hD_y)\right] v_c$$

$$= 2v_c \,.\mathrm{Cosh}.(h.(D_x + D_y))$$

Considering all the nodes surrounding c with their respective weightings and replacing hD_x and hD_y by θ and ϕ yields

$$v_c \left(\alpha\left[2\ \mathrm{Cosh}\ (\theta+\phi) + 2\ \mathrm{Cosh}\ (\theta-\phi)\right] + \beta\left[2\ \mathrm{Cosh}\theta + 2\ \mathrm{Cosh}\phi\right] \right) = v_c$$

i.e. $4\alpha\ \mathrm{Cosh}\theta\ \ \mathrm{Cosh}\phi + 2\beta\ (\mathrm{Cosh}\theta + \mathrm{Cosh}\phi) = 1$

expanding in series from

$$4\alpha\left[1 + \theta/2! + \text{----}\right]\left[1 + \phi/2! + \text{----}\right] + 2\beta\left[2 + (\theta+\phi)/2 + \text{---}\right] = 1$$

from which

$$\alpha = 1/4 \text{ and } \beta = 1/2$$

Thus

$$v_c = \tfrac{1}{2}\left[v_n + v_s + v_e + v_w\right] - \tfrac{1}{4}\left[v_{ne} + v_{se} + v_{sw} + v_{nw}\right]$$

Similarly it could be shown that for an end point

$$\alpha = 1/2;\quad \beta = 1/2 \quad \text{and} \quad \Upsilon = 1$$

and that

$$v_c = \tfrac{1}{2}\ (v_n + v_s) - \tfrac{1}{2}(v_{ne} + v_{se}) + v_e$$